

UMTA-MA-06-0100-83-1

DOT-TSC-UMTA-82-37



U.S. Department  
of Transportation

**Urban Mass  
Transportation  
Administration**

# **Design Recommendations for Concrete Tunnel Linings**

## Volume I: Results of Model Tests and Analytical Parameter Studies

---

S.L. Paul  
A.J. Hendron  
E.J. Cording  
G.E. Sgouros  
P.K. Saha

University of Illinois at Urbana-Champaign  
Department of Civil Engineering  
Urbana IL 61801

November 1983  
Final Report

This document is available to the public  
through the National Technical Information  
Service, Springfield, Virginia 22161.

**UMTA Technical Assistance Program**

**NOTICE**

This document is disseminated under the sponsorship of the Department of Transportation in the interest of information exchange. The United States Government assumes no liability for its contents or use thereof.

**NOTICE**

The United States Government does not endorse products or manufacturers. Trade or manufacturers' names appear herein solely because they are considered essential to the object of this report.

1. Report No. UMTA-MA-06-0100-83-1		2. Government Accession No.		3. Recipient's Catalog No.	
4. Title and Subtitle DESIGN RECOMMENDATIONS FOR CONCRETE TUNNEL LININGS - VOLUME I: RESULTS OF MODEL TESTS AND ANALYTICAL PARAMETER STUDIES				5. Report Date November 1983	
				6. Performing Organization Code DTS-77	
7. Author(s) S. L. Paul, A. J. Hendron, E. J. Cording, G. E. Sgouros, P. K. Saha				8. Performing Organization Report No. DOT-TSC-UMTA-82-37	
9. Performing Organization Name and Address University of Illinois at Urbana-Champaign* Department of Civil Engineering Urbana, Illinois 61801				10. Work Unit No. (TRAIS) UM476/R4642	
				11. Contract or Grant No. DOT-TSC-1504	
12. Sponsoring Agency Name and Address U.S. Department of Transportation Urban Mass Transportation Administration Office of Technical Assistance Washington DC 20590				13. Type of Report and Period Covered Final Report April 1978 - July 1981	
				14. Sponsoring Agency Code URT-10	
15. Supplementary Notes *Under Contract to:		U.S. Department of Transportation Research and Special Programs Administration Transportation Systems Center Cambridge, MA 02142			
16. Abstract <p>This report describes model tests and analytical studies that were performed to augment background information based on experience, interviews with design engineers, and review of the literature to propose design recommendations for concrete tunnel linings.</p> <p>Tests of model arches that represent underground stations and circular linings that represent continuous tunnels in rock-like media are described. Ten arches, 6 ft (1.8 m) diameter, were tested to investigate modes of failure and determine the effects of lining thickness, medium stiffness, lining stiffness, lining reinforcement, shear between the lining, and medium and active load shape. Tests are also described of five circular linings, 1.0 in. (25 mm) thick and 44 in. (1120 mm) diameter, in which the effects of lining reinforcement, medium stiffness, and joints in the lining are investigated.</p> <p>A computer based analysis is described that will simulate a concrete lining and include the nonlinear behavior due to material properties of the concrete and reinforcement and cracking of the concrete. In the analysis, the nonlinearity due to deformations can also be included. The medium around the lining can be represented by radial and tangential springs or by continuum elements, and in the latter case, a special interface element between the lining and medium may be used. This analysis was used to simulate the model tests to verify the program and the various input parameters, and then to investigate the various parameters that have a major influence on lining behavior and lining-medium interaction.</p>					
17. Key Words Tunnel Linings Concrete Linings Model Studies Ground/Structure Interaction			18. Distribution Statement  DOCUMENT IS AVAILABLE TO THE PUBLIC THROUGH THE NATIONAL TECHNICAL INFORMATION SERVICE, SPRINGFIELD, VIRGINIA 22161		
19. Security Classif. (of this report) Unclassified		20. Security Classif. (of this page) Unclassified		21. No. of Pages 520	22. Price





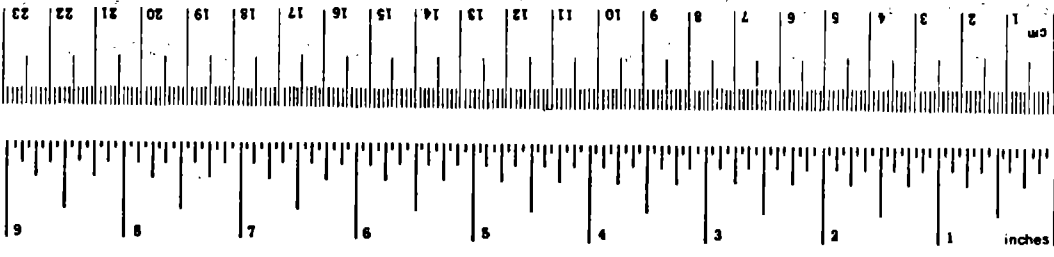


## PREFACE

The studies described in this report were performed by the staff of the Department of Civil Engineering of the University of Illinois at Urbana-Champaign, Urbana, Illinois during the period April 1978 to July 1981. The work was sponsored by the U.S. Department of Transportation, Urban Mass Transportation Administration under contract with the Transportation Systems Center, Cambridge, Massachusetts and performed under the technical direction of Mr. Gerald Saulnier and Ms. Beth Madnick. Their helpful suggestions, advice and patience are gratefully acknowledged. The authors also wish to acknowledge the special assistance and guidance of Professor C. P. Siess, for his help in interpretation and understanding of the concrete lining behavior, and Professor D.A.W. Pecknold, who offered invaluable guidance in development of the computer analysis.

# METRIC CONVERSION FACTORS

Approximate Conversions from Metric Measures		Approximate Conversions to Metric Measures	
When You Know	Multiply by	When You Know	Multiply by
Symbol	To Find	Symbol	To Find
<b>LENGTH</b>			
mm	inches	inches	mm
cm	inches	feet	cm
m	feet	yards	m
m	yards	miles	km
km	miles		
<b>AREA</b>			
cm <sup>2</sup>	square centimeters	square centimeters	cm <sup>2</sup>
m <sup>2</sup>	square meters	square meters	m <sup>2</sup>
km <sup>2</sup>	square kilometers	square yards	m <sup>2</sup>
ha	hectares (10,000 m <sup>2</sup> )	square miles	km <sup>2</sup>
	acres		ha
<b>MASS (weight)</b>			
g	grams	ounces	g
kg	kilograms	pounds	kg
t	tonnes (1000 kg)	short tons	t
<b>VOLUME</b>			
ml	milliliters	fluid ounces	ml
l	liters	pints	l
l	liters	quarts	l
l	liters	gallons	l
m <sup>3</sup>	cubic meters	cubic feet	m <sup>3</sup>
m <sup>3</sup>	cubic meters	cubic yards	m <sup>3</sup>
<b>TEMPERATURE (exact)</b>			
°C	Celsius temperature	°F	Fahrenheit temperature
			9/5 (then add 32)



Approximate Conversions to Metric Measures		Approximate Conversions from Metric Measures	
When You Know	Multiply by	When You Know	Multiply by
Symbol	To Find	Symbol	To Find
<b>LENGTH</b>			
inches	*2.5	cm	centimeters
feet	30	cm	centimeters
yards	0.9	m	meters
miles	1.6	km	kilometers
<b>AREA</b>			
square inches	6.5	square centimeters	cm <sup>2</sup>
square feet	0.09	square meters	m <sup>2</sup>
square yards	0.8	square meters	m <sup>2</sup>
square miles	2.6	square kilometers	km <sup>2</sup>
acres	0.4	hectares	ha
<b>MASS (weight)</b>			
ounces	28	grams	g
pounds	0.45	kilograms	kg
short tons (2000 lb)	0.9	tonnes	t
<b>VOLUME</b>			
teaspoons	5	milliliters	ml
tablespoons	15	milliliters	ml
fluid ounces	30	milliliters	ml
cups	0.24	liters	l
pints	0.47	liters	l
quarts	0.96	liters	l
gallons	3.8	liters	l
cubic feet	0.03	cubic meters	m <sup>3</sup>
cubic yards	0.76	cubic meters	m <sup>3</sup>
<b>TEMPERATURE (exact)</b>			
°F	Fahrenheit temperature	°C	Celsius temperature
			5/9 (after subtracting 32)

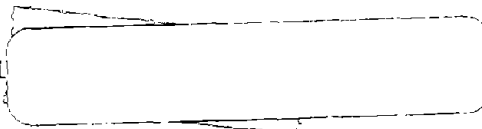
\*1 in = 2.54 (exact). For other exact conversions and more detailed tables, see NBS Misc. Publ. 286, Units of Weights and Measures, Price \$2.25, SO Catalog No. C13.10/286.

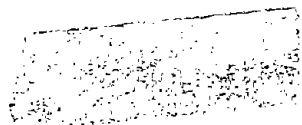
## TABLE OF CONTENTS

	<u>Page</u>
1. INTRODUCTION . . . . .	1
2. BACKGROUND . . . . .	6
2.1 EXPLANATION OF CONCEPTS . . . . .	6
2.2 PREVIOUS STUDIES . . . . .	18
2.3 MODEL LAWS AND SIMILITUDE CONSIDERATIONS . . . . .	24
2.3.1 Basic Considerations . . . . .	24
2.3.2 Similitude Considerations . . . . .	25
2.3.3 Applicability and Reliability of Results . . . . .	33
3. NUMERICAL MODELS . . . . .	36
3.1 INTRODUCTION . . . . .	36
3.2 REPRESENTATION OF THE LINING . . . . .	37
3.3 REPRESENTATION OF THE GROUND . . . . .	39
3.3.1 Beam-Spring Model . . . . .	39
3.3.2 Beam-Continuum Model . . . . .	40
3.4 SOLUTION TECHNIQUE . . . . .	42
3.5 COMPUTATION OF MOMENT-THRUST ENVELOPE . . . . .	44
4. MODEL TESTS OF ARCHES IN HARD MEDIUM . . . . .	46
4.1 PURPOSE OF THE TESTS . . . . .	46
4.2 DESCRIPTION OF THE TESTS . . . . .	50
4.2.1 Test Facility . . . . .	50
4.2.2 Loads . . . . .	63
4.2.3 In-Situ Plate Load Tests on the Medium . . . . .	65
4.2.4 Specimen Preparation . . . . .	72
4.2.5 Instrumentation and Test Procedure . . . . .	79
4.3 TEST RESULTS . . . . .	84
4.3.1 Behavior and Ultimate Capacity of the Linings . . . . .	84
4.3.2 Deformability and Cracking of the Linings . . . . .	97
4.3.3 Base Loads and Deformations . . . . .	126
4.3.4 Failure Mechanisms . . . . .	128

	<u>Page</u>
4.4 FINITE ELEMENT ANALYSIS AND COMPARISON WITH EXPERIMENTS . . . . .	149
4.4.1 Description of Input Data . . . . .	149
4.4.2 Comparison with Experimental Results . . . . .	156
4.5 DISCUSSION OF TEST RESULTS . . . . .	164
5. PARAMETER STUDY FOR ARCHES IN ROCK . . . . .	172
5.1 DESCRIPTION OF THE STUDY . . . . .	172
5.2 EFFECT OF LOADING SHAPES . . . . .	176
5.3 EFFECT OF FLEXIBILITY RATIO F . . . . .	178
5.4 EFFECT OF THE RATIO OF TANGENTIAL TO RADIAL STIFFNESS OF THE MEDIUM ( $K_t/K_r$ ) . . . . .	190
5.5 EFFECT OF REINFORCEMENT . . . . .	195
5.6 EFFECT OF RADIUS TO THICKNESS RATIO . . . . .	197
5.7 DESIGN IMPLICATIONS . . . . .	197
6. MODEL TESTS OF CIRCLES IN SOFT MEDIUM . . . . .	202
6.1 PURPOSE OF THE TESTS . . . . .	202
6.2 DESCRIPTION OF THE TESTS . . . . .	203
6.2.1 Test Facility . . . . .	203
6.2.2 Development of the Medium . . . . .	207
6.2.3 Specimen Preparation . . . . .	213
6.2.4 Instrumentation and Test Procedure . . . . .	217
6.3 TEST RESULTS . . . . .	221
6.3.1 Behavior and Ultimate Capacity of the Linings . . . . .	221
6.3.2 Deformability and Cracking of the Linings . . . . .	231
6.3.3 Failure Mechanisms . . . . .	247
6.4 FINITE ELEMENT ANALYSIS AND COMPARISON WITH EXPERIMENTS . . . . .	255
6.4.1 Description of Input Data . . . . .	255
6.4.2 Determination of the Medium Stiffness . . . . .	257
6.4.3 Comparison with Experimental Results . . . . .	260
6.5 DISCUSSION OF TEST RESULTS . . . . .	264
7. PARAMETER STUDY FOR CIRCULAR LININGS . . . . .	269
7.1 INTRODUCTION . . . . .	269
7.2 DESCRIPTION OF THE STUDY FOR LININGS IN ROCK . . . . .	270
7.2.1 Effect of Flexibility Ratio F . . . . .	274
7.2.2 Effect of the Ratio of Tangential to Radial Stiffness of the Medium ( $K_t/K_r$ ) . . . . .	290

	<u>Page</u>
7.2.3 Effect of Radius to Thickness Ratio (R/t) . . . . .	304
7.2.4 Effect of Reinforcement. . . . .	304
7.2.5 Discussion of Results. . . . .	309
7.3 DESCRIPTION OF THE STUDY FOR LININGS IN SOFT GROUND . . .	317
7.3.1 Effect of Interface Properties . . . . .	321
7.3.2 Effect of Water Pressure . . . . .	325
7.3.3 Effect of Loading Conditions . . . . .	329
7.3.4 Effect of Reinforcement. . . . .	339
7.3.5 Effect of Joints in Segmented Linings. . . . .	346
7.3.6 Discussion of Results. . . . .	348
8. SUMMARY OF RESULTS OF MODEL TESTS AND PARAMETRIC STUDIES . . .	352
8.1 MODEL TEST RESULTS. . . . .	352
8.2 PARAMETRIC STUDIES. . . . .	358
APPENDIX A: DETAILED DESCRIPTION OF EXISTING DESIGN PRACTICE FOR CONCRETE TUNNEL LININGS . . . . .	367
APPENDIX B: FORMULATION OF INTERFACE ELEMENT. . . . .	465
APPENDIX C: REPORT OF NEW TECHNOLOGY. . . . .	474
REFERENCES . . . . .	475





LIST OF FIGURES

FIGURE		<u>Page</u>
2.1	ANALYSIS SIMULATION WITH OVERPRESSURE AND EXCAVATION LOADING . . . . .	16
2.2	GEOMETRIC, LOADING AND RESPONSE VARIABLES . . . . .	28
3.1	NODAL DISPLACEMENT AND COORDINATE SYSTEM FOR THE BEAM-ELEMENT . . . . .	38
3.2	MATERIAL PROPERTIES REPRESENTATION FOR ANALYSIS . . . . .	38
3.3	QUADRATIC PARENT ELEMENT AND ISOPARAMETRIC ELEMENT . . . . .	41
3.4	INCREMENTAL-ITERATIVE NONLINEAR ANALYSIS . . . . .	41
4.1	PLAN VIEW OF TEST SETUP . . . . .	49
4.2	TOP VIEW OF THE TUNNEL OPENING . . . . .	51
4.3	TEST FACILITY WITH FORM IN PLACE FOR CASTING ARCH SPECIMEN . . . . .	53
4.4	RUBBER USED TO REDUCE EFFECTIVE MODULUS OF THE MEDIUM . . . . .	53
4.5	SERRATIONS ON THE MEDIUM SURFACE FOR MECHANICAL INTERLOCK WITH THE ARCH SPECIMEN . . . . .	54
4.6	MECHANICAL INTERLOCK ELIMINATED BY FILLING THE SERRATIONS IN THE MEDIUM . . . . .	54
4.7	TOP VIEW OF THE LOADING SYSTEM . . . . .	57
4.8	SIDE VIEW OF TEST RAMS . . . . .	58
4.9	OUTLINE OF HYDRAULIC SYSTEM . . . . .	60
4.10	HYDRAULIC ACTUATORS USED TO PRODUCE NON-UNIFORM LOADINGS . . . . .	61
4.11	SET-UP FOR RIGID BLOCK LOADING . . . . .	61
4.12	LOADING CONFIGURATIONS . . . . .	64
4.13	LOCATIONS OF IN-SITU PLATE LOAD TESTS . . . . .	66
4.14	POSITION OF DIAL GAGES DURING IN-SITU PLATE LOAD TESTS FOR ARCHES 1 TO 6 . . . . .	66
4.15	DIAL GAGE ARRANGEMENT FOR THE IN-SITU PLATE LOAD TESTS . . . . .	68
4.16	PLATE LOAD TEST IN PROGRESS . . . . .	68
4.17	TYPICAL IN-SITU PLATE LOAD TEST DATA FOR ARCHES 1 TO 6 . . . . .	70

**Preceding page blank**



	<u>Page</u>
4.18	FORM FOR CASTING SPECIMENS . . . . . 73
4.19	CASTING OPERATION FOR THE ARCH SPECIMENS . . . . . 75
4.20	REINFORCEMENT FOR ARCH-10 . . . . . 78
4.21	DIAL GAGE LOCATIONS IN TEST . . . . . 80
4.22	DIAL GAGES IN PLACE ON A SPECIMEN . . . . . 80
4.23	SIDE VIEW OF THE BASE MECHANISM . . . . . 82
4.24	TOP VIEW OF THE BASE MECHANISM . . . . . 82
4.25	BASE MECHANISM AS CONSTRUCTED . . . . . 83
4.26	DATA ACQUISITION AND CONTROL SYSTEMS . . . . . 83
4.27	TOTAL LOAD VS DEFORMATION AT CROWN AND BASE OF ARCH 1 AND 5 . . . . . 87
4.28	TOTAL LOAD VS DEFORMATION AT CROWN AND BASE OF ARCH 2 . . . 88
4.29	TOTAL LOAD VS DEFORMATION AT CROWN, BASE, AND 15R OF ARCH 3 . . . . . 90
4.30	TOTAL LOAD VS DEFORMATION AT CROWN, BASE, AND 15L OF ARCH 4 . . . . . 91
4.31	TOTAL LOAD VS DEFORMATION AT CROWN AND BASE OF ARCH 6 . . . 92
4.32	TOTAL LOAD VS DEFORMATION AT CROWN, BASE, 20 AND 30R OF ARCH 7 . . . . . 94
4.33	TOTAL LOAD VS DEFORMATION AT CROWN AND BASE OF ARCHES 1 AND 8 . . . . . 95
4.34	TOTAL LOAD VS DEFORMATION AT CROWN AND BASE OF ARCHES 9 AND 10 . . . . . 96
4.35	DEFORMATION OF ARCHES 1 AND 5 AT 50% LOAD . . . . . 101
4.36	DEFORMATION OF ARCHES 1 AND 5 AT 100% LOAD . . . . . 102
4.37	DEFORMATION OF ARCH 2 AT 96% LOAD . . . . . 103
4.38	DEFORMATION OF ARCH 2 AT 50% LOAD . . . . . 104
4.39	FIRST CRACKS IN ARCH-2 . . . . . 106
4.40	FIRST CRACKS IN ARCH-5 . . . . . 106

	<u>Page</u>
4.41	DEFORMATION OF ARCH 3 AT 100% LOAD . . . . . 107
4.42	DEOFRMATION OF ARCH 3 AT 50% LOAD . . . . . 108
4.43	DEFORMATION OF ARCH 4 AT 50% LOAD . . . . . 109
4.44	DEFORMATION OF ARCH 4 AT 100% LOAD . . . . . 110
4.45	DEFORMATION OF ARCH 6 AT 50% LOAD . . . . . 112
4.46	DEFORMATION OF ARCH 6 AT 95% LOAD . . . . . 113
4.47	DEFORMATION OF ARCH 7 AT 50% LOAD . . . . . 115
4.48	DEFORMATION OF ARCH 7 AT 100% LOAD . . . . . 116
4.49	SEPARATION BETWEEN THE LINING AND THE MEDIUM, ARCH-7 . . 117
4.50	FIRST CRACKING OF ARCH-7 . . . . . 117
4.51	DEFORMATION OF ARCHES 1 AND 8 AT 50% LOAD . . . . . 118
4.52	DEFORMATION OF ARCHES 1 AND 8 AT 97% LOAD . . . . . 119
4.53	FIRST CRACKING OF ARCH-8 . . . . . 120
4.54	DEFORMATION OF ARCHES 9 AND 10 AT 50% LOAD . . . . . 122
4.55	DEFORMATION OF ARCHES 9 AND 10 AT 100% LOAD . . . . . 123
4.56	INITIAL SHRINKAGE CRACKS IN ARCH-9 . . . . . 124
4.57	CRACKING OF ARCH-9 . . . . . 125
4.58	CRACKING OF ARCH-10 . . . . . 126
4.59	MAP OF DAMAGE TO ARCH-1 AT FAILURE . . . . . 129
4.60	ARCH-1 AT FAILURE . . . . . 130
4.61	FAILURE AT 35 DEGREES TO THE RIGHT OF THE CROWN OF ARCH-1 . . . . . 130
4.62	MAP OF DAMAGE TO ARCH-2 AT FAILURE . . . . . 131
4.63	COMPRESSIVE FAILURE ZONE OF ARCH-2 . . . . . 132
4.64	CROWN OF ARCH-2 AT FAILURE . . . . . 132
4.65	MAP OF DAMAGE TO ARCH-3 AT FAILURE . . . . . 134
4.66	FAILURE ZONE AT 35 DEGREES TO THE RIGHT OF THE CROWN IN ARCH-3 . . . . . 135
4.67	MAP OF DAMAGE TO ARCH-4 FAILURE . . . . . 136
4.68	COMPRESSION ZONE OF ARCH-4 AT FAILURE . . . . . 137
4.69	CROWN OF ARCH-4 AT FAILURE . . . . . 137

	<u>Page</u>
4.70	MAP OF DAMAGE TO ARCH-5 AT FAILURE . . . . . 139
4.71	ARCH-5 AT FAILURE . . . . . 140
4.72	FAILED REGION OF ARCH-6 . . . . . 141
4.73	MAP OF DAMAGE TO ARCH-6 AT FAILURE . . . . . 142
4.74	MAP OF DAMAGE TO ARCH-7 AT FAILURE . . . . . 143
4.75	ARCH-7 AT FAILURE . . . . . 144
4.76	ARCH-8 AT FAILURE . . . . . 144
4.77	MAP OF DAMAGE TO ARCH-8 AT FAILURE . . . . . 145
4.78	MAP OF DAMAGE TO ARCH-9 AT FAILURE . . . . . 147
4.79	ARCH-9 AT FAILURE . . . . . 148
4.80	ARCH-10 AT FAILURE . . . . . 148
4.81	MAP OF DAMAGE TO ARCH-10 AT FAILURE . . . . . 150
4.82	FINITE ELEMENT MODEL OF THE ARCH FOR SIMULATION OF TESTS . . . . . 151
4.83	INTERACTION DIAGRAM OF ARCH 1 . . . . . 160
4.84	INTERACTION DIAGRAM OF ARCH 3 . . . . . 161
4.85	INTERACTION DIAGRAM OF ARCH 7 . . . . . 162
4.86	EFFECTS OF LOADING SHAPE AND FLEXIBILITY RATIO ON THE THRUST RATIO . . . . . 168
4.87	FIRST CRACKING AS A FUNCTION OF FLEXIBILITY RATIO . . . . . 170
5.1a	FINITE ELEMENT MODEL FOR PARAMETER STUDIES OF ARCHES . . . . . 173
5.1b	CONCRETE STRESS-STRAIN CURVE USED IN THE PARAMETER STUDY . . . . . 174
5.2	MOMENT-THRUST PATHS FOR CRITICAL SECTION FOR VARIOUS LOAD SHAPES . . . . . 177
5.3	MOMENT-THRUST PATHS FOR $K_t/K_r = 0$ AND VARIOUS FLEXIBILITY RATIOS . . . . . 179
5.4	MOMENT-THRUST PATHS FOR $K_t/K_r = 12.5\%$ VARIOUS FLEXIBILITY RATIOS . . . . . 180
5.5	MOMENT-THRUST PATHS FOR $K_t/K_r = 25\%$ AND VARIOUS FLEXIBILITY RATIOS . . . . . 181

	<u>Page</u>
5.6	TOTAL LOAD VS FLEXIBILITY RATIO FOR ARCHES . . . . . 182
5.7	THRUST RATIO VS FLEXIBILITY RATIO FOR ARCHES . . . . . 183
5.8	THRUST RATIO VS TOTAL ULTIMATE LOAD FOR ARCHES . . . . . 185
5.9	VAIATION OF RADIUS CHANGE RATIO AT FAILURE WITH FLEXIBILITY RATIO . . . . . 186
5.10	THRUST DISTRIBUTION AT MAXIMUM LOAD FOR VARIOUS F AND $K_t/K_r$ . . . . . 187
5.11	MOMENT DISTRIBUTION AT MAXIMUM LOAD FOR VARIOUS $K_t/K_r$ AND FOR VARIOUS FLEXIBILITY RATIOS . . . . . 188
5.12	SHEAR DISTRIBUTIONS AT MAXIMUM LOAD FOR VARIOUS F AND FOR VARIOUS $K_t/K_r$ . . . . . 189
5.13	TANGENTIAL SHEAR STRESS AND RADIAL PRESSURE DISTRIBUTION FOR VARIOUS FLEXIBILITY RATIOS . . . . . 191
5.14	EFFECT OF $K_t/K_r$ ON MOMENT-THRUST PATHS FOR ARCHES . . . . 192
5.15	EFFECT OF $K_t/K_r$ ON THRUST RATIO FOR ARCHES . . . . . 194
5.16	TANGENTIAL SHEAR STRESS AND RADIAL PRESSURE DISTRIBUTION FOR VARIOUS $K_t/K_r$ . . . . . 196
5.17	EFFECT OF REINFORCEMENT ON MOMENT-THRUST PATHS FOR ARCHES . . . . . 198
5.18	EFFECT OF REINFORCEMENT ON THRUST RATIO FOR ARCHES . . . . 199
6.1	TEST SETUP FOR CIRCULAR LININGS . . . . . 204
6.2	VIEW OF THE LOADING RAMS . . . . . 206
6.3	CEMENT-FLY ASH-STYROFOAM BEAD MEDIUM IN THE PROCESS OF BEING REMOVED, CIRCLE-1 . . . . . 210
6.4	STRESS-STRAIN CURVE FOR MEDIUM OF CIRCLE-4 . . . . . 211
6.5	LINING DIMENSIONS AND REINFORCEMENT ARRANGEMENT FOR SEGMENTED LININGS . . . . . 215
6.6	REINFORCEMENT AND JOINT DETAILS, CIRCLE-4 . . . . . 216
6.7	OVERALL VIEW OF THE FORM . . . . . 216
6.8	DEFORMATION MEASURING DIAL GAGES . . . . . 218

	<u>Page</u>
6.9	JOINT ROTATION MEASURING DEVICE . . . . . 218
6.10	LOCATION OF STRAIN GAGES . . . . . 220
6.11	STRAIN GAGES INSTALLED ON THE LINING, CIRCLE-3 . . . . . 222
6.12	LOAD-DEFLECTION CURVES OF MONOLITHIC LININGS . . . . . 224
6.13	MOMENT-THRUST PATH AT CROWN AND LEFT SPRINGLINE OF CIRCLE-1 . . . . . 225
6.14	MOMENT-THRUST PATHS AT CROWN AND 70 DEGREES RIGHT OF CIRCLE-2 . . . . . 226
6.15	MOMENT-THRUST PATHS AT CROWN AND 70 DEGREES RIGHT OF CIRCLE-3 . . . . . 228
6.16	LOAD-DEFLECTION CURVES OF SEGMENTED LININGS . . . . . 229
6.17	MOMENT-THRUST PATHS AT CROWN AND 60 DEGREES RIGHT JOINT OF CIRCLE-4 . . . . . 230
6.18	MOMENT-THRUST PATHS AT CROWN AND 60 DEGREES RIGHT JOINT OF CIRCLE-5 . . . . . 232
6.19	COMPARISON OF LOAD-DEFLECTION CURVE OF MONOLITHIC AND SEGMENTED LININGS . . . . . 233
6.20	DEFLECTED SHAPES OF CIRCLE 1 AT 50 AND 100 PERCENT OF PEAK LOAD . . . . . 235
6.21	EFFECT OF AMOUNT OF REINFORCEMENT ON CRACK SIZE . . . . . 236
6.22	CRACKING PATTERN OF CIRCLE-1 . . . . . 237
6.23	DEFLECTED SHAPES OF CIRCLE 2 AND 5 AT 50 AND 100 PERCENT OF PEAK LOAD . . . . . 238
6.24	CRACKING PATTERN OF CIRCLE-2 . . . . . 239
6.25	DEFLECTED SHAPES OF CIRCLE-3 AT 50 AND 100 PERCENT OF PEAK LOAD . . . . . 241
6.26	CRACKING PATTERN OF CIRCLE-3 . . . . . 242
6.27	CRACKING PATTERN OF CIRCLE-4 . . . . . 243
6.28	LOAD VS JOINT ROTATIONS OF CIRCLE-4 . . . . . 244
6.29	DEFLECTED SHAPES OF CIRCLE-4 AT 50 AND 100 PERCENT OF PEAK LOAD . . . . . 245

	<u>Page</u>
6.30	CRACKING PATTERN OF CIRCLE-5 . . . . . 246
6.31	LOAD VS JOINT ROTATIONS OF CIRCLE-5 . . . . . 248
6.32	TYPE AND LOCATION OF FAILURE MODES IN CIRCLES . . . . . 249
6.33	CIRCLE-1 AT FAILURE . . . . . 250
6.34	CURVATURE VS DISTANCE FROM CROWN FOR CIRCLE-2 . . . . . 251
6.35	CIRCLE-2 AT FAILURE . . . . . 253
6.36	CIRCLE-3 AT FAILURE . . . . . 253
6.37	CIRCLE-4 AT FAILURE . . . . . 254
6.38	CIRCLE-5 AT FAILURE . . . . . 254
6.39	FINITE ELEMENT MODEL FOR SIMULATION OF CIRCLE TESTS . . . 256
6.40	IN-SITU PLATE LOAD TESTS FOR CIRCLES . . . . . 258
6.41	RESULTS OF RADIAL PLATE LOAD TEST ON MEDIUM FOR CIRCLE-4 . . . . . 259
6.42	STIFFNESS OF THE MEDIUM AND MEDIUM-LINING SYSTEM FOR DIFFERENT MODULI AND ELASTICITY . . . . . 261
6.43	COMPARISON OF EXPERIMENTAL AND ANALYTICAL RESULTS FOR CIRCLE-3 . . . . . 262
6.44	COMPARISON OF EXPERIMENTAL AND ANALYTICAL RESULTS FOR CIRCLE-4 . . . . . 263
7.1	FINITE ELEMENT MODEL OF CIRCULAR LINING FOR PARAMETRIC STUDIES . . . . . 271
7.2	LINING CAPACITY AS A FUNCTION OF FLEXIBILITY RATIO . . . 275
7.3	TOTAL LOAD VS FLEXIBILITY RATIO . . . . . 277
7.4	EFFECT OF FLEXIBILITY RATIO ON DIAMETER CHANGE . . . . . 278
7.5	EFFECT OF F ON MOMENT-THRUST PATHS AT CROWN . . . . . 280
7.6	EFFECT OF F ON THRUST AT MAXIMUM LOAD . . . . . 282
7.7	EFFECT OF F ON THRUST AT EQUAL LOAD . . . . . 284
7.8	EFFECT OF F ON MOMENT DISTRIBUTION AT MAXIMUM LOAD . . . 285
7.9	EFFECT OF F ON MOMENT AT EQUAL LOAD . . . . . 286
7.10	EFFECT OF F ON SHEAR AT MAXIMUM LOAD . . . . . 288
7.11	EFFECT OF F ON RADIAL PRESSURE AT MAXIMUM LOAD . . . . . 289
7.12	EFFECT OF F ON TANGENTIAL PRESSURE . . . . . 291

	<u>Page</u>
7.13	LINING CAPACITY AS A FUNCTION OF TANGENTIAL TO RADIAL STIFFNESS RATIO ( $K_t/K_r$ ) FOR $R/t = 11.83$ . . . . . 292
7.14	EFFECT OF $K_t/K_r$ ON DIAMETER CHANGE . . . . . 294
7.15	EFFECT OF $K_t/K_r$ ON MOMENT-THRUST PATHS AT CROWN . . . . . 295
7.16	EFFECT OF $K_t/K_r$ ON THRUST AT MAXIMUM LOAD . . . . . 297
7.17	EFFECT OF $K_t/K_r$ ON THRUST AT MAXIMUM LOAD . . . . . 298
7.18	EFFECT OF $K_t/K_r$ ON TANGENTIAL STRESS AT MAXIMUM LOAD. . . 299
7.19	EFFECT OF $K_t/K_r$ ON RADIAL STRESS AT MAXIMUM LOAD . . . . . 300
7.20	EFFECT OF $K_t/K_r$ ON MOMENT DISTRIBUTION AT MAXIMUM LOAD FOR $F = 7.5$ . . . . . 302
7.21	EFFECT OF $K_t/K_r$ ON MOMENT DISTRIBUTION AT MAXIMUM LOAD FOR $F = 6230$ . . . . . 303
7.22	EFFECT OF $K_t/K_r$ ON SHEAR AT MAXIMUM LOAD . . . . . 305
7.23	EFFECT OF REINFORCEMENT ON DIAMETER CHANGE . . . . . 307
7.24	EFFECT OF REINFORCEMENT ON MOMENT-THRUST PATHS . . . . . 308
7.25	EFFECT OF REINFORCEMENT ON THRUST DISTRIBUTION AT MAXIMUM LOAD . . . . . 310
7.26	EFFECT OF REINFORCEMENT ON MOMENT DISTRIBUTION AT MAXIMUM LOAD . . . . . 311
7.27	EFFECT OF REINFORCEMENT ON SHEAR DISTRIBUTION AT MAXIMUM LOAD . . . . . 312
7.28	EFFECT OF REINFORCEMENT ON TANGENTIAL STRESS DISTRIBUTION AT MAXIMUM LOAD . . . . . 313
7.29	EFFECT OF REINFORCEMENT ON RADIAL PRESSURE DISTRIBUTION AT MAXIMUM LOAD . . . . . 314
7.30	F.E. MODEL FOR PARAMETER STUDIES . . . . . 319
7.31	FINITE ELEMENT MODEL OF CIRCULAR LINING FOR PARAMETRIC STUDIES IN SOFT GROUND FOR LOOSENING LOAD . . . . . 320
7.32	THE IN-SITU STRESS STATE . . . . . 322
7.33	EFFECT OF $\phi$ AND $c$ ON RADIAL PRESSURE AND TANGENTIAL STRESS . . . . . 323
7.34	EFFECT OF $\phi$ AND $c$ ON AXIAL THRUST AND MOMENT . . . . . 324

	<u>Page</u>
7.35	EFFECT OF SLIPPAGE ON ULTIMATE LOAD . . . . . 326
7.36	EFFECT OF WATER PRESSURE ON MOMENT-THRUST PATHS . . . . . 327
7.37	RADIAL PRESSURE DISTRIBUTION FOR EXCAVATION LOADING . . . 330
7.38a	EFFECT OF LOADING CONDITION ON TOTAL ULTIMATE LOAD . . . 331
7.38b	EFFECT OF COEFFICIENT OF EARTH PRESSURE ON TOTAL LOAD . . 331
7.39	THRUST RATIO VS FLEXIBILITY RATIO FOR SOFT GROUND . . . . 333
7.40	COMPARISON OF LOADING CONDITIONS . . . . . 334
7.41	TOTAL LOAD VS DIAMETER CHANGE COEFFICIENT $\Delta D/D$ FOR EXCAVATION LOADING . . . . . 336
7.42	DIAMETER CHANGE COEFFICIENT VS FLEXIBILITY RATIO (LINEAR) . . . . . 337
7.43	DIAMETER CHANGE COEFFICIENT AT ULTIMATE LOAD VS FLEXIBILITY RATIO . . . . . 338
7.44	EFFECT OF NON-LINEARITY OF LINING ON TOTAL LOAD AND THRUST RATIO . . . . . 340
7.45	EFFECT OF REINFORCEMENT ON MOMENT-THRUST PATHS FOR OVERPRESSURE LOADING . . . . . 341
7.46	EFFECT OF REINFORCEMENT ON TOTAL LOAD AND CRACKING LOAD . . . . . 343
7.47	EFFECT OF REINFORCEMENT ON FIRST CRACKING FOR OVERPRESSURE LOADING . . . . . 344
7.48	EFFECT OF FLEXIBILITY RATIO ON FIRST CRACKING FOR EXCAVATION LOADING . . . . . 345
7.49	MOMENT COEFFICIENT VS MODULUS OF LINING FOR A MONOLITHIC LINING IN DIFFERENT SOIL MEDIA . . . . . 347
7.50	EQUIVALENT MODULUS OF ELASTICITY OF SEGMENTED LININGS . . 349
A.1	WMATA LOADING CRITERIA FOR HORSESHOE SHAPED TUNNELS IN SOFT GROUND . . . . . 373
A.2	WMATA LOADING CRITERIA FOR CIRCULAR SHAPED TUNNELS IN SOFT GROUND . . . . . 375



	<u>Page</u>
A.3	WMATA LOADING CRITERIA FOR RUNNING TUNNELS IN ROCK-- CASES AT I AND II . . . . . 378
A.4	WMATA LOADING CRITERIA FOR RUNNING TUNNELS IN ROCK-- CASES III AND IV . . . . . 379
A.5	WMATA LOADING CRITERIA FOR RUNNING TUNNELS IN ROCK-- CASE V . . . . . 380
A.6	WMATA LOADING CRITERIA FOR STATIONS IN ROCK--CASES I THRU IV . . . . . 382
A.7	WMATA LOADING CRITERIA FOR STATIONS IN ROCK--CASE V . . . 383
B.1	NODAL INTERFACE ELEMENT VISUALIZED AS A SET OF NORMAL AND TANGENTIAL SPRINGS . . . . . 467
B.2	GLOBAL ABSOLUTE DISPLACEMENT . . . . . 467
B.3	ORIENTATION OF THE NODAL INTERFACE ELEMENT . . . . . 468
B.4	MATERIAL PROPERTIES FOR INTERFACE ELEMENTS . . . . . 468

LIST OF TABLES

TABLE		<u>Page</u>
2.1	SIGNIFICANT VARIABLES. . . . .	29
2.2	DIMENSIONLESS pi-TERMS . . . . .	30
2.3	MODEL LAWS FOR A TRUE MODEL. . . . .	30
4.1	SUMMARY OF ARCH TESTS IN HARD MEDIUM . . . . .	47
4.2	TEST SPECIMEN CONCRETE MIXES . . . . .	74
4.3	TEST SPECIMEN THICKNESS AND CONCRETE PROPERTIES. . . . .	76
4.4	STRENGTH CHARACTERISTICS OF THE ARCHES . . . . .	86
4.5	DEFORMABILITY CHARACTERISTICS OF THE ARCHES. . . . .	99
4.6	CRACKING CHARACTERISTICS OF THE ARCHES . . . . .	100
4.7	COMPARISON OF MEASURED AND COMPUTED RESULTS. . . . .	157
4.8	SUMMARY OF ARCH TEST RESULTS . . . . .	165
6.1	SUMMARY OF CIRCULAR LINING TEST RESULTS. . . . .	212
7.1	EFFECT OF WATER PRESSURE ON VARIOUS PARAMETERS . . . . .	328

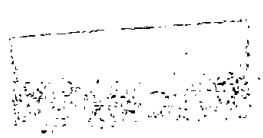


The first part of the document discusses the importance of maintaining accurate records of all transactions. It emphasizes that every entry should be supported by a valid receipt or invoice. This ensures transparency and allows for easy auditing of the accounts.

In the second section, the author details the various methods used to collect and analyze data. This includes both primary and secondary research techniques. The primary research involved direct observation and interviews with key stakeholders, while secondary research relied on existing industry reports and market analysis.

The third section provides a comprehensive overview of the findings. It highlights several key trends and insights that emerged from the data. These findings are crucial for understanding the current market landscape and identifying potential opportunities for growth.

Finally, the document concludes with a series of recommendations based on the research findings. These suggestions are designed to help the organization optimize its operations, improve its financial performance, and stay ahead of the competition in a rapidly changing market.



## LIST OF SYMBOLS

- A = area of the loaded surface in the plate load test
- C = compressibility ratio (Eq. 1.1)
- $C_o$  = arc length of the arch that is under compressive load from footing to the point where separation of arch and medium occurs for calculating the subgrade reaction
- $C_l$  = width of the footing of an underground arch
- D = diameter of the opening
- $E_{eq}$  = equivalent modulus used in segmented lining analysis
- $E_l$  = modulus of elasticity of the lining
- $E_m$  = modulus of elasticity of the medium
- $E_R$  = in-situ modulus of elasticity of a rock mass
- F = flexibility ratio (Eq. 1.2)
- $\underline{F}$  = fundamental dimension of force
- G = shear modulus of the medium at the lining-medium interface
- H = hydrostatic forces determined from maximum expected water level
- $I_l$  = moment of inertia of a unit length of lining

$K_F$  = stiffness of the spring that represents the footing of an underground arch

$K_o$  = coefficient of earth pressure at rest

$K_r$  = radial spring stiffness that represents the medium

$K_t$  = tangential spring stiffness that represents the medium

$L$  = surface line loads

$L$  = fundamental dimension of length

$P$  = total load on the loaded area

$P_{fc}$  = total load on the model test linings at first appearance of a flexural crack

$P_u$  = total load on the lining at failure

$R$  = mean radius of the lining

$R_m$  = maximum load expected (or overburden load) determined from local geology, thickness of rock above crown, width of opening, buoyancy and soil overburden

$R_T$  = typical rock loads determined from local geology, thickness of rock above crown, width of opening, buoyancy and soil overburden

$S$  = shape factor for loading used in the dimensional analysis

$T$  = fundamental dimension of time

$T_{eu}$  = prediction of ultimate thrust by linear analysis

- $T_o$  = failure thrust of the lining section due to axial load only
- $T_u$  = failure thrust of the lining section due to axial thrust and moment
- $W$  = weight of all structural components including fill of overbreak, back packing and grout to the rock line
- $\bar{W}$  = average displacement of the loaded surface in the plate load test
- $b$  = tunnel length that is represented by a spring
- $c$  = cohesion intercept describing the medium properties at the lining-medium interface
- $f'_c$  = compressive strength of concrete
- $f_2$  = confining stress of concrete in the lining
- $f_r$  = modulus of rupture of concrete
- $f'_{sp}$  = split-cylinder strength of concrete
- $k$  = modulus of subgrade reaction
- $\bar{m}$  = displacement coefficient dependent on the shape of the loaded surface and the distribution of load in the plate load test
- $p$  = internal pressure in a circular opening in a medium
- $q_u$  = unconfined compressive strength of a medium material
- $t$  = thickness of the lining

- $u$  = radial displacement of the lining in a medium  
 $\alpha$  = angle of repose of fresh concrete  
 $\theta$  = angular segment (in a plane perpendicular to the tunnel axis) for which the medium is represented by a spring  
 $\nu_l$  = Poisson's ratio for the lining  
 $\nu_m$  = Poisson's ratio for the medium  
 $\nu_R$  = in-situ-Poisson's ratio of a rock mass  
 $\pi$  = dimensionless term consisting of the physical variables in a dimensional analysis  
 $\phi$  = angle of internal friction of the medium material at the lining-medium interface  
 $\gamma_w$  = unit weight of water

## SUMMARY

The research described in this report was sponsored by the U.S. Department of Transportation, Urban Mass Transportation Administration and performed under the technical direction of the Transportation System Center, Cambridge, Massachusetts. The objective of the overall research effort was to formulate recommendations for the structural design of final concrete linings for tunnels and underground stations for mass transit use, that are based on ultimate strength concepts of concrete behavior and that take full advantage of interaction between the lining and ground. A need for some type of standards for design has been expressed by many designers. Also, there has been little uniformity of approach to lining designs in the past, that has led to widely varying strengths in similar ground conditions, and in some cases to over design and poor economy.

The report describing this work is in two volumes; in Volume II a summary of the research and the design recommendations are presented. In this report, Volume I, the model tests and analytic studies are described. In addition, the details of interviews conducted with 16 design firms are provided, to evaluate existing design practice. The results of these interviews helped to establish where problems exist in the design process and how recommendations can be integrated into the existing system.

Ten models of circular arches 6 ft 3 in. (1.9 m) outside diameter and 3.0 in. (76 mm) or 1.0 in. (25 mm) thick were embedded in a stiff medium that was intended to simulate rock, and loaded in the upper 60 deg region of the crown with hydraulic rams. The loads were applied directly to the lining and could be given various shapes. Other variables included lining reinforcement, medium stiffness, lining thickness and tangential shear between the medium and lining. Strength variation as a result of these variables is reported as a strength



ratio,  $T_u / T_o$ , where  $T_u$  is the thrust at failure in the test and  $T_o$  is the calculated thrust due to pure axial load; reduction of the ratio below 1.0 occurs due to moment and indicates the amount of moment resulting from the variable examined.

The load shape that gave the lowest  $T_u / T_o$  at a given medium stiffness was a symmetrical triangle with load concentrated at the center of the loaded area, and that giving the highest ratio was a uniform load; the range was from 0.60 to 0.69. With a softer medium, loads were applied uniformly or with a rigid block on the lining, and the  $T_u / T_o$  ratios were 0.42 and 0.37, respectively. All the failures were ductile and occurred at the crown due to combined flexure and thrust, except one in which the load was concentrated near the sides of the loaded area; in this case the failure was more sudden and the failure surface had a more diagonal surface, indicating a larger influence of shear on the failure.

Two specimens were tested that were comparable except that in one case serrations in the medium provided interlocking between the lining and medium, while in the other the shear was reduced on this surface; these tests showed the effect of shear stress between the lining and medium. Removal of the shear stress reduced  $T_u / T_o$  from 0.69 to 0.52 or 33 percent, increased the forces on the base footings and increased the crown deflections.

The rock modulus and lining stiffness can be incorporated into a single variable called the flexibility ratio  $F$ , which is the ratio of the two stiffnesses. Due to this variable and with uniform load  $T_u / T_o$  varied from 0.42 at the smallest value of  $F$  to 0.62 for the largest. It was also found that strength varied with  $F$  much more in the low  $F$  range than in the high  $F$  range.

Cracking did not occur in 4 tests, and in 5 of the remaining 6 tests they first appeared at a load that was 50 percent or more of the

ultimate load. In one test in which the lowest flexibility ratio was combined with the rigid block loading, cracking first occurred at 40 percent of the ultimate load. In the linings with reinforcement the cracks did not grow rapidly after first occurrence until near ultimate load. Reinforcement had little influence on the strength of the specimens, but in comparing the cracking it appears that reinforcement did result in a larger number of cracks that remained finer.

Five circular concrete linings 44 in. (1118 mm) diameter and 1.0 in. (25 mm) thick were embedded in a continuous medium and the surface of the medium that represented the ground surface was loaded, as the other sides were constrained. The medium was a styrofoam bead aggregate-cement mixture with low modulus that represented a soft or firm soil. Variables that were investigated included reinforcement, medium stiffness and joints in the lining. It was found that the modulus of the medium was the most important parameter, and overshadowed both the reinforcement and joints in the lining.

Reinforcement did not affect the first appearance of cracks, but once they started, it served to distribute them throughout the high moment region and thus keep them from opening as much as if there had been only one or two. First cracking appeared at 32 to 42 percent of the ultimate load in the monolithic linings and at 91 and 93 percent in the two segmented linings. The loads at which cracking first occurred would have been higher if the loads had been applied more slowly so that creep of the concrete could occur, however. In the ground, load would be applied to the final lining slowly since the ground is supported by the initial supports when the final lining is placed.

The medium stiffness was in the range for which the lining behavior is sensitive to changes in the medium; thus, an increase in medium stiffness increased the lining strength and decreased the cracking. The  $T/T_u$  ratio varied from 0.40 to 0.62, a lower range than for the arch tests because of the softer medium.

Joints in the lining act as preformed cracks and reduce the lining moments, so cracking did not occur until near failure. However, the joints did not appear to influence the failure loads significantly, compared with the linings without joints; the reduction in moments due to the joints tended to increase the thrust at failure which increased the load capacity, but the joints reduced the thrust capacity because the section was thinner and the reinforcement was not continuous through them; in these tests these factors tended to offset one another. The effect of joints in reducing moment increases as the medium becomes less stiff because the moments become larger in the jointed lining.

Failure occurred in the region 60 to 80 deg from the crown in all tests except one where it occurred at a joint 120 deg from the crown. In all cases failure began as a result of crushing of concrete on the inside compression face of the lining section that spread as loading continued, and was generally accompanied by cracking in the direction of compression stress as loading continued. Failure occurred at the joints in both of the segmented lining tests.

A computer based analysis was used to extend the range of parameters studied in the model tests after it was first used to simulate these tests to verify its adequacy. The program model includes the nonlinear behavior of the lining as a result of material behavior or geometry change, and the medium can be represented by radial and tangential springs or by continuum elements. In the latter case, a special interface element between the lining and medium can be used to model the partial slip condition at the surface. In general, the analysis reinforced the findings from the model tests and in some cases allowed additional parameters to be investigated.

The response of semicircular arches to interaction with the ground represented by radial and tangential springs and subjected to loosening rock loads was investigated by varying the relative medium to lining

stiffness, lining radius to thickness ratio, stiffness of the radial and tangential springs and shape of the applied load. Of the load shapes studied, the uniform load gave the smallest safety factor, though a triangular load caused larger moments at the crown.

When the medium was very stiff relative to the lining, as a result of either a stiff medium or flexible lining, then the strength was not sensitive to this relative stiffness. In the practical case, this condition indicates that great precision is not required in the determination of stiffness parameters. On the other hand, when the medium is soft relative to the lining, the analysis results are sensitive to the stiffness and great care should be exercised in determining the stiffnesses, in avoiding the condition or in increasing the safety factor.

Tangential stress between the lining and medium was studied by varying the ratio of tangential to radial spring stiffness, and it was found that the lining strength was increased greatly as the ratio was increased up to about 12 percent, and for larger values the strength increase was less dramatic. Thus, it is important to include the tangential shear stress in an analysis, and if the value used for the tangential springs is above 12 percent of the radial spring stiffness, errors in its determination become less important. Reinforcement in linings in amounts normally used did not increase the failure load appreciably.

The behavior of circular linings were also studied in rock with the model that represents the medium with springs. The effect of reinforcement, relative medium to lining stiffness and tangential spring stiffness was found to be similar to that for arches. It was also found that the radius to thickness ratio of the lining affects the strength near failure, though in the linear range there is no variation with this parameter.

The moment-thrust paths of critical sections combined with the moment-thrust failure envelope was used to show how the various parameters affect the strength. When the medium is soft, large deformation of the lining results and is accompanied by large moment at critical sections. The moment-thrust path of these sections reach the moment-thrust failure envelope below the balance point in structural terms, and in this range the structure is ductile so failure does not occur immediately; more load can be applied before the critical sections reach their rotational capacity and failure occurs. As the medium stiffness increases less deformation and thus less moment occurs at a given thrust; with less moment the thrust at failure is increased and the load is also increased since load and thrust at failure are nearly proportional. By comparing the moment-thrust paths and the envelopes of failure, the structures reaction to changing various parameters can be observed. The same process was used to show how reinforcement affects the lining behavior by comparing the paths and failure envelopes for linings with no reinforcement and with varying amounts.

Linings in softer continuous media, such as soil, interact with the ground differently from those subjected to loosening rock loads, because the load does not remain constant in magnitude and shape, but depends on the interaction process. The analysis in which the medium is represented by continuum elements was used to model this condition with two types of loading applied. An "overpressure" load was applied in which the lining is placed in an opening in the unstressed medium and then subjected to a surface pressure. Also, an "excavation" loading was applied in which the in-situ stresses are present when the opening is assumed to be made and the lining inserted instantaneously. In this case the lining is not subjected to the deformations resulting from the in-situ stresses, but must interact with the lining as a result of these stresses. The excavation loading is, therefore, less severe, because a larger overburden pressure would be required to cause lining failure. The loosening load results in much larger moment and

therefore, smaller loads at failure than either of these latter two types. However, loosening loads cannot occur in some medium types, and when it does occur the total load is limited in magnitude to the weight of some fixed depth of material above the crown. However, when it may occur it should be checked because of its severity.

The study of water pressure in addition to ground loads on the lining clearly indicated a beneficial effect on strength, because the uniform pressure increased the thrust while moment at the critical section remained the same. The thrust at failure, and consequently the load, was thus increased slightly.

An interface element between the lining and medium allowed a study of partial slip conditions on this surface. The interface element properties were controlled by assigning a cohesion and angle of internal frictions. Cohesion values in the practical range did not influence the lining behavior appreciably, but the angle of internal friction had an appreciable effect; high values increased the thrust at the springline and decreased it at the crown. Thus, for soft soil (and low internal friction angle) failure occurred at the crown, but for firmer soil the failure section shifted to the springline as the pressure at failure increased.

Lining capacity was improved by the nonlinear behavior over the value predicted by a linear analysis. For loosening loads the capacity was increased by a factor of 1.7 to 1.9 depending on the medium/lining stiffness. For excavation loading this factor was smaller except for low values of medium/lining stiffness. The larger difference between nonlinear and linear analyses occurs when moments are large and the moment-thrust path reaches the failure envelope near the moment axis; in this range the moment-thrust path can follow the failure envelope farther because the structure is more ductile.

In the report these studies are described to provide a better understanding of the lining-medium system behavior. This information will also be helpful in formulation recommendations for the structural design of linings.

## 1. INTRODUCTION

The research described in this report was funded by the Urban Mass Transportation Administration of the U.S. Department of Transportation and performed under the technical direction of the Transportation Systems Center, Cambridge, Massachusetts. The realization by these and other agencies that construction costs for underground transit facilities are increasing much more rapidly than other construction costs has led to a search for ways to reduce them. Excavation of the underground opening and its support is a significant part of the total costs, and therefore substantial savings might be realized by more efficient designs of the support system. In addition, review of the design of existing linings shows that there is little uniformity of approach, and though they are all safe, some are more efficient than others.

These considerations have led to the research effort described in this report, that has the twofold objective: 1) make recommendations for the structural design of final concrete linings that encompass ultimate strength concepts of concrete and take full advantage of interaction of the lining with the surrounding medium, and 2) improve the understanding of lining-medium interaction and lining behavior near the failure load range. The research is described in two volumes. Volume II, contains the design recommendations and a summary of the research findings. This report, Volume I, contains the details of model tests and parameter studies, that were performed to augment background information based on experience and literature review to formulate the design recommendations. In addition, interviews with a number of design engineers is described in an effort to summarize existing practice. The details of the interviews is described in Appendix A of this report and summarized in Volume II.

There is a lack of agreement among engineers concerning methods of design and analysis of concrete tunnel support systems. Many methods



used are extremely conservative, representing in an inadequate manner the beneficial effects of soil-structure interaction and of nonlinear behavior of real lining materials. As a result, lining costs are greater than they need to be in many cases. A number of examples could be cited in which tunnel linings are quite different in terms of thickness or reinforcement in essentially the same geologic environment and depth. New sewer tunnels have recently been connected with existing lines to find that the new design consisted of a thicker lining, or it was more heavily reinforced than the old one that had performed satisfactorily for years. Many miles of unreinforced concrete linings and precast segmented concrete linings have performed satisfactorily in both rock and soft ground, but in recent years it has been difficult to convince designers to accept these support systems, though they appear to be cost effective. There are probably several reasons for this situation. One is perhaps the lack of experience of the designers in dealing with the type of structures that are used underground. Probably a more important reason for a trend toward more conservative designs is the decaying legal position of the designer in case of support problems, even if they are not directly a result of inadequate design. If there are problems with the supports, under the present system there is little doubt that litigation will result and the designer will be involved.

The long-term objective of the present study is to develop guidelines and recommendations for structural design of concrete linings based on ultimate strength concepts for predicting structural capacity and on beneficial effects of interaction between the ground and the structure. It is recognized that the design of all tunnel linings cannot be improved, because the minimum constructable lining may be adequate, or factors other than strength govern the design. This is particularly true of running tunnels in good ground, but it is not the case in all tunnels. It is also recognized that great amounts of money cannot be saved on a tunnel project by rather substantial savings in the lining design because the lining cost is a fairly small

part of the overall tunnel cost. However, these savings should be realized if possible even if they are small in many cases. It has been stated that substantial reduction in cost can be achieved by expert planning and interpretation of exploratory programs in order that the tunnel designer and contractor are more aware of potential problems during construction. This is undoubtedly true, and it is in these potentially troublesome ground conditions that the lining designer can also benefit from a better understanding of the ground conditions and provide a more economical lining.

Aside from improved economics of lining design, a rational uniformly accepted design approach is needed to provide some consistency in designs and to prevent gross overdesign because of lack of experience. An approach is suggested in Volume II of the report; the concepts are not entirely new, and have been used or suggested for use in various forms similar to that proposed, but an effort has been made to put together a consistent logical approach that has been verified either by use or by the studies described in this report. Linings for running tunnels in soft ground and for running tunnels and large openings in rock are covered by the approach, which is similar to that used for aboveground concrete structures and therefore is familiar to most designers. Loads are selected and multiplied by load factors, an analysis is performed using these loads, and the resulting moments, thrusts and shears are compared with the ultimate strength of the lining. However, the load factors used and type of analysis performed depend on the type of loading assumed to act on the lining and the ground conditions. This volume contains descriptions of the studies performed to substantiate many of the recommendations.

In Chapter 2, the background associated with the lining design, structure-medium interaction and previous studies are discussed. The finite element analysis program used for the parameter studies on circular tunnel linings and Arches is described in Chapter 3. This analysis is intended to concentrate on the structural behavior of the

lining and those parameters that have the greatest influence on this behavior. The lining is modeled by a series of beam elements that can account for the nonlinear behavior of the concrete and the reinforcing steel if present, and can include the nonlinear behavior due to geometry change if the deformations are large. The medium can be represented by radial and tangential springs with linear or nonlinear properties, or it can be represented by linear isoparametric continuum elements. Also, in the latter representation an interface element can be included between the lining and the medium that has failure conditions defined by the cohesion and angle of internal friction, and elastoplastic stress-strain properties.

Load tests on ten physical models of semicircular underground arches are discussed in Chapter 4. The models were 3 ft (0.92 m) average radius and 3 in. (76 mm) or 1.0 in. (25 mm) thick embedded in a medium that simulated rock, so the linings were "flexible" relative to the medium. The purpose of these tests was to investigate the modes of failure and the strength and behavior of flexible arches when loaded near the crown by gravity loads that have various shapes. The 60 deg sector at the crown was loaded and the medium stiffness, shear between the lining and medium, and lining reinforcement were varied. The model tests were simulated with the analysis described in Chapter 3 and the results of the tests and analysis compared.

In Chapter 5 a parameter study is described in which one of the analytic models described in Chapter 3 is used to investigate the effects of load shape, medium stiffness, reinforcement and radius to thickness ratio on the strength and behavior of semicircular arches. The model that represents the medium by radial and tangential springs was used with the load applied directly to the lining to model the lining behavior in a rock that can loosen above the crown.

In Chapter 6 physical models of circular linings in a medium designed to simulate a soft ground were tested by applying load to the

ground surface. Three monolithic and two segmented linings were tested primarily to determine the modes of failure and failure locations, relative strength with varying deformability and ground stiffness, and effects of joints and reinforcement. It was also used to show that the computer program described in Chapter 3 that models the ground with isoparametric continuum elements can provide reasonably accurate results when the medium is soft and the deformations are much larger than they were in the arch tests.

Parametric studies of circular linings in soft ground are described in Chapter 7, using both the spring elements and the continuum elements to model the ground. In both cases the effects of medium stiffness, lining reinforcement and lining dimensions are investigated; and with the beam-continuum model it was also possible to study the influence of properties of the interface between the lining and medium and influence of different ways in which the load is applied to the lining-medium system. The various possible loadings and analysis techniques are compared and discussed in connection with the construction and support sequence.

Chapter 8 contains a summary of the model test results and parameter studies and a discussion of their implication on design.

## 2. BACKGROUND

### 2.1 EXPLANATION OF CONCEPTS

In the early use of reinforced concrete for above-ground structures, design and analysis were based on concepts of linear behavior and working stress design methods. Beginning with the studies of concrete columns at the University of Illinois and at Lehigh University in the 1930's, the significance of nonlinear concrete behavior and ultimate strength began to be recognized. Ultimate strength concepts began to influence column design, and by 1956 the American Concrete Institute Code for buildings allowed the use of ultimate strength methods for most aspects of design. By 1971 emphasis was placed entirely on ultimate strength design, though working stress methods were still allowed. In the ultimate strength method, the nonlinear concrete behavior is recognized in calculating the ultimate load, to which factors of safety in terms of load factors and capacity reduction factors are applied. This is a rational approach that provides a reasonable estimate of the factor of safety against failure. Though these concepts have been in use for some time, they have not been adopted for the design of underground structures except in scattered instances; they are equally applicable, however, and economies in design could result as they have for surface structures.

When the response of a structure goes beyond the linear range, the difference in behavior of a member in a statically indeterminate frame and that of an individual member is largely due to the interaction between members of the frame that allow shear and moment from highly stressed members to be redistributed to other members with lower stress because they are then more stiff comparatively. The current ACI Code (1977) contains recommendations that allow up to 20 percent moment redistribution in ductile flexural members (but not columns) to partially account for this effect. Considerable research has been performed in this area (Glanville and Thomas, 1939; Ferguson and Breen,

1966; Furlong and Ferguson, 1966; Blomeier and Breen, 1975) that shows the extent to which redistribution can occur in frames. These studies also show that ductility of the members is necessary for redistribution and that it is limited by the deformability of the critical member sections. Ferrera-Boza and Paul (1978) showed analytically how the forces on the critical sections behave to allow redistribution of moment, and how the limits of deformation can then be predicted. They also demonstrated that greater redistribution can occur when the thrust is small so the moment-thrust path intersects the moment-thrust failure envelope (interaction diagram) below the balance point, because concrete sections have greater ductility in this range.

There is greater potential for redistribution of moment in underground supports than in above-ground frames because the structure is more highly indeterminate. Ferrera-Boza and Paul (1978) report tests that verify its existence and their analysis that explains the mechanism. They show that the amount of redistribution depends on the relative stiffness of the medium and lining, because this relative stiffness dictates the moment-thrust ratio in the lining and therefore the ductility of the sections. Throughout the full range of relative stiffnesses the lining strength is larger than that predicted by a linear analysis of the lining, but the difference increases as the thrust decreases. At low thrust levels the strength may be 4 to 5 times that of the linear prediction. Consideration of these concepts in tunnel lining design would provide a better estimate of the factor of safety, and would contribute to more economic designs.

Medium-structure interaction concepts and the advantages that they provide have been recognized since the earliest days of tunnel construction. Terzaghi (1942) advocated the use of thinner, more flexible linings to take advantage of the interaction of the lining with the medium in the construction of the Chicago subway. The method of steel rib analysis outlined by Proctor and White (1946) is based on concepts of structure-medium interaction. Design procedures vary from

strictly empirical approaches that consider interaction in a very crude way to very complex analytical methods such as the finite element approach. Many of the less complex methods do not take adequate advantage of the benefits of interaction, and are more conservative than necessary. A realistic approach to interaction is obtained from the complex methods, provided the construction process is also considered in the analysis, and realistic ground properties can be obtained, but these approaches may not be available for routine tunnel design or may be too costly.

The concept of structure-medium interaction recognizes that as active ground loads come on a curved lining at one location where the ground tends to move inward, the lining deflects inward slightly at that loading point, and at the same time deflects outward against the ground at other locations. Where the lining deflects outward against the ground, the ground resists the movement, and passive ground pressures develop on the lining. The total system of active and passive pressures on the lining is a more favorable loading than the active pressures alone and result from the arch or curved shape of the structure. If this interaction is taken into account fully in the design, a thinner, more efficient lining can result.

There is an additional phase of the structure-medium interaction in a continuous medium that affects the active loads actually applied to the structure and depends on the overall relative stiffness of the lining and medium that it replaces. If the lining is less stiff than the medium, it will deform more than the medium that it replaces, and therefore, will resist less load. The additional load that would have been resisted by the replaced medium will arch around the lining and be resisted by the adjacent medium. This is termed positive arching. If the lining is more stiff than the medium it replaces, load adjacent to the lining will be attracted to it, because it will not deform as much as the medium it replaced. This is termed negative arching. The stiffness of the lining of concern here is the vertical

load-deformation properties, which depend on the axial and bending stiffness of the lining and the passive pressure that is developed laterally when the lining deforms. Also, the arching of stress around the lining affects the properties of the medium near the springlines and its passive resistance, so the two phases of arching are related or coupled. There is an additional component of interaction that occurs locally in the region of the crown and results in a change in shape of applied pressure on the lining due to interaction of the ground and lining in this region; the crown deflects more than adjacent points on the lining so the pressure is reduced there.

A so-called New Austrian Tunneling Method (NATM), which is a concept comparable to Terzaghi's observational approach, is based on the idea to preserve and utilize the inherent rock mass resistance as much as possible, that is, to take full advantage of interaction. Initial supports are applied as soon as possible mainly for their confining function, utilizing such adaptable supports as rock bolts and shotcrete. The support behavior is closely monitored, and criteria are developed to judge when they are performing inadequately, so that steps can be taken to provide additional support if needed. However, to allow the mobilization of selfsupport of the medium, significant movements may be tolerated as long as they do not become unsafe. To achieve satisfactory results, every stage of the tunneling operation, from planning to performance monitoring, should be carefully coordinated and controlled. Numerous examples of the application of this observational approach to support design can be found in the literature (Rabcewicz, 1964 and 1969; Wagner, 1970; Cording, 1974; Muller, 1978; Fernandez-Delgado, et al. 1979; and O'Rourke, 1978).

The above discussion of liner-medium interaction does not account for the construction process or the fact that there is often an initial lining placed in the opening that supports it until a final lining is placed after the excavation is completed. The process by which the final lining is loaded is somewhat different for a tunnel in soil and



for one in rock; these processes will be discussed to help clarify the actual loading.

In ground that is relatively soft and homogeneous such as soil, initial support is usually used as close to the heading as possible, and then either of two courses is normally followed. If the initial support is concrete segments, it may also be the final lining and no additional lining is added; if the initial support is steel ribs and timber lagging or steel liner plate, it may only serve to stabilize the opening until a final concrete lining can be placed after the mining operation is completed.

As the tunnel heading progresses, overburden stresses tend to push the face of the excavation inward, so there is both radial and longitudinal movement directly at the face. If no supports were placed to restrain the ground, the radial movement would increase with distance behind the face until a constant deformation is reached 2 to 3 tunnel diameters back. The deformation will also increase with time due to creep, the amount of increase depending on the type of soil. In soft clay the increase with time may be appreciable (up to full overburden), while with sandy soils it may be small (a fraction of the diameter of the tunnel). Interaction will clearly depend on when the lining is placed and how much ground movement has occurred before contact is made between the lining and ground, and this movement depends on the distance behind the face that the lining is placed and the size of the gap that is often left between the ground and the lining. An attempt is made to fill the gap with pea gravel and/or grout soon after the support is placed to reduce the soil movement before the ground-liner contact is made. The success of this attempt depends on the rate of movement of the soil and the care exercised during construction. Concrete segments and steel ribs are sometimes expanded against the ground to provide contact and support as soon as possible and reduce the effect of the gap. The interaction process with the initial supports cannot begin until full contact is

established between the lining and medium, and the deformation that has occurred in the soil affects its stress state and therefore the part of the load that the soil can resist through arching.

Final linings placed inside the initial supports are cast in a stable opening that has deformed, so the initial lining resists only part of the load and the soil mass is stabilized. The final lining is cast against the initial support so good contact is established, but it is initially unstressed. There are several ways that the final lining can subsequently receive load. If the final lining was placed under compressed air and the air pressure is removed, the external pressure will increase accordingly. If the soil has been dewatered, and the water level is subsequently raised, a nearly uniform water pressure will act on the outer surface. Little moment will result from either of these sources, but the thrust will increase correspondingly. Some moments may result if the tunnel is partially drained, and a water pressure gradient is established between the location of the drain and the undrained region. The passage of a second tunnel near the first will alter the stress pattern in the soil and thus alter the load on the existing lining. However, the final lining would normally be placed after the second tunnel has passed so the temporary lining can deform to accommodate the altered soil stresses.

It would seem then that pressure from the soil would never occur in the final lining. However, in some soils time-dependent relaxation may continue for an extended period and additional pressure may occur after the final lining is placed. This additional load is resisted by both the initial and final linings as a composite structure. However, many designers feel that the initial supports may rust away, and then the soil pressure that was originally resisted by them (or some portion of it) would be applied to the final lining. If this philosophy is adopted it is the most significant source of loads on the final lining and in most cases will control its design. In this case the load assumed to be resisted by the initial lining is critical in the final

lining design. The initial support was very flexible and therefore deformed so that the external pressure was nearly uniform, so it is this nearly uniform pressure that should be applied to the final lining. The final lining may be assumed to be in contact with the soil when this pressure is applied to it, because of casting the final lining against the initial one. In addition to this uniform pressure that acted on the initial supports, the soil relaxation after the final lining is placed can cause additional pressure that is larger in the vertical than in the horizontal direction. These pressures cause moment in the lining and their magnitude depends on the properties of the soil.

In certain soils with low cohesion, the shearing deformations during construction combined with the soil weight may cause a portion of soil above the crown of the lining to loosen after the lining is installed. If this occurs, the weight of the loosened material will bear directly on the lining resulting in what is called in this report a "loosening" load. If an additional final lining is installed later and the initial one is assumed to rust away, the same load will rest on the final lining as well. Not more than about one diameter height of this material above the crown is likely to loosen, but the distribution is such that it could cause a critical condition at the crown in some cases.

Rock excavation is performed primarily by various drill and blast techniques or by tunnel boring machines, and in the former case an irregular surface on the interior of the opening is usually created while a fairly smooth surface is created in the latter; also vibrations from the drill and blast operation are likely to loosen the remaining rock more than the tunnel boring machine. Rock will normally support itself around an opening if it contains few joints, so a structural lining may not be necessary. The geologic settings of interest then are those in which sufficient jointing, bedding planes, faults or fractures exist so that rock blocks and wedges may loosen and bear on

the supports provided. In these cases initial support must be provided to protect the excavation operation. It is well established that the loading that actually occurs depends in most cases on how quickly and well the temporary supports are provided; if they are placed quickly after excavation and loosening is prevented, the loads will be much smaller than if the rock blocks are allowed to move and loosen before they are supported.

Running tunnels in rock are likely to be excavated and supported temporarily, with the final lining placed after excavation is completed; large openings in rock are likely to be supported temporarily by rock bolts and steel ribs shotcreted in place, with the steel ribs and shotcrete becoming part of the final support when additional shotcrete is added. In both cases the final lining is placed in reasonably good contact with the rock and the opening is stable when the final lining is placed. There is little tendency for loosening loads to arch around the opening because the loosened rock is partially or completely detached from the rock mass; also the magnitude of loosening loads is not likely to change appreciably with lining deformation. Therefore, it is reasonable in analysis to apply the loads directly to the lining rather than letting the load be the result of deformation of the medium. Lateral stress in the rock at the sides of the opening have been relieved by the excavation and do not act on the final lining when it is placed. Therefore, the only source of passive pressure at the sides of the lining result from outward movement of the lining toward the rock.

Tangential shear stress between the lining and rock influences the lining behavior a great deal and is difficult to evaluate. If the lining is cast directly against the irregular surface resulting from the drill and blast technique, it seems reasonable to assume that there would be no relative tangential deformation or no-slip. Often, however, there is wood blocking behind the steel ribs that may be left in place, soil remains on the rock surface, or voids are left in the

deep overbreak areas that reduce the effective shear stress between the lining and rock, and the actual conditions are somewhere between the no-slip and full-slip conditions. The full-slip condition allows larger deformation of the lining and therefore large moments occur, but this condition is unrealistic in most cases; the no-slip condition is overly optimistic, so a partial slip condition would represent the actual behavior more accurately. By whatever means the partial slip condition is taken into account, it is reasonable to assume that it acts to some extent in the region of the lining where the load is applied if the rock loading on the lining occurs in large blocks, but if it is very highly fractured, the tangential stresses in the loaded area would be negligible.

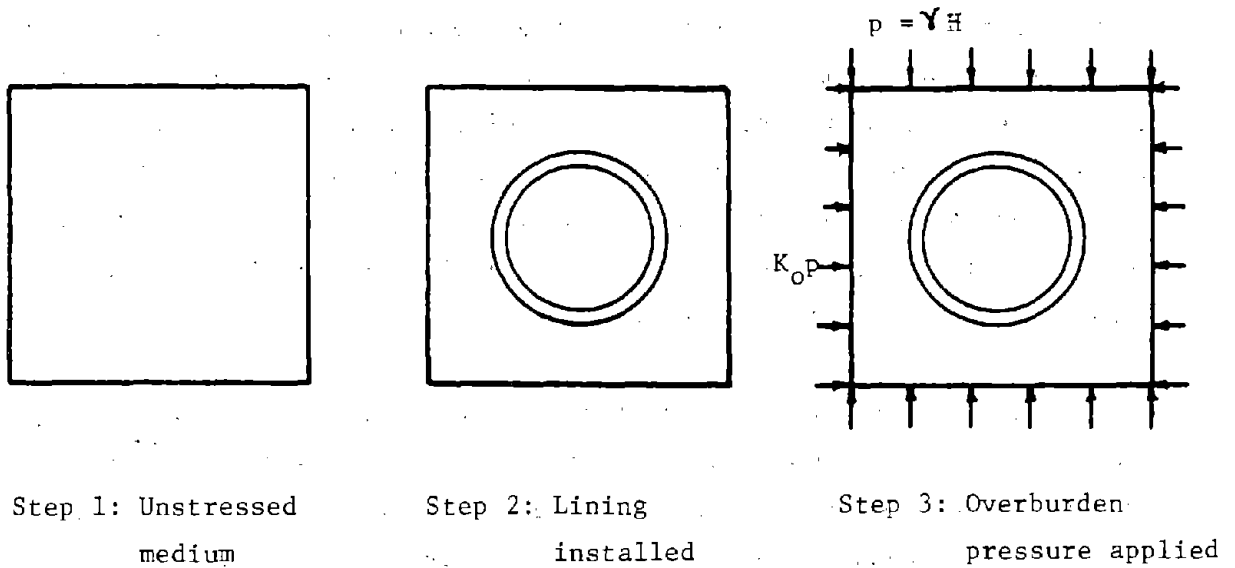
Loads applied by loosening rock can have different shapes, depending on the geology of the rock mass. Highly fractured layered strata that loosen may apply load uniformly over the crown region, or triangular rock wedges may load the lining that give maximum pressure at the crown decreasing laterally. Larger blocks or systems of blocks may remain relatively rigid as they rest on the lining; deflection at the crown would then reduce the load there and allow the block to rest primarily at each side of the crown, resulting in a pressure pattern that is minimum at the crown and increasing laterally in both directions. An oblique system of joints in the rock may cause the load to be concentrated at one side of the crown region or to be applied on the side of the lining. If the geologic conditions are known well enough to draw the pattern of joints that exist at the site on the tunnel cross-sections, it will be possible to predict the shape and magnitude of loadings that are likely to occur.

In view of this discussion of the construction sequence, initial support and source of loads, it is clear that determining the actual loads that occur on a final lining is difficult. For analysis purposes it is necessary to make some assumption about the loading, and in this report three types are considered that are called overpressure loading,

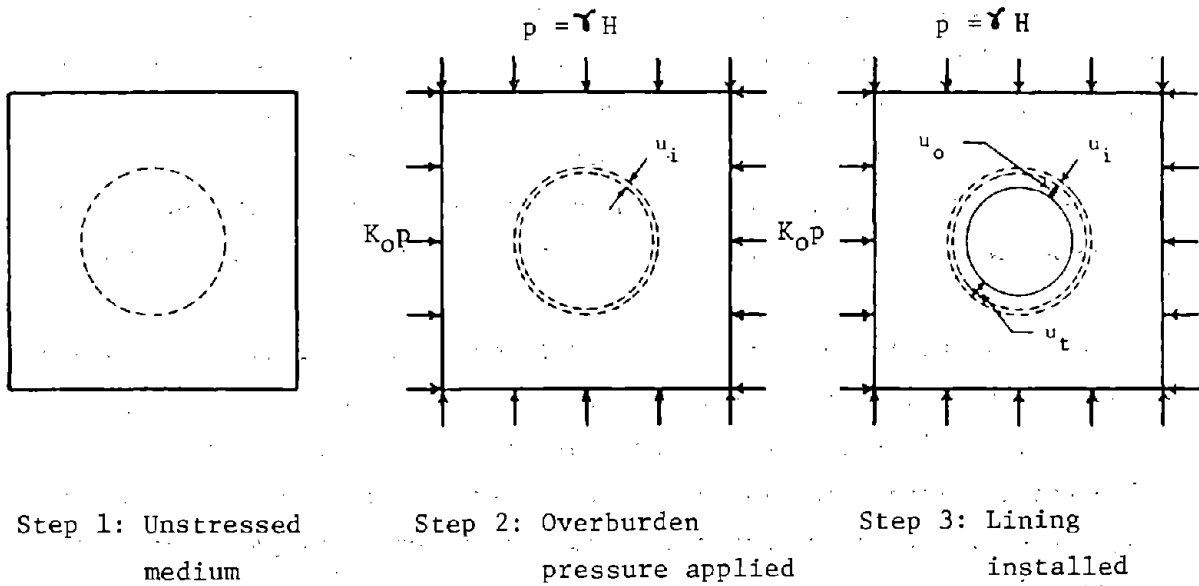
excavation loading and loosening loads. In the overpressure loading a region of the medium containing a lined opening is isolated and a pressure is applied to the upper surface. The lining was placed in the medium when it was unstressed and the lining and medium interact as the surface pressure is applied, as shown in Fig. 2.1a. Lateral stress in the medium is normally handled by applying a lateral pressure to the medium. This loading represents the vertical stress in the soil at the tunnel level due to the overburden.

In reality the lining is never placed in an unstressed medium, but the excavation is made in the medium with the overburden stresses present so some medium deformation occurs when the tunnel is excavated as shown in Fig. 2.1b. The initial lining is then placed in the opening immediately after this overburden deformation has occurred so that it fits perfectly, and before any additional deformation occurs due to the excavation. This is called the "excavation" loading and is different from the overpressure loading in that the lining is not subjected to the medium deformation that occurs due to the in-situ stress before the opening is excavated. The moment and thrust in the lining resulting from the excavation loading are smaller than those from the overpressure loading. However, the excavation loading still ignores the deformation in the medium due to the excavation and the gap between the lining and medium in soft ground tunnels discussed above.

In rock and in some types of soil material above, the opening loosens and rests directly on the lining, resulting in a loading equal to the full weight of the loosened material. This is referred to as a "loosening" load and is applied directly to the lining with constant magnitude, while the overpressure and excavation loadings result from deformation of the medium, and their magnitude and distribution depend on the properties of the medium and deformation of the lining. All the loadings are approximations to the actual conditions and the best approximation depends on the ground conditions and method of construction.



a) Sequence of events for analysis with overpressure loading



b) Sequence of events for analysis with excavation loading

FIGURE 2.1 ANALYSIS SIMULATION WITH OVERPRESSURE AND EXCAVATION LOADING

In deriving a closed-form solution for the interaction of a linear elastic lining with a linear elastic medium subjected to the overpressure or excavation loading, two ratios are used to define the relative properties of the medium and lining provided they are both continuous and homogeneous and the lining is circular (Peck, Hendron, and Mohraz, 1972). Both ratios appear in the equations for response of the lining, but one of them called the flexibility ratio  $F$  dominates in the moment equation and the other, called the compressibility ratio  $C$ , dominates in the thrust equation. The compressibility ratio is the ratio of stiffnesses of the medium to that of the lining in the radial direction when both the lining and the corresponding hole in the medium are subjected to a uniform radial pressure, and is given by

$$C = \frac{E_m / (1 + \nu_m) \cdot (1 - 2\nu_m)}{E_l t / (1 - \nu_l^2) \cdot R} \quad (2.1)$$

where the subscript  $m$  is for the medium and  $l$  for the lining, and

- $E$  = modulus of elasticity
- $\nu$  = Poisson's ratio
- $t$  = lining thickness
- $R$  = mean radius of the lining.

The flexibility ratio is a measure of the flexural stiffness of the medium to that of the lining and is obtained as the ratio of the stiffness of medium to that of the lining, when the lining and the corresponding hole in the medium are each subjected to pressures corresponding to a state of pure shear in the medium. The ratio is given by

$$F = \frac{E_m / (1 + \nu_m)}{6 E_l I_l / (1 - \nu_l^2) \cdot R^3} \quad (2.2)$$

where  $I_l$  = moment of inertia per unit length of lining



In the discussions and plots in subsequent chapters, the flexibility ratio is used as the variable defining the liner-medium properties when strength is considered, because it is more prominent in determining moment and it is the moment that influences strength most by reducing the thrust capacity. Though the derivation is for linear materials,  $F$  is also used as the independent variable when strength is determined in the nonlinear range;  $F$  provides a unique definition of the system initially even though the effective  $F$  changes as the stiffnesses of the lining and medium change with cracking and nonlinear stress-strain response of the materials. Though the flexibility ratio derivation was for circular linings, it is also used to define the relative stiffness for arches as if the lower part of the structure is still present, and appears to provide the correct combination of variables to describe the system.

## 2.2 PREVIOUS STUDIES

Solution of the structure-medium interaction problem may take many forms that include closed-form solutions, various types of finite element models, and tests of models of full scale support systems. Closed-form solutions have been discussed by Craig and Muirwood (1978) and by Ranken, Ghaboussi and Hendron (1978) and are summarized later in this section. They generally apply to circular linings only, linear material behavior and allow either full-slip or no-slip between the lining and medium. In two cases approximations are made for the partial slip case and in one solution a visco-elastic method of analysis for the medium is included that enable the time-dependent effects to be taken into account. Several studies of interaction using small-scale physical models have also been performed.

The finite element method has been used extensively to simulate interaction of the ground with lined and unlined openings; its great value lies in the ability to consider nonlinear, time-dependent and jointed ground behavior and the construction sequence. The technique

for simulating the construction process was developed by Clough and Woodward (1967), and has been used in the analysis of the incremental construction of earth dams by Kulawy, et al. (1969), for large open excavations by Duncan and Dunlop (1968) and braced excavations by Christian and Ing (1973). Duncan (1979) simulated the interaction of a long-span metal culvert during incremental backfilling around and over the structure using hyperbolic stress-strain relationships for the backfill material. Hayashi and Hibino (1970) used a visco-plastic material model to investigate the behavior of underground supports during the progress of excavation. Ranken, Ghaboussi and Hendron (1978) investigated the effect of depth from the surface of a lined tunnel in an elastic medium, the stresses and yield zones in an elastoplastic medium with an advancing tunnel lined at various distances behind the heading, stresses around two parallel advancing tunnels with linear and elastoplastic mediums, and internal forces in a lining subjected to gravity loadings in an elastic medium.

The effect of constructing tunnels in layered rock was studied by Goodman (1966), using elastic plane strain finite elements. Karshenas and Ghaboussi (1979) developed a two-dimensional finite element program which is capable of handling problems with geometric, material, and boundary nonlinearities in conjunction with a study of the behavior of tunnels in soft ground during and after construction.

A joint element was described by Goodman, Taylor and Brekke (1968) to model a series of rock blocks rather than a continuum. Zienkiewicz, et al. (1970) modeled jointed rock as a continuum with no tension and a special element to account for joint thickness and volume change during shear. Ghaboussi, Wilson and Isenberg (1973) developed a joint element that would represent a wide range of joint properties, including positive or negative dilatancy and slip in both directions. Roberds and Einstein (1978) described a general purpose behavioral model to represent elastic, visco-plastic behavior in which a change in stress or time or both will lead to a change in shape and volume. Dolcetta

(1971) and Judd and Perloff (1971) used linear material models to study the displacements and stresses in large underground chambers. A computer program that can model the behavior of assemblages of discrete rock blocks and visually display the behavior on the screen of a cathode ray tube was described by Voegelé, et al. (1977).

The medium was modeled by springs in a study by Dixon (1971) similar to some of the studies reported herein, though only radial springs were used. Brierley (1975) used both radial and tangential springs for the medium in a study to match the measurements made on the Dupont Circle Station lining of the Washington Metro.

Accurate simulation of the ground-liner interaction using the finite element approach is very complex, if all the relevant nonlinear aspects of the lining and medium are considered as well as discontinuities in the medium and the construction process. Because of limitations of computer capabilities and knowledge of material behavior, it is necessary to simplify the problem and concentrate on some specific aspects of it. In most of the studies described above, a large region of the medium is represented by elements so that the medium boundary will not interfere with the stresses near the opening and a fairly simple model is used for supports within the opening. This allows the modeling of both aspects of the interaction problem; the change in external stresses on the lining due to deformation and the shifting of load onto or around the lining due to the differences in overall stiffness of the lining and the medium it replaces. In the numerical models described in Chapter 3, the details of structural behavior of the lining were to be studied so the lining is represented by a nonlinear element in some detail, while the medium is represented by tangential and radial springs or by linear continuum elements.

Use of the finite element method as an aid in design has grown in recent years. Several of the Washington Metro stations were checked during the design stage by representing the lining by a series of beam elements and the medium by spring elements. Large underground caverns in rock are often checked with finite continuum element models to help determine the opening shape and examine high stress areas.

Many early studies of underground structures using physical models were performed in connection with the design of protective structures for blast loading. Newmark (1965) examined the feasibility of modeling cavity behavior in jointed rock masses. Tener (1964) tested 5 geometrically similar, semicircular aluminum arches with diameters ranging from 8 to 24 in. (203 to 610 mm) buried in dense dry sand and loaded with dynamic surface pressure to investigate modeling procedures for small-scale buried structures. These tests verified the modeling procedure for the range of parameters investigated. Meyer and Flathau (1967) performed static and dynamic tests on reinforced fixed-end arches buried in dry sand. Kennedy and Ballard (1967) applied dynamic loads to model flexible-arch-type protective shelters with a scaling ratio of 1:4.5 in dense dry sand. Heuer and Hendron (1969) performed tests on small-scale circular linings in a modeled homogeneous rock; Hendron, Engeling, Aiyer and Paul (1972) continued this study with a jointed rock medium; and Hendron and Engeling (1973) continued it further by strengthening the jointed rock mass by chemical adhesive simulating grouting of the medium. Wallace (1973) investigated the behavior of horizontally oriented, steel-lined cylindrical openings in both jointed and unjointed model rock masses subjected to static surface pressure; the results of six tests are discussed. Norman and Prendergast (1973) tested 9 horizontally oriented stiff cylinders buried at shallow depth in dense dry sand subjected to surface pressure. The primary variables were lining stiffness and depth of burial. Munn, Carre and Kennedy (1970) investigated the failure of footing-supported buried steel arches loaded statically in sand in which the variables were footing width, arch flexibility and depth of

burial. The influence of soil modulus on the behavior of cylinders in sand was investigated by Allgood and Ciani (1968) and Kennedy and Lindberg (1978) performed model tests to study the plastic response of lined tunnels.

At the Cambridge University, Caincross (1973) used models to study the deformations around tunnels in stiff clay. Atkinson, Brown and Potts (1975) describe an investigation of the collapse of shallow unlined tunnels in dense sand in which a uniform pressure was applied and the opening was supported by a uniform internal pressure. These studies were extended to include lined openings by Atkinson, Orr and Potts (1975). Orr (1976) studied the behavior of lined and unlined models in stiff clay, and Potts (1976) performed similar studies in sand.

Ferrera-Boza and Paul (1978) tested circular linings that were 10 ft (3.0 m) outside diameter and 6 in. (152 mm) thick loaded radially at 12 equally spaced locations by hydraulic rams. The ram loads were controlled to simulate active loading near the crown and invert, and passive loadings near the springlines that could be controlled in terms of stiffness. The passive stiffnesses and lining reinforcement were varied and with the known loads and strains measured at critical sections, it was possible to determine the influence of these variables on the internal thrust, moment and shear for the lining. These tests were useful to test the analytic model for the lining developed concurrently. It also allowed the assessment of the effect of passive stiffness, but the peak loads obtained may be conservative because of the detrimental effects of the lack of continuous distribution of the active and passive forces, and the lack of tangential shear forces on the lining.

Several approaches to support selection for circular openings based on closed-form solutions are discussed in some detail by Craig and Muirwood (1978) and by Ranken, Ghaboussi and Hendron (1978). Ebaid and Hammad (1978) compare the closed-form solutions for circular tunnels and discuss their implications to design. Solutions for linings placed in an unstressed medium to which a surface pressure is then applied, have been obtained by Burns and Richard (1964), Schulze and Duddeck (1964), Hoeg (1968), Morgan (1971), Peck, et al. (1972), Dar and Bates (1974), Muirwood (1975) and Curtis (1976). These solutions differ by various other assumptions that are made about the lateral pressure intensity and representation for the lining. The Muirwood (1975) and Curtis (1976) solutions contain approximations for the case of partial slip between the medium and lining while the others contain only solutions for the full and/or no-slip cases. Ranken, et al. (1978) and Einstein and Schwartz (1979) have developed solutions for the case of a lining placed deep in a medium that is already stressed by the overburden and show that this correction to the representation for tunnel excavation and support can reduce the support loads by 50 to 100 percent. Anderson, Haelsig, and Reifel (1966) considered both homogeneous and reinforced concrete rings subjected to nonuniform external pressure in connection with loading resulting from blast, and a nomograph is presented to determine the required reinforced concrete section properties for a given loading.

Salamon (1970) introduces a closed-form solution for the maximum axial stress in the liner, considering the effect of yielding support and delayed installation of support. Nonlinear stress-strain relationships with time effects were considered by adopting the Bingham-Voigt model. A ratio of shear modulus between liner and rock was introduced as a relative stiffness. Ladangi (1974) presents a closed-form solution accounting for linear and nonlinear failure envelopes of the rock mass, strength decrease with time and effect of volume dilation.

## 2.3 MODEL LAWS AND SIMILITUDE CONSIDERATIONS

### 2.3.1 Basic Considerations

Observations of tunnel liner behavior in the field require extensive instrumentation which is expensive and time-consuming to install, and the interpretation of the field data is difficult because many relevant variables which influence the liner behavior cannot be controlled or are unknown. Furthermore, any field condition is unique in terms of geologic as well as construction conditions, leading to lack of generality, and in most cases loads never approach the strength of the support. On the other hand, analytic techniques inevitably involve simplifications and assumptions, and require verification against other theoretical solutions, field data or results of model tests. Model tests allow the control of most of the test variables, can be carried to failure and are generally much less costly than full scale tests so more variables can be investigated through a larger number of tests. Therefore, in the overall quest for understanding of underground support behavior, the model investigation has a definite place. In this study the model tests are used to verify the analytic models, determine the modes of failure under various load conditions and investigate a few of the parameters that influence the lining-medium behavior. However, model tests also present problems in interpretation, especially if the scale is small, because of the possible effect of change of size of the structure on its behavior.

A structural model is defined by ACI Committee 444 (1979) as "any physical representation of a structure or a portion of a structure by any other structure differing in material strength or dimensions," and often employed with the purpose, (1) to study the general behavior of a structure and identify significant controlling factors, (2) to examine the validity of simplifications and assumptions inherent to a particular analytical technique, or (3) to predict the behavior of a

prototype correctly and qualitatively by satisfying the model laws and similitude conditions.

The theoretical basis for model studies in general (for example, Murphy, 1950; Langhaar, 1951; Massey, 1971), geologic and geotechnical models in particular (for example, Hubert, 1937; Rocha, 1957; Mandel, 1963; Fumagalli, 1968; Roscoe, 1963 and 1968) and structural models (for example, Rocha, 1955, 1958 and 1965; Fumagalli, 1960; Obert and Duvall, 1967), has been well established. Theoretical and practical problems in modeling of concrete structures were reviewed by ACI Committee 444 (1979) and also at the RILEM Symposium in 1959 and the ACI Los Angeles Symposium in 1968. An annotated bibliography on the subject until 1968 was compiled by Ady and Carpenter (1970).

### 2.3.2 Similitude Considerations

Fundamentals: The theory by which the behavior of prototype structures or systems is predicted from a corresponding model is called the similitude relationships. This theory is concerned with the relationship between the physical variables that describe the model and prototype. By physical variables is meant those quantities such as length, weight, thickness, etc. that describe the structure. These physical variables have dimensions, or in a few cases are ratios of quantities that have dimensions such as Poisson's ratio.

If all the dimensions of a model bear a constant ratio to the prototype, the two systems are said to be geometrically similar. This is a desirable attribute in structural models and is considered to exist in the model studies described later in this report. For many hydraulic models it is necessary to reduce vertical and horizontal dimensions by a different constant, in which case a distorted model is said to exist. It sometimes occurs that some characteristic that has insignificant effect on the behavior of the prototype becomes very



important in the model. Such a disturbing influence is called a scale effect.

If a theory for analyzing a system is not available or is too complex, but the phenomenon is understood well enough that the physical variables affecting it are known, then a dimensional analysis can be performed. This analysis is based on the concept expressed by the Buckingham pi theorem (Murphy, 1950), which states that any dimensionally homogeneous equation involving the physical variables that describe the system can be reduced to a relationship between a complete set of dimensionless products. From this it is clear that any physical phenomena may be stated in terms of an equation involving dimensionless pi terms of the form

$$\pi_0 = f(\pi_1, \pi_2, \pi_3, \dots, \pi_n), \quad (2.3)$$

where  $f$  indicates some function that may not be known for the particular phenomena, and each  $\pi_i$  (pi) is a dimensionless term involving the physical variables.

Two systems are said to be similar with respect to a particular set of physical variables when the dimensionless pi terms developed from these variables are the same at every corresponding point in the two systems; that is, the pi terms are equal in the model and prototype. Also, the original set of (n) physical variables describing the phenomena can be transformed to another set of (n-r) dimensionless pi terms, where (r) denotes the number of distinct fundamental dimensions, such as force, length and time. Thus, the number of variables involved in a particular problem is reduced in this way.

Significant Variables: As an example of the application of this theory, assume that the significant variables controlling the ultimate behavior of a concrete liner interacting with a geologic medium under localized loading in the vicinity of the crown, are those shown on Fig.

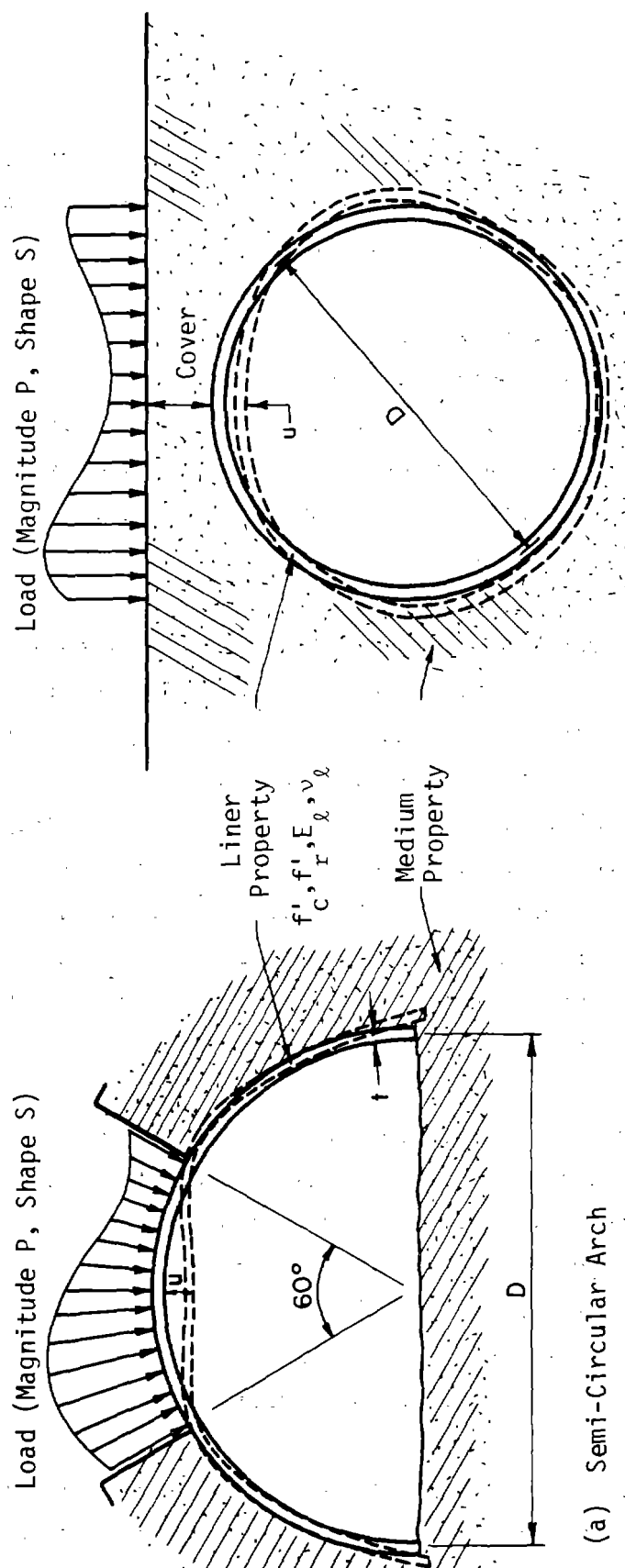
2.2 and defined in Table 2.1 by fundamental dimensions of force,  $F$  and length,  $L$ . The time dimension,  $T$  is not considered, since the time-dependent behavior is not a subject of the model tests directly.

The gravity load exerted by sliding blocks of rock was converted to a surface load on the lining defined by its magnitude  $P$  and dimensionless shape factor  $S$ . The medium is represented by two strength parameters, cohesion intercept  $c$  or compressive strength  $q$  and angle of internal friction  $\phi$ . Two deformation parameters, modulus  $E_m$  and Poisson's ratio  $\nu_m$ , are considered.

The concrete compressive strength  $f'_c$  or the ultimate thrust capacity of a section without moment  $T_c$  is selected as strength parameters of the concrete lining, and the modulus  $E_c$  as well as Poisson's ratio  $\nu_c$  are chosen as deformation parameters. Observed lining response are deformations, strains and crack geometry. The selection of significant variables is a compromise between need to reduce the number of variables to a working minimum and need to include all the relevant variables in regard to the objective of a particular model test. The variables selected here are comparable with those compiled by Heuer and Hendron (1969) and Zia, et al. (1970).

Model Laws: Assuming that the behavior of the concrete liner can be adequately described by the variables listed in Table 2.1, a set of independent pi terms (dimensionless ratios) can be determined as shown in Table 2.2. The procedure to determine pi terms is described in various text books such as Murphy (1950), Langhaar (1951), and Massey (1971), but often a fair amount of knowledge of the behavior of models and judgment is required to assure adequate forms of these terms.

For a model to reproduce the prototype behavior correctly, that is, for a model to be "similar" to the prototype, the pi terms should be identical for the model and the prototype. Then, it can be shown that there should be certain relationships between the ratio of each of the



(a) Semi-Circular Arch

(b) Circular Tunnel

FIGURE 2.2 GEOMETRIC, LOADING AND RESPONSE VARIABLES

TABLE 2.1 SIGNIFICANT VARIABLES

	Variables	Dimensions
1. Load		
a. Magnitude;	P, total applied load	$\underline{F}$
b. Loading shape;	S	—
2. Medium Properties		
a. Strength parameters;	c or $q_u$ cohesion or Unconfined Compressive Strength	$\underline{FL}^{-2}$
	$\phi$ , Angle of Internal Friction	—
b. Deformation parameters;	$E_m$ , Modulus of Medium	$\underline{FL}^{-2}$
	$\nu_m$ , Poisson's Ratio	—
3. Lining Concrete Properties		
a. Strength parameters;	$f'_c$ or $T_o$ , Compressive Strength of Concrete or Ultimate Thrust Capacity of the Section without Moment	$\underline{FL}^{-2}$ or $\underline{F}$
	$f_r$ , Modulus of Rupture of Concrete	$\underline{FL}^{-2}$
b. Deformation parameters;	$E_l$ , Modulus of Concrete	$\underline{FL}^{-2}$
	$\nu_l$ , Poisson's Ratio	—
4. Geometry of the Opening		
a. Size;	D, Diameter of Opening	$\underline{L}$
	t, Thickness of Lining	$\underline{L}$
b. Position;	C, Cover of Medium over Crown	$\underline{L}$
5. Response of Lining		
a. Force or Stress;	$T_u$ or $\sigma$ , Maximum Thrust at the Critical Section or Stresses (radial, tangential and shear)	$\underline{F}$ or $\underline{FL}^{-2}$
b. Deformations;	u, deformations (radial, tangential and shear)	$\underline{L}$
	$\theta$ , Rotation	—
c. Strains;	$\epsilon$ , Strains (radial, tangential and shear)	
d. Crack formation	w, Crack Width	$\underline{L}$
	s, Average Crack Spacing	$\underline{L}$

TABLE 2.2 DIMENSIONLESS pi-TERMS

Defining Load Level	$P/T_o, S$
Defining Medium Properties	$\phi, \nu_m, E_m/q_u$
Defining Lining Concrete Properties	$E_\ell/E_m$ (modular ratio), $\nu_\ell, f_r/f'_c$ $\frac{E_m(1-\nu_\ell^2) R}{E_\ell(1+\nu_m)(1-2\nu_m)t}$ (compressibility ratio) $\frac{E_m(1-\nu_\ell^2) R^3}{E_\ell(1+\nu_m) t^3}$ (flexibility ratio)
Defining Response of Lining	$\sigma/f'_c$ or $T_u/T_o$ (thrust ratio) $u/D, \epsilon, \theta, w/D, s/D$
Defining Geometry of Opening	$t/D$

TABLE 2.3 MODEL LAWS FOR A TRUE MODEL

Linear Dimensions, L	$S_L = S_D = S_u = S_t = S_w = S_s =$ dimensional scale factor
Stresses, $\sigma$	$S_\sigma = S_{\sigma_j} = S_{q_u} = S_{f_r} = S_{f'_c} = S_{E_j} = 1$
Forces, P	$S_P = S_{T_j} = S_\sigma \cdot (S_L)^2$
Strains, $\epsilon$	$S_\epsilon = S_{\epsilon_j} = S_{\nu_j} = 1$
Angles, $\phi$	$S_\phi = S_\theta = 1$
Shape Factor, S	$S_S = 1$

where: j = l or m

physical variables in the model and the corresponding one in the prototype. These ratios are called scale factors and the relationships between them are the model laws. They are obtained by equating the pi terms for the model and prototype, and solving for the ratios of the individual variables chosen for the problem and are shown in Table 2.3 where  $S$  denotes the scale factor. The scale factor,  $S_i$  is defined as the ratio of any physical variable in the prototype to the corresponding one in the model. For example, the scale factor for stresses,  $S = (\sigma)_{\text{prototype}} / (\sigma)_{\text{model}}$ , and scale factor of linear dimension,  $S_L = (\text{Length})_{\text{prototype}} / (\text{Length})_{\text{model}}$ . The scale factor for linear dimension is the inverse of conventional use of scale; for example, the  $S_L$  for a 1/4-scale model is 4.

Model Material Requirements: In order for the scale factors defining the response to be as described above, the model materials selected must also satisfy the previously described model laws; that is, the material must have a similar stress-strain relationship to failure and the same Poisson's ratio, not only in a monotonic loading condition but also in any loading-unloading-reloading path along which the prototype may follow, in order to have a strength determined by the model ratio of stresses. Other factors such as ease of handling, ease of instrumentation and economy must also be considered. It has been suggested by a number of researchers such as Rocha (1961 and 1965), Serafim and Azvedo (1961), and ACI Committee 444 (1979) that the problems of rupture or behavior of a concrete structure beyond its elastic range should be studied on models made of materials which have physical properties very close to those of the prototype, such as micro-concrete, or the same material whenever possible, thereby eliminating a rigorous procedure in search of a material satisfying the model laws in the complicated post-yield behavior. Introduction of different materials may require additional considerations of the influence of temperature, humidity and time, etc. On the other hand, the use of the same material simplifies the similitude considerations and also eliminates the need for assuming a certain failure criteria.

The model materials selected for the concrete liner for the tests performed in this study were intended to represent the same materials in the field and were chosen within the practical range of their properties. For the lining, concrete was used with aggregate that was scaled approximately by the geometric scale factor; in arches, the compressive strength  $f'_c$  ranged from 3500 to 5700 psi (24 to 40 MPa) and the tensile strength from split cylinder tests ranged from 247 to 460 psi (1.7 to 3.2 MPa). In circles, the compressive strength ranged from 2240 to 2760 psi (15.4 to 19 MPa), and the tensile strength from split cylinder tests ranged from 181 to 294 psi (1.2 to 2.0 MPa).

Modeling the geologic materials presents the greatest difficulty; however, if the lining behavior is the major concern, then only the load-deformation that the lining "sees" at the lining-medium interface must be considered. To represent the medium in the first six arch tests, a weak concrete was used for the medium and in the last four arch tests a layer of medium adjacent to the lining was replaced with strips of rubber. However, the load-deflection behavior at the surface of the medium adjacent to the lining was measured in place and the properties of an infinite, homogeneous medium determined that would give the same load-deformation properties at the interface. It was the properties of this infinite, homogeneous medium that were used to interpret the model test results. The actual load-deformation of the medium is affected by lack of confinement in the longitudinal direction, properties of the materials, and boundary conditions around the medium, but all these factors are considered by measuring the load-deformation of the medium interface in place and converting that behavior to properties of ground in the field. The same approach was used when circular lining models were tested in a medium consisting of cement, fly ash and styrofoam beads.

### 2.3.3 Applicability and Reliability of Results

If the lining material in the model and prototype are similar as in this study, the model laws are much simpler, and the stresses, strains and all the scaled non-dimensional terms listed in Table 2.2 for the model correspond directly to those in the prototype as shown in Table 2.3. If the linear scale factor  $S_L$  is selected as 10, for example, and the load on the model has the same location and shape as the prototype, then the load on a prototype at a given stage in the test would be  $10^2$  times that on the model, the deflection, crack width and average crack spacing would be 10 times that in the model, while the stresses, strains and rotations at corresponding points would be the same as in the model.

The accuracy and reliability with which the predicted behavior from any model test results match the actual prototype behavior, depend in general on two factors:

- 1) The degree of accuracy with which the selected significant variables describe the phenomenon (Table 2.1); and
- 2) The accuracy with which the model laws and similitude conditions are satisfied (Tables 2.2 and 2.3).

Errors due to the above two factors are generally known as "size effects" and tend to become larger as the geometric scale becomes smaller.

The model tests reported herein were not scaled from a specific prototype but from dimensions of the typical transportation tunnels and stations. The model arches had a diameter of 6 ft (1.8 m) and thicknesses of 1.0 in. (25 mm) and 3 in. (76 mm). A typical station in rock has a diameter of 60 ft (18 m) and a thickness of 15 to 40 in. (380 to 1016 mm). These dimensions correspond to a model scale of



about 1/10. The scale and minimum dimension of the model are reasonable; minimum scale for ultimate strength concrete modeling is considered as ranging from 1/15 to 1/20, and the minimum dimension is often limited to about 1.0 in. (25 mm) (ACI Committee 444, 1979). The models of circular linings were 44 in. (112 cm) diameter and 1.0 in. (25 mm) thick, while a typical running tunnel has a diameter of about 19 ft (5.8 m) and is 10 to 15 in. (250 to 380 mm) thick; the dimensional scale for diameter is about 1/5, while that for thickness is about 1/10. This distortion of the model was necessary to obtain lining failure with the medium strength used. These scale factors and dimensions are still within the limits considered acceptable by ACI Committee 444 for ultimate strength models of concrete structures.

Model studies on reinforced concrete (Alami and Ferguson, 1963; Borges and Lima, 1960; Rocha, 1965) indicate that the failure mode, crack width, average crack spacing, maximum deflection and ultimate stress at failure can be simulated by a model as small as 1/4 scale provided bond failure is not the primary or secondary reason for failure. Their studies and also those of Serafim and Azevedo (1969), Carpenter, et al. (1970), Little, et al. (1970), and Harris, et al. (1970) indicate that as the model ratio of linear dimension becomes smaller, the model behaves stiffer, especially at low stress levels, and the width and the average spacing of cracks become wider. The reasons for the phenomena were given as:

- a) Inadequate bond properties of steel reinforcement in the model,
- b) Different stress level in the steel reinforcement,
- c) Reduced effective side concrete cover over the reinforcement,
- d) The relatively higher tensile strength of model concrete than that of the prototype of the same compressive strength, and

- e) Inadequacy of the method of observing cracks; that is, the usual methods such as by eye or with a magnifying glass under intense light may not be as effective in detecting the initiation of cracks in the small scale models.

Small scale direct models with scales ranging from 1/10 to 1/15 for tensile cracking studies (Harris, et al. 1970) indicate that the average spacing of cracks can be compared closely with the prototype results when appropriate deformed wires are used as reinforcement. For the test series reported herein, either plain concrete or reinforced concrete of low reinforcement ratio was used for the model liner. The reinforcement was steel wire of the same strength as standard reinforcing bars ( $f_y = 40$  ksi, 275 MPa) and deformed in the laboratory using a device similar to those reported by Harris, et al. (1970). The concrete tensile strength is in the normal range for prototype concrete compared to the compressive strength. Therefore, cracking similitude should be satisfied in the model lining, and any discrepancies are primarily because of reduced effective concrete cover.

### 3. NUMERICAL MODELS

#### 3.1 INTRODUCTION

The finite element analysis program used to represent the lining for the parameter study and the computations associated with the model arch and circle tests consider the nonlinear behavior of the lining due to geometry change and nonlinear stress-strain behavior of the material, and includes interaction of the lining and the medium. The lining is analyzed as a planar structure; that is, all the deformations and forces occur in a plane perpendicular to the longitudinal axis of the tunnel. Also, the thickness to radius ratio of practical tunnel linings is sufficiently small that plane sections may be assumed to remain plane, and deformations due to shear strains may be neglected. The program is a modified version of the nonlinear finite element program developed by Ferrera-Boza and Paul (1978). The earlier version featured a nonlinear beam element to represent the lining and one-dimensional spring element to represent the ground. In the modified version of the program two more finite elements, the two-dimensional quadratic isoparametric element to represent the ground and a newly devised interface element, have been incorporated. These elements are described in the following sections. The modification of the program also allowed for additional features in the solution technique for multi-level substructuring and static condensation.

The modified finite element program thus can represent the ground-lining interaction problem in two different numerical models that differ in the way the ground is represented, while the lining is represented by the same beam element in both; they are called the beam-spring and beam-continuum models and are described in Sections 3.3.1 and 3.3.2. Each model is appropriate for certain ground conditions as discussed in connection with the parameter studies described in Chapters 5 and 7.

### 3.2 REPRESENTATION OF THE LINING

The lining is represented by a series of one-dimensional beam elements in the circumferential direction. In most of the computations only one-half of the lining was included in the model, with appropriate boundary conditions at the crown and invert for circular lining or crown and footing for the arches. In the arch model vertical displacement was allowed, but not horizontal displacement and rotation at the crown to account for symmetry about the vertical axis. The same conditions were applied at the crown and invert in circular linings.

The beam element, shown in Fig. 3.1, has 3 nodes and 7 degrees of freedom, with one node at each end and one at midlength. The formulation of this beam-element is based on the derivations reported by Aldstedt and Bergan (1974). A local Cartesian coordinate system passing through the end nodes follows the element during deformation of the structure. The "X" axis passes through the plastic centroid of the cross-sections, and the "Z" axis coincides with the principal axis. Each end node has three degrees of freedom; one displacement in the axial direction ("X" direction), one displacement perpendicular to the "X" axis ("Z" direction), and one rotation in the "XZ" plane. The middle node has one displacement degree of freedom in the axial direction ("X" direction). The use of the internal degree of freedom  $u_3$  at midlength, renders a parabolic distribution of axial displacement, and therefore, the strain due to axial displacement is of the same degree as the strain due to flexure. Forces are assumed to be applied only at the joints.

Stress-strain curves for the concrete and reinforcing steel in the lining is described by a discrete number of points and a linear interpolation is performed between the points as shown in Fig. 3.2a. Thus, the modulus of elasticity is considered constant between points as shown in Fig. 3.2b. The concrete stress-strain curve can have a tensile component, and either the tension or compression curves can

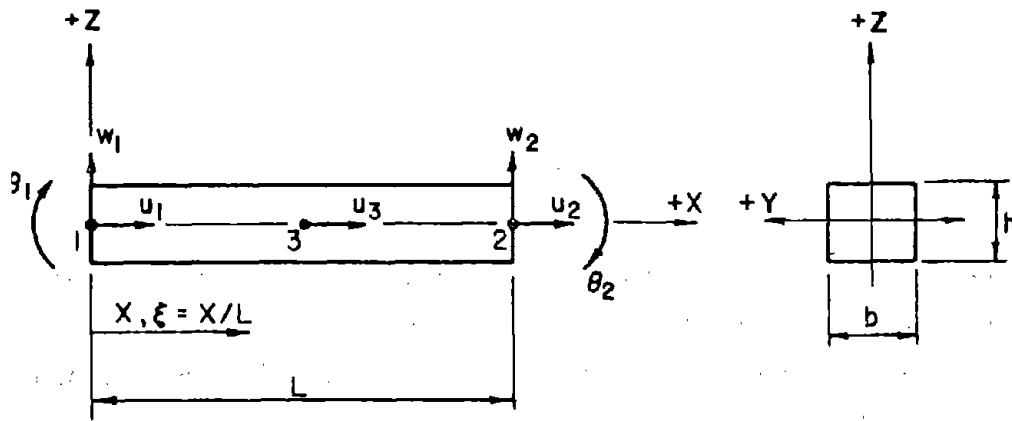
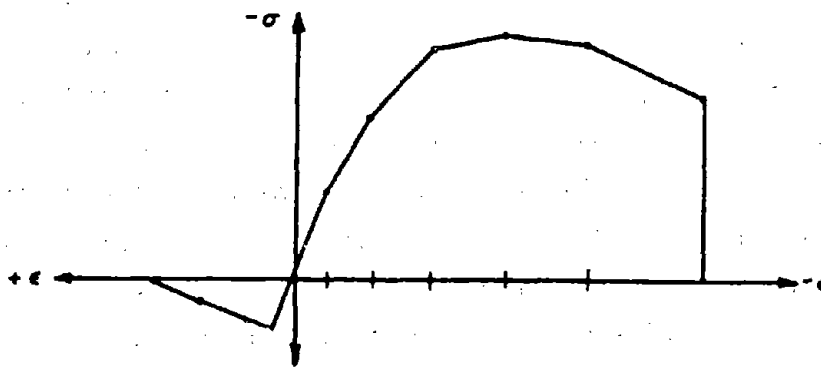
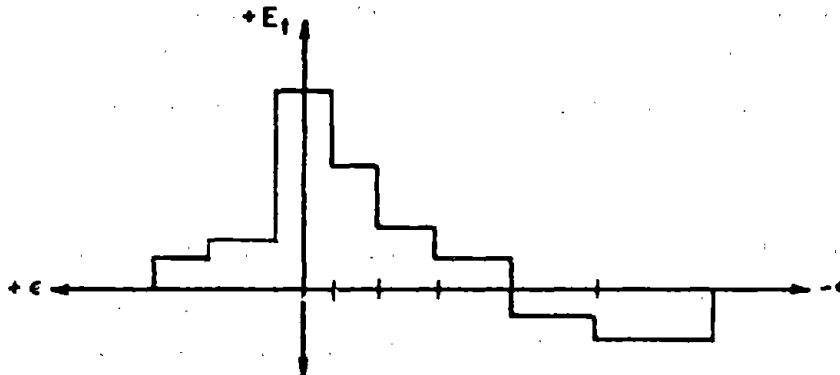


FIGURE 3.1 NODAL DISPLACEMENT AND COORDINATE SYSTEM FOR THE BEAM-ELEMENT



a) Representation of Stress-Strain Relationship for Analysis



b) Representation of Tangent Modulus-Strain Relationship Used in the Analysis

FIGURE 3.2 MATERIAL PROPERTIES REPRESENTATION FOR ANALYSIS

have a descending branch or cutoff. The descending branch of the compression stress-strain curve for the concrete is particularly important in obtaining the reduction in moment that occurs after the moment-thrust path reaches the failure envelope. The reinforcing steel stress-strain curve can have a plastic region followed by strain hardening if desired.

### 3.3 REPRESENTATION OF THE GROUND

#### 3.3.1 Beam-Spring Model

In this analytic model the ground surrounding the lining was idealized by spring elements attached to the end nodes of the lining elements oriented in the radial and tangential directions. These springs represent the radial passive pressure of the ground and the tangential shear between the ground and the lining. The springs are given load-deformation curves described by a series of points and can be linear or nonlinear. In studies with this model, the radial springs were assumed to have negligible tensile strength, while the tangential springs had equal stiffness in tension and compression to represent equal resistance to tangential movement in either direction. The spring elements were one-dimensional with one extensional degree-of-freedom in the direction of the elements.

This numerical model in which the medium is represented by springs takes into account only part of the interaction between the medium and the lining. The part of the interaction process that results in a change in lateral pressure between the lining and medium as a result of lateral lining deformation is adequately modeled, while the phase of the interaction process that concerns the change in active loads on the lining as a result of the difference in stiffness between the lining and the medium it replaces is not represented. Therefore, the loads that are used with this model should be considered to be those that are applied to the structure after this latter phase of the interaction

process has occurred. It is believed, however, that the spring model represents the lining behavior adequately when the final lining is placed in a stable opening and loads are applied by loosening rock blocks or soil above the lining.

### 3.3.2 Beam-Continuum Model

In order to accurately represent all phases of the interaction process for the ground assumed as a continuous homogeneous medium, the medium must be represented by continuum elements. The two-dimensional quadratic isoparametric element used for the medium in this model is shown in Fig. 3.3. It has four corner nodes and four mid-side nodes, and each has two translational degrees-of-freedom. The displacement at any point within the element is defined in terms of the generalized nodal coordinates of the element and is given by shape functions. The stiffness matrices for the elements are formulated, using virtual work concepts and writing transformation matrices. The numerical integration is performed over Gauss integration points. The formulation of the isoparametric elements is documented in several references, such as Zienkiewicz (1977).

This model in which the medium is represented by continuum elements, does not allow debonding and slip along the interface between the lining and the medium, and parametric studies indicate that the tangential stresses at the interface between the lining and medium can become unrealistically high. Also, the loading in discontinuous or fractured rock media where loosening of the ground near the crown is a more usual condition cannot be applied. Application of this loading in the model requires separation of the lining from the medium near the crown region and consequently abandoning interaction in the loaded portion of the lining. Hence, it is important to incorporate debonding and slip along the lining-medium interface.

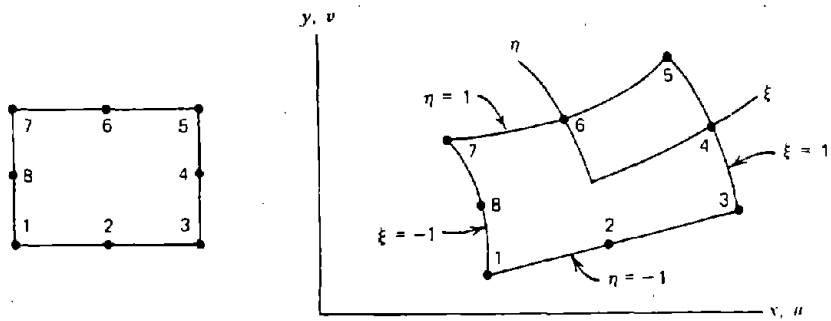


FIGURE 3.3 QUADRATIC PARENT ELEMENT AND ISOPARAMETRIC ELEMENT

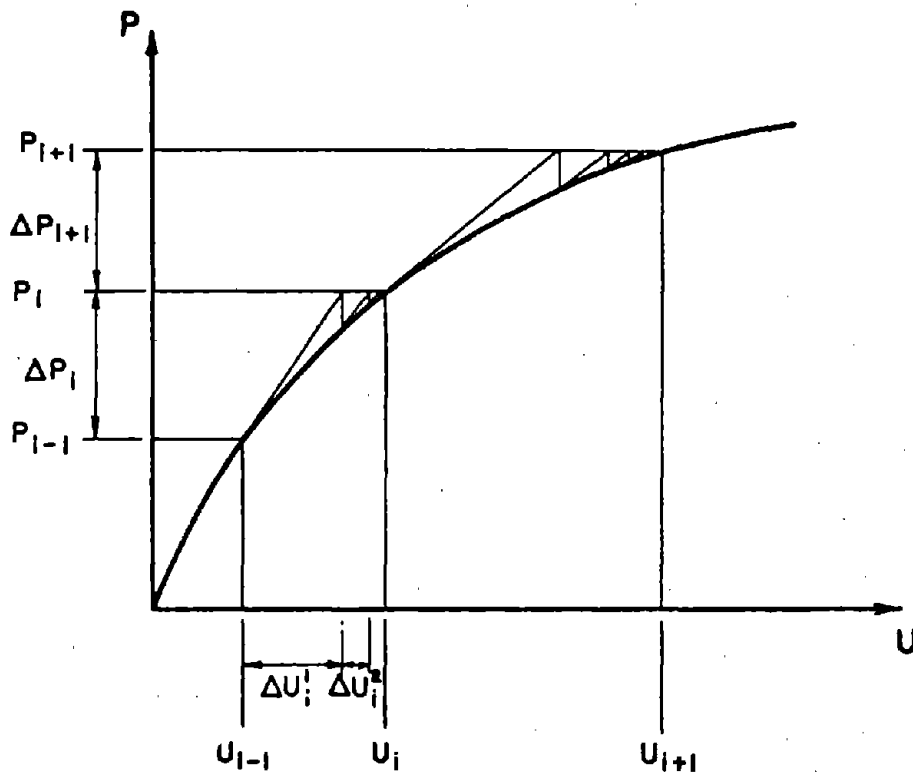


FIGURE 3.4 INCREMENTAL-ITERATIVE NONLINEAR ANALYSIS



An attempt to incorporate a commonly used joint element (Ghabboussi, Wilson and Isenberg, 1973) between the lining and medium resulted in nonconvergence problems because of the limitation of these elements to straight joints. The geometry used in the element was not compatible with a curved joint consisting of a series of straight segments, because a shearing deformation along the segment results in a relative normal deformation at the joint in the adjacent element. Hence, a different interface element was devised that is placed at each node and oriented tangent to the actual curved lining. This interface element has been modeled with two relative displacement degrees of freedom, one in the normal and the other in the tangential direction, and zero stiffness is assigned to the joint elements when separation occurs. For the purpose of parametric studies, only nondilatant joint properties were given. Very high normal stiffness is assigned to the element to model contact and a Mohr-Coulomb criterion is used to model the elastoplastic tangential shear deformation at the interface. A detailed description of the formulation of this element is given in Appendix B.

### 3.4 SOLUTION TECHNIQUE

An incremental-iterative procedure is used for the analysis. The load is subdivided into small increments that are applied successively. The response of the structure to each increment is computed by an iterative procedure. The element stiffness matrices are computed at the current state of stresses at the beginning of each load increment and at specified iterations within an increment. The increment in displacement for each node is calculated and added to the total displacement from the beginning of the loading process. When the member end forces are computed using these displacements, equilibrium at the structure nodes is not necessarily satisfied because of the approximate value of stiffness used for the previous iteration, so unbalanced forces remain at the nodes. The structure is then loaded with these unbalanced forces in the next iteration to compute

additional increments in displacements that are added to the previous totals. This process is repeated until equilibrium is approximated to some acceptable degree. The procedure is shown graphically in Fig. 3.4.

Since the medium represented by continuum elements is considered to remain elastic throughout the solution, a multiple-level substructuring technique has been adopted to economize solution time and for efficient handling of large problems. The basic concept of substructuring and the computations associated with the static condensation procedure are described in detail by Przemieniecki (1968). However, for a perspective view of the use of hierarchy in multi-level substructuring and its efficient application to nonlinear finite element analysis, the reader may refer to Dodds, Lopez and Pecknold (1978) or Anand and Shaw (1980). The medium is divided into a number of linear substructures whose stiffness matrices are assembled using the direct stiffness approach. All nodes of each substructure except the ones interfacing with another substructure or the lining are condensed out by the Gauss elimination process in a banded format. The condensed stiffness matrices and the equivalent load vectors for the various substructures are placed in peripheral storage for repeated use in different problems having the same medium geometry. This process of substructuring and static condensation can be continued sequentially at subsequent higher levels, reducing the size of the total structural stiffness matrix for the medium to a size that can be used more efficiently. The nonlinear solution of the overall system remains essentially the same as described earlier except for the modification required for substructuring. The condensed stiffness matrix of the substructure that never changes for a particular load increment is assembled into the main structural stiffness matrix by the direct stiffness method, whenever an updating of the stiffness matrix is required in the iterative process. However, the stiffness of any particular portion of the medium represented by a substructure can be changed by performing a

restart at a desired load level and by specifying the elastic modulus of that region.

Deformations are taken into account in the solution process by updating the coordinates of the lining each time a new increment in displacements is computed. The geometric nonlinearity in the analysis results because of the continuously changing transformation matrix between local and global coordinates for forces and displacements.

The structure is loaded in increments until the maximum load capacity is reached; as this maximum is approached, the load increments are made smaller. Failure is predicted when the forces in the structure can no longer balance an additional load increment, however small, so equilibrium is never achieved.

### 3.5 COMPUTATION OF MOMENT-THRUST ENVELOPE

An additional computer program was used to calculate the moment-thrust failure envelopes (moment-thrust interaction diagrams) used in the parameter studies and arch and circle model studies. These diagrams are a property of the section and represent the combinations of moment and thrust that will cause failure. Failure can be defined in several ways, but perhaps the most meaningful one would be the maximum moment that can occur at any given thrust; this is the definition used to construct the failure envelopes in these studies.

In order to obtain the envelopes, moment-curvature curves at a constant thrust were calculated and the maximum moment picked from each curve. This moment and the corresponding thrust provided one point on the moment-thrust envelope. Another moment-curvature curve at a different constant thrust was then calculated to provide a second point, and so on. In addition to giving the failure envelope, these moment-curvature curves help to understand other aspects of section behavior and consequently the behavior of the structure.

The program was written to calculate moment-curvature curves for a specified axial load by assuming a linear strain distribution and an arbitrary curvature (slope of the strain distribution on the section); the stress distribution over the section was then obtained from the given stress-strain relationship for the materials. The thrust on the section was then calculated by integrating numerically the stress over the section area; since the strain distribution was assumed, the thrust may not be that desired for the curve being calculated, so the strain distribution was changed by translating it without changing the curvature, and the thrust was recalculated. This process was repeated until the desired thrust was calculated, and then the moment was computed. One point on the moment-curvature curve at the constant thrust resulted. The curvature was changed and the process repeated to obtain another point, until the curve is completed. After this curve was completed, another thrust was selected and the process repeated.

This program also allows any shape of stress-strain curve in tension and compression for the materials to be defined by a series of points with linear distribution of stress between. Descending branches of the stress-strain curves can be handled as well.

## 4. MODEL TESTS OF ARCHES IN HARD MEDIUM

### 4.1 PURPOSE OF THE TESTS

The objective of the model arch tests was to determine the overall behavior and failure modes for concrete linings in rock and their implications to design. In particular, the effects of loading shape, medium modulus, thickness of the lining, flexibility ratio (Eq. 2.1), lining reinforcement and tangential shear between the lining and medium were investigated. The model tests were also used to verify the numerical model, described in Chapter 3, for this type of underground structure. A summary of the tests and the parameters that were varied are shown in Table 4.1.

Strength of the test linings is reported in terms of the thrust ratio  $T_u/T_o$ , where  $T_u$  is the ultimate thrust that occurred at the critical section and  $T_o$  is the thrust capacity of the section without moment. Representation of capacity by this dimensionless ratio accounts for different concrete compressive strengths and reinforcement, and allows the comparison of strength to be based only on the parameters being evaluated. The reduction in thrust capacity below the pure axial value occurs because of moment at the section, so the thrust ratio provides a measure of the moment that occurs at the critical section and its effect on strength due to the parameter under study.

Serviceability is evaluated by monitoring deformations, the first appearance of cracks, and the distribution and size of cracks. Ten arches labelled Arches-1 to 10 were tested. They were cast-in-place, semicircular, unreinforced and reinforced concrete arches, 1.0 ft (0.3 m) long with a mean diameter of 6.0 ft. (1.8 m). The thickness varied

TABLE 4.1 SUMMARY OF ARCH TESTS IN HARD MEDIUM

Designation	Loading Shape	Thickness in (mm)	Rock Modulus psi (10 <sup>6</sup> )	Tang. Shear	Reinforced
ARCH-1		3(76)	1.68x10 <sup>6</sup> (11575)	YES	NO
ARCH-2		3(76)	1.68x10 <sup>6</sup> (11575)	YES	NO
ARCH-3		3(76)	1.68x10 <sup>6</sup> (11575)	YES	NO
ARCH-4		3(76)	1.68x10 <sup>6</sup> (11575)	YES	NO
ARCH-5		3(76)	1.68x10 <sup>6</sup> (11575)	NO	NO
ARCH-6		3(76)	1.68x10 <sup>6</sup> (11575)	YES	NO
ARCH-7		3(76)	0.17x10 <sup>6</sup> (1170)	YES	NO
ARCH-8		3(76)	0.17x10 <sup>6</sup> (1170)	YES	NO
ARCH-9		1(25)	0.17x10 <sup>6</sup> (1170)	YES	NO
ARCH-10		1(25)	0.17x10 <sup>6</sup> (1170)	YES	YES

from 3 in. (76 mm) for Arches-1 to 8 to 1 in. (25 mm) for Arches-9 and 10.

The rock-like medium surrounding the arches was simulated with low strength concrete, and in two tests with a layer of rubber added between the medium and the lining. The arrangement, shown in Fig. 4.1, models the configuration of subway stations and roughly represents the critical upper half of circular running tunnels. Instrumentation for these tests included measurement of deformations, loads and relative movement between the lining and the surrounding medium. The active loads were applied by 10 hydraulic rams over a 60 deg segment, centered at the crown region; the loading arrangement could simulate loads applied by rock wedges near the crown, either symmetrical or unsymmetrical.

The effects of loading shape were assessed by comparing the behavior of Arches-1, 2, 3, 4 and 6, which had the same medium and shear condition between the medium and lining, but the shape of the active load was varied. Medium modulus effects were evaluated by comparing Arch-6 to 7 and Arch-1 to 8. Both pairs had the same loading shape, but different modulus of the medium. The extent of damage and rotational capabilities of thinner linings were obtained from the comparison of Arches-8, 9, and 10, the first being 3 in. (76 mm) and the last two 1 in. (25 mm) thick. The effects of flexibility ratio were assessed by comparing the thrust ratios of all arches at failure. An attempt to describe the effects of reinforcement on ultimate and service load behaviors was made by comparing Arches-9 and 10 test results.

Another variable considered in the tests was the tangential shear stress between the lining and the medium. The influence of these stresses was evaluated by comparing tests Arch-1 and Arch-5. Both tests were subjected to uniform loading, but full mechanical interlock between the lining and the medium were provided in Arch-1, while they

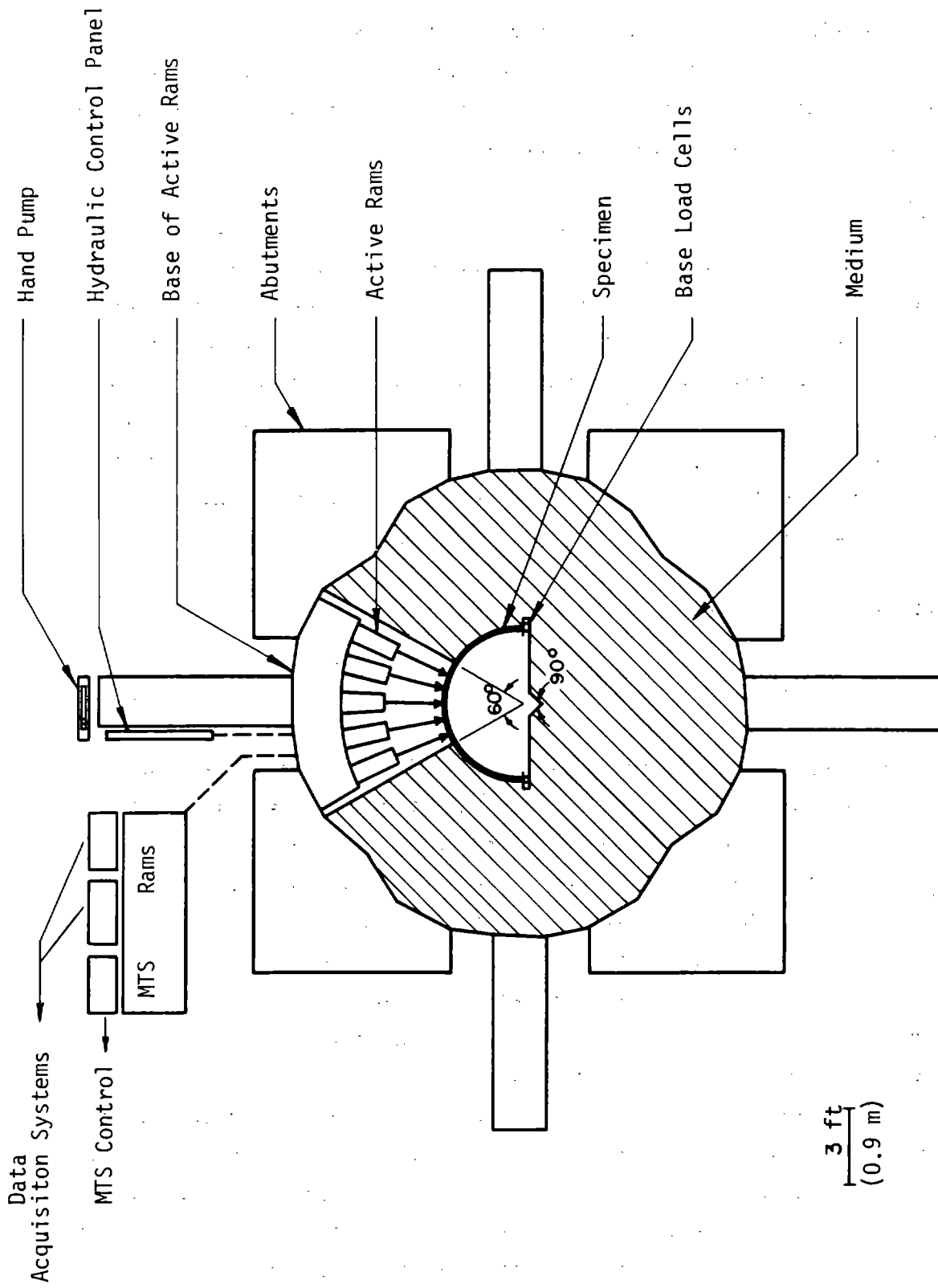


FIGURE 4.1 PLAN VIEW OF TEST SETUP



were essentially eliminated in Arch-5. The load reaching the base of the arches was measured, so the load retained as shear resistance between the lining and the medium could be estimated by subtracting the base load from the total applied active load.

The beam-spring numerical model was used in the analysis of the tests, because the radial and the tangential shear stresses between the lining and medium were not measured, so the internal lining forces could not be calculated directly. Therefore, the known parameters were used in the analysis and the tangential and radial spring stiffnesses that represent the medium were varied until the calculated lining deflections and footing loads matched the measured ones. The internal thrust, moment and shear at each section of the arch were then obtained from the analysis.

## 4.2 DESCRIPTION OF THE TESTS

### 4.2.1 Test Facility

Dimensions: The test facility consisted of 8 separate massive concrete abutments bolted to a very stiff test floor within which the arch model and medium surrounding it were cast, as shown in Fig. 4.1. An opening with a diameter of about 6 ft (1.8 m) was selected, based on consideration of the available space within the abutments, and the need to provide an adequate thickness of medium around the lining, while keeping the arch as large as possible to reduce the influence of scaling effects, discussed in Section 2.3. The thickness of the medium around the lining ranged from about 5.5 to 8.5 ft (1.7 to 2.6 m). The opening dimensions are shown in Fig. 4.2. The outer radius is 37.5 in. (952 mm) and provides a scale factor of about 13 for the DuPont Circle Station in the Washington Metro System which has an average radius of 40 ft (12 m). That station lining was designed with a thickness of 30 in. (762 mm), and applying the same scale factor would give a thickness

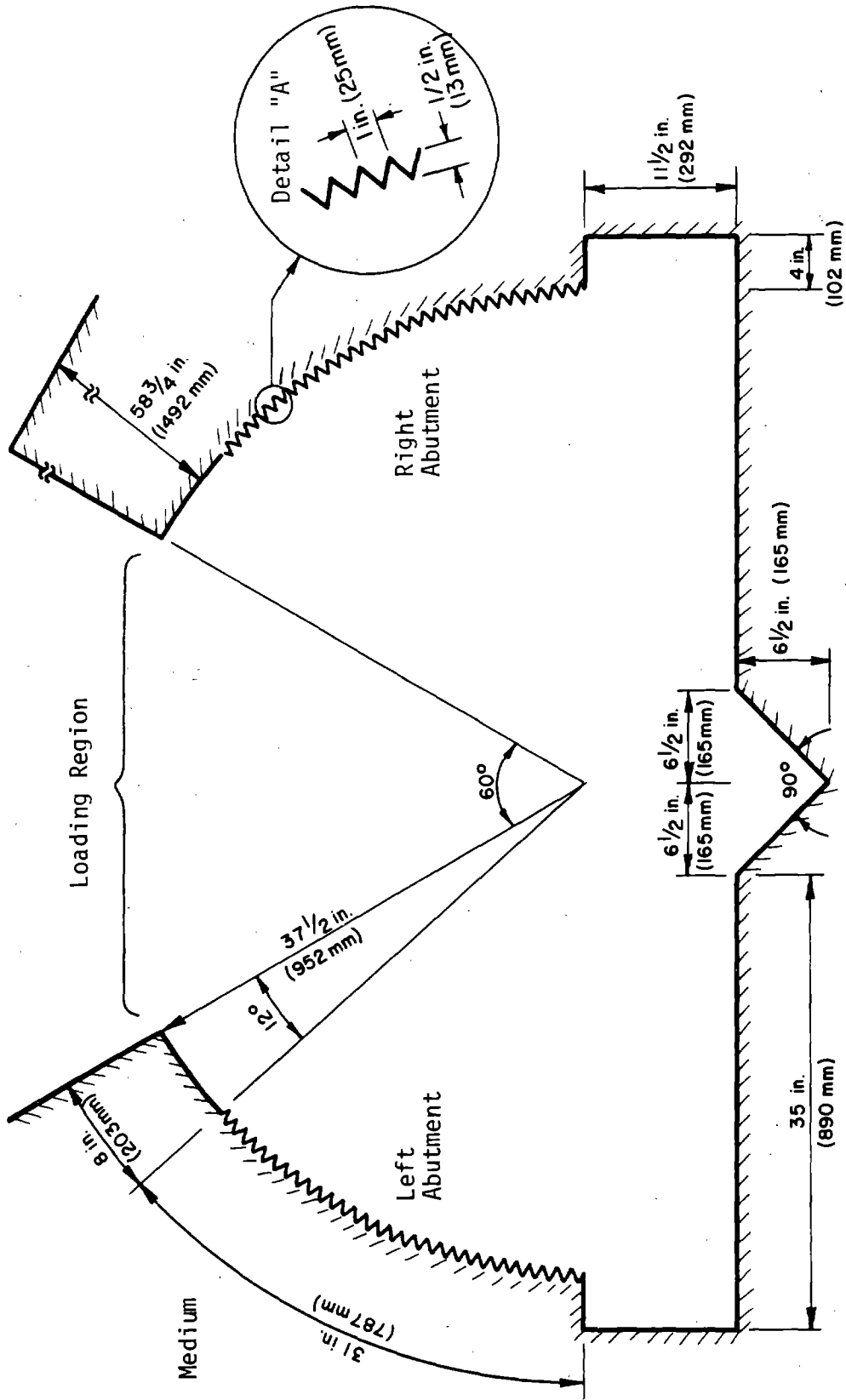


FIGURE 4.2 TOP VIEW OF THE TUNNEL OPENING

of 2.3 in. (58 mm) for the model. A thickness of 3.0 in. (76 mm) was used for Arches-1 to 8 and of 1 in. (25 mm) for Arches-9 and 10.

The 4 x 11.5 in. (101 x 292 mm) pockets at the base of the arch opening were provided to accommodate load cells to measure the footing reactions. The notch at the center at the bottom of the opening was to accommodate the base of a ram in order to measure the in-situ medium stiffness with plate load tests. A 60 deg opening at the top of the medium was left to apply loads to the crown region of the model with hydraulic rams.

Medium: A flexible lining was to be represented in these tests, which implies that the flexural stiffness of the medium is much larger than that of the lining, and low moments would result in the lining. In addition, the medium should exhibit nearly elastic behavior in order for the test conditions to be reproducible; that is, the medium should load along the same path each time loads are applied. Two different mediums were used. For Arches-1 to 6 low strength concrete was selected to provide a modulus representative of a medium quality rock mass with an equivalent elastic modulus of  $E_R = 1.68 \times 10^6$  psi (11575 MPa). The test setup for this series of tests is shown in Fig. 4.3. The medium modulus was reduced for Arches-7 to 10 by lining the side of the medium opening with 1 in. (25 mm) thick strips of rubber, as shown in Fig. 4.4. Three horizontal strips were used to reduce the Poisson's effect of the rubber that would cause lateral tensile stresses on the specimen. The combined effective modulus of rubber and concrete was  $E_R = 0.17 \times 10^6$  psi (1170 MPa), representing low quality rock.

The lining-medium interface was simulated by two limiting conditions for Arches-1 to 6. To represent full bond and mechanical interlock for Arches-1, 2, 3, 4 and 6, serrations were formed on the surface of the medium opening as shown in Fig. 4.5. This type of condition exists in the field when the surface of the opening is rough and irregular, as a result of overbreak during excavation. Thirty

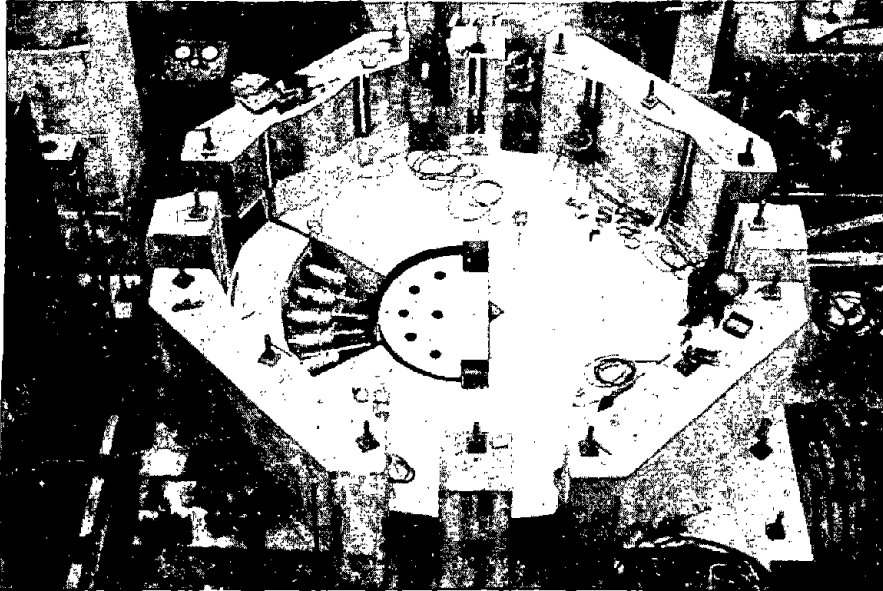


FIGURE 4.3 TEST FACILITY WITH FORM IN PLACE FOR CASTING ARCH SPECIMEN

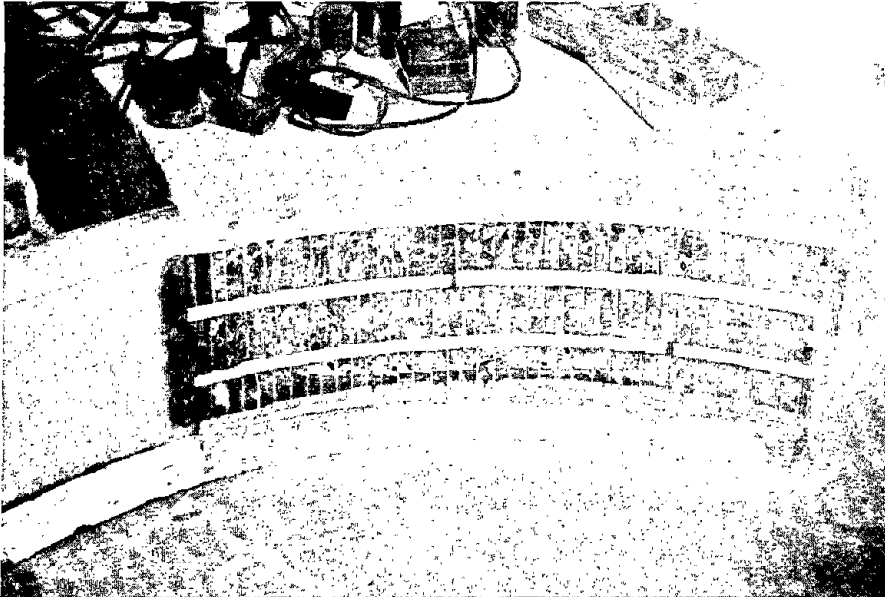


FIGURE 4.4 RUBBER USED TO REDUCE EFFECTIVE MODULUS OF THE MEDIUM



FIGURE 4.5 SERRATIONS ON THE MEDIUM SURFACE FOR MECHANICAL INTERLOCK WITH THE ARCH SPECIMEN

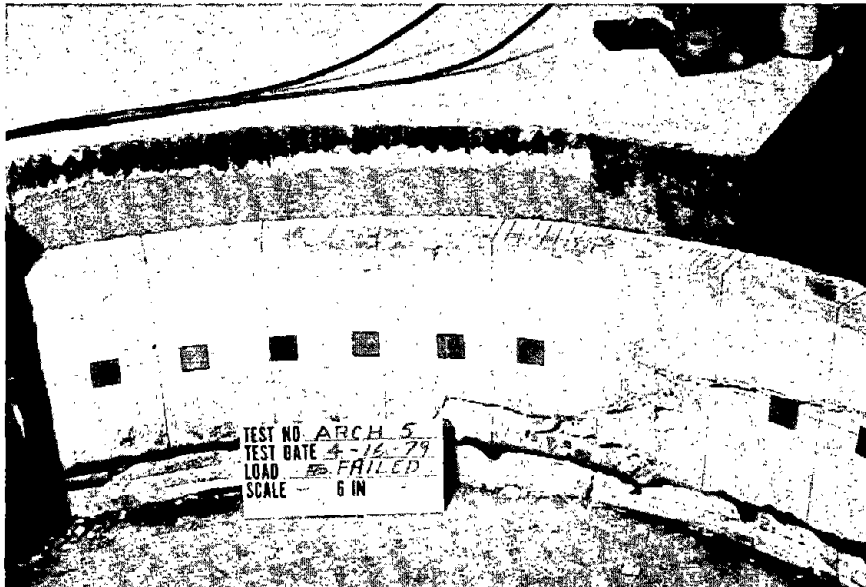


FIGURE 4.6 MECHANICAL INTERLOCK ELIMINATED BY FILLING THE SERRATIONS IN THE MEDIUM

serrations of triangular shape 1 in. (25 mm) wide and 1/2 in. (13 mm) high were formed on the sides of the opening. This was achieved by nailing pieces of wood of triangular shape on the outside surface of the plywood form. There was concern that these serrations might not withstand the induced shearing stresses during loading of the specimens. Shearing off of some of the serrations during testing would change the boundary conditions for the remaining load increments and cause difficulty in interpretation of the results. Also, subsequent tests would not have the same interlocking mechanism. Two measures were taken to assure that this would not occur. First, serrations were not formed in the first 8 in. (203 mm) of the medium adjacent to the loading region. Secondly, the serrations and about 3 in. (76 mm) of the medium adjacent to the opening were cast with a higher strength concrete.

To represent no bond or mechanical interlock (full-slip) conditions for Arch-5, the serrations were eliminated by filling them with cement paste and providing a double sheet of plastic with grease between over the surface, as shown in Fig. 4.6. Full-slip conditions might be approached in the field in a TBM (Tunnel Boring Machine) excavated tunnel in good quality rock with minimum amount of overbreak. In reality, linings in the field are between the full-slip and full interlock conditions.

Some degree of bond and mechanical interlock at the interface of medium and lining for Arches-7 to 10 was reproduced by cutting 1/4 in. (6 mm) vertical grooves on the surface of the rubber strips.

To cast the concrete representing the medium, a wooden form was constructed along the boundaries of the opening. The floor and abutments were covered with thin plastic sheet to prevent bonding of the medium to these elements. Bonding of the medium to the floor was not desirable because it would cause the straining of the medium to be unsymmetrical about its midheight since the top surface was free.

Preventing bond to the abutments would also facilitate removal. The medium was cast in two halves, 2 days apart. The concrete was cured by keeping it wet and covered with burlap and plastic sheet for 7 days. The compressive strength for the two halves at 28 days were 3380 psi (23 MPa) and 3600 psi (25 MPa).

For reasons mentioned earlier, the serrations were made of a stronger concrete mix than the medium, 9200 psi (63 MPa) versus about 3500 psi (24 MPa). To form the serrations, a 3 in. (76 mm) void was maintained during casting along the outer surface of the form for the opening, by using a curved metal sheet. The metal sheet served as a divider between the low-strength concrete for the medium and the higher-strength concrete for the serrations. The void between the sheet metal and the form was filled with the higher-strength concrete, whereas the space between the sheet metal and the rigid abutments was filled with the lower-strength concrete. The concrete on both sides of the sheet metal was vibrated until it reached the top of the divider; the sheet metal was then withdrawn, and the interface between the two mixes was vibrated once more.

Loading Systems: The active loads were provided by ten 60-ton (534 kN) capacity rams arranged radially in two rows as shown in Fig. 4.7. The rams were arranged radially, since a vertical loading direction would create a tangential frictional component along the outside surface of the crown portion of the arch. The cylindrical seat for each individual ram was bolted to a steel plate embedded in a specially constructed concrete base. The load was transmitted through a load cell, to a load centering mechanism, and then to a 1-1/2 in. (38 mm) thick 6 x 18 in. (152 x 457 mm) steel plate. The bottom edge of these plates rested on a friction-reducing system on the floor, consisting of two sheets of plastic with a lubricant between. At each loading position, two rams were spaced 8 in. (203 mm) apart vertically as shown in Fig. 4.8. To assure uniform load transfer from the steel plates to the arch model, a 1.0 in. (25 mm) thick layer of hard rubber curved to

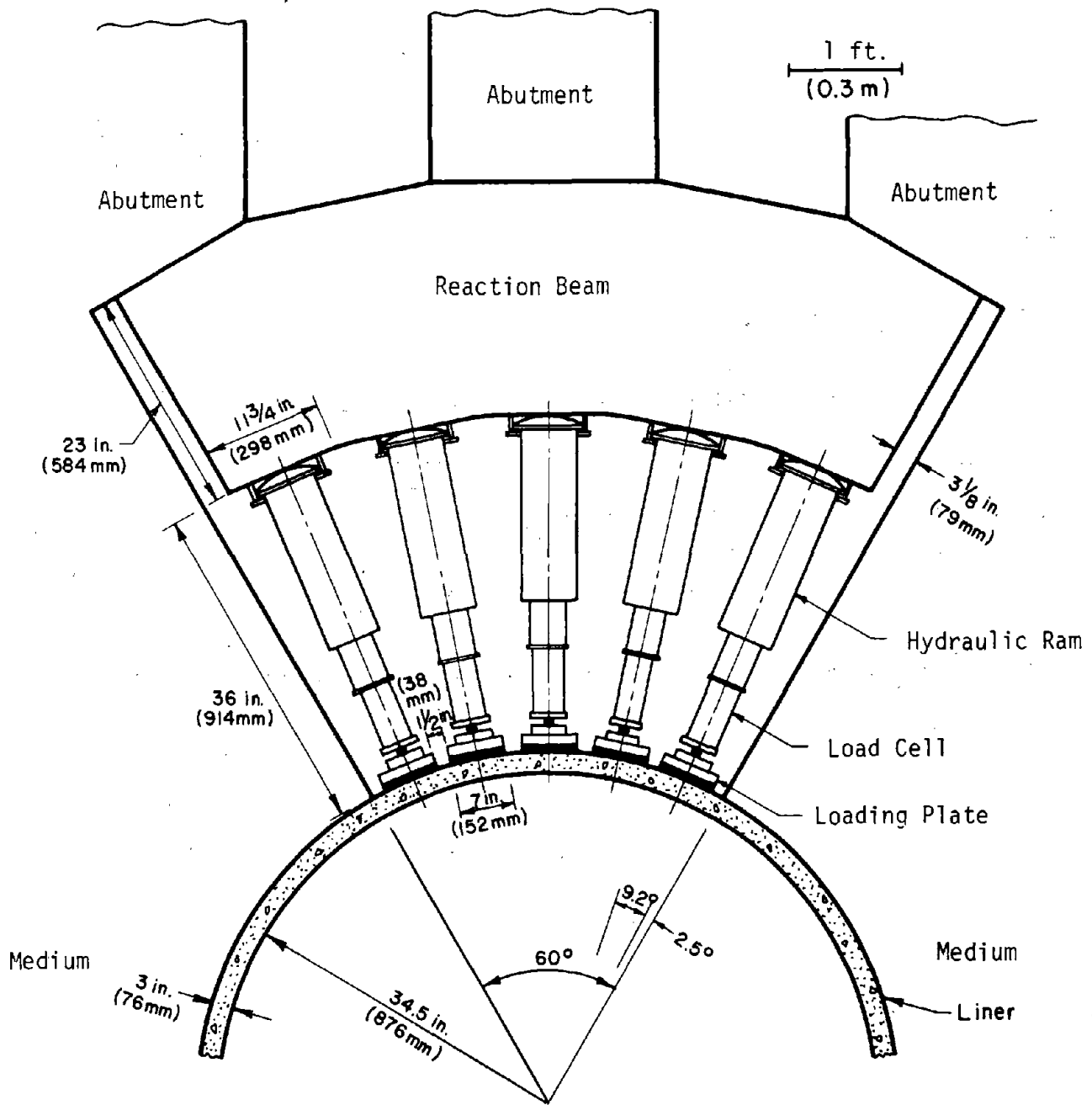


FIGURE 4.7 TOP VIEW OF THE LOADING SYSTEM



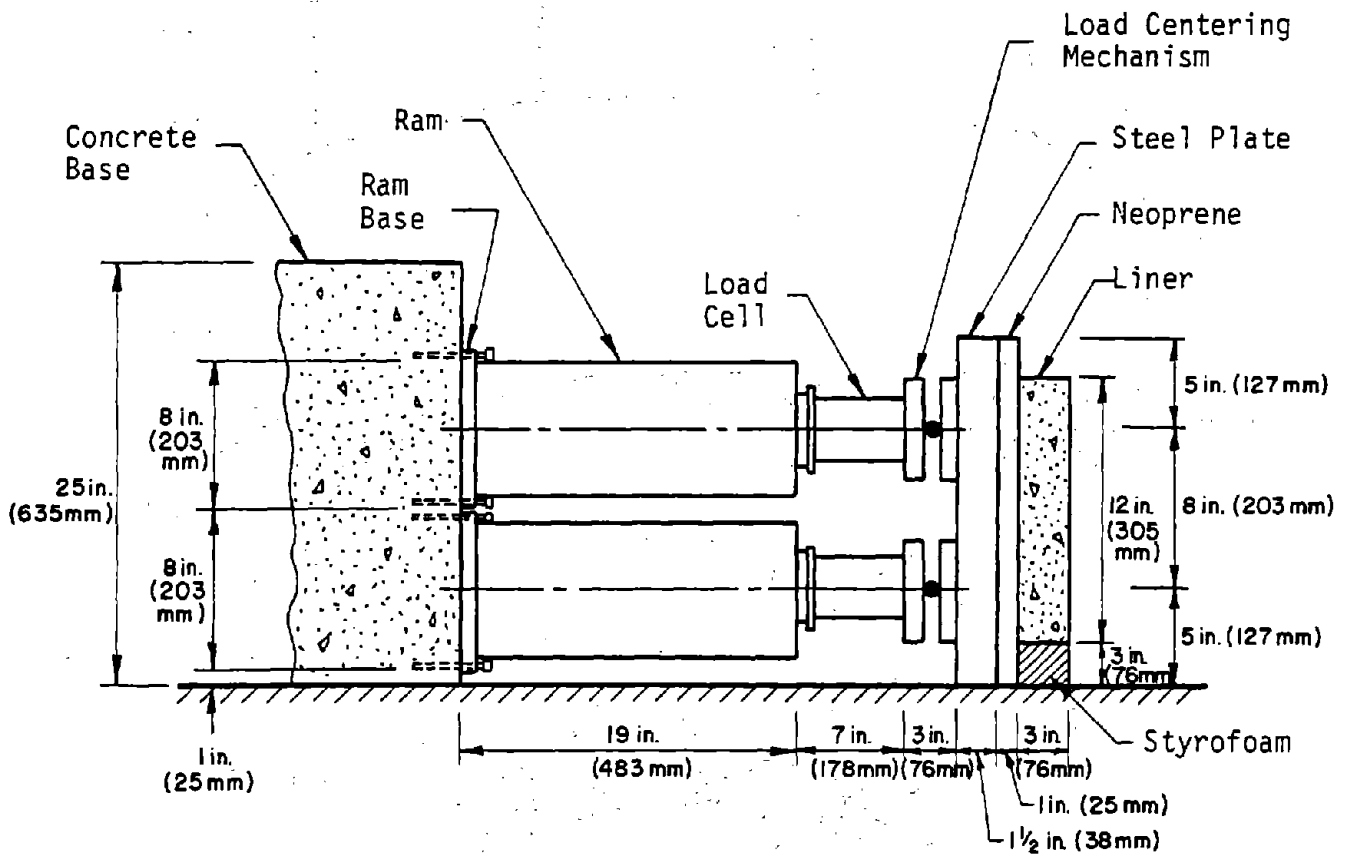


FIGURE 4.8 SIDE VIEW OF TEST RAMS

the shape of the specimen surface was glued to the loading plate. Thus, even though the curvature of the arch would vary at high load levels, which would tend to concentrate the applied load toward the edges of the loading plate, additional deformation of the rubber in these regions would result in a more uniform distribution of the applied pressure. The vertical separation of the loading rams and the dimensions of the loading plates were designed to permit testing linings 1.0 ft (0.3 m) or 1.5 ft wide (0.46 m). The five loading plates used with 1.5 in. (38 mm) spacing provided almost complete confinement of the concrete in the loaded portion of the arch. The rams were numbered counter-clockwise 1-3-5-7-9 for the upper five, and 2-4-6-8-10 for the lower five. The same numbering system was followed for the corresponding load cells.

To obtain the nonuniform load distribution for tests Arch-2 and Arch-3 (shown in Table 4.1), the two outer pairs of rams, 1-2 and 9-10 were connected hydraulically, the two intermediate ones 3-4 and 7-8 formed another group and the middle ones 5-6, the third group (Fig. 4.9). Different pressures were necessary for each group of rams. Three hydraulic actuators, two of 25 kips (111 kN) and one of 6 kips (27 kN) capacity, operating both in tension and compression, were employed. These actuators are MTS hydraulic rams with built in load cells that allow the electronic control of loads by adjusting the hydraulic pressures in the rams with servo-controlled valves. They were set vertically to react against a steel frame (Fig. 4.10). By adjusting the reaction load in each of the actuators, the oil pressure within their individual oil compartments was adjusted proportionately. At their capacity load, the maximum oil pressure in each one was 3000 psi (21 MPa) on one side of a movable piston within the oil compartment and 0 psi (0 MPa) on the other. By reducing the reaction load, the oil pressure on one side of the piston would increase and on the other side it would decrease. At zero load, the pressures on both sides of the piston would be equal. Thus, by starting at the fully extended position (full compression) of the hydraulic actuators and retracting

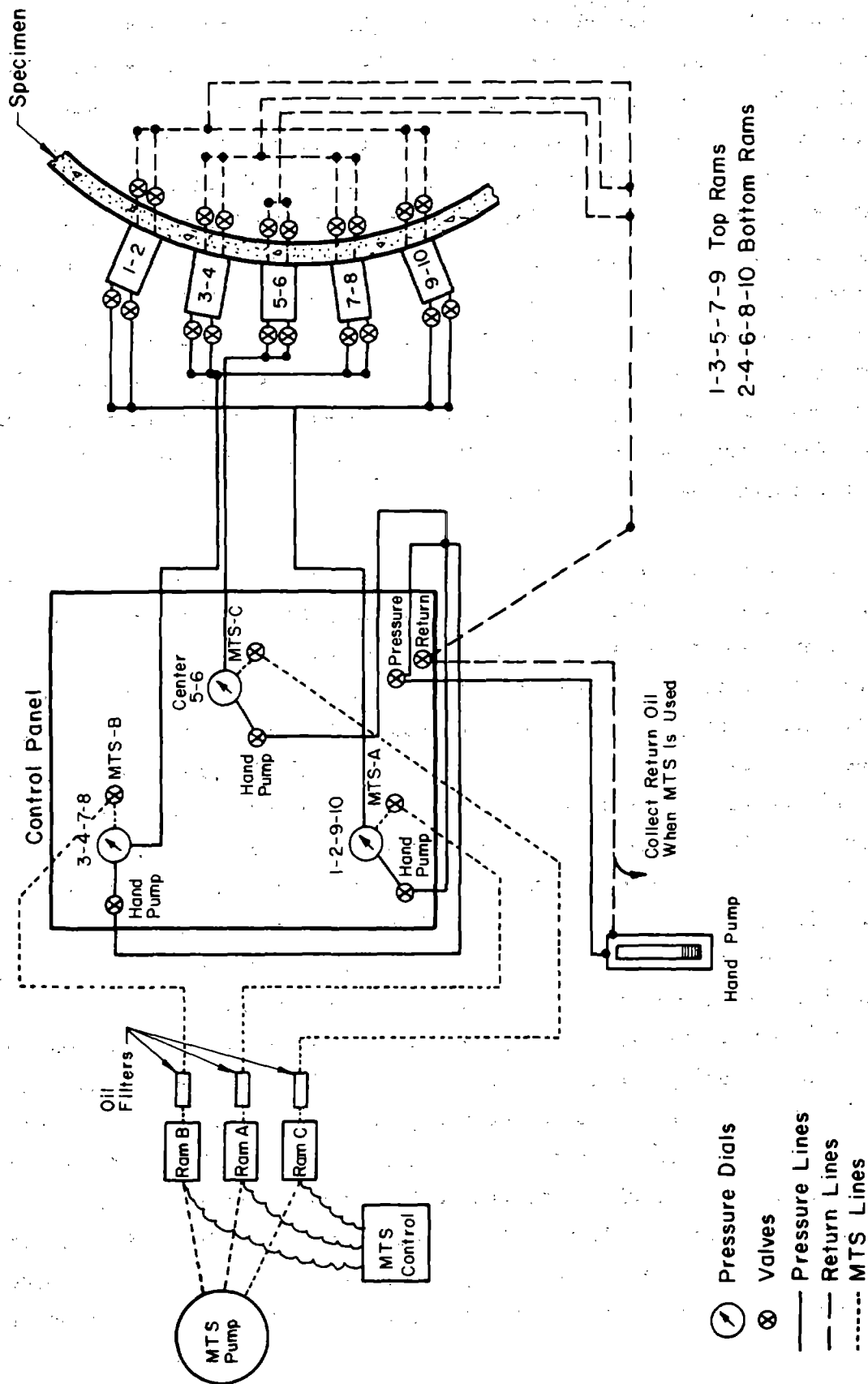


FIGURE 4.9 OUTLINE OF HYDRAULIC SYSTEM

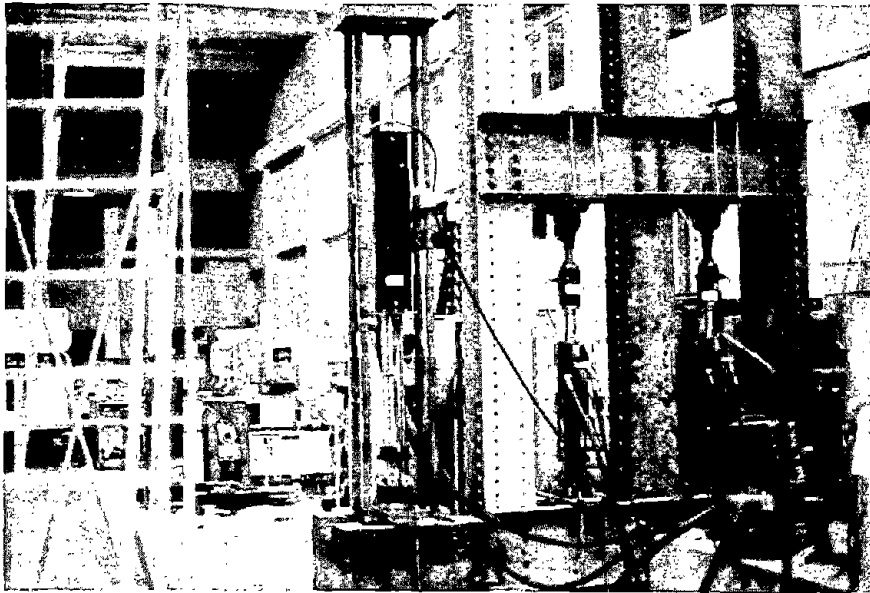


FIGURE 4.10 HYDRAULIC ACTUATORS USED TO PRODUCE NON-UNIFORM LOADINGS

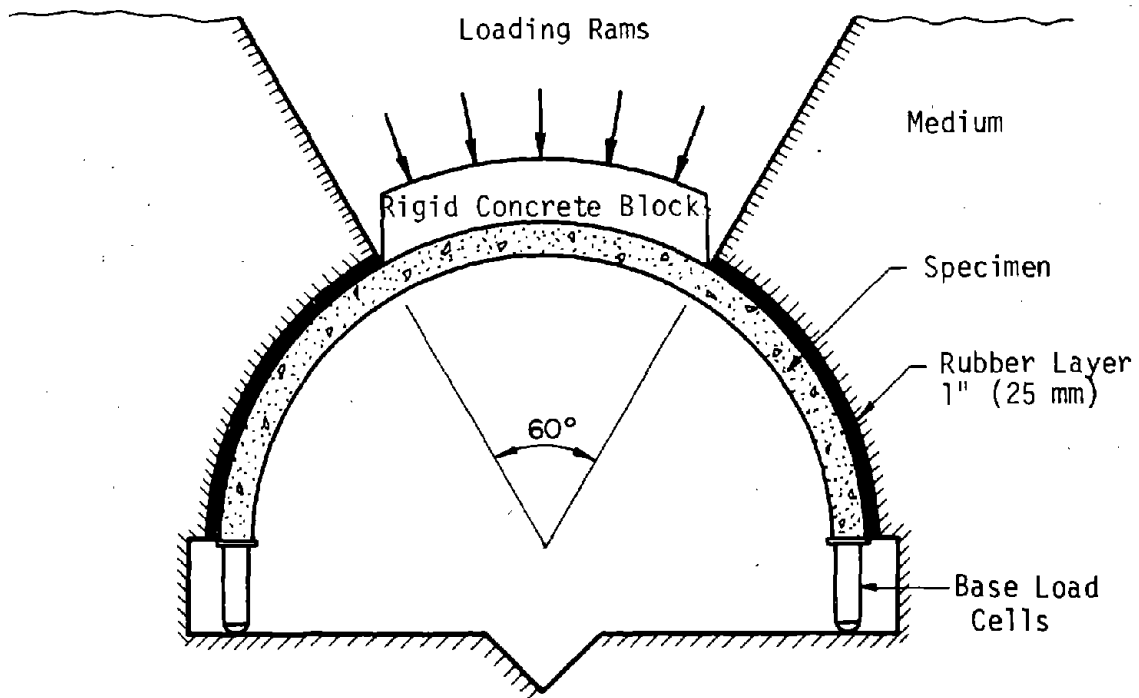


FIGURE 4.11 SET-UP FOR RIGID BLOCK LOADING

them by applying tension in their rigid supports, the pressure at the top portion of the oil compartment would vary from 0 psi (0 MPa) to 3000 psi (21 MPa). By connecting them to a control console, the actuators could be adjusted to operate at a portion of their total capacity. Since three different, equally increasing ratios of pressure were desired, the three hydraulic actuators were pre-programmed to operate at 33, 66, and 100 percent of capacity. Consequently, at the same input pressure, provided by an MTS pressure pump, three different pressures could be generated within the oil compartments of the hydraulic actuators. As the input pressure was increased, the pressure in each actuator was increased, but their ratios remained constant. These three different pressures were fed separately into the outer pairs of rams, the intermediate ones and the middle pair. If Arch-2 loading was desired, the outer pressure would be the lowest, the intermediate one the next higher and the middle one the highest. For loading of Arch-3, the magnitudes of pressure were reversed.

In the case of Arch-4, where five different pressures were necessary, the three actuators generated pressures of 100, 80 and 60 percent capacity which were fed to the three successive pairs of rams 9-10, 7-8, and 5-6. The last two pairs, 3-4 and 1-2, were connected to two hand pumps providing the 40 and 20 percent of maximum pressure. To assure that the ratios of pressure were the desired ones, a digital readout of a load cell from each pair of rams was continuously monitored. Any necessary adjustments in pressure were made manually.

In order to achieve uniform loading conditions, as desired for Arches-1 and 5, the same hydraulic pressure was fed to all 10 of the rams. Thus, the loads varied only slightly due to difference in ram friction. The pressure for the two uniform loading cases was provided by a hand pump.

To represent a field condition in which a rigid rock block is loosened from the medium and rests on the lining, a heavily reinforced

concrete block 6 in. (152 mm) thick was cast at the crown of Arches-6 and 7, as shown in Fig. 4.11. Loading was applied by pushing this rigid block with the hydraulic rams against the specimen.

The hydraulic system was interconnected and could either be operated using the hand pump, or the MTS control system, through a control panel with hydraulic valves and pressure gages. For fast retraction of the hydraulic rams, an electric pump was used in place of the hand pump. Thus, the hydraulic system could be operated either manually, electrically, or electronically.

#### 4.2.2 Loads

Since the tests were intended to model openings in rock, the loads imposed were chosen to represent certain realistic, though idealized, geologic conditions that could exist within a rock mass in which an opening is excavated. In these tests, the loads were assumed to be caused by loosening rock. The distribution remained constant, and the magnitude was increased until the lining failed. Squeezing and swelling type loads were not considered. The loading shapes and their geologic idealizations are shown in Fig. 4.12. The loading for Arches-1, 5, 8, 9 and 10 represents a highly jointed or weathered rock over the crown that would result in a fairly uniform distribution. Test Arch-2 depicts the case of a tunnel in rock with a symmetrical triangular wedge formed over the crown that moves downward as a unit. This condition could be typical in highly jointed rock where the conjugate joint sets offer ample opportunity for formation of this type of wedge. Arch-3 could be in the same rock conditions as Arch-2, but with either the wedge being of comparable size relative to the width of the opening or with the joints running vertical. The massive rigid block on the top of the tunnel lining would transfer most of its load toward the edges because of the lining deforming in the center portion of the crown. Arch-4 represents a tunnel in highly jointed or foliated rock in which the joint or shear zone orientation is such that

Idealized Geologic Condition

Corresponding Loading Pattern

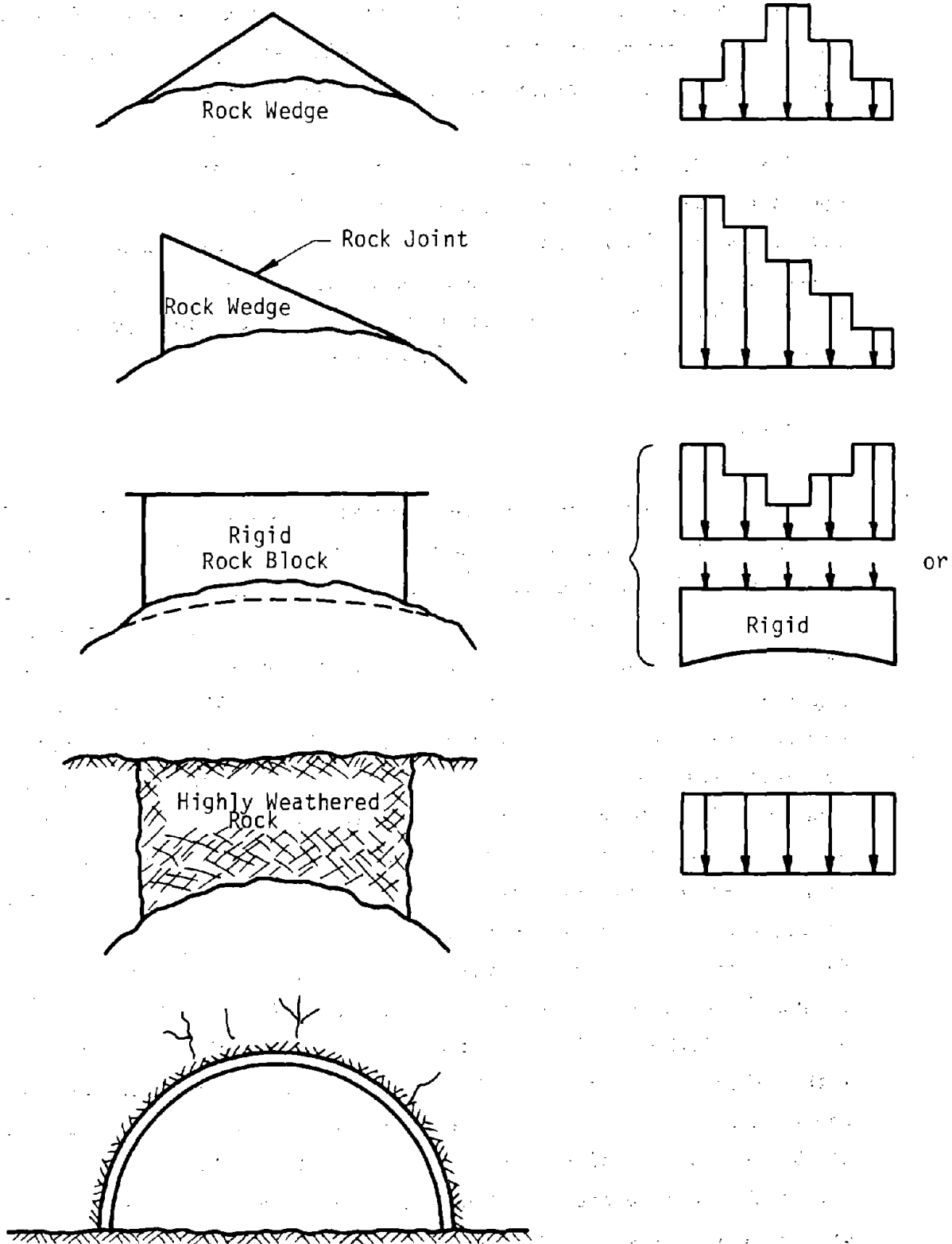


FIGURE 4.12 LOADING CONFIGURATIONS

formation of an unsymmetrical wedge is favored. As a result, more load would be transferred at one end of the wedge than the other. The same loading could result if a steeply dipping shear zone intersects the sides of the opening. Arch-5 had the same loading as Arch-1, but the side friction was eliminated.

The rigid block loading used in Arches-6 and 7 represents the same type of loading as in Arches-2, 3, and 4 in a different way. Applying the load through a rigid concrete block caused higher rotations and higher bending moments at the edges of the loading block. Furthermore, the effect of this loading condition on the shear capacity of the lining could be evaluated.

#### 4.2.3 In-Situ Plate Load Tests on the Medium

Although the concrete stress-strain curve and the initial tangent modulus were obtained for the medium using 6 by 12 in. (152 by 205 mm) cylinder tests, a better approximation of the stiffness of the medium in place was considered necessary.

The cylinder tests of intact rock specimens invariably leads to overestimation of stiffness of the in-situ rock masses due to the effect of the inherent geologic discontinuities present in the rock mass. Visible discontinuities within the concrete medium did not exist, but in-situ deformability tests were conducted to account for the three dimensional behavior of the concrete, and to evaluate the effects of shrinkage cracks within the concrete mass or between the edges of the concrete medium and the abutments, and the deformation of the abutments. In-situ plate load tests were performed at two locations on the right side of the medium. It was assumed that the left side would behave similarly, considering the fact that the same concrete mix and the same curing procedure were employed. Position A located 12-5/8 in. (320 mm) from the edge, (Fig. 4.13) was intended to account for the open boundary effects. Position B was located 30 in.



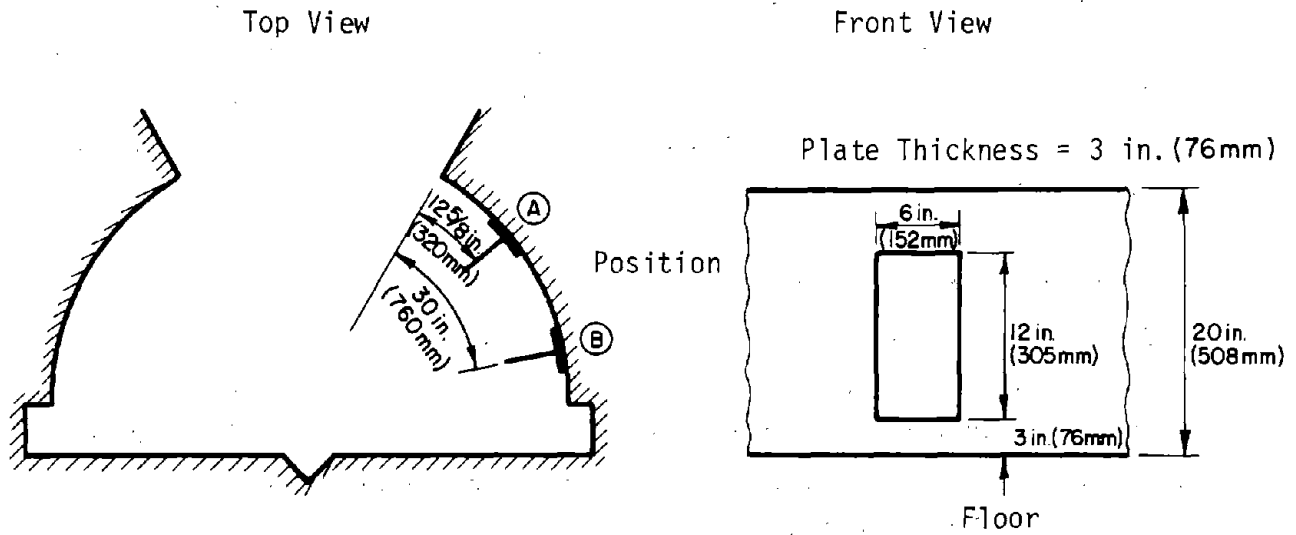


FIGURE 4.13 LOCATIONS OF IN-SITU PLATE LOAD TESTS

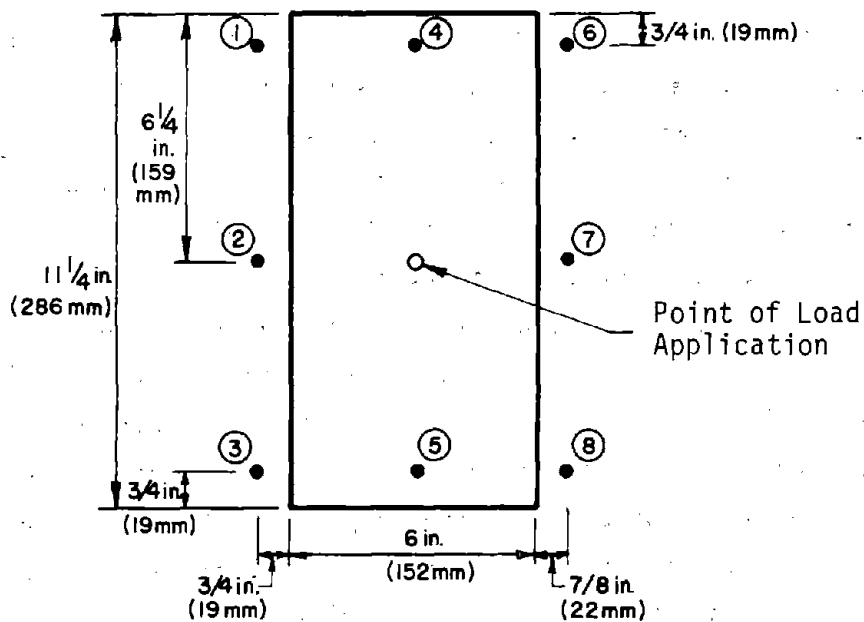


FIGURE 4.14 POSITION OF DIAL GAGES DURING IN-SITU PLATE LOAD TESTS FOR ARCHES 1 TO 6

(760 mm) from the edge. For Arches-1 to 6 a 3 in. (76 mm) thick steel plate, 6 by 12 in. (152 by 305 mm) was placed at the positions A and B and loaded at the center by a hydraulic ram. The plate was grouted with a 1 in. (25 mm) thick layer of grout to distribute the applied load evenly on the plate. For Arches-7 to 10 additional tests with 11-3/4 by 11-3/4 in. (298 by 298 mm) plates were performed as well to reduce the edge effects around the plate. A slightly higher modulus was obtained with the larger loading plate.

In the case of a uniformly loaded rectangular area on the plane surface of an elastic medium, the displacement at the center is larger than that at the corners. The magnitude of the maximum displacement depends largely on the distribution of load. In contrast, the magnitude of the average displacement is less dependent on the load distribution, depending mainly on the total load as described by Waldorf, et al. (1963).

Since it is much easier to measure the total load than to try to assess the pressure distribution underneath a loading plate, it is usually preferable to measure the average rather than the maximum displacement, assuming uniform load distribution. The error in assuming uniform load distribution is less than 5 percent.

For Arches-1 to 6, eight dial gages were used, six of them measuring the deformations outside the vertical edges of the plate and two of them on the plate, as shown in Figs. 4.14 and 4.15. For Arches-7 to 10, only deformations on top of the plate were measured, since the rubber close to the edges of the loading plate was deforming outwards and thus the readings would be meaningless.

The load was applied by a hydraulic ram reacting against the base of the arch opening and the right abutment, as shown in Fig. 4.16, and measured by a load cell inserted between the end of the ram and the loading plate. Several loading-unloading cycles were performed



FIGURE 4.15 DIAL GAGE ARRANGEMENT FOR THE IN-SITU  
PLATE LOAD TESTS

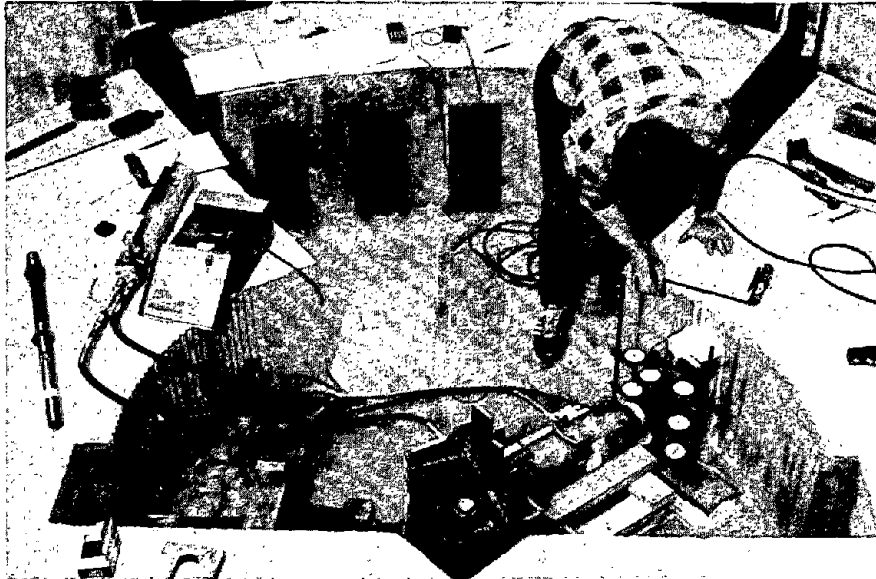


FIGURE 4.16 PLATE LOAD TEST IN PROGRESS

revealing hysteresis as shown in Fig. 4.17. The concrete appeared to stiffen after a few cycles, probably because of the closing of the shrinkage cracks. For Arches-1 to 6 the average of all the dial gages on the concrete and the average of all eight dial gages were plotted. The average total deformation was slightly larger than the deformation of the concrete at any given load level, since it contained the deformation of the grout between the loading plate and the concrete surface. For computing the modulus, only the average deformation of the concrete was used for Arches-1 to 6. For Arches-7 to 10, only the deformation on the plate was measured and used.

Although neither rock nor concrete is homogeneous or elastic, it is customary to interpret test results on the basis of the theory of elasticity and to assign the mass an equivalent value of Young's Modulus,  $E_R$ , because the stress-strain curve is roughly linear at the moderate stress levels usually encountered in the medium.

Integrating the Boussinesque solution as given by Timoshenko and Goodier (1970), for the normal displacement of the surface of a semi-infinite elastic solid under the action of a point normal load, the average displacement becomes:

$$\bar{W} = \frac{\bar{m} \cdot P(1 - \nu_R^2)}{E_R \cdot \sqrt{A}} \quad (4.1)$$

where

$\bar{W}$  = average displacement of the loaded surface

$\bar{m}$  = displacement coefficient dependent on the shape of the loaded surface and the distribution of the load

A = area of the loaded surface

P = total normal load

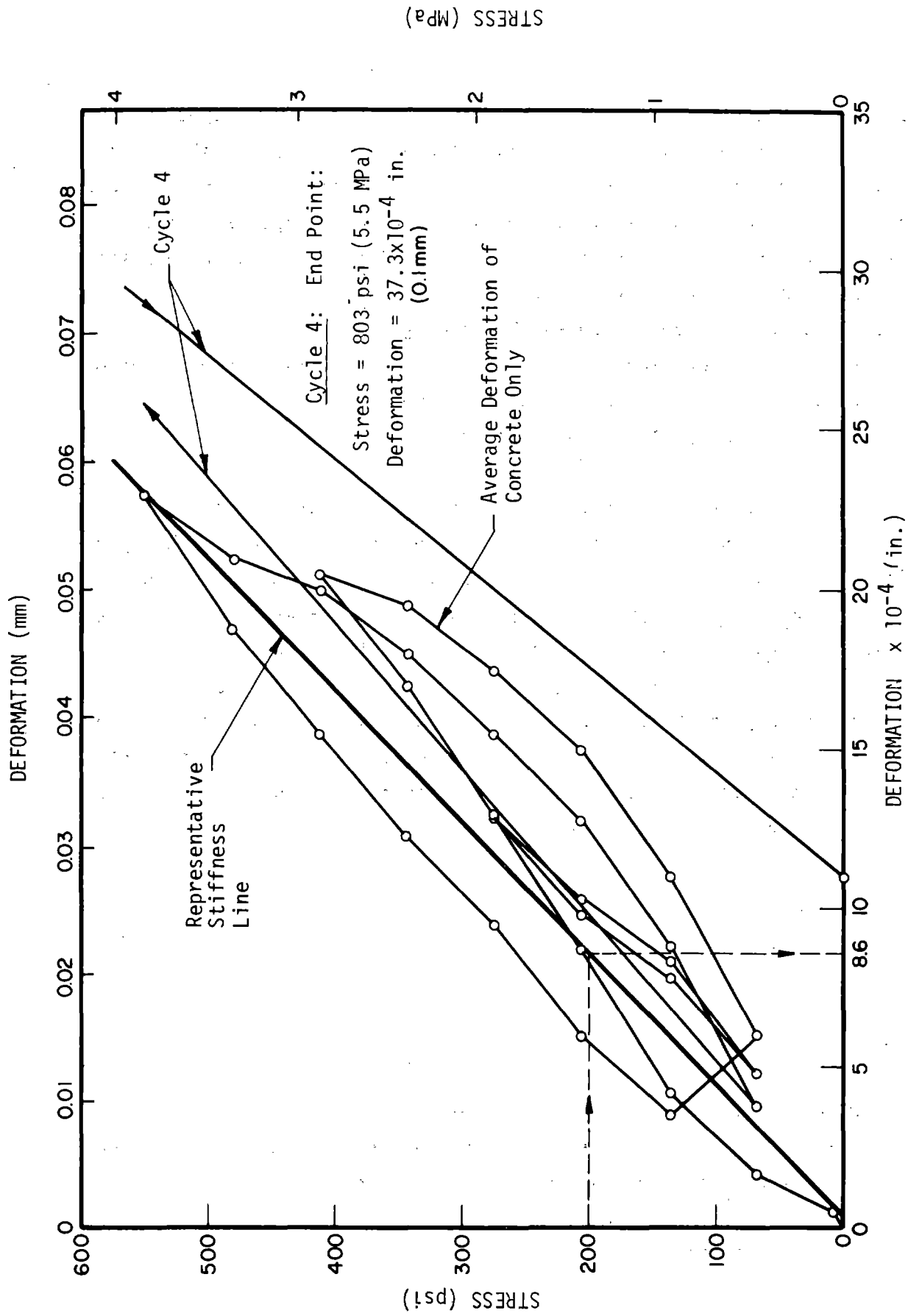


FIGURE 4.17 TYPICAL IN-SITU PLATE LOAD TEST DATA FOR ARCHES 1 TO 6

$\nu_R$  = in-situ Poisson's ratio of the rock (medium) mass  
 $E_R$  = in-situ modulus of elasticity of the rock (medium) mass

A "representative stiffness" line was used to define the loading path after a few loading cycles as shown in Fig. 4.17. The estimate of modulus of elasticity was obtained from Eq. 4.1, assuming Poisson's ratio  $\nu_R = 0.17$  and  $\bar{m} = 0.92$  for Arches-1 to 6 and  $\nu_R = 0.45$  and  $\bar{m} = 0.95$  for Arches-7 to 10. These shape factors are given by Stagg and Zienkiewicz (1978). The resulting modulus of the medium was used to obtain the flexibility ratio for the particular test lining that represents its flexural stiffness in the ground.

The maximum radial pressure level expected in each test was estimated, and the "representative stiffness line" from the load deformation curves was used to determine the displacement for use in Eq. 4.1 to calculate  $E_R$ . These pressures were 200 psi (1.4 MPa) for Arches-1 to 8, and 80 psi (0.5 MPa) for Arches-9 and 10.

For Arches-1 to 6 the estimates of modulus of elasticity of the medium were: Position A,  $E_R = 1.46 \times 10^6$  psi (10,060 MPa) and Position B,  $E_R = 1.89 \times 10^6$  psi (13,020 MPa). For classification purposes and for computing the flexibility ratio, an average value of  $E_R = 1.68 \times 10^6$  psi (11,575 MPa) was used. The value at Position A is lower due to the proximity to the free edge.

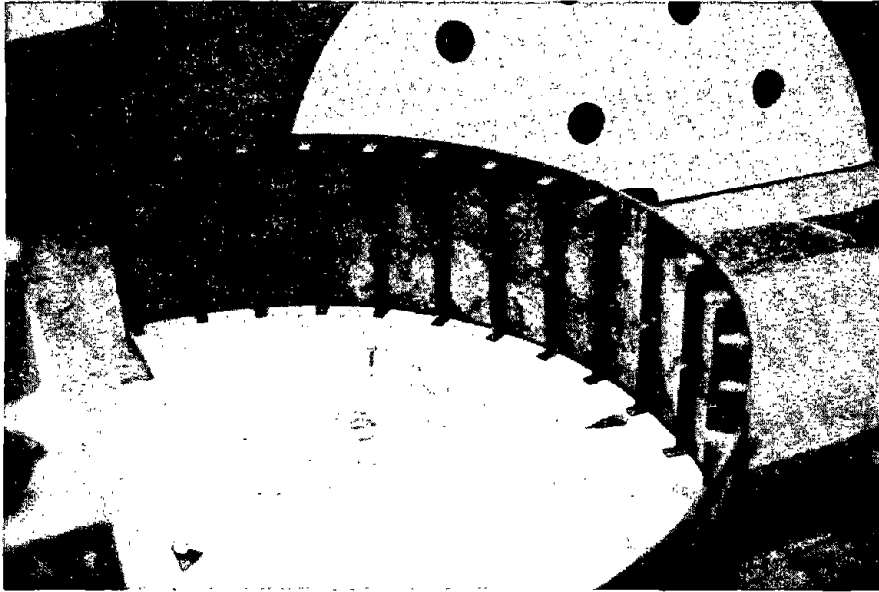
The modulus of elasticity of the medium used for Arches-7 to 10 was the average of the two tests with different plate sizes, with the larger plate test yielding a slightly larger value. The values were  $E_R = 150,000$  psi (1030 MPa) at Position A and  $E_R = 200,000$  psi (1380 MPa) at Position B. The value used for computing the flexibility ratio was  $E_R = 170,000$  psi (1170 MPa).

#### 4.2.4 Specimen Preparation

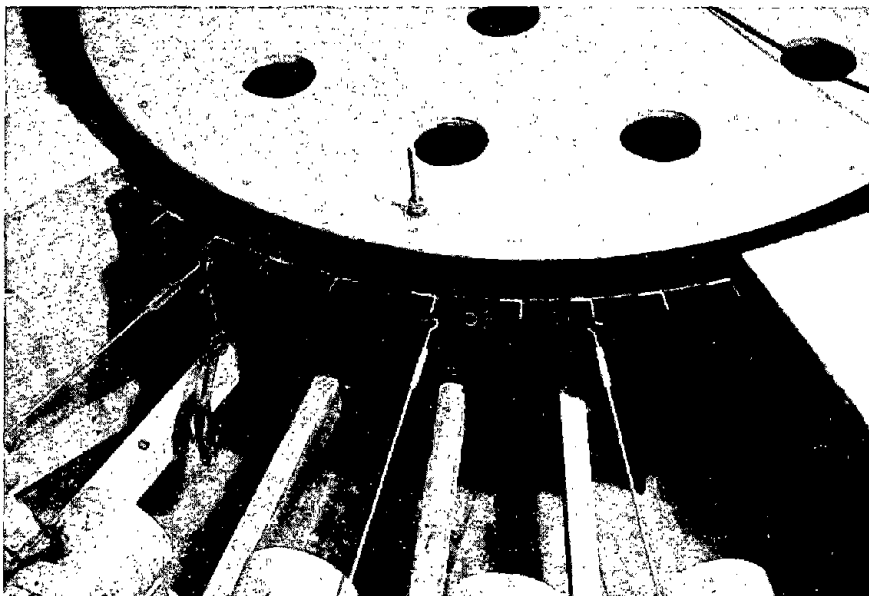
Nine unreinforced concrete arches designated as Arches-1 to 9 and one reinforced one designated Arch-10 were tested. The outside diameter of the specimen was 6 ft 3 in. (1.9 m) and the width 12 in. (305 mm). The nominal thickness was either 3 in. (76 mm) or 1 in. (25 mm). The measured thicknesses are shown in Table 4.2.

The arches were of semi-circular shape, cast-in-place against the sides of the opening with 1/8 in. (3 mm) thick steel form. The form, shown in Fig. 4.18, was assembled outside the test facility by fastening the metal sheet to three plywood sheets at the top, bottom, and midheight. The entire assembly was placed inside the medium opening and bolted to the floor, leaving a 3 in. (76 mm) void between the outer portion of the form and the sides of the medium. To achieve the 1 in. (25 mm) thickness for Arches-9 and 10, the inside surface of the form was lined with thin matboard using 2 in. (51 mm) spacers, between the new and the old surface. The 60 deg opening at the crown of the lining was closed with another metal form shored against the base of the rams. The form was completed by using two 5 x 18 x 1 in. (127 x 457 x 25 mm) steel plates at the bases of the arch shored against the medium. To insure that the specimen would not adhere to the sides of the medium and to facilitate its removal after testing, a layer of gloss finish polyurethane paint was applied to the face of the medium when the concrete medium was used. The inside of the form was oiled before placing the concrete.

The concrete was prepared in one 10 ft<sup>3</sup> (0.3 m<sup>3</sup>) batch in the laboratory; the mix proportions are given in Table 4.2. It was placed in two layers (Fig. 4.19) and vibrated. The form was removed the following day, and the specimen was kept moist and covered for seven more days. To expedite the experimental program, testing of the specimen followed about two weeks after casting. The exact age of each specimen on test day is given in Table 4.3. Arches-9 and 10 were



(a) Form Assembling Process



(b) View of the Crown Portion of the Form

FIGURE 4.18 FORM FOR CASTING SPECIMENS



TABLE 4.2 TEST SPECIMEN CONCRETE MIXES

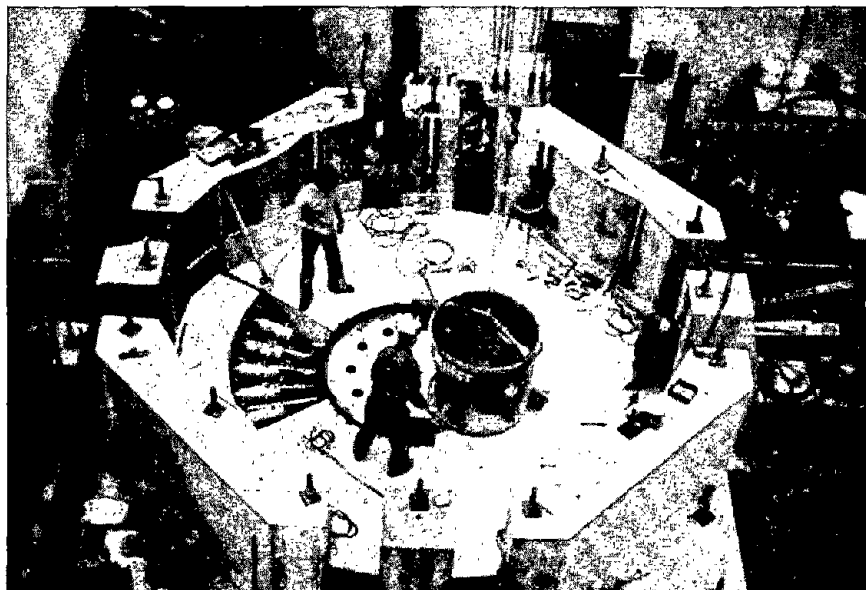
a) Arches 1 to 8\*

	Weights			
	Dry		Saturated, Surface Dry	
Coarse Sand, 1b (kg)	1360	(617)	1380	(626)
Cement Type 1, 1b (kg)	494	(224)	494	(224)
Water, 1b (kg)	312	(141)	272	(123)
Gravel:				
3/16-3/8 in. (0.2-0.4 mm), 1b (kg)	200	(91)	200	(91)
3/8-3/4 in. (0.4-0.8 mm), 1b (kg)	1580	(717)	1600	(726)
Water/Cement Ratio:	0.55		0.55	
Slump, in. (mm)	5-7	(127-178)	5-7	(127-178)

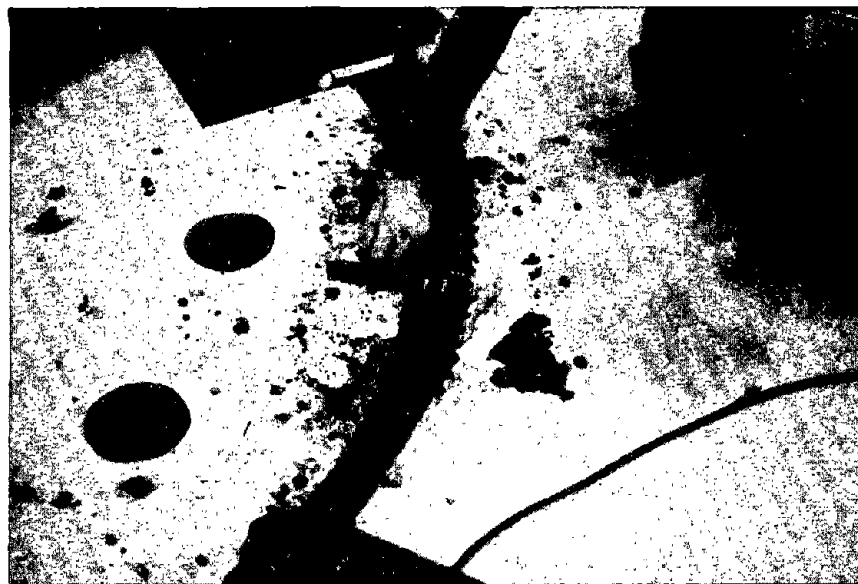
b) Arches 9 and 10\*

Coarse Sand, 1b (kg)	2230	(1011)	2260	(1025)
Fine Sand, 1b (kg)	522	(237)	562	(255)
Cement Type 1, 1b (kg)	624	(283)	624	(283)
Water, 1b (kg)	570	(259)	500	(227)
Water/Cement Ratio:	0.80		0.80	
Slump, in. (mm)	3	(76)	3	(76)

\* Mixes for 1 yd<sup>3</sup> (0.8 m<sup>3</sup>) of concrete.



(a) Placing the Concrete



(b) Finishing the Top Surface to Assure Uniformity in Width

- FIGURE 4.19 CASTING OPERATION FOR THE ARCH SPECIMENS

TABLE 4.3 TEST SPECIMEN THICKNESS AND CONCRETE PROPERTIES

Specimen Number	Measured Thickness, in. (mm)		Age on Test Day (days)	$f'_c$ psi (MPa)	$f_{sp}$ psi (MPa)
	Crown	Sides			
Arch-1	3 (76)	3-1/4 (82)	18	5740(39) <sup>1</sup>	450(3.1) <sup>3</sup>
Arch-2	3-1/16 (78)	3-1/8 (79)	12	4880(34) <sup>2</sup>	430(3.0) <sup>3</sup>
Arch-3	3-1/8 (79)	3-3/16 (81)	12	5350(37) <sup>2</sup>	460(3.2) <sup>3</sup>
Arch-4	3 (76)	3-1/8 (79)	11	4337(30) <sup>2</sup>	450(3.1) <sup>3</sup>
Arch-5	3-1/16 (78)	3-1/8 (79)	12	4495(31) <sup>2</sup>	440(3.1) <sup>4</sup>
Arch-6	3-3/8 (86)	3-1/8 (79)	15	5155(35) <sup>2</sup>	444(3.0) <sup>3</sup>
Arch-7	2-15/16(75)	3 (76)	10	4880(34) <sup>2</sup>	417(2.9) <sup>3</sup>
Arch-8	2-7/8 (73)	2-7/8 (73)	14	4925(34) <sup>2</sup>	394(2.7) <sup>3</sup>
Arch-9	1 (25)	1 (25)	27	3522(24) <sup>2</sup>	249(1.6) <sup>3</sup>
Arch-10	13/16 (21)	13/16 (21)	26	3978(27) <sup>2</sup>	247(1.7) <sup>3</sup>

<sup>1</sup> Using ten 6 x 12 in. (152 x 305 mm) cylinders.

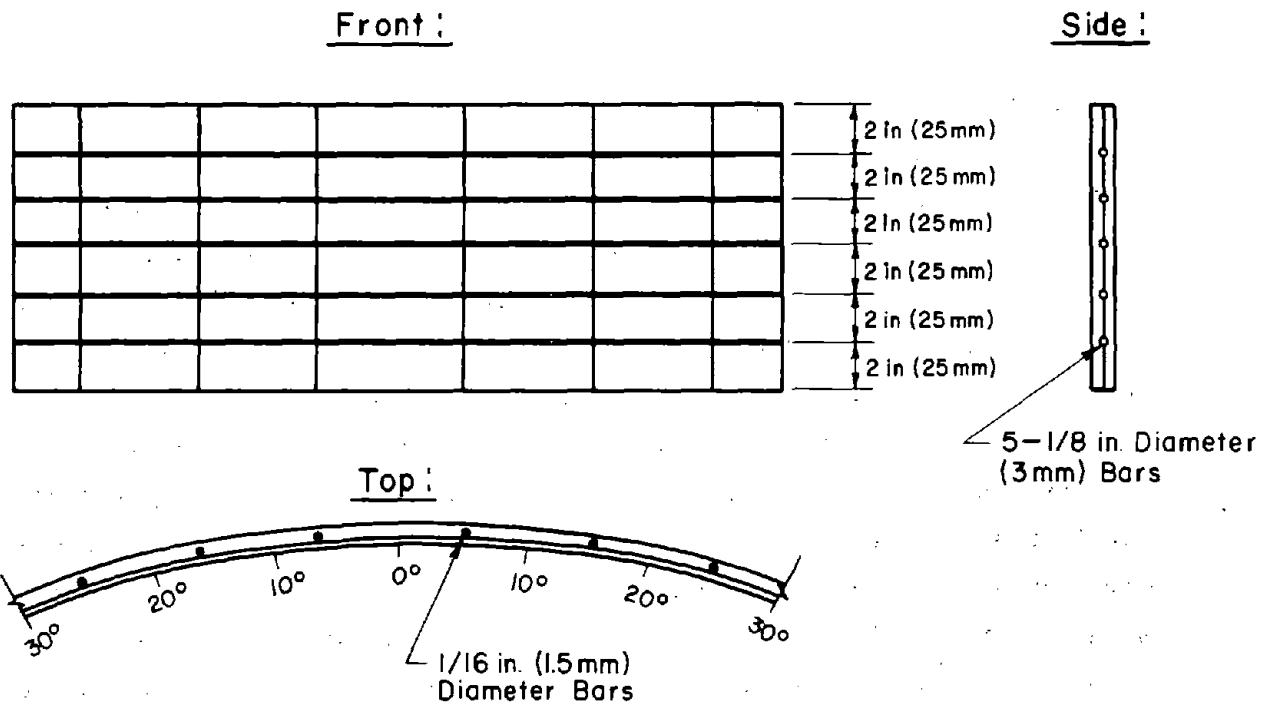
<sup>2</sup> Using ten 4 x 8 in. (102 x 203 mm) cylinders.

<sup>3</sup> Using ten 6 x 6 in. (152 x 152 mm) cylinders.

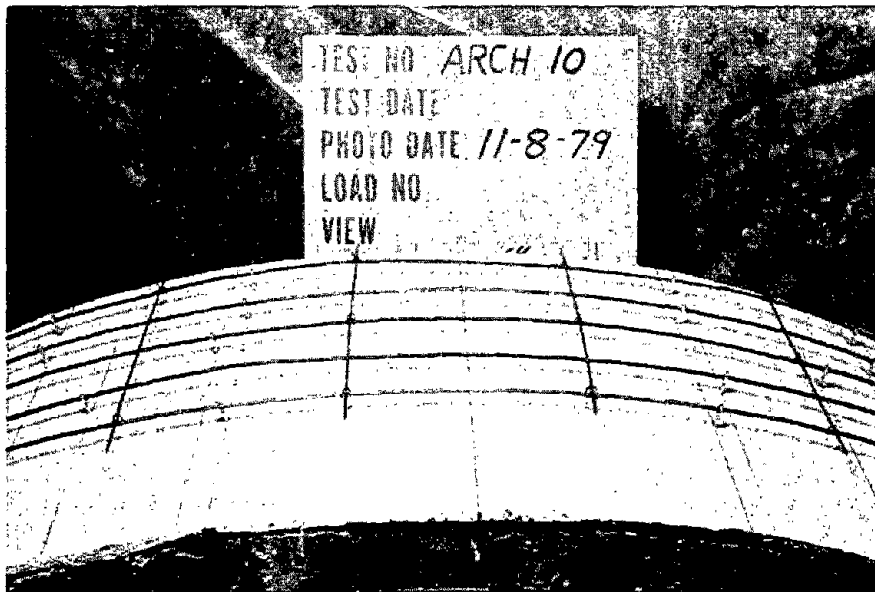
<sup>4</sup> Estimated.

tested at a later time to allow the concrete to gain strength. Although the concrete was still gaining strength when the tests were performed, the concrete properties were obtained at the time of the model test. From the stress-strain curves obtained for cylinders from each batch, the strains at peak load varied from 0.004 to 0.005 in./in. or about twice the traditional value of about 0.002 in./in. obtained at 28 days and a faster load rate. Ten 6 by 6 in. (152 by 152 mm) cylinders for split-cylinder tests and ten 6 by 12 in. (152 by 305 mm) compressive test cylinders for Arch-1 and 4 by 8 in. (102 by 203 mm) for Arches-2 to 10, were obtained from each batch. These cylinders were cured in the same way and tested on the same day as the arch models. The results of these tests are given in Table 4.2. Although care was exercised to assure uniformity in mixing, placing and curing the specimens, it is observed that Arch-3, at the same age as Arches-2 and 5, attained higher strength. This could be the result of more wetting during curing for Arch-3. Also, it should be noted that for specimens Arches-2 to 10, 4 by 8 in. (102 by 203 mm) cylinders were used for determination of compressive strength because their size was more nearly the correct scaled size of the 6 by 12 in. (152 by 305 mm) cylinders used for actual linings. The split cylinder test was employed for determination of the tensile strength of the specimens because of its simplicity. The flexural tensile strength measured by the modulus of rupture,  $f_r$ , is related to the tensile strength by the equation  $f_r = (1.25-1.75) f_{sp}'$ , as given by Neville (1971). The lower coefficient corresponds to higher strength concrete. For analysis purposes the modulus of rupture was taken as  $f_r = (1.5) f_{sp}'$ .

Arch-10 was reinforced with five 1/8 in. (3 mm) diameter steel wires as shown in Fig. 4.20. The reinforcement was placed at midheight of the specimen using eye hoops fastened to the form. The steel wire was deformed in the laboratory to provide better bond between it and the concrete. The yield strength of the deformed bar was  $f_y = 40$  ksi (275 MPa).



(a) Details of Reinforcement



(b) Reinforcement in Place on the Form

FIGURE 4.20 REINFORCEMENT FOR ARCH-10

#### 4.2.5 Instrumentation and Test Procedure

The instrumentation had two objectives: to determine the overall behavior of the arches in terms of loads and deformations and to provide measurements to check the results of the analytic model. Once agreement between the experimental and the analytical results was established, a complete analysis for internal forces at any section of the arch could be performed.

Measurements were made of the active loads on the lining, the loads that reached the bases of the arch, the deformations of the lining around its periphery, the base movements, and the relative movement of the lining with respect to the medium. For Arches-9 and 10 strain measurements at the crown and at 35 deg left were taken as well.

The overall structural response was monitored by measuring the radius changes relative to the floor with 23 dial gages. Twelve dial gages were used on the left half and six on the right, as shown in Fig. 4.21. The dials were mounted on a steel frame bolted to the floor. Deformation measurements were taken at midheight of the specimen as shown in Fig. 4.22. Thin steel plates, 1.0 by 1.0 in. (25 by 25 mm) lubricated with oil, were bonded to the concrete surface at the contact points of the dial gage plungers, to minimize the friction when the specimen moved in the tangential direction. The four steel angles in the crown region, bolted vertically to the support frame, served as a protective shield for the dial gages.

Two additional dials were attached to the top of specimens Arches-1 to 4 at 35 deg right and at 35 deg left of the crown to measure the relative movement between the specimen and the medium. In the case of Arch-5, where the side friction was eliminated, three additional dial gages were placed at 40, 45, and 50 deg on the right side. For Arches-6 to 10, where the medium was softer, three more dials at 60, 70 and 80 deg were installed.

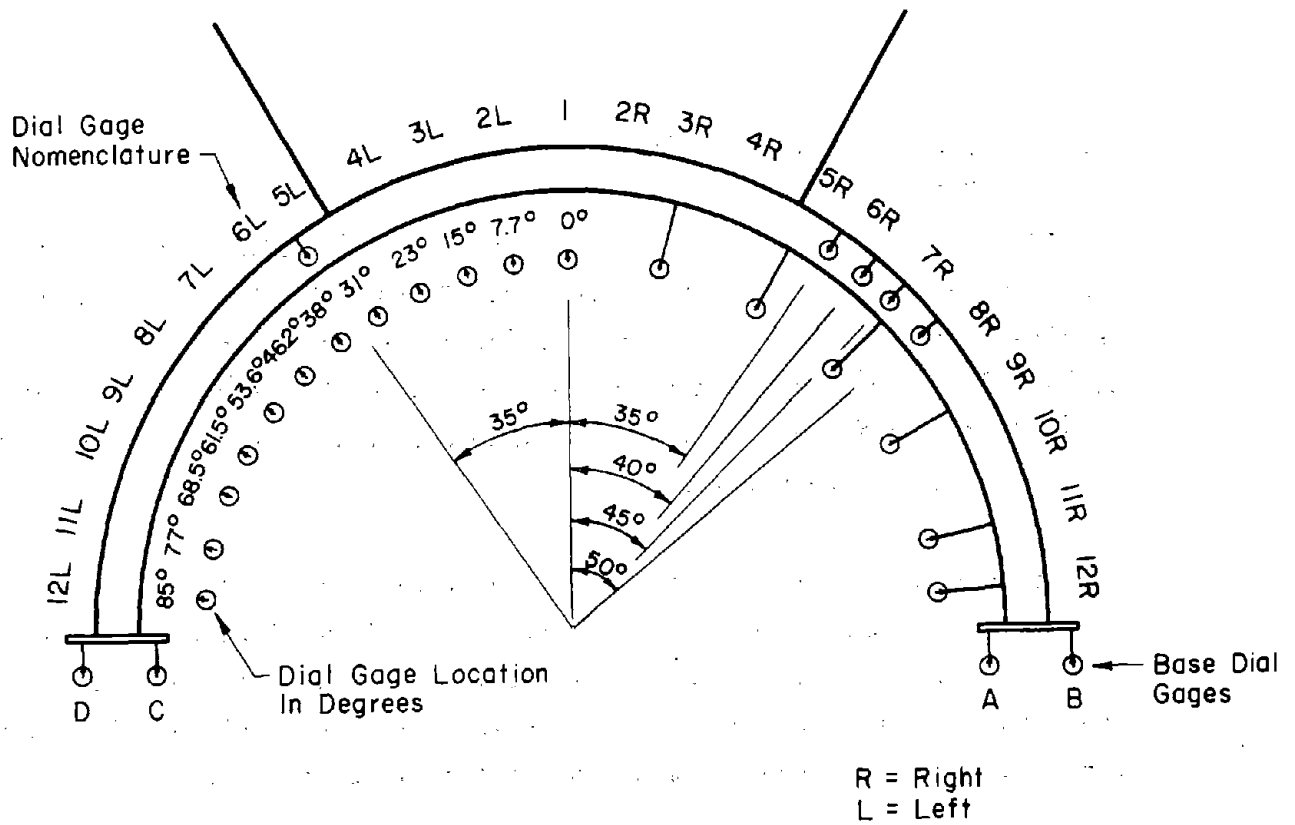


FIGURE 4.21 DIAL GAGE LOCATIONS IN TEST

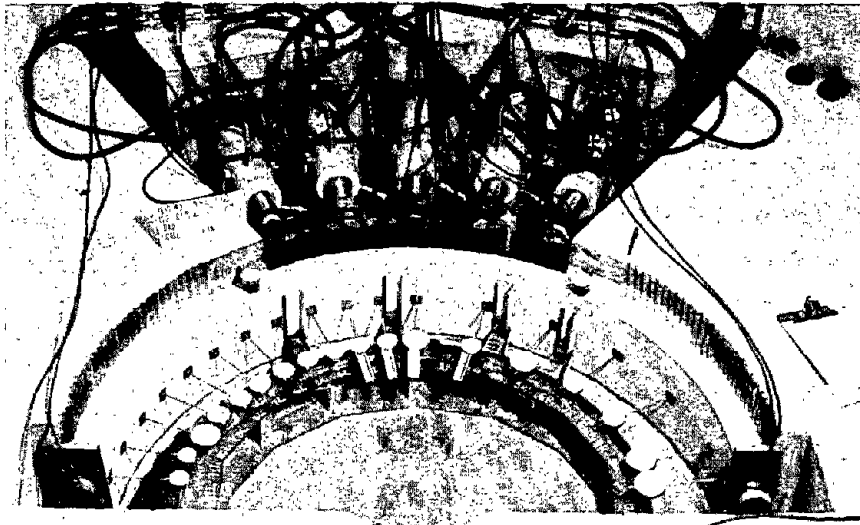


FIGURE 4.22 DIAL GAGES IN PLACE ON A SPECIMEN

In order to evaluate the portion of the active load that reached the base and thus to estimate the portion of the load resisted by friction and interlock between the lining and the medium, the base mechanism shown in Figs. 4.23, 4.24, and 4.25 was constructed. It consisted of two load cells, placed between two steel plates. One of the plates was 1.0 in. (25 mm) thick against which the specimen was cast to assure good contact, and the other, 3/4 in. (19 mm) thick, was bolted to the medium to obtain better distribution of the reactions. The reactions were transmitted through two half-cylinder steel seats. A threaded pin with a nut in the system was used to apply a small initial load to the base cells to assure that bearing on the base load cells was uniform at the start of the test. The stiffness of the base mechanism was comparable to that of the medium as discussed in a subsequent section. The relative movement of the entire lining with respect to the floor at the base was measured with two dial gages on each side 3.0 in. (76 mm) apart at midheight of the specimen as shown in Fig. 4.23.

The load cells were hollow aluminum cylinders with a full strain gage bridge bonded to them. The load cells and strain gages were connected to automatic recording equipment shown in Fig. 4.26. The first unit from the left in the figure was connected to the load cells and strain gages and provided means for calibration of the excitation voltage. The second unit provided digital readout of the load or strain in microvolts. Voltages read by the equipment were automatically recorded by the teletype which produced a typed copy. The last two units on the right side of Fig. 4.26 were the control consoles for adjusting the pressures in the hydraulic actuators, whenever a non-uniform loading was applied.

At the beginning of the test, it was necessary to assure that all the rams were in contact with the model so that proportional loading would begin immediately for all rams. Therefore, a small uniform load (about 2 percent of the total) was applied by the 10 active rams, with



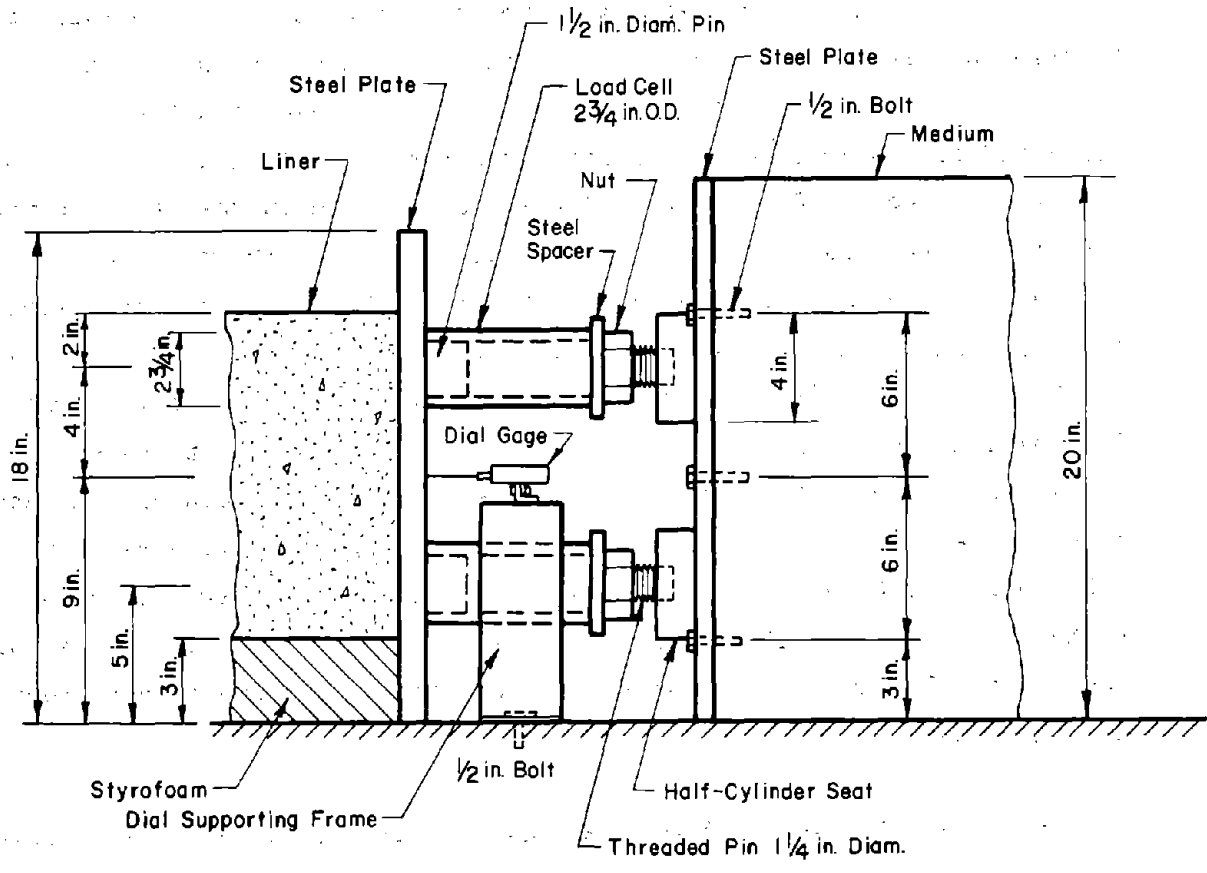


FIGURE 4.23 SIDE VIEW OF THE BASE MECHANISM

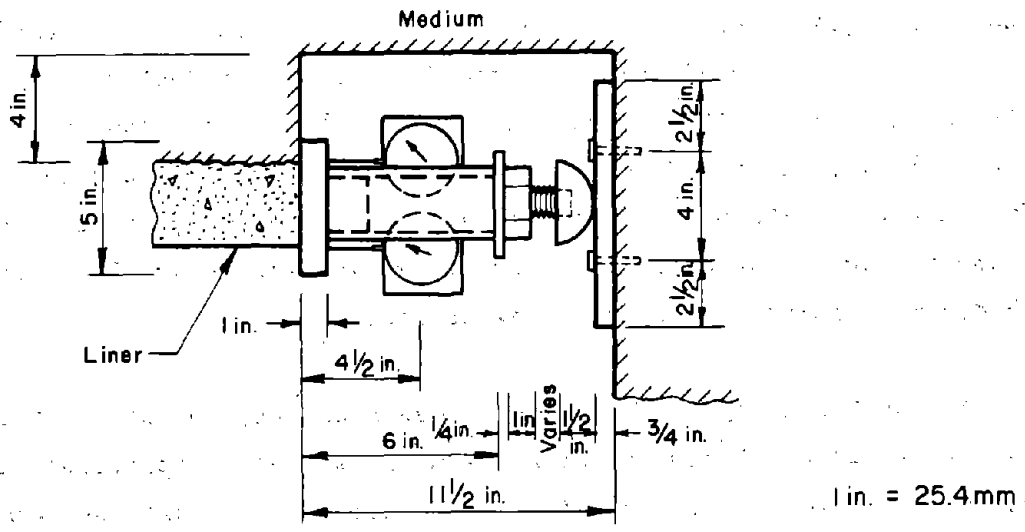


FIGURE 4.24 TOP VIEW OF THE BASE MECHANISM

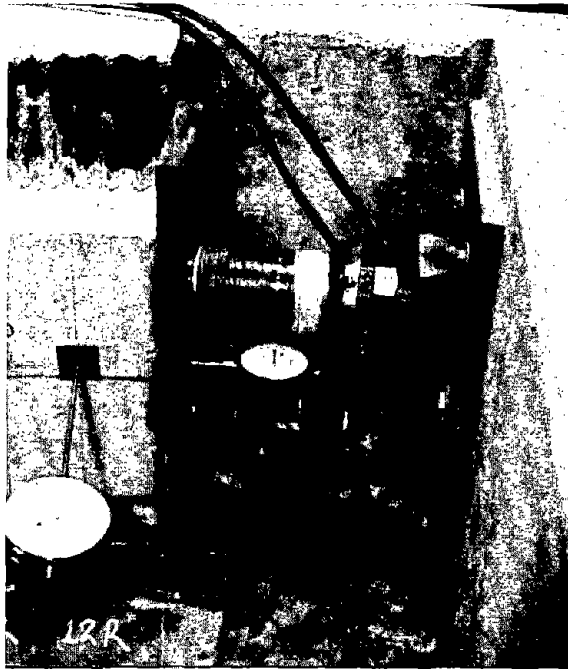


FIGURE 4.25 BASE MECHANISM AS CONSTRUCTED

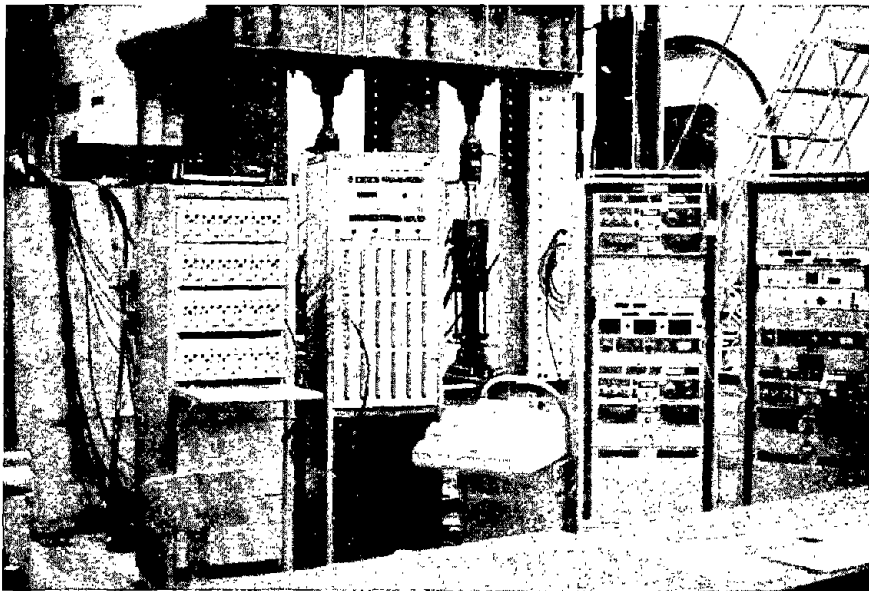


FIGURE 4.26 DATA ACQUISITION AND CONTROL SYSTEMS

each ram loaded separately to a predetermined level. The individual ram valves were then closed. After every active ram had been preloaded, the central pressure valve was closed, and the individual ram valves opened. Following pressure equalization within the active rams, the base load cells were tightened to equal contact load levels, usually 200 lb (~1 kN) per cell. The test proceeded by increasing pressure in the active rams. The first two increments were small, and then they were increased to 10 kips (44 kN) until the peak load was approached, when they were decreased to 5 kips (22 kN). The load data recorded by the teletype were checked for comparability and the desired reading for the next load increment was selected. A plot of total load versus maximum deflection was maintained as the test progressed as a guide to predict when the failure load was being approached, indicated by a flattening of the load-deflection curve. A complete set of deformation and strain measurements were taken at each load increment. In addition, progress of concrete cracking and crushing was monitored. The entire process took about 20 min. per load increment, and the total duration of the test, with a crew of 5, was 4.5 to 6.0 hours.

#### 4.3 TEST RESULTS

##### 4.3.1 Behavior and Ultimate Capacity of the Linings

Direct comparison of the ultimate load between the linings is not possible because of the variation in the concrete strengths from specimen to specimen as indicated in Table 4.2. In the following paragraphs two values of ultimate load will be reported, the one measured during testing and the one normalized with respect to the strength of the concrete in Arch-1.

The average base deflection reported is the average of all four base dial gages, even though in some cases the deflection on one side of the arch was larger than on the other as a result of the loading configuration or the difference in movement along the interlocking

sides of the specimen. In the following paragraphs the results from each test will be discussed separately; they are summarized in Table 4.4.

Arch-1 Specimen Arch-1 was loaded uniformly; it reached a total ultimate load of 180 kips (800 kN). Since the concrete strength for this specimen will be the basis for normalizing the specimen capacities, the normalized failure load will also be 180 kips (800 kN).

The ram forces were nearly equal; a small variation in the forces occurs because of differences in the friction between the ram piston and housing. The total load-crown deformation curve is nearly linear to a load of 160 kips (712 kN), when it becomes flatter as shown in Fig. 4.27. There was no slippage observed between the lining and the medium.

Arch-2 The load in Arch-2 was higher at the crown and became smaller toward the sides; an ultimate load of 117 kips (520 kN) was reached. The normalized ultimate load is 138 kips (614 kN). At a total load of 92.5 kips (411 kN), the right side of the specimen began to move at a larger rate relative to the medium; this is reflected in the crown and base movements shown in Fig. 4.28. Because of the shape of the serrations, this downward movement at the base was accompanied by an inward movement. In the next increment, at a total load of 107 kips (476 kN), the rate of movement increased at the left side also. The slippage was detected by a visible crack forming along the contact of the lining and the medium and by the sudden increase in the applied load that reached the base.

Arch-3 Arch-3 had larger loads at the sides of the loaded area than at the center. A total ultimate load of 174 kips (774 kN) was reached, which is equivalent to a normalized load of 187 kips (829 kN). The loading ratios were provided by the MTS servo-controlled rams. In some instances during loading, manual adjustments of the loads was

TABLE 4.4 STRENGTH CHARACTERISTICS OF THE ARCHES

Test	Load Shape	Flex.		Ultimate		% of Load Reaching Base	Critical Sect. deg
		Ratio, F	Tang. Shear	Load kips (kN)	Normalized Ult. Load kips (kN)		
ARCH-1		1200	YES	180 (800)	180 (800)	5.5	35 RIGHT
ARCH-2		1200	YES	117 (520)	138 (614)	21.0	CROWN
ARCH-3		1200	YES	174 (774)	187 (832)	21.0	35 RIGHT
ARCH-4		1200	YES	119 (529)	157 (698)	20.0	15 LEFT & 40 LEFT
ARCH-5		1200	NO	114 (507)	146 (649)	120.0	35 LEFT
ARCH-6		1200	YES	190 (845)	212 (943)	30.0	35 RIGHT
ARCH-7		120	YES	104 (463)	122 (543)	121.0	30 RIGHT
ARCH-8		120	YES	111 (494)	129 (574)	134.0	35 LEFT & CROWN
ARCH-9		3650	YES	27 (120)	44 (196)	176.0	35 LEFT
ARCH-10		3650	YES	31 (138)	45 (200)	165.0	CROWN

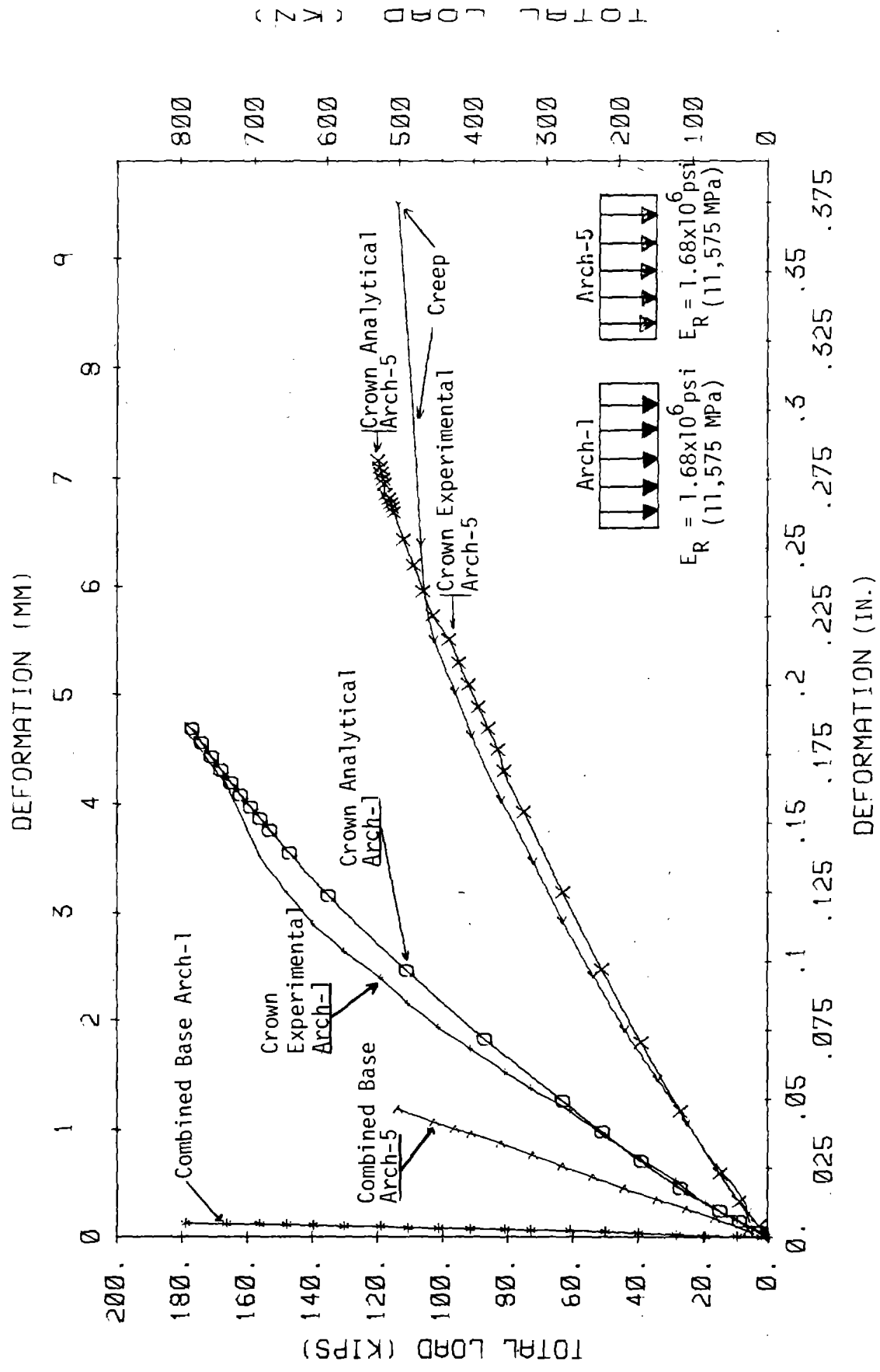


FIGURE 4.27 TOTAL LOAD VS DEFORMATION AT CROWN AND BASE OF ARCH 1 AND 5

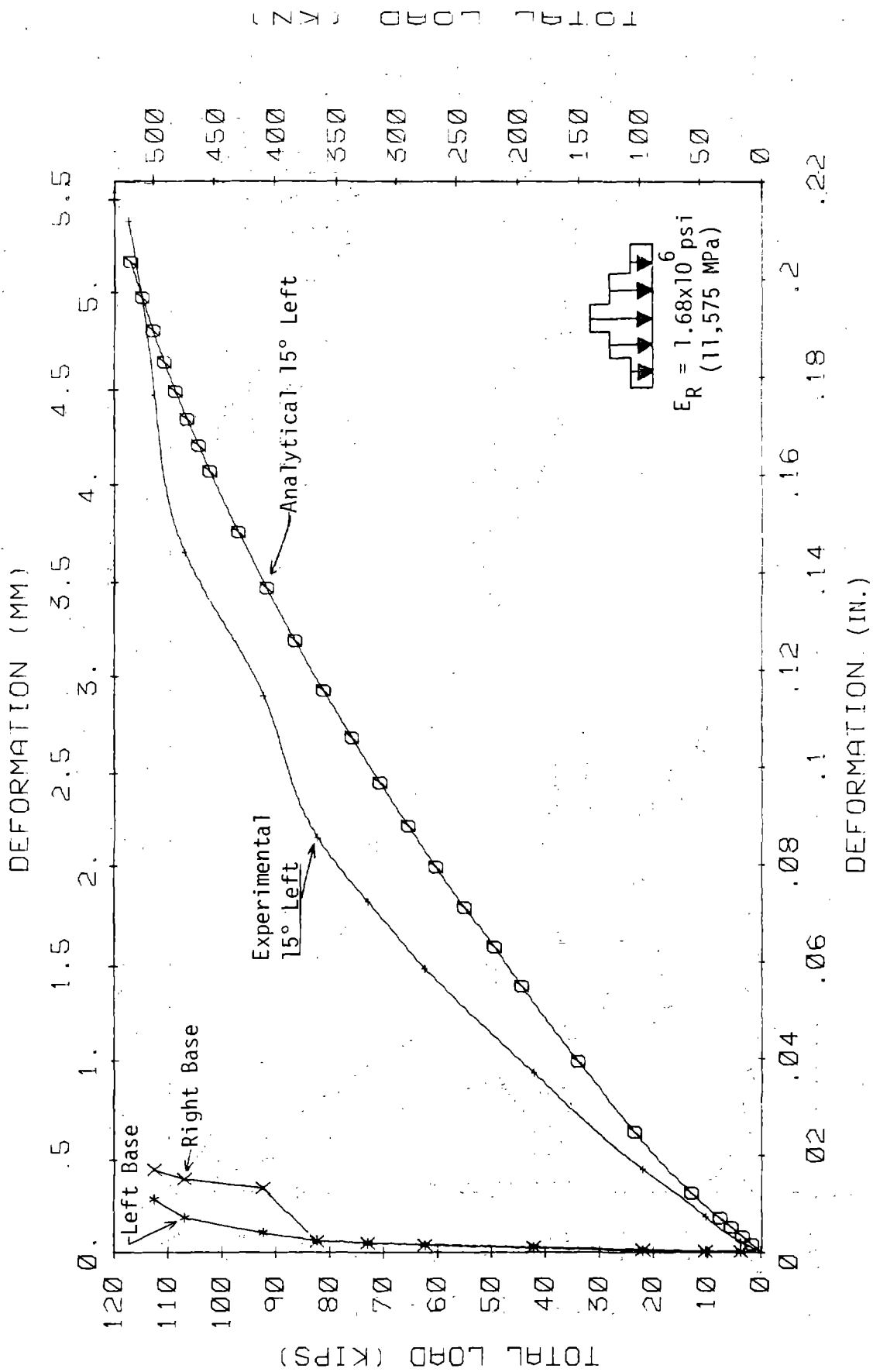


FIGURE 4.28 TOTAL LOAD VS DEFORMATION AT CROWN AND BASE OF ARCH 2

necessary, although the overall performance of the MTS system in maintaining the loading shape was excellent. At a load level of 102 kips (454 kN), the rate of movement of the specimen relative to the medium increased at both sides of the arch. The occurrence of slippage can be observed on the load-deformation curve shown in Fig. 4.29, where a noticeable change in slope occurs at that load level. The load-deflection curve for the crown of Arch-3 is slightly stiffer than the one for Arch-1 and considerably stiffer than the one for Arch-2.

Arch-4 Arch-4 was loaded with the five-step triangular configuration with the maximum load on one side. A small uniform load was applied at first (300 lb (1.3 kN) per position) and then the loading ratios were adjusted to their final values for additional loading. An ultimate total load of 119 kips (529 kN) was reached, which corresponds to a normalized load of 157 kips (698 kN). Slippage between the lining and the medium did occur at a load of 90 to 100 kips (400 to 445 kN). The load deformation curve shown in Fig. 4.30 exhibits more curvature than those of the other tests.

Arch-5 The side friction between the lining and the medium was eliminated for this test, and a uniform load was applied. To compare the load-deformation curve with that of the case of full-side friction and mechanical interlock, the curve is plotted with that for Arch-1 in Fig. 4.27. An ultimate load of 114 kips (507 kN) was reached, which corresponds to a normalized ultimate load of 146 kips (649 kN). The load-deformation curve for the crown deflection exhibits lower stiffness than that of Arch-1, because of the greater movement between the specimen and the medium in Arch-5.

Arch-6 Loading in this case was applied through a rigid block of concrete; a maximum load of 190 kips (845 kN), corresponding to a normalized load of 212 kips (943 kN) was reached as shown in Fig. 4.31. This is the highest load level reached by any of the arches. At a load level of 70 kips (311 kN) separation between the lining and the medium



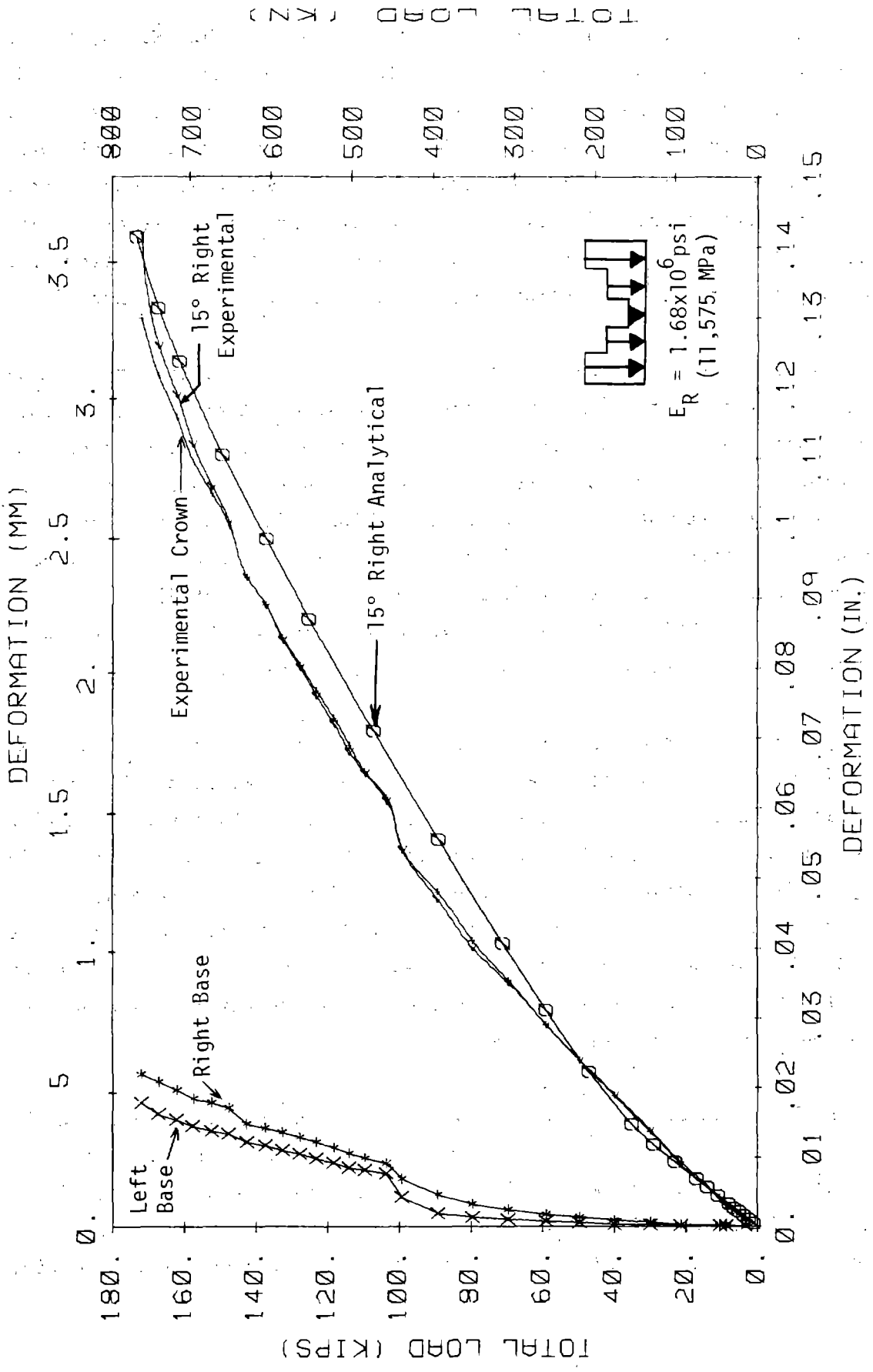


FIGURE 4.29 TOTAL LOAD VS DEFORMATION AT CROWN, BASE, AND 15R OF ARCH 3

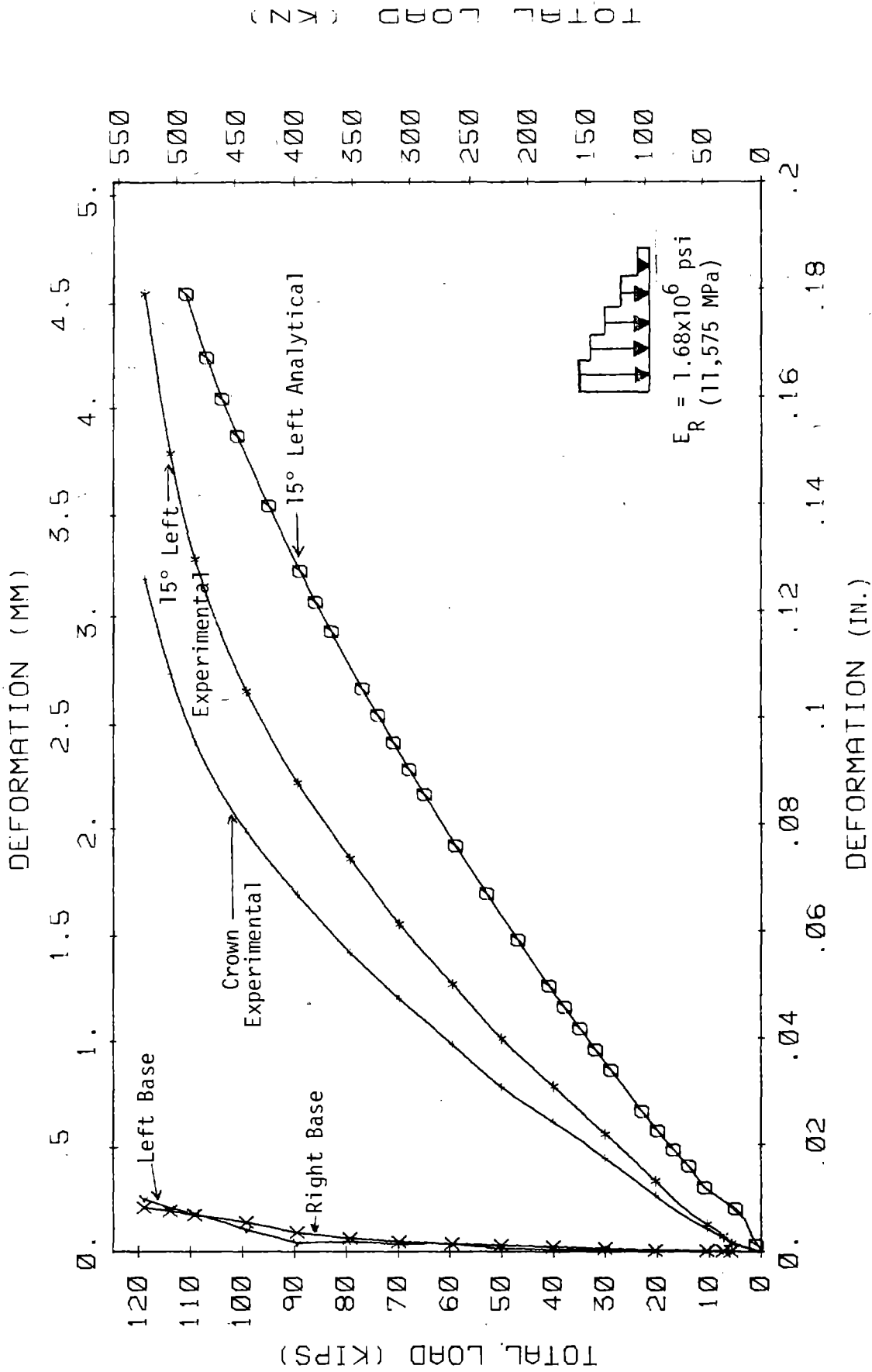


FIGURE 4.30 TOTAL LOAD VS DEFORMATION AT CROWN, BASE, AND 15L OF ARCH 4

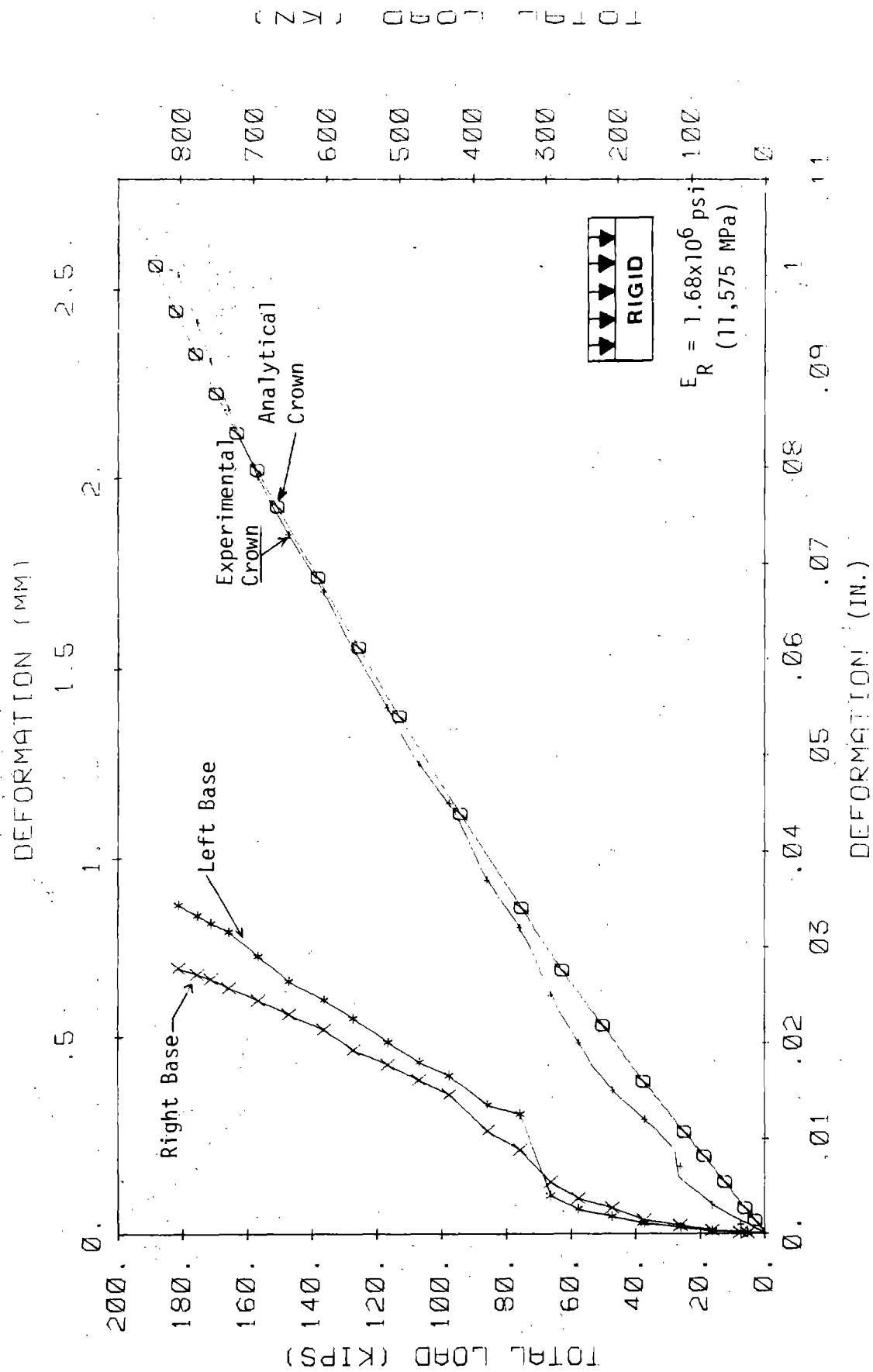


FIGURE 4.31 TOTAL LOAD VS DEFORMATION AT CROWN AND BASE OF ARCH 6

occurred as indicated by the sudden increase in base deformation in Fig. 4.31. The initial curving of the load-deformation curve was caused by the adjustment of the base load cells to equalize the load distribution within them.

Arch-7 Load was applied the same way as in the previous test, although the modulus of the medium was about one tenth as great. A maximum load of 104 kips (463 kN), corresponding to a normalized load of 122 kips (543 kN), was reached as shown in Fig. 4.32. The shape of the crown load-deformation curve is linear, because the failure region is outside the crown region although its slope is not as steep as that of Arch-6. No visible separation between the lining and the medium was observed.

Arch-8 A uniform load was applied in this case to compare the shape of the load-deformation curve. The plot for Arch-8 is shown with that of Arch-1 in Fig. 4.33. The slope of Arch-8 load-deformation curve is about one half that of Arch-1. The maximum load reached was 111 kips (494 kN) or a normalized load of 129 kips (574 kN). Separation between the lining and the medium occurred on the left side at a load level of about 50 kips (222 kN) and on the right side at a load level of 70 kips (311 kN). These events are noticeable on the load-deformation curve where the slope changes at those load levels. The initial steepening of the load-deformation curve is caused by the tightening of the base load cells to equalize the load distribution.

Arch-9 A uniform load was applied on Arch-9. To compare the effects of reinforcement Arch-9 is plotted with Arch-10 as shown in Fig. 4.34. Since the thickness was only 1 in. (25 mm), the maximum load reached was 27 kips (120 kN) or a normalized load of 44 kips (196 kN). No visible separation between the lining and the medium was observed in this case.

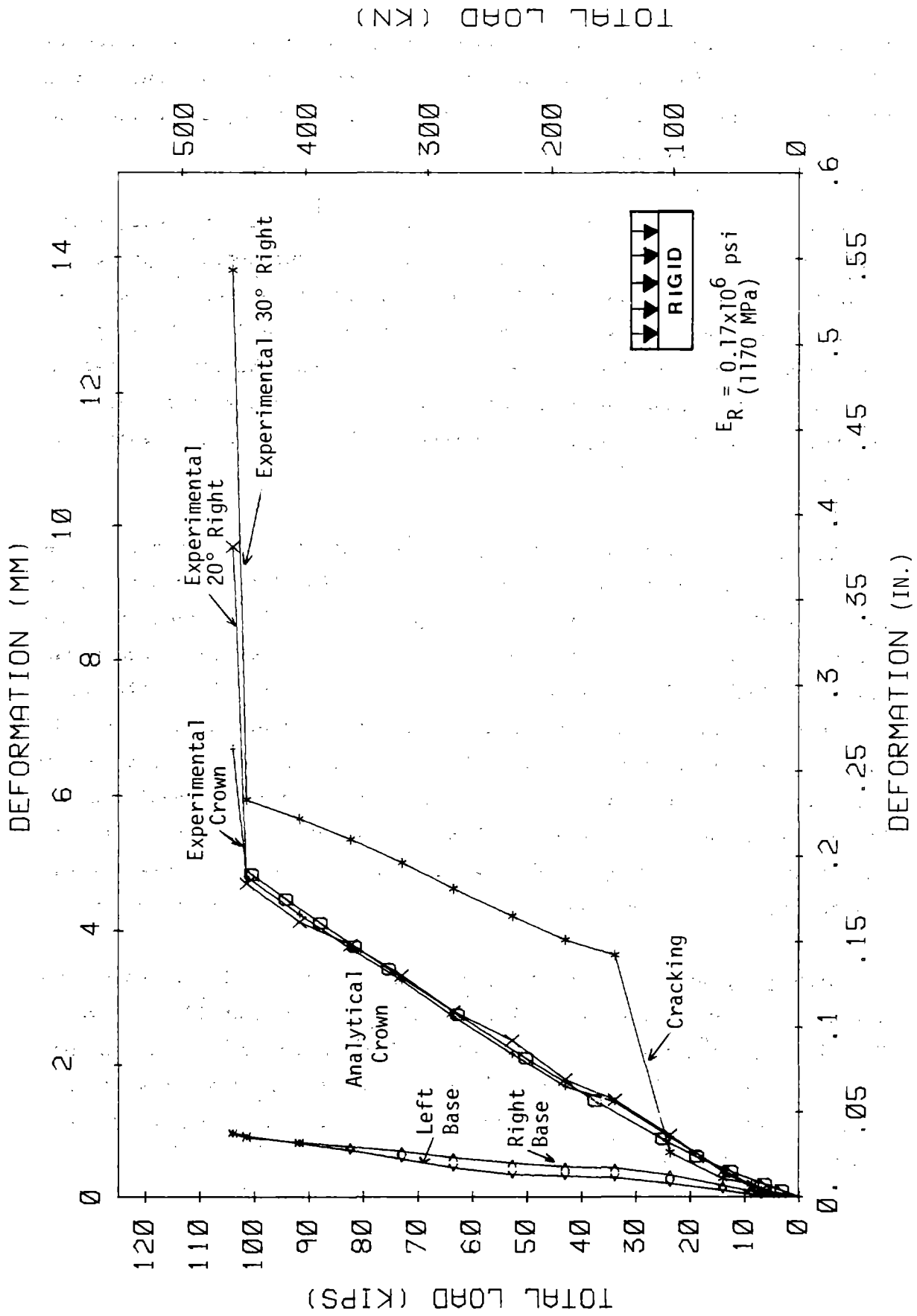


FIGURE 4.32 TOTAL LOAD VS DEFORMATION AT CROWN, BASE, 20 and 30R OF ARCH 7

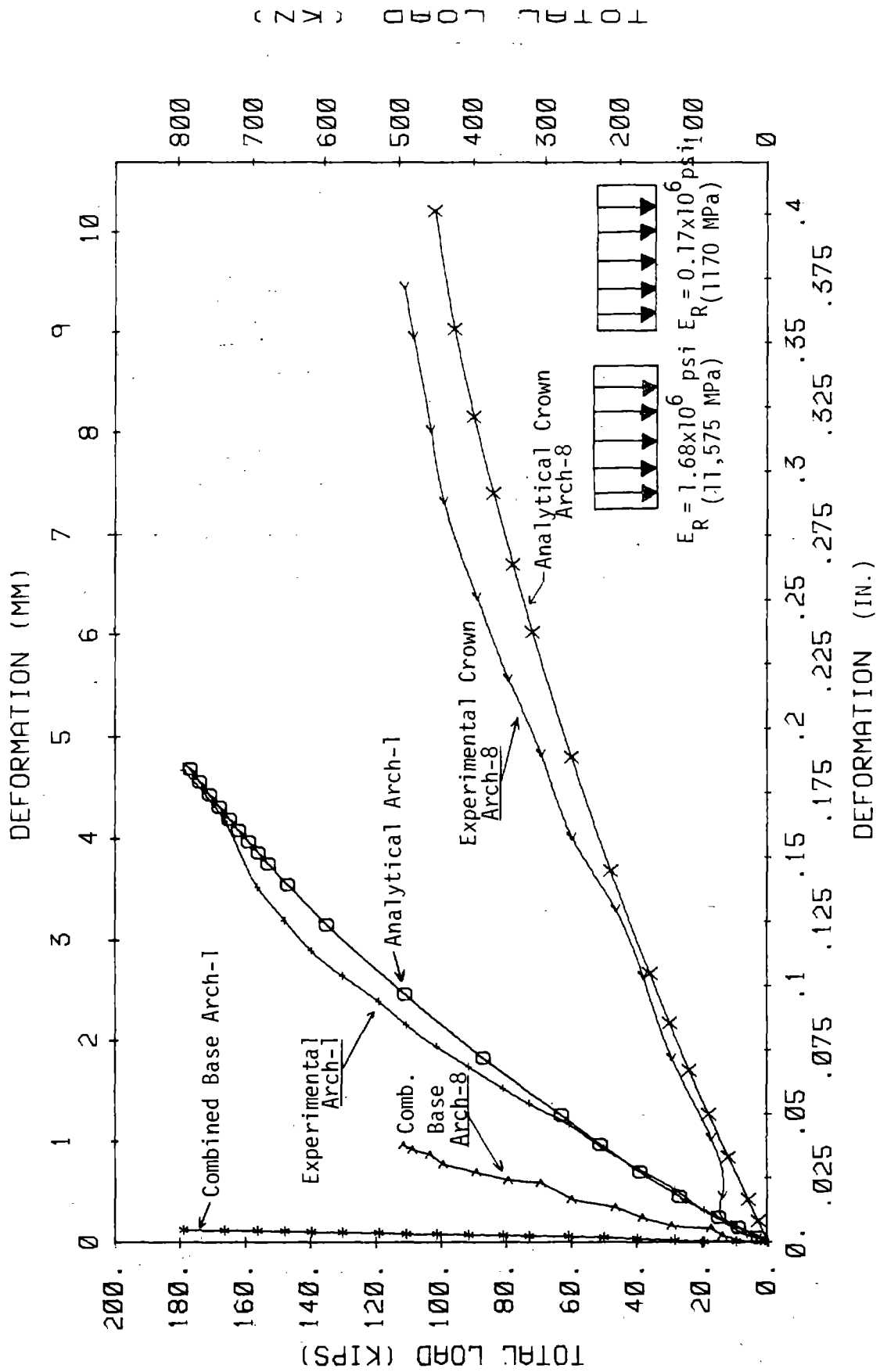


FIGURE 4.33 TOTAL LOAD VS DEFORMATION AT CROWN AND BASE OF ARCHES 1 AND 8

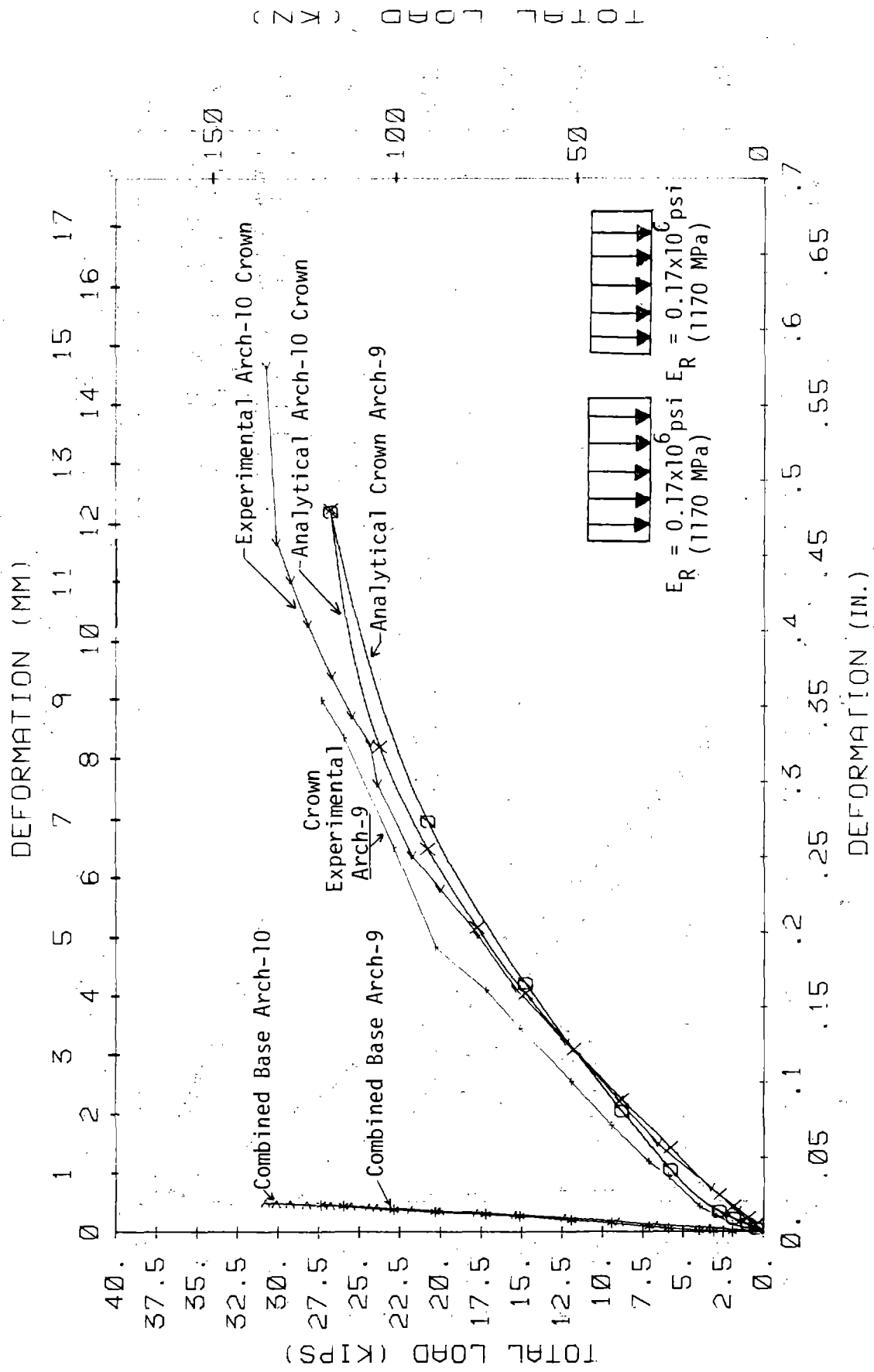


FIGURE 4.34 TOTAL LOAD VS DEFORMATION AT CROWN AND BASE OF ARCHES 9 AND 10

Arch-10 The applied load which was uniform for Arch-10 was reinforced with 1.0 percent longitudinal reinforcement at mid-depth of the 1 in. (25 mm) thick section. The effects of the reinforcement are obvious in Fig. 4.34, where the slope of the load-deformation curve is similar to that for Arch-9 but the observed ultimate deformation was larger. No visible deformation between the lining and the medium was observed. A maximum load of 31 kips (138 kN) was reached, corresponding to a normalized load of 45 kips (200 kN).

#### 4.3.2 Deformability and Cracking of the Linings

The flexural deformation of a tunnel lining depends on the flexibility ratio  $F$ , defined by Eq. 2.2, which relates the modulus of elasticity of the medium with that of the lining. For these tests, the modulus of elasticity of the medium was  $E = 1.68 \times 10^6$  psi (11,575 MPa) for Arches-1 to 6 and  $E = 0.17 \times 10^6$  psi (1170 MPa) for Arches-7 to 10. The modulus of elasticity of the lining material changed very little, because the same concrete mix was used, but the equivalent value based on the stiffness of the lining, depends on the amount of cracking in the specimen and the stress level. The modulus for the lining used for computing the flexibility ratio was based on the initial concrete modulus of elasticity of the uncracked specimen. The ACI formula  $E_c = 57,000 \sqrt{f'_c}$  (where  $f'_c$  is the unconfined compressive strength of concrete in psi) was used for computing the concrete modulus. For Arches-1 to 8, a concrete modulus of  $E = 4.0 \times 10^6$  psi (27,500 MPa) and for Arches-9 and 10 an  $E = 3.6 \times 10^6$  psi (21,200 MPa) were used. For computing the flexibility ratio, the Poisson's ratios for the lining and the medium were taken as 0.17. The values of the flexibility ratios were computed as  $F = 1200$  for Arches-1 to 6,  $F = 120$  for Arches-7 and 8, and  $F = 3650$  for Arches-9 and 10. These values are in the range of flexible linings; this means that they will easily deform with the medium, and the moments in the linings will be relatively low. In the following paragraphs, the deformability and



cracking of each lining are discussed and summarized in Tables 4.5 and 4.6.

Arch-1 The maximum deformation of 0.184 in. (4.7 mm) for Arch-1 occurred at the crown and corresponded to a relative change in the radius of the arch of  $\Delta R/R = 0.53$  percent. The final deflection occurred 30-40 sec after application of the final load, as the concrete continued to creep. The deflected shapes at 50 and 100 percent of the ultimate load are shown in Figs. 4.35 and 4.36. From about 45 deg downward on either side of the crown, the specimen moved outward into the medium. Deflections measured below about 45 deg from the crown are very small relative to those at the crown. No visible cracks were noticed during the course of loading Arch-1.

Arch-2 The maximum crown deformation of 0.212 in. (5.4 mm) corresponds to a  $\Delta R/R = 0.61$  percent and is larger than the one occurring in Arch-1. The deflected shape at 96 percent of the ultimate load shown in Fig. 4.37 implies that the specimen is moving inwards relative to its initial position. This is the result of the slippage that occurred between the lining and the medium. The riding of the lining over the serrations caused an inward movement of the specimen which was larger than the outward deformation of the medium, and thus a net inward deflection resulted. Deflection at the right side is more than at the left because slippage occurred first at the right side. An outward deformation at the sides is noted in Fig. 4.38 at 50 percent of the ultimate load just before slippage. At 35 deg from the crown on the left side of the specimen the lining and the medium moved together (compressed), whereas at 35 deg right between loads of 80-90 kips (345-400 kN) when slippage occurred, they separated. The first cracks appeared at a load of 62.4 kips (277 kN) on the inside surface near the crown. At a load of 92.5 kips (411 kN) the cracks extended all the way down the inside crown surface, and crushing was observed on the top surface of the crown of the specimen at the edge opposite the tension cracks. The appearance and extent of first cracking are shown in Fig.

TABLE 4.5 DEFORMABILITY CHARACTERISTICS OF THE ARCHES

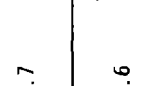

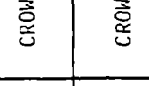
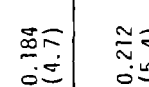
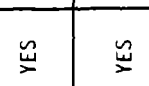
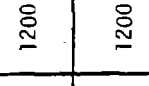

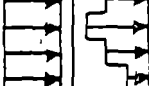
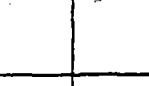
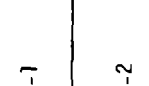
Test	Load Shape	Flex. Ratio, F	Tang. Shear	Maximum Deflection in. (mm)	Location Max. Defl. deg	Base Defl. % of Maximum	Location Liner-Medium Separation
ARCH-1		1200	YES	0.184 (4.7)	CROWN	2.7	45
ARCH-2		1200	YES	0.212 (5.4)	CROWN	6.6	35
ARCH-3		1200	YES	0.142 (3.6)	15 RIGHT	14.1	45
ARCH-4		1200	YES	0.179 (4.5)	15 LEFT	5.0	45 LEFT 20 RIGHT
ARCH-5		1200	NO	0.375 (9.5)	CROWN	12.3	45
ARCH-6		1200	YES	0.105 (2.7)	CROWN	29.5	50
ARCH-7		120	YES	0.543 (13.8)	30 RIGHT	6.8	50
ARCH-8		120	YES	0.372 (9.4)	CROWN	10.2	43
ARCH-9		3650	YES	0.370 (9.4)	CROWN	5.0	45
ARCH-10		3650	YES	0.570 (14.5)	CROWN	3.5	45

TABLE 4.6 CRACKING CHARACTERISTICS OF THE ARCHES

Test	Load Shape:	Flex. Ratio	Tang. Shear	First Occurrence of Cracks			Max. Size Crack Ult. Load in (mi)
				Crack- ing	% Ult. Load	% Max. Deformation	
ARCH-1		1200	YES	NO	---	---	---
ARCH-2		1200	YES	YES	50	26	NOT MEASURED
ARCH-3		1200	YES	NO	---	---	---
ARCH-4		1200	YES	NO	---	---	---
ARCH-5		1200	NO	YES	80	47	NOT MEASURED
ARCH-6		1200	YES	NO	---	---	---
ARCH-7		120	YES	YES	40	28	0.01 (0.3)
ARCH-8		120	YES	YES	60	44	0.01 (0.3)
ARCH-9		3650	YES	YES	85	71	0.04 (1.0)
ARCH-10		3650	YES	YES	80	34	0.01 (0.3)

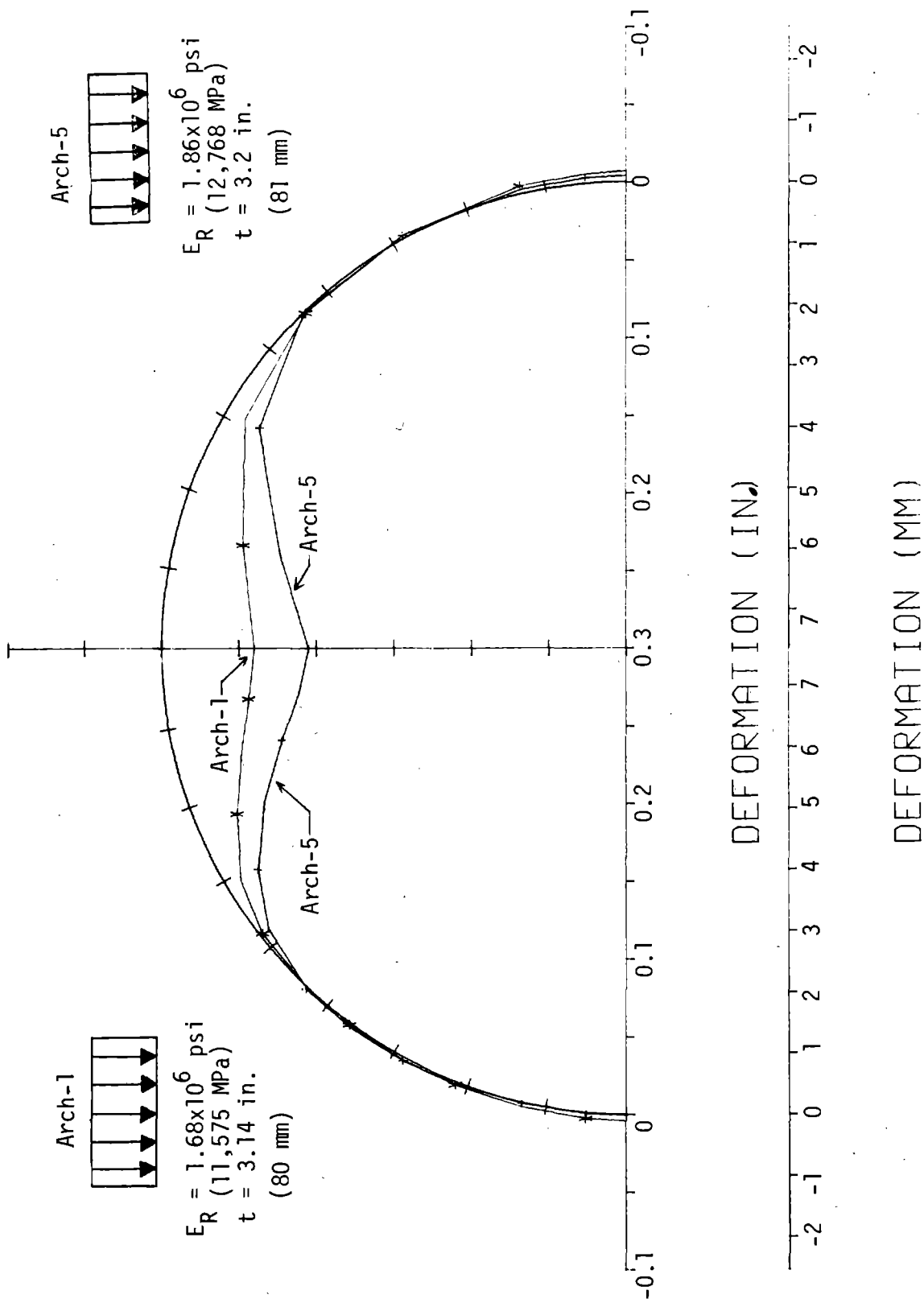


FIGURE 4.35 DEFORMATION OF ARCHES 1 AND 5 AT 50% LOAD

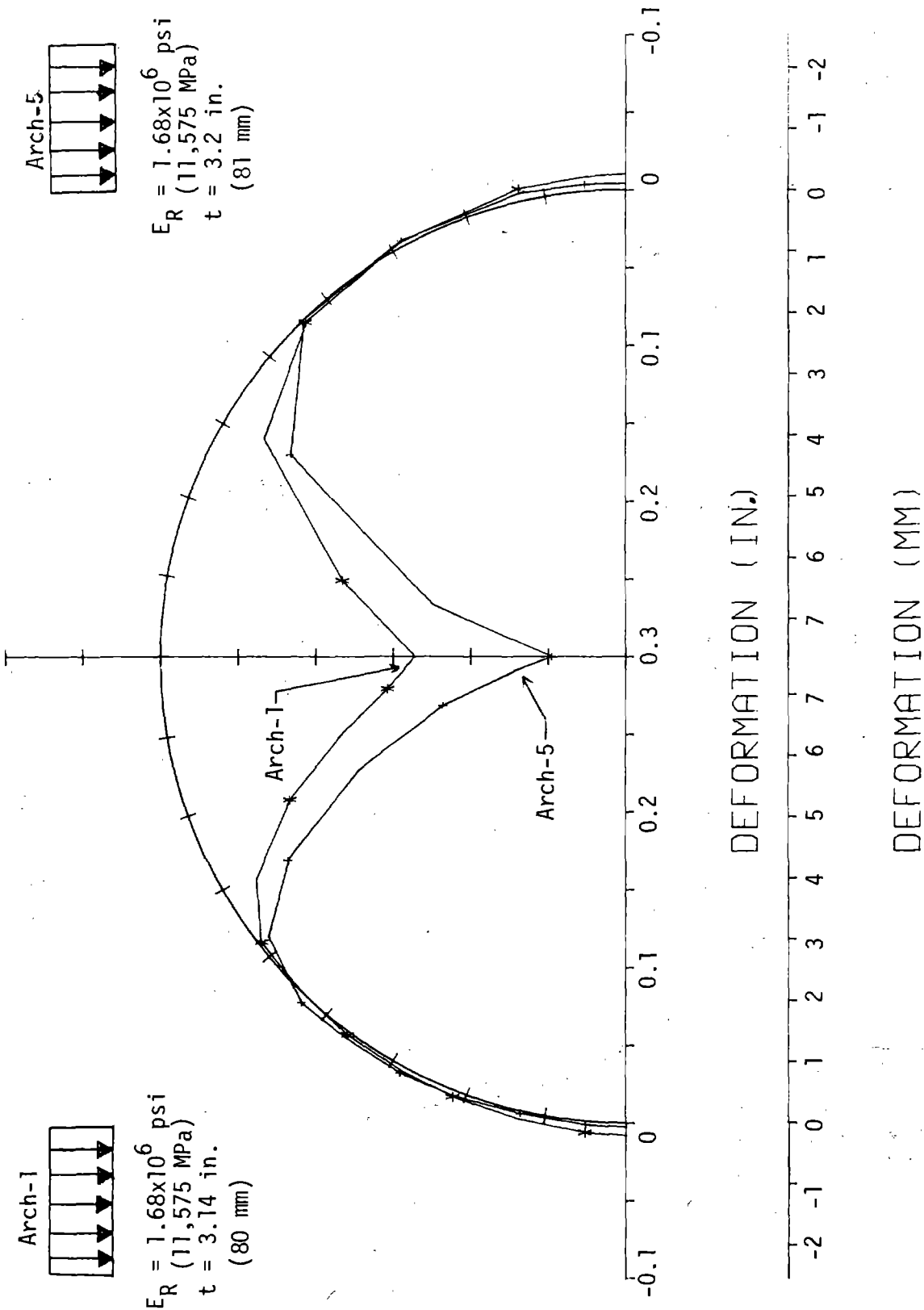
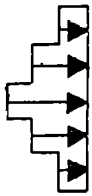


FIGURE 4.36 DEFORMATION OF ARCHES 1 AND 5 AT 100% LOAD



$E_R = 1.68 \times 10^6 \text{ psi}$   
 (11,575 MPa)  
 $t = 3.1 \text{ in.}$   
 (79 mm)

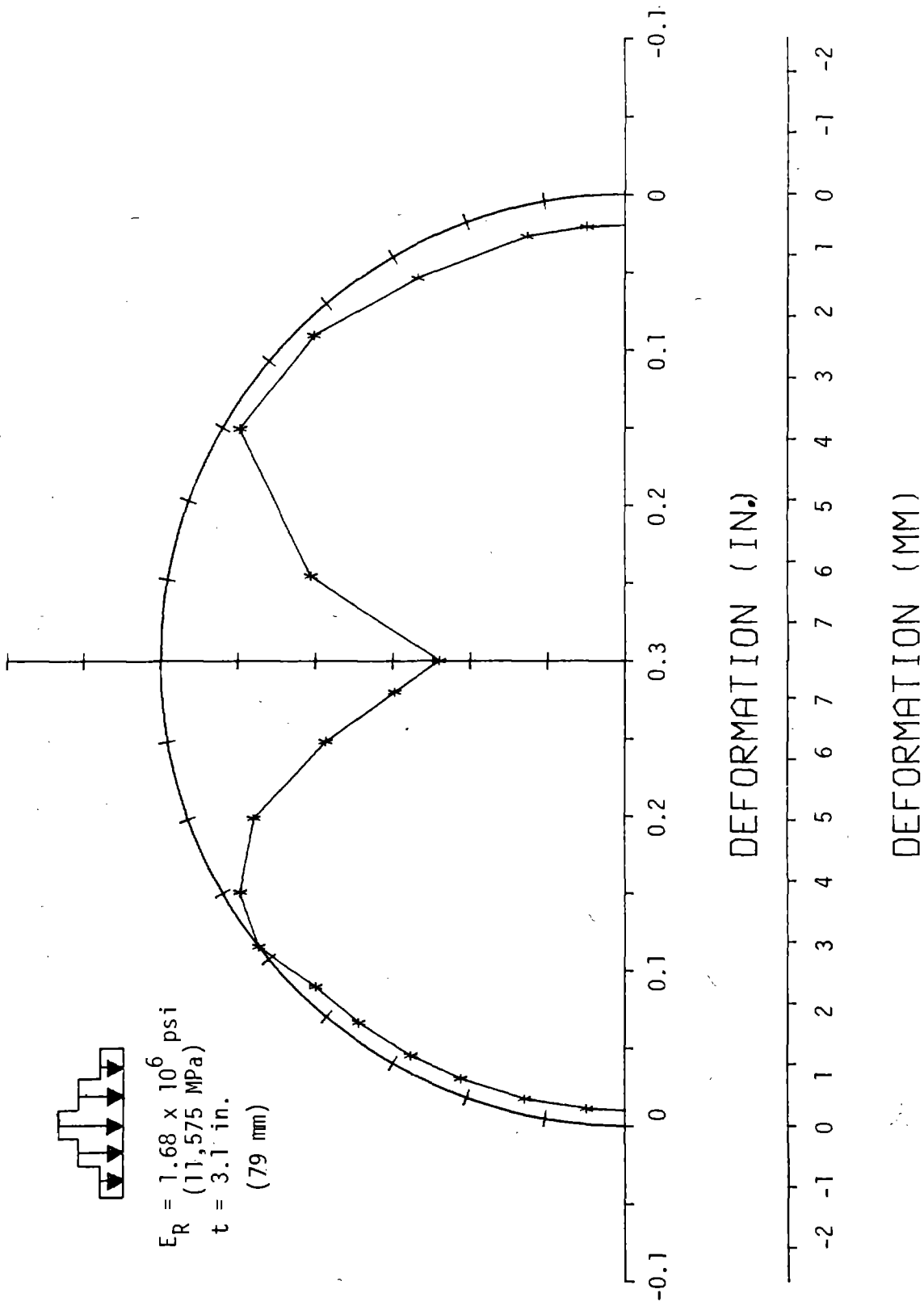


FIGURE 4.37 DEFORMATION OF ARCH 2 AT 96% LOAD

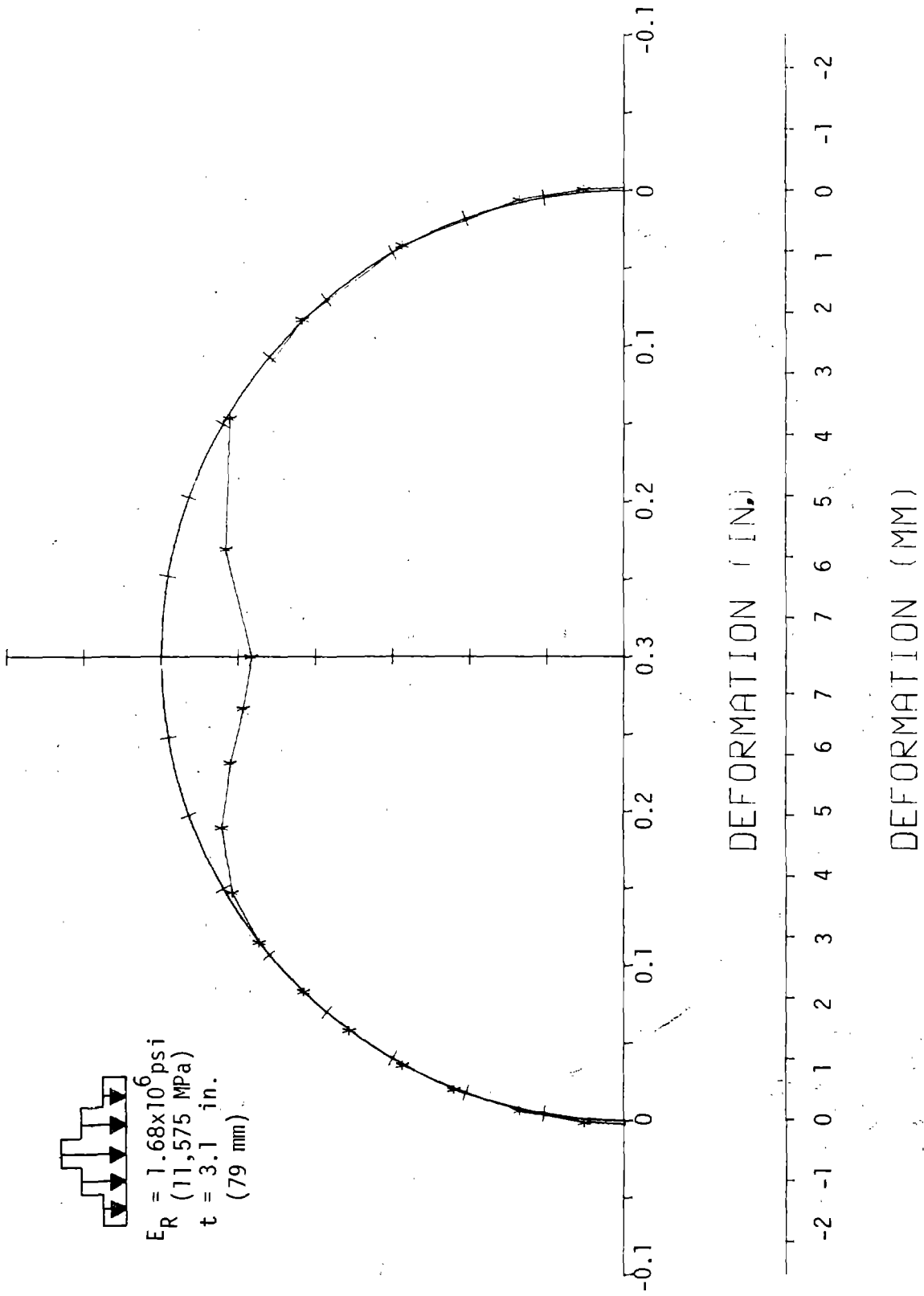


FIGURE 4.38 DEFORMATION OF ARCH 2 AT 50% LOAD

4.39. At a load of 112.6 kips (500 kN) more spalling of the concrete was observed on the top outer surface at the crown, whereas the inside vertical tension crack widened (Fig. 4.40). Failure occurred at the next load increment at a total load of 117 kips (520 kN).

Arch-3 The maximum deformation for Arch-3 was observed consistently at 15 deg to the right of the crown. Although the loading is symmetrical and maximum deformations should be symmetrical, the fact that maximum deflection occurred to the right might be due to a local weakness in the concrete matrix or due to the difference in stiffnesses between the base cells at the left and right sides. The value of maximum deformation of 0.142 in. (3.6 mm) corresponds to a  $\Delta R/R = 0.41$  percent. As in the case of Arch-2, the slippage which occurred at a load of 105 kips (467 kN), caused the specimen to deform inward at the ultimate load as shown in Fig. 4.41. At 50 percent of the ultimate load and before slippage, no such effects are observed as shown in Fig. 4.42. At 45 deg on either side of the crown the lining and medium separated. Tension cracking was not detected in this test.

Arch-4 The unsymmetrical loading pattern of Arch-4 caused the maximum deflection to occur 15 deg to the left of the crown. The magnitude of maximum deflection was 0.179 in. (4.5 mm) corresponding to a  $\Delta R/R = 0.52$  percent. Slippage between the lining and the medium occurred after 50 percent of the load had been applied, as is evident by comparing the deflected shapes at 50 and 100 percent (Figs. 4.43 and 4.44). At 50 percent of the load, Fig. 4.43, the lining deflected outward, whereas at 100 percent (after separation) the lining deflected inward. The shape of the load distribution caused the specimen to move away from the medium at 45 deg to the left of the crown but toward the medium at 20 deg to the right. Tension cracking was not detected in this specimen.

Arch-5 The lack of shearing resistance between the lining and medium resulted in a value for the maximum deflection at the crown



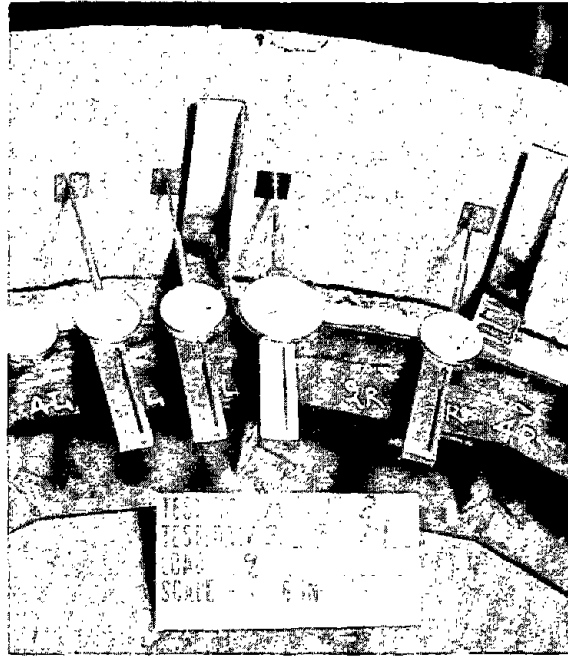


FIGURE 4.39 FIRST CRACKS IN ARCH-2

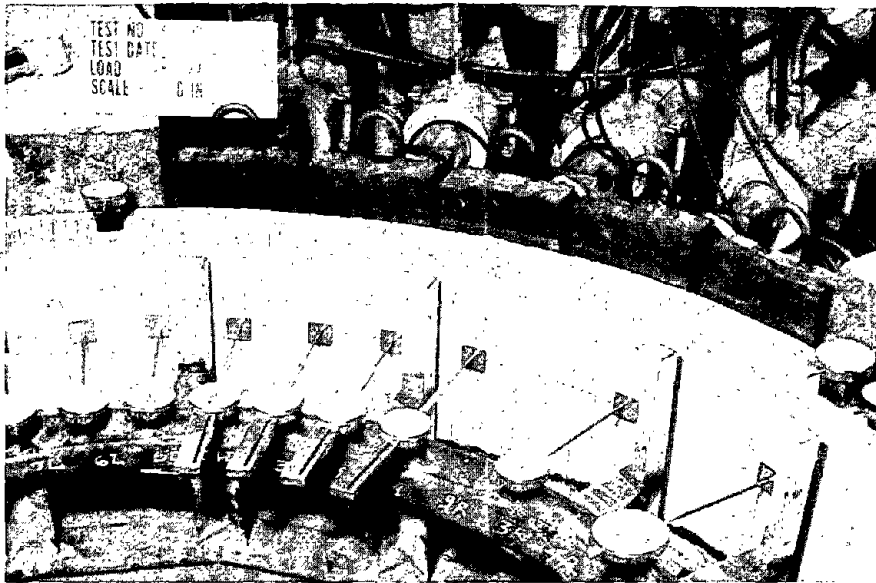
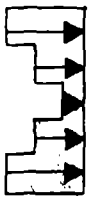


FIGURE 4.40 FIRST CRACKS IN ARCH-5



$E_R = 1.68 \times 10^6 \text{ psi}$   
 (11, 575 MPa)  
 $t = 3.15 \text{ in.}$   
 (80 mm)

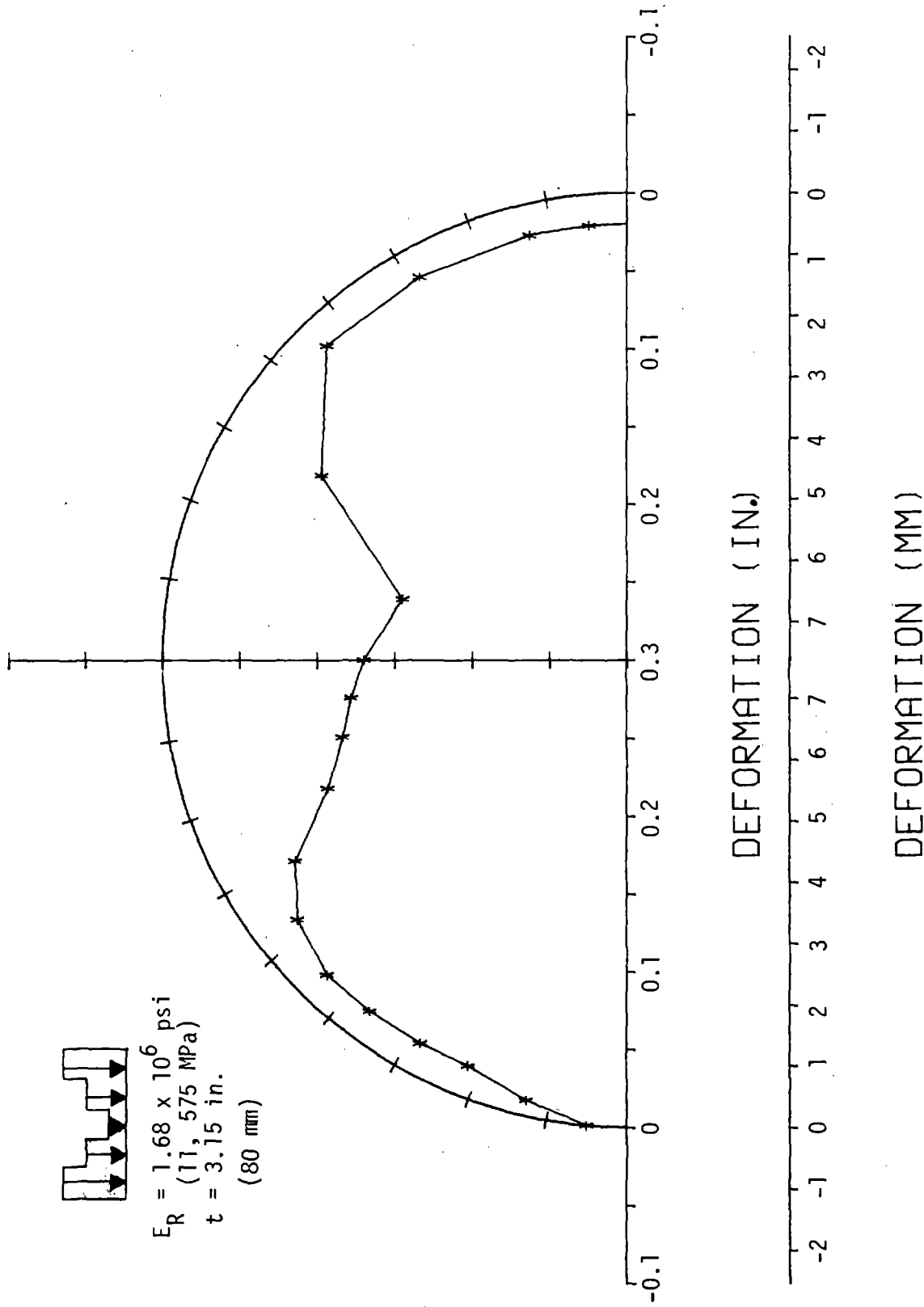


FIGURE 4.41 DEFORMATION OF ARCH 3 AT 100% LOAD

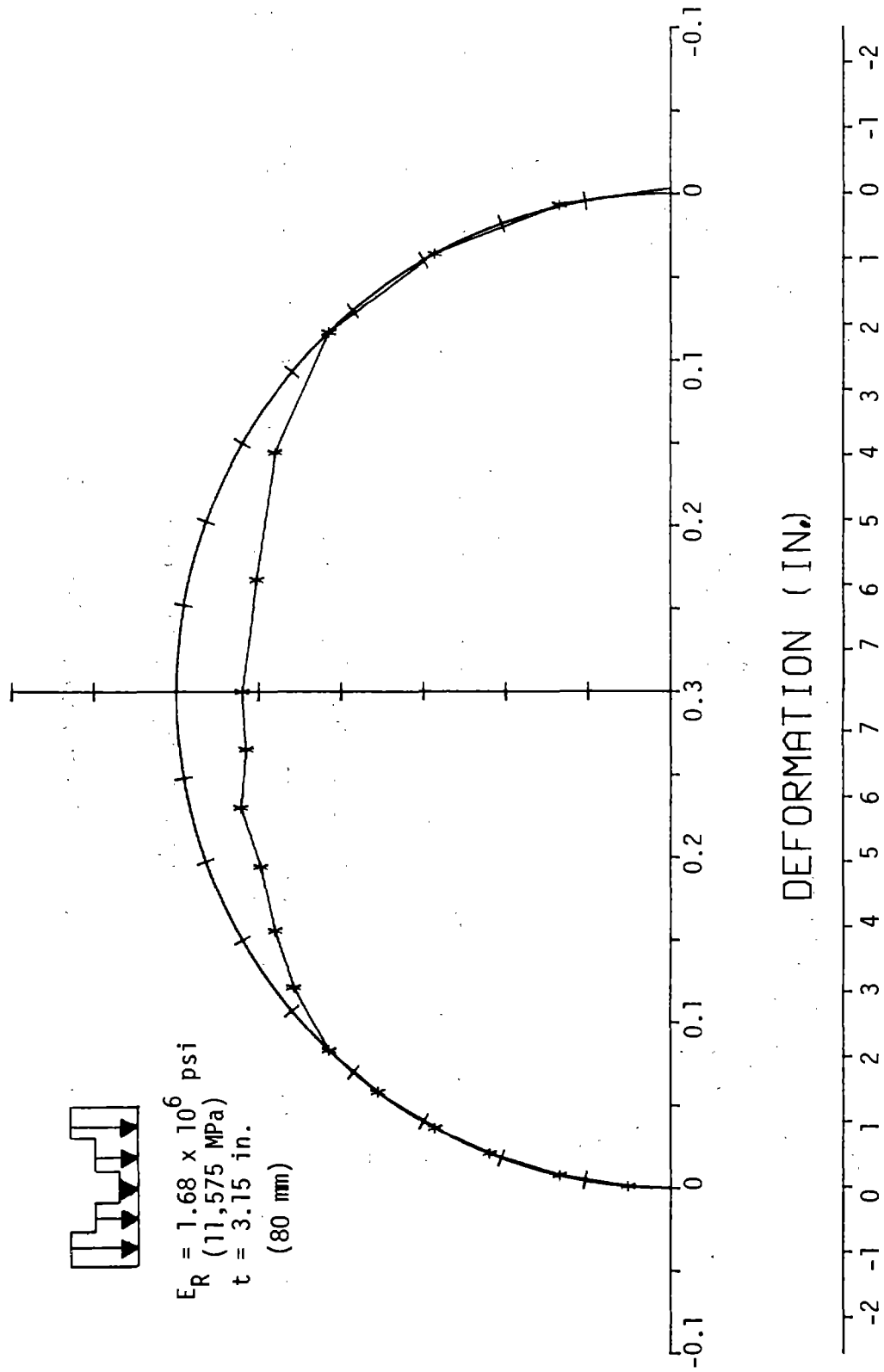


FIGURE 4.42 DEFORMATION OF ARCH 3 AT 50% LOAD

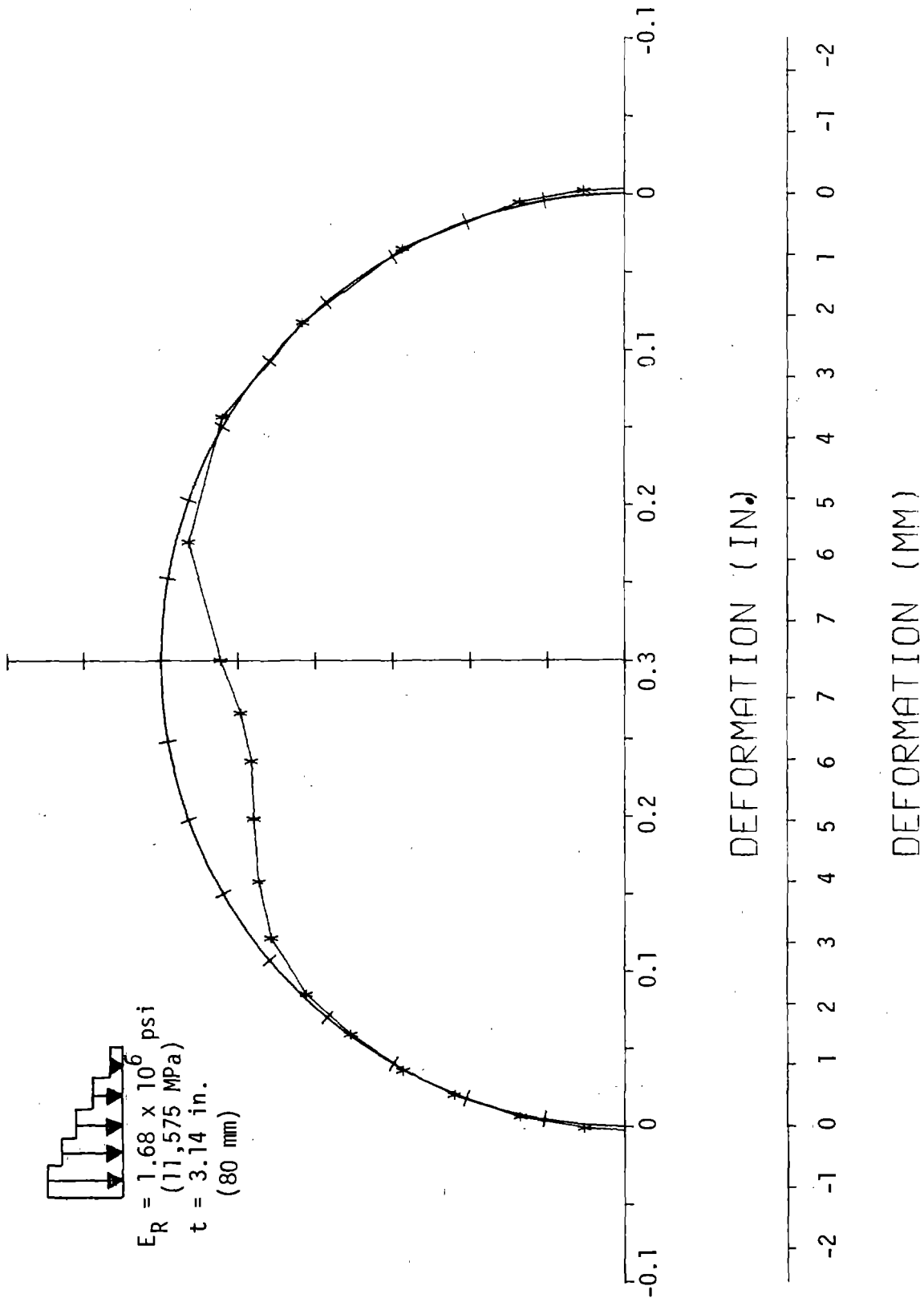


FIGURE 4.43 DEFORMATION OF ARCH 4 AT 50% LOAD

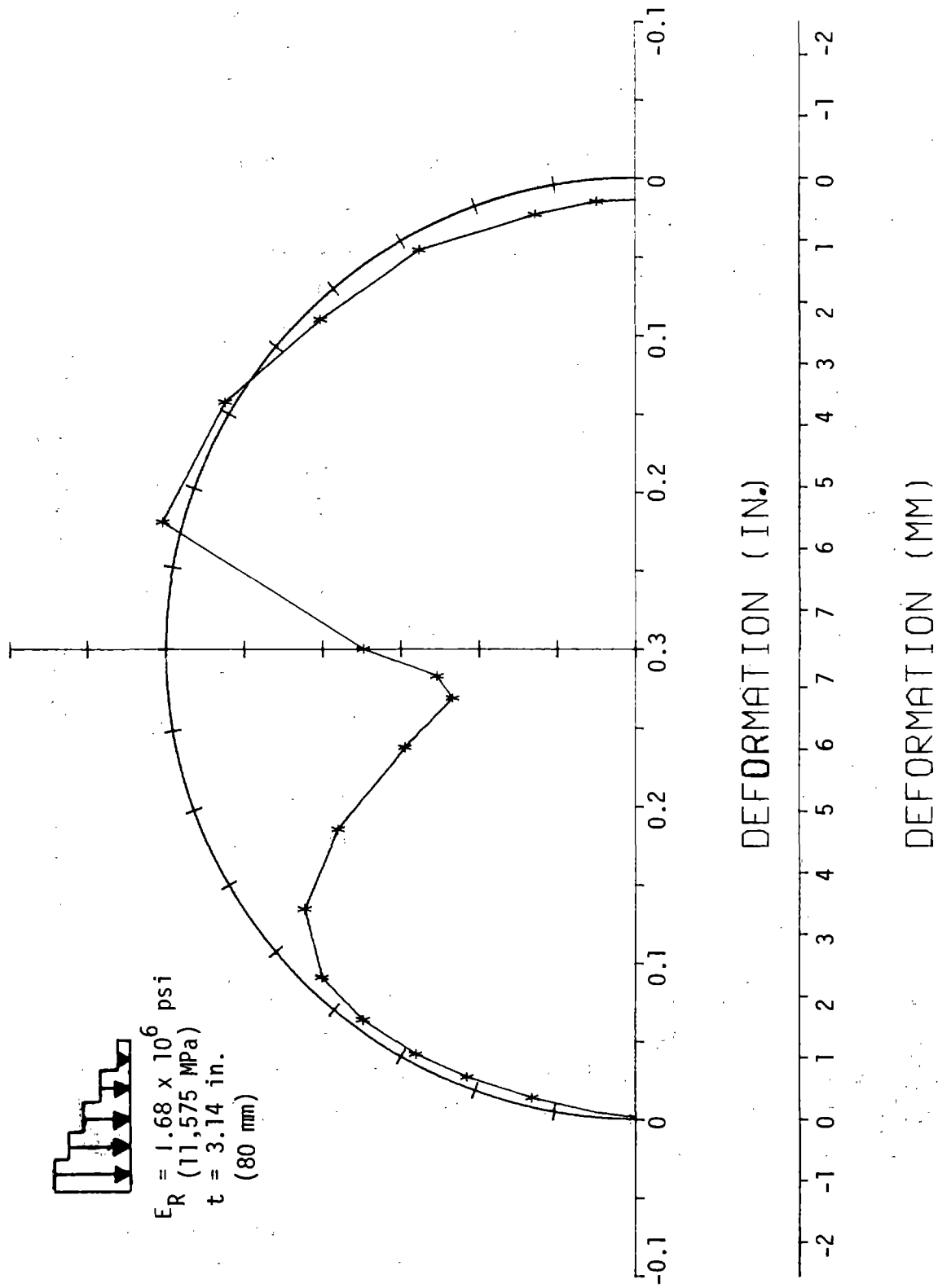


FIGURE 4.44 DEFORMATION OF ARCH 4 AT 100% LOAD

equal to 0.375 in. (9.5 mm) corresponding to a  $\Delta R/R = 1.09$  percent. The deflection from 0.252 in. (6.4 mm) to the maximum occurred at a constant load of 113.7 kips (506 kN) as a result of creep of the concrete. Deflected shapes of the arch at 50 and 100 percent of the ultimate load indicate that the lining moved outward at the sides as shown in Figs. 4.35 and 4.36. The maximum observed crown deflection for Arch-5 was twice that observed for Arch-1, where shear and mechanical interlock were present. For this test relative movement between the lining and the medium was monitored at 35, 40, 45, and 50 deg to the right of the crown and at 35 deg to the left. It was concluded from these measurements that the point where the lining does not deflect relative to the medium lies at about 45 deg. Tension cracks on the inside of the crown region, similar to those observed in Arch-2, were detected at 91.2 kips (406 kN) load as shown in Fig. 4.40. These cracks continued to open as ultimate load was approached, and at 113.7 kips (506 kN) additional tension cracks in the crown region were observed.

Arch-6 The maximum deformation of Arch-6 was 0.105 in. (2.7 mm) at the crown, the smallest one observed in any of the tests. Thus, this arch was the least ductile with a  $\Delta R/R = 0.30$  percent. The deflected shapes at 50 and 100 percent of the ultimate load are shown in Figs. 4.45 and 4.46. The effects of slippage between the lining and the medium are more obvious at 100 percent of the load, where the inward deformation is higher. Because of the rigid block loading the lining separated from the medium at about 50 deg from the crown instead of the range of 35-45 deg observed for other loading shapes. No tension cracks were observed in this test, except for a diagonal hairline crack at the top of the specimen, 35 deg to the right of the crown, at a load level of 166 kips (739 kN). This is where the failure occurred, at a load level of 190 kips (845 kN).

Arch-7 The reduction in rock modulus caused considerable increase in deformation (about 5 times) between Arches-6 and 7 under the same

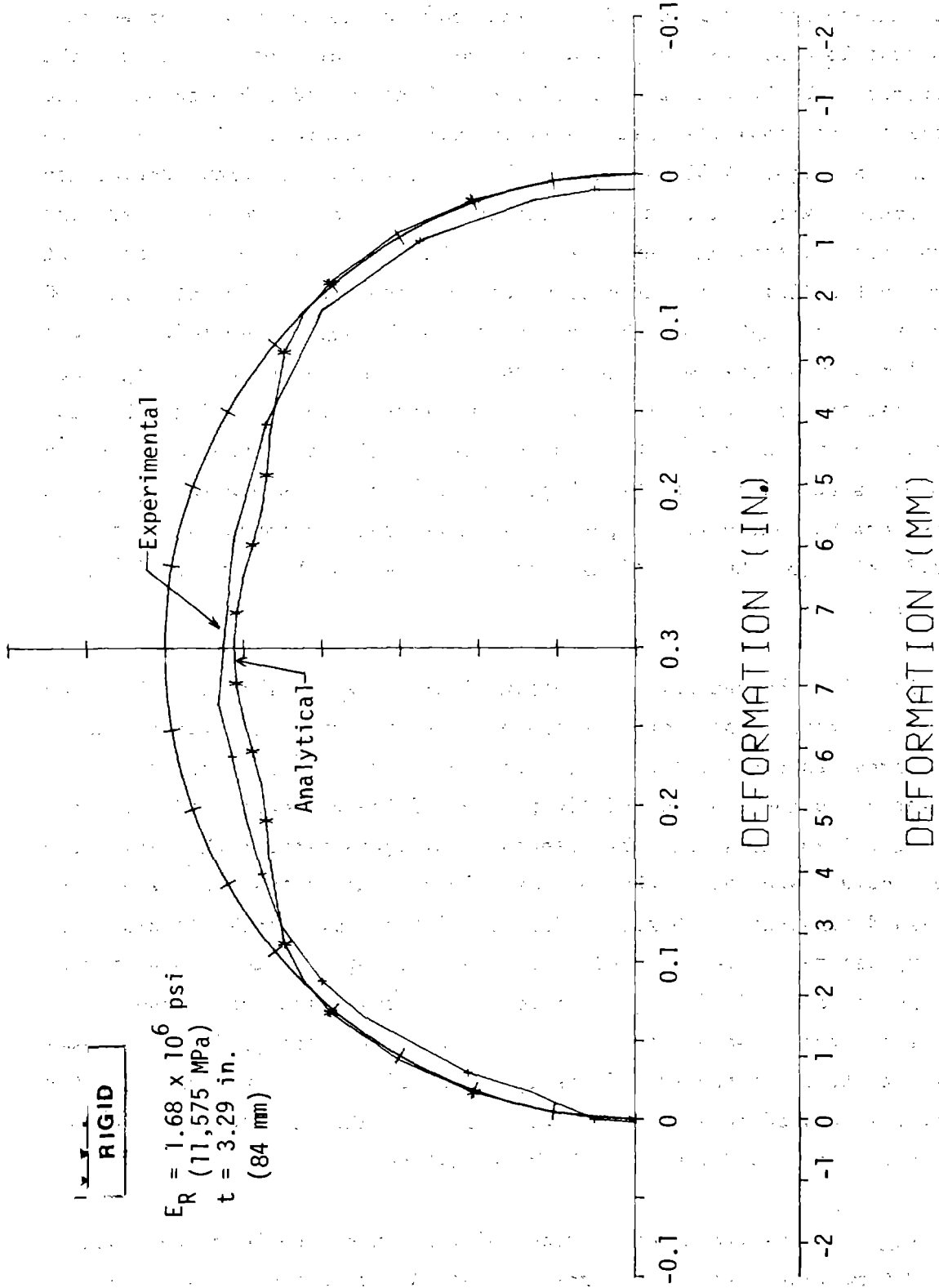


FIGURE 4.45 DEFORMATION OF ARCH 6 AT 50% LOAD

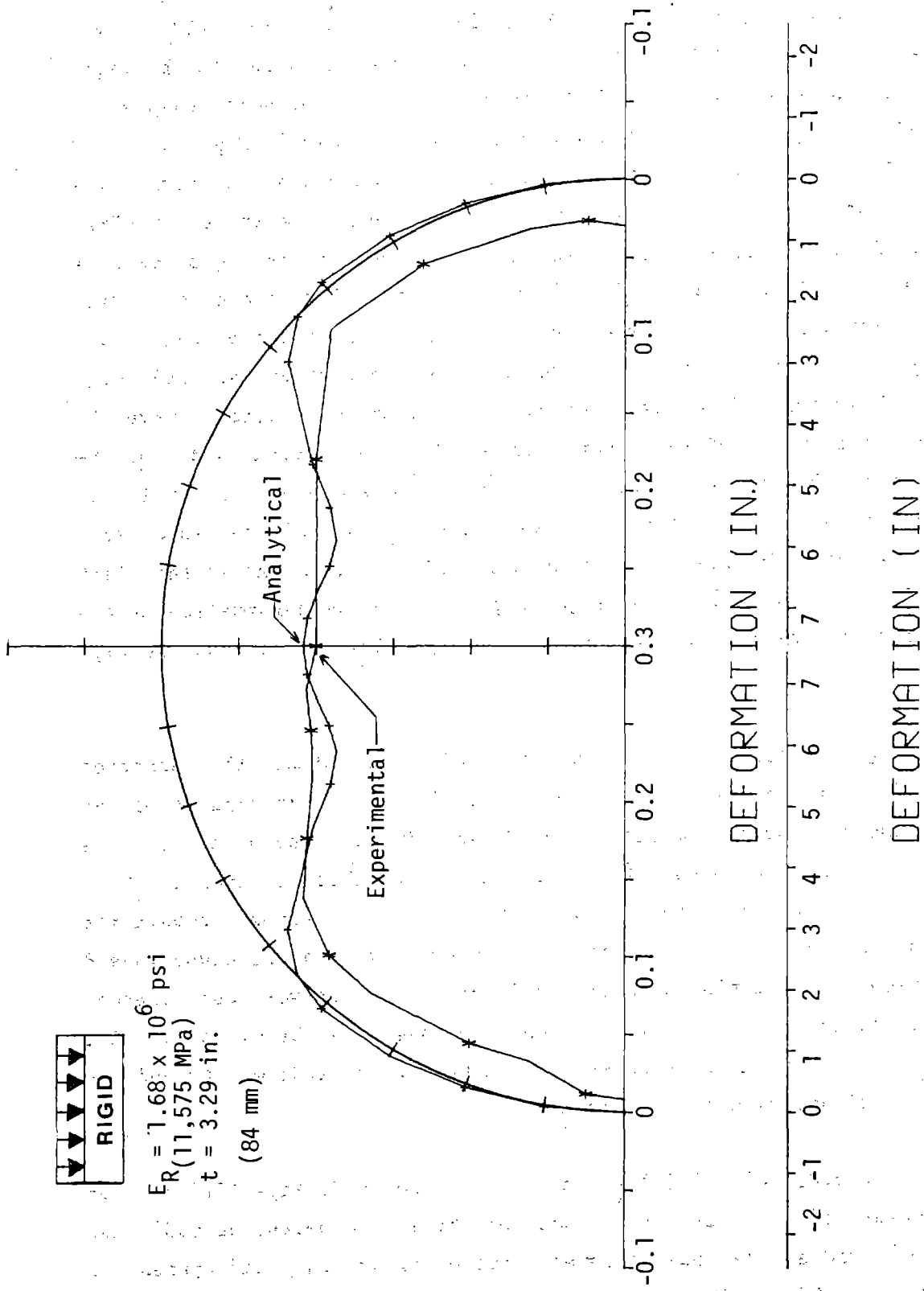


FIGURE 4.46 DEFORMATION OF ARCH 6 AT 95% LOAD



type of loading. The maximum deformation of 0.543 in. (13.8 mm), corresponding to a  $\Delta R/R = 1.50$  percent, occurred at 30 deg to the right of the crown under the edge of the loading block. Deflected shapes at 50 and 100 percent of the maximum load are shown in Figs. 4.47 and 4.48. Separation between the lining and the medium did not occur. The lining moved away from the medium at about 50 deg from the crown (Fig. 4.49). First cracks occurred under the edges of the loading block at a load of about 35 kips (156 kN) or 40 percent of ultimate load (Fig. 4.50). The influence of the crack at 30 deg to the right of the crown is obvious in the deflected shape at 100 percent of the load (Fig. 4.48). This same effect is observed in the load deformation curve 30 deg to the right of the crown (Fig. 4.32). The initial width of the cracks was 0.002 in. (0.05 mm) at the left edge and 0.004 in. (0.1 mm) at the right. At a load level of 101 kips (449 kN), one load level before failure, the cracks had opened to 0.01 in. (0.3 mm) at the left and 0.008 in. (0.2 mm) at the right edge. Extensive deformation at the crown occurred at a constant load of 111 kips (434 kN) as shown in Fig. 4.32.

Arch-8 To compare the effects of medium modulus, the deformed shape for Arch-8 is plotted with that for Arch-1 in Figs. 4.51 and 4.52. The maximum deformation of 0.372 in. (9.5 mm) occurred at the crown, and it is about twice as much as that for Arch-1. This deformation corresponds to a  $\Delta R/R = 1.03$  percent. Although separation between the lining and medium did occur, it did not cause inward deflection of the lining because the large serrations were not present on the surface of the medium (as was the case in Arches-1 to 6). The inward relative movement between the lining and the medium extended to 43 deg on either side of the crown.

First cracks (Fig. 4.53) appeared at a load of 70 kips (311 kN) or 60 percent of the ultimate load, on the inside measuring 0.002 in. (0.05 mm), and at one load increment before failure they had opened to a width of 0.008 in. (0.2 mm).



$E_R = 0.17 \times 10^6 \text{ psi}$   
 (1170 MPa)  
 $t = 2.96 \text{ in.}$   
 (75 mm)

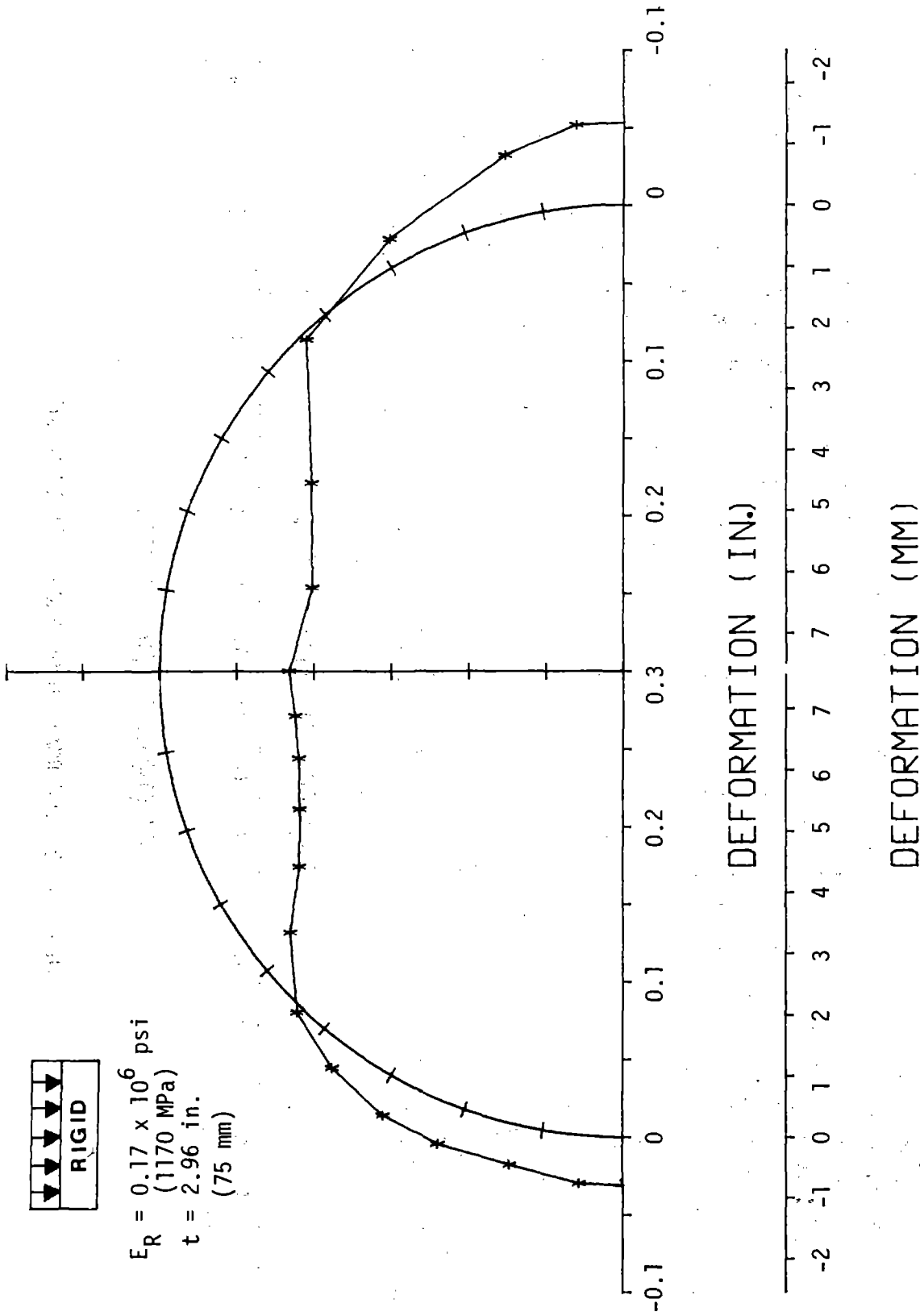


FIGURE 4.47 DEFORMATION OF ARCH 7 AT 50% LOAD



$E_R = 0.17 \times 10^6$  psi  
(1170 MPa)  
 $t = 2.36$  in.  
(60 mm)

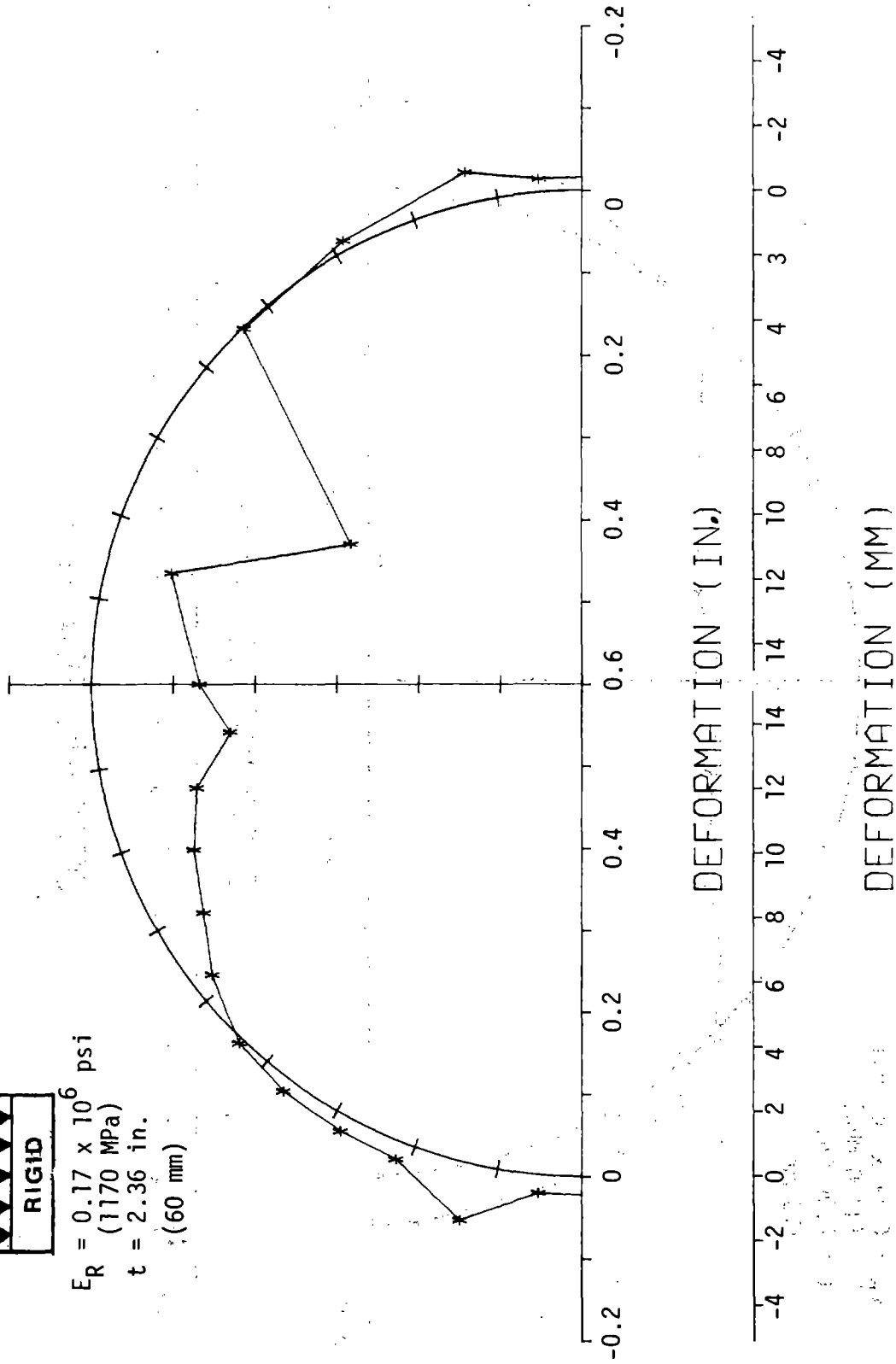


FIGURE 4.48 DEFORMATION OF ARCH 7 AT 100% LOAD

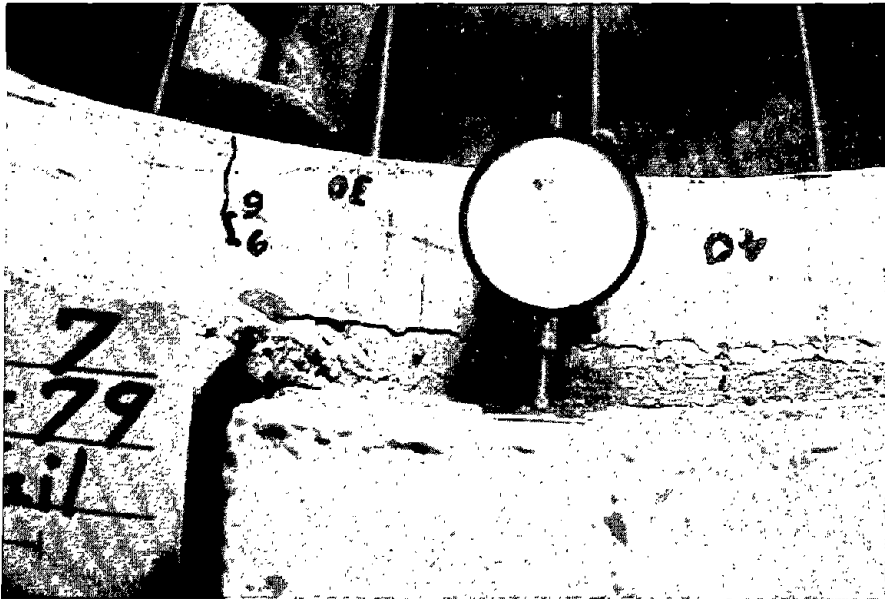


FIGURE 4.49 SEPARATION BETWEEN THE LINING AND THE MEDIUM, ARCH-7

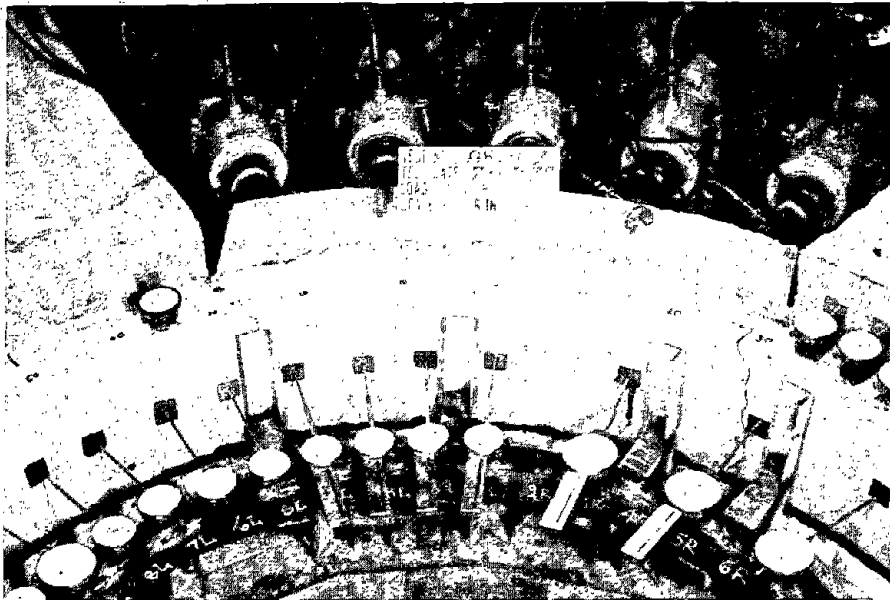


FIGURE 4.50 FIRST CRACKING OF ARCH-7

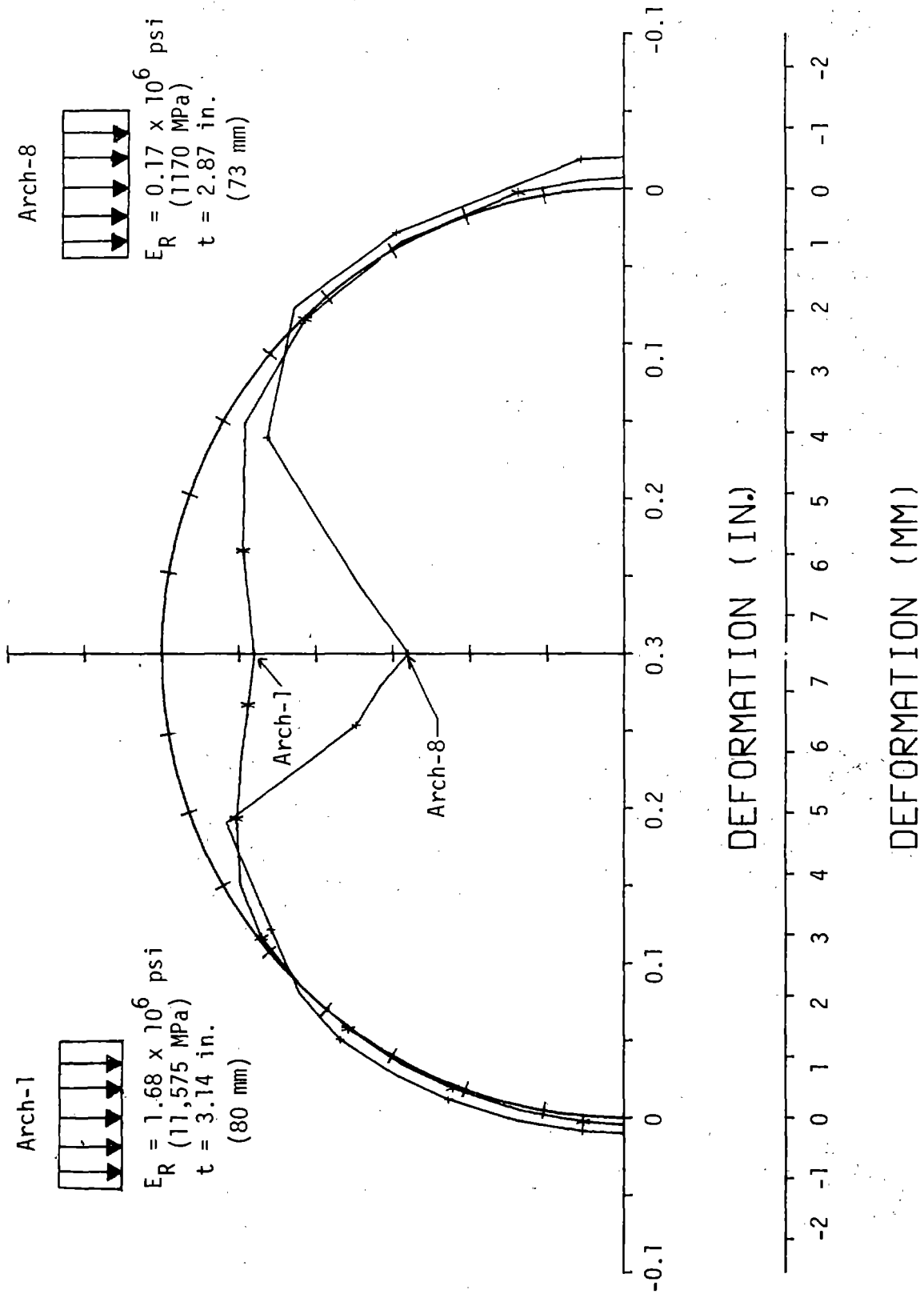


FIGURE 4.51 DEFORMATION OF ARCHES 1 AND 8 AT 50% LOAD

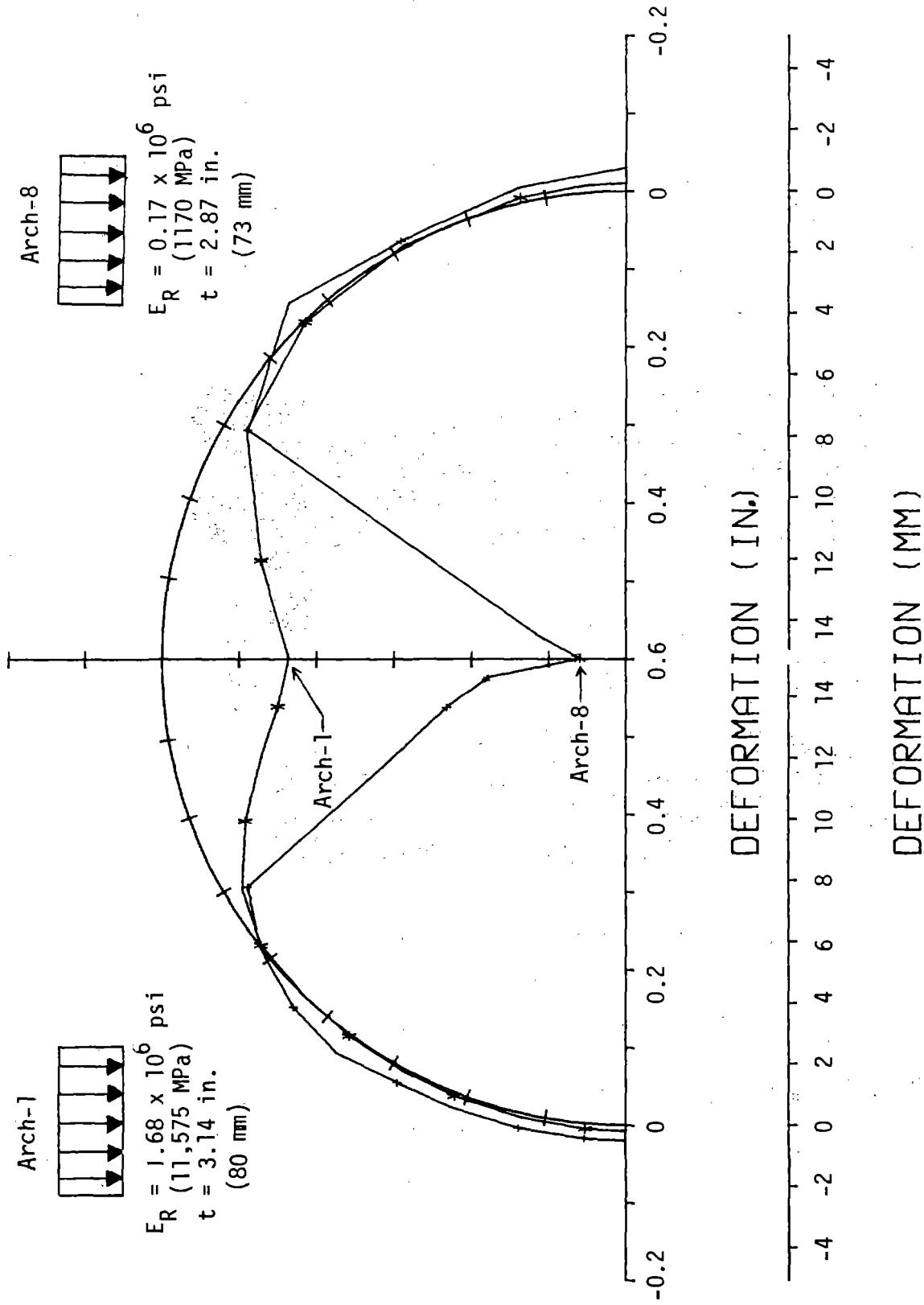


FIGURE 4.52 DEFORMATION OF ARCHES 1 AND 8 AT 97% LOAD

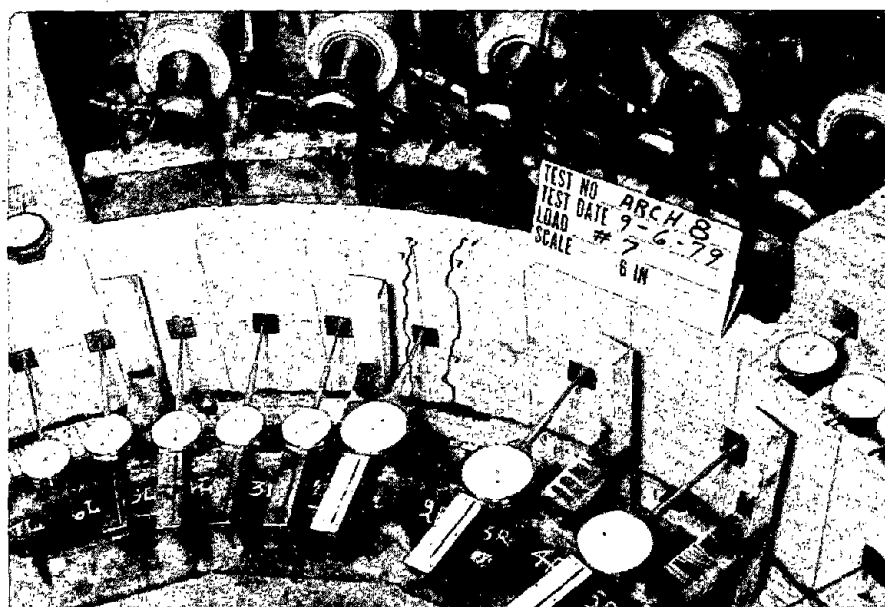


FIGURE 4.53 FIRST CRACKING OF ARCH-8

Arch-9 To assess the effects of reinforcement on the deformability of the lining, deflected shapes for Arch-9 are plotted with those for Arch-10 in Figs. 4.54 and 4.55. Before loading Arch-9 three shrinkage cracks 0.002 in. (0.05 mm) wide existed at the crown region as shown in Fig. 4.56. These shrinkage cracks closed once loading started and did not open again to influence the overall behavior of the lining. A maximum crown deformation of 0.370 in. (9.4 mm) was observed ( $\Delta R/R = 1.03$  percent). Separation between the lining and the medium did not take place during this test. The lining moved inward until 45 deg on either side of the crown.

The first damage to the specimen consisted of a horizontal crack that began near the crown and propagated in both directions toward the supports (Fig. 4.57). It first appeared at about 22 kips (98 kN) or 85 percent of the ultimate load and at failure it had propagated to 30 deg on each side of the crown. The width of the crack increased from 0.002 in. (0.05 mm), when it first appeared, to 0.04 in. (1 mm) just before failure. Since the horizontal crack started at the crown and resulted from a vertical tension, it is suspected that it was caused by the Poisson effect in the rubber pads between the steel loading plates and the specimen. As the rubber was compressed, it tended to move laterally and since the concrete was in contact with the rubber, it tried to pull it along.

Arch-10 To avoid the horizontal cracking observed in Arch-9, two additional measures were taken before loading Arch-10. First, horizontal slots were cut in the rubber pads so that when the rubber tended to expand horizontally each rectangular portion could move laterally and fill the slots. Secondly, fine vertical wires were cast in the specimen (Fig. 4.20) that could resist the vertical tension forces if they occurred. The maximum deformation of 0.570 in. (14.5 mm) was measured at the crown. This is the maximum deformation of all tests, corresponding to a  $\Delta R/R = 1.6$  percent. Consequently, the effects of reinforcement in improving the ductility of the specimen are



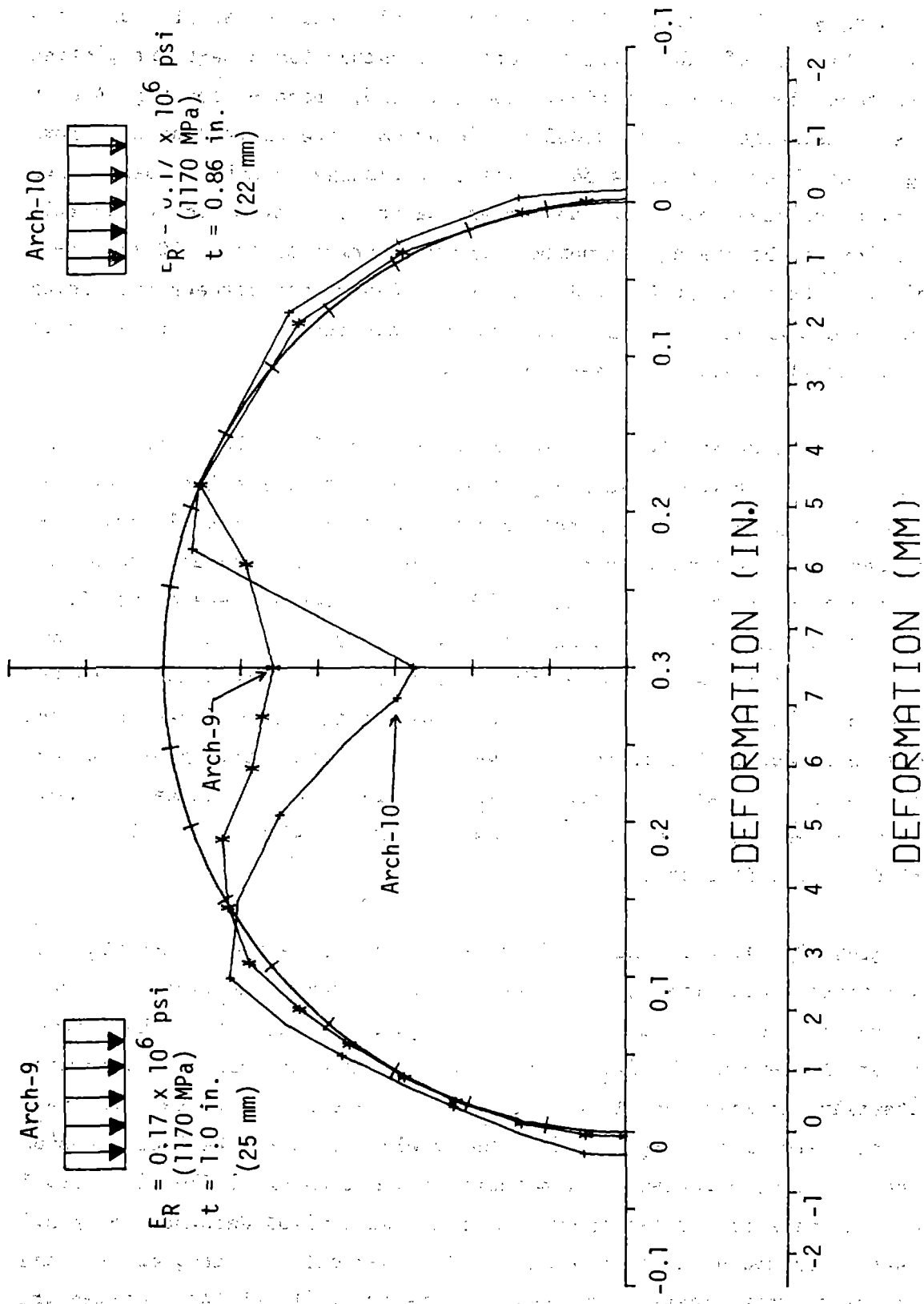


FIGURE 4.54 DEFORMATION OF ARCHES 9 AND 10 AT 50% LOAD

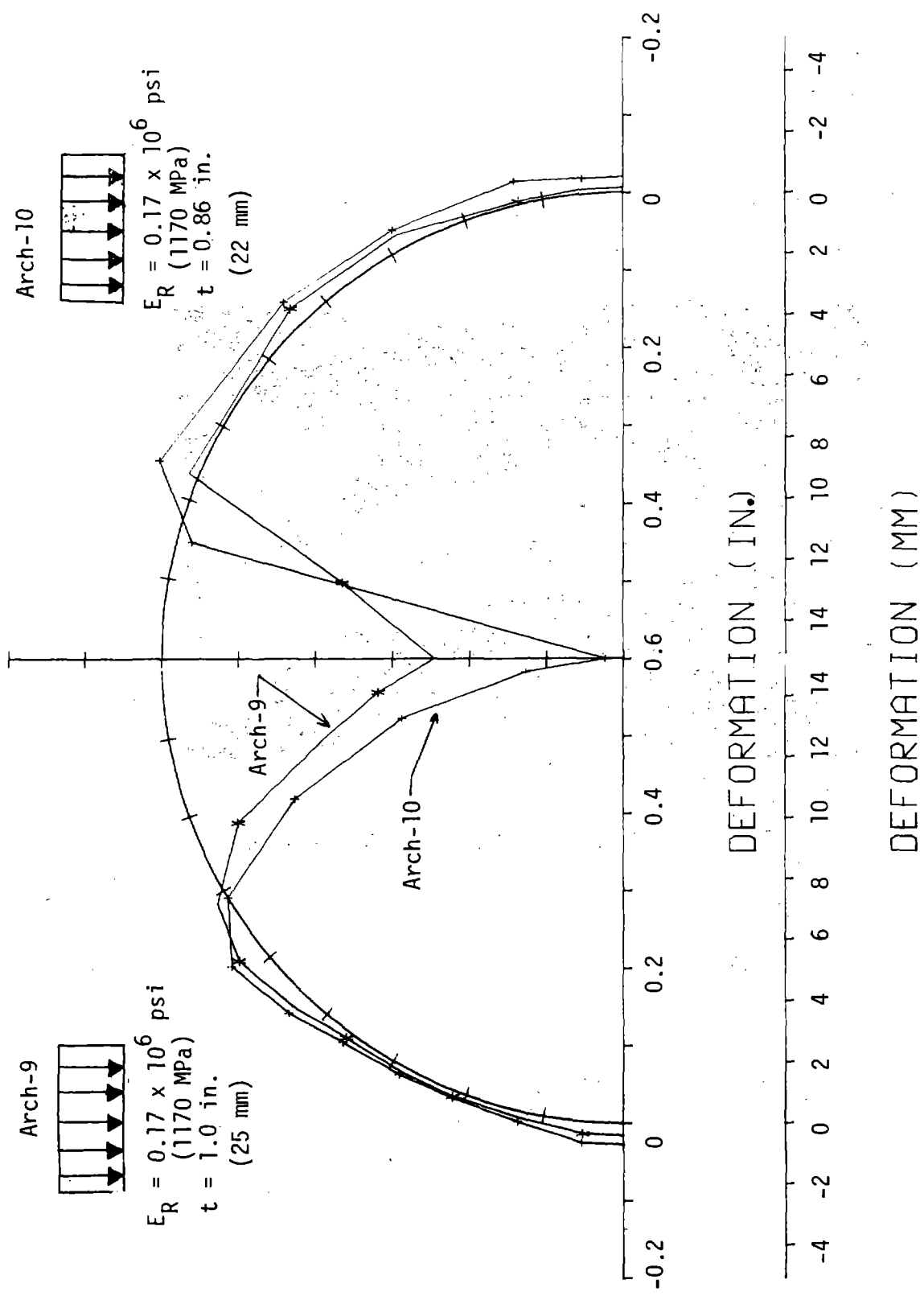


FIGURE 4.55 DEFORMATION OF ARCHES 9 AND 10 AT 100% LOAD

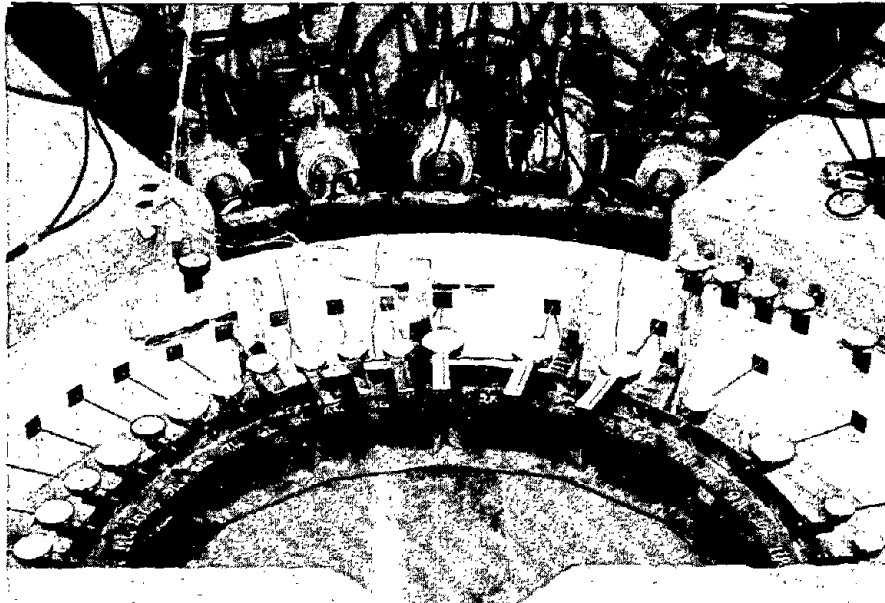


FIGURE 4.56 INITIAL SHRINKAGE CRACKS IN ARCH-9

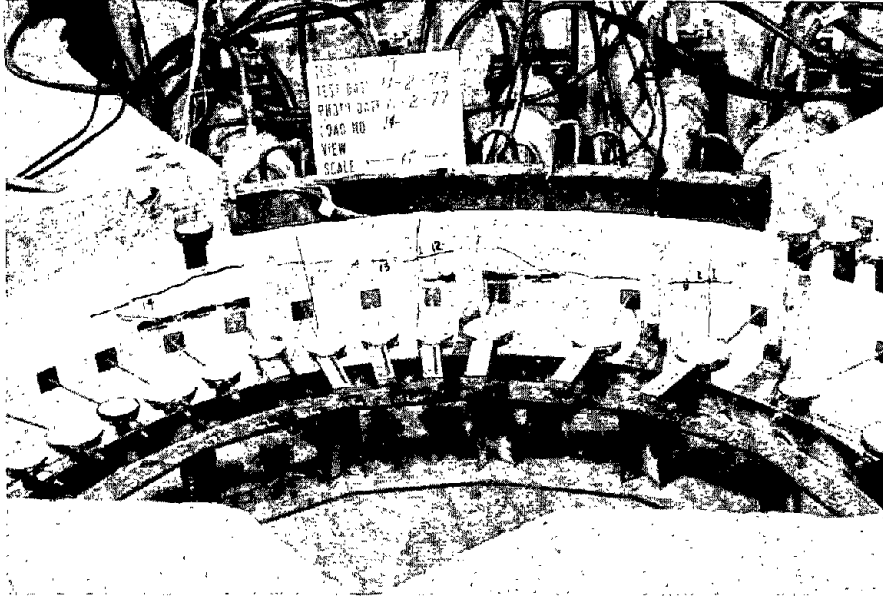


FIGURE 4.57 CRACKING OF ARCH-9

obvious. This conclusion is verified by comparing the deformed shapes of Arches-9 and 10 at 50 and 100 percent of the applied load in Figs. 4.54 and 4.55. No separation between the lining and medium was observed during this test. The inward movement of the lining relative to the medium extended 45 deg on either side of the crown.

Flexural cracks occurred on the inside surface near the crown at a load of about 25 kips (111 kN) corresponding to 80 percent of the maximum applied load (Fig. 4.58). The size of the cracks increased from 0.002 in. (0.05 mm) to 0.01 in. (0.3 mm) just before failure. The size of the cracks is one third as large as that observed in Arch-9, and thus, the beneficial effects of reinforcement on reducing crack size are clear.

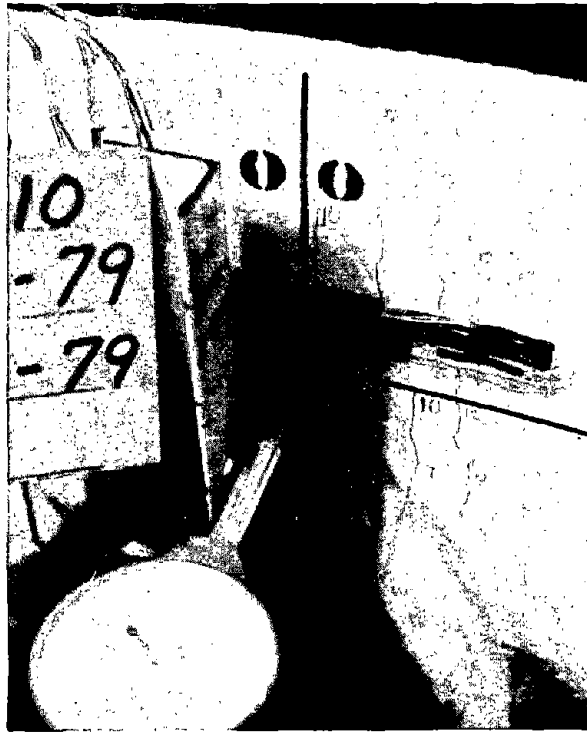


FIGURE 4.58 CRACKING OF ARCH-10

#### 4.3.3 Base Loads and Deformations

The stiffness of the base mechanism was determined by dividing the load transmitted to the base cell by the average deformation recorded by the base dial gages at each loading increment; the average stiffness for the entire base mechanism, consisting of the base plates, load cells and concrete of the medium, was calculated for the right and the left sides. The stiffnesses obtained from the first two or three load increments were not considered in order to discount the effects of seating of the base mechanism at the beginning of the loading sequence. The values of base stiffness given below were used to determine the stiffness of the base springs used in the analysis described in Section 4.4.1.

<u>Specimen Number</u>	<u>Left Base Stiffness</u> K/in. (kN/mm)		<u>Right Base Stiffness</u> k/in. (kN/mm)	
Arch-1	1100	(194)	1048	(158)
Arch-2	875	(155)	568	(100)
Arch-3	832	(147)	1074	(190)
Arch-4	1170	(207)	1537	(272)
Arch-5	1329	(235)	1547	(273)
Arch-6	671	(119)	915	(162)
Arch-7	1805	(319)	1428	(252)
Arch-8	2047	(362)	1296	(229)
Arch-9	1075	(190)	1056	(187)
Arch-10	906	(160)	1038	(183)

The variation in values of the overall base stiffnesses occurred because of the difference in stiffness of the individual base cells and the distribution of load reaching the bases.

The amount of total applied load that reached the base varied from about 5 percent before slippage between the lining and medium, to 20-30 percent after slippage for the tests in which the medium was serrated. In the case of Arch-5, where little side friction existed, 120 percent of total applied load reached the base. The load above 100 percent results from the vertical component of the radial reaction of the medium against the lining. The same argument applies for the test that had a layer of rubber between the concrete medium and the lining and had more load in the base load cells than was applied. The component of radial pressure between the medium and lining toward the base was larger than the load removed by tangential stress in the rubber, even though there was no-slip between the rubber and the lining. This occurred in tests Arches-7 to 10.

The base deformations are plotted with the crown deformations in Figs. 4.27-4.34. The deformations measured at the base were 3 to 30

percent of those at the crown (Table 4.5). The values of base deflection for Arches-1, 7, 9 and 10 are low because no-slippage occurred between the lining and the medium. For the tests in which there was slippage, the base deflections are still relatively low, because movement toward the base could only occur with a corresponding inward deflection along the serrations.

#### 4.3.4 Failure Mechanisms

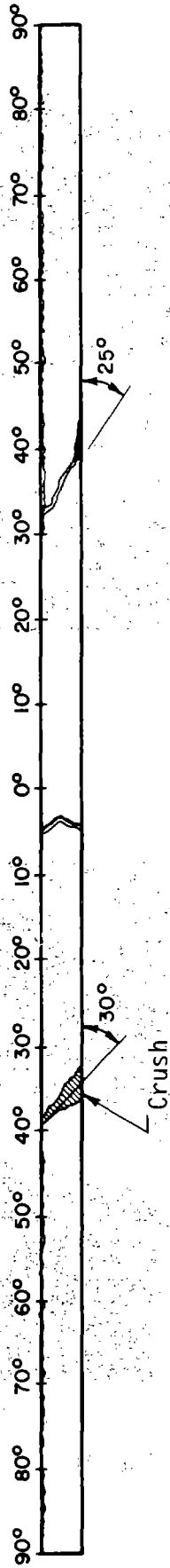
Arch-1 Failure of Arch-1 occurred 30 to 40 sec after the ultimate load was reached. The failure was initiated 35 deg to the right of the crown and the upper half of the specimen from 35 deg to the left to 35 deg to the right broke away from the rest of the specimen, as shown in Figs. 4.59 and 4.60. The orientation of the sheared section is shown in Fig. 4.61. The failure was sudden and without cracking or other warning. The loads recorded by the upper base load cells were slightly higher than those at the bottom. Consequently, the upper half of the specimen may have been stressed more, resulting in failure in the upper portion of the specimen. The loads on the active rams were in close agreement, so the imbalance at the base resulted from a difference in stiffness of the two base load cells. In addition the upper portion of the specimen may have been slightly weaker than the lower portion because of migration of water to the top during casting and curing.

Arch-2 The shape of the loading in this case was more concentrated at the center, causing more rotation of the arch in the crown region and flexural cracks on the inside surface of the crown. The higher rotation also caused higher compressive strains on the outside surface of the crown as confirmed by the localized crushing zone shown in Fig. 4.62. This zone was restricted to the upper surface of the arch because the confinement, provided by the loading pads, increased the compressive strength of the concrete in the rest of the crown region. The combination of high moment and thrust in the crown region resulted in the compression failure shown in Figs. 4.63 and

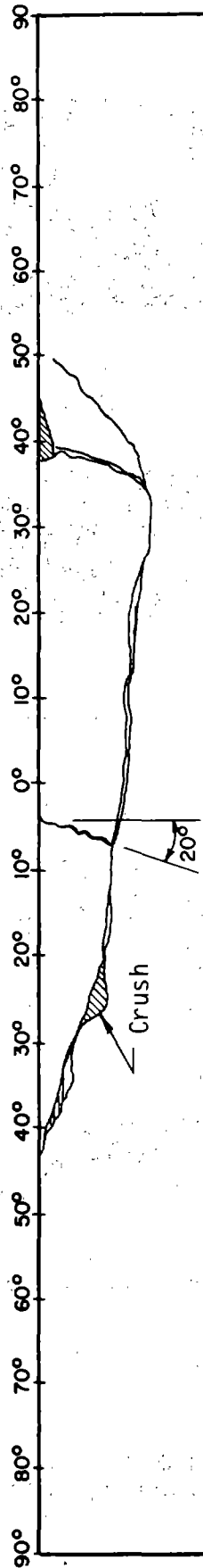
LOADING



Inside: Top View



Side View



Outside

Side View

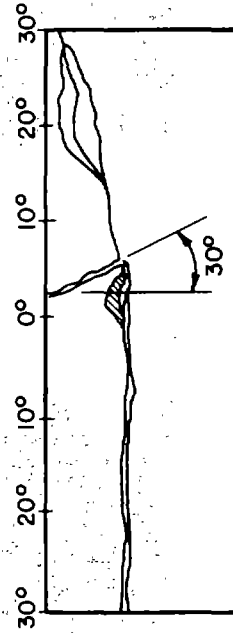


FIGURE 4.59 MAP OF DAMAGE TO ARCH-1 AT FAILURE



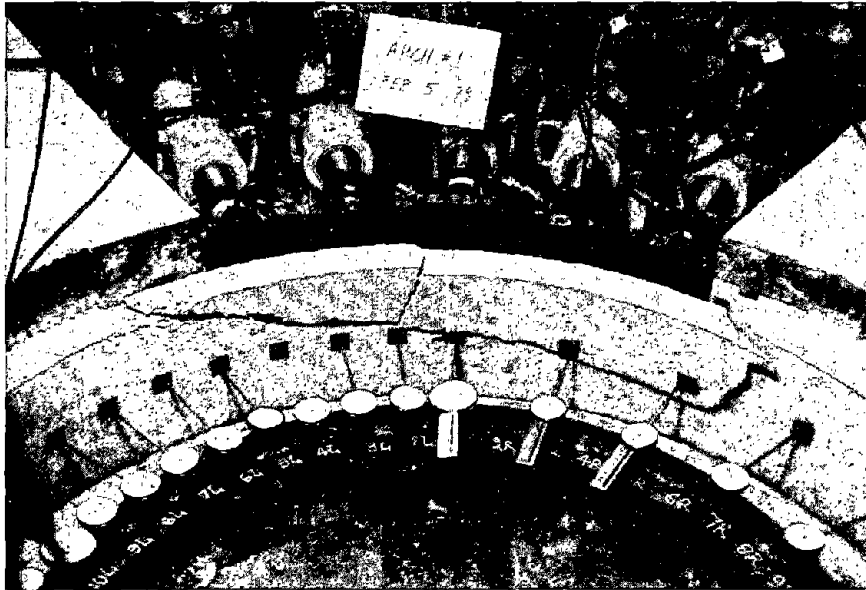


FIGURE 4.60 ARCH-1 AT FAILURE

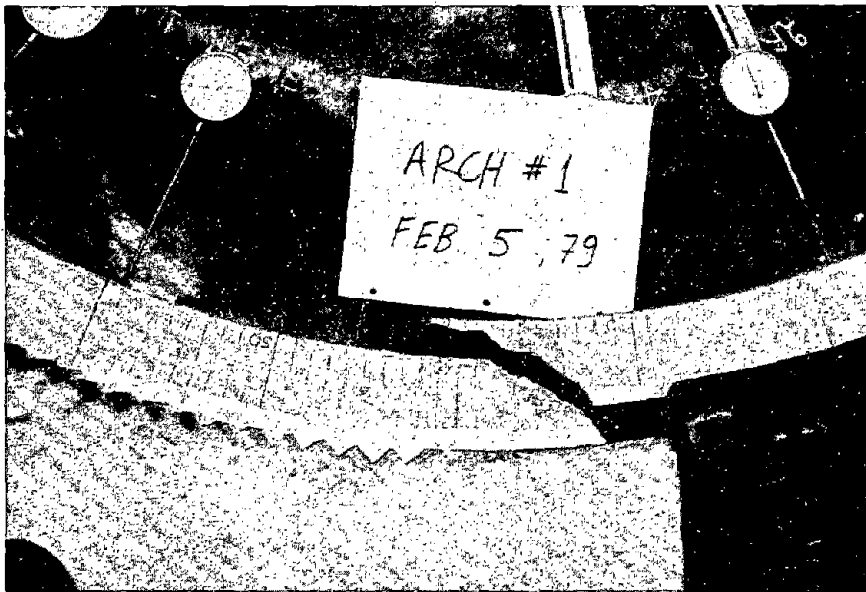
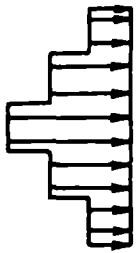


FIGURE 4.61 FAILURE AT 35 DEGREES TO THE RIGHT OF THE CROWN OF ARCH-1

LOADING



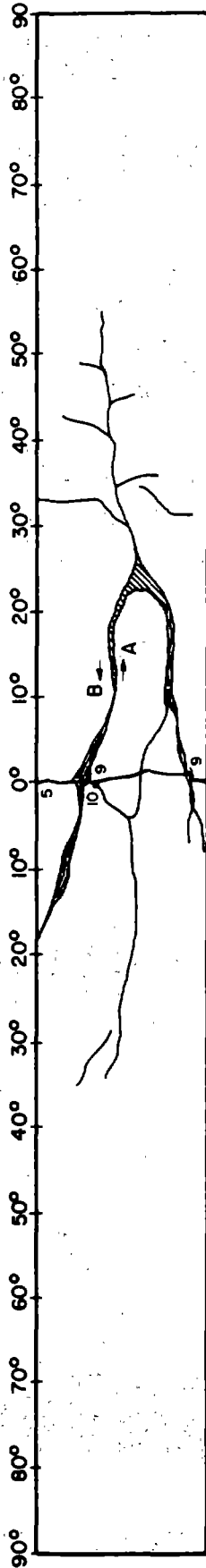
End of Abutment

Crushing Up to a  
Depth of 0.5 in.  
(13 mm)

Inside: Top View

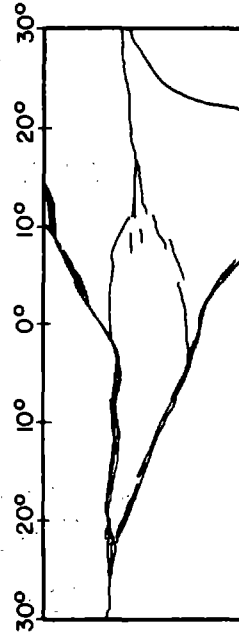


Side View



Outside

Side View



Inside

FIGURE 4.62 MAP OF DAMAGE TO ARCH-2 AT FAILURE

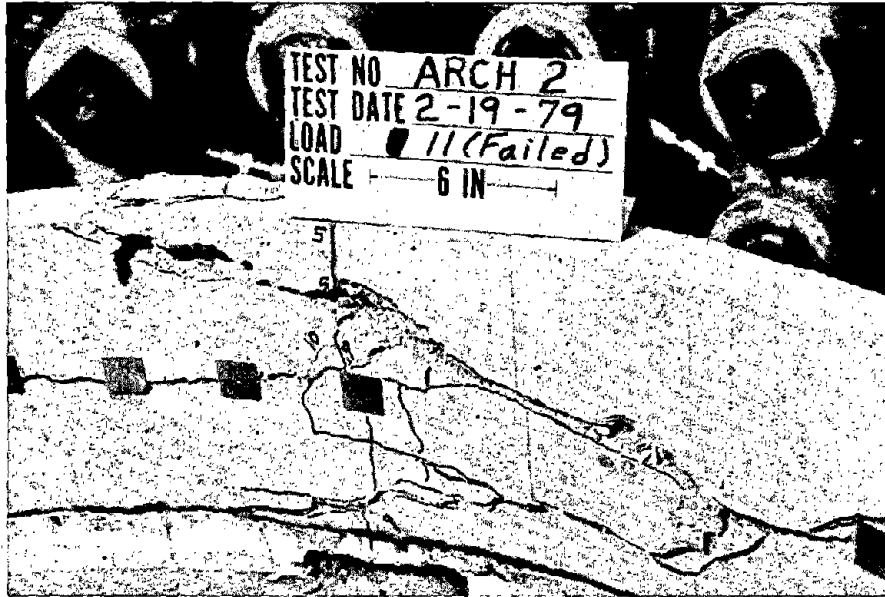


FIGURE 4.63 COMPRESSIVE FAILURE ZONE OF ARCH-2



FIGURE 4.64 CROWN OF ARCH-2 AT FAILURE

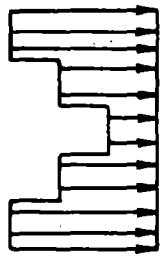
4.64. The shape of the failed surface is similar to those observed in the compression cylinders that were tested to determine the strength of the concrete used in the lining.

Arch-3 The failure of Arch-3, as in Arch-1, was sudden. No tension cracking was detected before the ultimate load was reached. Failure was initiated by a diagonal crack at about 35 deg to the right of the crown (Fig. 4.65) and a horizontal crack about 4 in. (109 mm) from the top surface. Separation of this upper portion was followed by the crushing at 35 deg at the right of the crown and complete failure as shown in Fig. 4.66. Thus, the failure began with a diagonal crack near the top edge and continued by crushing and splitting below the diagonal crack. The reason for failure initiating near the top surface was probably due to the weakness of concrete in this area, resulting from migration of water to the upper portion during casting. The corresponding top and bottom active ram loads were in good agreement, so the loads applied to the top and bottom of the specimen were very nearly the same.

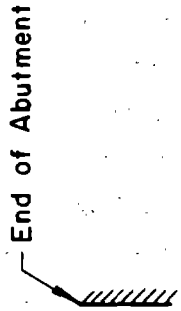
Arch-4 The loading imposed on Arch-4 was concentrated on the left side of the crown. This caused the critical portion of the arch to occur between 40 deg to the left of the crown and 15 deg to the right, as shown in Fig. 4.67. At failure, compressive crushing at 40 deg left and tension cracking at 15 deg right on the inside surface caused these two points A and B to serve as rotational hinges; therefore, the portion between these sections resisted most of the imposed load in compression as a very flat arch. This resulted in compressive failure of the center portion of this flat arch 15 deg to the left of the crown as shown in Figs. 4.68 and 4.69.

Arch-5 The lack of shear resistance between the specimen and medium caused more crown deflection and flexural cracking in this test. The additional moment resulting from the larger deformation caused compressive crushing due to combined compression and flexure on the

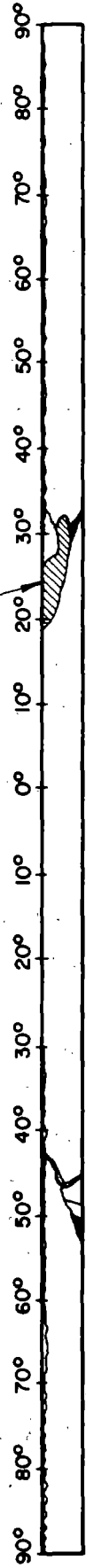
LOADING



Inside: Top View



Initiation of Crushing at Failure

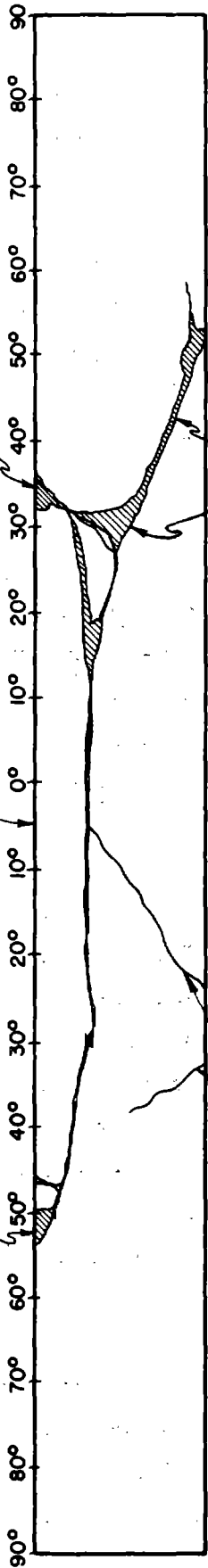


Side View

I

II

I



Thin Cracks

Outside

Side View

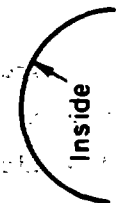
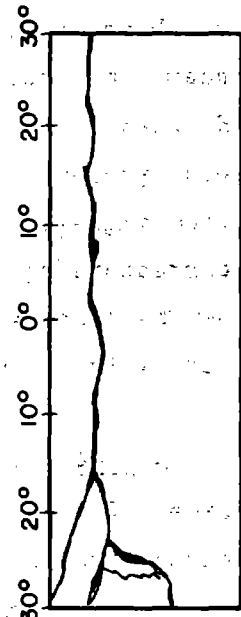
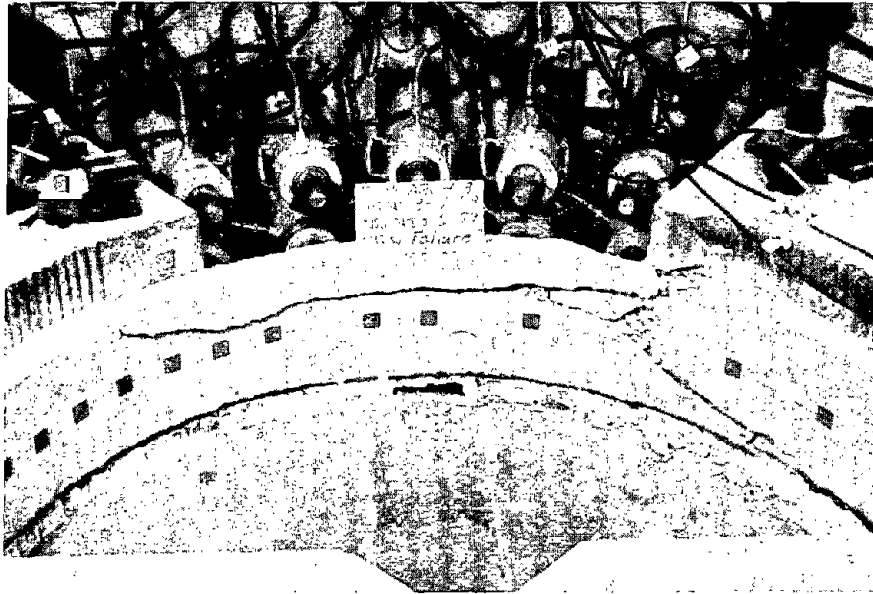
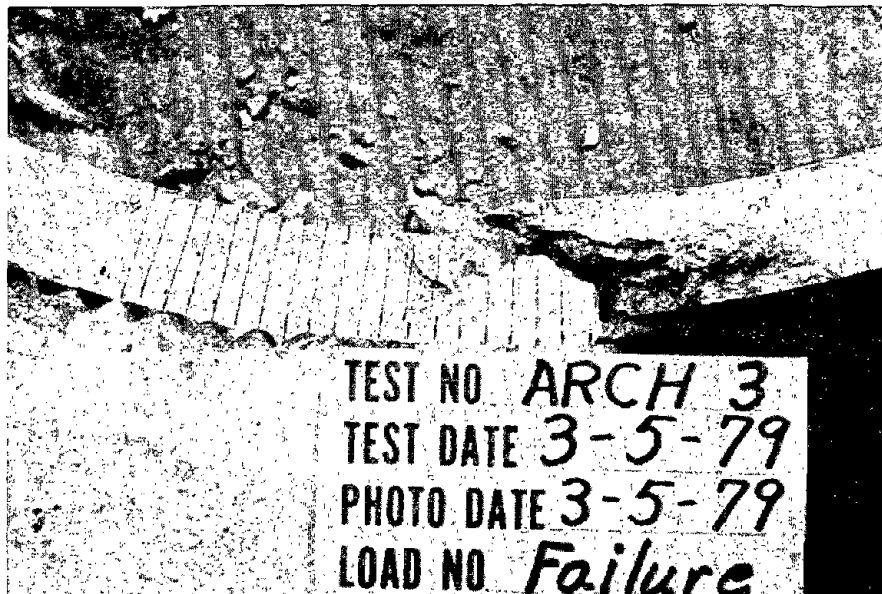


FIGURE 4.65 MAP OF DAMAGE TO ARCH-3 AT FAILURE



(a) Front view



(b) Top view

FIGURE 4.66 FAILURE ZONE AT 35 DEGREES TO THE RIGHT OF THE CROWN IN ARCH-3

LOADING

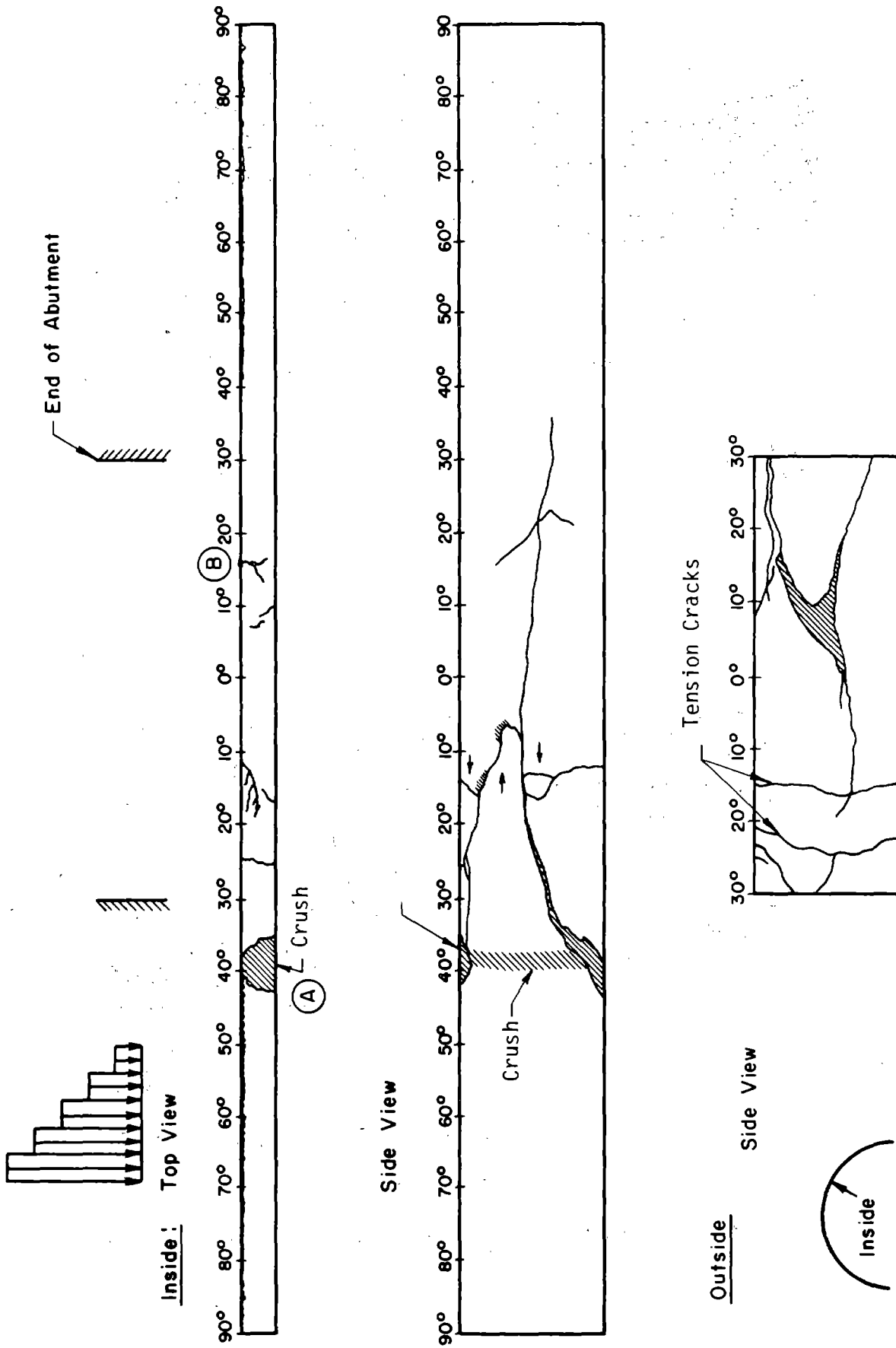


FIGURE 4.67 MAP OF DAMAGE TO ARCH-4 AT FAILURE

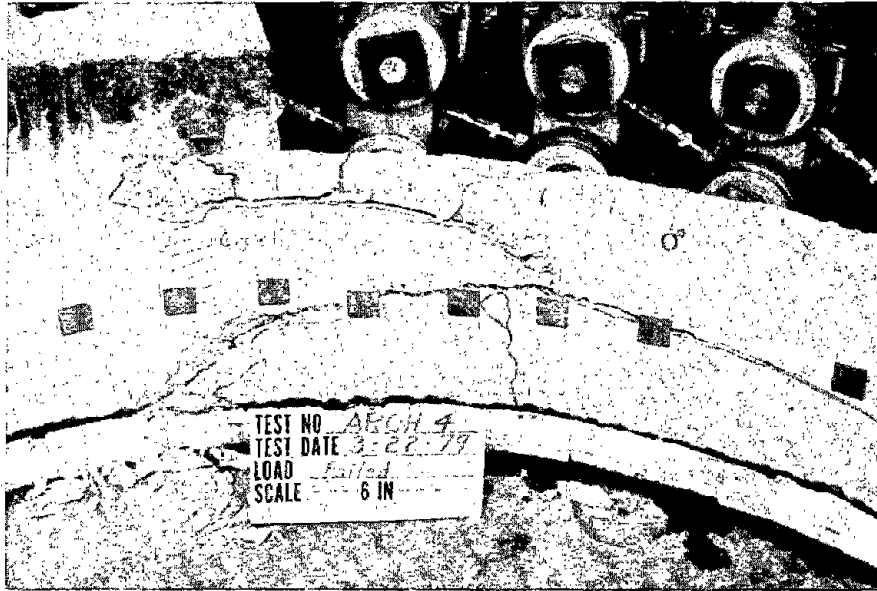


FIGURE 4.68 COMPRESSION ZONE OF ARCH-4 AT FAILURE



FIGURE 4.69 CROWN OF ARCH-4 AT FAILURE



inside at 35 deg left of the crown and on the outside surface at about 2 deg left of the crown, as shown in Figs. 4.70 and 4.71. Tension cracks occurred opposite these compression failure regions before the crushing began. Failure resulted primarily from compressive failure of the concrete accompanied by splitting in the direction of compressive stress.

Arch-6 The rigid block loading of Arch-6 caused load to be concentrated near the edges of the loaded area. Failure was sudden without cracking or other type of warning and occurred at 35 deg to the left of the crown at the edge of the loading block (Fig. 4.72). The orientation of the failed section (Fig. 4.73) resembled that of a shear failure, although it was caused by the combined effects of shear, moment and thrust at that particular region.

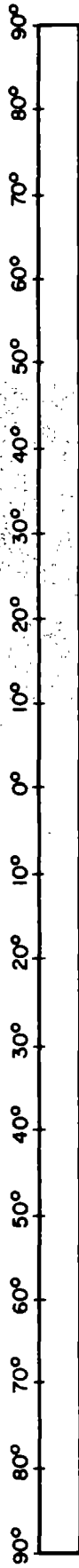
Arch-7 Although loading was the same as that used in Arch-6, the softer medium allowed more deformation and thus some flexural cracking before failure, as shown in Fig. 4.74. However, the failure mechanism and its location were the same with that of Arch-6, as shown in Fig. 4.75.

Arch-8 The load applied on Arch-8 was uniform as in Arches-1 and 5. Compressive failure occurred simultaneously at the outside surface near the crown (under the loading plates) and at the inside surface 35 deg to the left of the crown (Figs. 4.76 and 4.77). The concrete that was confined by the loading pads near the crown had a higher effective compressive strength than on the inside, so the stress conditions near the crown had to be more severe in order to cause simultaneous failures at the two locations. Though failure appeared to occur simultaneously at the two regions, it is possible that there was a small time difference between them and the failure at one location, and the corresponding additional deformation precipitated failure at the other location.

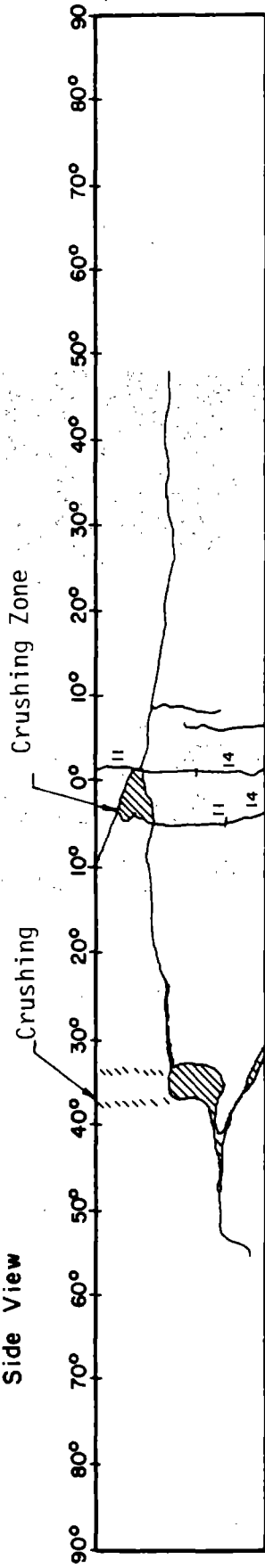
LOADING  
NO-SHEAR



Inside: Top View



Side View



Outside: Side View

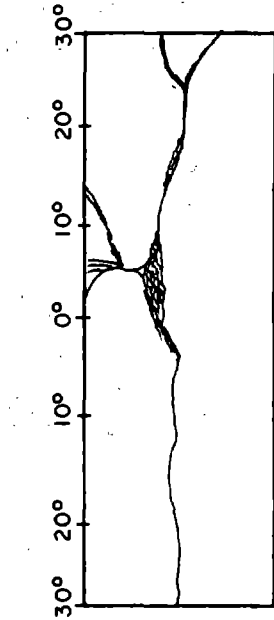


FIGURE 4.70 MAP OF DAMAGE TO ARCH-5 AT FAILURE

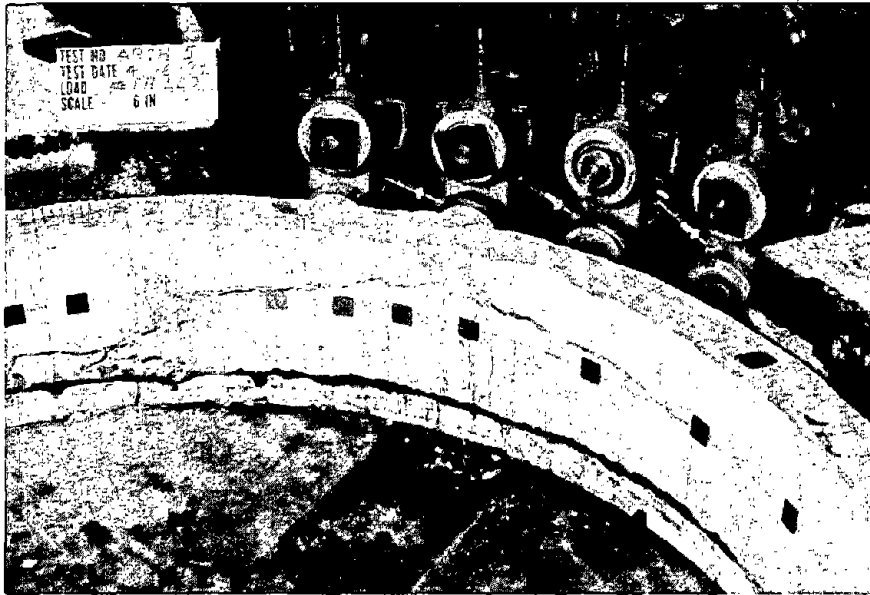


FIGURE 4.71 ARCH-5 AT FAILURE

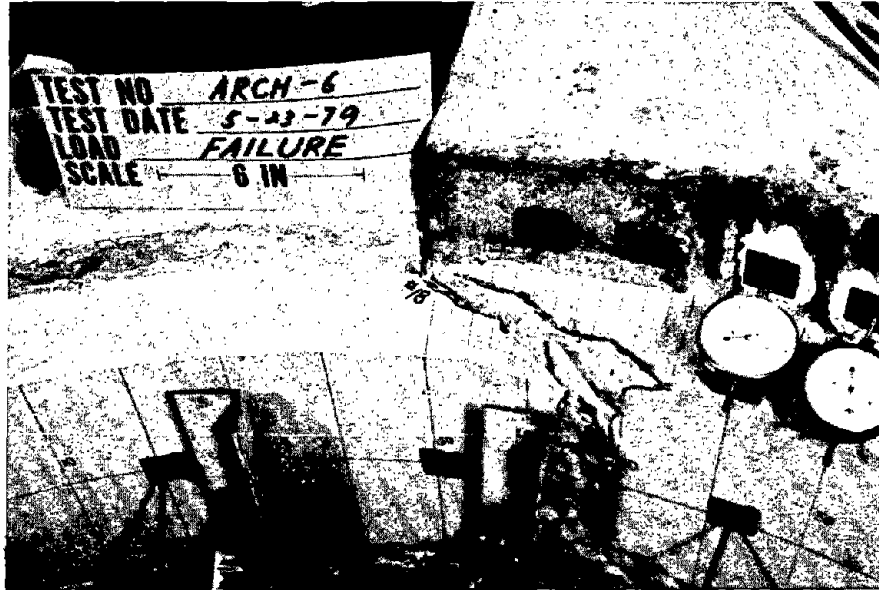
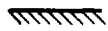
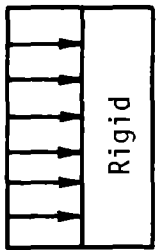


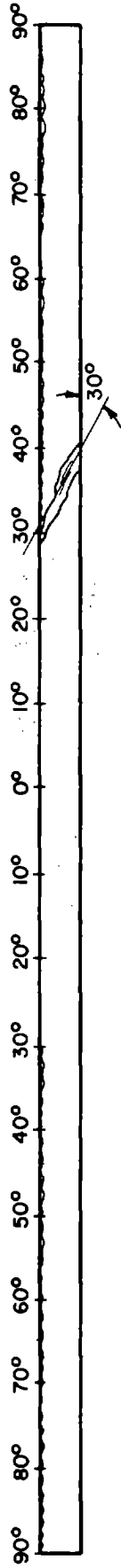
FIGURE 4.72 FAILED REGION OF ARCH-6

LOADING



End of Abutment

Inside: Top View



Side View

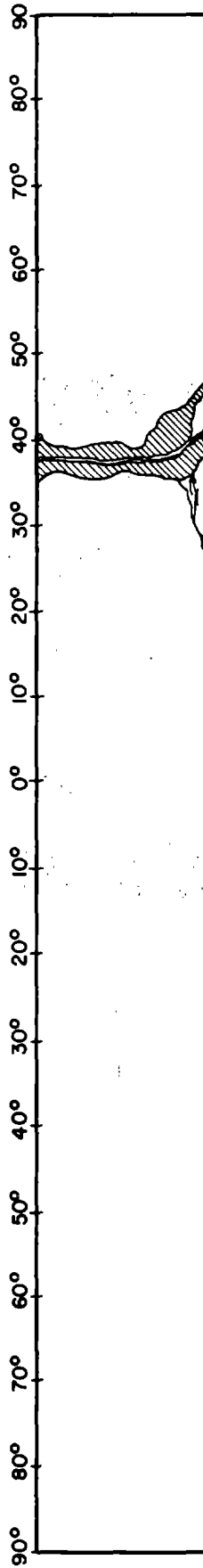
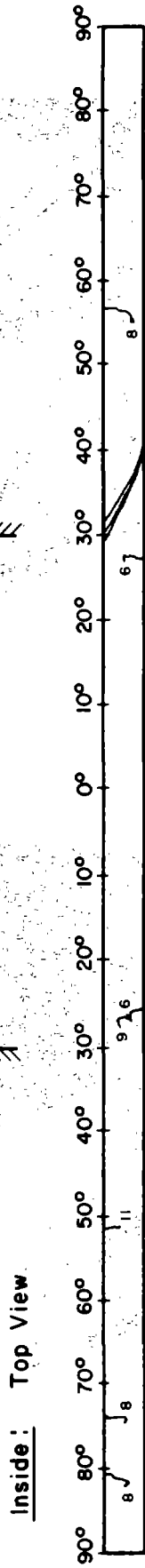
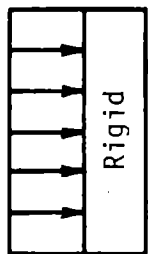


FIGURE 4.73 MAP OF DAMAGE TO ARCH-6 AT FAILURE

LOADING



Side View

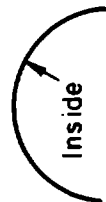
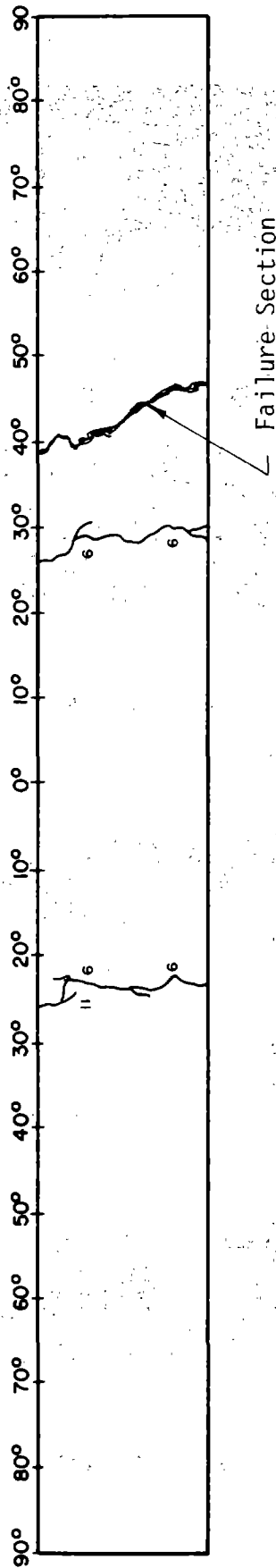


FIGURE 4.74 MAP OF DAMAGE TO ARCH-7 AT FAILURE



FIGURE 4.75 ARCH-7 AT FAILURE

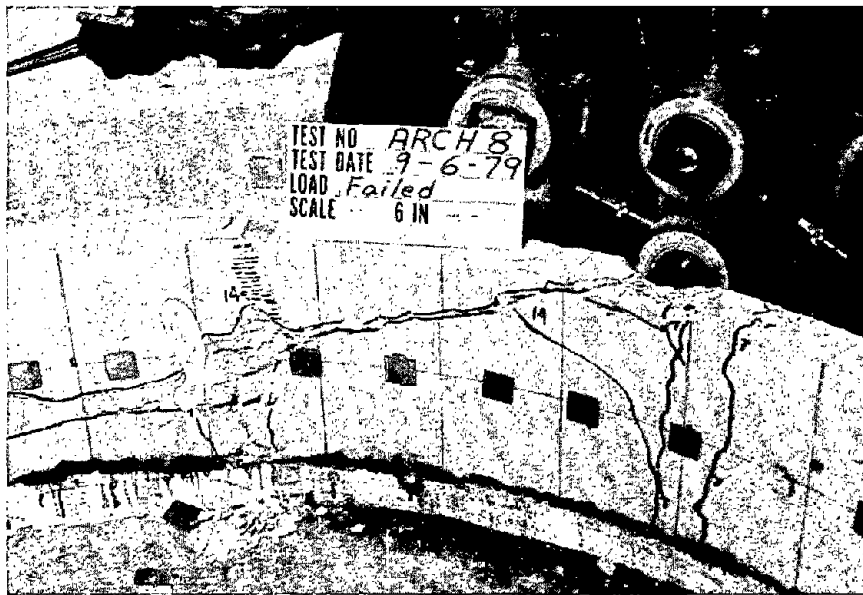
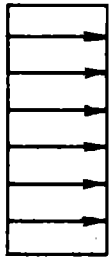
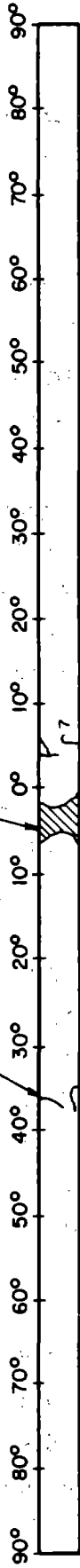


FIGURE 4.76 ARCH-8 AT FAILURE

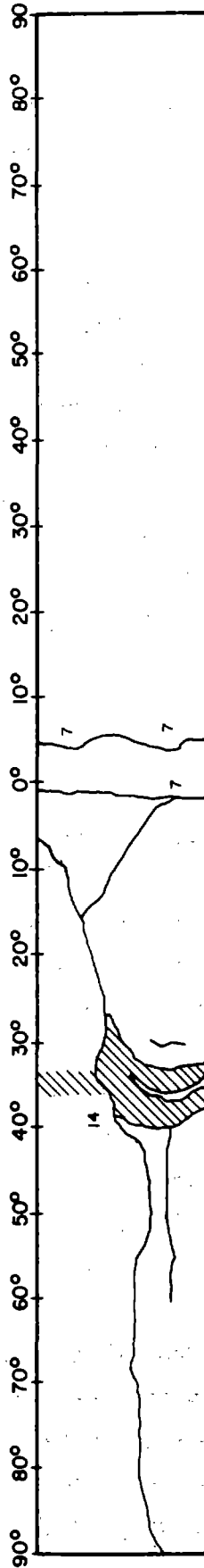
LOADING



Inside: Top View



Side View



Outside:

Side View

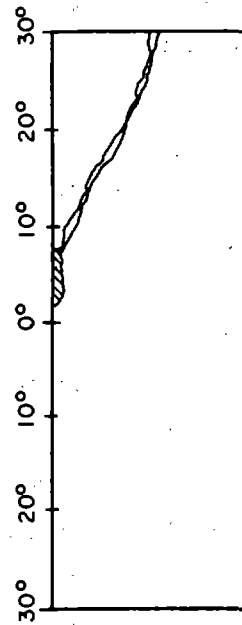


FIGURE 4.77 MAP OF DAMAGE TO ARCH-8 AT FAILURE



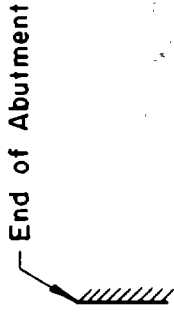
The failure mechanism was different from that observed in Arches-1 and 5 for the same loading condition but with interlock (Arch-1) and full-slip (Arch-5).

Arch-9 The three shrinkage cracks existing in Arch-9 before loading (Fig. 4.78) closed as soon as load was applied. They did not open during the test, because the uniform compression component through the section was sufficient to overcome any tension that would tend to open them. Furthermore, they were not in the failure region, so they did not affect the behavior or failure mechanism of the specimen. The first damage to the specimen consisted of a horizontal crack that began near the crown and propagated in both directions toward the supports (Fig. 4.79). Failure occurred at 35 deg to the left of the crown primarily in the upper portion of the specimen above the horizontal crack.

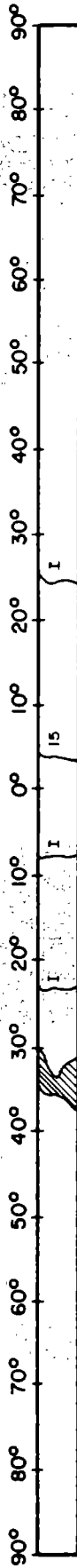
Crushing began at the inside surface and the right side of the region of crushing (crown side) moved inward relative to the left as the two sides of the crushed region tried to move past one another. The resulting deformation caused the portion of the specimen on the crown side of the failure region and above the horizontal crack to break away, but the lower portion was still resisting considerable load. The gages were removed and the load increased until the crushing continued at the same location through the lower part of the specimen. It is not clear whether the horizontal crack reduced the specimen strength. In any case, it did not affect the failure mode which was a classical compression failure in the region where it would be expected; similar to the one observed in the thicker specimens.

Arch-10 This specimen was the only one reinforced with 1.0 percent longitudinal reinforcement at mid-depth. The applied load was uniform, as in Arch-9. A compression failure occurred suddenly at the crown from top to bottom of the specimen. The crushed concrete fell away, and the reinforcing bars buckled (Fig. 4.80). Very fine flexural

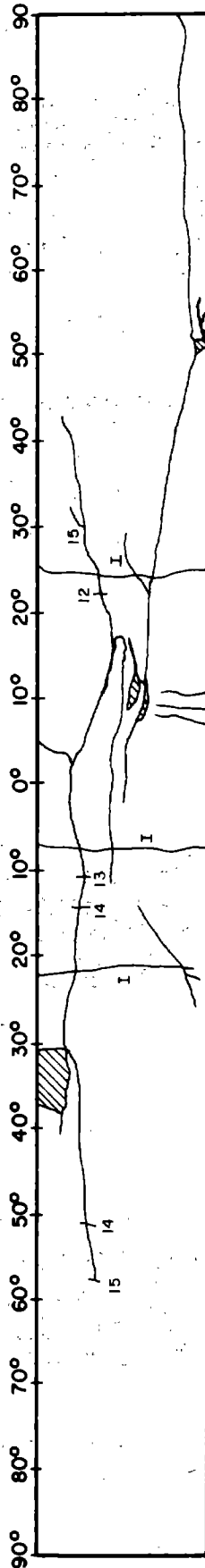
LOADING



Inside: Top View



Side View



I = Shrinkage Cracks

Outside:

Back View

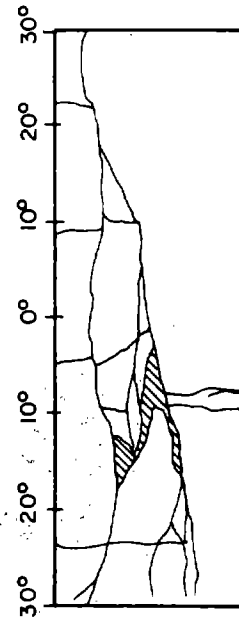


FIGURE 4.78 MAP OF DAMAGE TO ARCH-9 AT FAILURE

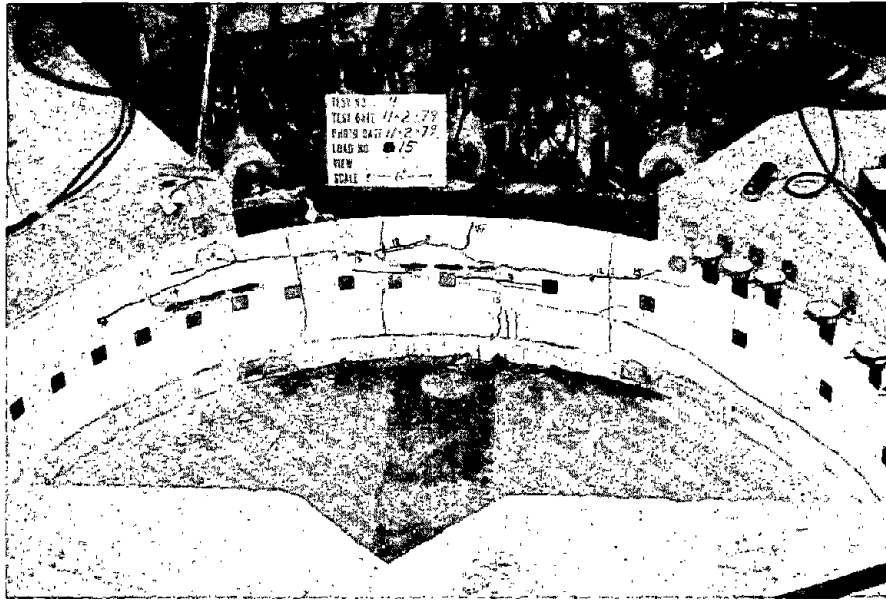


FIGURE 4.79 ARCH-9 AT FAILURE

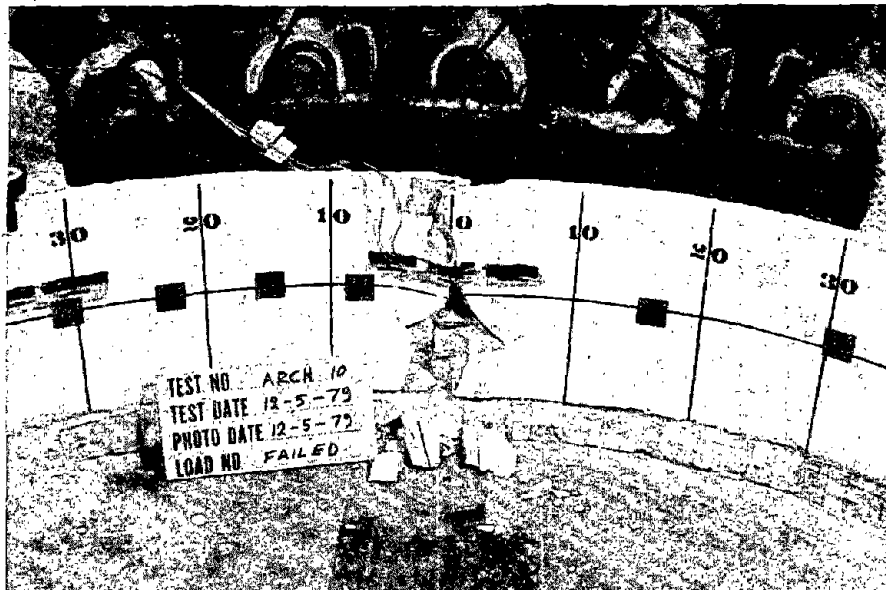


FIGURE 4.80 ARCH-10 AT FAILURE

tension cracks first appeared at 80 percent of total load on the inside surface of the crown, but they never widened as the compression component of internal force grew as fast as the moment keeping the cracks small. Tension strains were measured on the inside surface; they showed an increase in strain up to the approximate load when cracks were detected, and then a reduction of strain as loading continued. There were no horizontal cracks in Arch-10 as shown in Fig. 4.81.

#### 4.4 FINITE ELEMENT ANALYSIS AND COMPARISON WITH EXPERIMENTS

##### 4.4.1 Description of Input Data

The analysis described in Section 3.3.1 was used to simulate the arch tests. In the analysis, the lining was represented by the three-node beam element and the surrounding medium by a series of radial and tangential springs. Since the loading conditions as well as the configuration of the arches for all tests, except Arch-4, were symmetrical about the vertical axis through the crown, only one half the lining was modeled for these tests as shown in Fig. 4.82. The symmetry dictates a boundary condition at the crown (node No. 1) in which vertical deflection was permitted, while horizontal deflection and rotation were restrained. Each element corresponds to an arc of 5 deg except for elements 1 and 2, that correspond to an arc of 2.5 deg. The active loads were applied to the nodes at the crown region, and their magnitudes were proportional to the load on the tributary area. For test Arch-4, where the loading condition was not symmetrical about the center line, it was necessary to model the entire arch.

The radial spring stiffnesses were determined using the modulus of elasticity of the medium from the plate load tests. These values of modulus are given in Section 4.2.3. Values obtained at Position A were used to model the radial springs from 35 to 50 deg from the crown, and

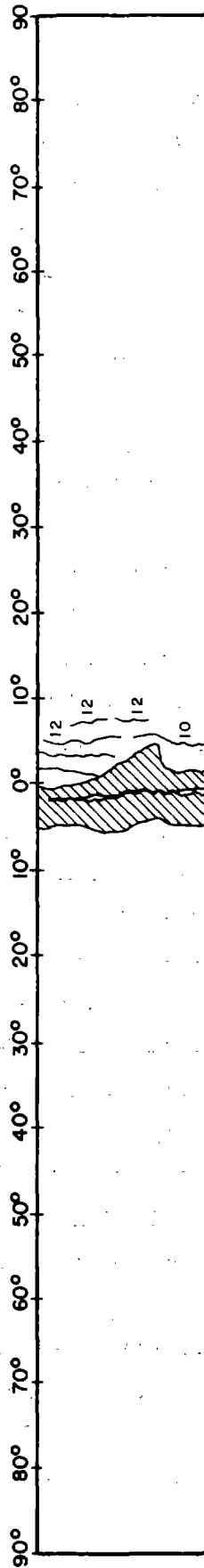
LOADING



Inside: Top View



Side View



Outside:

Back View

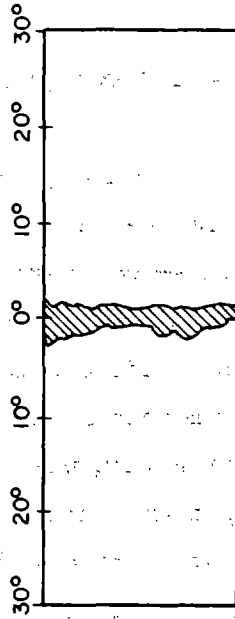


FIGURE 4.81 MAP OF DAMAGE TO ARCH-10 AT FAILURE

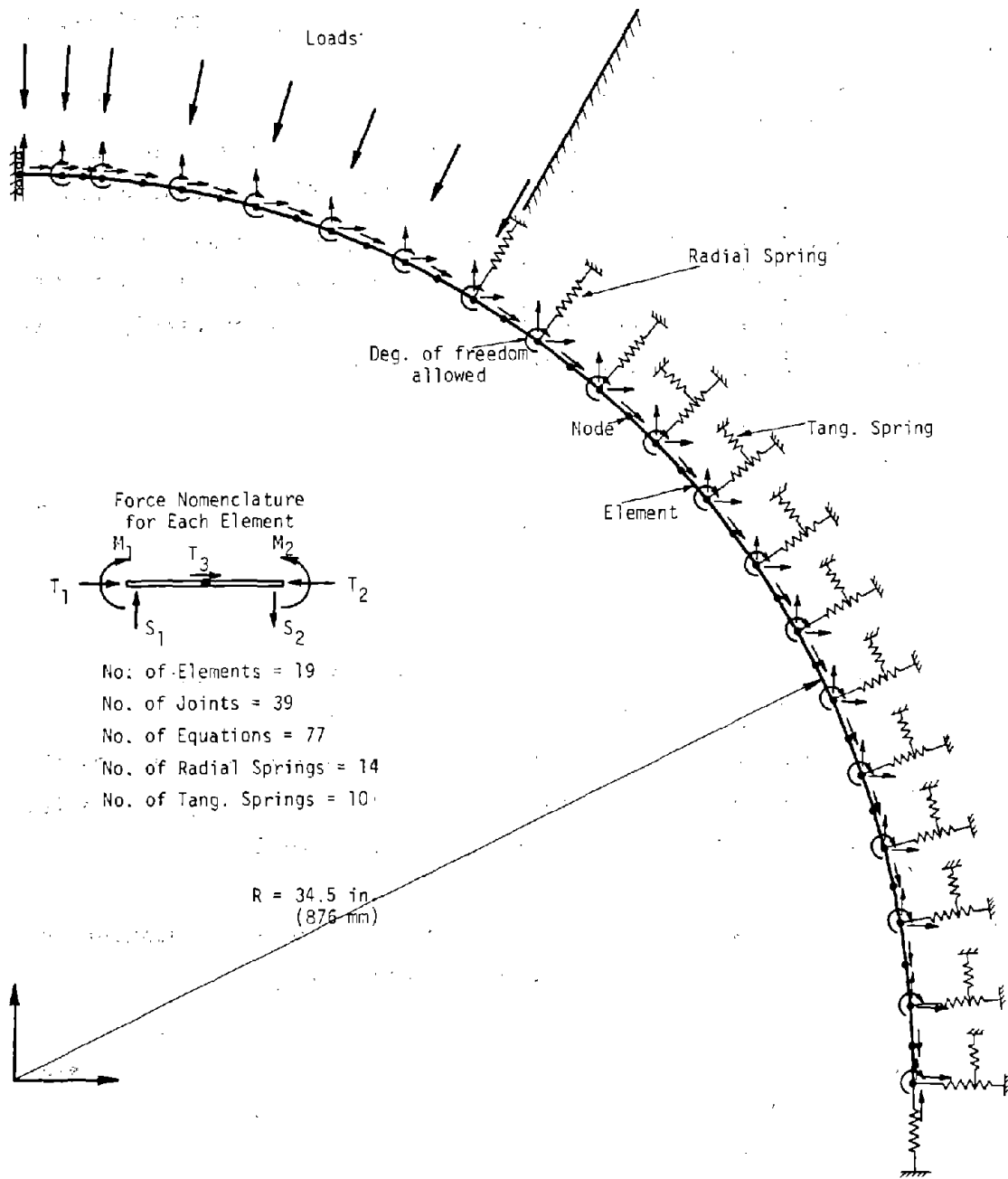


FIGURE 4.82 FINITE ELEMENT MODEL OF THE ARCH FOR SIMULATION OF TESTS

the values at Position B were used for the springs between 50 and 90 deg.

The modulus of subgrade reaction of the medium was approximated from the plain strain formulation of a semi-infinite elastic medium subjected to uniform pressure on a portion of its boundary. Once the shape of the loaded area is taken into account and also the fact that average rather than maximum deformations are considered, this approximate modulus of subgrade reaction is given by:

$$k = \frac{E_R}{2 C_o} \quad (4.2)$$

where

$E_R$  = in-situ modulus of elasticity of the rock mass (medium)

$k$  = modulus of subgrade reaction of the medium

$C_o$  = arc length of the arch that is under compressive load from the footing to the point where separation of lining and medium occurs (45 deg used, as indicated in Table 4.5).

The spring stiffness was obtained by multiplying the modulus of subgrade reaction by the tributary area for each spring:

$$K_r = k R b \theta \quad (4.3)$$

where

$K_r$  = radial spring stiffness representing the medium included by angle  $\theta$

$R$  = mean radius of the lining

$b$  = tunnel length under consideration

$\theta$  = angle subtended by the tributary area of spring.

The stiffness of the springs used varied from 86 kips/in. (15 kN/mm) for Arches-7 to 10 (with the lower modulus) to 1300 kips/in. (230 kN/mm) for Arches-1 to 6.

To determine the values for the tangential springs, the above radial springs were first used for the analysis of Arch-5 which did not need tangential springs; good correlation with the experimental results was obtained. A number of trial runs was then performed for the analysis of Arch-1, assigning a range of values for tangential spring stiffness. A tangential spring stiffness corresponding to 50 percent of the radial spring stiffness resulted in fairly good agreement with the experimental data in terms of failure load and crown deformation, though the analytic model gave larger deflections through the midrange of the loading. The value of 50 percent of the radial spring stiffness was then used in the analysis of Arches-1, 2, 3, and 4. For Arches-7 to 10 a tangential spring stiffness of 33 percent of the radial stiffness was obtained by first matching the experimental results for Arch-6, using the same tangential spring stiffness that was used in Arches-1 to 4. Once good agreement was obtained for Arch-6, the rigid block loading was reproduced by loading the center 30 deg region with 18 percent of the load at the outer 15 deg regions. This load shape was used in Arch-7 to assess the stiffness of the tangential springs.

The stiffness of the base springs that represent the load cell mechanism was determined from the measured base loads and deformations which were discussed in Section 4.3.3. The thickness of the specimens used in the analysis was the measured average thickness rather than the nominal values. These thickness values are given in Table 4.2.

The base spring stiffness used in the analysis for each test were the following:



Arch. No.	Base Spring Stiffness	
	k/in.	(kN/mm)
1	1050	(185)
2	800	(141)
3	1000	(177)
4	1350	(239)
5	1550	(274)
6	800	(141)
7	1620	(286)
8	1670	(295)
9	1065	(188)
10	1065	(188)

The stress-strain curve for the concrete was discretized as discussed in Chapter 3. The stress-strain curve was obtained by testing 6 by 12 in. (152 by 305 mm) cylinders in a 600 kip (2669 kN) capacity closed loop MTS hydraulic testing machine. The rate of the head movement was adjusted to 0.01 in./min (.2 mm/min). The ability to control the strain rate of the machine and its large stiffness relative to the specimen prevented destruction of the specimen at the peak load.

As described by Hudson, et al. (1971) in relation to rock specimens, "by using a testing machine with a relatively high longitudinal stiffness the sudden displacement accelerations are avoided as the machine elastically releases the stored strain energy during specimen failure." In other words, the energy that would be released by the stiff machine in an increment of displacement is insufficient to break the specimen, because the machine unloads more slowly than the specimen. If the testing machine is also closed-loop servo-controlled, a constant strain rate is achieved by the continuous operation of the closed-loop as the actual experimental condition is adjusted to coincide with a programmed constant strain rate; the machine can reduce the load faster than the specimen breaks, and sudden

failure is avoided. Combination of the stiff and servo-controlled characteristics provided complete stress-strain curves for the cylinders.

Cylinder deformation was measured with a 6 in. (152 mm) gage length compressometer centered at the midheight of the specimen. The compressometer consisted of two metal rings, 6 in. (152 mm) apart, attached to the specimen with 3 pointed set screws with provisions for measuring the relative movement of the rings with two diametrically opposite LVDT's (Linear Variable Differential Transformers). The output of the load cell of the testing machine, and the average output of the two LVDT's were plotted on the respective axes of an X-Y recorder. Thus, a continuous recording of the load and deformation was achieved.

The stress-strain curve was obtained from one of the load-deformation curves by dividing the load by the area of the cylinder, and the deformation by the 6 in. (152 mm) gage length. The maximum compressive strength determination may not be the same, since two different rates of loading are required for the two different types of tests.

Two compression stress-strain curves, one corresponding to the unconfined condition and the other corresponding to the confined condition near the crown were used. The peak of the confined curve was obtained by applying the results of tests performed by Richart, Brandtzaeg and Brown (1928). The applied contact pressure, was taken as equivalent hydrostatic confining pressure, and the new peak stress was calculated as  $f'_c + 4.1f_c$  where  $f'_c$  is the peak stress of the unconfined curve and  $f_c$  is the confining pressure. Once the peak of the confined curve was established, the descending branch was drawn following the shape of the unconfined curve, and the peak strain was increased according to the value obtained from the data presented by the authors noted above. Since the elements in the crown region were

confined by the loading plates, the confined stress-strain curve was used for these elements. The two curves were assumed to reach zero stress at very high strain, and to merge at that value. The tensile stress portion of the curves was assumed to have the same modulus as the initial slope of the compression curve, up to a peak stress equal to the modulus of rupture and then to maintain a horizontal slope thereafter. The value of modulus of rupture  $f^I$  was assumed to be 1.5 times the split tensile strength,  $f'_{sp}$  described in Section 4.2.4.

Very small load increments were used for the initial iterations, then subsequently larger values but no larger than 12 kips (53 kN) per increment were used. As the failure load was approached, the load increments were again reduced to a small value so that a better estimate of the failure load would be obtained.

#### 4.4.2 Comparison with Experimental Results

Load-deflection curves for the crown obtained from the analysis are compared with the test results in Figs. 4.27 through 4.34. In Table 4.7 the failure loads, maximum deflections and position of critical sections are compared. The load-deflection curves show good agreement between the initial slopes and load and deflection at failure, but in the midrange of loading, the deflections obtained from the analysis are larger than those from the tests. The agreement between location of failure sections in the tests and that predicted is quite acceptable. Better agreement could have been attained if some parameters were adjusted for each test, but this was not done to ensure uniformity. The radial and tangential spring stiffnesses discussed in Section 4.4.1 were used. The measured average stiffness was used for the springs at the footings in each test. The measured stress-strain curve for each test was used, and the same procedure was applied to this curve to obtain the confined concrete curve.

TABLE 4.7 COMPARISON OF MEASURED AND COMPUTED RESULTS

Test	Load Shape	Maximum Load kips (kN)		Maximum Deflection in. (mm)		Critical Secl., deg Meas.	Max. Shear Magnitude kips (kN)	Max. Shear Location deg
		Meas.	Comp.	Meas.	Comp.			
ARCH-1		180 (800)	183 (814)	0.184 (4.67)	0.184 (4.67)	35 RIGHT	13.2 (58.7)	30
ARCH-2		117 (520)	117 (520)	0.212 (5.38)	0.204 (5.18)	CROWN	12.7 (56.5)	15
ARCH-3		174 (774)	173 (770)	0.142 (3.61)	0.144 (3.66)	35 RIGHT	14.5 (64.5)	30
ARCH-4		119 (529)	112 (498)	0.179 (4.55)	0.179 (4.55)	15 & 40 LEFT	15.9 (70.7)	30
ARCH-5		114 (507)	120 (534)	0.375 (9.53)	0.282 (7.16) (CREEP)	35 LEFT	12.4 (55.1)	30
ARCH-6		190 (845)	188 (836)	0.105 (2.67)	0.101 (2.57)	35 RIGHT	23.1 (102.7)	30
ARCH-7		104 (463)	100 (445)	0.543 (13.79)	0.189 (4.80) (CREEP)	30 RIGHT	14.3 (63.6)	30
ARCH-8		111 (494)	102 (454)	0.372 (9.45)	0.401 (10.19)	35 LEFT & CROWN	10.7 (47.6)	30
ARCH-9		27 (120)	27 (120)	0.370 (9.40)	0.479 (12.17) (CRACKS)	35 LEFT	0.8 (3.6)	30
ARCH-10		31 (138)	27 (120)	0.570 (14.48)	0.481 (12.22) (CREEP)	CROWN	0.6 (2.7)	30

Near failure the agreement between measured and calculated load is better than the deformation in this range. The deformations near failure are very difficult to calculate and to measure, however. When the stress is very high, there is creep of the concrete after loading stops, so at each load increment the deflection depends on when the readings were taken, and how close to failure the load actually is. Also, when load stops and deformation continues, the load drops off. The computer analysis does not take into account concrete creep other than by modification of the stress-strain curve at high stress to give larger strain at a given stress. This is partially included by performing the cylinder tests from which the stress-strain curves were obtained very slowly, but the strain rate is still not the same as in the test; the rate is faster in the cylinder test than the average rate in the model tests. Therefore, good agreement of deformation near failure should not be expected.

Though the agreements between calculated and measured ultimate loads are good, there are reasons why they can be different. There is a time effect associated with the strength as well as deflection. There is a strength associated with a certain constant load rate; if a load, say 10 percent less than this, is applied and maintained, then failure will probably occur after some time has elapsed. If the load had been only 5 percent less than the constant rate strength, failure would also occur, but less time would be required. Consequently, the actual peak load measured depends on how close to the ultimate load the last increment happens to be and how long it is maintained. It has been found in column tests that failure will occur after considerable time when the load is 15 percent less than the short time ultimate.

The maximum shear was predicted by the analysis to occur at the edge of the loaded area for every test except Arch-2, which had the symmetrical triangular load, and for this one it occurred 15 deg on each side of the crown. The maximum computed shear from all the tests occurred in Arch-6, where the rigid block loading was used, because of

the greater concentration of load near the edges. Also, in the test of Arch-6 the failure appeared to have a greater shear component indicated by the diagonal failure surface, though the moment and thrust were quite high there also.

Prediction of failure by the analysis is demonstrated by the moment-thrust path and its location relative to the moment-thrust failure envelope or interaction diagram. Representative curves are shown in Figs. 4.83 to 4.85 for Arches-1, 3, and 7. Two envelopes are shown; one is calculated using the measured stress-strain curve for the concrete and the other using the same curve but with the stress and strain increased to account for the effect of confinement in compression by the loading plates (see Section 4.4.1). The confined curve only corresponds to failure conditions in the region near the crown (30 deg each side). The peak stress is sensitive to the confining pressure, and the magnitude of confining pressure selected for the curve may not be the actual one. The maximum value calculated from the peak load at the crown divided by the area loaded was used, but in reality the confining pressure varies with the load. This outer envelope should therefore, be considered an outer limit of the moment-thrust combinations in the crown region even though these combinations can go outside the inner envelope, which does not include the effects of confinement. On the other hand, the moment-thrust path for the lower part of the arch, where maximum compression stress occurs on the inside surface, should not go outside the inner envelope.

In Fig. 4.83 the moment-thrust path for the 35 deg section of Arch-1, where failure occurred in the test, terminates near the inner envelope indicating failure; the final point is slightly outside the envelope because of inaccuracies in calculating the envelope for these tests. The crown section path goes outside the inner envelope, but within the outer one so it does not indicate that failure would have occurred at the crown. These paths show that the moment was larger at the crown than at the 35 deg section.

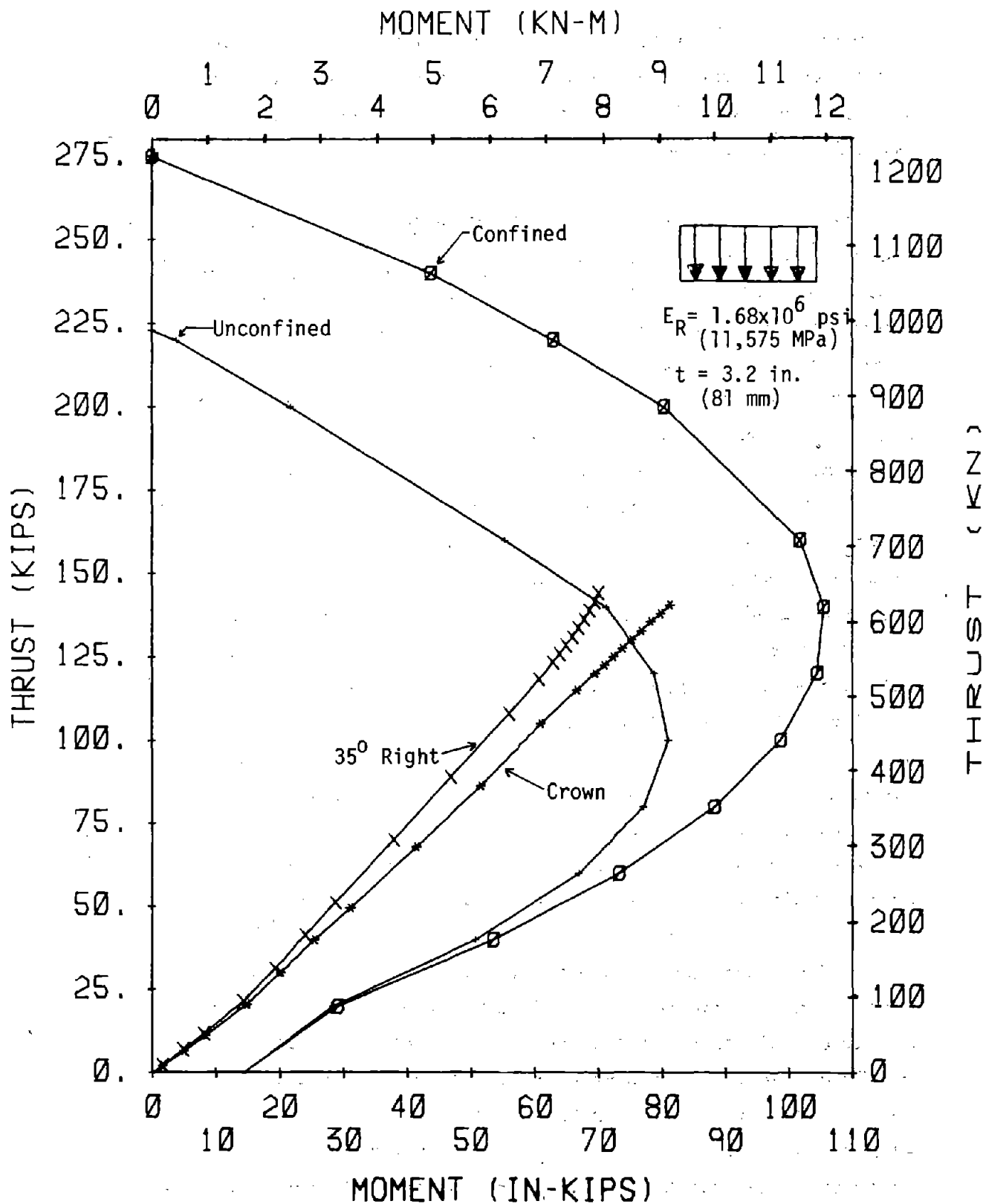


FIGURE 4.83 INTERACTION DIAGRAM OF ARCH 1

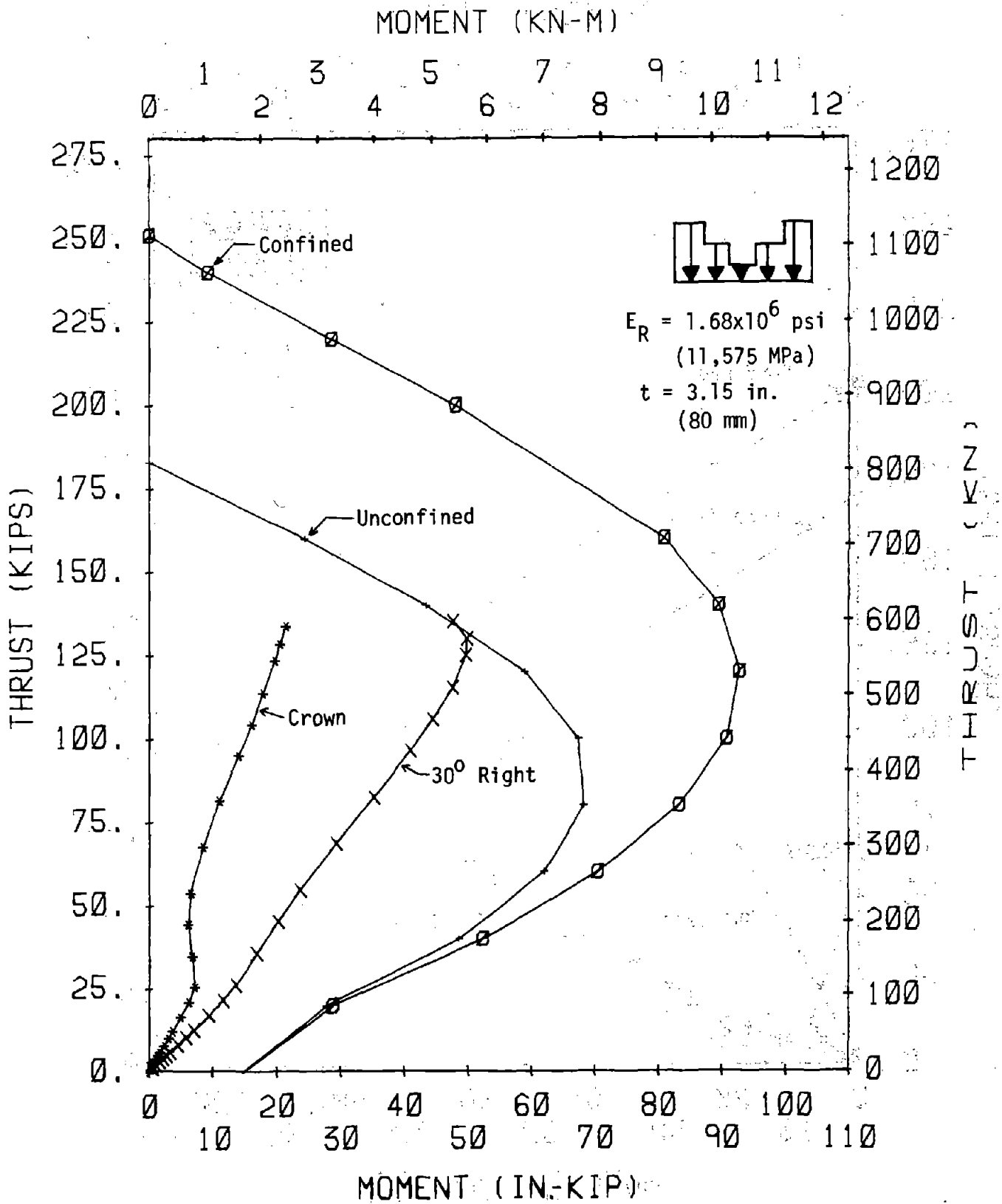


FIGURE 4.84 INTERACTION DIAGRAM OF ARCH 3



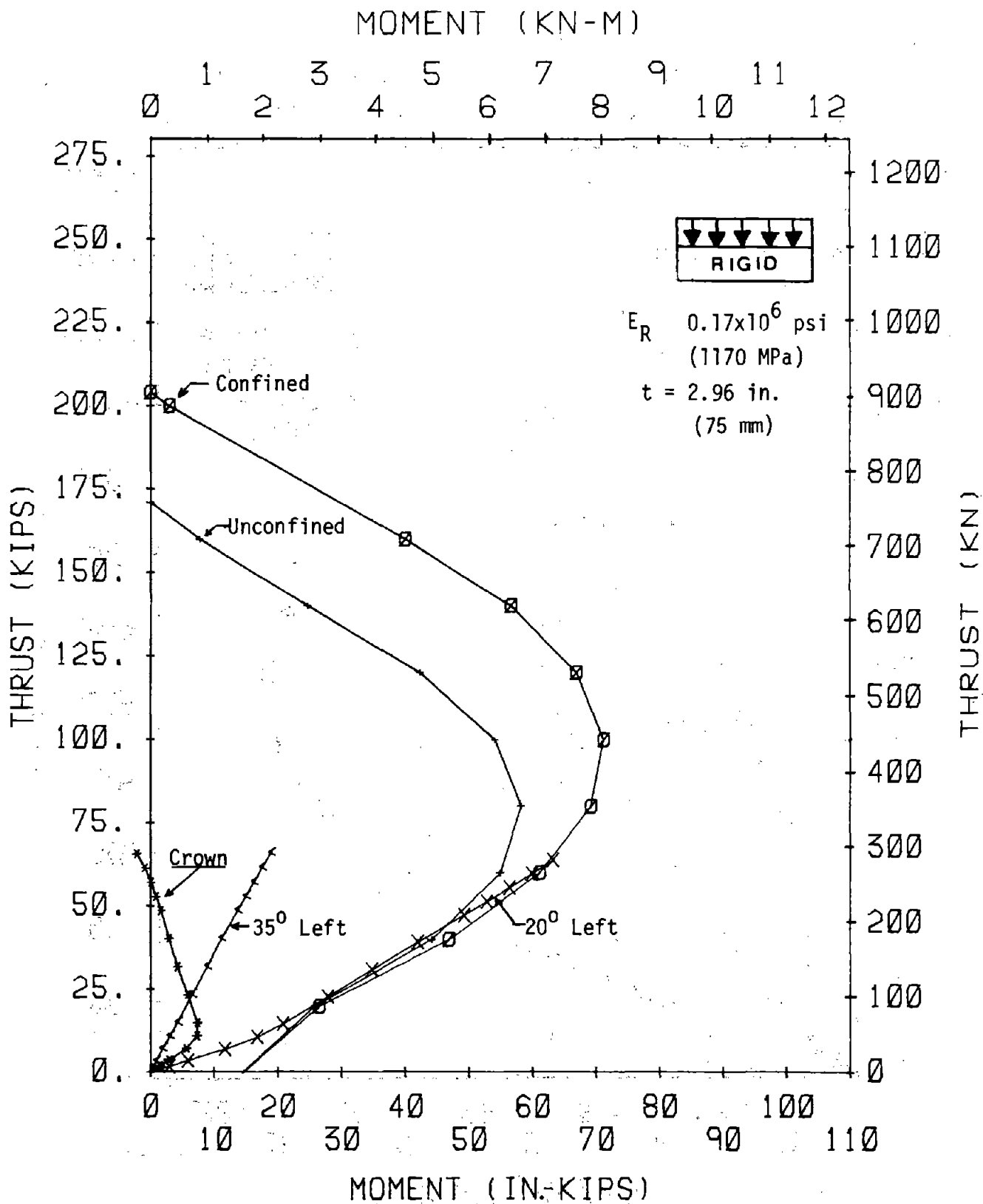


FIGURE 4.85 INTERACTION DIAGRAM OF ARCH 7

The crown and 30 deg section moment-thrust paths are shown for Arch-3 in Fig. 4.84 and indicate failure at the 30 deg section as occurred in the test. The load in this case was large at the sides of the loaded area and low at the center. This reduced the moment at the crown so that it was much less than that at the 30 deg section, so the crown section did not even reach the inner envelope. Also, this loading condition results in smaller moment at a given thrust at the 30 deg section than in Arch-1.

The moment-thrust paths for three sections in Arch-7 are shown in Fig. 4.85. This test was one of the two with the lowest flexibility ratio (the arch was stiffest relative to the medium) and the rigid block loading was applied. The results of this condition are shown by the moment-thrust paths and indicate a moment condition with steep gradients, because the moment is largest at 20 deg and much less at 35 deg and at the crown. Moment at the crown is small, indicating that the load was small there, and in fact the moment actually reversed its sign near failure. This is not unreasonable for this loading condition, and the deflected shape actually shows a reversal in curvature in this region in Fig. 4.48. The moment-thrust path at the failure section (20 deg) intersected the outer envelope below the balance point; in all other tests the intersection point for the critical section was above or only slightly below the balance point. For Arches-2, 5 and 8 the intersection was slightly below the balance point. This is significant because a linear analysis provides a reasonable estimate of the intersection point when it is above or near the balance point. This can be seen by extending the moment-thrust paths through the lower linear portions to an intersection and discounting the curvature near failure. In addition, the 20 deg moment-thrust path for Arch-7 followed the envelope in the low thrust region, and failure did not occur until the thrust reached about 65 kips (289 kN). This is characteristic of cases in which the path first reaches the envelope at a low thrust, and a linear prediction of the failure thrust would be much too low. In these cases a linear analysis

should not be used, but this case can be detected by examining the intersection points that result from the linear analysis.





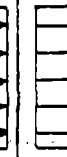


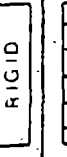
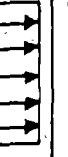

Prediction of failure by the analysis is good in all tests, provided it is realized that the outer envelope is a limiting case and when failure occurs at or near the crown, the moment-thrust must lie between the two envelopes.

#### 4.5 DISCUSSION OF TEST RESULTS

The test results are summarized in Table 4.8. In Section 2.3 the applicability of model test results to full scale structures was discussed. It was found that conclusions drawn by comparing the model tests may be applied to full scale arches in the ground once appropriate scale factors are applied, the loads are applied to the arch in the same way as the model, and certain other conditions concerning material properties are satisfied. Also, in the comparisons it should be realized that there is scatter in test results because of unknown factors. If any particular test was duplicated several times, the same result would not be obtained each time. Only one test was performed for each condition, and it is not certain whether the result of that test is at the high, low or middle of the range that would result from several tests. This experimental error should be kept in mind. Any disturbing influence that affected the test results is probably present equally in all tests so the comparison among tests is valid.

The load shape that gave the lowest  $T_u/T_o$  ratio was the symmetrical triangle for the test with  $F = 1200$  and interlocking at the sides (Table 4.8). However, the range was only from 0.60 to 0.69 with the uniform load providing the largest ratio; this is only a variation of 15 percent. This comparison is made for a particular flexibility ratio of 1200, but at a value of 120, two load shapes were tested (Arches-7 and 8), and the  $T_u/T_o$  was 0.37 and 0.42 or a difference of 14 percent.

TABLE 4.8 SUMMARY OF ARCH TEST RESULTS

Test Designation	Loading Shape	Flexib. Ratio	Tang. Shear	Reinf.	Thrust Ratio $P_u/P_c$	$\Delta R/R\%$	Cracking Load % of Ultimate
ARCH-1					0.69	0.53	NO CRACKS
ARCH-2			YES		0.60	0.61	50
ARCH-3		1200			0.67	0.41	NO CRACKS
ARCH-4				NO	0.64	0.52	NO CRACKS
ARCH-5			NO		0.52	1.09	80
ARCH-6					0.64	0.30	NO CRACKS
ARCH-7		120			0.37	1.50	40
ARCH-8			YES		0.42	1.03	60
ARCH-9		3650			0.62	1.03	85
ARCH-10				YES	0.65	1.60	80

so the above conclusion may be valid for lower flexibility ratios as well. Comparing the  $T/T_u$  ratio does not tell the full story when comparing load shapes because the load depends on the geology and opening size, and the total load that can occur is not the same for each shape. This will be discussed in more detail in Chapter 5.

The load shape did have a pronounced effect on the failure mechanism of the linings. In Arch-2, where the load was of triangular shape, the lining exhibited a more ductile "flexural" type of failure whereas Arches-1, 3 and 4 failed more abruptly. This could be significant in the field where a triangular type of loading may provide some indication of lining distress near failure (i.e., cracking) whereas other load shapes may cause sudden failure without preliminary signs or warning. With the exception of the case where load was concentrated in the middle (Arch-2) and in Arch-10 (reinforced w/uniform load), where failure occurred by crushing at the crown, failure took place at the edge of the loaded region (35 deg from the crown).

The load shape also had an effect on the deformability of the lining with the rigid block loading (Arch-6) exhibiting the smallest ductility as shown in Table 4.8.

The effect of tangential shear is shown by comparing Arches-1 and 5 which have the same flexibility ratio. Removal of the tangential interlock reduced  $T/T_u$  from 0.69 (Arch-1) to 0.52 (Arch-5) or a reduction of 33 percent. In an actual tunnel the tangential stress conditions are somewhere between full interlock and full-slip. Consequently, the thrust ratio should be expected to be between these two values for the same range of flexibility ratio.

The removal of tangential shear leads to larger deflection of the arch which allows the crown region to flatten more.

The flatter arch leads to greater thrust but the deflection results in even larger moment so the moment-thrust path is lower on the moment-thrust interaction diagram. It can also be said that the eccentricity of thrust in the arch, which is the moment divided by the thrust, is larger.

Tangential shear between the lining and medium also affects the amount of applied load that reaches the base of the arch. This base load varied from 5 percent, when no-slippage occurred between the lining and the medium, to 20-30 percent after slip occurred. The base load increased to more than 100 percent in the case of low tangential shear (Arch-5) and low rock modulus (Arches-7 to 10). Reasoning for this large base load was provided in Section 4.3.3. The magnitude of applied load reaching the base could be important in determining the size of the footings.

The medium modulus and lining thickness are incorporated in the flexibility ratio, which has a marked effect on  $T_u/T_o$  as shown in Fig. 4.86. There is a problem with the comparison, however, because at  $F = 1200$  the full interlock and no interlock cases were tested, while at  $F = 120$  and  $3650$  the rubber was used between the lining and medium, which would be equivalent to a partial interlock between these extremes. By trial and error, in trying to match the analysis with experimental results, it was determined that these latter cases with the rubber corresponded to a tangential shear stiffness that was about 33 percent of the radial stiffness, so the curve shown in Fig. 4.86 is drawn 1/3 of the way between Arch-5 (full-slip) and Arch-1 (full interlock). The resulting curve is then for the same interlock condition and uniform loading. For this loading case  $T_u/T_o$  varied from 0.42 at  $F = 120$  to 0.62 at  $F = 3650$  or a range of 0.20. Also, the curve is rather flat beyond  $F = 2000$ , which would indicate that there is an upper limit for  $T_u/T_o$  which is about 0.62 for the uniform load case in good quality rock. This conclusion is based on the assumption made at  $F = 1200$  to draw the curve, but any assumption made will result in a fairly flat

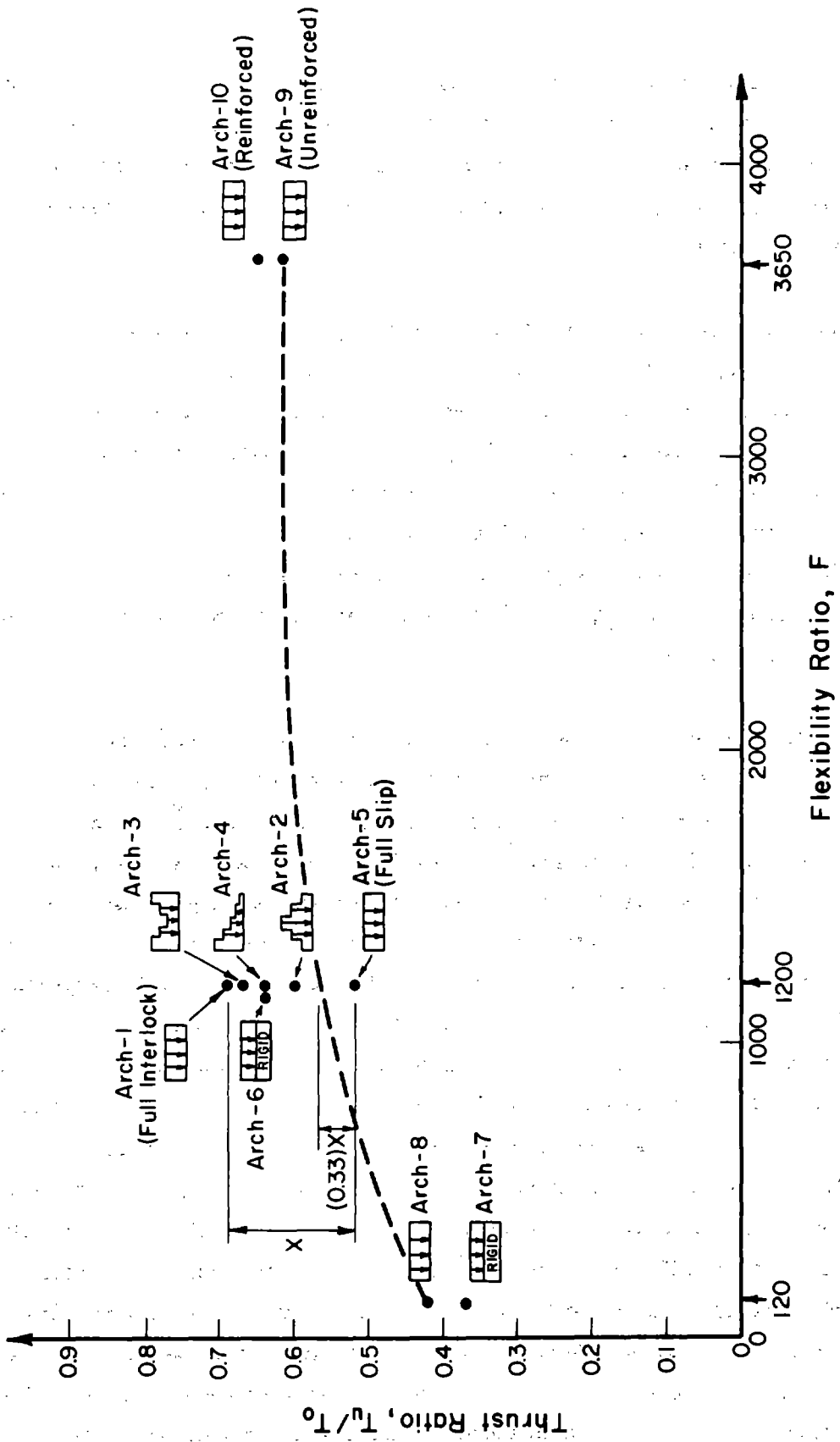


FIGURE 4.86 EFFECTS OF LOADING SHAPE AND FLEXIBILITY RATIO ON THE THRUST RATIO

curve. It may reasonably be expected that there is a similar limit for other load shapes or other tangential shear conditions. Therefore, a minimum amount of moment should be expected in the lining, no matter how high the value of rock modulus. This moment causes the thrust ratio to drop from 1.0 (no moment) to 0.62.

Cracking characteristics of the test specimens are summarized in Table 4.6 and Fig. 4.87. Flexural tension cracks did not occur in 4 tests. In all tests that had cracking except Arch-7, it first appeared at or above 50 percent of the ultimate load. In these cases if there existed a safety factor against failure of at least 2.0, then the working load would be below 50 percent of the ultimate, so cracking would not occur at service load. In reality cracks would be less likely to occur in the ground due to flexure than shown by these model tests because creep was less in the tests. When the compression zone of the concrete section creeps with time as the load is applied slowly, this zone shortens and the tension stress present on the other side of the section is relieved. Also, if the tension stress is applied over a long period, the concrete can creep in tension and a larger strain is required to cause cracking than would have occurred if the tension had been applied faster.

There is a definite increase in the tendency toward cracking as the flexibility ratio becomes smaller, as shown in Fig. 4.87. This results from larger deformation and larger moment, which is consistent with the effect of flexibility ratio discussed above. In Arch-7 where cracking occurred at 40 percent of the ultimate load, the smallest flexibility ratio was combined with the loading that provided the greatest concentration. In most of the tests in which cracking occurred, the width of the crack remained small during loading, and only started to open significantly near failure.

Reinforcement had little influence on the strength of Arch-10, which was the companion test of uniformly loaded Arch-9 that did not



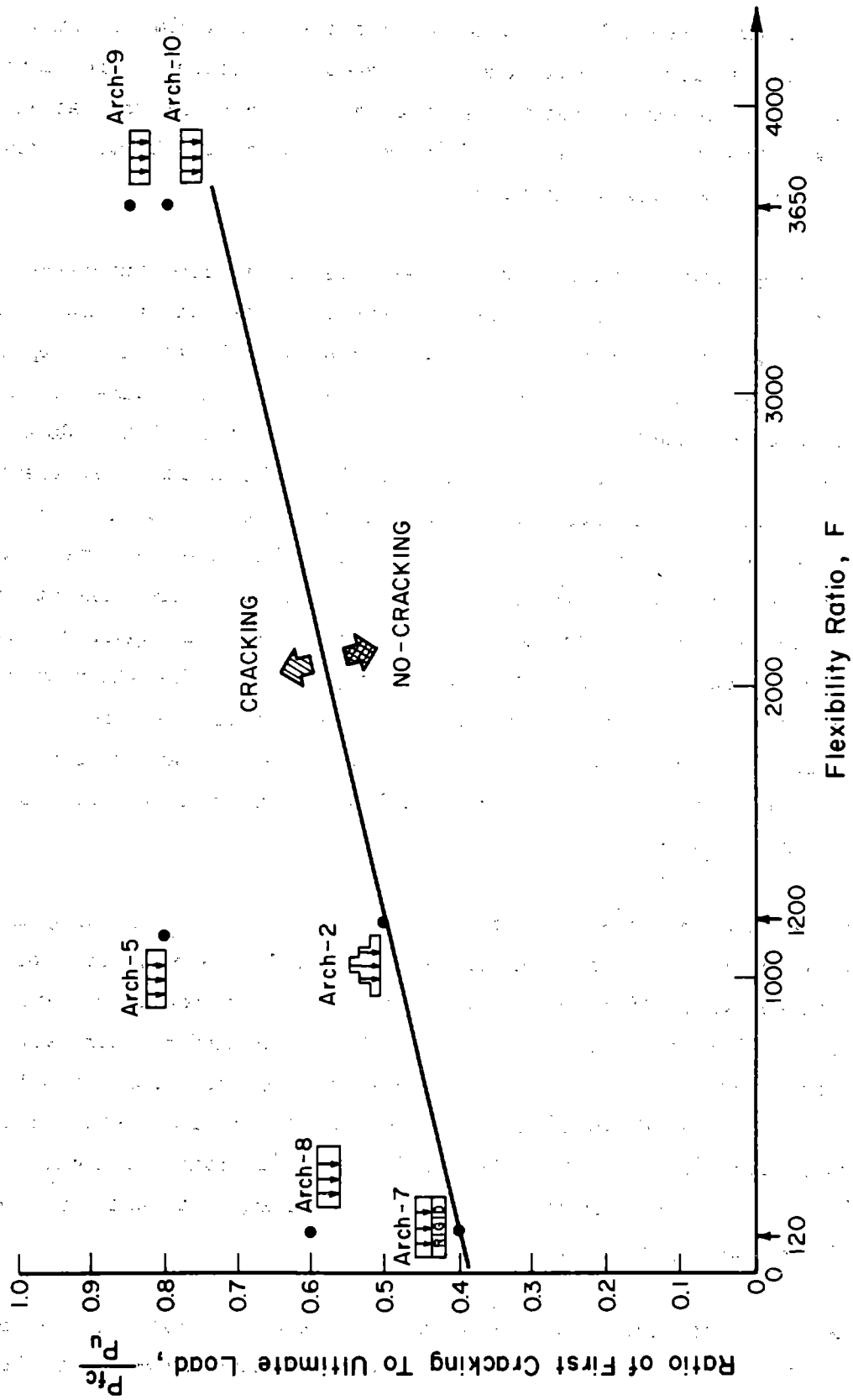


FIGURE 4.87 FIRST CRACKING AS A FUNCTION OF FLEXIBILITY RATIO

have reinforcement. The normalized load for Arch-9 was 44 kips (196 kN), while that for Arch-10 was 45 kips (200 kN). The reinforcement ratio was 0.010 and the reinforcement area was then  $0.0614 \text{ in.}^2$  ( $42 \text{ mm}^2$ ); if all the bars reached their yield stress they could resist a thrust of 2.5 kips (11 kN) so it is reasonable that this thrust would result in a small increase in load. By comparing the general appearance of the cracks for Arch-10 in Fig. 4.58 with those of Arch-2 in Fig. 4.39 and Arch-5 in Fig. 4.40, it appears that the reinforcement serves to distribute the cracks and by so doing keep them finer. When no reinforcement was present only one or two cracks appeared in a high moment region, and when there were more than one, generally only one of them opened significantly while the others remained fairly small. However, in Arch-10 with reinforcement, 4 cracks formed that were approximately evenly spaced and each of them opened at about the same rate. This observation can be made from other tests of reinforced concrete members as well, but it is not as clear from comparing Arches-9 and 10, from which the assessment of effects of reinforcement was intended to be made because there was little flexural cracking in Arch-9. This is consistent with other measurements, however; for example the deflection was not as great in Arch-9 as shown by the load-deflection curves that are compared in Fig. 4.34. These curves demonstrate also that near failure reinforcement helped the failed region hold together for a little more deflection at nearly constant load.

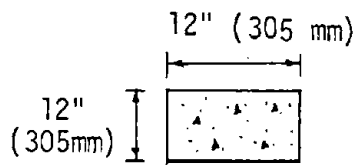
It can be concluded that from a purely strength point of view, reinforcement does not seem to improve the load carrying capacity of the lining. However, as size of the tunnel opening increases and the degree of design uncertainty increases as well, the inclusion of reinforcement might be necessary to guard against localized failures.

## 5. PARAMETER STUDY FOR ARCHES IN ROCK

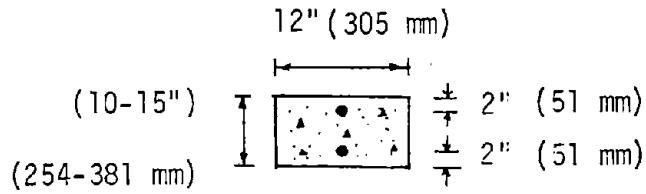
### 5.1 DESCRIPTION OF THE STUDY

The analysis program described in Chapter 3 was used to investigate the effects of flexibility ratio  $F$ , radius divided by thickness  $R/t$ , tangential stiffness to radial stiffness ratio for the medium  $K_t/K_r$  and load shape on typical full scale station configurations using a beam-spring model. The finite element model used is shown in Fig. 5.1a and has radii of 20, 25 and 30 ft (6.1, 7.6, 9.1 m), thicknesses of 10, 12 and 15 in. (254, 305, 381 mm) and a concrete compressive strength of 4000 psi (27.6 MPa) with a curve shape similar to that in Fig. 5.1b. Most of the study was performed for a typically 12 in. (305 mm) thick arch of 25 ft (7.6 m) radius with a uniform load across the full arch, and several problems were worked with a symmetrical triangular load over the center 60 deg portion of the arch; to investigate further the effect of load shape one problem with uniform load over the 60 deg portion and one with uniform load over the right one-half of the arch were worked. The radius and thickness were varied in some problems to study their effects, while keeping the  $K_t/K_r$  ratio constant at 0.25. These solutions were for arch sections with one-half percent reinforcement in each face, and then a series of solutions were obtained for an unreinforced section for the full range of flexibility ratios and one value of tangential shear stiffness ratio ( $K_t/K_r = 25$  percent).

The medium has been represented by radial and tangential springs. The tangential springs are assigned certain percentages of the radial spring stiffnesses to represent the shear transfer between the lining and rock. The radial spring stiffness is derived from reasonable approximations of the plain strain formulation of the modulus of subgrade reaction which takes into account the area loaded. This approximate modulus of subgrade reaction is given by Eq. 4.2 and the spring stiffness by Eq. 4.3.



$f'_c = 4.0 \text{ ksi (28 MPa)}$   
 $T_o = 576 \text{ ksi (2562 kN)}$



$f'_c = 4.0 \text{ ksi (28 MPa)}$   
 $f_y = 40 \text{ ksi (276 MPa)}$   
 $A_s = A'_s = 0.48 \text{ in}^2 (3.0 \text{ mm}^2)$   
 $T_o = 5.8.4 \text{ kips (2036 kN)}$   
 $A_s = A'_s = 0.78 \text{ in}^2 (503 \text{ mm}^2)$   
 $T_o = 782.4 \text{ kips (3480 kN)}$

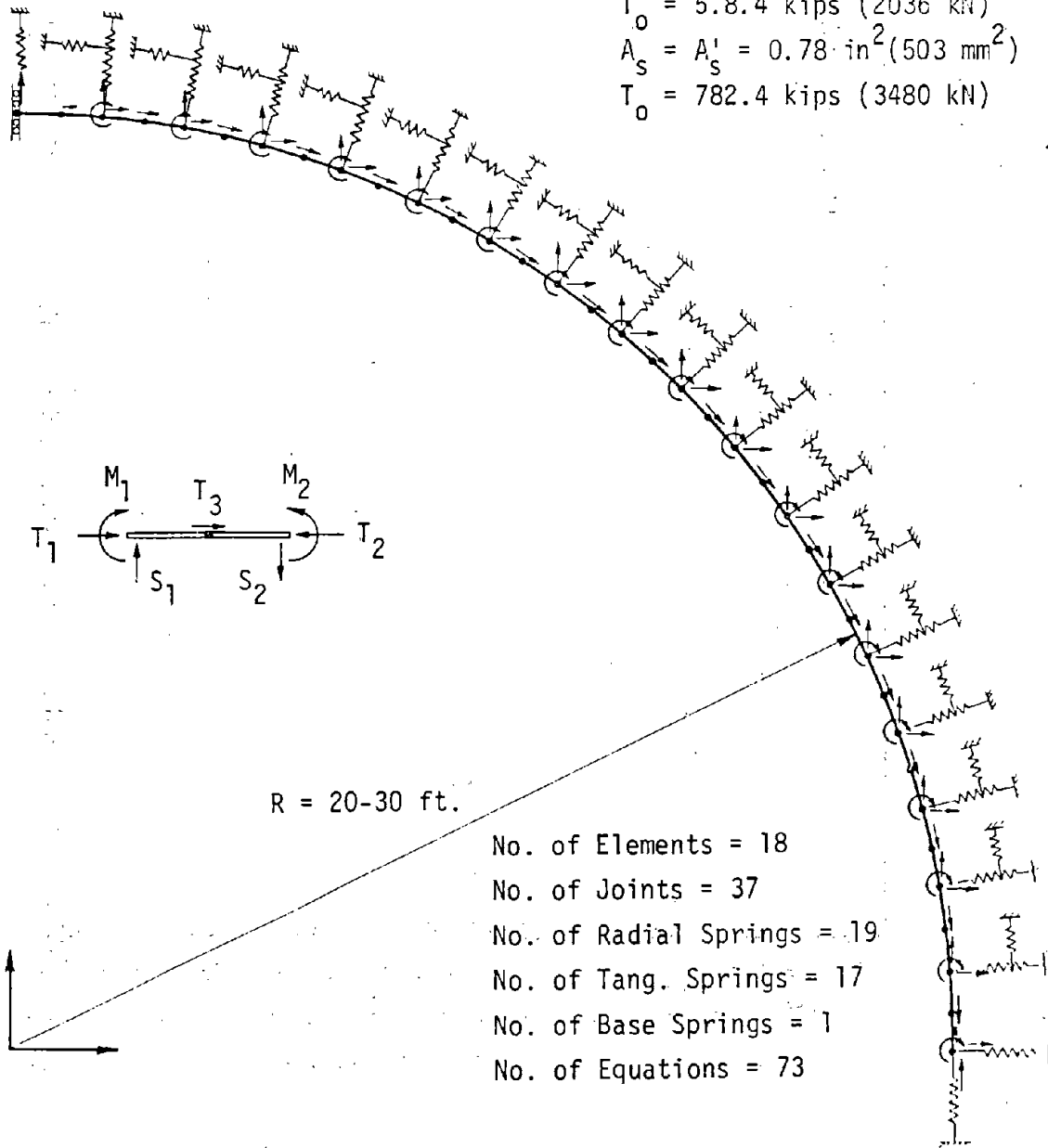


FIGURE 5.1a FINITE ELEMENT MODEL FOR PARAMETER STUDIES OF ARCHES

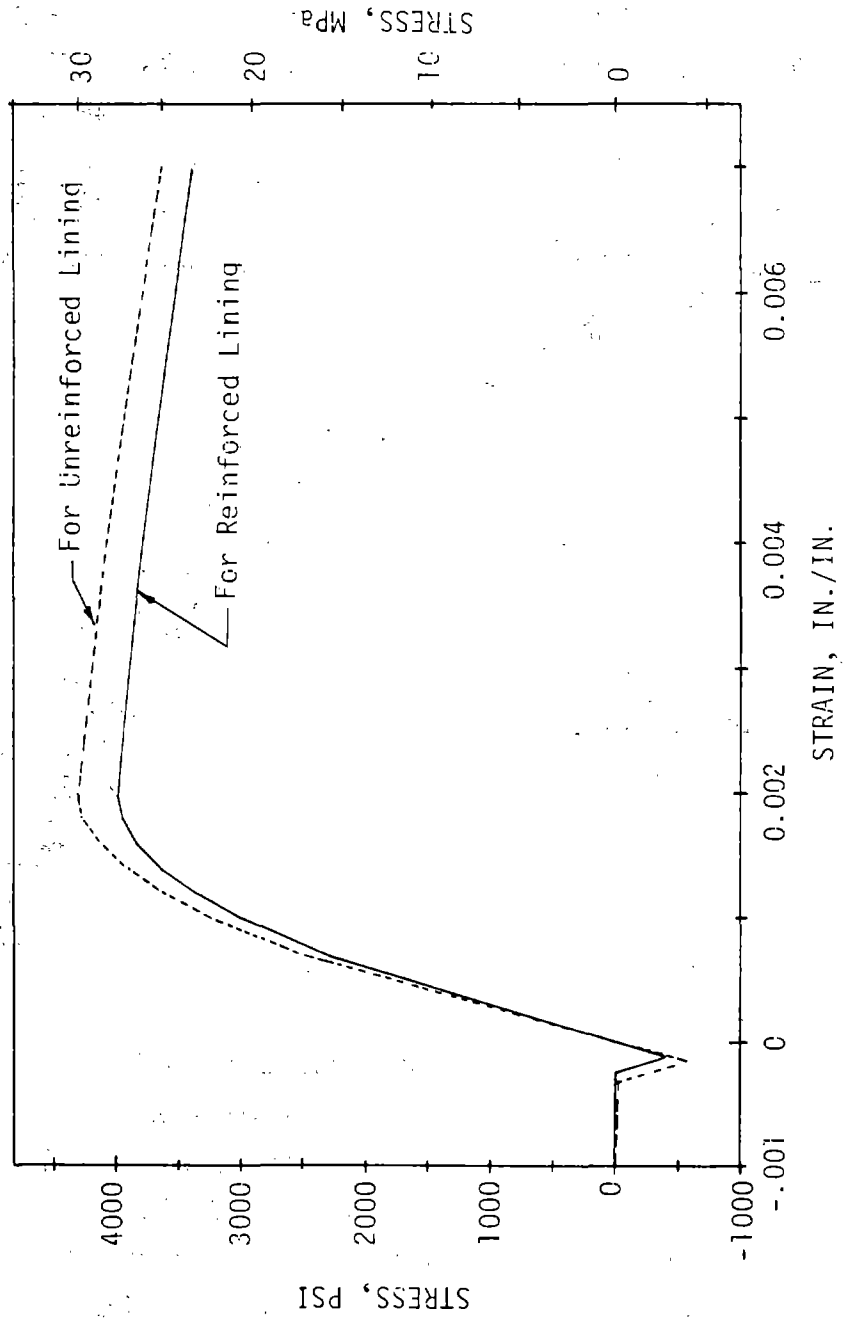


FIGURE 5.1b CONCRETE STRESS-STRAIN CURVE USED IN THE PARAMETER STUDY

The medium under the footing of the arch is also represented by a spring. The stiffness of this base spring is computed from the subgrade modulus as below:

$$K_F = k \cdot C_1 \cdot b = \frac{E_R}{2 \cdot C_1} (C_1 \cdot b) = \frac{E_R \cdot b}{2}$$

where

$K_F$  = stiffness of the base spring that represents the footing, kips/in. (kN/mm)

$k$  = modulus of subgrade reaction, lb/in.<sup>3</sup> (N/mm<sup>3</sup>)

$C_1$  = width of the footing, in. (mm)

$b$  = tunnel length under consideration

$E_R$  = in-situ modulus of elasticity of the rock mass.

The shear stress at the interface depends on degree of roughness of the exposed rock surface, size and shape of the asperities, strength of the rock, magnitude of radial stress, etc. For this study the ratio of tangential stiffness to radial stiffness ( $K_t/K_r$ ) of the springs was varied from 0 to 0.25 to investigate the effect of this parameter.

Vertical loosening or gravity type loading has been used by applying them directly to the lining at the nodes joining each beam element. Thus, the representation of the medium by springs combined with the loosening type of loading does not allow that part of the medium structure interaction to be represented that allows arching in the ground around the lining as discussed in Chapter 2. However, since a loosening type loading is the reasonable type of loading that actually reaches the arches in rock, the spring model represents the interaction quite adequately.

## 5.2 EFFECT OF LOADING SHAPES

In Fig. 5.2 the moment-thrust paths are shown on the interaction diagram for a flexibility ratio of 3500, lining thickness of 12 in. (305 mm), radius of 25 ft (7.6 m) and various load shapes. The symmetrical uniform load that covers the full span induces the smallest moment and therefore the largest thrust before failure. The triangular load over the central 60 deg arc induces the largest moment at the crown and consequently the smallest thrust and load at failure. The other two loading conditions fall between these two extremes with the unsymmetrical uniform load causing very nearly as much moment as the triangular load. However, maximum loads that can occur depend on the geologic conditions that tend to cause various loads as described in Section 4.2.2; if joint sets are assumed to occur in both directions relative to the vertical, a triangular wedge of rock depicted by the triangular load could occur about one radius wide at the base and have a height of about one-third diameter. The total weight per foot of tunnel for 50 ft (15.2 m) diameter would then be 31.25 kips (139 kN) if the rock is assumed to weigh 150 lb/ft<sup>3</sup> (2400 kg/m<sup>3</sup>). The total load at failure from the analysis was 277 kips (1232 kN), so there is a safety factor of 8.8 against failure. If, however, the uniform load completely across the lining is assumed to represent a vertical depth of rock of one diameter, the total weight is 375 kips (1668 kN) per foot of tunnel. At failure the load was 992.5 kips (4415 kN) so the safety factor is 2.6 for this loading. This comparison shows that the triangular load is less critical though it produces more moment in the lining and thus results in failure at a smaller thrust and smaller total load (Fig. 5.2). The following summary of safety factors, for all four loads in which the vertical dimension of the rock block is assumed to be the same as the horizontal dimension for the uniform loads, show that the loading providing the smallest safety factor is the uniform load across the arch.

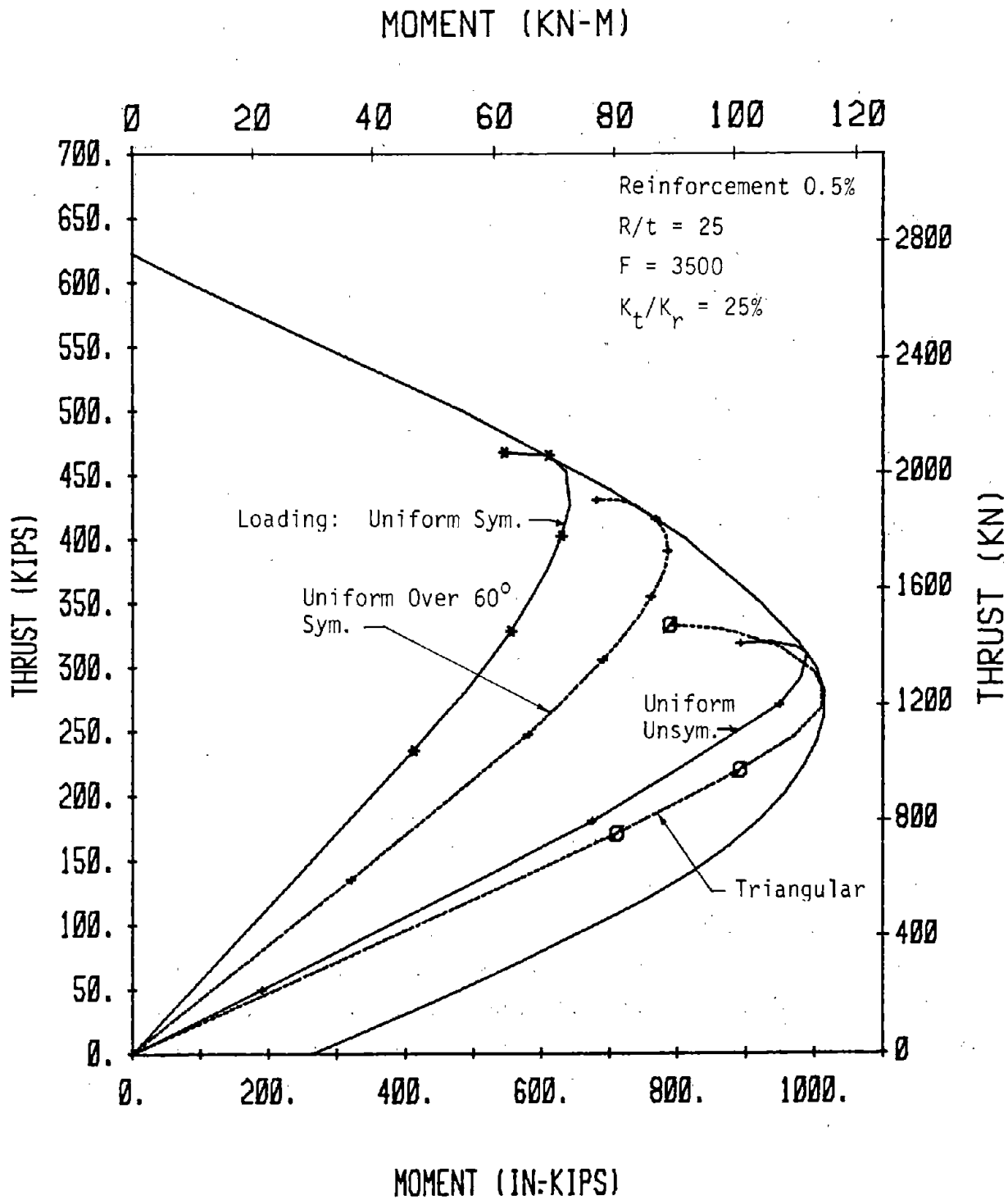


FIGURE 5.2 MOMENT-THRUST PATHS FOR CRITICAL SECTION FOR VARIOUS LOAD SHAPES



Load Shape	Rock Load		Failure Load from Analysis		Safety Factor
	kips	(kN)	kips	(kN)	
Triangle	31.25	(139)	277	(1232)	8.8
Partial, uniform Symmetrical	93.75	(417)	468	(2082)	5.0
Partial, uniform Unsymmetrical	93.75	(417)	452.5	(2013)	4.8
Full uniform	375.0	(1668)	992.5	(4415)	2.6

Arbitrary dimensions of rock blocks have been assumed, and in reality they would depend on actual field conditions, but they are reasonable and show that the condition providing the greatest total load tends to be most severe. For all the symmetrical loadings the critical section occurred at the crown, and for the unsymmetrical one it occurred on the loaded side of the crown.

### 5.3 EFFECT OF FLEXIBILITY RATIO F

Figures 5.3, 5.4 and 5.5 show the effect of flexibility ratio on the moment-thrust paths and consequently on the strength and behavior of the 12 in. (305 mm) thick lining for the three values of  $K_t/K_r$  and the full uniform load. In Fig. 5.3, where  $K_t/K_r = 0$  the effect of F is smaller than in the other two figures where  $K_t/K_r$  is 0.125 and 0.25. Therefore, part of the increase in strength that appears to result from increasing F in the latter figures actually result from increased shear stiffness.

The effect of F on total load on the lining for two loading shapes are shown in Fig. 5.6 where the same comparison concerning  $K_t/K_r$  is apparent. The vertical axis is changed to  $T_u/T_o$  in Fig. 5.7, but the curve shapes are very similar because the total load and the ratio

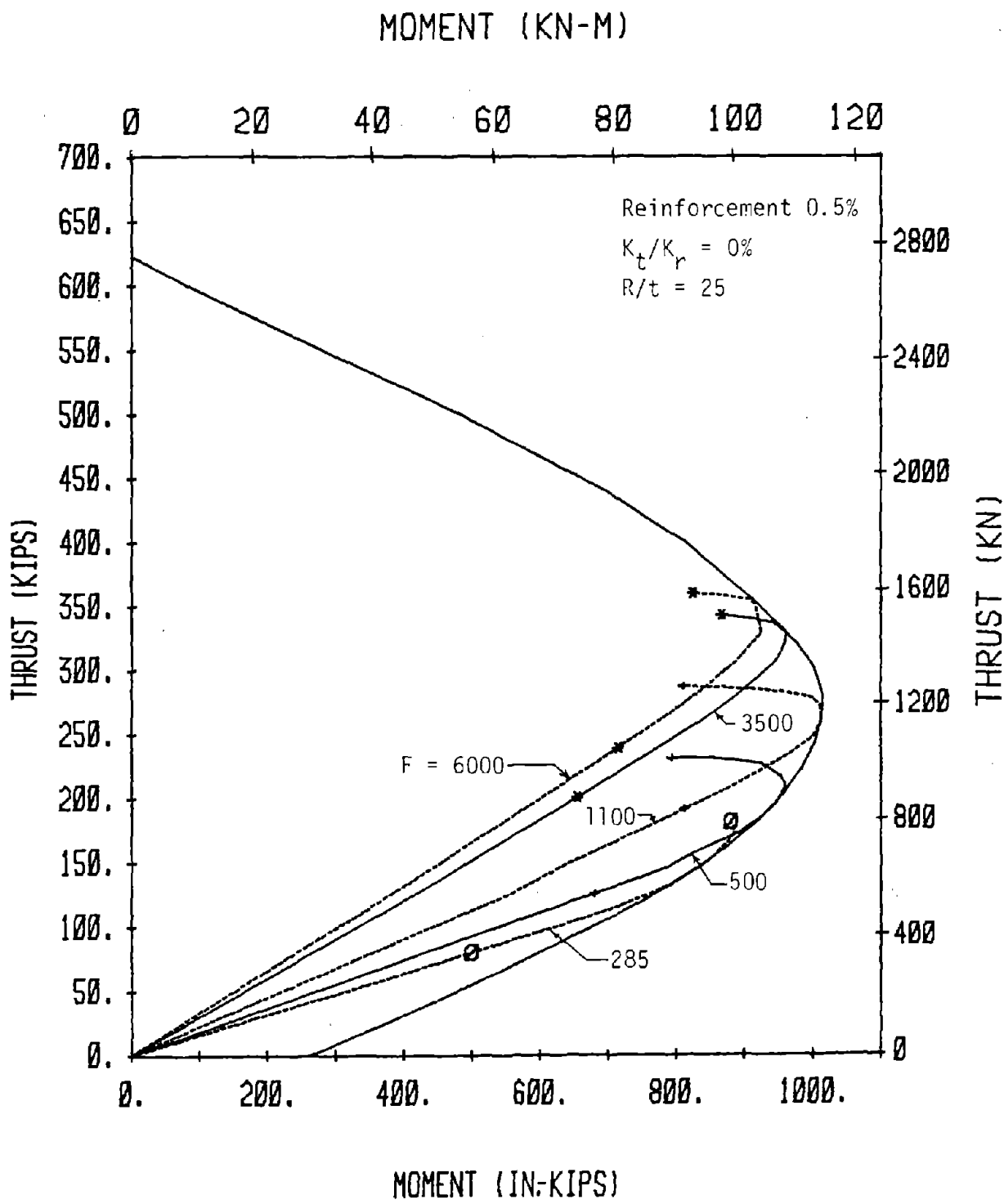


FIGURE 5.3 MOMENT-THRUST PATHS FOR  $K_t/K_r = 0$  AND VARIOUS FLEXIBILITY RATIOS

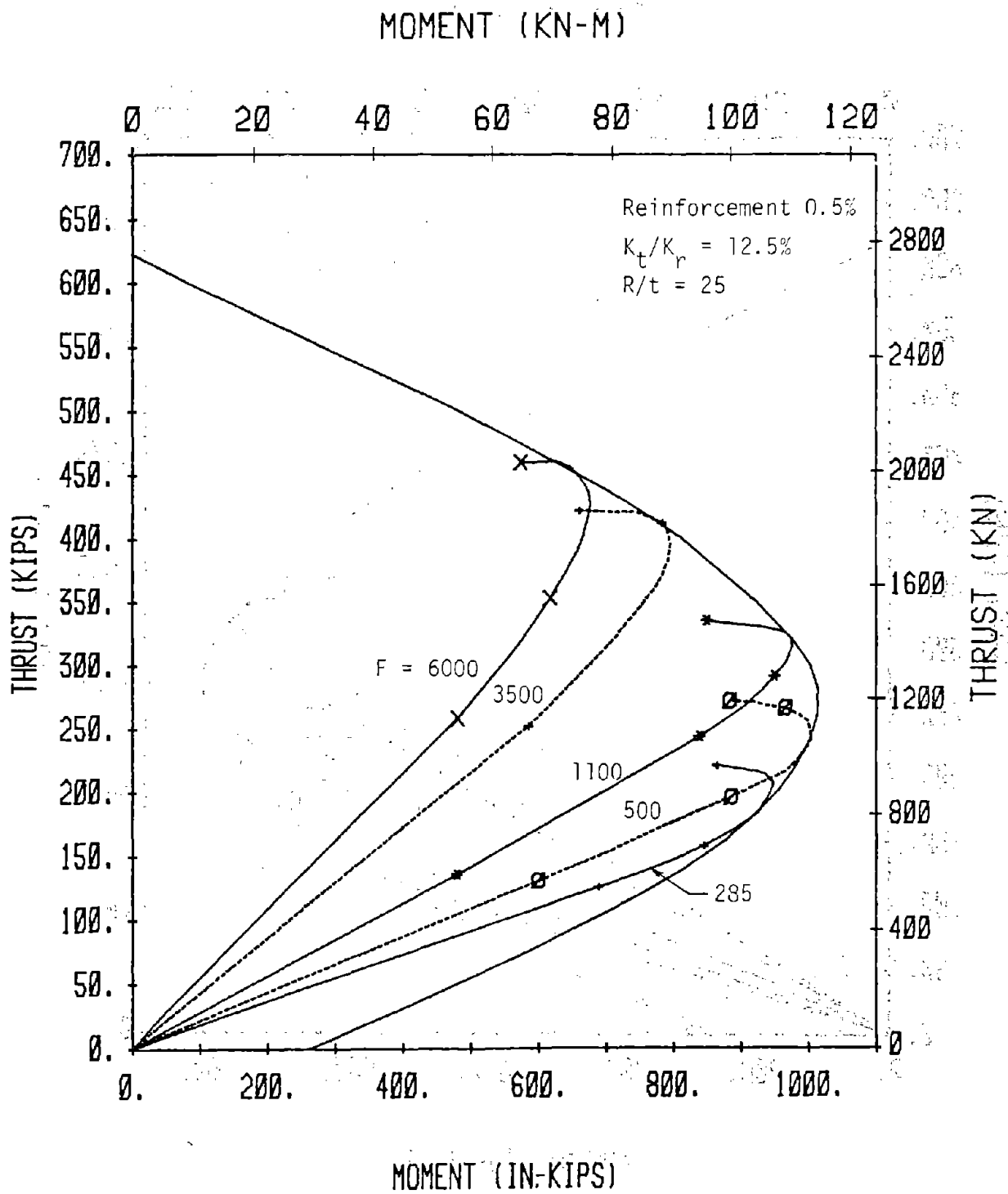


FIGURE 5.4 MOMENT-THRUST PATHS FOR  $K_t/K_r = 12.5\%$  AND VARIOUS FLEXIBILITY RATIOS

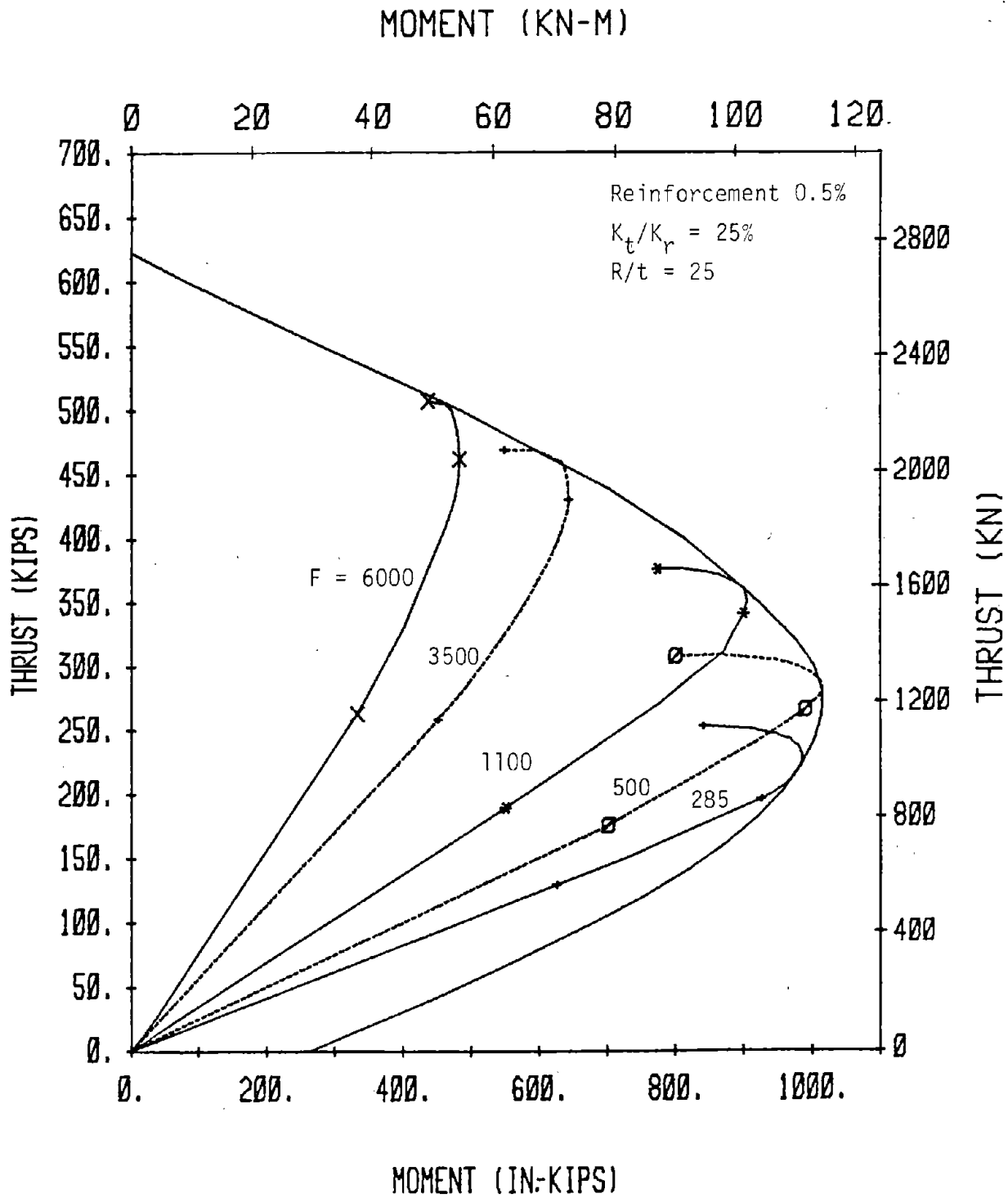


FIGURE 5.5 MOMENT-THRUST PATHS FOR  $K_t/K_r = 25\%$  AND VARIOUS FLEXIBILITY RATIOS

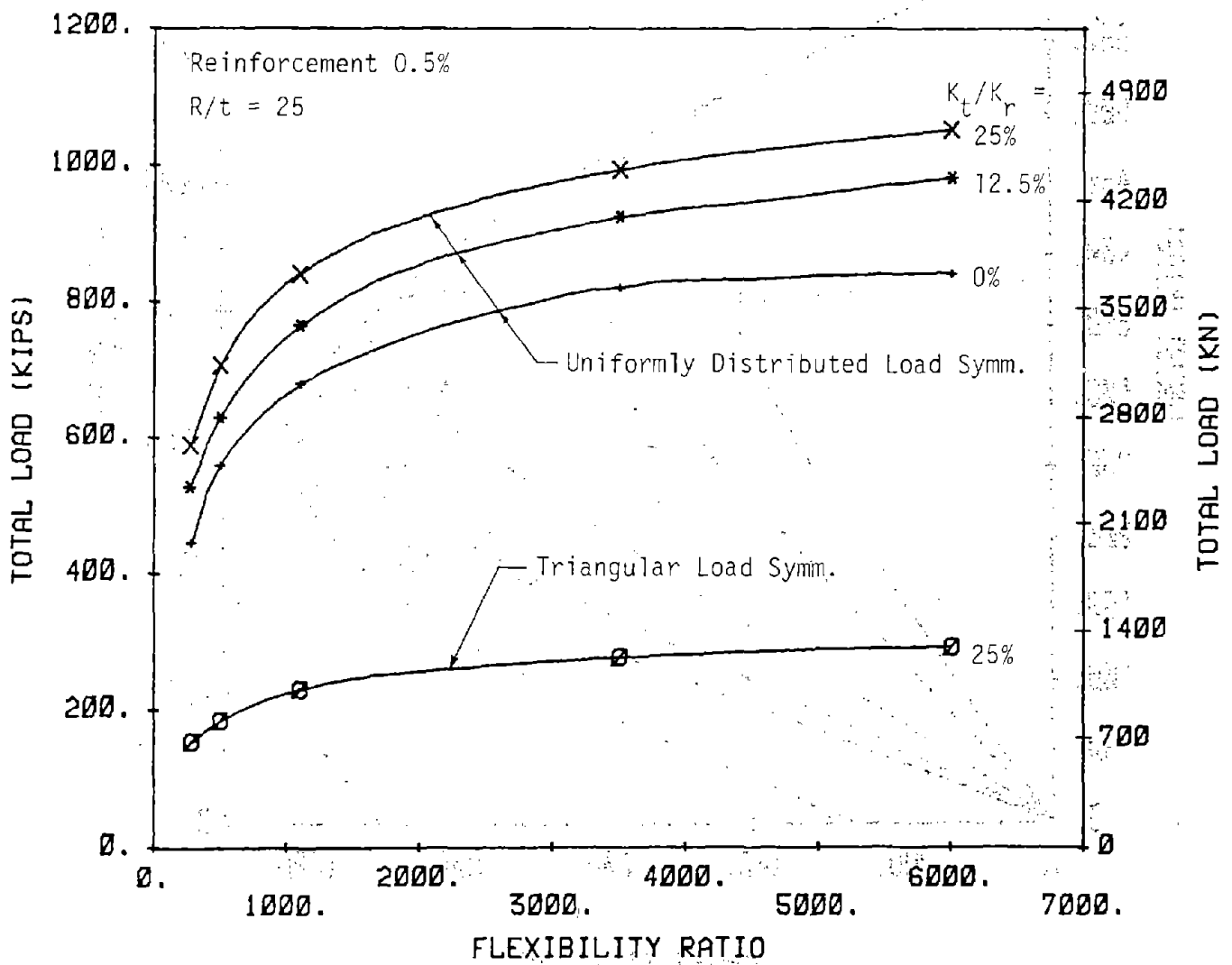


FIGURE 5.6 TOTAL LOAD VS FLEXIBILITY RATIO FOR ARCHES

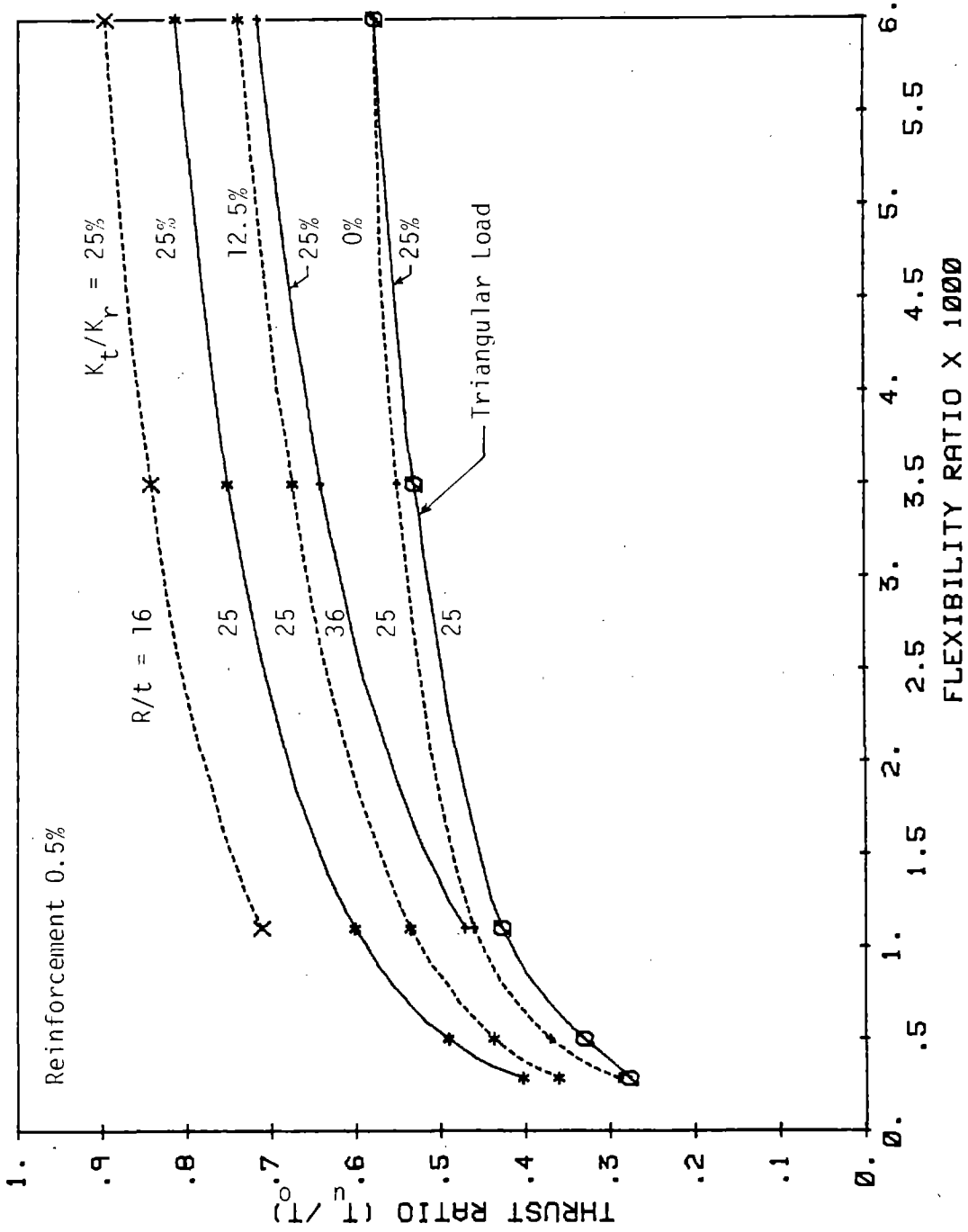


FIGURE 5.7 THRUST RATIO VS FLEXIBILITY RATIO FOR ARCHES

13

$T_u / T_o$  are almost proportional for a given load shape. This proportionality is shown in Fig. 5.8, and depends very little on the  $K_t / K_r$  ratio. With this in mind, Fig. 5.7 can be considered the variation of load with  $F$  for different  $K_t / K_r$  ratios and load shapes. The curve is not as flat as that obtained from the model tests, but shows a definite decrease in sensitivity to  $F$  at larger values of  $F$ . In this range determining accurate values of rock and lining stiffness for calculating  $F$  are not as critical as it is in the low range where the curve is steep.

The influence of  $F$  on the ratio of change in radius to radius ( $\Delta R / R$ ) at failure in the direction of loading is shown in Fig. 5.9. Linings in a soft medium or low  $F$  show considerably higher deformation, which decreases sharply as the flexibility ratio becomes larger. The deformations are also considerably higher for the case of no tangential shear than for other values of  $K_t / K_r$  ratios.

The distribution of thrust around the arch is shown in Fig. 5.10. For the low flexibility ratios the thrust is nearly constant, and decreases from crown to base for high values of  $F$ ; this variation for the larger  $F$  values is essentially due to the effect of tangential shear stresses. As  $F$  becomes higher so does the medium modulus  $E_r$ , and the tangential shear stiffness increases, thus removing more thrust from the lining.

The internal moment and shear distribution around the arch are shown in Figs. 5.11 and 5.12, respectively, for various flexibility ratios. The moments at the critical sections are larger for smaller flexibility ratios because of larger bending in a softer medium. For  $F$  of 900 and 285 the moment-thrust paths for the crown reached the envelope near the balance point, so there is little difference in the crown moments. However, for  $F = 6000$  the moment-thrust path for the crown reached the envelope above the balance point, and so the crown moment is considerably smaller. The moment is slightly larger at a

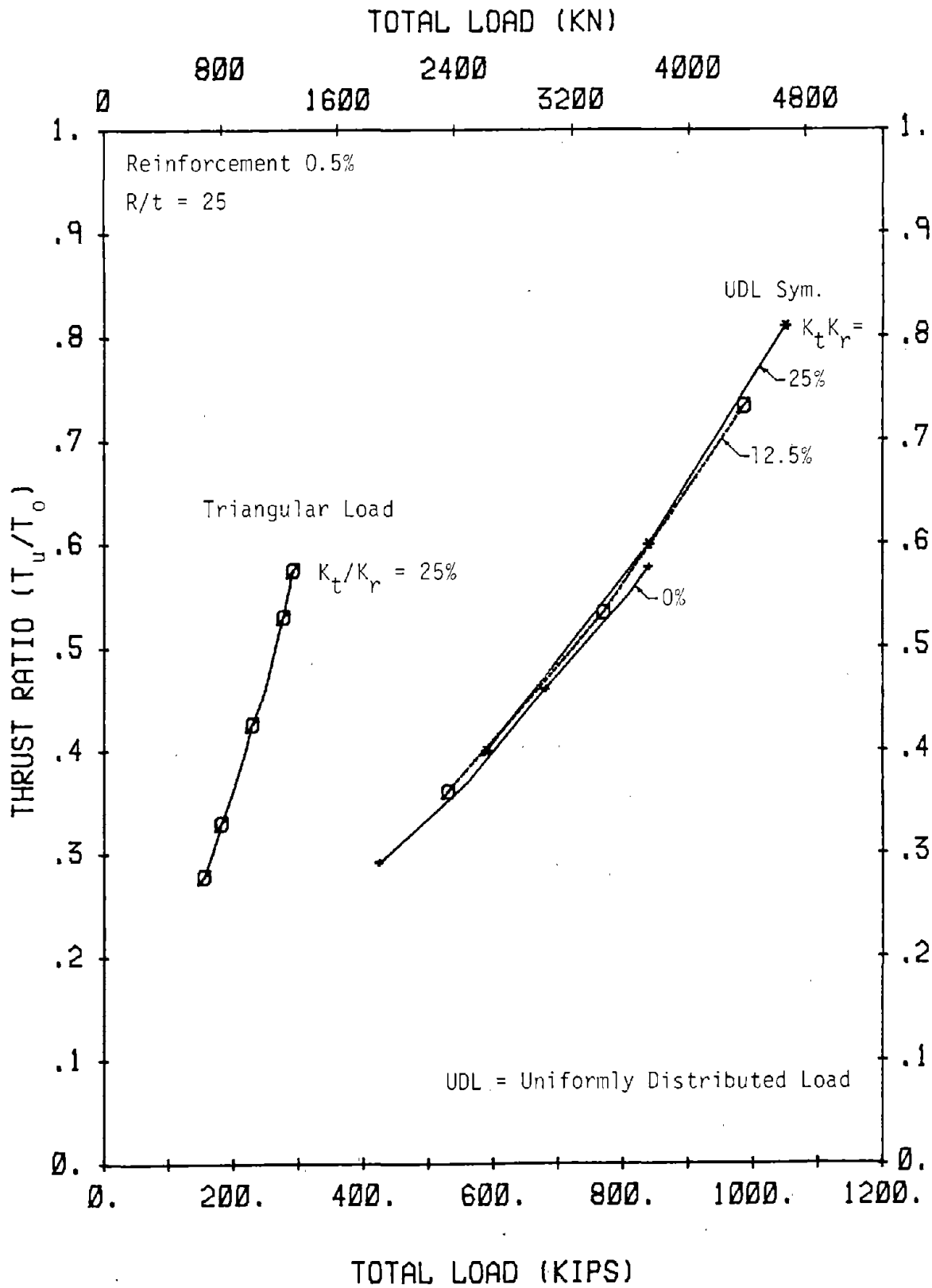


FIGURE 5.8 THRUST RATIO VS TOTAL ULTIMATE LOAD FOR ARCHES



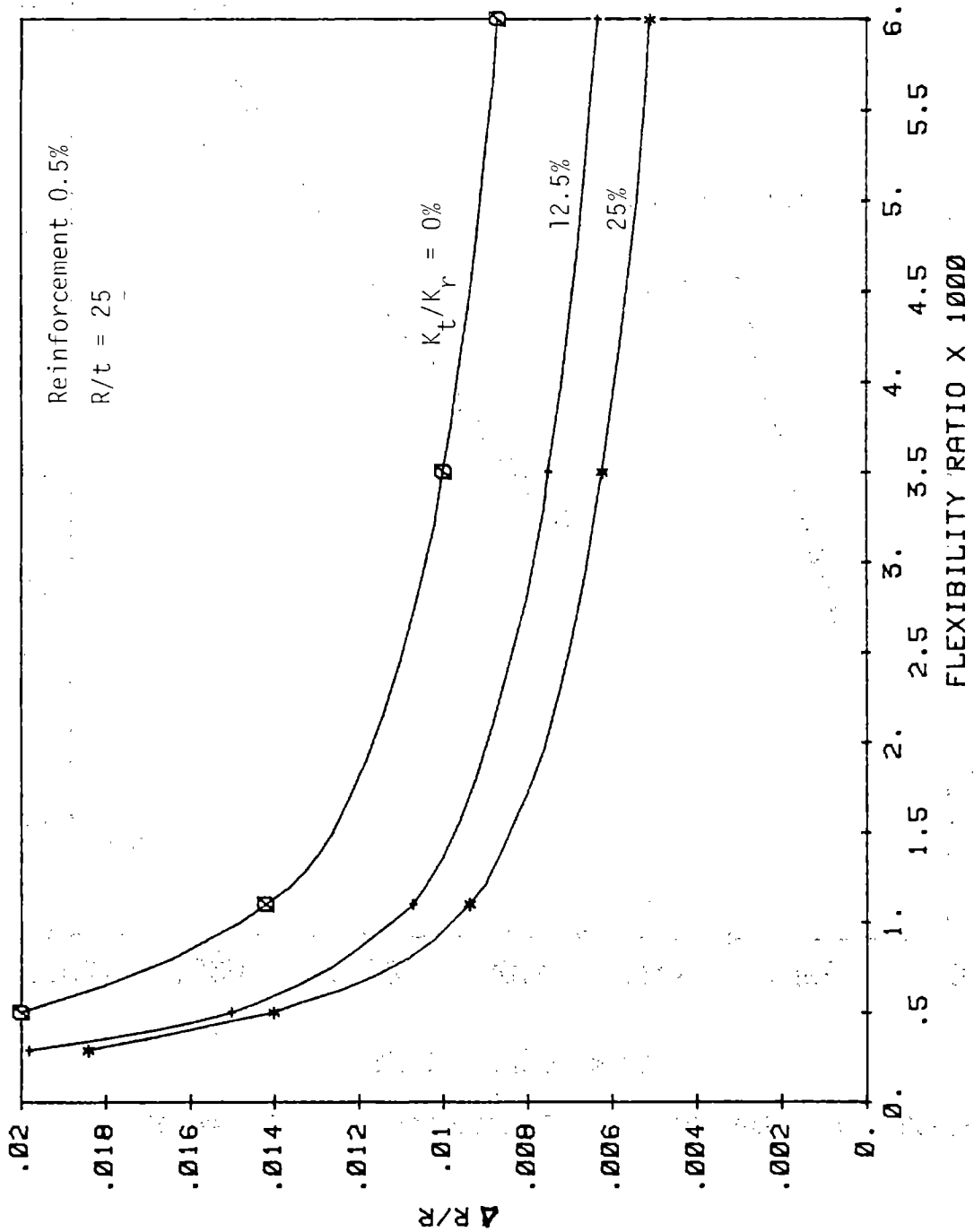


FIGURE 5.9 VARIATION OF RADIUS CHANGE RATIO AT FAILURE WITH FLEXIBILITY RATIO

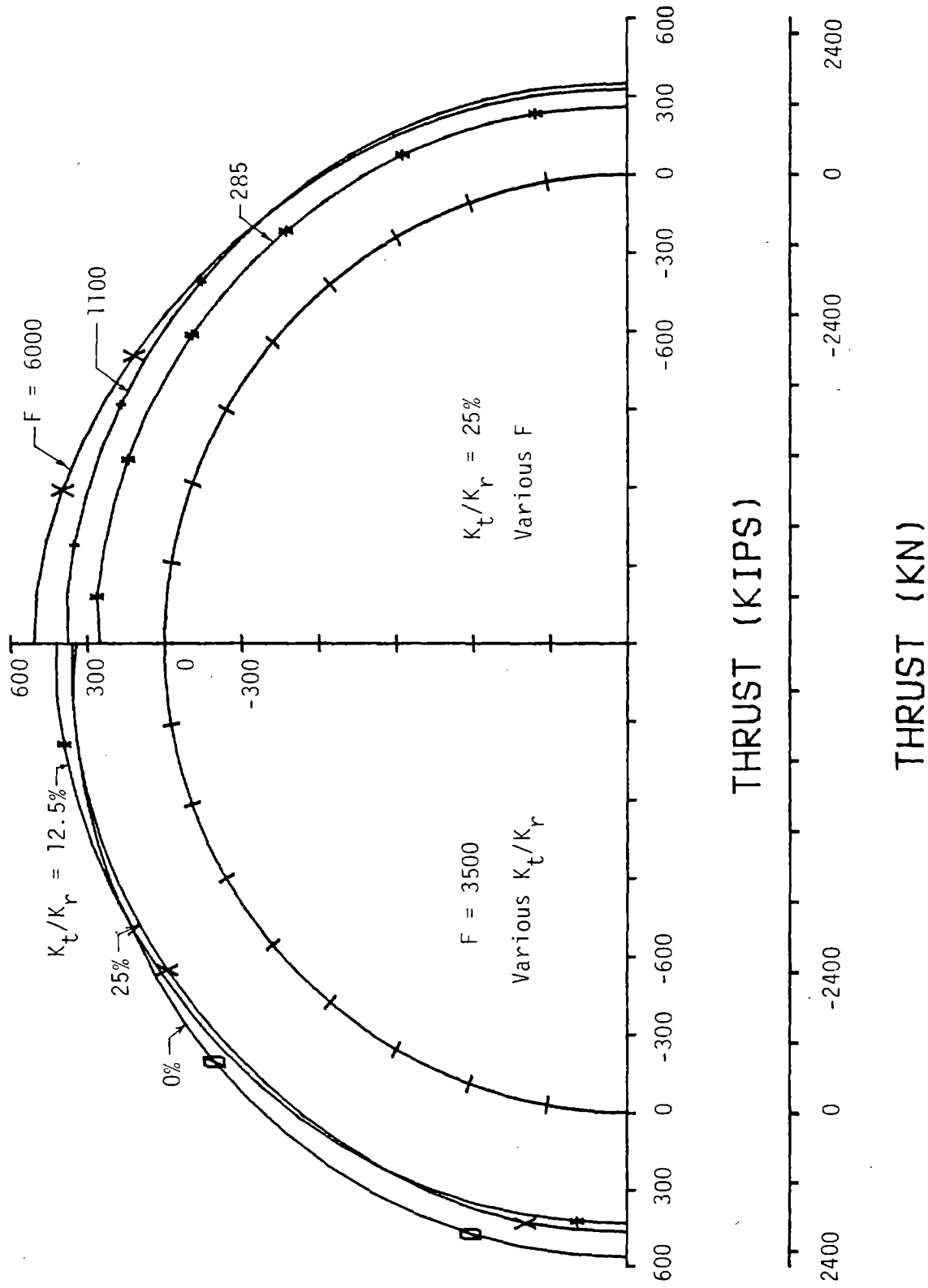


FIGURE 5.10 THRUST DISTRIBUTION AT MAXIMUM LOAD FOR VARIOUS F AND  $K_t/K_r$

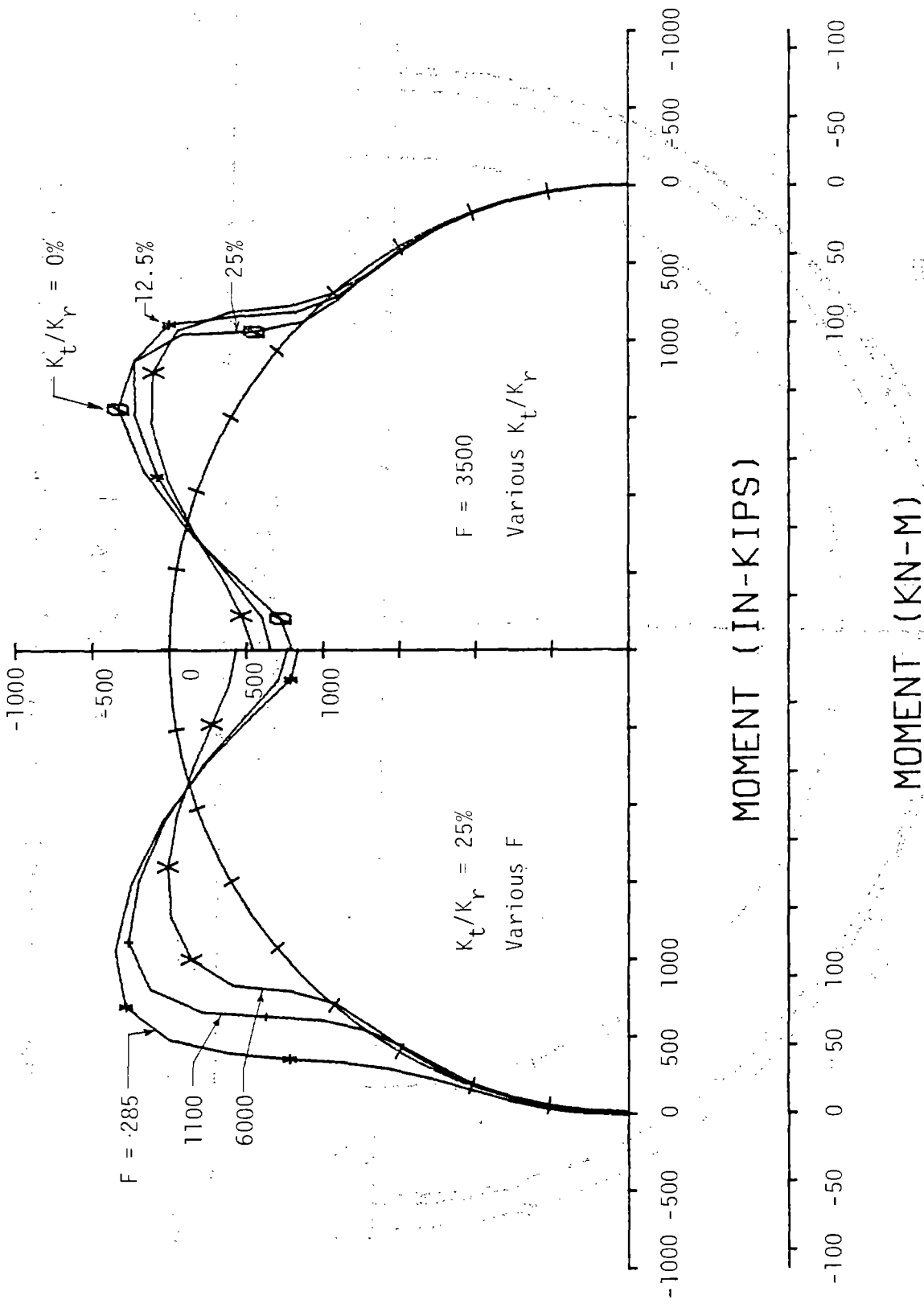


FIGURE 5.11 MOMENT DISTRIBUTION AT MAXIMUM LOAD FOR VARIOUS  $K_t/K_r$  AND FOR VARIOUS FLEXIBILITY RATIOS

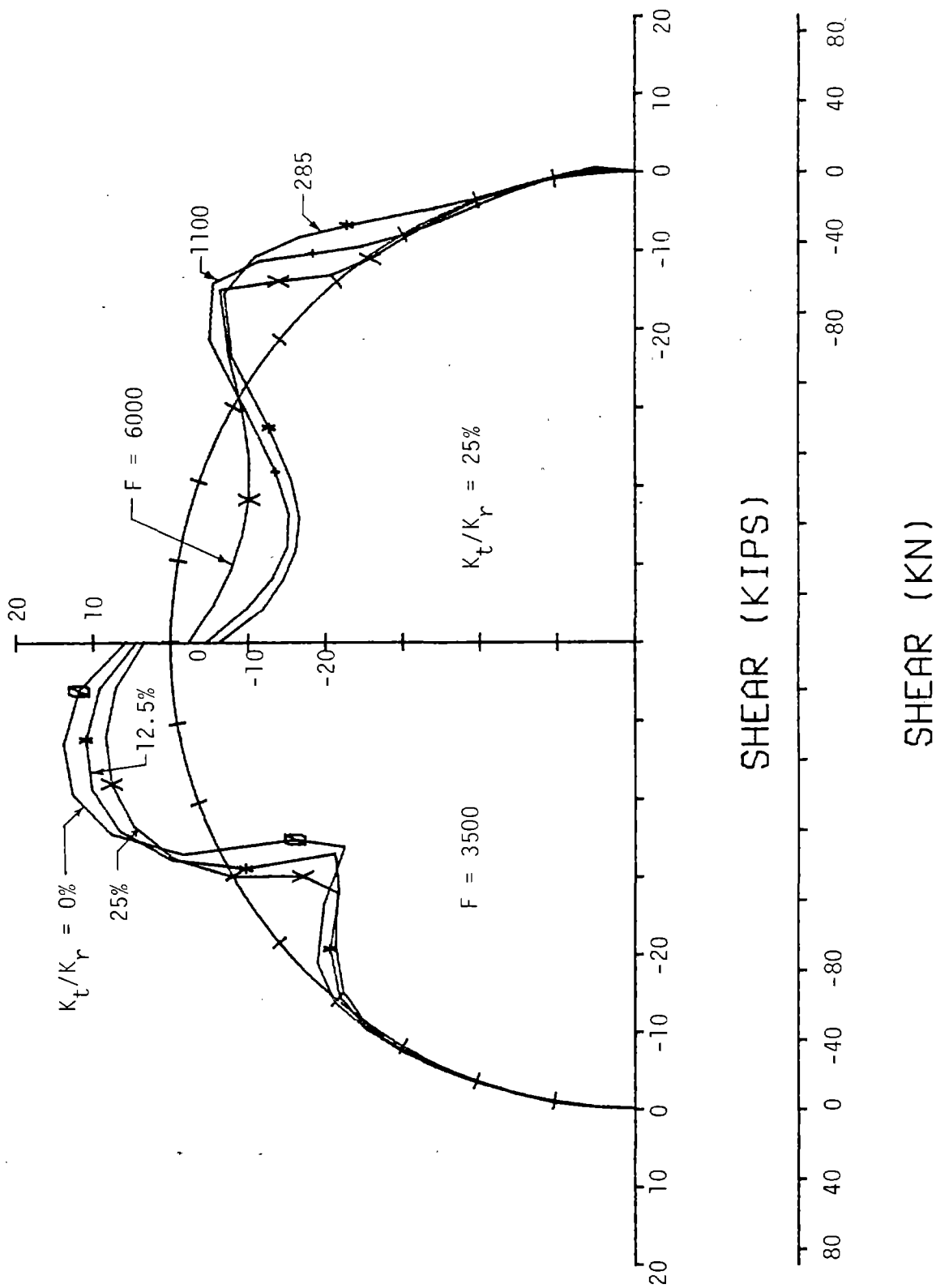


FIGURE 5.12 SHEAR DISTRIBUTIONS AT MAXIMUM LOAD FOR VARIOUS F AND FOR VARIOUS  $K_t/K_r$

section 30 to 40 deg from the crown than at the crown, but, this is not the critical section, as the moment-thrust path had not reached the failure envelope when the crown section had failed.

Near the base of the arch the moment is nearly zero, though the section at which the moment becomes small varies with  $F$ . The crown region of the 180 deg arch behaves like a pin-based flatter arch with the lower portion resisting only the thrust. The internal shear distribution has peaks near 15 deg and 40 deg, but the one nearer the crown is likely to be more critical because it corresponds to a punching of the crown into the tunnel. The shear is equal to the slope of the moment distribution and therefore is zero at 30 to 35 deg from the crown where the moment peaks. It is nearly zero near the base of the arch.

The horizontal component of reaction for the arch is resisted by the tangential and radial pressure on the outer surface between the lining and medium that is shown in Fig. 5.13. The tangential shear varies with  $F$ ; it is zero at the crown for all values of  $F$  and increases more for larger  $F$ . At the base the shear stress is nearly the same again for all values of  $F$ . The radial passive pressure on the arch at the outer surface is about the same for all values of  $F$ , increasing from zero at about 40 deg from the crown to a maximum value at the base.

#### 5.4 EFFECT OF THE RATIO OF TANGENTIAL TO RADIAL STIFFNESS OF THE MEDIUM ( $K_t / K_r$ )

Figure 5.14 shows the effect of tangential shear stiffness  $K_t / K_r$  on the moment-thrust behavior for the two extreme values of  $F$  equal to 6000 and 285, and the full uniform loading. For both values of  $F$  the curves are shown for  $K_t / K_r$  of 0, 0.125 and 0.25. For each value of  $F$  the radial spring stiffness remains the same, and the tangential

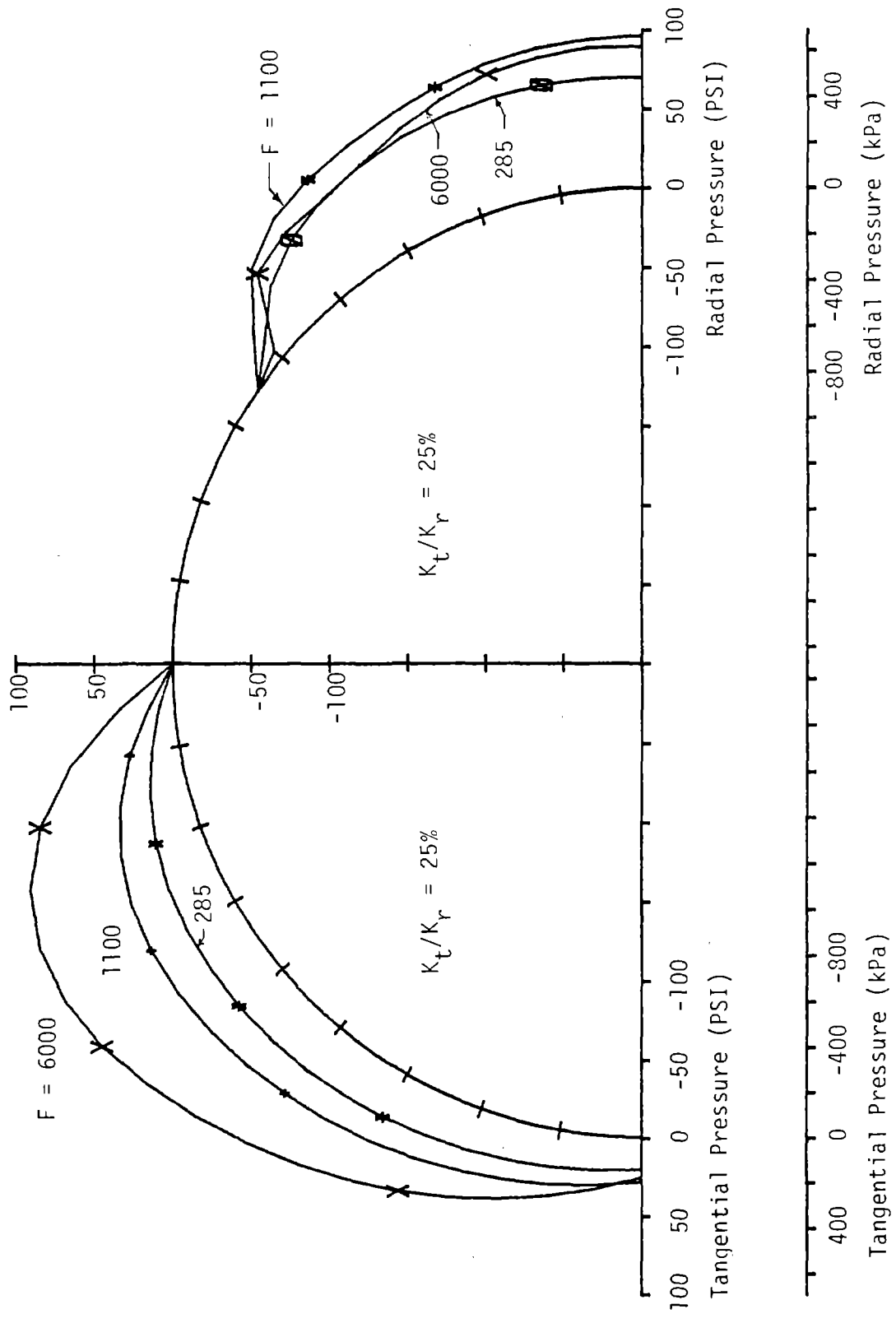


FIGURE 5.13 TANGENTIAL SHEAR STRESS AND RADIAL PRESSURE DISTRIBUTION FOR VARIOUS FLEXIBILITY RATIOS

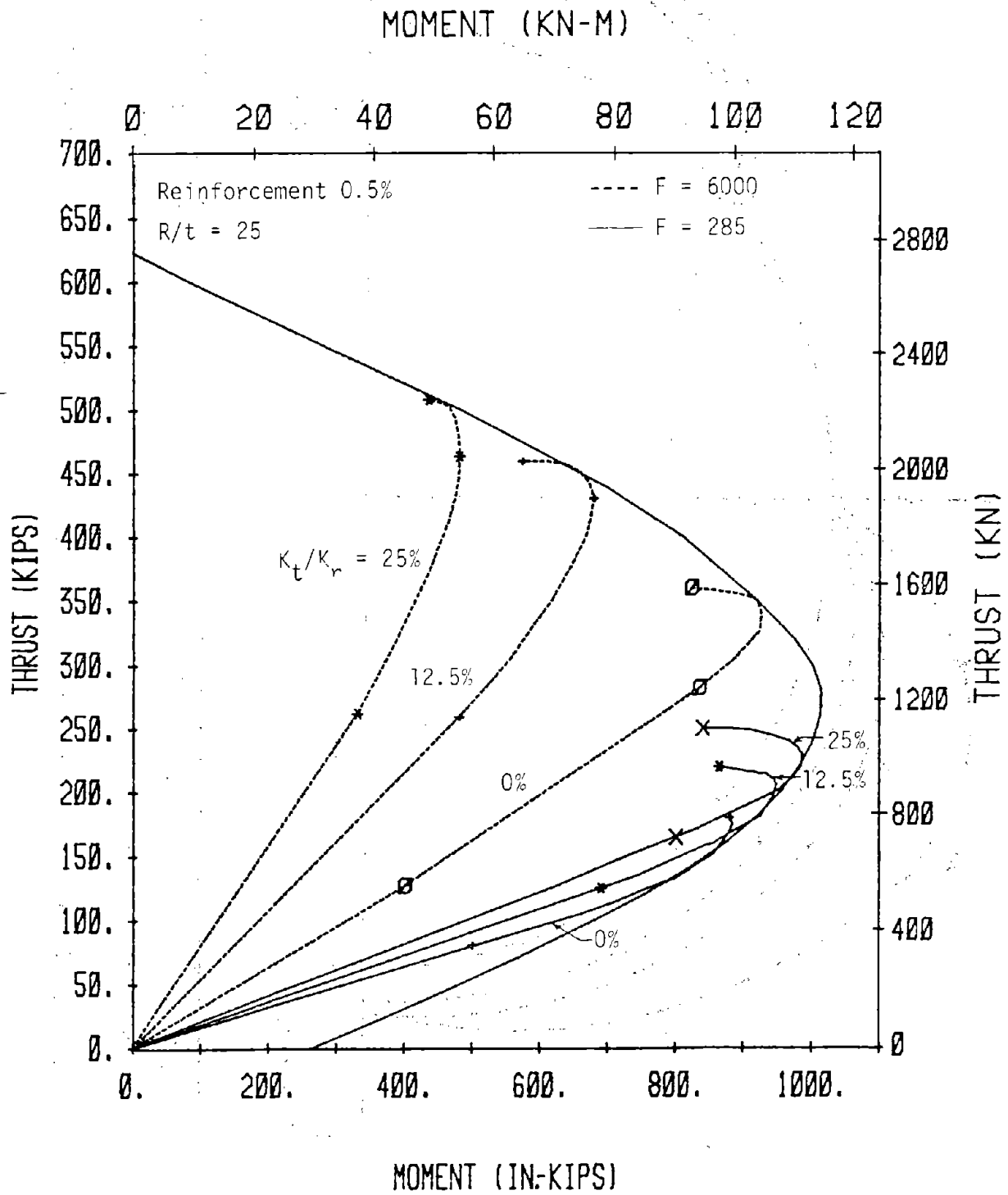


FIGURE 5.14 EFFECT OF  $K_t/K_r$  ON MOMENT-THRUST PATHS FOR ARCHES

stiffness changes. The following table shows the increase in total load for the two cases.

$F$	$K_t/K_r$	Total Load kips (kN)	Increase from $K_t/K_r = 0$ Case kips (kN)	Percent Increase from $K_t/K_r = 0$ Case
6000	0	840.0 (3737)	0 ( 0)	0
6000	12.5	983.5 (4375)	143.5 (638)	17.0
6000	25	1050.0 (4671)	210.0 (934)	25.0
285	0	445.5 (1982)	0 ( 0)	0
285	12.5	529.0 (2353)	83.5 (371)	18.7
285	25	588.5 (2618)	143.0 (636)	32.1

From this comparison it is clear that the absolute value of increase in load due to tangential shear is larger for the larger flexibility ratio, but the relative increase becomes smaller. It also indicates that the increase in load for an increment of  $K_t/K_r$  from 0 to 12.5 percent is greater than that when  $K_t/K_r$  is increased from 12.5 to 25 percent. This effect is more pronounced for large flexibility ratios. The same trend is shown by the variation of thrust ratio ( $T_u/T_o$ ) when plotted against  $K_t/K_r$  in Fig. 5.15.

The effect of  $K_t/K_r$  on deformation of the lining at maximum load is shown in Fig. 5.9, where the ratio of change in radius to radius ( $\Delta R/R$ ) in the direction of loading is plotted against  $F$  for various values of  $K_t/K_r$ . The deformations become smaller as  $K_t/K_r$  increases. In fact, the decrease in  $\Delta R/R$  for an increment of  $K_t/K_r$  from 0 to 12.5 percent is greater than that for the increment of 12.5 to 25 percent.

The distribution of internal thrust in the arch is shown in Fig. 5.10 as  $K_t/K_r$  is varied. The thrust increases from crown to base when there is no tangential shear at the interface because of the



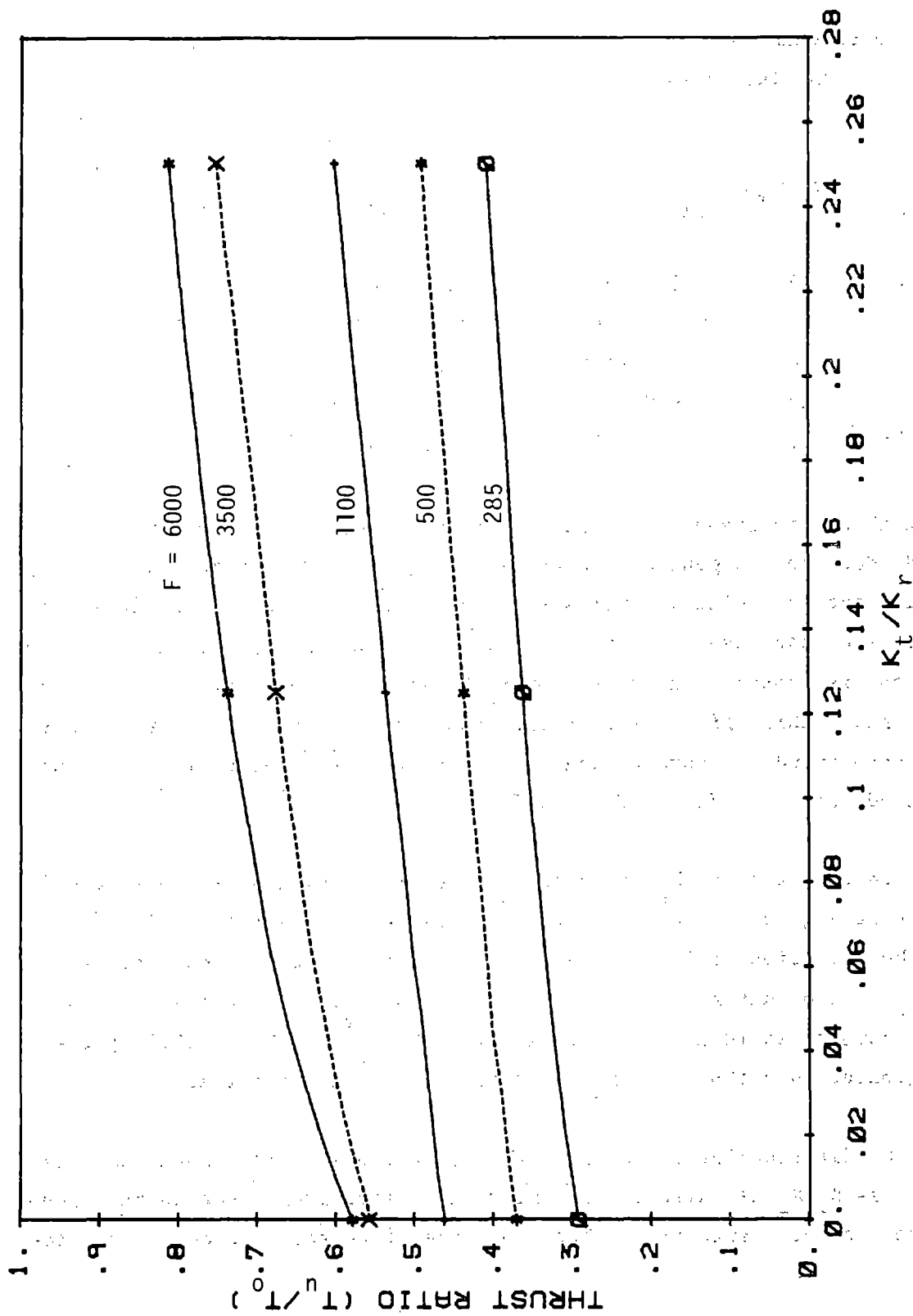


FIGURE 5.15 EFFECT OF  $K_t/K_r$  ON THRUST RATIO FOR ARCHES

contribution of vertical component of the radial pressure to the external load. However, when the tangential shear is present, it reduces the thrust and so for  $K_t/K_r$  equal to 0.125 and 0.25 the thrust decreases from crown to the base. The reduction increases as the value of  $K_t/K_r$  increases. For these cases the increase in thrust due to the increased radial pressure is still present, but is overcome by the larger influence of removal of thrust by the shear stress.

The moment and shear distribution around the arch are shown in Figs. 5.11 and 5.12, respectively. The moment increases with the decrease in  $K_t/K_r$ , as deformations become larger as shown earlier. The moments are nearly zero from about 45 deg from the crown to base and have peak values at the crown and at about 30 deg from the crown. The maximum shear decreases with increases in  $K_t/K_r$  and occurs at about 10 to 15 deg and 30 to 40 deg from crown. The shear remains almost zero below the 40 deg section to the base.

The distribution of tangential shear stress and passive radial pressure at the rock-lining interface are shown in Fig. 5.16. The tangential shear stress increases with the increase of  $K_t/K_r$  ratio when the flexibility ratio is kept constant; the maximum occurs at about 25 to 30 degrees from the crown. The passive radial pressure is zero in the loaded region near the crown and to the point where separation of the lining from the medium has occurred, though there is an active radial pressure component in this region that is not shown. The passive radial pressure increases toward the arch base from zero at about 35 deg from the crown.

## 5.5 EFFECT OF REINFORCEMENT

A lining with the same dimensions and concrete stress-strain curve was investigated without reinforcement. The ultimate pure thrust capacity ( $T_o$ ) reduces to 576 kips (2562 kN). The moment-thrust envelope for the unreinforced lining is also smaller than the

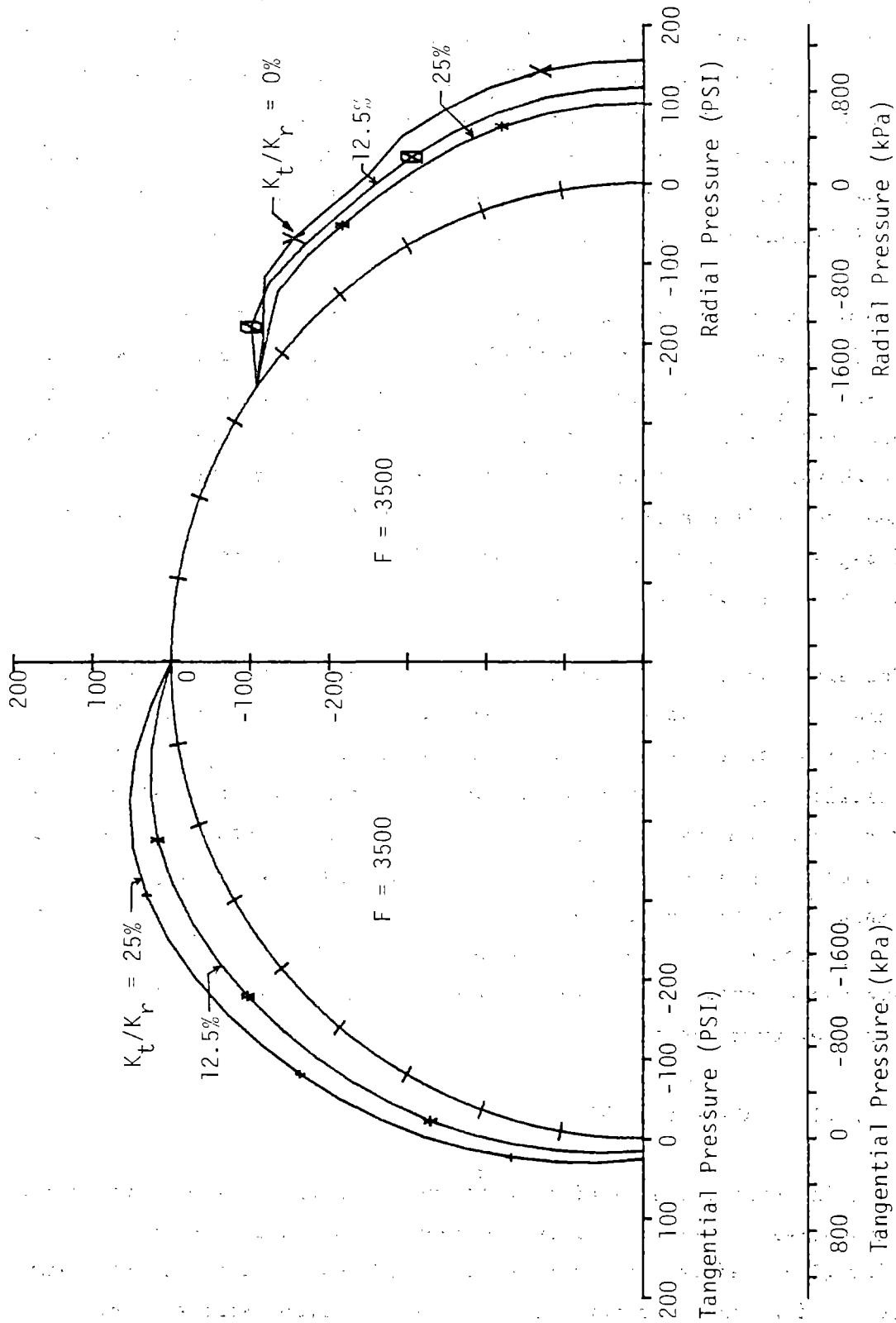


FIGURE 5.16 TANGENTIAL SHEAR STRESS AND RADIAL PRESSURE DISTRIBUTION FOR VARIOUS  $K_t/K_r$

reinforced one in Fig. 5.17 where the moment-thrust paths for different flexibility ratios and for  $K_t/K_r = 0.25$  and  $R/t = 25$  are shown. The moment in the unreinforced lining is slightly smaller at a given thrust than that in the reinforced one because the lining became less stiff and therefore at essentially the same deformation the moment is less. Another way to look at this is that removal of the reinforcement decreased the lining stiffness and therefore increased flexibility ratio, and an increase in  $F$  causes a decrease in moment. However, this difference in the initial moment-thrust ratio is small. As the moment-thrust paths approached their respective failure envelopes, the ultimate thrust ( $T_u$ ) and correspondingly the maximum load for the reinforced lining was higher than the unreinforced lining because the envelope was higher. However, the ratio  $T_u/T_o$  increases for the unreinforced lining by a small amount as shown in Fig. 5.18. This difference in  $T_u/T_o$  for the two cases would be reduced, however, if the actual value of  $F$  were computed for the reinforced section based on the transformed section.

## 5.6 EFFECT OF RADIUS TO THICKNESS RATIO

Values of radius to thickness ratio of 16, 25, and 36 were used based on radii from 20 to 30 ft (6.1 to 9.1 m) and thicknesses from 10 to 15 in. (254 to 381 mm). The effect of the  $R/t$  ratio was studied by keeping the  $K_t/K_r$  at 25 percent, the reinforcement ratio at 0.5 percent and varying the dimensions. Figure 5.7 shows that as the  $R/t$  ratio increases, thrust ratio decreases when  $F$  and  $K_t/K_r$  are kept constant. The variation of  $R/t$  from 16 to 25 and from 25 to 36 renders similar changes in thrust ratio. Thus, linear interpolation is possible for intermediate values of  $R/t$  and the same  $F$  and  $K_t/K_r$ .

## 5.7 DESIGN IMPLICATIONS

The parameter study indicates that a uniform loading across the entire arch gives the smallest safety factor against collapse for the

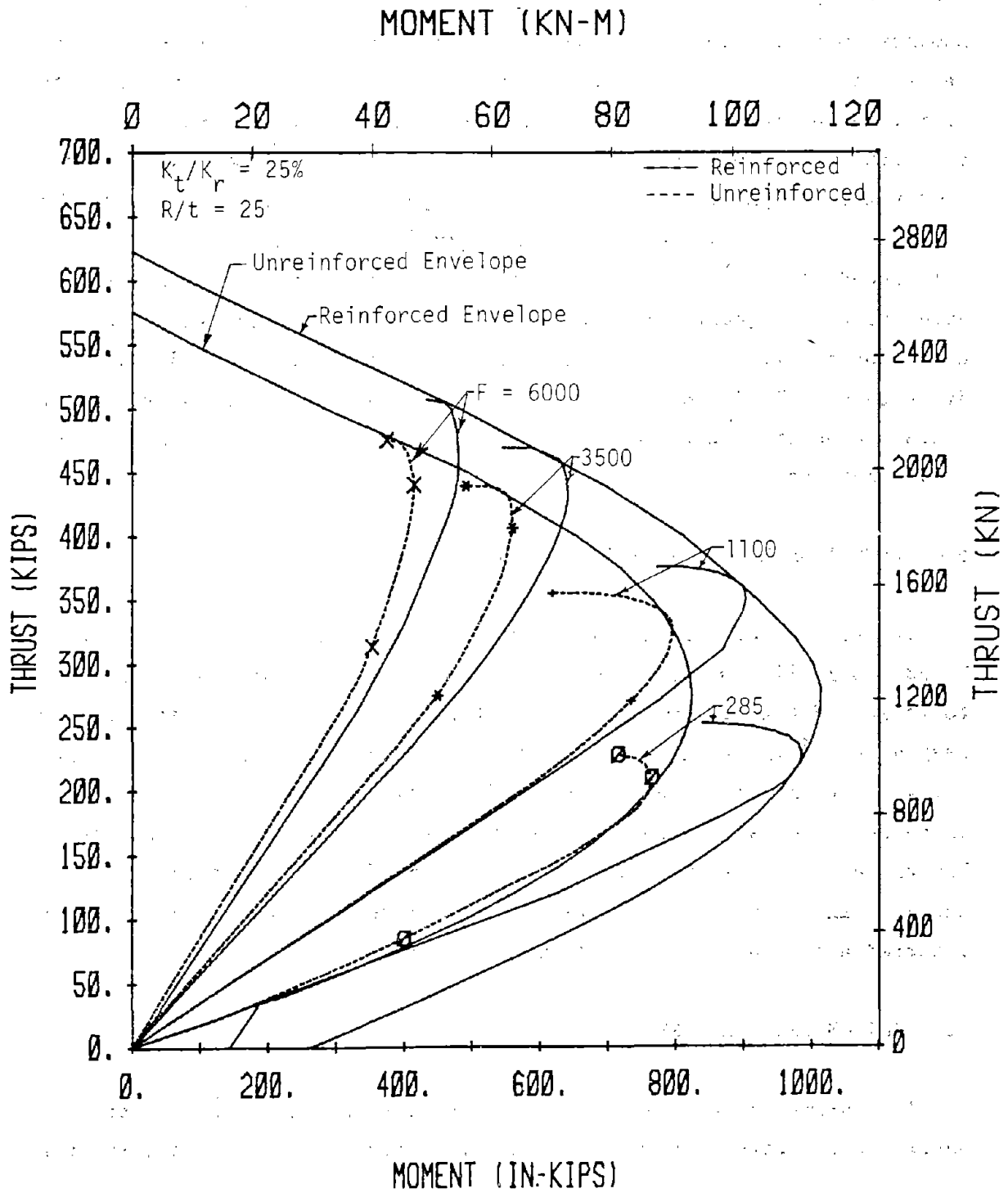


FIGURE 5.17 EFFECT OF REINFORCEMENT ON MOMENT-THRUST PATHS FOR ARCHES

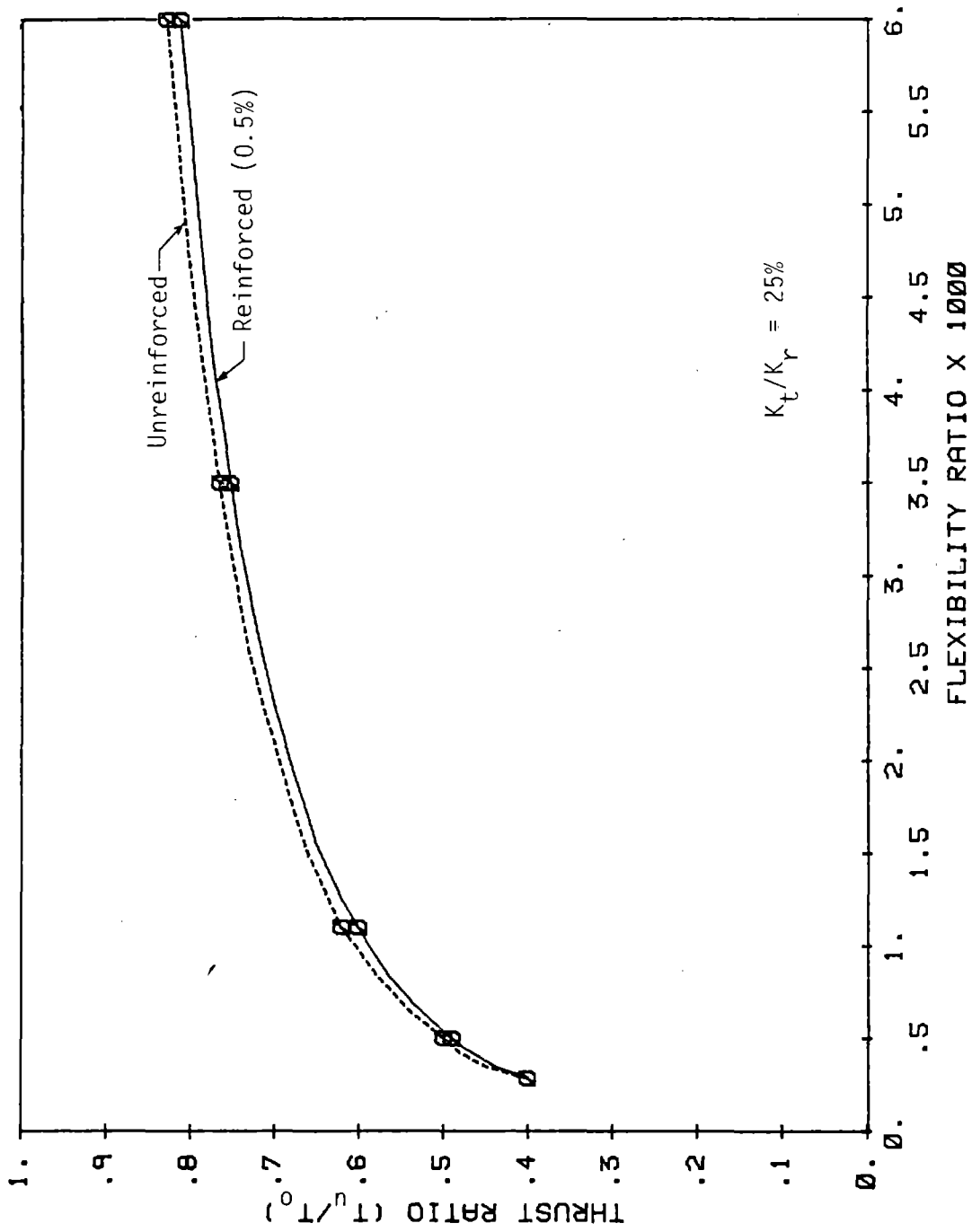


FIGURE 5.18 EFFECT OF REINFORCEMENT ON THRUST RATIO FOR ARCHES

particular conditions investigated. Though a triangular and unsymmetrical uniform loading provide lower values of  $T/T_u$ , they still had larger safety factors for the particular rock block dimensions selected. This study was not broad in its coverage of parameters, however, and the unsymmetrical loadings should be investigated at a particular site. In the tests the  $T/T_u$  varied from 0.60 to 0.69 for various load shapes while the parameter study gave a wider range because at low  $F$  the values from the parameter study were quite a lot lower; for a uniform load over the center 60 deg sector of the arch the parameter study gave 0.69 for  $F = 3500$ , while the same value was obtained at  $F = 1200$  in the model tests. Though these values do not correspond closely, they are reasonable and there were other differences such as tangential and footing spring stiffnesses that represent the medium. At the very low values of  $F$  the parameter study gives much lower  $T/T_u$  values than obtained in the model study; for example, the  $T/T_u$  value obtained for  $F = 285$  and a uniform load over the center 60 deg sector was 0.40 from the parameter study and 0.42 from the model tests at  $F = 120$ . The calculated values are more conservative. The practical cases of arches in rock will lie above the  $F = 285$  value, where the model study and calculations are in general agreement.

Both the model tests and calculations show that strength increases with  $F$ , though the increase indicated in the parameter study is slightly larger. There is a definite flattening of the curve in Fig. 5.7 above  $F = 1000$ , indicating less sensitivity to the calculation of  $F$  in the practical case. An increase in shear stress between the lining and medium results in a definite increase in strength of the lining as shown by both the model tests and parameter study. This increase is constant, as  $F$  varies from  $K_t/K_r$  of 0.125 to 0.25 as shown by the parallel curves in Fig. 5.7, but for an increase from zero to 0.125 the increase is larger at larger  $F$  than in the previous interval. Also, for this latter interval of  $K_t/K_r$  the curves do not remain parallel. but the increase in  $T/T_u$  is smaller, as  $F$  becomes smaller, as shown

also in Fig. 5.15 where the curves for small  $F$  are flatter. Therefore, it is essential to include the shear stress in the analysis of the lining to obtain a realistic prediction of strength, especially for larger values of  $F$ , but the strength is not highly sensitive to  $K_t/K_r$  as shown by the flatness of the curves in Fig. 5.15.

Reinforcement increases the absolute strength approximately as would be indicated by an analysis of the section, but both the model tests and parameter studies show that the effect on the  $T_u/T_o$  ratio is very small. That is,  $T_u$  and  $T_o$  increase in the same ratio, so the reinforcement has no effect other than its obvious effect on strength. The absence of reinforcement does not lead to premature failure due to other causes such as lack of ductility, for example. In the model tests it appeared that the lining could deform a little more at the peak load before total collapse with reinforcement, however. Also, in the low  $F$  range where cracking occurred near peak load, the reinforcement distributed the cracks more uniformly and consequently caused them to remain smaller. This may not be significant, however, if cracking begins well above the working load so that in the practical case it is unlikely to occur.



## 6. MODEL TESTS OF CIRCLES IN SOFT MEDIUM

### 6.1 PURPOSE OF THE TESTS

The objective of the circular lining model tests was to examine the overall behavior and failure modes for concrete tunnel linings in a soft medium. In particular, the effects of amount of reinforcement, medium stiffness and presence of joints in the lining were investigated. Linings in the field are seldom loaded to failure, because of the safety factor incorporated in their design, so the behavior of linings at ultimate load can only be observed by performing model tests. Furthermore, the test results were used to verify the finite element model that was then used to perform parametric studies.

Both strength and serviceability of the linings are examined. Strength is reported either in terms of the maximum load taken by the lining or in terms of the thrust ratio  $T^u/T^o$  defined in Section 4.1. Serviceability is evaluated by monitoring deformations, first appearance of cracks and distribution and size of cracks.

Five circular concrete linings, 3 monolithic and 2 segmented, 44 in. (112 cm) in diameter, 1.0 in. (25 mm) thick and 12 in. (305 mm) long were tested. The ground around the tunnel was represented by a cement-fly ash-styrofoam bead mix with the requirement that its deformations should be comparable to those of soil under the same load.

The effects of reinforcement were assessed by comparing Circle-2 (1.0 percent reinforcement) and Circle-3 (0.6 percent reinforcement) with Circle-1 (no reinforcement). The influence of the medium stiffness was examined by comparing Circle-4 to Circle-5 with similar lining properties but different stiffness of the medium and Circles-1, 2 and 3, which all had different medium stiffnesses, but different amounts of reinforcement as well. The presence of joints in the lining was evaluated by comparing Circle-2 (monolithic) to Circle-5

(segmented). Measurements of the applied loads, lining strains, lining and medium deformations, joint rotations as well as crack monitoring were performed during the tests.

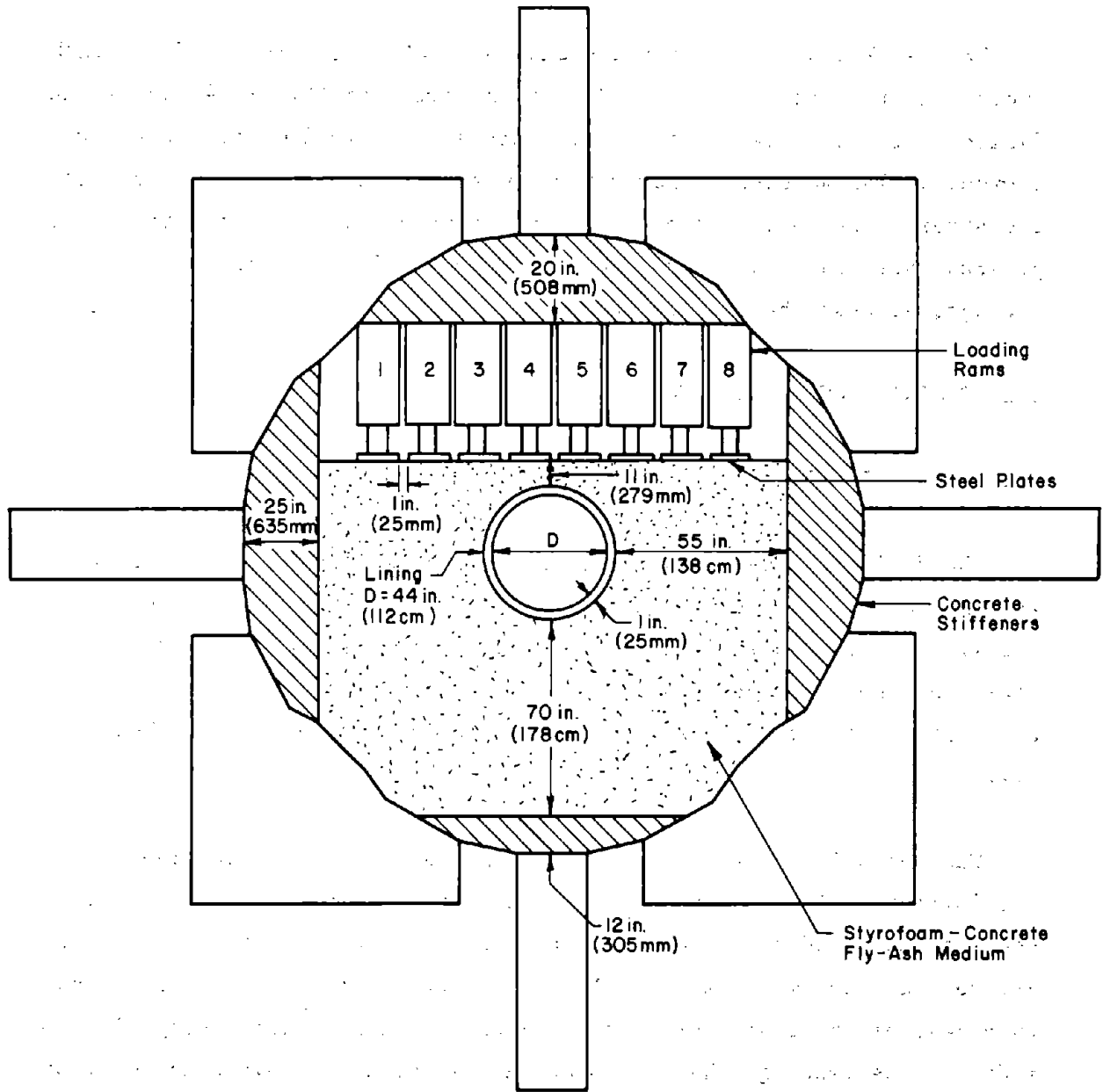
The results are shown for the analysis of one lining from each group, a monolithic (Circle-3) and a segmented (Circle-4) using the finite element program that represents the medium as continuum elements. The measured deformations, moments and thrusts computed from the strain data were matched with the finite element results. The program was then used to perform parametric studies for circular linings, as described in Chapter 7.

## 6.2 DESCRIPTION OF THE TESTS

### 6.2.1 Test Facility

The facility used in the testing of circular linings was the same as the one used in the testing of arches, described in Section 4.2.1, but with several modifications. The concrete medium used to represent rock in the arch tests was removed, and four concrete stiffeners were cast next to the abutments to form a rectangular opening as shown in Fig. 6.1.

The objective of the circular lining tests was to obtain a low flexibility ratio (defined in Eq. 2.2), preferably less than 10. This could be achieved by either decreasing the radius of the lining, increasing the modulus of elasticity of the lining, increasing the thickness of the lining or decreasing the modulus of elasticity of the medium. Decreasing the radius of the lining would have been the most effective way to proceed, since it appears in the flexibility expression in the third power. However, a radius of lining less than 2 ft (0.6 m) would have made it very difficult to install strain and deformation measuring gages on the inside. Furthermore, modeling and similitude considerations were taken into account. Correlation of



Active Rams: 3, 4, 5, 6  
 Passive Rams: 1, 2, 7, 8

FIGURE 6.1 TEST SETUP FOR CIRCULAR LININGS

failure modes, crack width, average crack spacing between model and prototype have been performed with scale factors as small as 1/4 (Alami and Ferguson (1963), Borges and Lima (1960), Rocha (1965)). Consequently, a mean radius of 22 in. (559 mm) was selected, which provided a scale factor of about 1/5 for transportation tunnels (typical diameters 18 to 20 ft (5.5 to 6.1 m)), and adequate space inside the lining to install instrumentation.

Increasing the thickness of the lining would have required higher loads to be transmitted through the medium in order to fail the lining, a requirement which was not easily fulfilled considering the low modulus and low strength medium used in the tests. Thus, the minimum constructable dimension of 1 in. (25 mm) suggested by the ACI Committee 444 (1979) was used. The resulting diameter to thickness ratio of 44 is a little higher than the normal range of 20 to 30 observed in actual tunnels but still reasonable, since there is a tendency toward thinner linings especially with the introduction of precast segmented construction. The modulus of elasticity of the lining concrete is a function of the compressive strength of the concrete, and was about  $2.8 \times 10^6$  psi (19,290 MPa) for the range of concrete strengths used. With the above parameters fixed, the attention of lowering the flexibility ratio to represent a stiff lining in a soft medium was turned to lowering the modulus of elasticity of the medium. Development of the medium is discussed in Section 6.2.2.

The real distribution of the load transmitted to the lining by the soil is not known. Thus, instead of applying the loads directly on the lining (in which case the proper load distribution had to be known), a medium cover of 11 in. (279 mm) was provided to permit load distribution and arching and to allow enough load to reach and fail the lining. Loads were applied through a single row of loading rams shown in Fig. 6.2. Only the middle four rams 3, 4, 5, and 6 were applying load, whereas the remaining four provided passive resistance to the loading surface during testing. This loading might be thought of as a

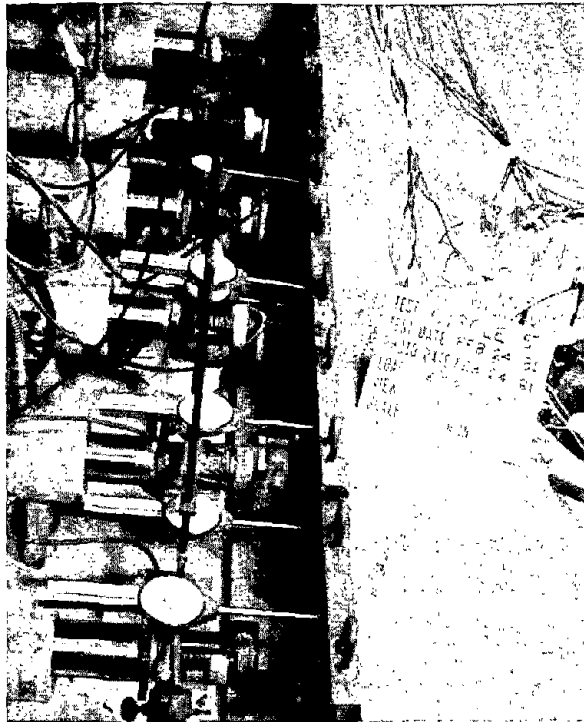


FIGURE 6.2 VIEW OF THE LOADING RAMS

case between overpressure and loosening conditions, as described in Section 2.1. The loads were transmitted to the loading surface through eight 12 by 15 in. (305 by 381 mm) plates 1 in. (25 mm) thick, loaded at their centers and resting on steel rollers to limit friction with the floor. The length of the test section was limited to 12 in. (305 mm) in order to reduce the magnitude of the required failure loads. The concrete lining was cast and instrumented first and then the medium was cast around it.

#### 6.2.2 Development of the Medium

In order for the medium material to be satisfactory, it had to fulfill the following requirements:

a) Its modulus of elasticity should be as low as possible within the range of 2,000 to 30,000 psi (13.8 to 206.7 MPa) in order to deform the same as soil. As discussed in the previous section, the modulus of the medium had to be low for the flexibility ratio to be low. It should be kept in mind that the original objective of the tests was to investigate the behavior of the lining, while undergoing a certain degree of deformation with as realistic passive resistance and applied loads as possible. Consequently, any material that would allow the desired deformations in the lining to develop ought to be satisfactory.

b) It should have adequate unconfined compressive strength to be able to transmit sufficient load to fail the lining (estimated at 60 psi (410 kPa)). Furthermore, it should possess enough cohesion and low Poisson's ratio so that lateral confinement would not be necessary. Providing confinement would have increased the complexity of the tests, because of the large area that had to be confined. This is one of the reasons that soil was not used.

c) Its properties ought to be easily reproduced, and since it had to be cast and replaced in every test, it ought to be easy and relatively inexpensive to place and remove.

Styrofoam balls 1/8 in. (3.2 mm) in diameter were used as aggregate and were mixed with different pastes, made of cement, Hydrocal, plaster and cement and fly ash combined. Cylinders 4 by 8 in. (102 by 203 mm) were cast in 3 layers and compacted with a 2 in. (51 mm) diameter glass rod with 5 blows per layer. The void ratio of the styrofoam beads compacted without the paste (volume of voids over the volume of beads) was 0.53. The volume of paste relative to the volume of voids was varied between 50 and 70 percent.

Measurements of unconfined compressive strength and initial tangent modulus of elasticity were taken by loading the cylinders in a uniaxial compression machine and controlling the loading head movement at 0.022 in./min (0.6 mm/min). The tests were repeated at 7, 14, and 28 days after casting without showing any appreciable variation of the parameters of interest with time. At 14 days after casting, unconfined compressive strengths varied from 26 to 60 psi (180 to 410 kPa) and initial modulus of elasticity obtained from the slope of the stress-strain curves varied from 2,500 to 50,000 psi (17.2 to 344.5 MPa). The higher unconfined strengths and moduli values were given by mixes with beads, cement, fly ash and water (with cement weight twice the weight of the fly ash).

It was observed that adding fly ash increased the unconfined compressive strength of the mix, a conclusion consistent with the one reached by Berry and Malhotra (1980). Addition of fly ash also improved the cohesiveness of the mix, a desirable property since it was very difficult for the paste in the mixes without fly ash to adhere to the styrofoam beads causing mix segregation. Thus, to increase the unconfined compressive strength of the mixes, additional tests with increased fly ash content were performed. Finally, a mix with weight

of cement three times the weight of the fly ash, water to cement ratio of 0.5 and volume of paste 60 percent the volume of voids was selected.

Because of the large quantities of medium material involved in the tests, a concrete mixer truck was brought into the laboratory with a predetermined amount of cement and then the beads, fly ash and water were added and mixed for 20 minutes. The mix was then placed and hand compacted with wooden tampers in three layers around the lining. Both the medium and the lining were removed and recast after each test as shown in Fig. 6.3. The quantities of material required in each cast are given below:

Volume of Beads:	164 ft <sup>3</sup> (4.64 m <sup>3</sup> )
Cement, Type I:	2587 lb (1174 kg)
Fly ash:	865 lb (392 kg)
Water:	1305 lb (592 kg)

The same mix was used for all tests, except in the case of Circle-5, where 30 lb (136 kg) of water were added to intentionally lower the modulus of the medium.

Testing of 4 by 8 in. (102 by 203 mm) cylinders of the medium from the final mix during the development stage gave an initial tangent modulus in the range of 5,000 to 10,000 psi (34.4 to 69 MPa), resulting in a range of flexibility ratios between 35 and 70. This range is higher than the one originally intended, but by observing a typical stress-strain curve for the medium shown in Fig. 6.4, it is seen that it exhibits a pseudo-elastoplastic behavior maintaining the peak strength of 100 psi (0.7 MPa) long after it was initially reached. Thus, if during loading of the specimen the medium experienced a strain of more than about 0.01 in./in., a secant instead of the initial tangent modulus should be used. This value will be lower and thus it will also lower the effective flexibility ratio. The value of modulus of elasticity for the medium shown in Table 6.1 was obtained by





FIGURE 6.3 CEMENT-FLY ASH-STYROFOAM BEAD MEDIUM IN THE PROCESS OF BEING REMOVED, CIRCLE-1

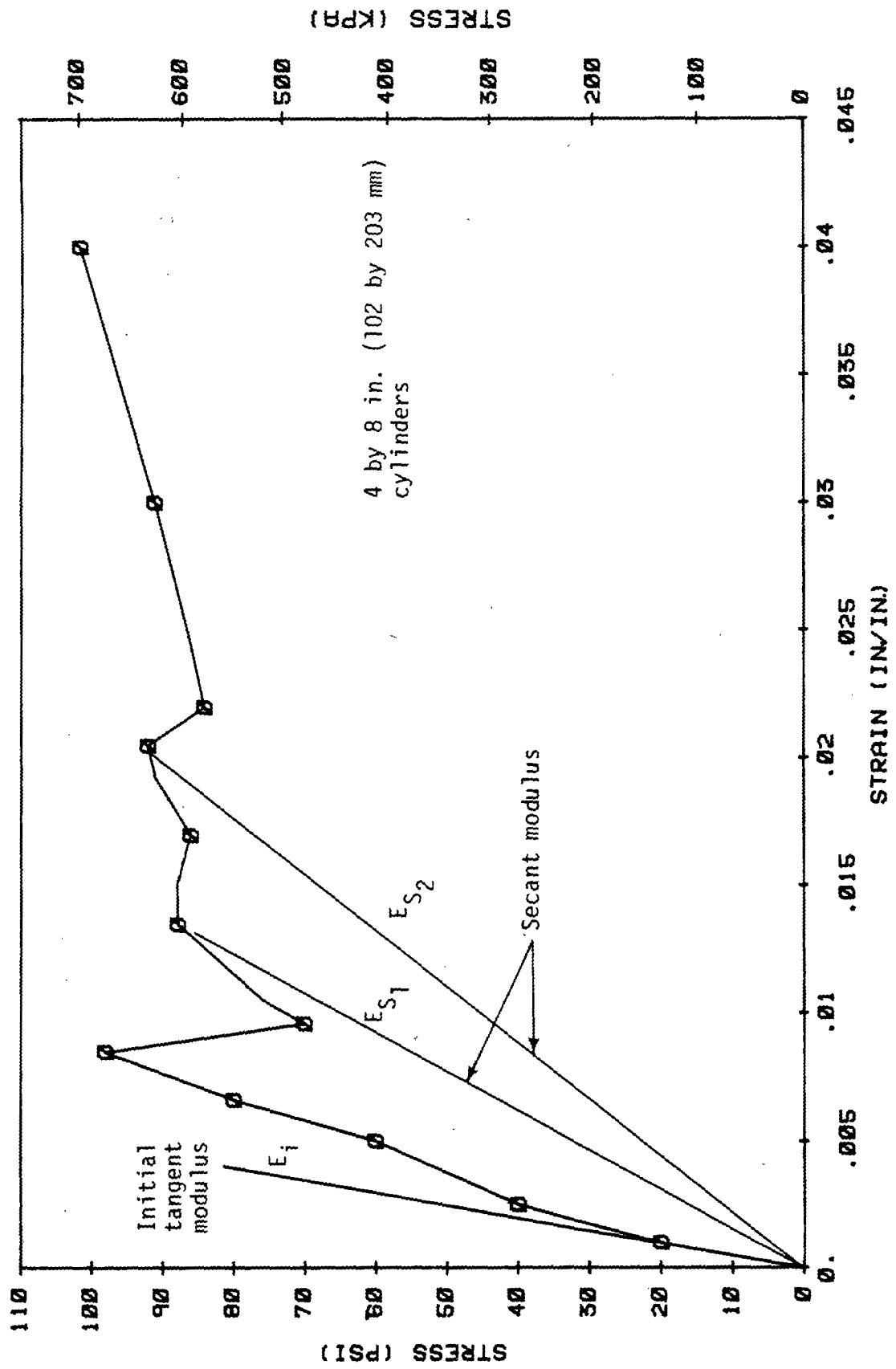


FIGURE 6.4 STRESS-STRAIN CURVE FOR MEDIUM OF CIRCLE-4

TABLE 6.1 SUMMARY OF CIRCULAR LINING TEST RESULTS

Type of Lining	Circle-1		Circle-2		Circle-3		Circle-4		Circle-5	
	Monolithic		Monolithic		Monolithic		Segmented		Segmented	
Amount of Reinforcement (%)	0		1		0.6		1		1	
Initial Equivalent Elastic Modulus of Medium psi (MPa)	25,000 (172.2)		35,000 (241.1)		40,000 (275.6)		45,000 (310)		35,000 (241.1)	
Compressive Strength of Lining Concrete f <sub>c</sub> , psi (MPa)	2,760 (19)		2,560 (17.6)		2,240 (15.4)		2,720 (18.7)		2,280 (15.7)	
Peak Load Kips, (KN)	48.4 (215)		73 (325)		90 (400)		77 (342)		70 (311)	
Change in Diameter $\frac{\Delta D}{D}$ (%)	0.36		0.43		0.25		0.41		0.36	
	At 50% of Peak Load		At 100% of Peak Load		At 100% of Peak Load		At 100% of Peak Load		At 100% of Peak Load	
First Flexural Cracking Load, % of Peak Load	42		36		32		91		93	
Failure Section, Degrees from Crown	80-Left		70-Left		65-Right		60-Right		120-Left	
Initial Flexibility Ratio, F	170		250		300		310 <sup>1</sup>		260 <sup>1</sup>	
Thrust Ratio ( $T_u/T_o$ ) at Failure	0.51 <sup>3</sup>		0.56 <sup>3</sup>		0.62 <sup>3</sup>		0.56 <sup>2</sup>		0.40 <sup>3</sup>	

<sup>1</sup> Monolithic flexibility, joints not taken into account.

<sup>2</sup> Measured.

<sup>3</sup> Estimated.

performing in-situ plate load tests as explained in Section 6.4.2 and is the equivalent modulus of an infinite elastic medium that would give the same load-deformation at the side of the specimen. These values are considerably higher than the ones obtained during the development stage from the cylinder tests. There are many possible reasons for this. Namely, the amount of cement in the concrete truck was probably higher than specified, the degree of dryness of the inside surface of the mixing barrel of the truck varied, and the strength of the mix was very sensitive to the mixing time. The lower modulus of Circle-1 is due to the fact that an older batch of beads was used, which were the ones used for the development testing. It is suspected that the new batch of beads used in Circles-2, 3, 4, and 5 absorbed more water, resulting in higher modulus. However, as will be explained in Section 6.3.3, parts of the medium did go into the "plastic" range, which lowered the effective modulus of the medium. Furthermore, once the finite element program was calibrated, it was used to investigate the behavior in the range of lower flexibility ratios (less than 10).

The value of Poisson's ratio for the medium material, determined by measuring the lateral deformations during testing of the cylinders ranged from 0.018 to 0.020. This low value limited the effects of the non-confinement in the longitudinal direction.

### 6.2.3 Specimen Preparation

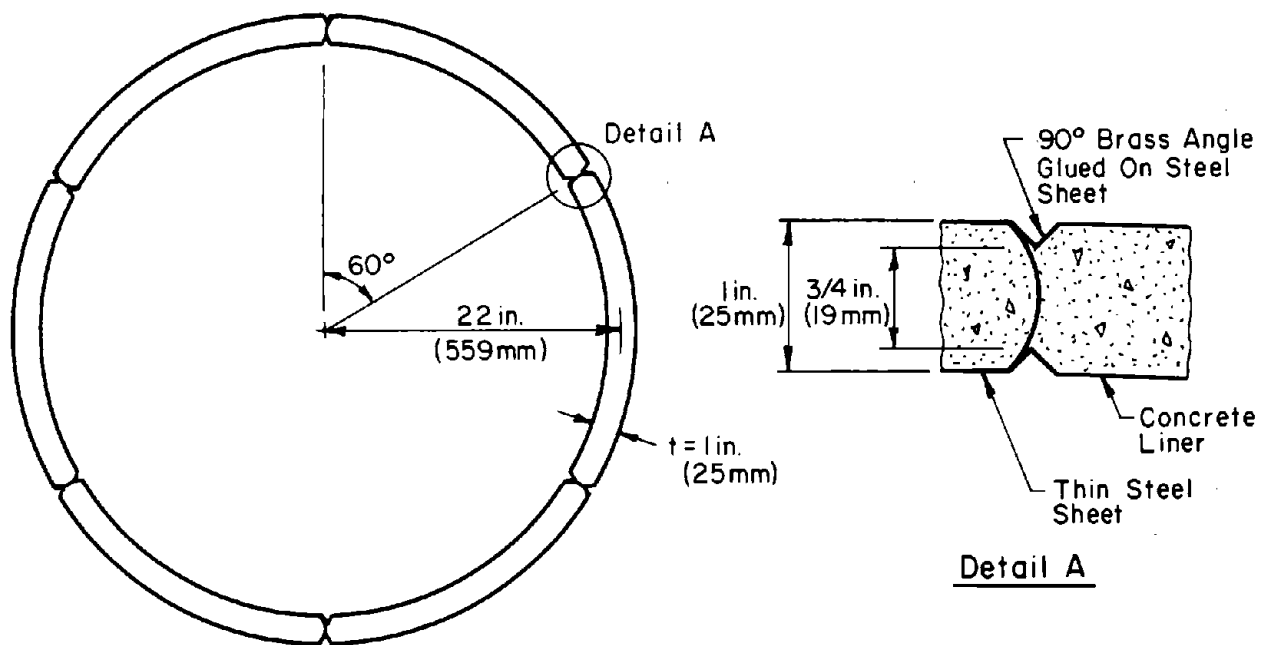
Five circular concrete linings with 44 in. (112 cm) mean diameter, 1 in. (25 mm) thick and 12 in. (305 mm) long, were tested. A list of the specimens tested and their properties is listed below:

<u>Specimen</u>	<u>Type of Construction</u>	<u>Percent Reinforcement</u>	<u>Age on Test Day (Days)</u>	<u><math>f'_c</math> (psi (MPa))</u>	<u><math>f'_{sp}</math> (psi (MPa))</u>
Circle 1	Monolithic	0.0	56	2760 (19 )	253 (1.7)
Circle 2	Monolithic	1.0	27	2560 (17.6)	294 (2.0)
Circle 3	Monolithic	0.6	29	2240 (15.4)	181 (1.2)
Circle 4	Segmented	1.0	29	2720 (18.7)	254 (1.7)
Circle 5	Segmented	1.0	18	2280 (15.7)	205 (1.4)

The procedure for casting monolithic and segmented linings was similar. However, in the case of segmented linings, thin strips of metal and brass angles were incorporated into the lining at 60 deg intervals, as shown in Fig. 6.5 to form the joints. They acted as preformed cracks allowing more rotation, and at the same time reduced the effective thickness of the specimen to represent the caulking groove in large scale linings. The slight curvature of the joint surface was provided to reduce the possibility of shear failure at the joint.

Reinforcement consisted of 1/8 in. (3.2 mm) steel wires. Five wires were used in Circles-2, 4, and 5 as shown in Fig. 6.5, and three in Circle-3. The reinforcement wires were deformed in the laboratory to provide better bond between them and the concrete and were held in place at midheight of the specimen by steel hoops fastened to the form from the inside. Vertical wires 1/16 in. (1.6 mm) in diameter were also placed every 4.5 in. (114 mm) as shown in Fig. 6.6 to limit horizontal cracking. The yield strength of all the steel wires used was 40 ksi (275 MPa).

The steel form consisted of two circular surfaces; the inside one was attached to a wooden form, and the outside one was held by spacers 1 in. (25 mm) wide between the two forms at the bottom and top as shown in Fig. 6.7. The form could be taken apart by first removing the outside form, the inside wooden supports, the steel hoops supporting the reinforcement, and finally the inside metal sheet. The top spacers were removed during casting, and the bottom ones were left in place with the circumferential spaces between them filled with styrofoam sheets 1 in. (25 mm) thick and 2 in. (51 mm) high. The entire lining and medium assembly was sitting on 2 in. (51 mm) thick styrofoam to limit friction with the floor. The form was assembled in place, and the styrofoam that the medium would be cast on was then placed around it.



Reinforcement Per Segment:

Horizontal Bars:  
5 of 1/8 in. (3.17 mm)

Vertical Bars:  
4 of 1/16 in. (1.59 mm)

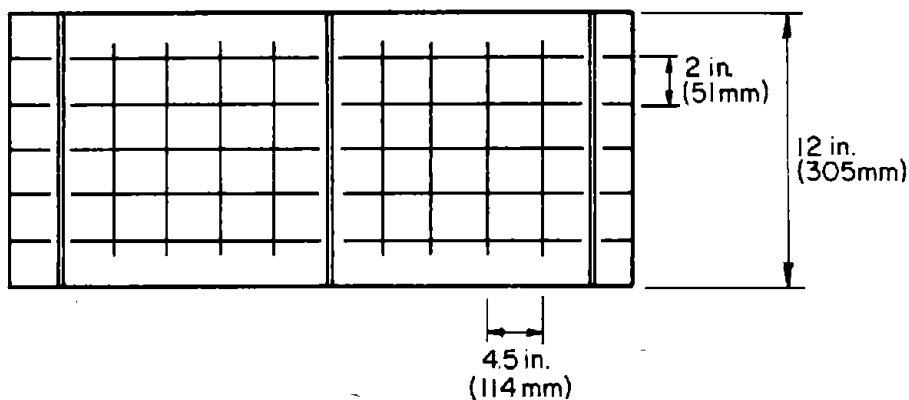


FIGURE 6.5 LINING DIMENSIONS AND REINFORCEMENT ARRANGEMENT FOR SEGMENTED LININGS

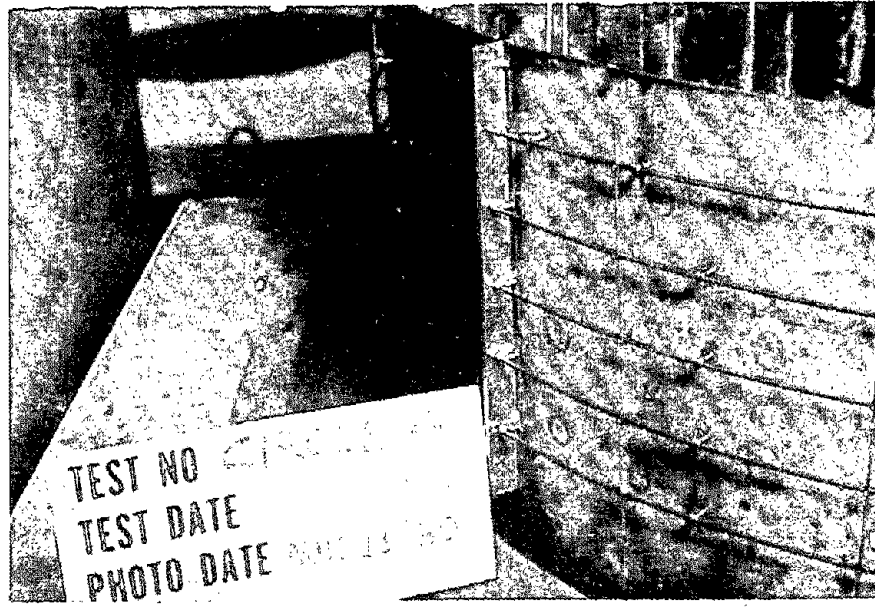


FIGURE 6.6 REINFORCEMENT AND JOINT DETAILS, CIRCLE-4

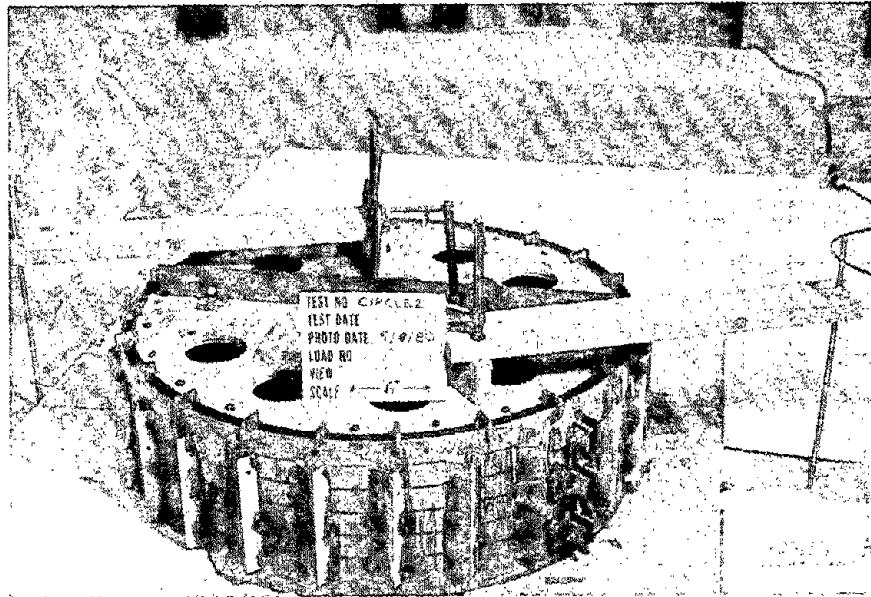


FIGURE 6.7 OVERALL VIEW OF THE FORM

The concrete for the specimen was prepared in one 2 ft<sup>3</sup> (0.06 m<sup>3</sup>) batch in the laboratory; the mix proportions for 1 yd<sup>3</sup> (0.8 m<sup>3</sup>) of concrete are given below:

	<u>Aggregates, Dry Weight</u>
Coarse Sand, lb(kg)	2365 (1073)
Fine Sand, lb(kg)	592 ( 269)
Cement Type I, lb(kg)	571 ( 259)
Water, lb(kg)	514 ( 233)
Water/Cement Ratio	0.90
Slump, in.(mm)	7-10 (178-254)

The concrete was placed in three layers, rodded, and the outside of the form vibrated. The form was removed the following day, and the specimen was kept moist and covered for five more days. Strain gages were installed and waterproofed, as described in the following section, and then the medium was placed. Testing followed about ten days after placement of the medium. Determination of the compressive and tensile properties of the lining concrete was performed by the same processes used for the arch models described in Section 4.2.4.

#### 6.2.4 Instrumentation and Test Procedure

Measurements were taken of the applied loads, deformation of the lining, deformations of the loaded surface, strains on the lining and rotation at the joints of the two segmented linings. The magnitude of applied loads was monitored by load cells between the loading rams and the loading plates as shown in Fig. 6.2. Lining deformations were measured by 16 dial gages, placed radially on the inside of the lining at midheight of the specimen as shown in Fig. 6.8. Thin lubricated steel plates, 1.0 by 1.0 in. (25 by 25 mm), were bonded to the concrete surface at the contact points of the dial gage



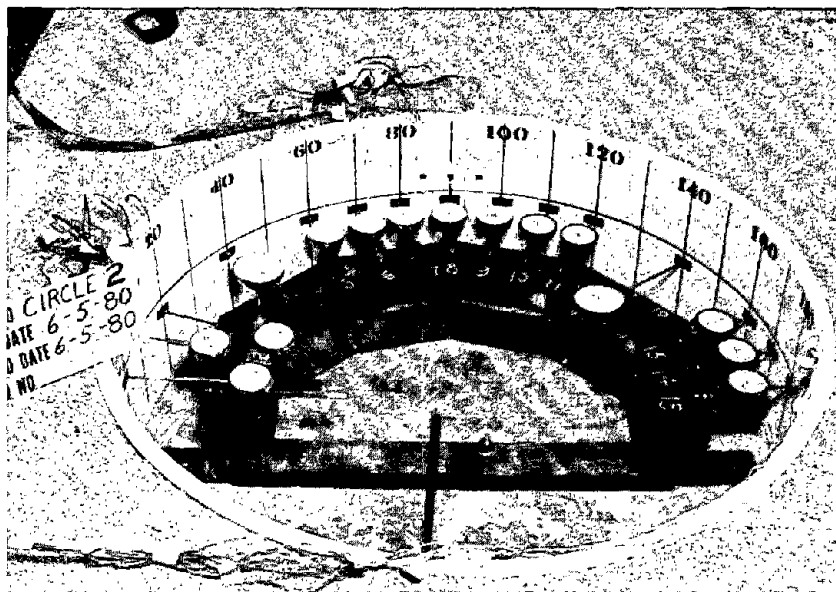


FIGURE 6.8 DEFORMATION MEASURING DIAL GAGES

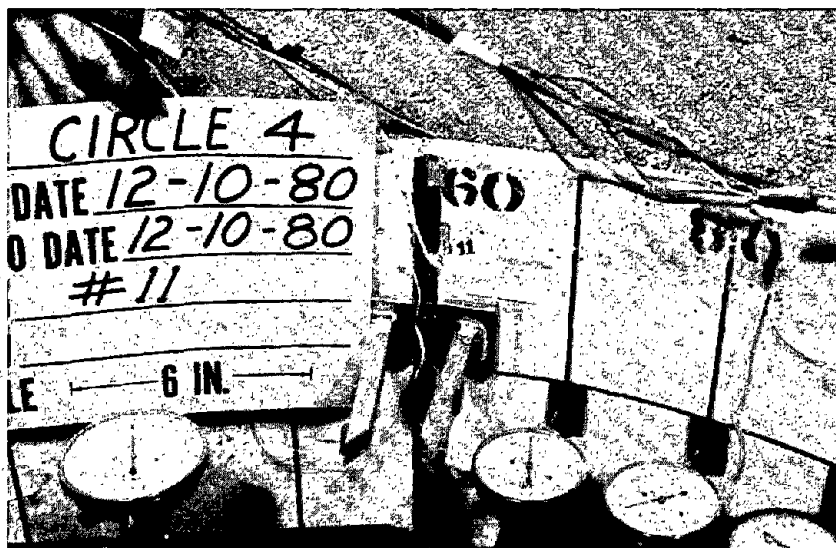


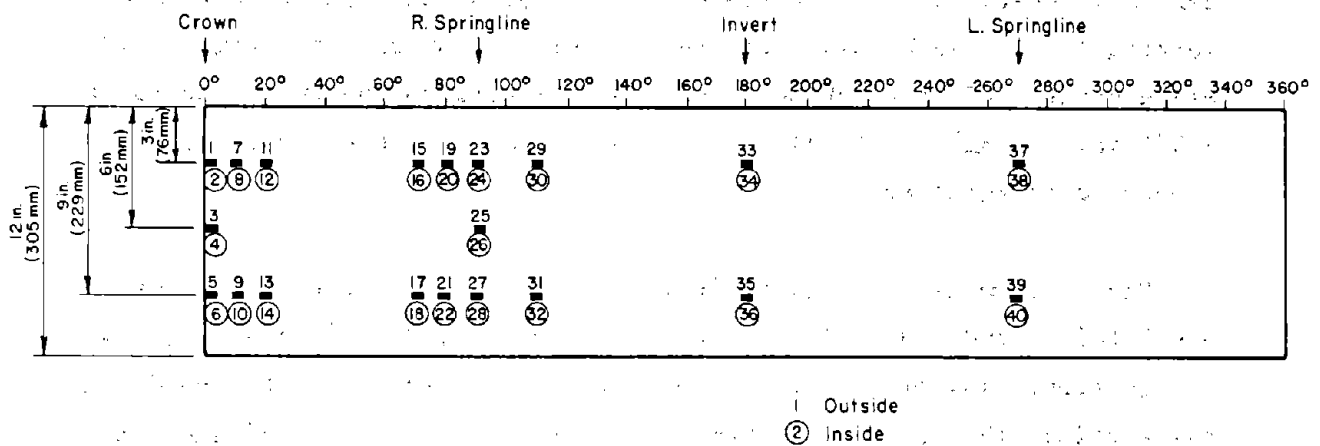
FIGURE 6.9 JOINT ROTATION MEASURING DEVICE

plungers, to minimize friction. Deformation dials were also used to measure the deflection of the loaded surface as shown in Fig. 6.2.

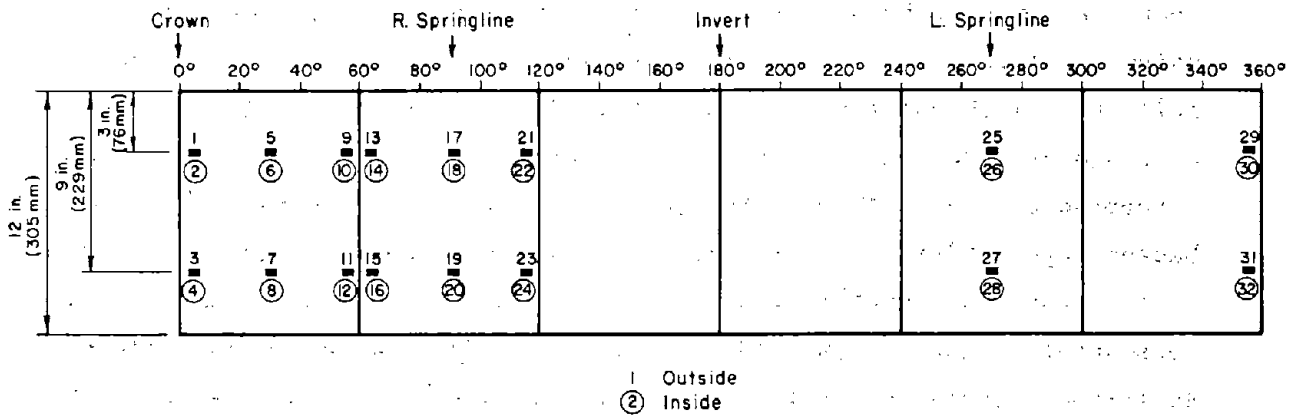
In the two segmented linings, rotations at the crown, 60 deg, 120 deg, and invert joints were measured. Two aluminum channels were glued vertically on each side of the joint as shown in Fig. 6.9. Measurements of the change in distance between the two channels at 2-3/4 in. (70 mm) and 4-3/4 in. (121 mm) from the lining surface were converted to rotations.

The instrumentation plan included 40 strain gages for the 3 monolithic and 32 for the two segmented linings, placed circumferentially on the inside and outside surfaces to be used in calculating the thrusts and moments. The location of the strain gages is shown in Fig. 6.10.

A problem to be resolved was the proper functioning of the outside surface gages, because the styrofoam bead concrete was cast around the specimen, and the moisture from this material would penetrate the specimen and perhaps affect the gage behavior. Tests were conducted using two types of gages, a wire gage with paper backing and a metal foil gage with polyimide film backing. The two gages were installed on concrete cylinders made with the same concrete mix as the specimen, waterproofed, and then immersed in water for 24 hours. The paper backed gage exhibited an increase in resistance, whereas the polyimide film backed gage exhibited no change in resistance from the immersion. Consequently, the 1/2 in. (13 mm) long metal foil gages were chosen. Additional tests were performed to select an adhesive, as the one used in the above tests did not seem to adhere well after the concrete became wet. An adhesive called M-Bond AE-10/15, with a curing time of about 6 hours at room temperature, proved to be more effective in keeping the gages dry than the M-Bond 200 that was used previously. In addition, the area around the gages that was waterproofed was increased in the actual installation. The outside surface gages were installed,



a) In Monolithic Linings



Note: Gages At Joints Are Two Inches Away  
 End of Gage To the Edge of the Joint

b) In Segmented Linings

FIGURE 6.10 LOCATION OF STRAIN GAGES

and protective caps made of metal were placed over them to protect them from direct pressure, as shown in Fig. 6.11.

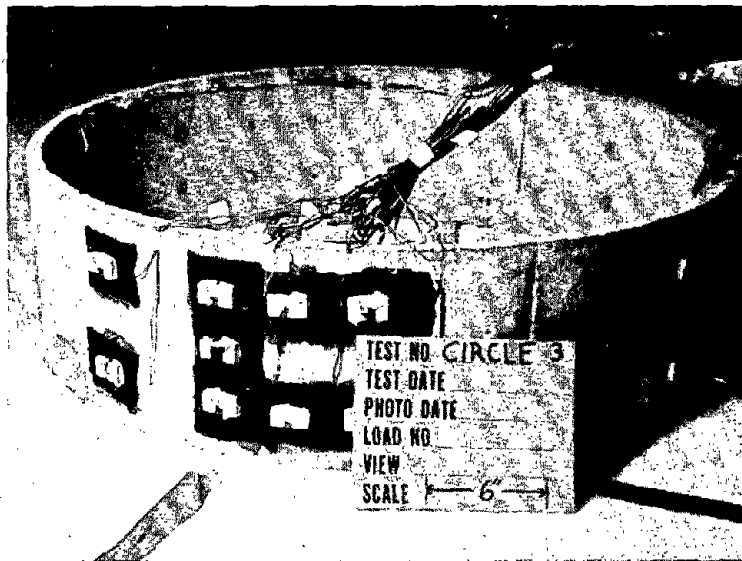
The test procedure, was the same as that used in the testing of the arches and described in Section 4.2.5. The total duration of the test, with a crew of 5, was 5 to 6 hours.

### 6.3 TEST RESULTS

#### 6.3.1 Behavior and Ultimate Capacity of the Linings

Capacity of the lining is expressed in terms of the total peak load applied through the four center rams. However, because of arching through the medium, only a portion of the load reaches the lining. Consequently, in order to estimate the magnitude of the internal forces in the lining, the moment-thrust paths at the crown and the critical sections are plotted. Moments and thrusts at a section are computed from the measured strains and using the stress-strain curve of the lining concrete to obtain the internal distribution of stress on the section. The thrust ratio  $T_u / T_o$  is an indication of the amount of moment at the critical section at the ultimate load. Thrust ratios for the segmented linings are computed from strain measurements at the full 1.0 in. (25 mm) sections and then converted to thrusts at the reduced joint regions (the joint being the critical section).

The relative stiffness between the lining and the medium is defined by the nondimensional flexibility ratio  $F$ . Since the initial equivalent elastic modulus of the medium was used, the value of the flexibility ratio computed represents an initial flexibility subject to change as the modulus of the medium and lining change with load. The initial flexibility ratio for the segmented models is defined by discounting the presence of the joints and treating them as monolithic linings. The joints do not influence the behavior of the lining beyond



(a) Overall View



(b) Close-up View

FIGURE 6.11 STRAIN GAGES INSTALLED ON THE LINING, CIRCLE-3

a certain value of the modulus of elasticity of the medium, as explained in Chapter 7, and believed to be the case here.

In the following paragraphs the results from each test will be discussed separately and are summarized in Table 6.1.

Circle-1 Specimen Circle-1 with an initial flexibility ratio of 170, reached a total ultimate load of 48.4 kips (215 kN). The total load-crown deflection curve is shown in Fig. 6.12. It is observed that because of the high degree of indeterminacy of the structure, extensive moment redistribution took place so stability and load were maintained long after the peak load was reached even though the lining was unreinforced. The moment-thrust paths for the crown and the left springline are shown in Fig. 6.13. The left springline was the closest instrumented section to the failure zone (80 deg left of the crown). The crown moment-thrust path lies under the springline path, indicating higher crown moments at the same thrust level. A thrust ratio of  $T_u / T_o = 0.51$  was estimated by extending the initial portion of the left springline path until it intersected the envelope for the lining section. The envelope provides the bounds for the moment-thrust combinations that the section can take. In this case the maximum measured moment and thrust remained well within the envelope, since they did not represent the critical section.

Circle-2 Circle-2 was reinforced with 1.0 percent circumferential reinforcement. It reached a total ultimate load of 73 kips (325 kN) with an initial flexibility ratio of 250. The peak load for Circle-2 is higher than that for Circle-1 as shown in Fig. 6.12. This is a result of two factors: higher modulus of the medium and inclusion of the reinforcement.

The moment-thrust paths for the crown and the section 70 deg to the right of the crown are shown in Fig. 6.14. Once again, the failure section (70 deg to the left of the crown) was not instrumented.

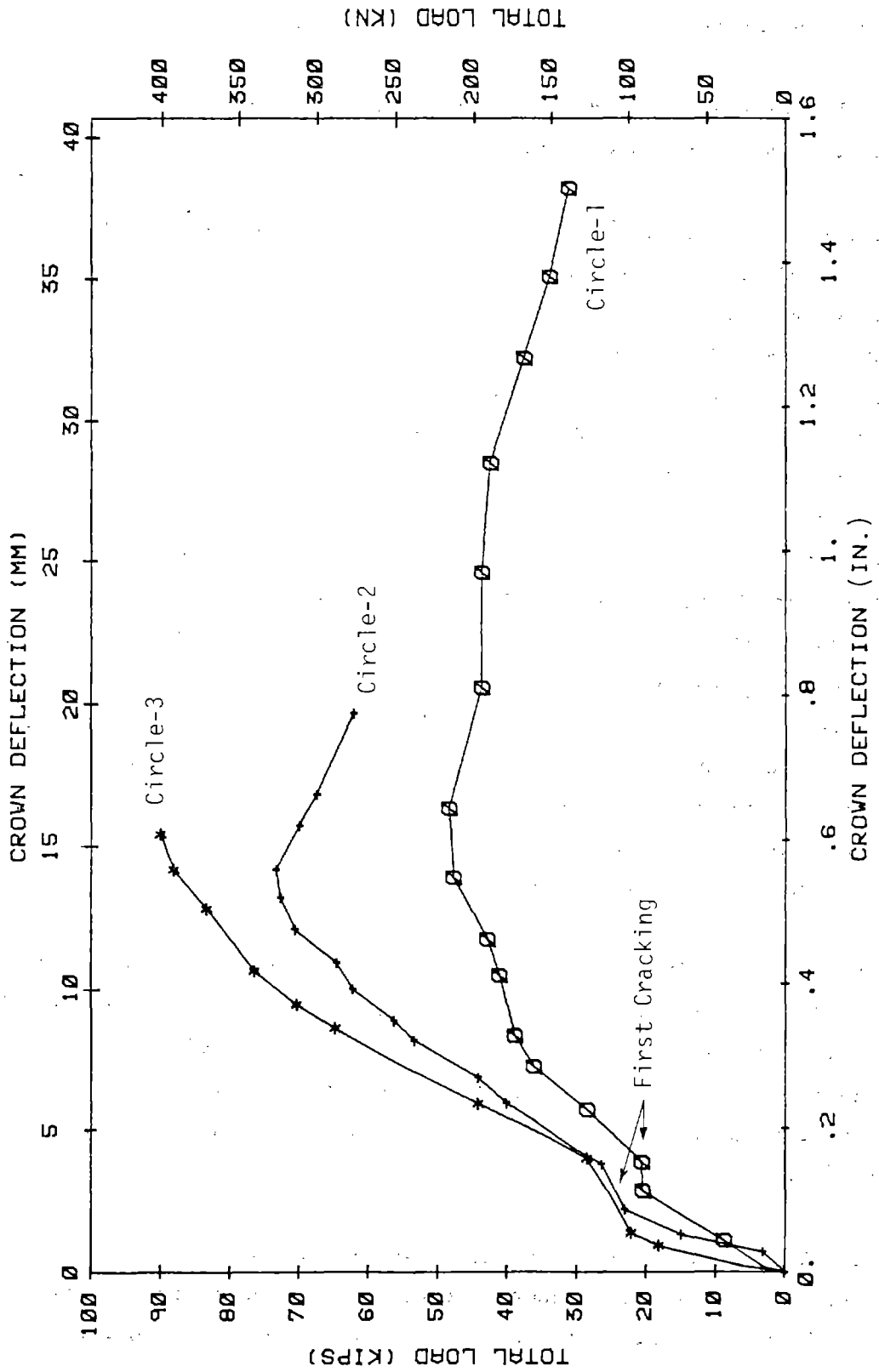


FIGURE 6.12 LOAD-DEFLECTION CURVES OF MONOLITHIC LININGS

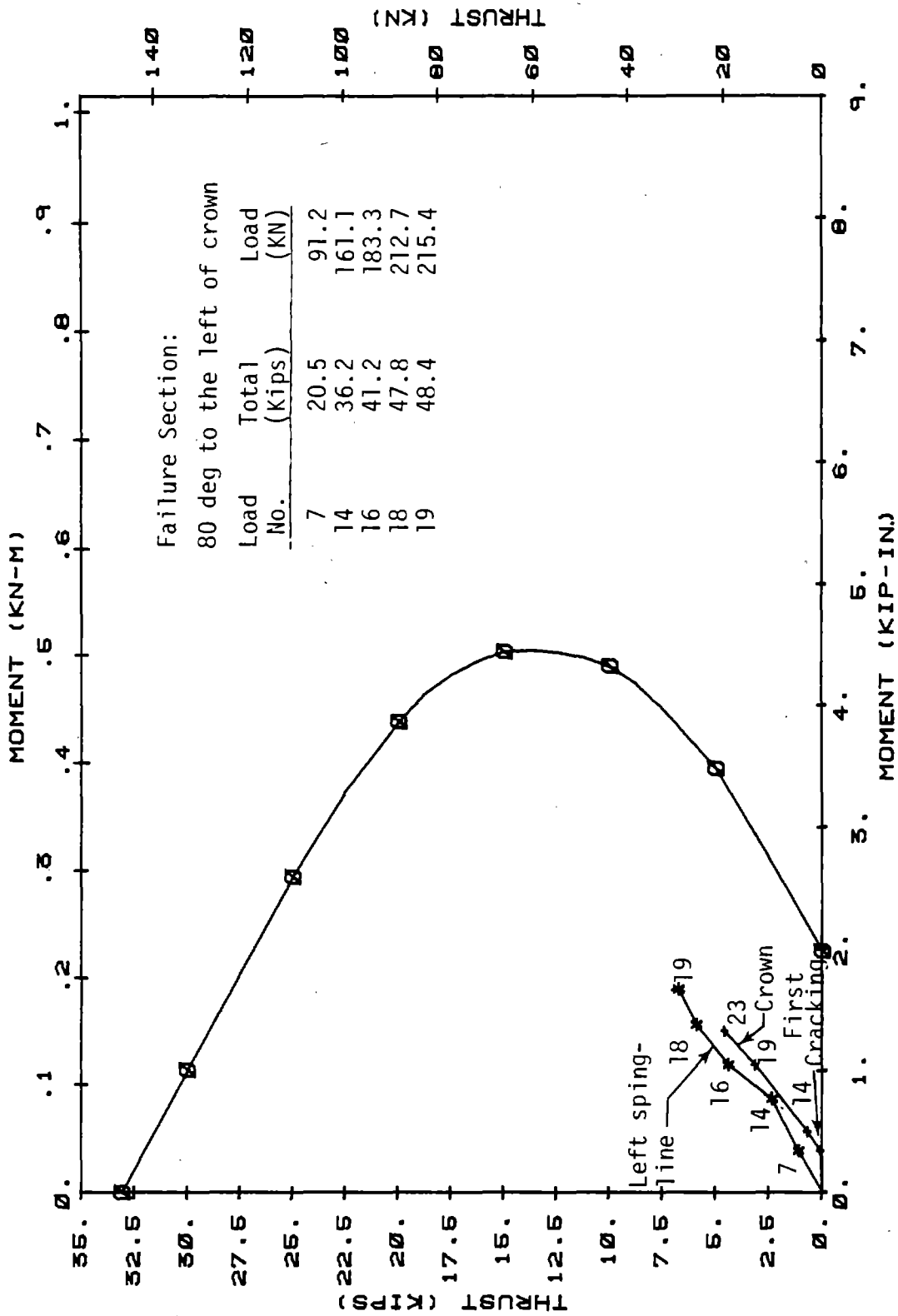


FIGURE 6.13 MOMENT-THRUST PATH AT CROWN AND LEFT SPRINGLINE OF CIRCLE 1



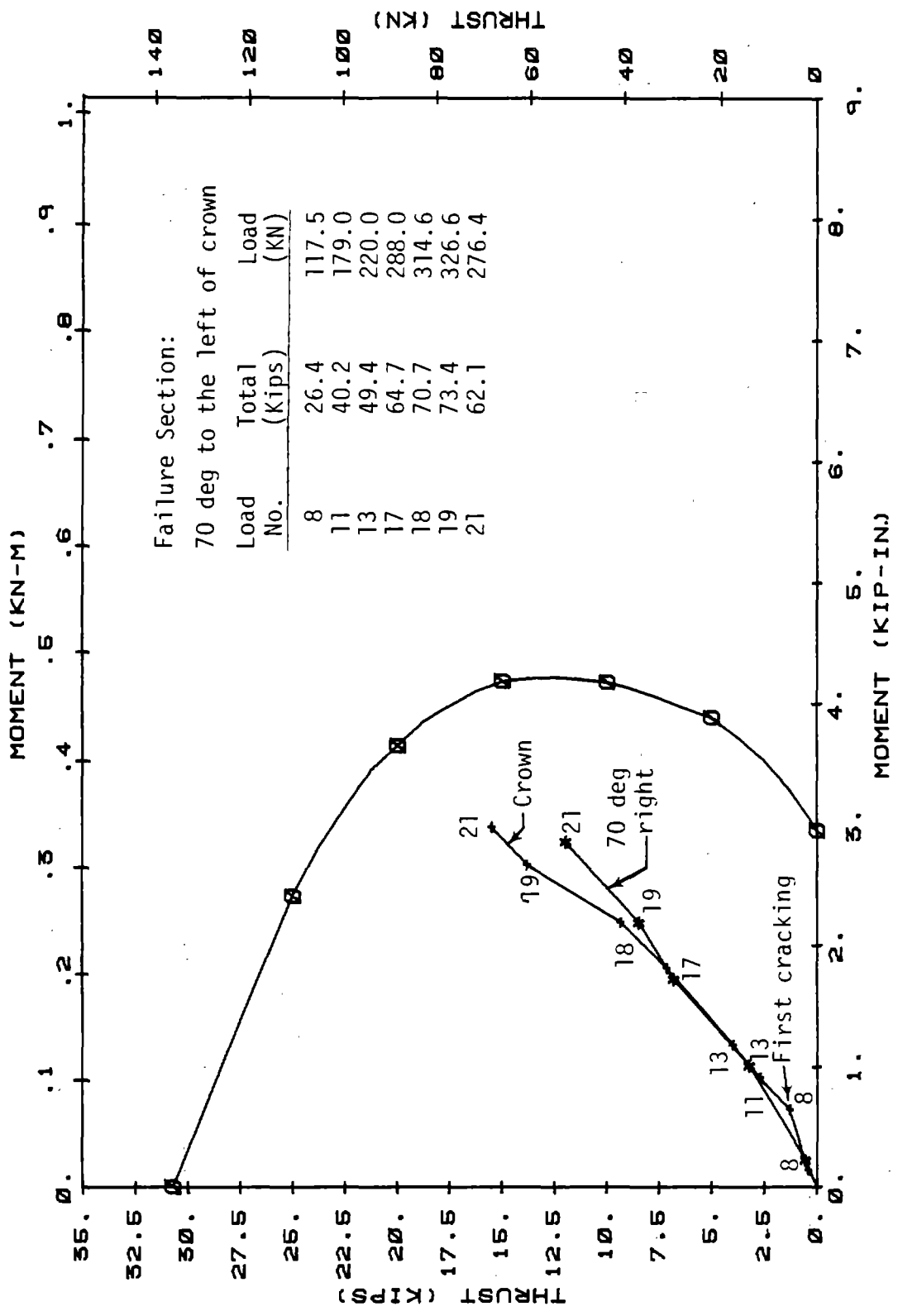


FIGURE 6.14 MOMENT-THRUST PATHS AT CROWN AND 70 DEGREES RIGHT OF CIRCLE-2

However, moment and thrust of the corresponding section on the right side of the lining were plotted, assuming that use of symmetry is reasonable. The value of the thrust ratio of  $T_u/T_o = 0.56$  was estimated by extending the moment-thrust path for the section 70 deg to the right of the crown, until it intersected the envelope. The higher value of the thrust ratio for Circle-2 indicates less moment at the critical section than that of Circle-1.

Circle-3 Circle-3 was the last of the monolithic linings tested, and it was reinforced with 0.6 percent circumferential reinforcement. It reached a total load of 90 kips (400 kN) with an initial flexibility ratio of 300. The medium modulus for this test was higher than that for Circles-1 and 2, and this resulted in higher total load for Circle-3, as shown in Fig. 6.12, even though the amount of reinforcement was less than that in Circle-2. The moment-thrust paths for the crown and for a section 70 deg to the right of the crown are shown in Fig. 6.15. In this case the critical section occurred within the instrumented portion of the lining, and so the moment-thrust path for the failure section stops on the envelope. The thrust ratio of  $T_u/T_o = 0.62$  is then obtained directly by dividing the thrust at the point of intersection A by the pure thrust capacity of the section at point B in Fig. 6.15. The thrust ratio for Circle-3 is the highest one obtained in all monolithic linings tested.

Circle-4 Circle-4 was the first of the two segmented linings tested. It had the higher medium modulus of 45,000 psi (310 MPa) as compared to 35,000 psi (241.1 MPa) for Circle-5. With the exception of the modulus of the medium, all other parameters were the same for the two tests. The lining, with an initial flexibility ratio of 310, failed at a total load of 77 kips (342 kN) as shown in Fig. 6.16. The moment-thrust paths for the crown and the joint at 60 deg to the right of the crown are shown in Fig. 6.17. Two envelopes are plotted, one for the reinforced 1.0 in. (25 mm) thick section of the segments and another for the unreinforced 0.82 in. (21 mm) thick section of the

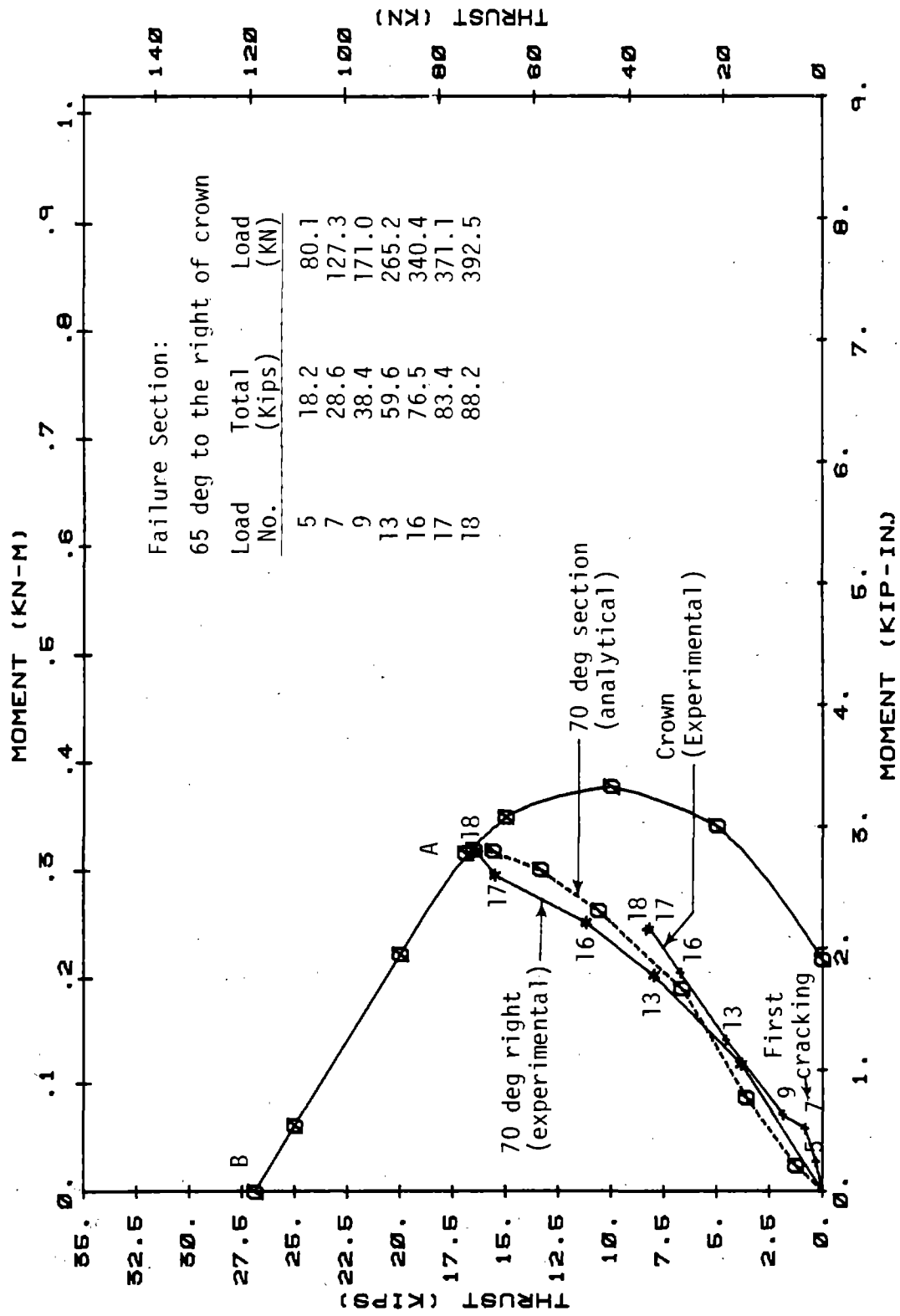


FIGURE 6.15 MOMENT-THRUST PATHS AT CROWN AND 70 DEGREES RIGHT OF CIRCLE-3

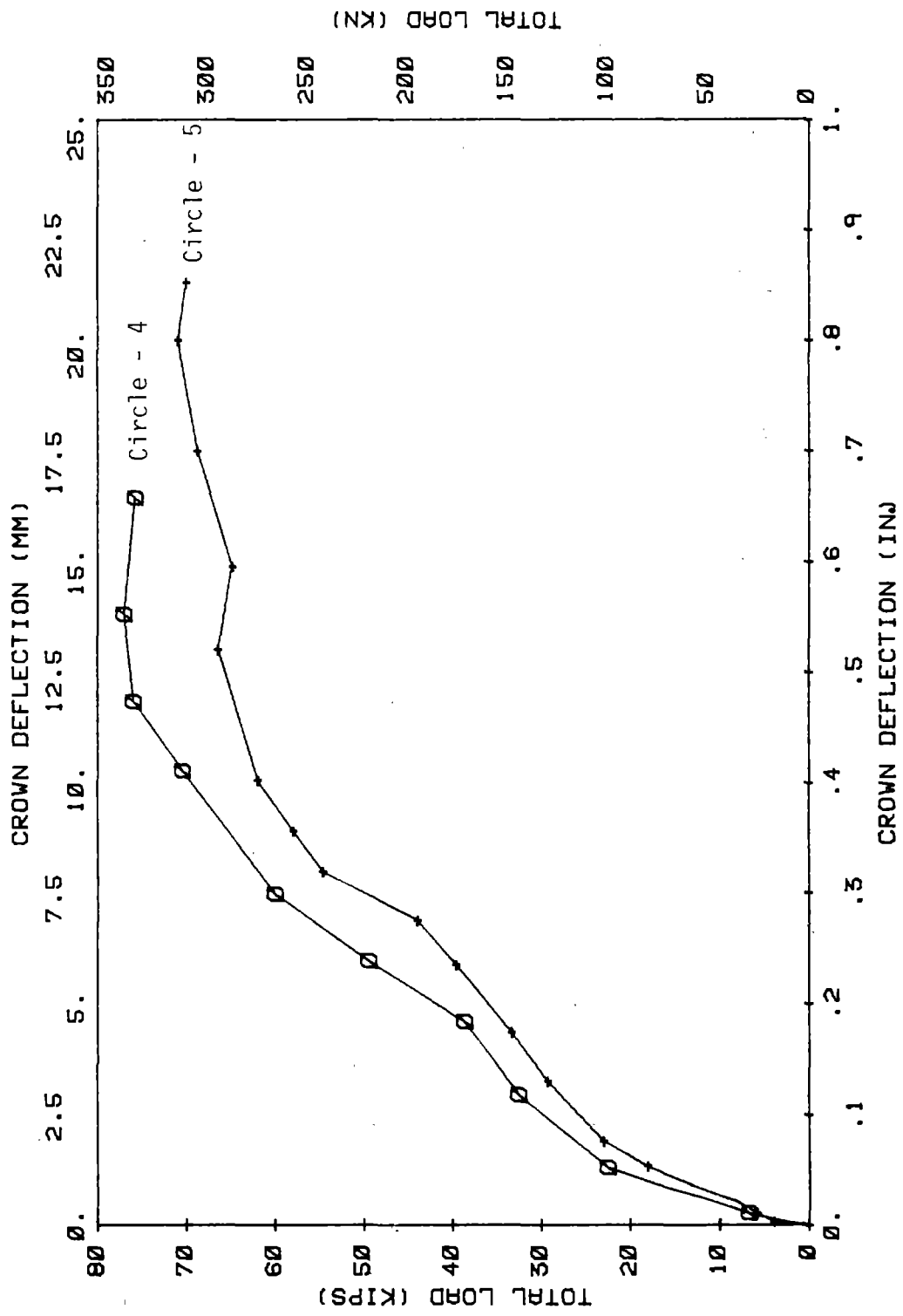


FIGURE 6.16 LOAD-DEFLECTION CURVES OF SEGMENTED LININGS

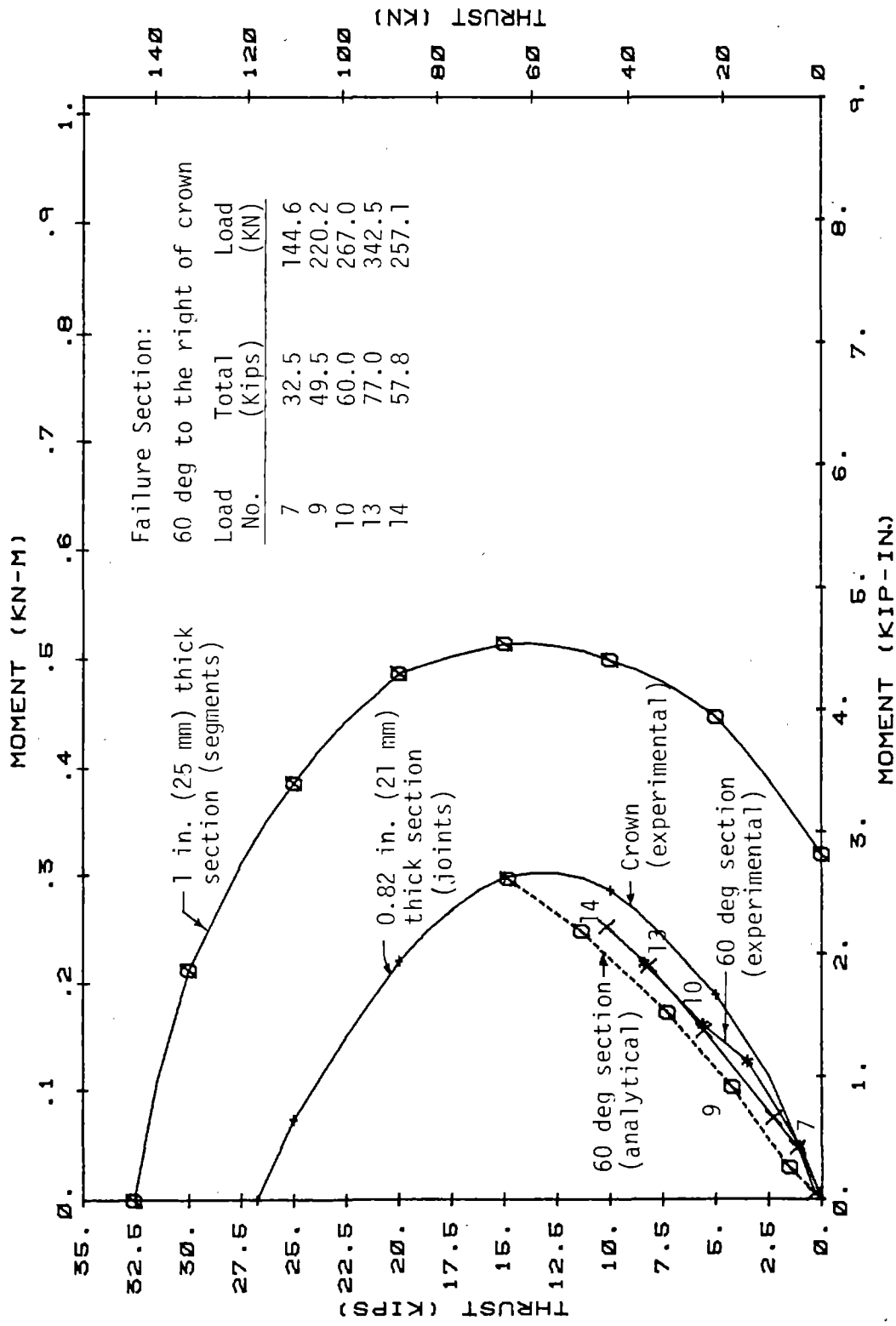


FIGURE 6.17 MOMENT-THRUST PATHS AT CROWN AND 60 DEGREES RIGHT JOINT OF CIRCLE-4

joints. Ideally, since failure occurred right at the 60 deg joint, the moment-thrust path should intersect the inside envelope. However, because of concrete spalling after load 11, the gages became inoperative so that no reliable strain data were available to complete the moment-thrust path. The thrust ratio of  $T_u/T_o = 0.56$  was obtained by extending the moment-thrust path at 60 deg right until it intersected the inside envelope.

Circle-5 Circle-5, with an initial flexibility ratio of 260, reached a total load of 70 kips (311 kN), as shown in Fig. 6.16. The thrust ratio of  $T_u/T_o = 0.40$  was obtained at the 120 deg right joint, rather than at the failure section (120 deg to the left of the crown), because the failure section was not instrumented. The peak load, the initial slope of the load-deflection curve and the thrust ratio are lower than in Circle-4, because of the lower modulus of the medium. Moment-thrust paths for the crown and 60 deg joints are shown in Fig. 6.18. It is observed that the moment-thrust paths for the segmented linings are generally steeper than the corresponding sections in the monolithic. However, when comparing a monolithic lining (Circle-2) with the segmented (Circle-5) having the same amounts of reinforcement and medium modulus, it is observed that their load carrying capacities are very close, as shown in Fig. 6.19.

### 6.3.2 Deformability and Cracking of the Linings

The amount of deformation and cracking in concrete tunnel linings are very important design considerations. Lining deformations reflect the magnitude of the moments in the lining section. Consequently, many tunnel designers use expected lining deformations as design criteria to ensure adequacy of the lining to withstand moments. Cracking is usually related to the amount of allowable water leakage in a tunnel. Obviously, more and wider cracks will permit more leakage. The time of appearance of first cracks is also an important design consideration, but if adequate load factors are integrated into the design, the lining

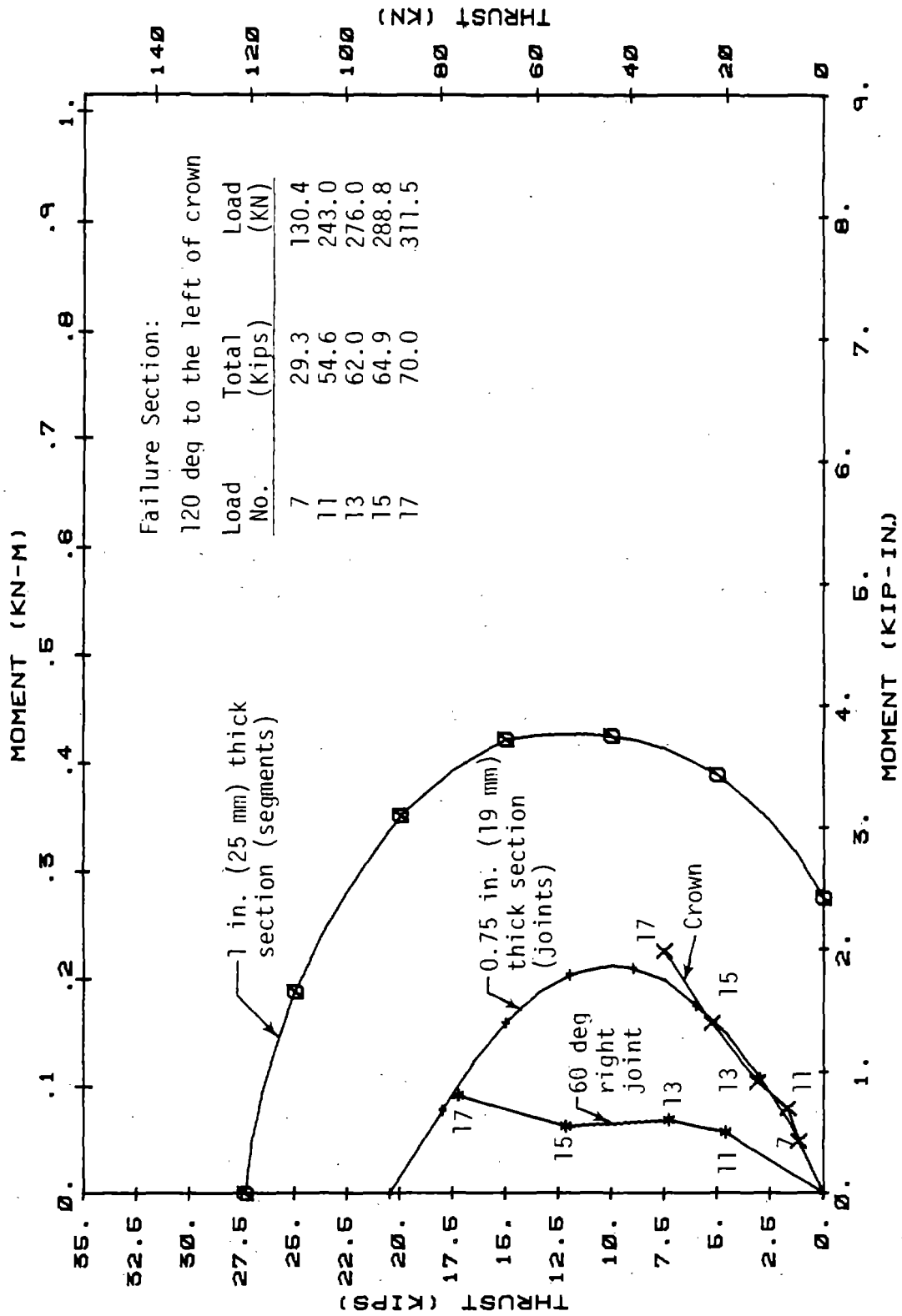


FIGURE 6.18 MOMENT-THRUST PATHS AT CROWN AND 60 DEGREES RIGHT JOINT OF CIRCLE-5

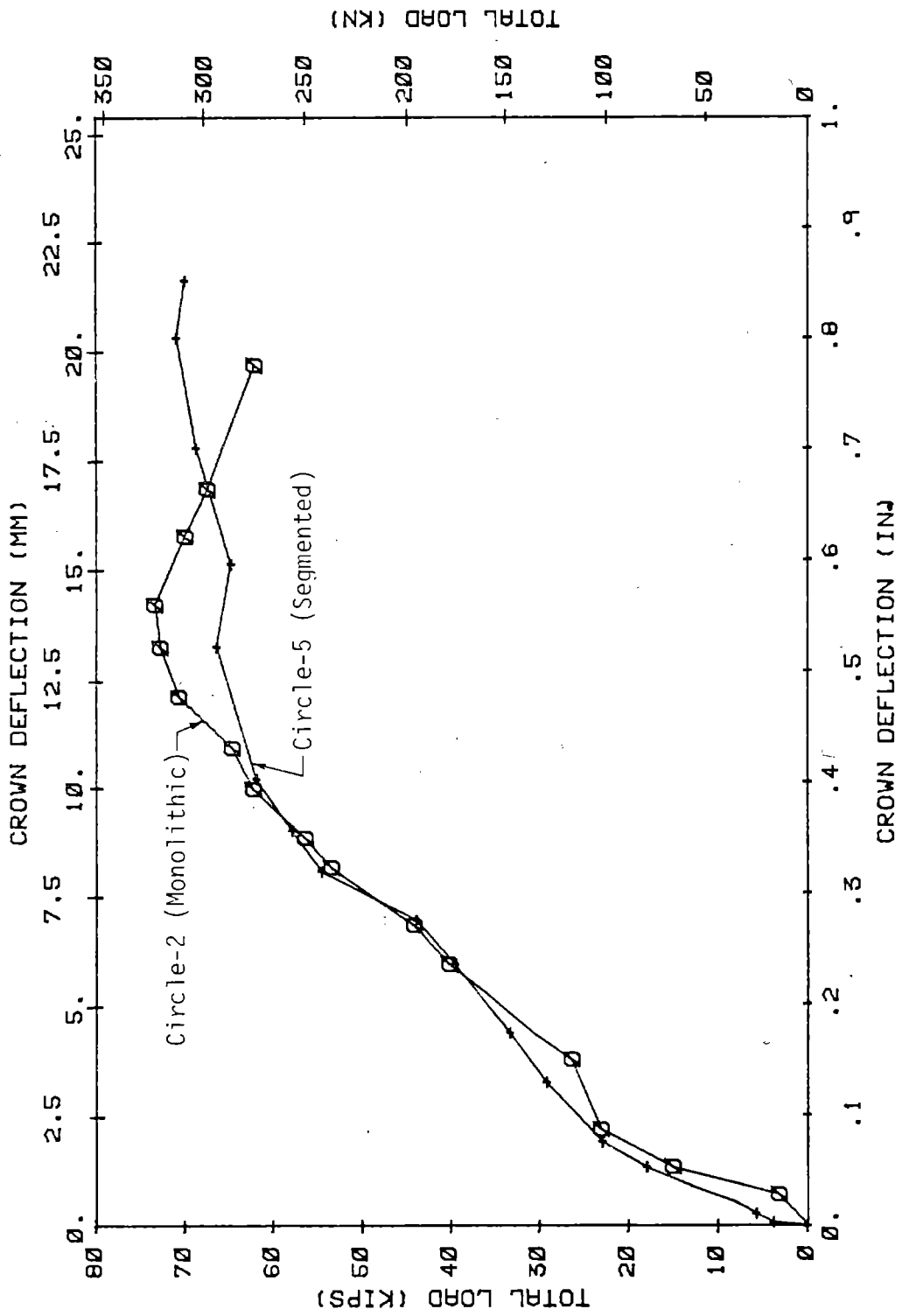


FIGURE 6.19 COMPARISON OF LOAD-DEFLECTION CURVE OF MONOLITHIC AND SEGMENTED LININGS



might never experience high enough loads to result in cracking. In the following paragraphs the deformability and cracking of each lining are discussed and summarized in Table 6.1.

Circle-1 Cracks first appeared in the crown region of Circle-1 at a load of 20 kips (89 kN), or 42 percent of the peak load. Because of this, a kink appears in the load-deflection curve of Circle-1 at that load level, as shown in Fig. 6.12. Deflection of the lining increased with the applied load reaching a maximum value of 0.643 in. (16 mm) or a  $\Delta D/D$  of 1.27 percent at peak load (after accounting for the invert deflection). The deflected shapes at 50 percent and at peak load are shown in Fig. 6.20. The crack at the crown opened with increasing load as shown in Fig. 6.21. At the same time more cracks appeared at the invert and in the left springline region; the crack pattern is shown in Fig. 6.22, where numbers next to every crack denote the load number at which they first appeared with a low number indicating that the crack appeared early in the loading process. The load numbers are related to the corresponding applied loads in the figures showing the moment-thrust paths for each lining.

Circle-2 Cracks first appeared at the crown at a load of 26.4 kips (109.5 kN) or 36 percent of the peak load, which is evident from the sudden change in slope of the crown-deflection curve in Fig. 6.12 at that load level. The crown deflection reached a value of 0.560 in. (14 mm) at peak load or a  $\Delta D/D$  of 1.2 percent as shown in Fig. 6.23. The sequence of cracking is shown in Fig. 6.24, where the crown cracks were followed by cracks at the invert and in the vicinity of the failure region, 70 deg to the left of the crown. The presence of reinforcement (1.0 percent) kept the major cracks at the crown and invert from opening, the crack-width remaining in the range of 0.002 in. (0.05 mm), as shown in Fig. 6.21. It should be kept in mind however that the medium modulus was higher in Circle-2 than in Circle-1, which also contributed to keeping deformations and cracking at lower levels.

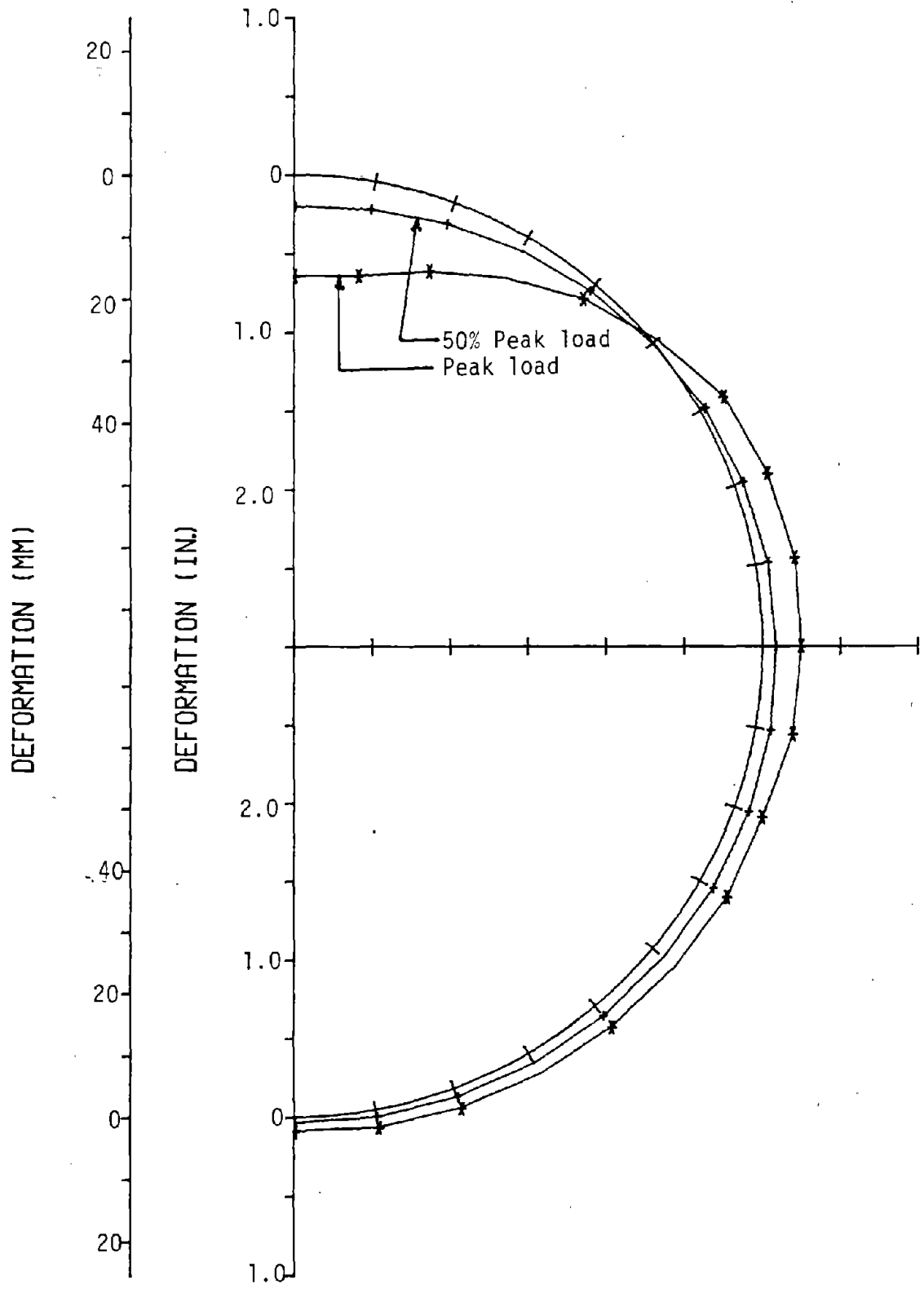


FIGURE 6.20 DEFLECTED SHAPES OF CIRCLE 1 AT 50 AND 100 PERCENT OF PEAK LOAD

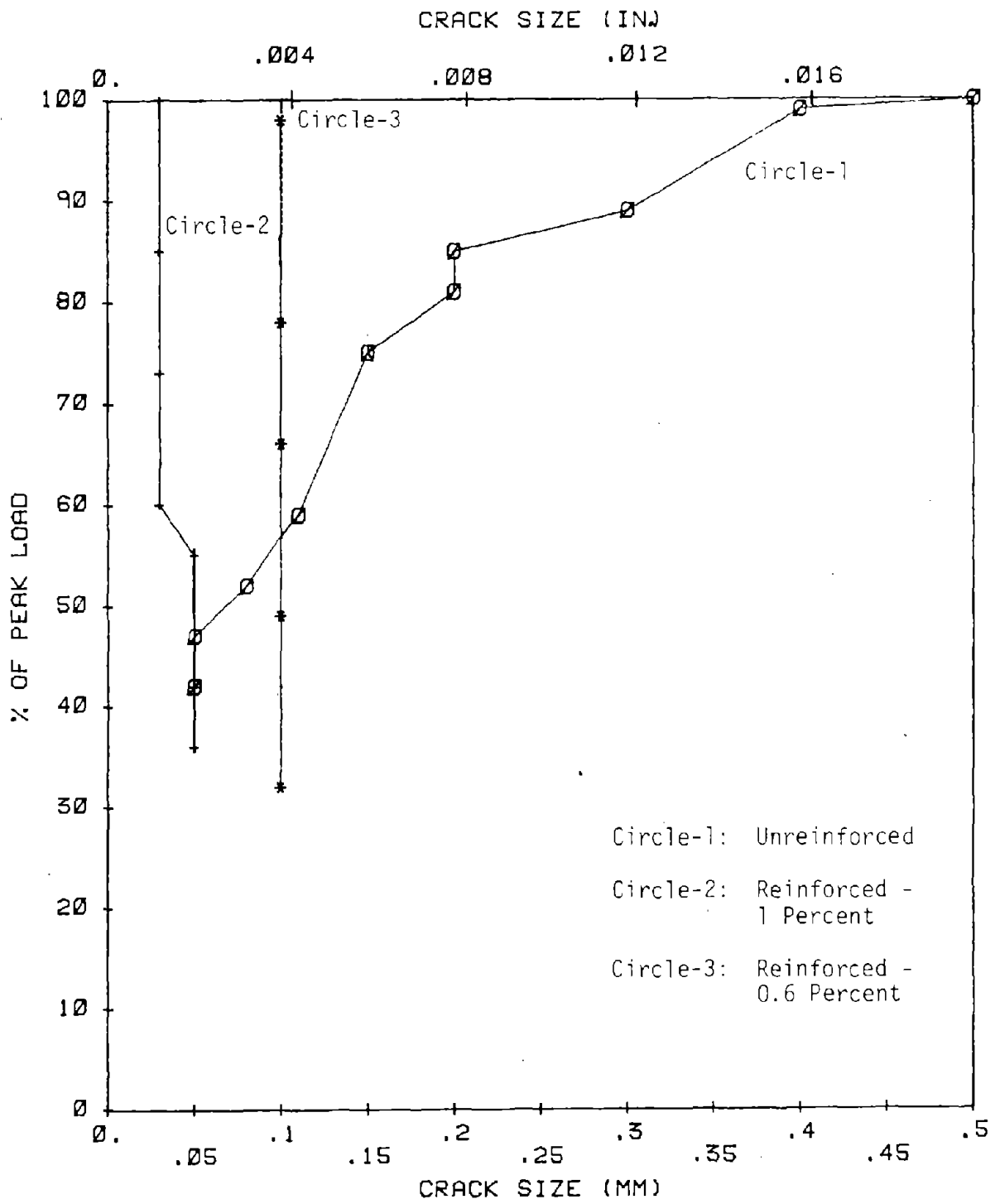


FIGURE 6.21 EFFECT OF AMOUNT OF REINFORCEMENT ON CRACK SIZE

Top View



Side View

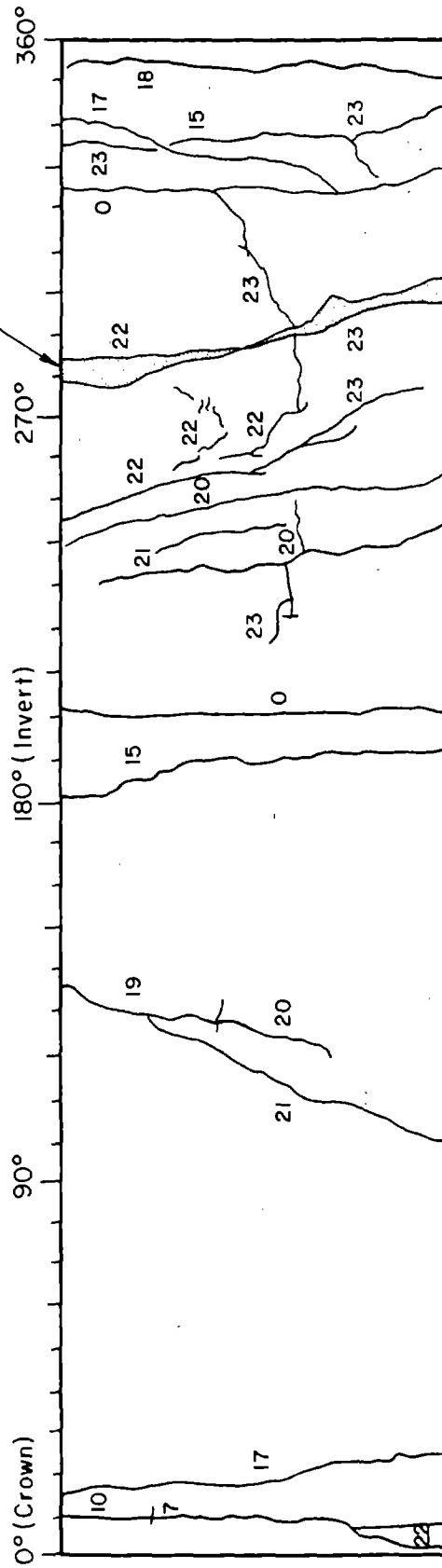


FIGURE 6.22 CRACKING PATTERN OF CIRCLE 1

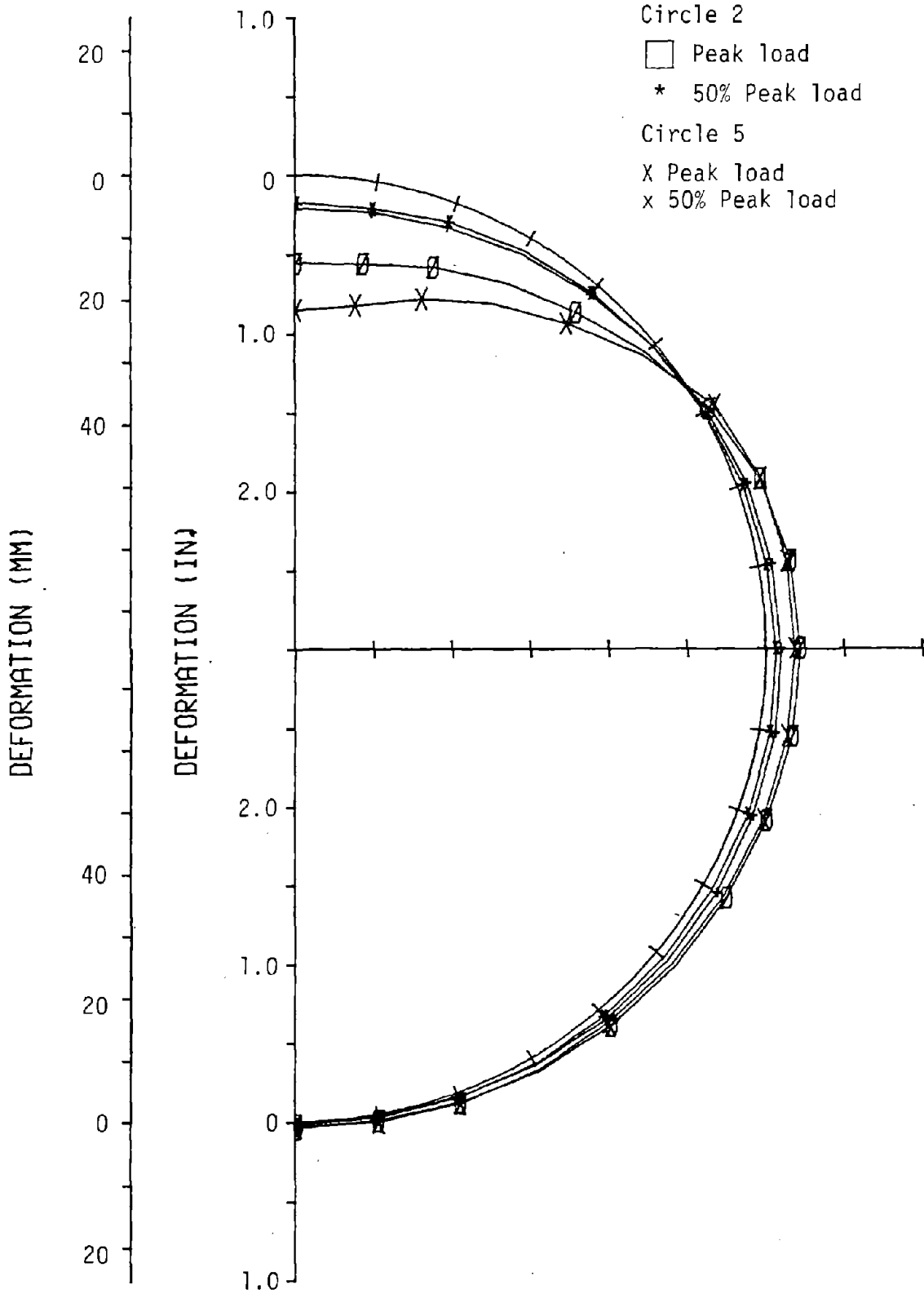


FIGURE 6.23 DEFLECTED SHAPES OF CIRCLE 2 AND 5 AT 50 AND 100 PERCENT OF PEAK LOAD

Top View



Side View

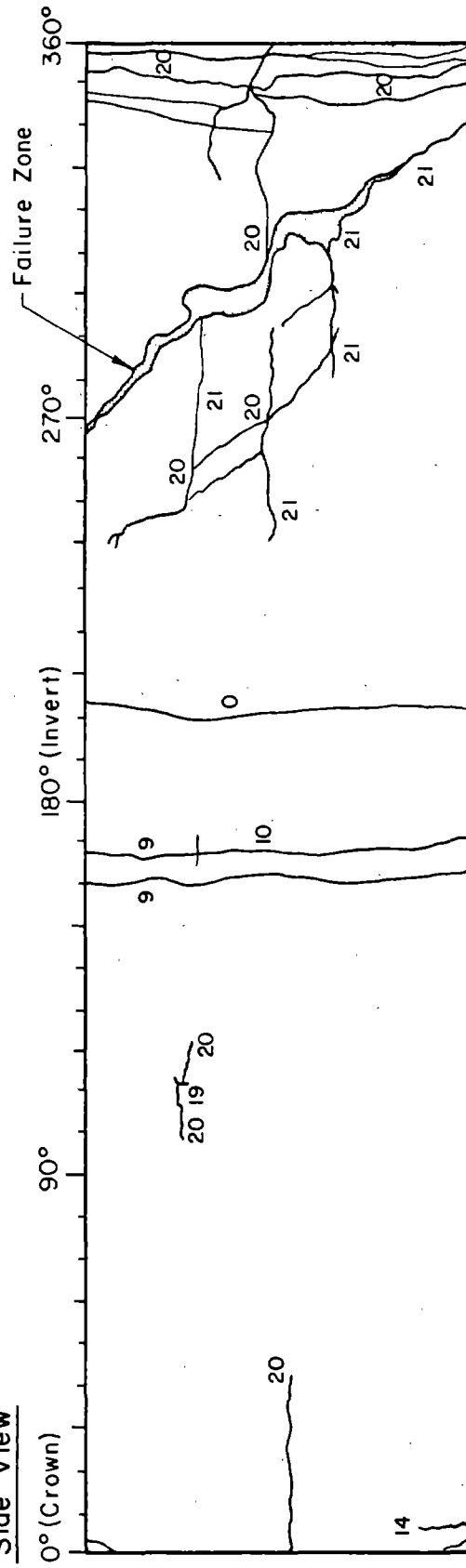


FIGURE 6.24 CRACKING PATTERN OF CIRCLE-2

Circle-3 First cracks appeared at the crown and invert at the same time, at a load of 28.5 kips (126.8 kN) or 32 percent of the peak load. Once again, first cracking caused a change in the slope of the load-deflection curve at that load level as shown in Fig. 6.12. The crown deflection reached a value of 0.610 in. (15 mm) at the peak load or a  $\Delta D/D$  of 1.3 percent as shown in Fig. 6.25. The deflection at peak load is of comparable magnitude for all three monolithic linings. However, the amount of cracking is drastically reduced in Circle-3 because of higher modulus of the medium, as shown in Fig. 6.26. The beneficial effects of reinforcement are shown in Fig. 6.21, however, where the size of the cracks in the crown region are larger in Circle-3 than in Circle-2.

Circle-4 First cracks appeared at a load of 70 kips (311.4 kN) or 90 percent of the peak load and the number of cracks was reduced as shown in Fig. 6.27. Failure was initiated in the vicinity of the joint 60 deg to the right of the crown, rather than at the crown and invert regions as was the case in the monolithic linings. Cracking initiated in the form of concrete in the vicinity of the joints 60 deg to the right of the crown, rather than at the crown and invert regions as was the case in the monolithic linings. Moments were reduced in those regions by the rotation of the joints as shown in Fig. 6.28. Crown and invert joints rotated about the outside edge of the lining and thus reduced tensile strains and cracking on the inside face, whereas the joints at the 60 and 120 deg rotated about the inside edge of the lining and thus reduced the tensile strains on the outside face. The deflected shapes of Circle-4 at 50 and 100 percent of the peak load are shown in Fig. 6.29. The crown deflection at peak load reached a value of 0.553 in. (14 mm) or a  $\Delta D/D$  of 1.2 percent.

Circle-5 First flexural cracks appeared at a load of 64.8 kips (288.2 kN) or 93 percent of the peak load as shown in Fig. 6.30. The joints were very effective once again in delaying the time of appearance of the first cracks and limiting their number and size.

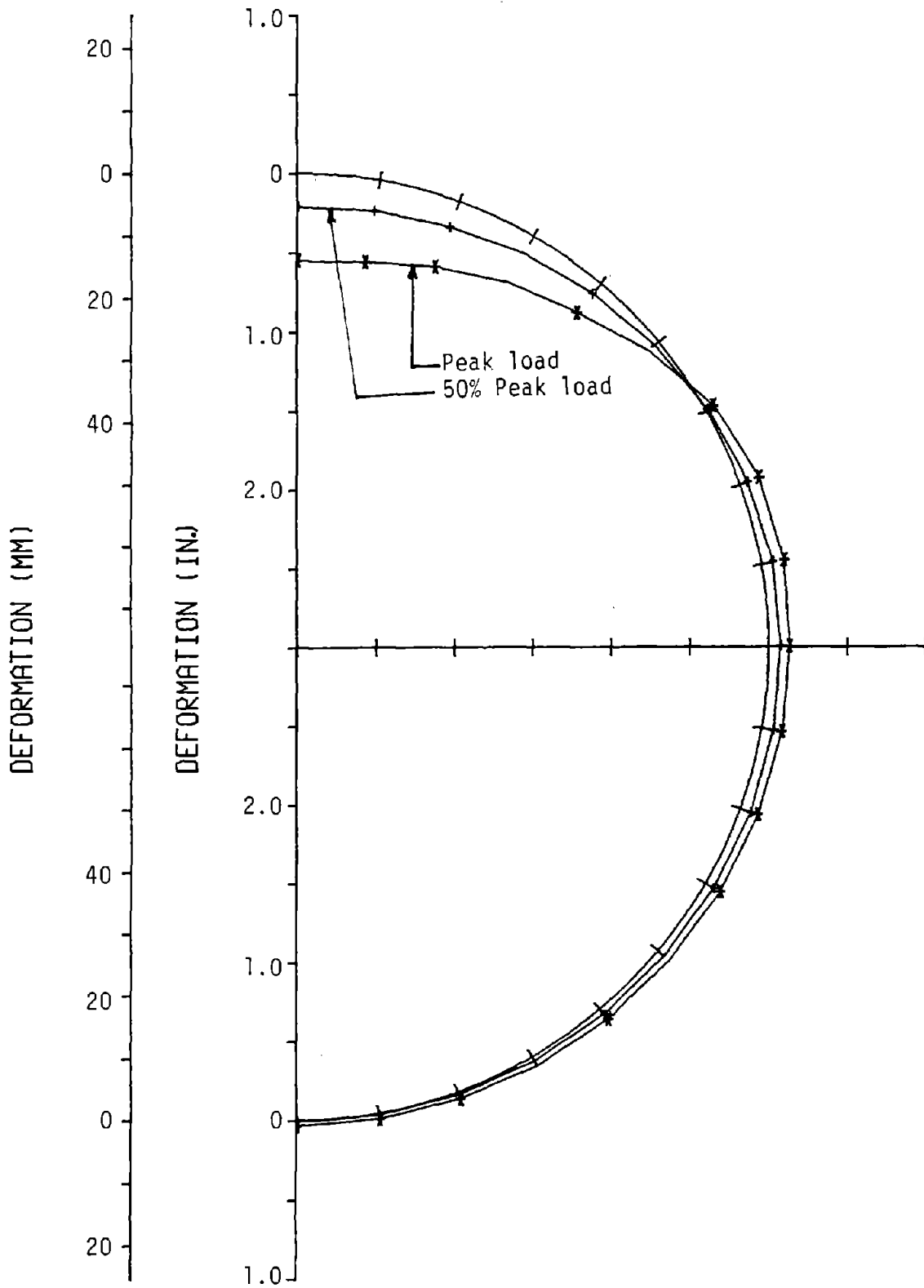


FIGURE 6.25 DEFLECTED SHAPES OF CIRCLE-3 AT 50 AND 100 PERCENT OF PEAK LOAD



Top View



Side View

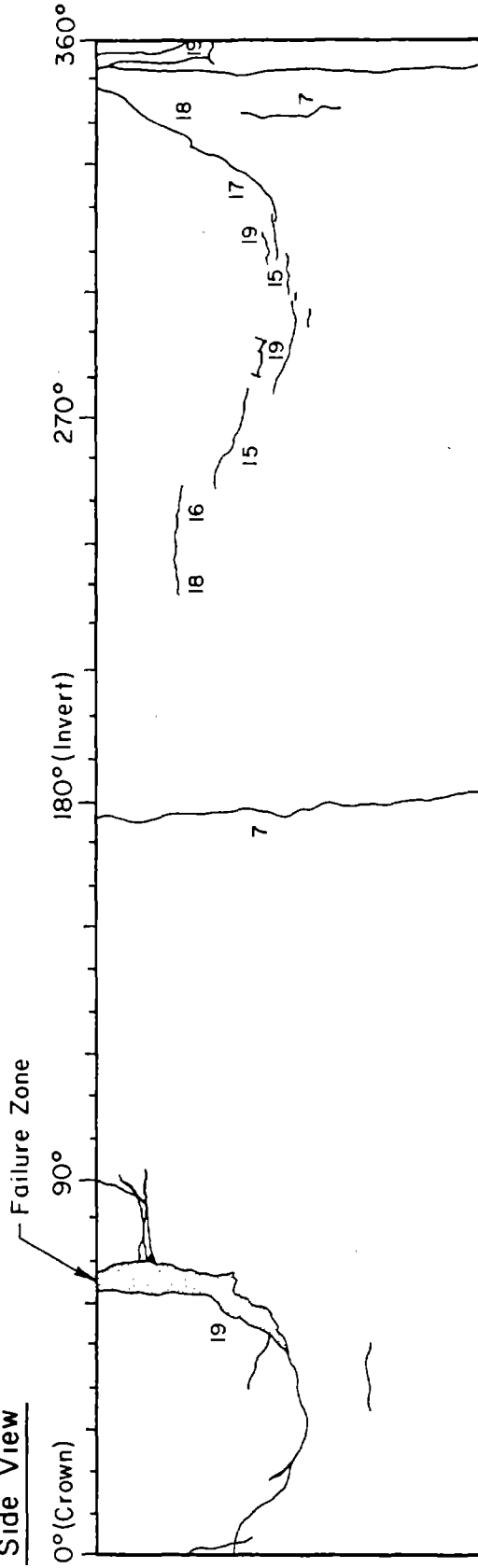


FIGURE 6.26 CRACKING PATTERN OF CIRCLE-3

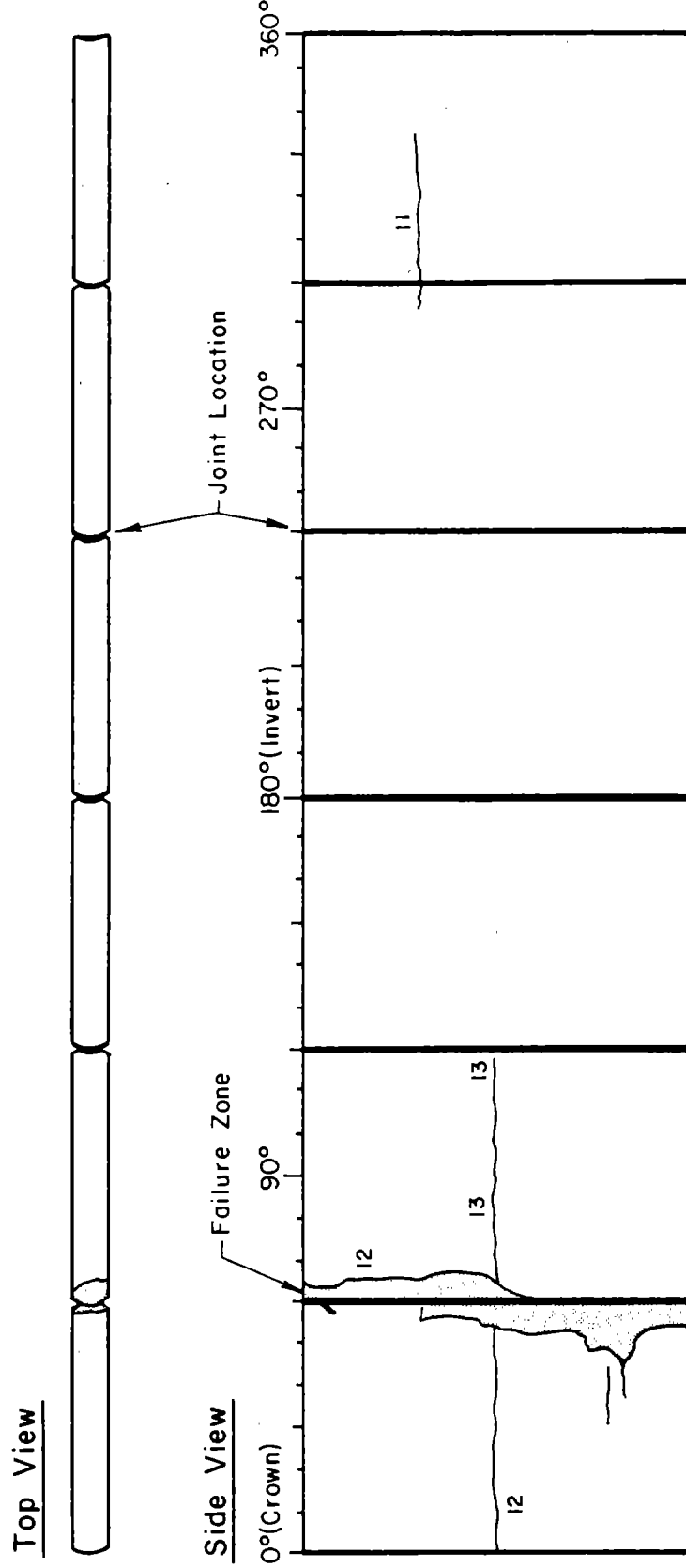


FIGURE 6.27 CRACKING PATTERN OF CIRCLE-4

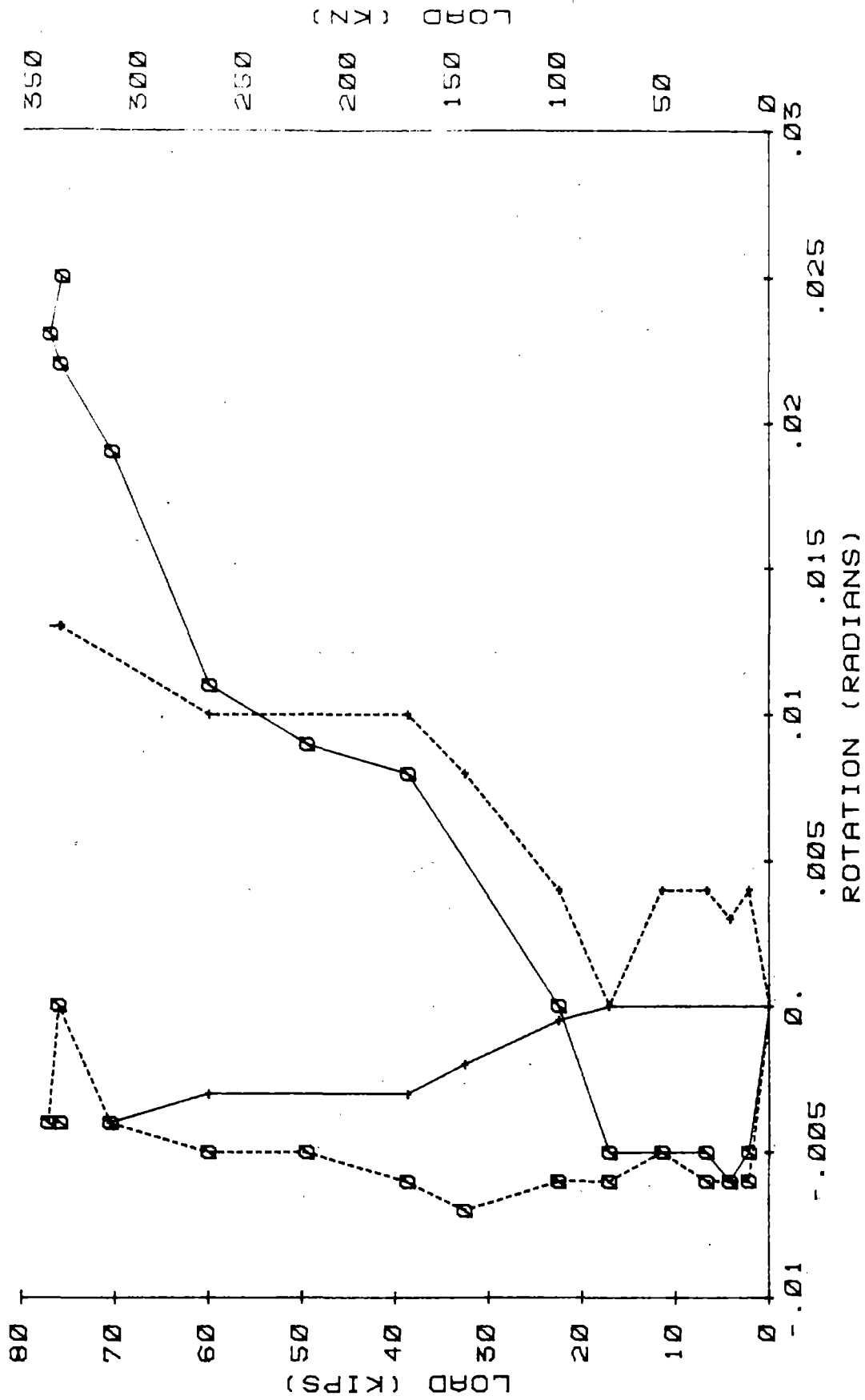


FIGURE 6.28 LOAD VS JOINT ROTATIONS OF CIRCLE-4

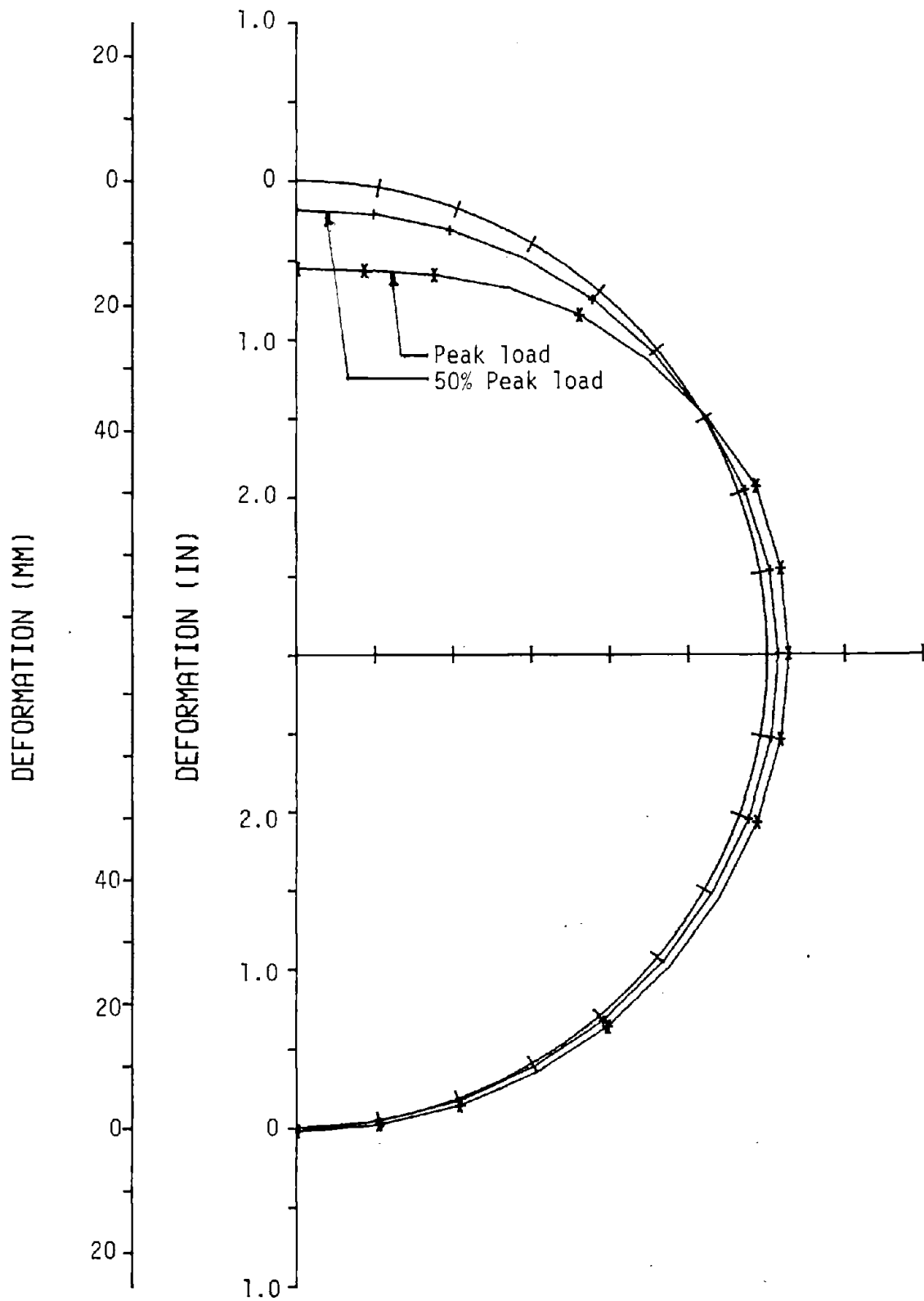


FIGURE 6.29 DEFLECTED SHAPES OF CIRCLE-4 AT 50 AND 100 PERCENT OF PEAK LOAD

Top View



Side View

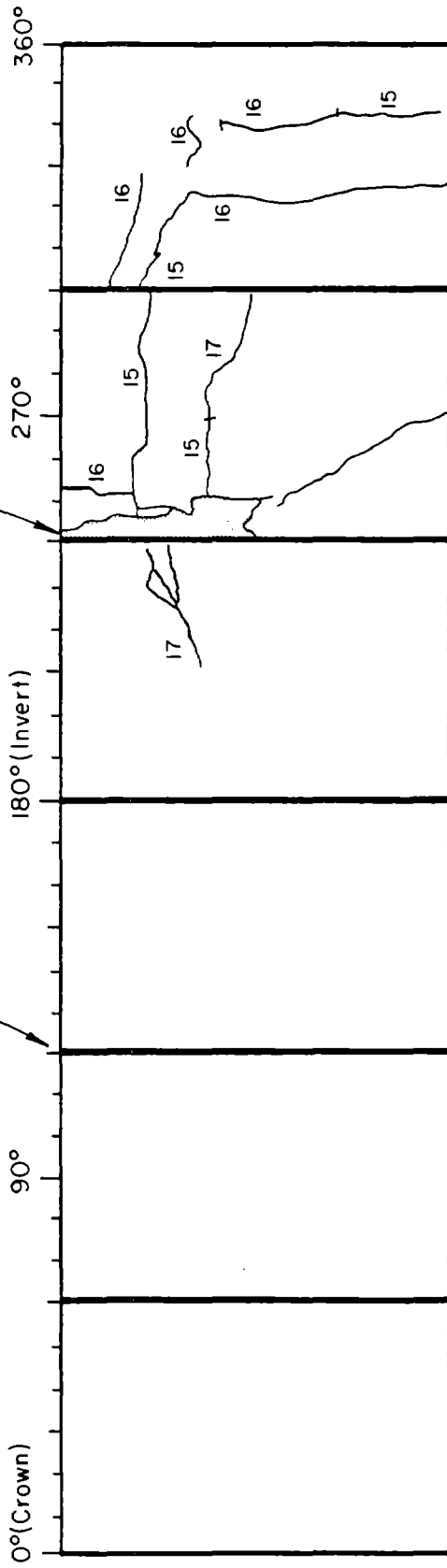


FIGURE 6.30 CRACKING PATTERN OF CIRCLE-5

Joint rotations for Circle-5 are higher than those of Circle-4, because of the lower value of the modulus of the medium, as shown in Fig. 6.31. The deflected shapes of Circle-5 are compared in Fig. 6.23 with those of Circle-2, the monolithic lining with the same amount of reinforcement and about the same modulus of the medium. As observed the crown deflection of 0.852 in. (22 mm) or  $\Delta D/D$  of 1.86 percent for Circle-5 is much higher than the value of 0.559 in. (14 mm) observed in Circle-2. This is the result of the presence of the joints which allow more rotation and thus deflection under the same load. However, comparing deflections at peak load may be misleading, because of the effect of test procedure on behavior at peak loads, such as time required to take readings and size of load increments near peak load. For these reasons, the change in diameter of the linings at fifty percent of the peak load are also provided in Table 6.1. As observed, the change in diameter of Circle-2 ( $\Delta D/D$  of 0.43 percent) is of similar magnitude to that of Circle-5 ( $\Delta D/D$  of 0.36 percent).

### 6.3.3 Failure Mechanisms

Monolithic Linings: All three monolithic linings Circles-1, 2 and 3 failed at a region between 65 to 80 deg from the crown, as shown in Fig. 6.32. In the process of loading, the lining was deflecting inward at the crown and outward at the sides. This outward movement caused visible deformation and cracking in the medium that was more pronounced in Circle-1 with the lower modulus and strength shown in Fig. 6.33. Because of high compressive stresses at the medium-lining interface, the medium exceeded its peak strength and entered into the "plastic" state shown in Fig. 6.4. The extent of this "plastic" zone is estimated by plotting the section curvatures along the lining calculated from the strains. As observed in Fig. 6.34 for Circle-2, a sharp increase in curvatures of the lining is observed in a zone extending from 50 to 90 degrees from the crown. Similar observations were made in all linings tested. The reduction of stiffness of the

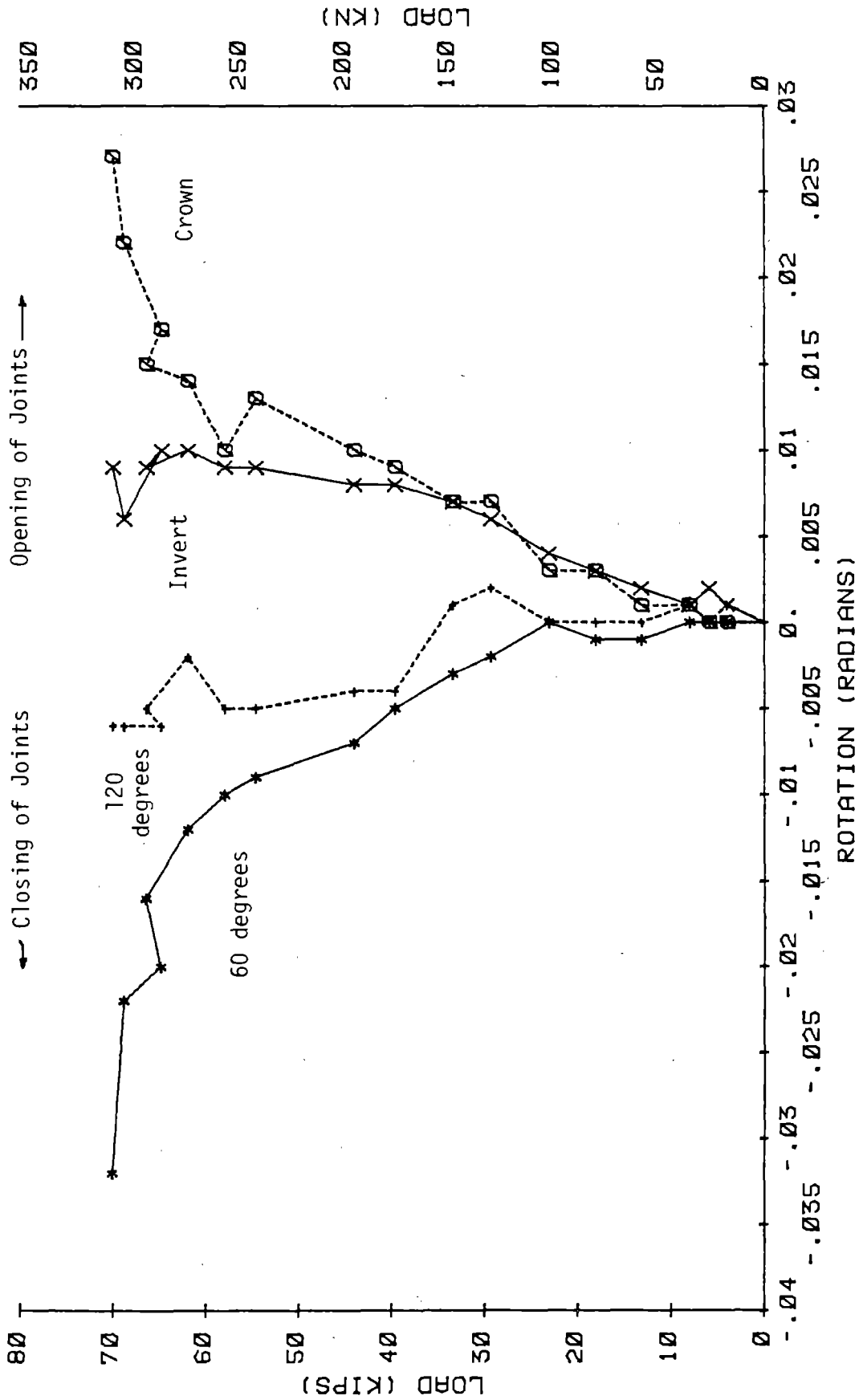


FIGURE 6.31 LOAD VS JOINT ROTATIONS OF CIRCLE-5

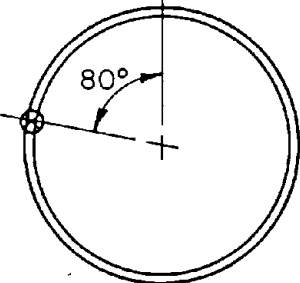
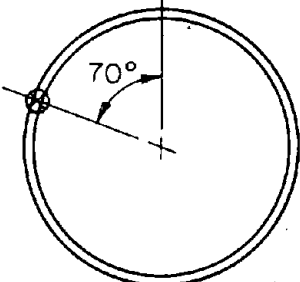
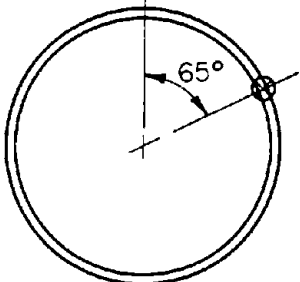
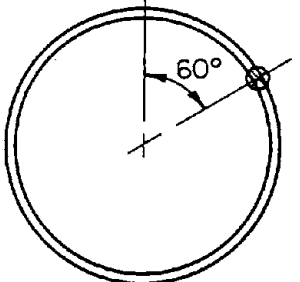
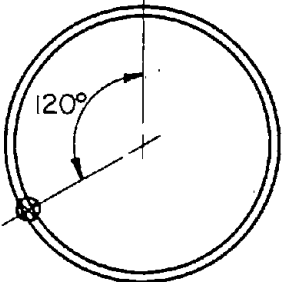
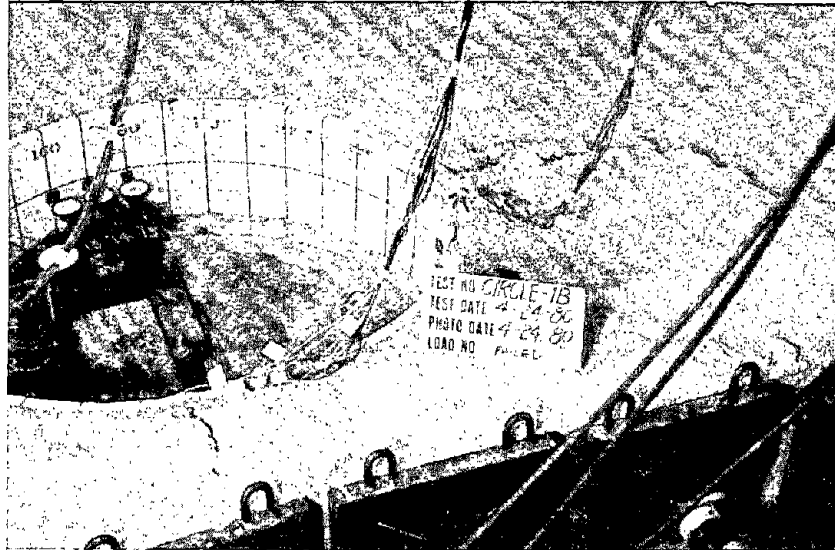
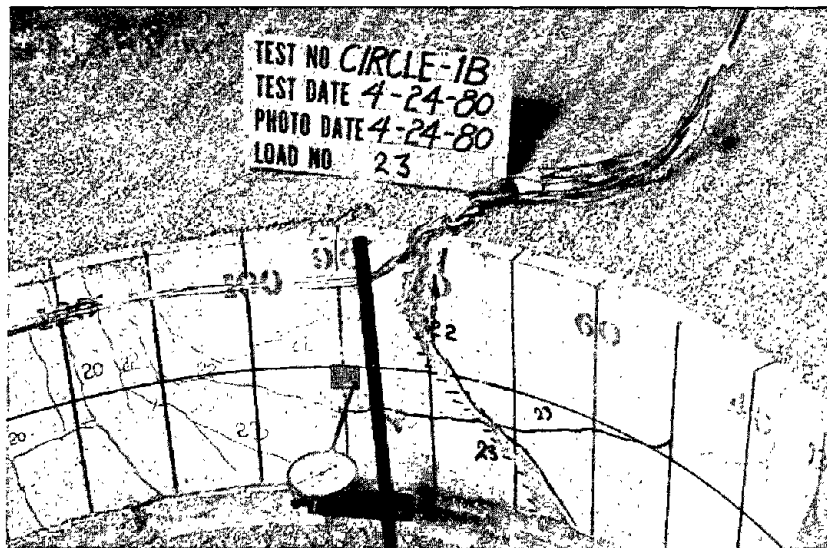
SPECIMEN	FAILURE LOCATION	FAILURE MODE
CIRCLE-1		CRUSHING OF CONCRETE MOMENT - THRUST
CIRCLE-2		CRUSHING OF CONCRETE MOMENT - THRUST
CIRCLE-3		CRUSHING OF CONCRETE MOMENT - THRUST
CIRCLE-4		CRUSHING OF CONCRETE BUCKLING OF R-BARS PRIMARILY COMPRESSION
CIRCLE-5		CRUSHING OF CONCRETE BUCKLING OF R-BARS PRIMARILY COMPRESSION

FIGURE 6.32 TYPE AND LOCATION OF FAILURE MODES IN CIRCLES





(a) Medium Failure



(b) Lining Failure

FIGURE 6.33 CIRCLE-1 AT FAILURE

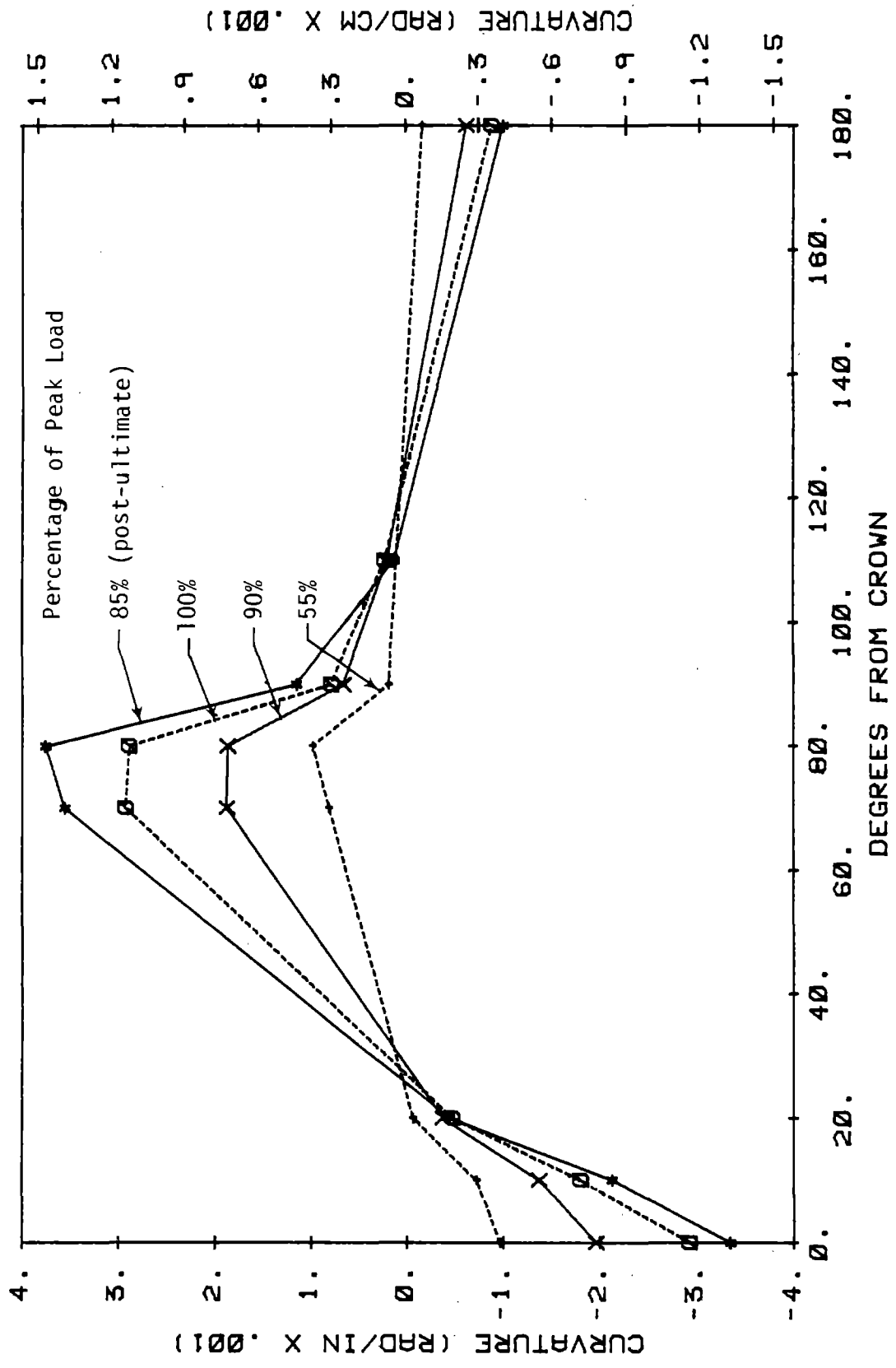


FIGURE 6.34 CURVATURE VS DISTANCE FROM CROWN FOR CIRCLE-2

medium in this region induced high moment in the linings, which in combination with the thrust caused failure.

The location of the failure section is also a function of the type and nature of the applied load. A more concentrated loosening type load in the crown region would tend to shift the failure section toward the crown, whereas a more overpressure type loading (explained in Section 2.1) would tend to shift the section toward the springline. In these experiments the loading condition was between loosening and overpressure and this provides another justification for the location of the failed zone. The failed sections are shown in Fig. 6.33 for Circle-1, Fig. 6.35 for Circle-2 and Fig. 6.36 for Circle-3.

Segmented Linings: Both segmented linings Circle-4 and Circle-5 failed at a joint. Circle-4 at the 60 deg to the left of the crown joint and Circle-5 at the 120 deg to the right of the crown joint, as shown in Fig. 6.32. In the case of Circle-4 failure occurred within the same region as in the monolithic linings between 50 and 90 deg from the crown. It is believed that a localized weakness in the medium mass caused failure at the 120 deg joint rather than at a 60 deg joint in Circle-5. The failure in Circle-4 (Fig. 6.27) started at the upper right side of the 60 deg joint with concrete spalling at about 90 percent of peak load and migrated to the lower left region of the joint. Spalling of the concrete eliminated the cover over the reinforcing bars which buckled and eventually caused crushing of the entire joint region as shown in Fig. 6.37. A horizontal crack in Circle-5, isolated the upper portion of the joint 120 deg to the left of the crown. Concentration of thrust in the region caused concrete spalling, elimination of the cover, buckling of the reinforcing bars and eventual failure, as shown in Fig. 6.38.

Thrust was a more predominant factor in the failure of the segmented linings, as it is implied by the steeper slopes of the moment-thrust paths at the critical regions and by the lesser amount of flexural cracks present.

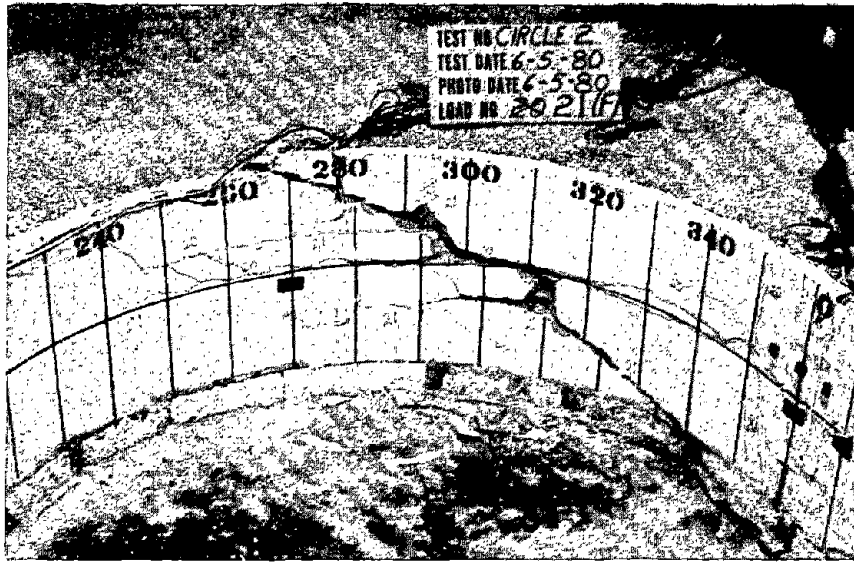


FIGURE 6.35 CIRCLE-2 AT FAILURE

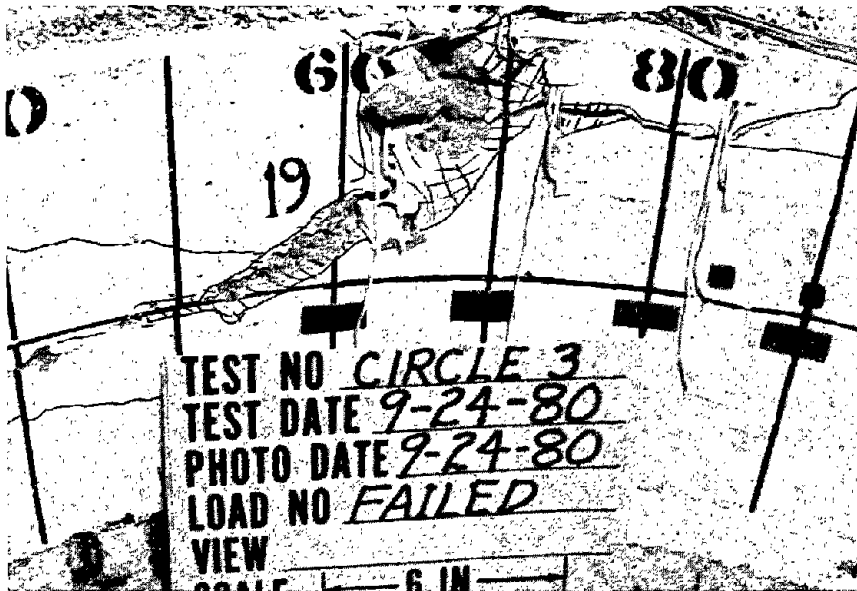


FIGURE 6.36 CIRCLE-3 AT FAILURE

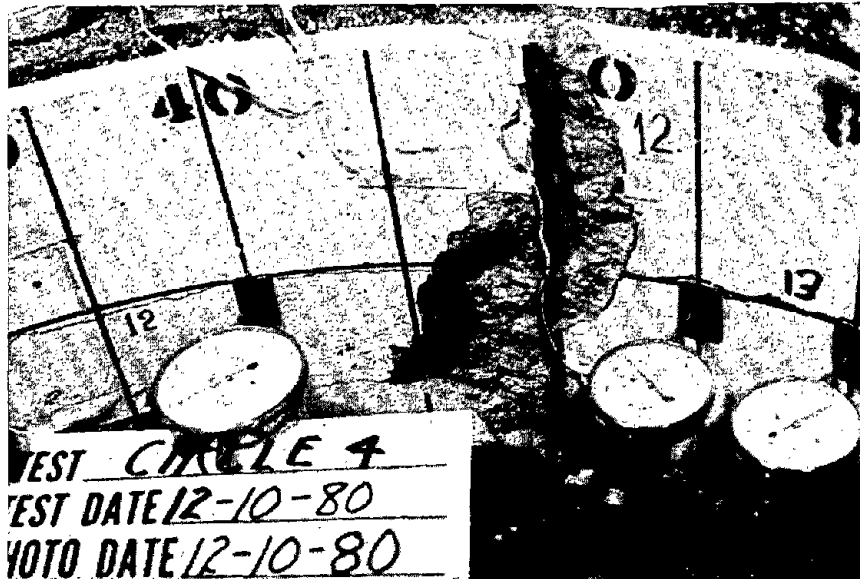


FIGURE 6.37 CIRCLE-4 AT FAILURE

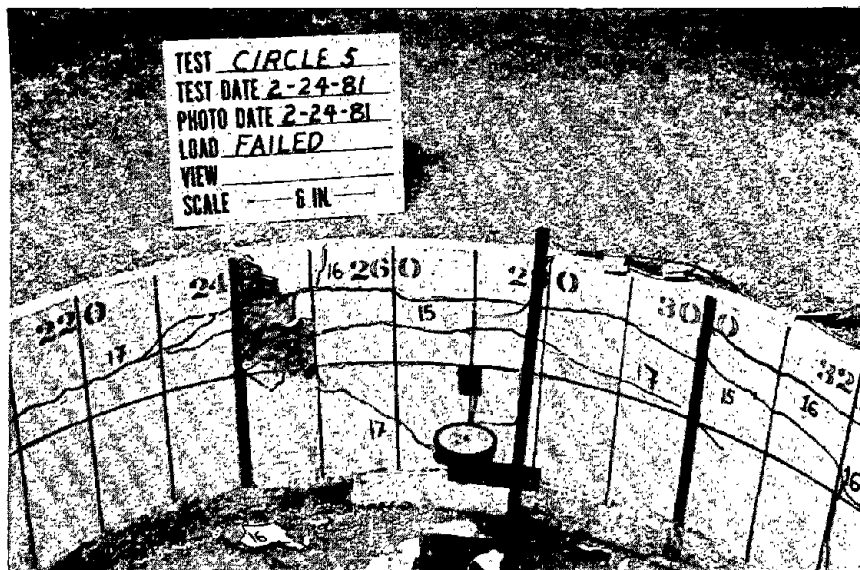


FIGURE 6.38 CIRCLE-5 AT FAILURE

## 6.4 FINITE ELEMENT ANALYSIS AND COMPARISON WITH EXPERIMENTS

The beam-continuum model, described in Section 3.3.2, was used to analyze the model tests and to determine the initial modulus of the medium in conjunction with the plate load tests. The stress-strain curve for the medium material shown in Fig. 6.4 obtained from in-situ plate load tests indicates that after a certain stress level the medium becomes essentially plastic. The nonlinear behavior of the medium during the model tests was verified by plotting the lining curvatures in Fig. 6.34. Certain portions of the medium reached a plastic state while other regions remained elastic. For purposes of comparison among the tests and in order to define the flexibility ratio, a value of initial elastic modulus of the medium was needed, however. The determination of this equivalent elastic modulus is discussed in Section 6.4.2. Once a value of the medium modulus was determined, the finite element model was used to reproduce the test results for Circles-3 and 4, discussed in Section 6.4.3. This substantiated the adequacy and validity of the program which was subsequently used to perform parametric studies described in Chapter 7.

### 6.4.1 Description of Input Data

The same basic finite element model shown in Fig. 6.39 was used to determine the elastic modulus of the medium and to simulate the test results. The general details applicable to both the medium modulus determination and the simulation of the tests will be discussed here. The lining was represented by a series of one-dimensional beam elements described in Section 3.2. Sections of the lining with high moment gradients near the crown were modeled using 5 deg elements, and 10 deg elements were used for the rest of the lining. The stress-strain curve and the tensile properties of the concrete were obtained, using the same procedure described in Section 4.4.1 for the arches, and discretized as discussed in Section 3.2.

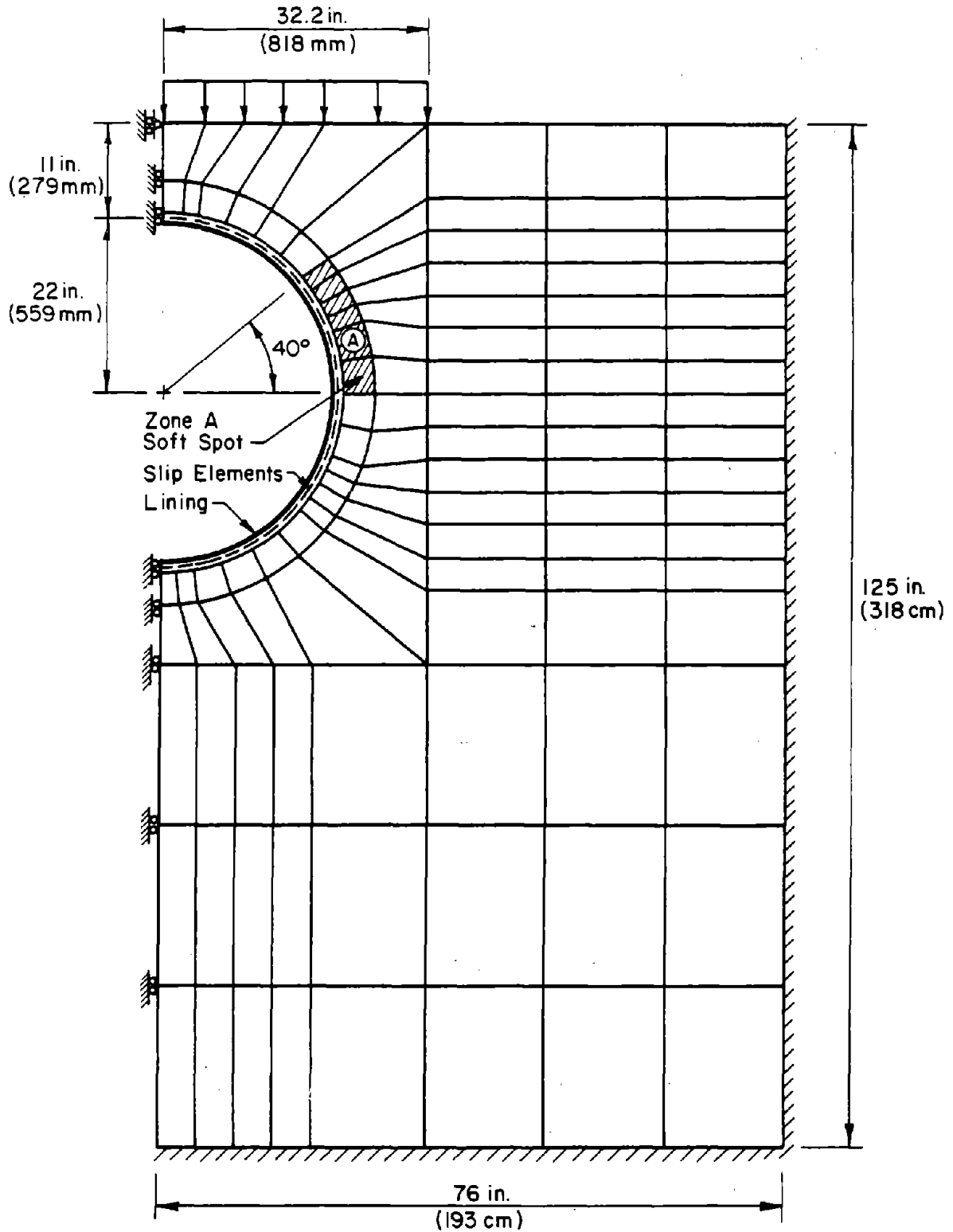


FIGURE 6.39 FINITE ELEMENT MODEL FOR SIMULATION OF CIRCLE TESTS

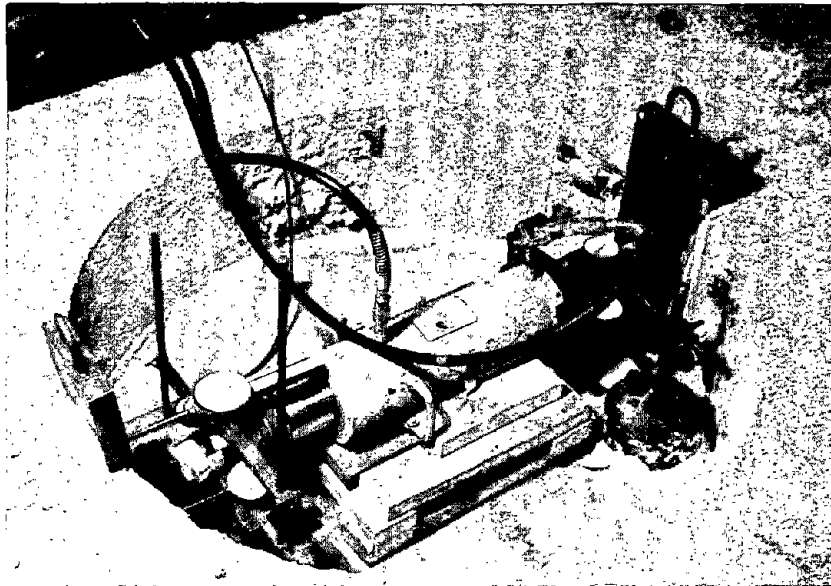
Joints between the segments in the segmented lining models were represented by very short beam elements, only 0.10 in. (2.5 mm) long, but with the reduced thickness of the joint, with no tension in the concrete and without reinforcement, since the segment reinforcement did not pass through the joint. The medium was represented by the two-dimensional quadratic isoparametric elements described in Section 3.3.2. Distributed loads were applied as uniform pressure on the element surfaces as shown in Fig. 6.39. The interface element described in Section 3.3.2 was used between the lining and the medium to model the interface stress conditions.

#### 6.4.2 Determination of the Medium Stiffness

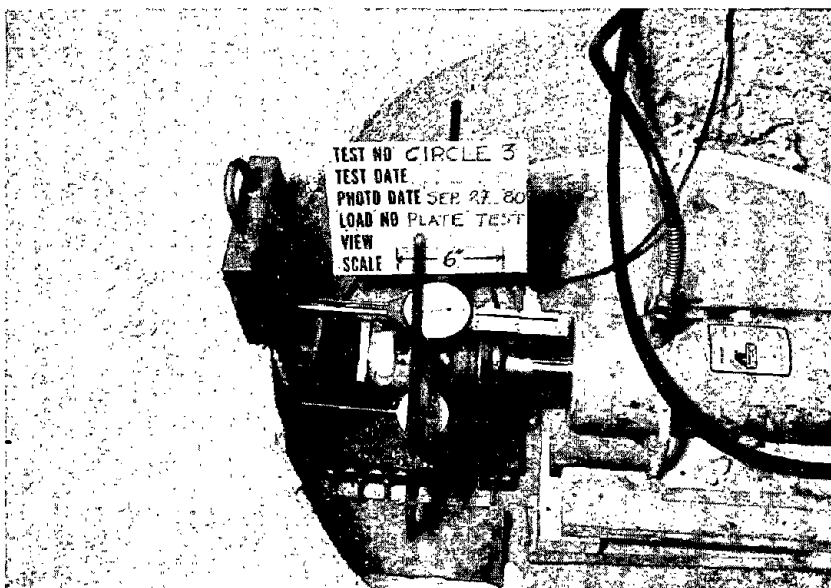
The equivalent elastic modulus of the medium was obtained by using both actual test data and the finite element model. In-situ radial plate load tests were performed on the medium in tests, Circles-3, 4 and 5. A 2 in. (51 mm) thick steel plate 7 by 12 in. (178 by 305 mm) was placed on the springline region of the medium once the test of the lining was completed and the lining removed, as shown in Fig. 6.40. The plate was grouted with a layer of Hydrocal to distribute the applied load evenly and a hydraulic ram equipped with a load cell was used to push the plate against the medium. Deformations were obtained, using three mechanical dial gages one at the top and two at the sides of the loaded plate. The test procedure was the same as that used for the arches and described in Section 4.2.3, and resulted in a load (stress)-deformation curve similar to that shown in Fig. 6.41. The initial stiffness of the load-deflection curve was then obtained as shown in the figure. In the two tests where radial plate load tests were not performed (Circles-1 and 2), the total load-crown deflection curves for the medium-lining system were used to obtain an initial stiffness (for the medium-lining system in this case).

The finite element model was used to reproduce the plate load tests for Circles-3, 4 and 5 and the medium-lining system for Circles-1 and 2.





(a) Overall View



(b) Close-up View

FIGURE 6.40 IN-SITU PLANT LOAD TESTS FOR CIRCLES

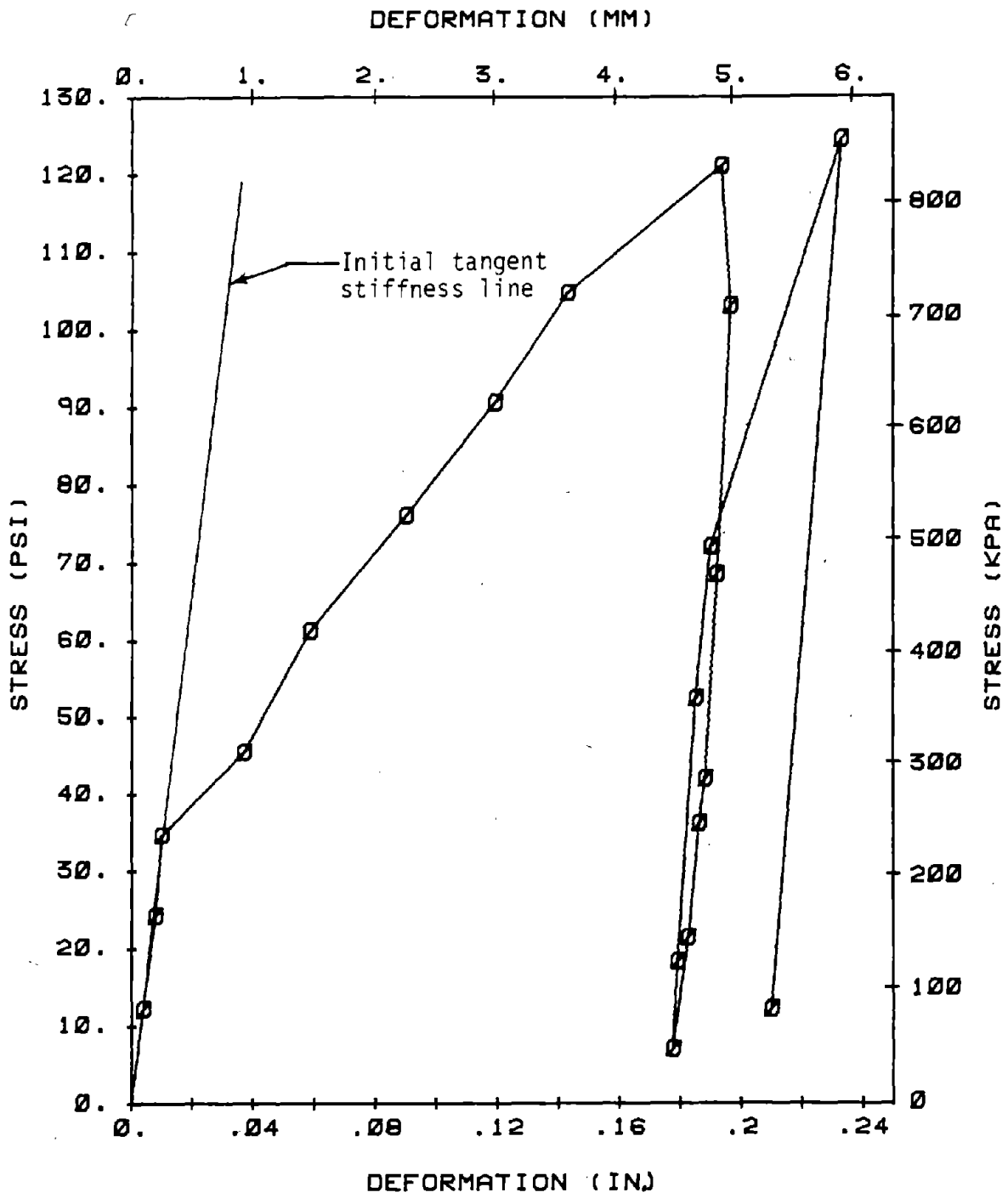


FIGURE 6.41 RESULTS OF RADIAL PLATE LOAD TEST ON MEDIUM FOR CIRCLE-4

and to match the corresponding load-deflection stiffness to obtain the medium modulus. When the plate load tests were modeled, the lining was not present and the loads were applied at the springline region of the model over an area equal to the actual plate area. Using these two systems (the plate load and the medium-lining) the elastic modulus of the medium was varied from 5 to 50 ksi (34.5 to 344.5 MPa), and for every solution with a different elastic modulus a point was obtained on Fig. 6.42. The plate load test results plotted on straight line A, whereas the medium-lining system results plotted within a narrow band between lines B and C. The initial tangent stiffnesses obtained from the actual test results were then entered in this graph on the vertical axis, and the corresponding value for the elastic modulus of the medium obtained. They were termed initial equivalent elastic modulus and are listed in Table 6.1.

#### 6.4.3 Comparison with Experimental Results

The finite element model shown in Fig. 6.39 was used to simulate tests Circles-3 and 4. The initial modulus of elasticity used for the medium was the one determined in the previous section. However, as discussed in Section 6.3.3 a zone of the medium between 50 and 90 deg from the crown entered the plastic state during the tests. Consequently, in simulating the test results, the modulus of the medium in the shaded region called Zone A in Fig. 6.39, was reduced gradually as loads were applied to simulate the reduced stiffness in this region.

In the simulation of Circle-3 the medium modulus in the soft spot region was gradually reduced from 40 to 3 ksi (275.6 to 20.8 MPa) whereas in Circle-4 it was reduced from 45 to 3 ksi (310 to 20.8 MPa). In simulating the tests full slip conditions were used between the lining and the medium. The total applied loads and corresponding changes in diameter of the lining for the analysis and the tests are compared in Figs. 6.43 and 6.44. The general slope of the test results is reproduced well, but sudden changes in the slope due to cracking of

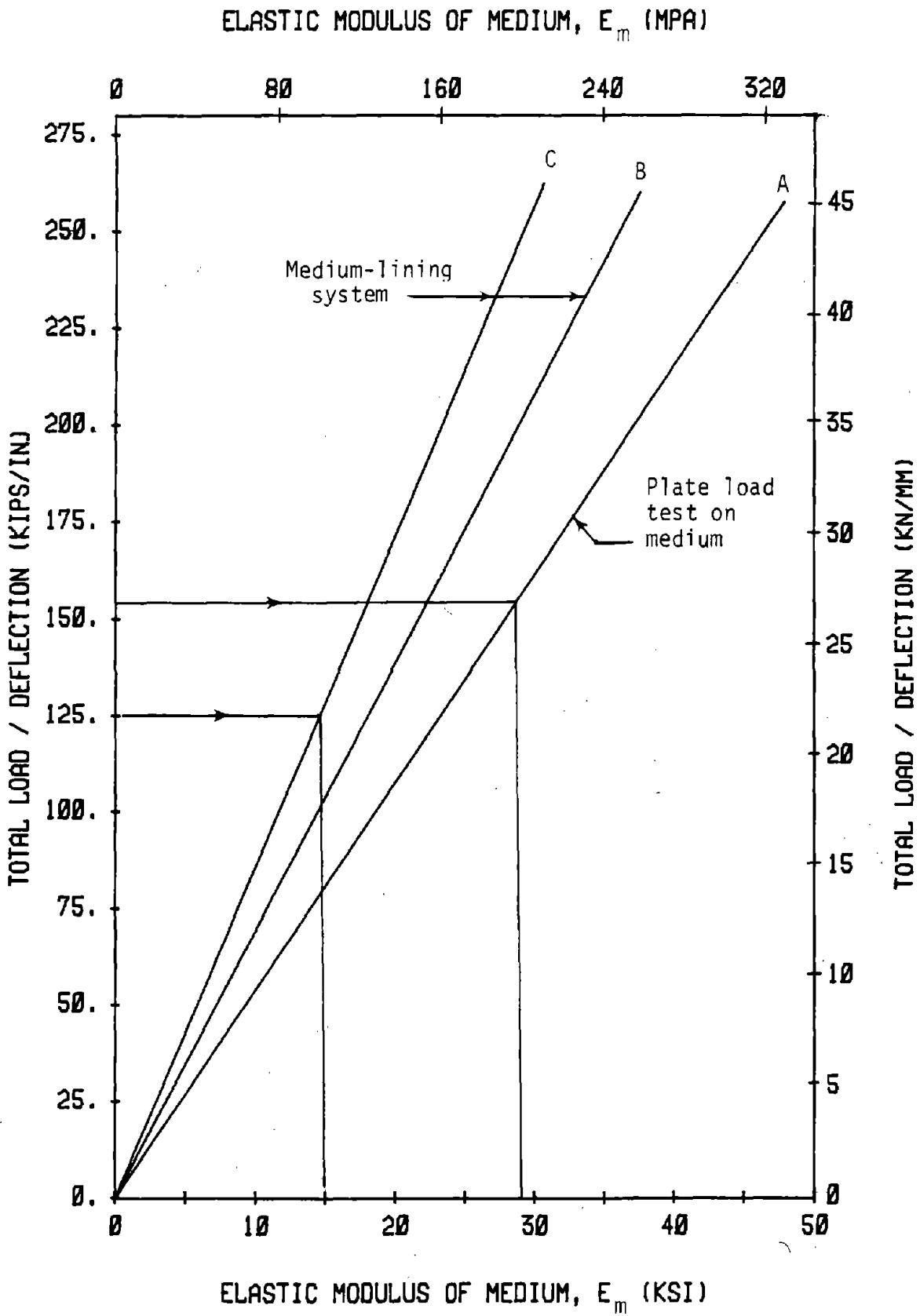


FIGURE 6.42 STIFFNESS OF THE MEDIUM AND MEDIUM-LINING SYSTEM FOR DIFFERENT MODULI AND ELASTICITY

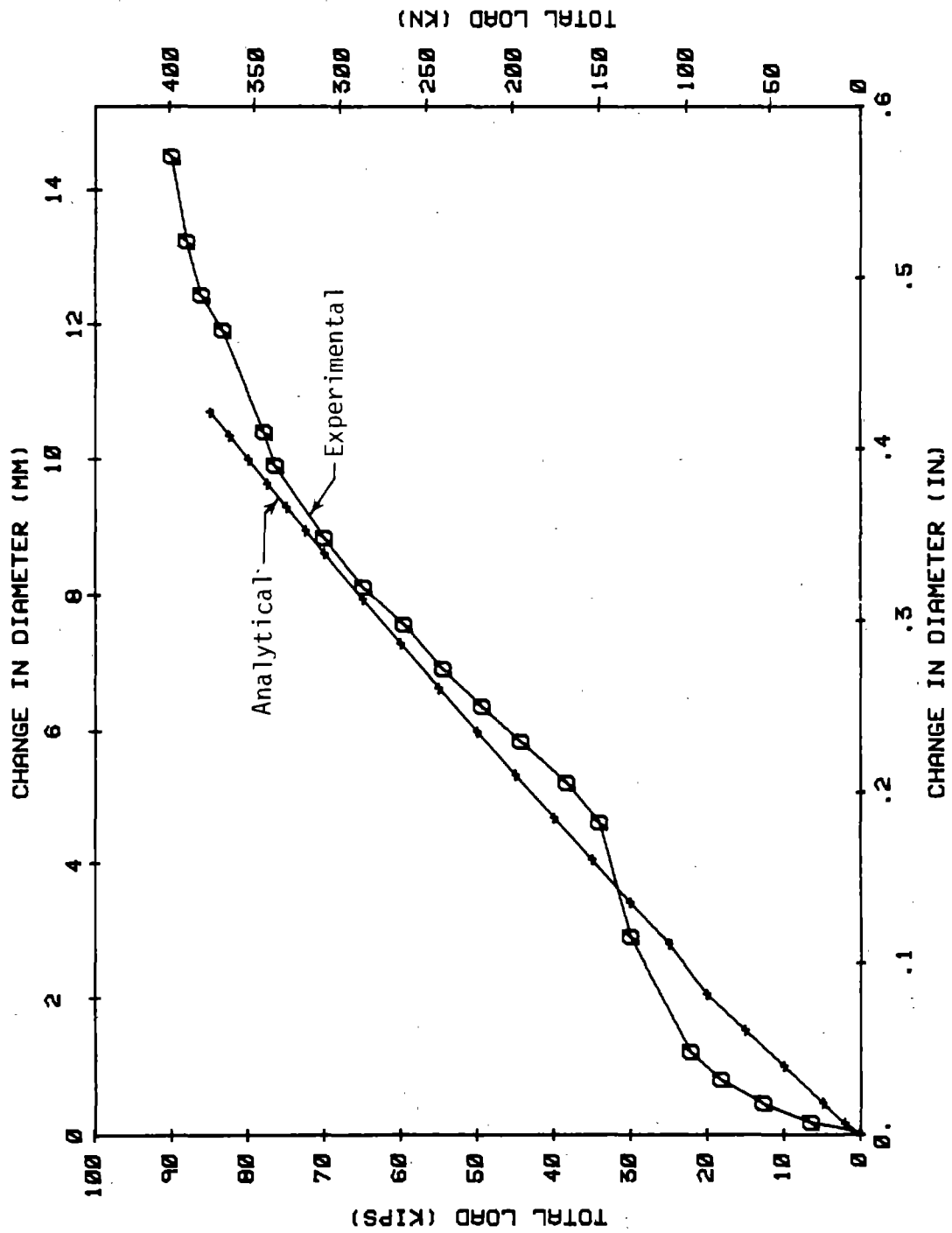


FIGURE 6.43 COMPARISON OF EXPERIMENTAL AND ANALYTICAL RESULTS FOR CIRCLE-3

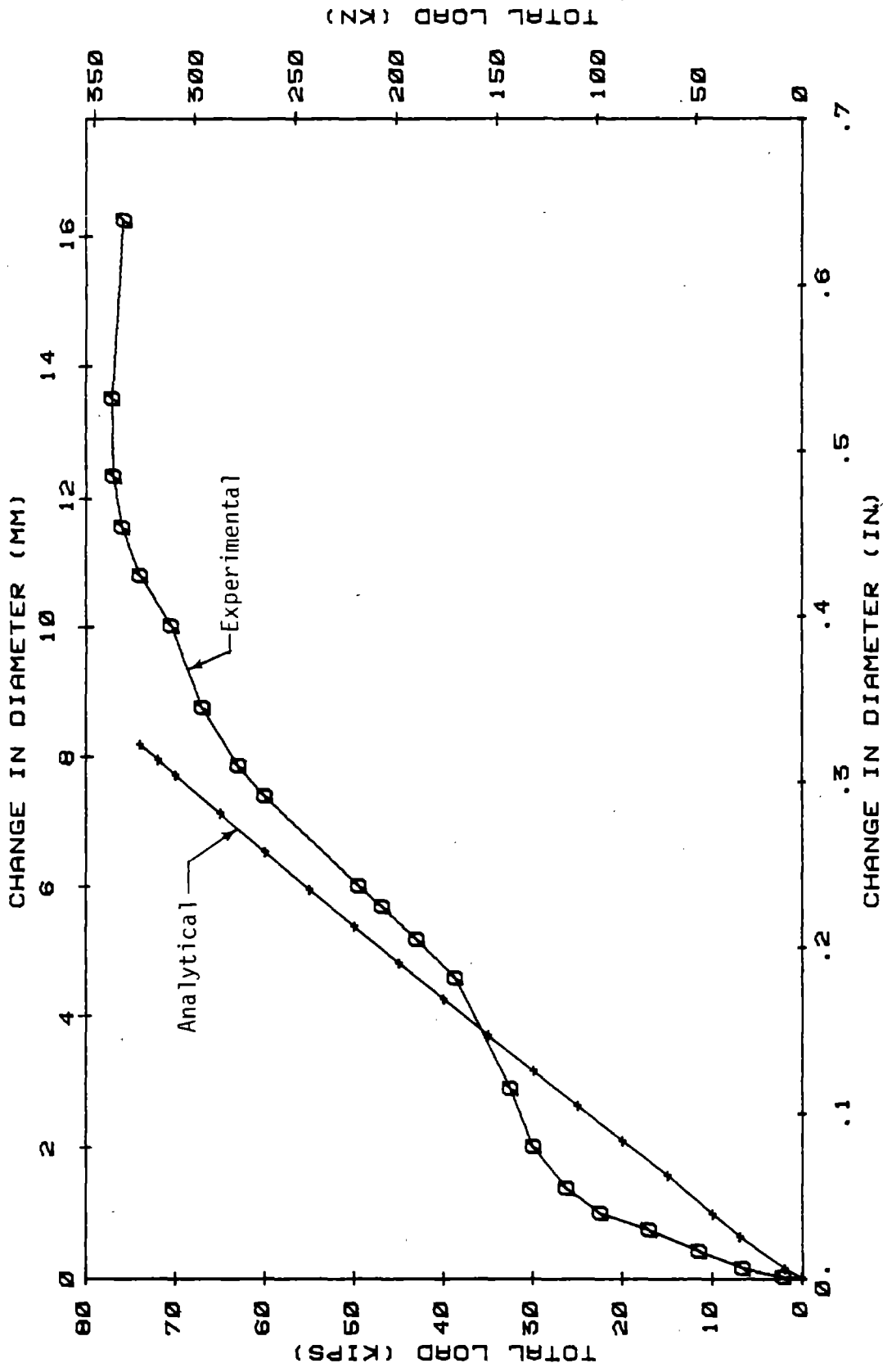


FIGURE 6.44 COMPARISON OF EXPERIMENTAL AND ANALYTICAL RESULTS FOR CIRCLE-4

the lining or "yielding" of the medium are not matched. The peak load predicted by the analysis was in the range of 95 percent of the one obtained in the tests.

The moment-thrust paths at the critical sections are also compared in Fig. 6.15 for Circle-3 and Fig. 6.17 for Circle-4, where the location of the critical section was the same in the tests as in the analysis (identified by high strains). The slopes of the moment-thrust paths match quite well, and the failure of the lining is predicted correctly by the analysis since the paths stop on the corresponding envelopes. It can be concluded that the finite element model simulated the lining tests satisfactorily; thus, the finite element program was used to perform parametric studies in order to investigate a wider range of parameters for full-sized linings and for lower values of the flexibility ratio.

## 6.5 DISCUSSION OF TEST RESULTS

Applicability of model test results to full scale tunnels was discussed in Section 2.3. It was pointed out that conclusions drawn from the model tests may be applied to full scale circular tunnels once appropriate scale factors are applied, the loads are applied in the same way as the model, and certain other conditions concerning material properties are satisfied. However, in view of the limitations imposed by problems with producing and testing an exact scale model, extrapolation of the test results to full scale tunnels should be done with caution.

The greatest value of the test results lies in the fact that they provided information about the overall behavior and failure modes of concrete tunnel linings near or at the ultimate load level. Linings in the field are never loaded close to failure, because of the safety factors incorporated in their design. Model tests provide the opportunity to examine the behavior at ultimate load, improve the

understanding of the overall behavior and eventually improve the design for service load conditions.

It was not possible to test linings with initial flexibility ratios less than 10, but because of local yielding of the fly ash medium (and thus reduction of its equivalent modulus of elasticity) the value of the flexibility ratios at failure of the lining was much less than those given in Table 6.1 (perhaps as low as ten percent). The finite element model used to simulate the test results is utilized in Chapter 7 to examine the behavior of full scale circular linings with flexibility ratios less than 10. Furthermore, most of the conclusions drawn from the overall test results discussed below, are valid at the lower flexibility ratios.

It was found that the load carrying capacity of the lining is more sensitive to variations in the modulus of the medium than to variations of any other parameter. The greater the value of the modulus of the medium, the greater the capacity of the lining as confirmed by the results of both the monolithic and the segmented tests as well as the parameter study. Thus, even though the amount of circumferential reinforcement was less in Circle-3 (0.6 percent) than in Circle-2 (1.0 percent) the load carrying capacity of Circle-3 was higher because the modulus of the medium was higher. The same trend was observed in the values of the thrust ratios  $T/T_u$  (an indication of the amount of moment present at the critical section). The higher the modulus of the medium the smaller the moment in the lining and thus the higher the thrust ratio. In the monolithic linings, the thrust ratio varied from 0.51 for Circle-1 to 0.62 for Circle-3, whereas in the segmented from 0.56 for Circle-4 to 0.40 for Circle-5. It is observed that the thrust ratio for a segmented lining is lower than a monolithic one with the same characteristics, primarily because of localized reductions of cross-section in the joint regions. The tendency for cracking appears to be influenced more by the stiffness of the medium than by the reinforcement as well. Thus, as the stiffness of the medium increased,



the number of cracks decreased in Circles-1, 2 and 3, irrespectively of the amounts of reinforcement present.

Circumferential reinforcement does little to improve the load carrying capacity of the lining, because the reinforcement is most effective in tension, and for the flexibility ratio range examined most of the lining section was in compression. The beneficial effects of reinforcement are shown in Fig. 6.21, however, where the size of cracks in the crown region are larger in Circle-1 (unreinforced) than in Circle-3 (reinforced with 0.6 percent) and even larger than in Circle-2 (reinforced with 1 percent). Larger amounts of reinforcement distribute cracks and in so doing keep them finer. Thus, the higher the amount of reinforcement the smaller the size of cracks. Cracking is usually related to the amount of water leakage through the concrete lining, as more and wider cracks will permit more leakage. Improving the ground stiffness around the tunnel opening (by grouting, effective backpacking, etc.) and reinforcing the lining will reduce the number and size of load-related cracks, respectively.

The time of appearance of first cracks is also an important design consideration, since adequate load factors incorporated into the design, might never allow the lining to experience loads large enough to result in cracking and thus leakage. Initial cracking is affected little by the amount of reinforcement, since it is a function of the cracking strain of the concrete. All monolithic linings cracked at the crown and invert at a load level between 32 and 42 percent of the peak load. The conclusions regarding reinforcement and cracking concern short term load-related cracking; the effects of reinforcement on temperature, shrinkage or long-term cracking of the lining cannot be obtained from these short term tests. If the loads were applied slowly and the concrete was allowed to creep during the load application, the cracks would occur at higher loads and would not open as much.

Lining moments are related to the magnitude of deformation of the lining. Consequently, many tunnel designers use expected lining deformations as design criteria to ensure that moments are limited. The values of the percent change in lining diameter ( $\Delta D/D$ ) at 50 percent and 100 percent of the peak load are very close for the monolithic and the segmented linings. The range of  $\Delta D/D$  for 50 percent of the load is from 0.25 to 0.43 percent and for the peak load from 1.20 to 1.27 percent (Circle-5 excluded). It is believed that comparing the deflections at 50 percent of the load is more meaningful than comparing them at peak load, because of the effect of test procedure on behavior at peak loads such as time required to take readings and size of load increments near peak load. These uncertainties are reflected in the high value of  $\Delta D/D$  for Circle-5. Furthermore, the values of  $\Delta D/D$  at 50 percent of peak load are more reasonable for design at service load conditions.

In comparing the behavior of monolithic and segmented linings several observations are made. Namely, cracks in segmented linings appeared at a later stage in the loading process, at about 90 percent of peak load vs about 30 percent for the monolithic. Furthermore, the number of cracks present was drastically reduced, because the rotation of the joints during loading reduced the moment in the lining and thus the flexure related strains and cracking. The effect of joints in reducing moments in the lining is magnified as the stiffness of the medium becomes lower, since the rotations increase. This magnification of the effect of joints with reduction of stiffness of the medium is further discussed in Chapter 7. In comparing a monolithic (Circle-2) with a segmented (Circle-5) lining, having the same amounts of reinforcement and modulus of medium, it is observed that their load carrying capacity are very close. The slightly lower load reached by the segmented lining is believed to be due to the reduction of the lining cross-section in the joint region.

Failure of the linings occurred between 60 and 80 deg from the crown with the exception of Circle-5 where it occurred 120 deg from the crown at a joint, probably because of a local weakness in the medium. All the model lining failures resulted from crushing of concrete that began at the inside surface in some small region and with additional load spread both through the depth of the section and longitudinally in the lining. The initiation of crushing was generally accompanied by cracking parallel to the direction of compressive stress (circumferential in the lining) typical of compression failures in concrete and to be expected in a specimen only 1.0 in. (25 mm) thick. Crushing occurred at a joint in both segmented lining models. The joints constitute a weak section because of the reduced cross-section and the lack of reinforcement. There was no indication of high shear stress contributing to the initiation of failure or contributing to the spread of failed concrete after initiation, as might be indicated by a radial offset each side of the failure region if shear were a contributing factor.

## 7. PARAMETER STUDY FOR CIRCULAR LININGS

### 7.1 INTRODUCTION

The finite element program described in Chapter 3 was used to investigate the effects of various parameters on the behavior of concrete circular linings in rock and in soft ground. The studies for linings in rock are described in Section 7.2 and those for soil in Section 7.3. Different analytic models were used for the two medium types. Loading on a lining in rock is usually the loosening type gravity loading which is due to the presence of intersecting joint sets and shear zones, that allow rock blocks to loosen and come to rest on the lining. The ground-lining interaction problem with this type of loading on a circular lining in an already stressed medium can be analyzed by using either a beam-spring model or a beam-continuum model with the load applied directly to the lining, though actual formation of the rock loads is not simulated. Since the beam-spring model is sometimes used in practice, and it adequately represents the interaction problem in rock, it was selected for the parameter study of circular linings in rock. A comparison of the beam-spring model with the continuum model with full-slip at the ground-lining interface showed excellent agreement in results when proper spring stiffnesses were used as computed by the formula given by Dixon (1971) and described in Section 7.2.

In the analysis of linings in soft ground, one of the greatest uncertainties lies in the way the ground loads reach the lining. Some of the commonly used loading conditions are described in Chapter 2 and are termed as i) overpressure loading, ii) excavation loading, and iii) loosening or gravity loading. The beam-spring model does not properly represent the overpressure or the excavation loading conditions because the load must be applied directly to the lining, and it does not account for arching of loads around or onto the lining. Hence, for better representation of the medium as well as to be able to

handle various other loading conditions, the beam-continuum model was used for parameter studies of circular linings in soft ground.

## 7.2 DESCRIPTION OF THE STUDY FOR LININGS IN ROCK

The beam-spring model was used to determine the internal moment, thrust and shear and the external shear and radial pressure for a circular lining as certain parameters varied. The varying parameters were flexibility ratio  $F$  as defined in Chapter 2, relative stiffness of the radial and tangential springs ( $K_r/K_t$ ), radius to thickness ratio ( $R/t$ ), and the lining reinforcement. For most of the parameter study a particular lining was considered that is typical of current designs. It was a uniform cast-in-place type, 9 in. (229 mm) thick; however, the thickness and the radius were varied in order to study the effects of these variables. The finite element model used to represent the lining is shown in Fig. 7.1. The reinforced concrete section contained concrete with compressive strength of 4000 psi (28 MPa) and 0.5 percent deformed bar reinforcement in each face, 2 in. (51 mm) from the surfaces. The resulting axial thrust capacity ( $T_u$ ) was 465 kips (2068 kN) for the typical 9 in. (229 mm) thick lining. In order for the axial thrust capacity to be the same for the unreinforced section of the same thickness, the compressive strength was increased to 4310 psi (30 MPa). This was done so that the difference between the reinforced and unreinforced case would be due to the additional bending strength and stiffness from the reinforcement. The objective was to determine if the added bending strength and stiffness would contribute appreciably to the moment redistribution and ductility of the lining.

For this study, the flexibility ratio was considered to influence  $T_u/T_o$  more than the compressibility ratio, because it is a better measure of the moment that will occur in the lining, and the strength is heavily influenced by the moment. To cover a range of relative stiffness ratios, that would correspond to linings in hard clay to competent rock, values of  $F$  equal to 7.5, 75, 415, 1250, 3760 and 6230

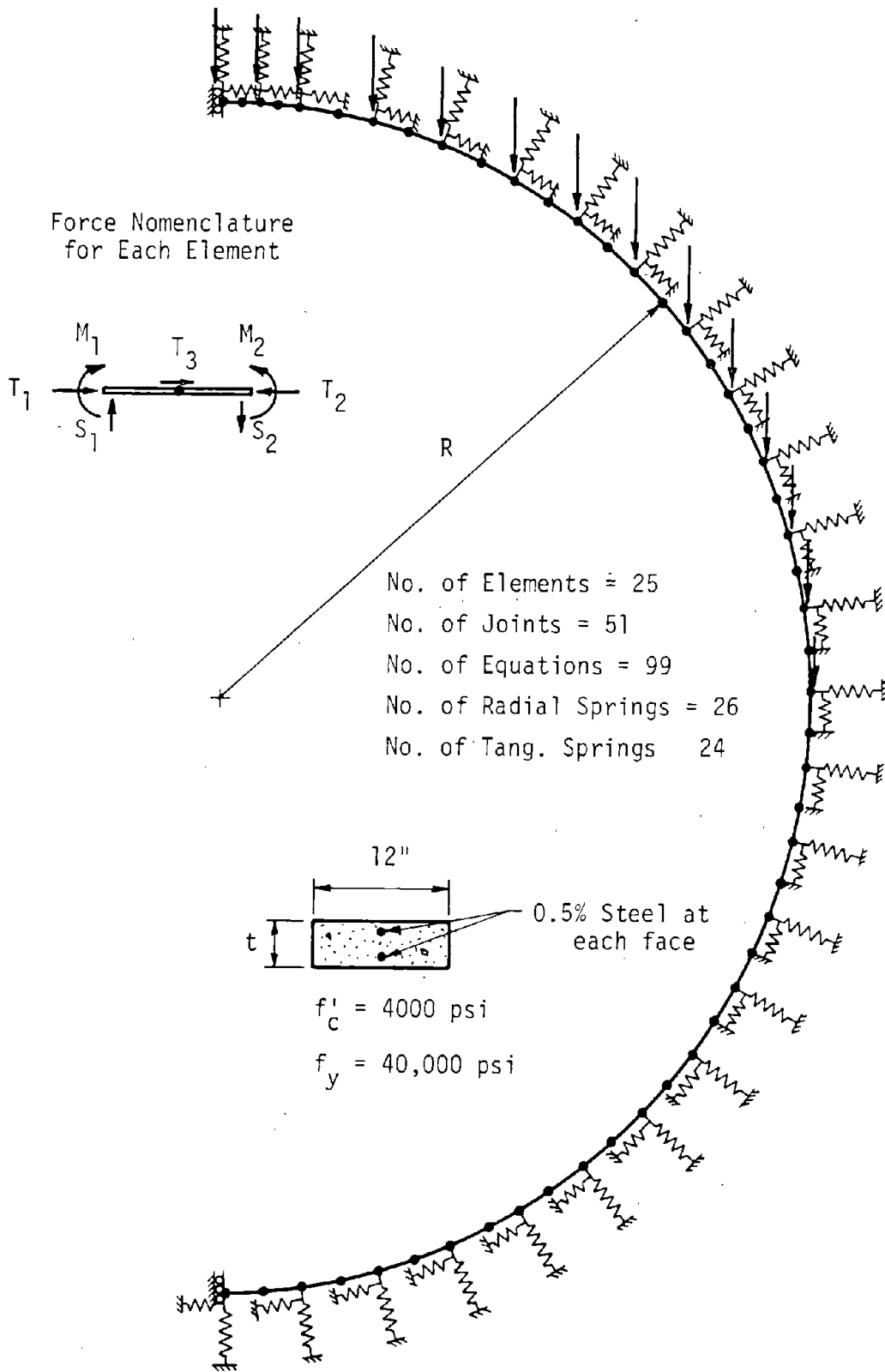


FIGURE 7.1 FINITE ELEMENT MODEL OF CIRCULAR LINING FOR PARAMETRIC STUDIES

were selected, the lower values corresponding to softer ground and stiff linings.

The medium has been idealized by radial springs, similar to a Winkler-type foundation used for the analysis of beams on elastic foundations, and by tangential springs that represent the shear transfer between the lining and medium. The radial spring constant was computed by the equation given by Dixon (1971)

$$K_r = \frac{E_m}{1 + \nu_m} b \theta \quad (7.1)$$

where

$b$  = tunnel length that is represented by a spring

$\theta$  = angular segment (in a plane perpendicular to the tunnel axis) for which the medium is represented by a spring

$E_m$  = elastic modulus of the medium

$\nu_m$  = Poisson's ratio of the medium.

This expression has been developed from the pressure-deformation ratio ( $p/u$ ) of a circular opening of radius "R" in a homogeneous medium subjected to an internal pressure "p" resulting in the radial displacement "u" to obtain an effective modulus of elasticity given by

$$p/u = \frac{E_m}{R(1 + \nu_m)}$$

which is then multiplied by the contact area between the lining and medium to yield Eq. 7.1. The tangential spring constants were taken as a percentage of the radial constants.

The concrete stress-strain curves for the lining used in the parameter study are shown in Fig. 5.1b. Different curves were used for the reinforced and unreinforced sections as discussed above; both curves were represented in the analysis by a discrete number of points.

The shape of the curve was obtained by using the parabolic equation due to Hognestad (1951) for a compressive strength of 4000 psi initial tangent modulus for the curve with 4000 psi (28 MPa) compressive strength was 3300 ksi (22700 MPa) and that for the 4310 psi (30 MPa) curve was 3560 ksi (24500 MPa). The reinforcing steel stress-strain curve was elastoplastic with a yield stress of 40,000 psi (275 MPa) and an elastic modulus of 29,000 ksi (200,000 MPa). In the present study, the medium springs were linear (though they could be nonlinear), but the lining was given nonlinear behavior as a result of the material properties and geometry change. Consequently, the relative stiffness of the medium and lining changed continuously as loading progressed, but the initial lining stiffness is used to describe the parameters for the problem. This change of relative stiffness with loading is observed in real tunnels as well, the effect being more pronounced in stiff linings.

Shear stress between the medium and lining in a tunnel depends on the material properties of the medium and on the bond between the two materials. The shearing resistance at the interface depends on the type of material and, if it is a rock, on the joint orientation and, spacing, degree of roughness of exposed surfaces, size and shape of the asperities, strength of the medium, magnitude of the radial stress, etc. Brierley (1975) estimated the relative stiffness of the radial to tangential springs  $K_t/K_r$  at Dupont Circle Station on the Washington, DC Metro System as 0.5 to give reasonable agreement with field measurements. Test results described in Chapter 4 indicated 0.5 as an upper limit for the  $K_t/K_r$  ratio to represent the material in those tests. For the present study, values of 0.0125, and 0.25 were selected to show the effect of variation of this parameter. Some solutions were also obtained for values of 0.05 and 0.08. In the selection of values to be used in a particular case, the bond between the lining and medium should also be considered because this bond may fail before the full shear stress in the medium can be developed. Bond failure can occur in a rock medium with a rough surface by shearing of



the interlocking roughness of the rock. If a rock surface is smooth, slip may occur at a lower shear stress by slipping along the surface, and for soils the shear strength may be exceeded in the medium or on the surface between the medium and lining. The interface in these cases would be highly nonlinear, and a change in behavior of the lining would occur when bond failure occurred.

Loads were applied vertically to the lining at the nodes between each beam element to represent a uniformly distributed pressure from the rock. This load represents the gravity load from the medium that actually reaches the lining. That is, the representation of the medium by springs does not allow that part of the medium-structure interaction to be represented that allows arching in the ground around the lining as discussed in Chapter 2.

In general, all combinations of the variables discussed above were considered except for certain cases in which the lining was unreinforced, the flexibility ratio  $F$  was low, and the tangential to radial spring ratio was low or zero. In these cases, problems with convergence were encountered before the moment-thrust path reached the failure envelope. This led to the conclusion that the peak load had not been reached but an instability occurred in the analysis. Therefore, these solutions have not been included in the discussion that follows.

#### 7.2.1 Effect of Flexibility Ratio $F$

Thrust Ratio  $T_u/T_o$ : The relationship between the thrust ratio  $T_u/T_o$  and the flexibility ratio  $F$  is shown in Fig. 7.2. To establish a frame of reference consider a concrete lining with initial modulus of 3300 ksi (22700 MPa); the modulus of the medium, corresponding to the various flexibility ratios and radius to thickness ratios, is fixed, and the corresponding medium types along the horizontal scale vary from a soft soil at the left, to a hard rock at the right. These curves

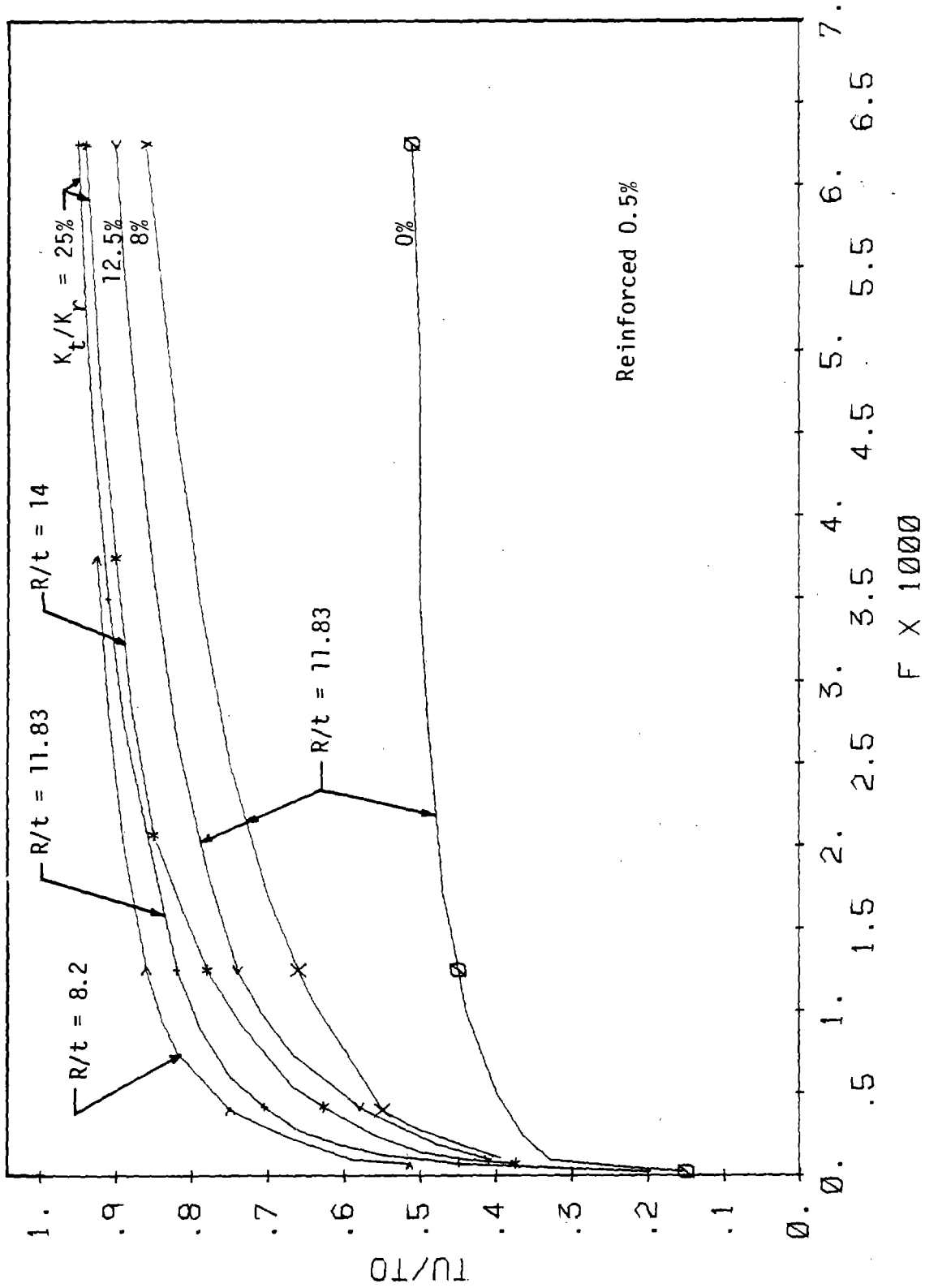


FIGURE 7.2 LINING CAPACITY AS A FUNCTION OF FLEXIBILITY RATIO

(Fig. 7.2) show that for a soft medium with a low effective modulus, the lining strength ( $T_u / T_o$ ) is sensitive to the flexibility ratio and consequently to the medium stiffness for any  $R/t$  ratio, increasing rapidly with the flexibility ratio. The rate of increase is greater for higher relative values of tangential stiffness ( $K_t / K_r$ ), an effect that will be discussed later. The curves become essentially horizontal for large values of flexibility ratio, indicating that as the flexibility ratio reaches a certain value, further increase does little to increase the lining strength. Each curve becomes asymptotic to a constant value of thrust ratio that depends on the shear stiffness between the medium and lining. Although this behavior was expected, the magnitude of the variation from these calculations provides a more thorough representation of the lining behavior. However, it is instructive to study other aspects of the lining behavior in order to understand why the strength varies as discussed above, and how serviceability aspects are influenced by the flexibility ratio.

The most important parameter affecting the strength and behavior of a given lining is the medium stiffness because of its major influence on the lining deformation and on the flexibility ratio. As the flexibility ratio increases, total load also increases as shown in Fig. 7.3. Strength of the lining depends on the combination of moment and thrust at the critical section where failure will eventually occur; the moment-thrust combination controls the cracking and potential serviceability problems at lower loads as well. In the discussion that follows, representative curves will be used for the reinforced lining case with a radius to thickness ratio of 11.8 to demonstrate the influence of flexibility ratio on the lining response.

Deformation: The influence of flexibility ratio on diameter change in the direction of loading is shown in Fig. 7.4. The diameter change at failure is about 5 in. (127 mm) for the lining in a soft medium ( $F = 7.5$ ) and on the order of 1/4 in. (6.5 mm) for a hard medium ( $F = 6230$ ) with an increase in strength of the lining by a factor of

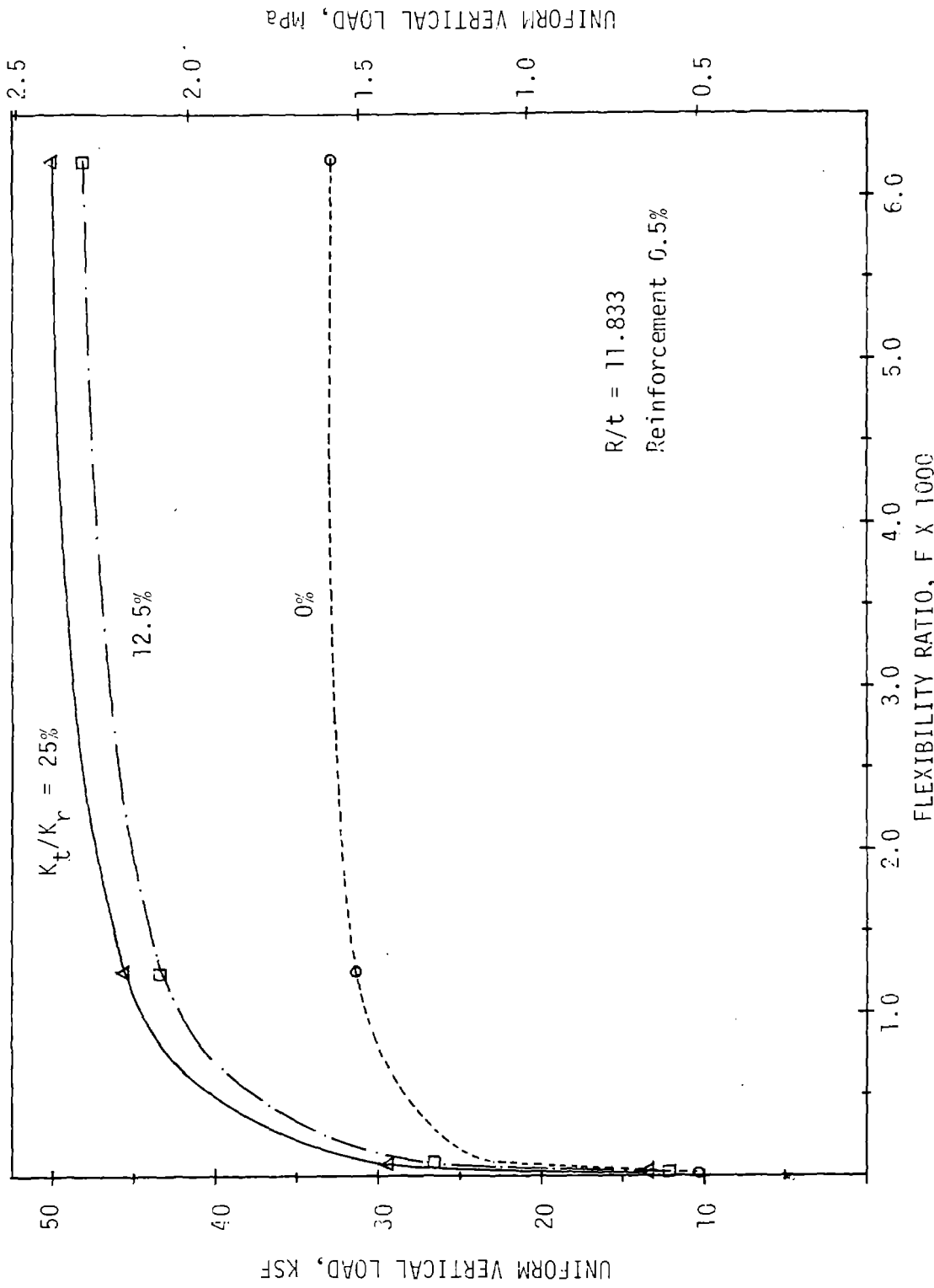


FIGURE 7.3 TOTAL LOAD VS FLEXIBILITY RATIO

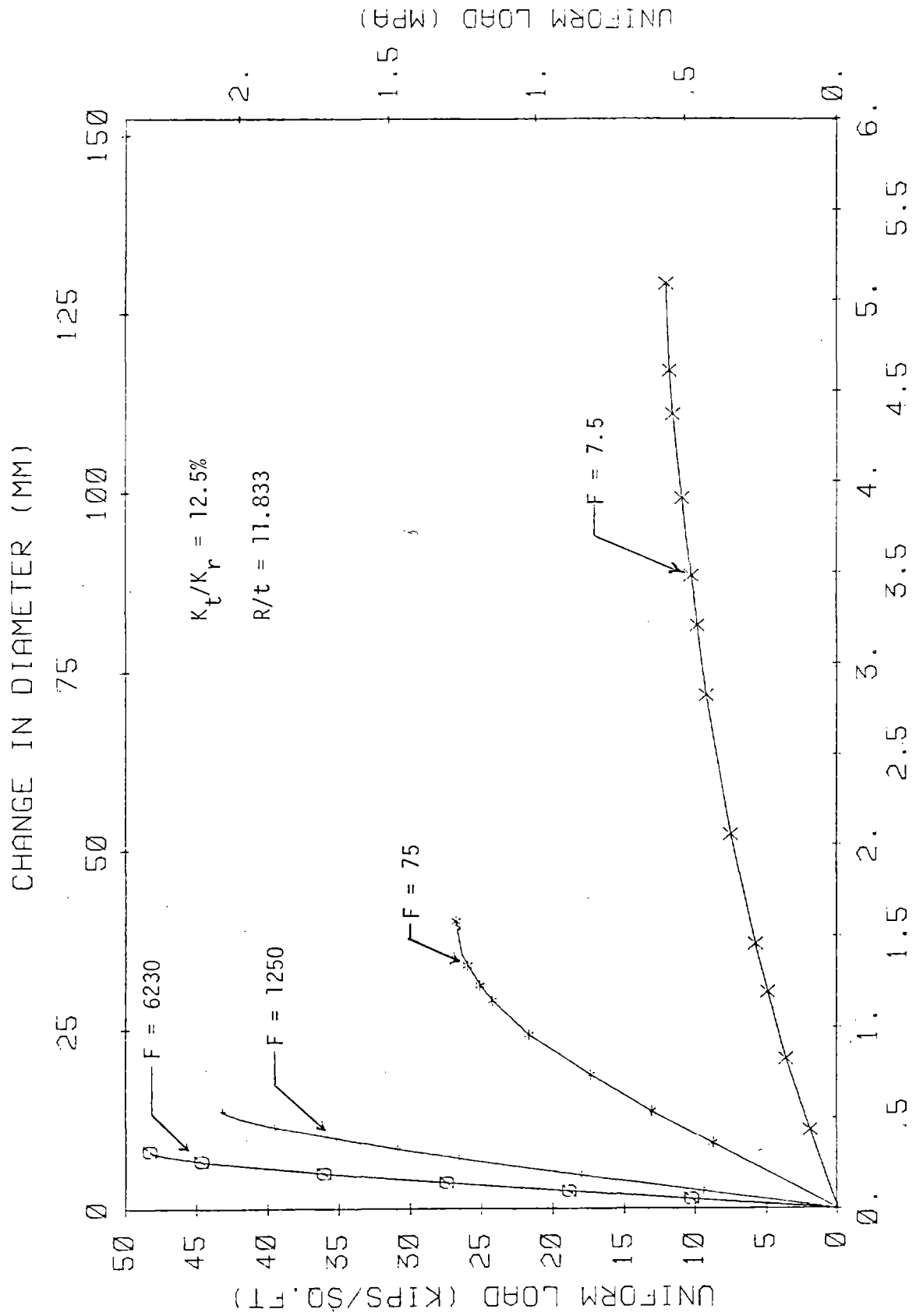


FIGURE 7.4 EFFECT OF FLEXIBILITY RATIO ON DIAMETER CHANGE

about 4. In addition the curves show considerably more ductility and nonlinearity of deformation for the two lower values of flexibility ratio; the two curves for higher flexibility ratio are nearly linear to failure.

Moment-Thrust Path: Deformation of the lining and moment in the lining is closely related, and the moment-thrust paths of the critical sections shown in Fig. 7.5 provide additional insight into the effect of flexibility ratio on strength and behavior. When the flexibility ratio is low, and therefore, the deformation and moment are large, the moment-thrust paths reach the failure envelope below the balance point. However, if the materials are ductile, as are concrete and steel, failure does not occur immediately. Instead, the moment-thrust ratio changes, and the moment-thrust path follows the envelope. When the concrete begins to crush on the compression side, the thrust resultant must shift inward toward the center of the section which reduces the internal lever arm and the corresponding moment, but the thrust can continue to increase. Thus, the moment-thrust path turns inward toward the thrust axis as shown for  $F = 7.5$  and  $75$  in Fig. 7.5. This behavior is related to the deformation allowed by the soft medium, because the large deformation results in a large moment at the critical section, resulting in a large moment-thrust ratio. The maximum thrust and thus, the peak load is finally reached when the rotational capacity of the critical section is reached.

When the flexibility ratio is large as for the curves shown in Fig. 7.5,  $F = 1250$  and  $6230$ , the liner deformation is smaller, therefore the moment is smaller. In this case, the moment-thrust path reaches the failure envelope above the balance point; sections that have such a small moment-thrust ratio because of a large thrust do not have as large a rotational capacity, and the limiting rotation is reached essentially when the failure envelope is reached. The failure thrust is considerably larger than that resulting from a linear analysis

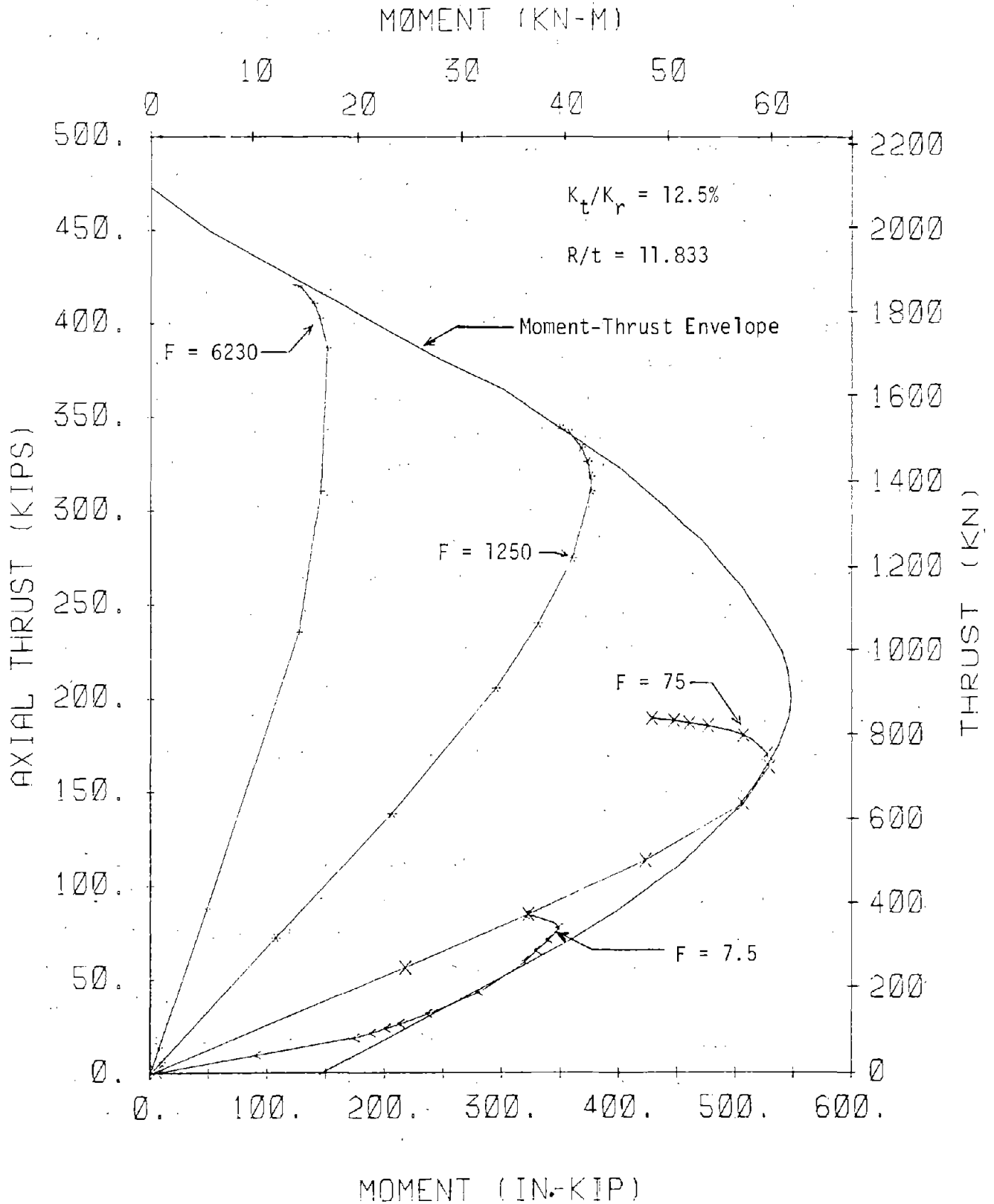


FIGURE 7.5 EFFECT OF F ON MOMENT-THRUST PATHS AT CROWN

because of the curvature of the moment-thrust path toward the thrust axis.

Figure 7.5 also demonstrates how moment influences the strength; the load capacity is nearly proportional to the thrust capacity, and the thrust capacity depends on where the moment-thrust path reaches the failure envelope. The smaller the moment, the higher the thrust at the intersection point and therefore, the larger the load. Cracking of the lining also depends on the moment-thrust ratio. If the moment is small, the compressive stress due to the thrust is larger than the tensile stress due to bending so tension cracks do not occur, while these cracks do occur at a low load when the moment is large. Also, from Fig. 7.5, it is clear that the relationship between stiffness of the medium and intersection of the moment-thrust path with the envelope is highly nonlinear; this is even more apparent from the curves in Fig. 7.3.

Thrust Distribution: The thrust distribution around the lining at the maximum load for various flexibility ratios appears in Fig. 7.6 and shows considerable variation. It will be found later that the shear stiffness between the medium and lining is a more important parameter in the thrust distribution, but for a constant shear stiffness ratio  $K_t/K_r$  of 12.5 percent there is almost constant thrust at the lowest medium stiffness, and when the medium is stiff, the thrust is largest at the crown and nearly zero at the invert. The reason for this variation cannot be separated from the tangential shear between the lining and medium, because the tangential shear stiffness was always taken as a percent of the radial medium stiffness. Therefore, when the radial stiffness becomes larger, so does the tangential stiffness. The tangential shear stress mechanism removes thrust from the lining and transmits it to the medium; hence, the thrust becomes smaller from crown to invert. The amount of thrust removed from the lining depends on the tangential stiffness and the relative tangential movement between the lining and medium. Thus, the largest variation of thrust



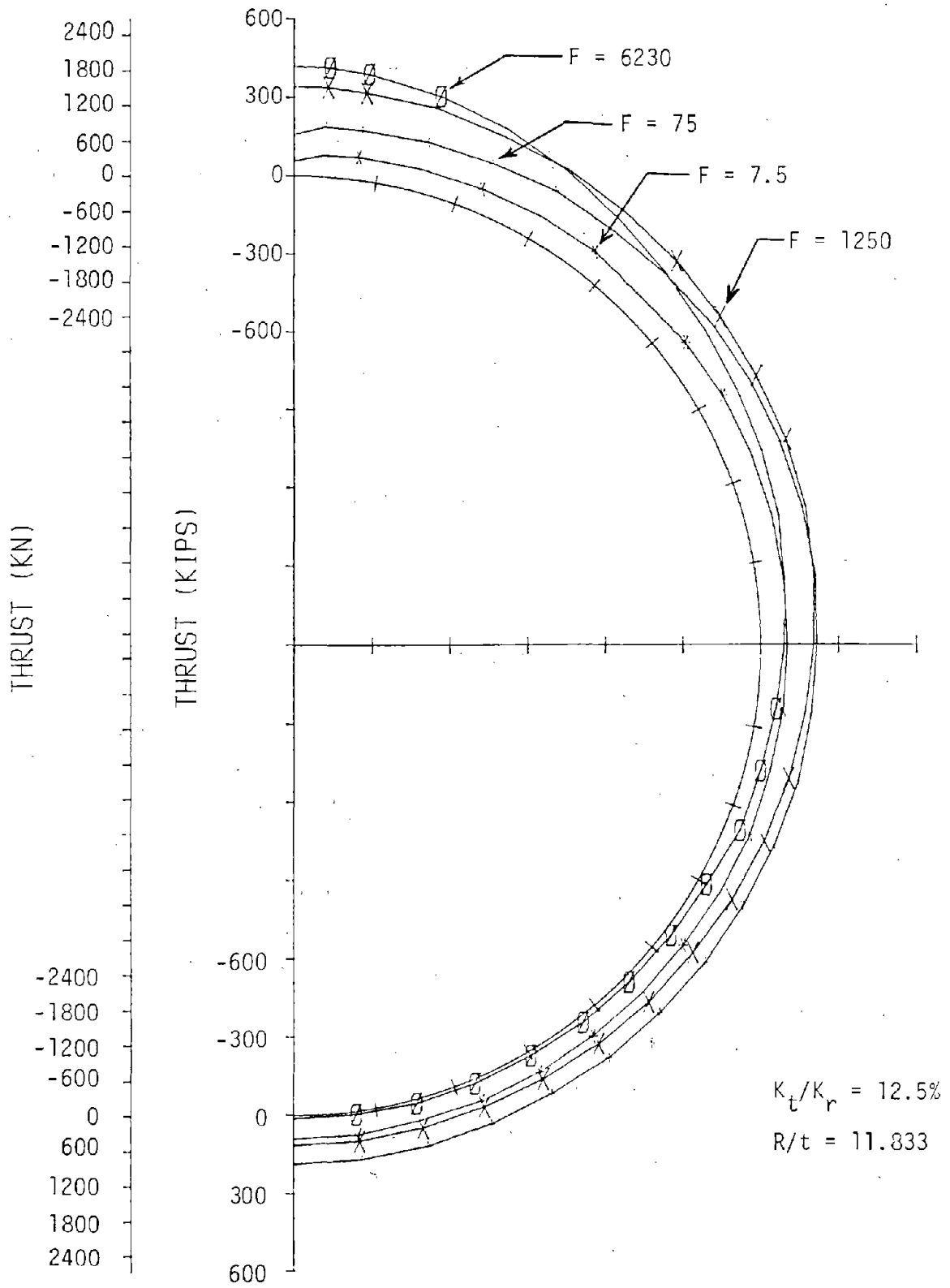


FIGURE 7.6 EFFECT OF F ON THRUST AT MAXIMUM LOAD

occurs with the largest medium stiffness. Also, if the thrust at the crown is considered, it is largest when the medium stiffness is largest. One reason for this is that the maximum load for which the thrust curves are drawn also increases with an increase in flexibility ratio. In Fig. 7.7 the thrust distribution is drawn for a constant load, and it shows that at the crown the thrust varies little with flexibility ratio. However, it becomes smaller toward the invert as the flexibility ratio increases, because the tangential medium stiffness is also increasing, as discussed earlier.

Moment Distribution: The moment distribution around the lining at the maximum load is shown in Fig. 7.8 for various flexibility ratios. For  $F = 7.5$  and  $75$ , the moment-thrust path reached the failure envelope below the balance point (Fig. 7.5), where an increase in thrust increased the moment capacity; therefore, the moment is larger for the larger flexibility ratio because the thrust was higher. On the other hand, for  $F = 1250$  and  $6230$ , where the moment-thrust paths reached the envelope above the balance point, (Fig. 7.5), an increase in thrust reduced the moment capacity, so the moment is smaller for the larger flexibility ratio. As shown in Fig. 7.8, the moment is slightly larger at a section 40 to 50 deg from the crown than at the crown and the thrust is equal to or slightly smaller at the 40 to 50 deg section (Fig. 7.6); therefore, this peak moment section is likely to have a larger moment to thrust ratio than the crown section.

The moment is almost zero at about 65 deg in Fig. 7.8 for the large flexibility ratio and remains negligible to the invert. On the other hand, for the soft medium cases the moment approaches zero at about 90 deg from the crown and below this point has appreciable magnitude of the opposite sign.

The moment distributions in Fig. 7.8 are drawn for different maximum loads on the lining, while those in Fig. 7.9 are drawn for the same load level for each  $F$  and therefore, show the effect of

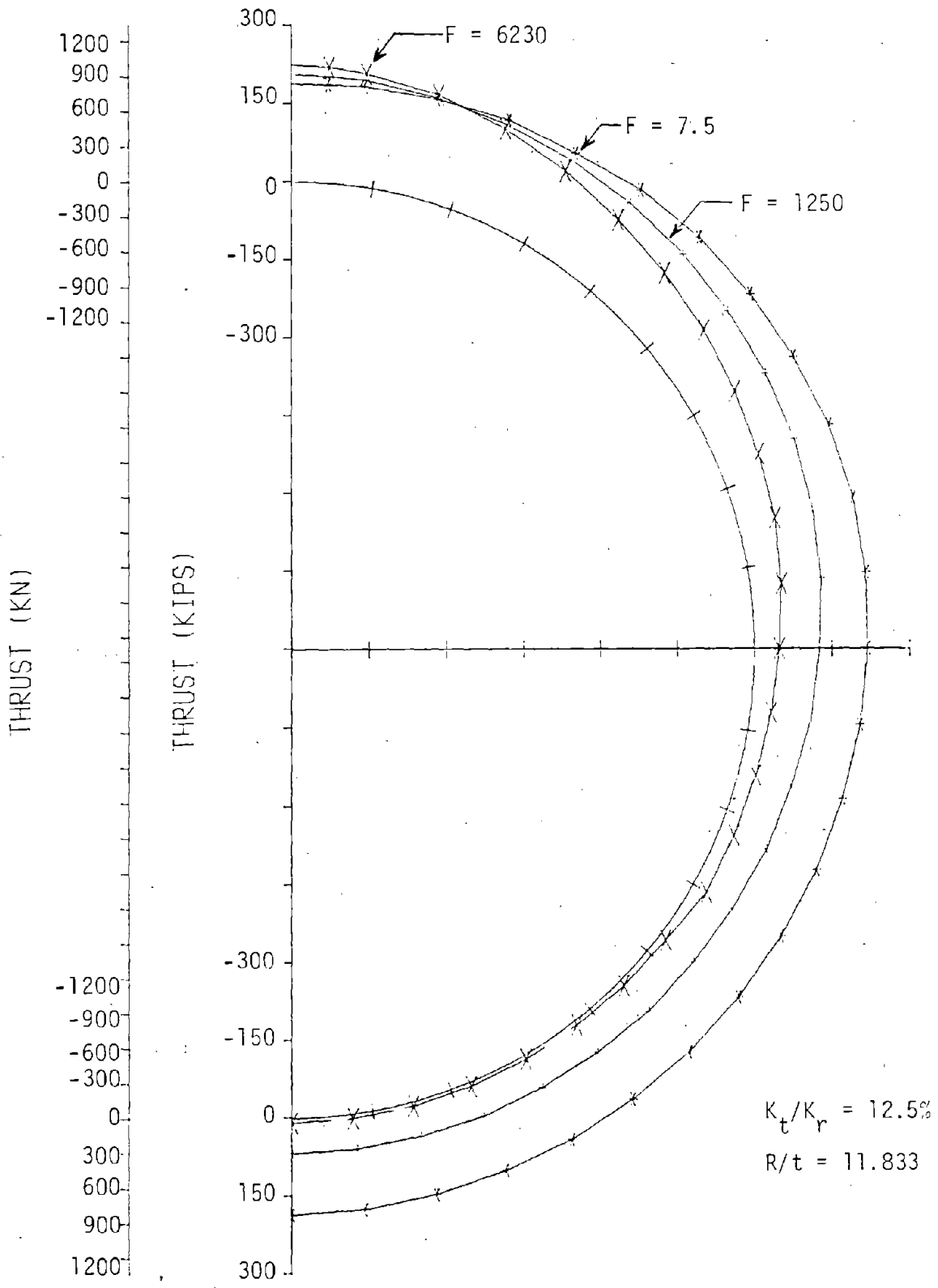


FIGURE 7.7 EFFECT OF F ON THRUST AT EQUAL LOAD

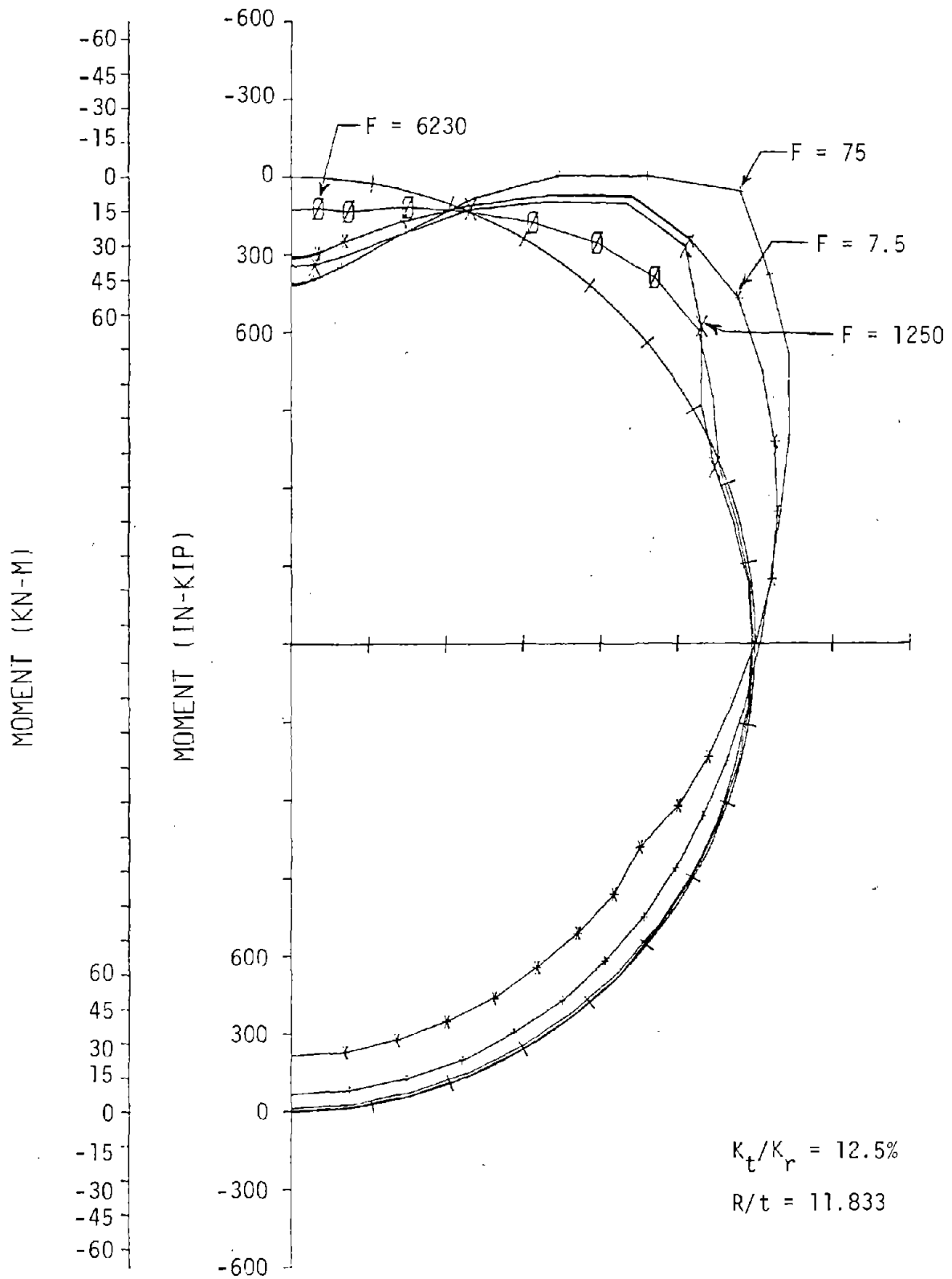


FIGURE 7.8 EFFECT OF F ON MOMENT DISTRIBUTION AT MAXIMUM LOAD

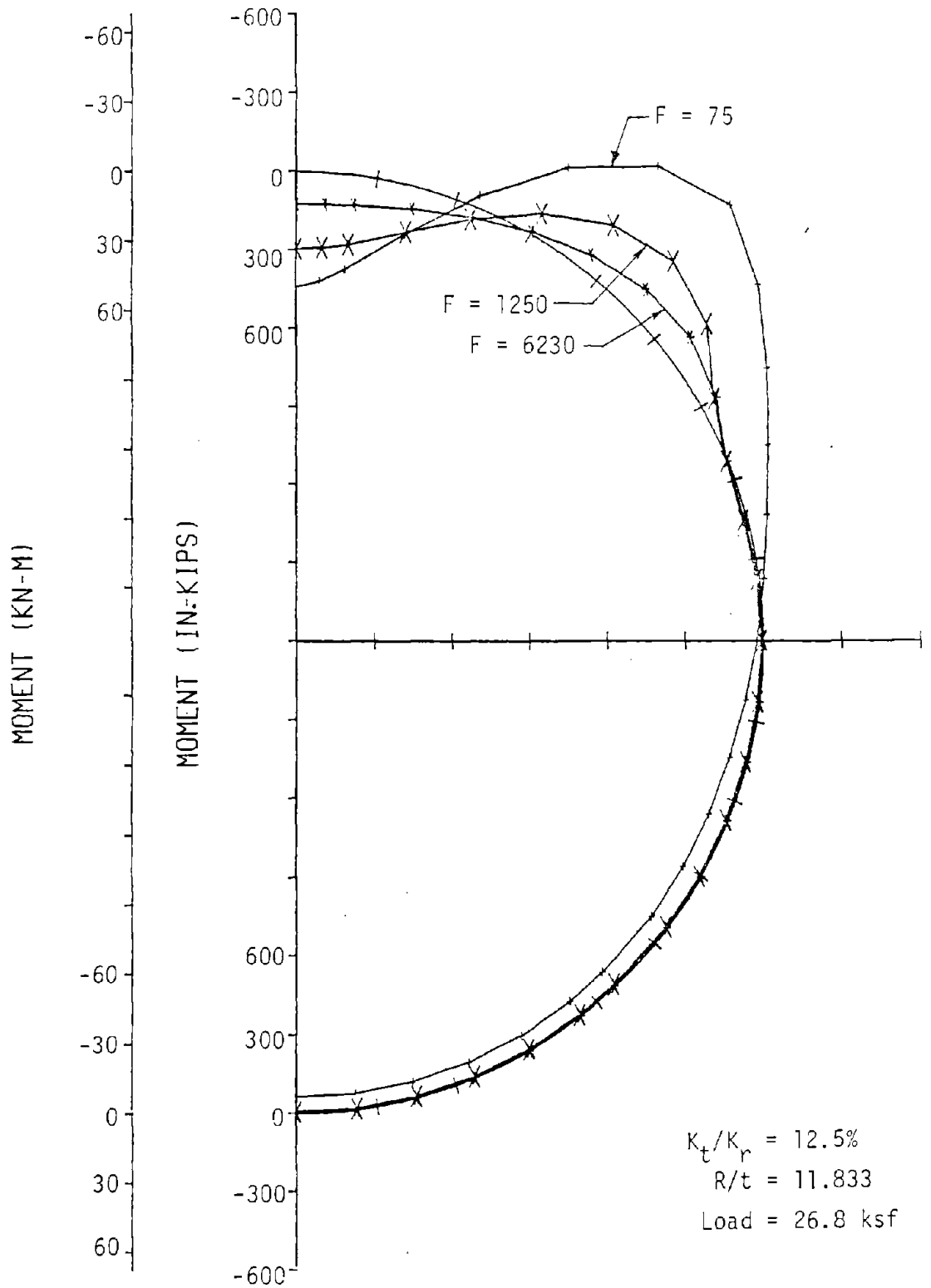


FIGURE 7.9 EFFECT OF F ON MOMENT AT EQUAL LOAD

flexibility ratio on the magnitude, and the complete change of character of the distribution at high values of flexibility ratio. It is clear in this figure that the softer medium corresponds to larger moment magnitude at a given load because the soft medium allows greater bending in the lining. The case for  $F = 7.5$  is not shown in the figure, because the selected load level exceeds the capacity of the lining for this value.

Internal Shear Distribution: The internal shear distribution induced in the lining is shown in Fig. 7.10 for the maximum load in each case. There are regions of peak shear near 20 deg and from 45 to 60 deg from the crown. For high values of flexibility ratio, the shear is larger at the 45 to 60 deg sections while for low flexibility ratio the 20 deg section has larger shear. The sections closer to the crown are likely to be more critical in all cases, however, because the direction of the diagonal tension at this section leads to movement into the tunnel of the loaded region near the crown. Internal shear is related to the slope of the moment distribution diagrams of Fig. 7.8 and therefore, depends on the shape of these diagrams. The shear is zero where the moment curves peak and have maximum values between the moment peaks where they have maximum slopes.

Radial Pressure Distribution: The external radial passive pressure between the medium and lining at the maximum load is shown in Fig. 7.11 and is seen to increase in magnitude with decreasing flexibility ratio. As the deformation increases, the radial pressure on the lining becomes larger. This may be easier to understand if the medium stiffness is considered to remain constant. Then as the stiffness of the lining decreases ( $F$  increases), it deforms more under the same load, causing larger passive pressure in the medium.

The radial pressure distribution varies from a maximum at 60 to 70 deg from the crown and becomes smaller toward the invert. The reduction toward the invert is greater for the larger flexibility ratio

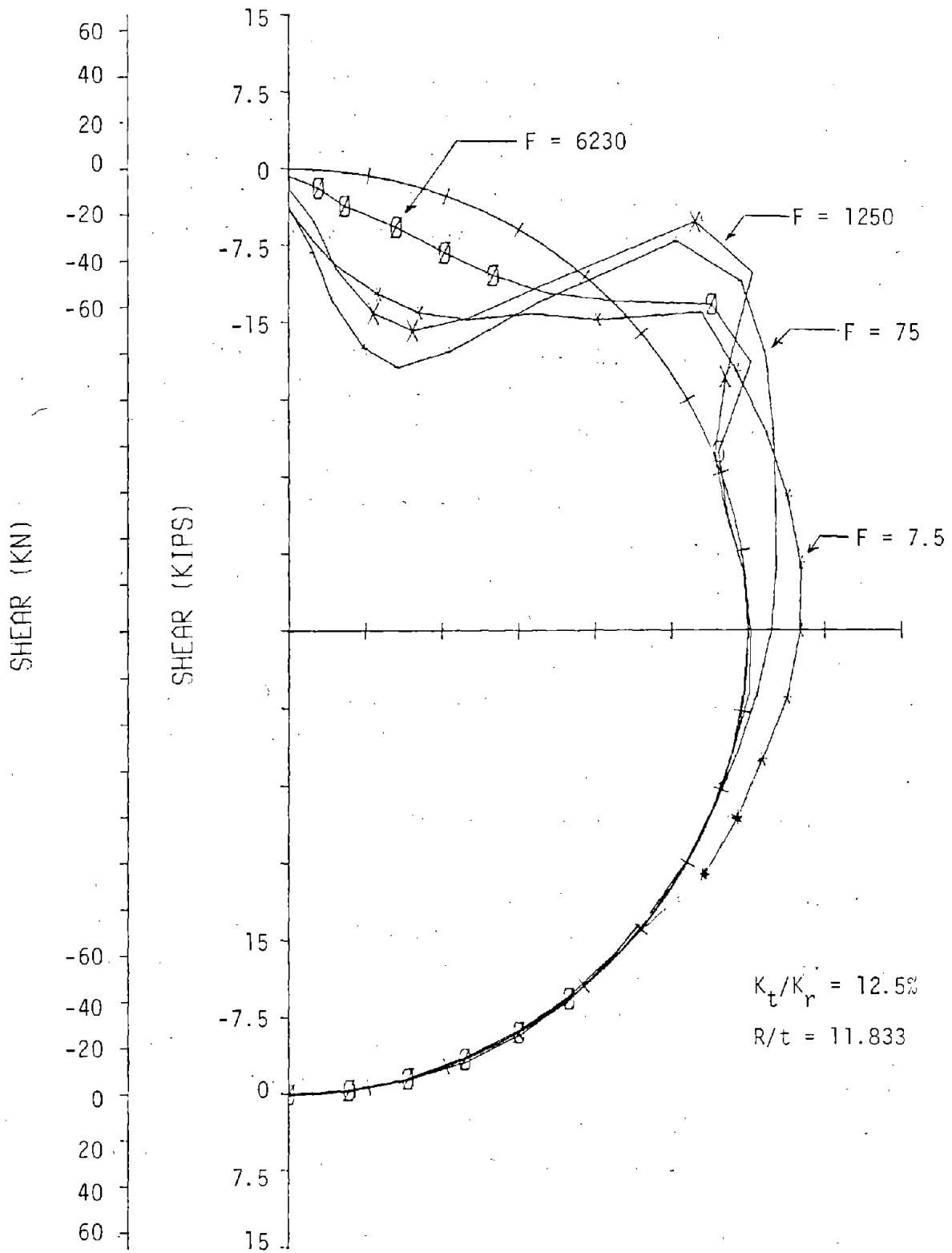


FIGURE 7.10 EFFECT OF F ON SHEAR AT MAXIMUM LOAD

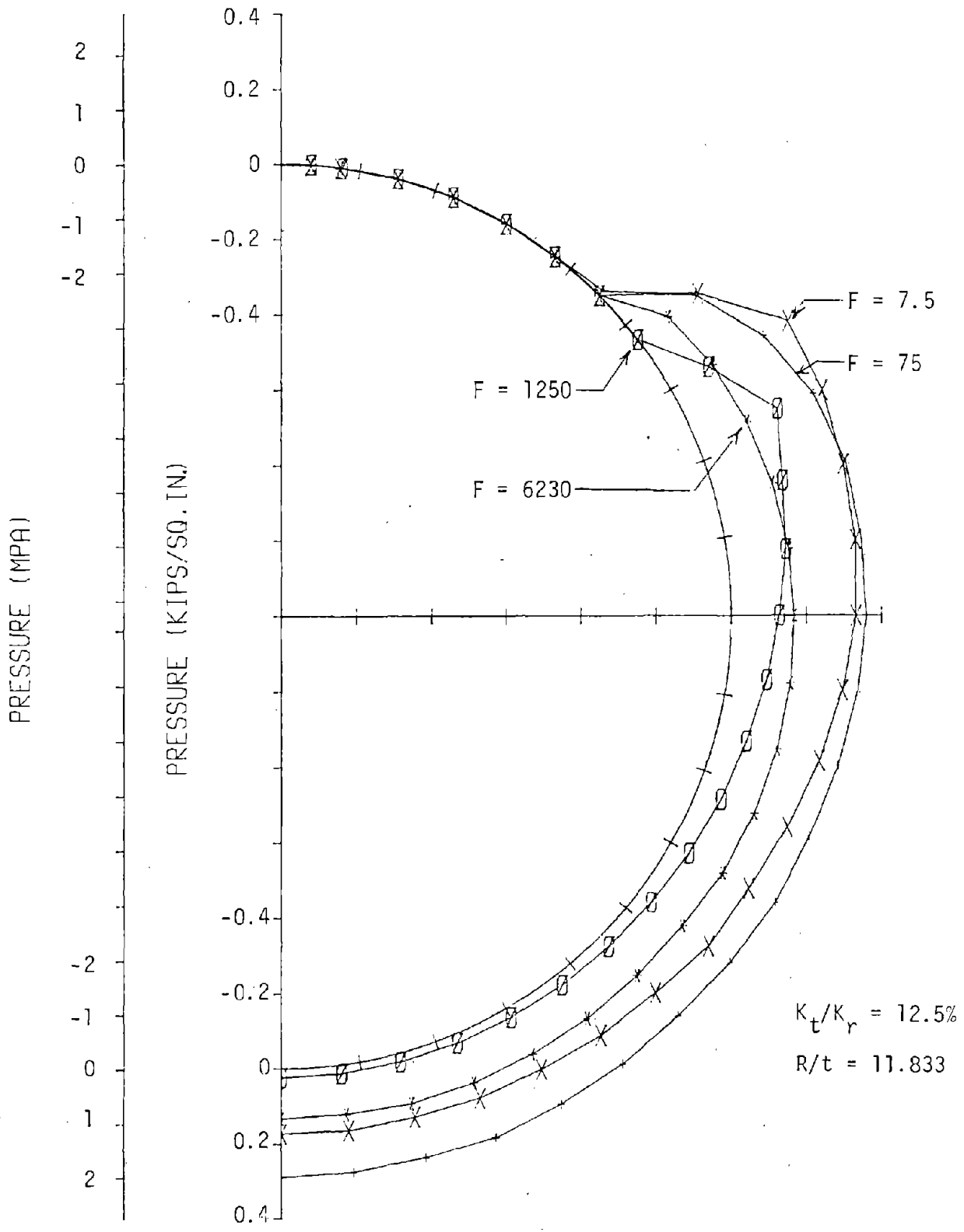


FIGURE 7.11 EFFECT OF F ON RADIAL PRESSURE AT MAXIMUM LOAD



and almost negligible for small flexibility ratio. This is related to the increase in tangential stiffness of the medium which is proportional to the radial medium stiffness. As the medium becomes stiffer, the increased stiffness of the tangential shear mechanism removes thrust from the lining toward the invert, so less force remains to push the lining downward into the medium at the invert, resulting in less radial pressure between lining and medium.

Tangential Stress Distribution: The tangential stress distribution between the lining and medium is shown in Fig. 7.12 for various flexibility ratios, but this stress is more closely related to the tangential shear stiffness, which is also changing with the radial stiffness, as discussed earlier. The shear stress is maximum 30 to 40 deg from the crown, largest for the largest flexibility ratio and becomes smaller as the medium stiffness is decreased because the maximum loads are decreasing in the same way. For all cases, the shear stress becomes smaller from the peak at 30 to 40 deg to zero at the invert and the crown, where the relative tangential displacement between the lining and medium is zero due to symmetry.

#### 7.2.2 Effect of the Ratio of Tangential to Radial Stiffness of the Medium ( $K_t / K_r$ )

Thrust Ratio  $T_u / T_o$ : Variation of the thrust ratio  $T_u / T_o$  with the ratio of tangential to radial medium stiffness  $K_t / K_r$  is shown in Fig. 7.13. Each curve corresponds to a particular flexibility ratio  $F$  and indicates that an increase in the shear stiffness ratio increases the lining strength ( $T_u / T_o$ ). This effect is much more pronounced for higher flexibility ratio values. For example, the curves for  $F$  equal to 6230 increase more rapidly than the other curves. However, the curves become almost horizontal for values of shear stiffness ratio  $K_t / K_r$  greater than about 12.5 percent. This indicates a tendency for

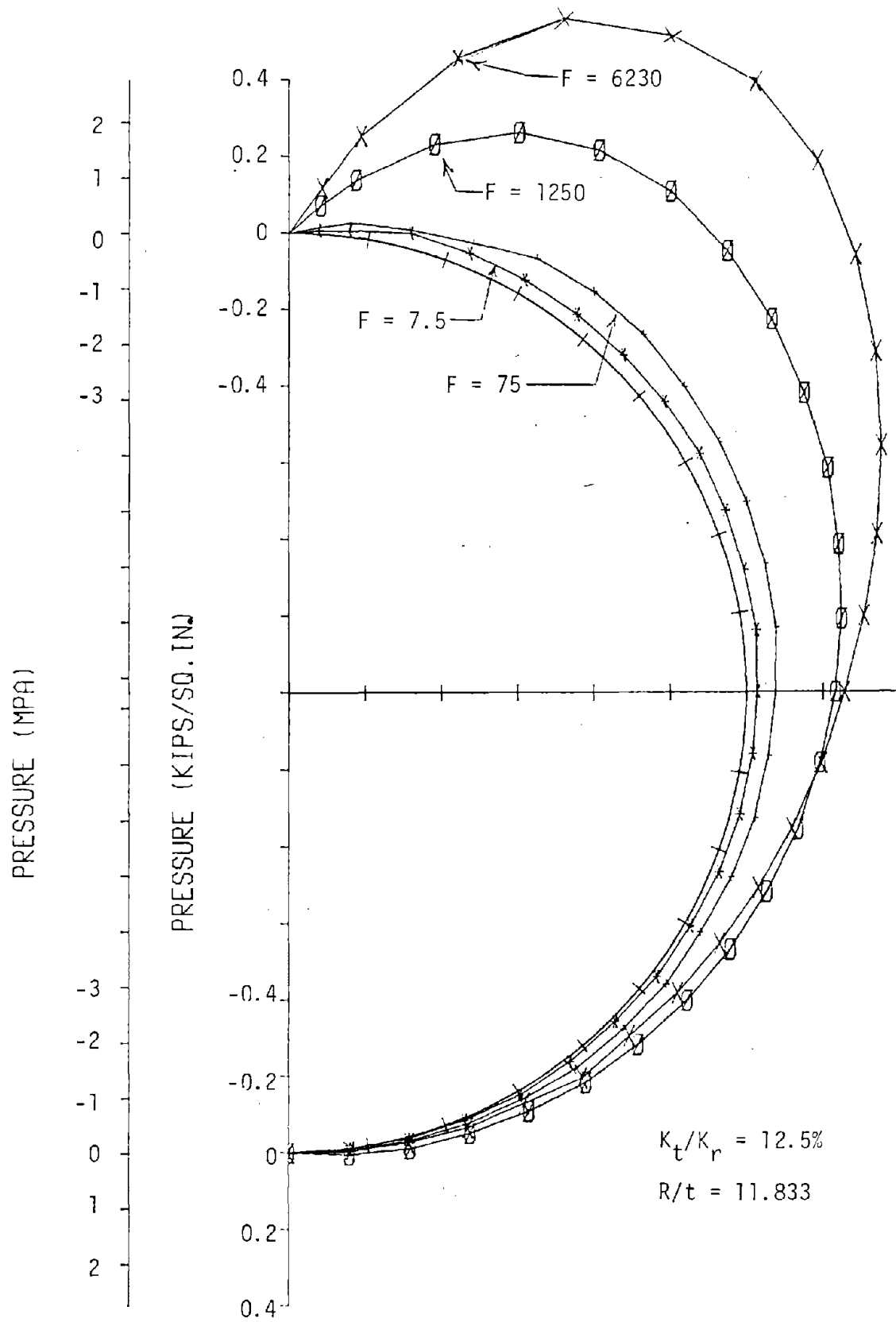
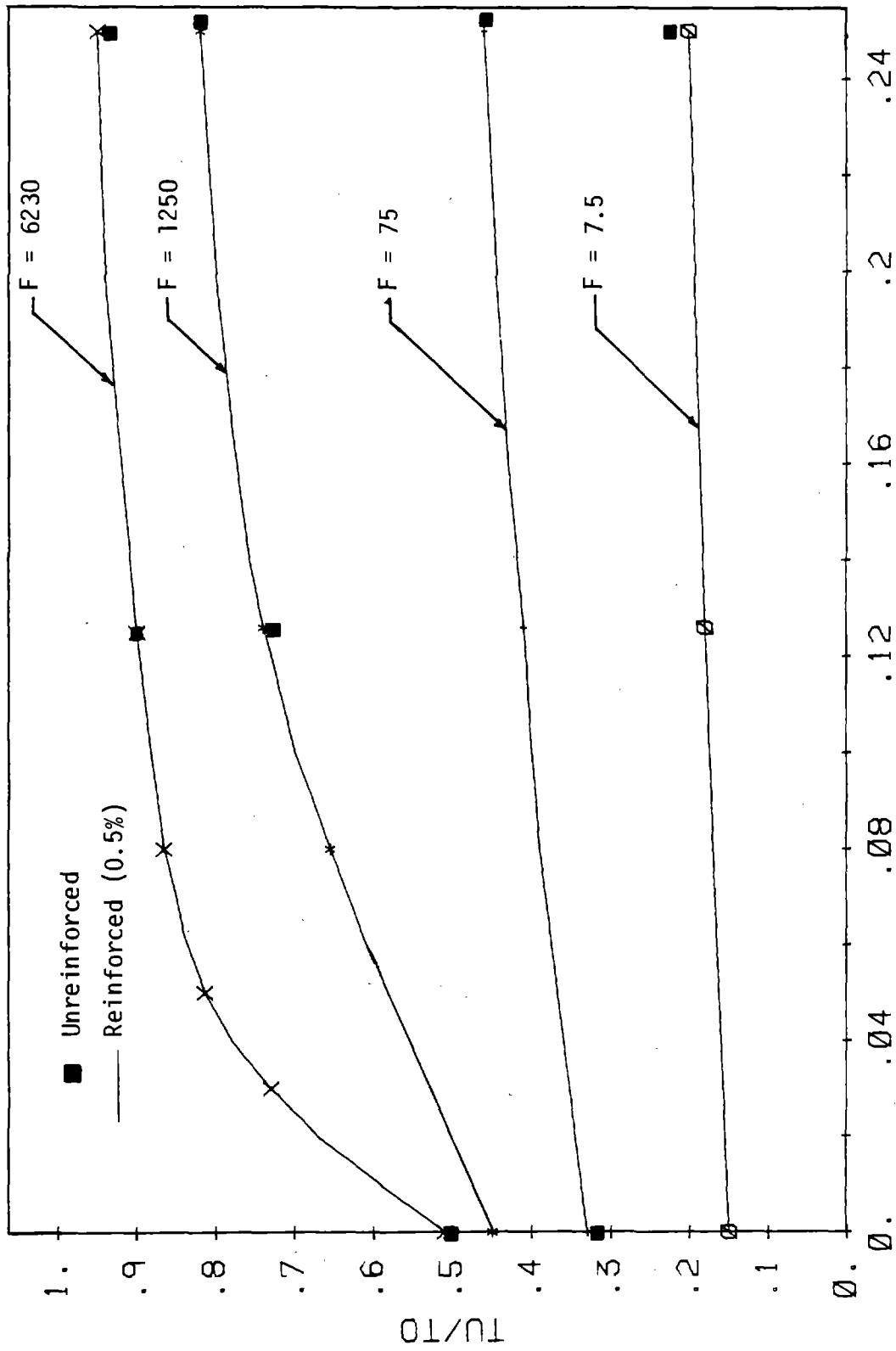


FIGURE 7.12 EFFECT OF F ON TANGENTIAL PRESSURE.



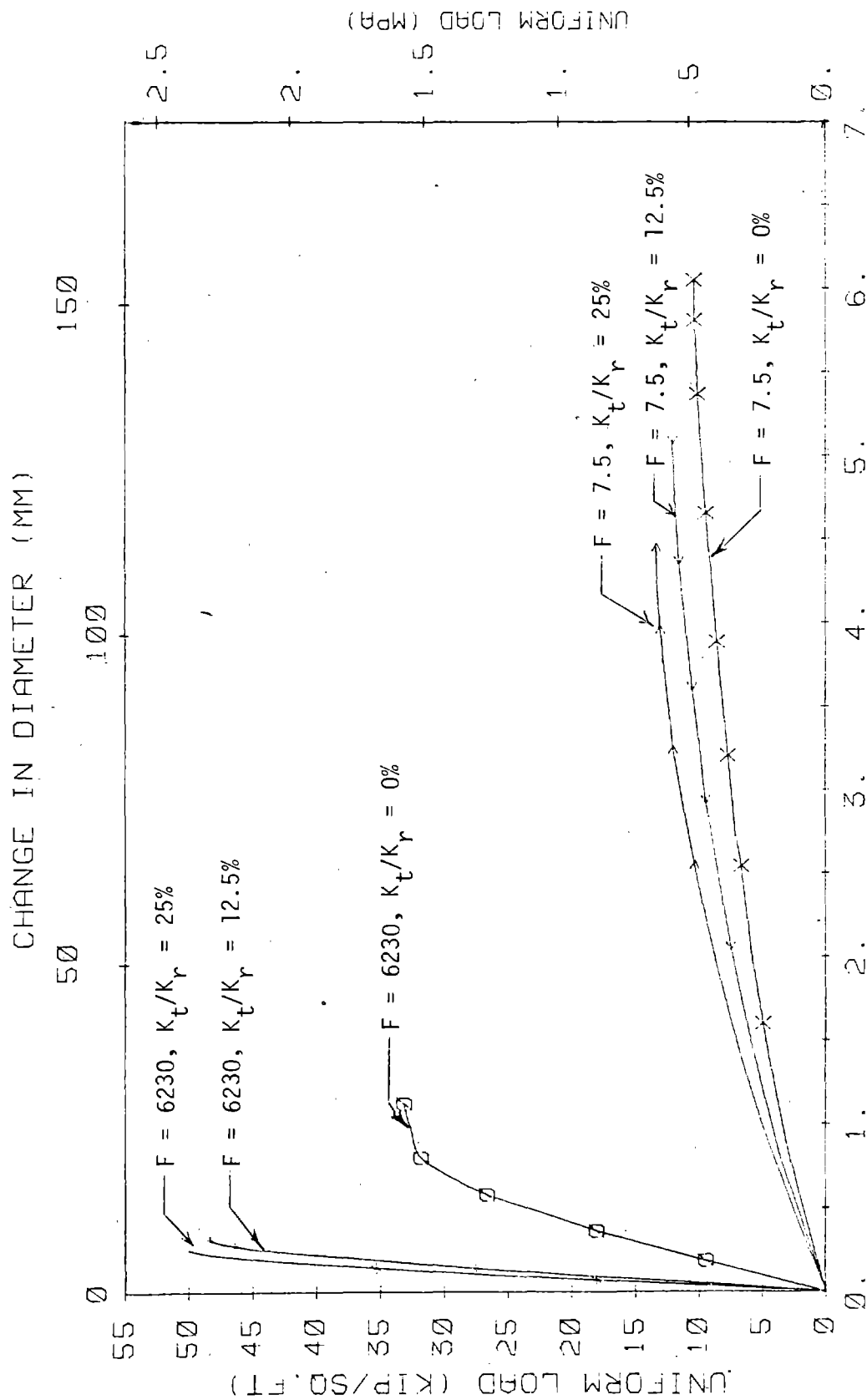
$KT/KR$

FIGURE 7.13 LINING CAPACITY AS A FUNCTION OF TANGENTIAL TO RADIAL STIFFNESS RATIO ( $K_t/K_r$ ) for  $R/t = 11.83$

the curves to approach asymptotically a constant ratio that depends on  $F$  and radius to thickness ratio.

Deformation: The effect of the shear stiffness ratio  $K_t/K_r$  on the diameter change in the direction of active loading is also pronounced as shown in Fig. 7.14, where the load-diameter change curves are shown for the extreme value of flexibility ratio. For a hard medium ( $F = 6230$ ) the load at failure increases from 33 to 51 ksf (1580 to 2440 kPa) when  $K_t/K_r$  increases from zero to 25 percent, while the diameter change at failure decreases from about 1.2 to 0.3 in. (30 to 7.6 mm). For a soft medium ( $F = 7.5$ ) the variation is similar but not nearly as large. The maximum load increases from 10.5 to 14 ksf (500 to 670 kPa), while the maximum deflection decreases from 6.2 to 4.4 in. (160 to 110 mm).

Moment-Thrust Path: The effect of  $K_t/K_r$  on the moment-thrust path for the extreme values of  $F$  are shown in Fig. 7.15. For the small flexibility ratio  $F = 7.5$  changing the shear stiffness ratio  $K_t/K_r$  does not affect the initial slope of the path very much, but has a greater influence on the upper portion of the curve near failure, where the failure thrust increases with increasing shear stiffness ratio because of a greater tendency for the moment-thrust path to follow the envelope. Also, the moment decreases more before failure occurs. If the limiting lining strength is considered to occur when the moment-thrust path first reaches the envelope, then  $K_t/K_r$  would have essentially no effect on the capacity, but the actual thrust at failure is 2 to 3 times this value. For the large flexibility ratio ( $F = 6230$ ) the effect of shear stiffness ratio  $K_t/K_r$  changes the initial slope of the moment-thrust path a great deal, and consequently, the lining capacity. The effect is large enough that for intermediate flexibility ratios the path may be changed to intersect above the balance point rather than below by increasing the  $K_t/K_r$  ratio. For  $F$  equal to 6230 the thrust capacity increased from 240 to 440 kips (1070 to 1960 kN) with an increase in  $K_t/K_r$  from zero to 25 percent. For  $K_t/K_r$  equal to



CHANGE IN DIAMETER (IN.)

FIGURE 7.14 EFFECT OF  $K_t/K_r$  ON DIAMETER CHANGE

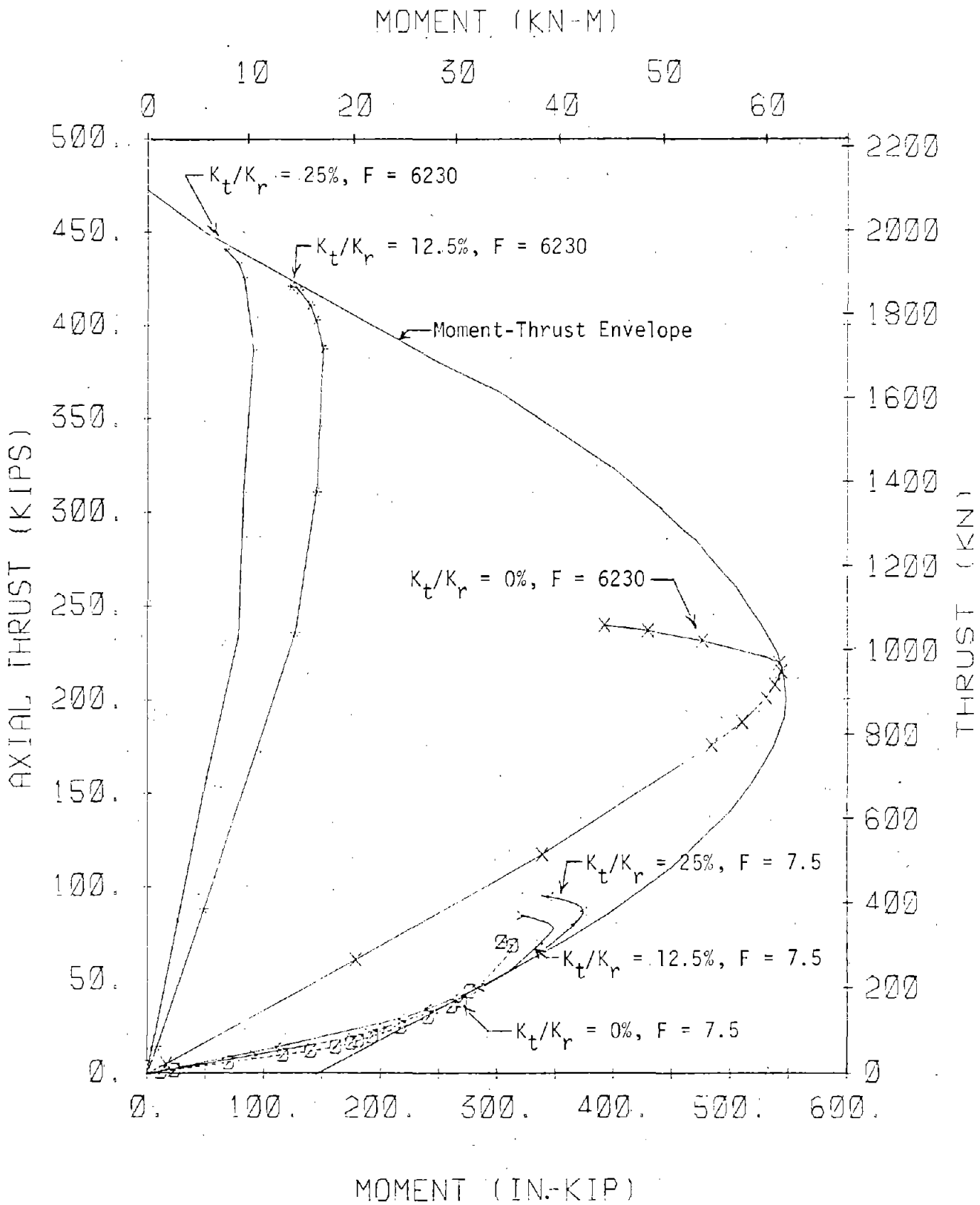


FIGURE 7.15 EFFECT OF  $K_t/K_r$  ON MOMENT-THRUST PATHS AT CROWN

zero the moment-thrust path reaches the failure envelope near the balance point and the moment decreases considerably with a small increase in thrust. For the larger  $K_t/K_r$  values, failure occurs when the envelope is reached. For all these cases with the larger flexibility ratio, the percent increase in thrust over that obtained from a linear analysis is smaller than for the small flexibility ratio, though the absolute value of increase may be larger.

Thrust Distribution: The thrust distribution in the lining is influenced primarily by the tangential shear stiffness; the effect is more pronounced when the medium stiffness is high, as shown in Figs. 7.16 and 7.17, because the tangential shear stiffness is also higher in that case. The tangential shear mechanism between the lining and medium reduces the thrust in the lining from crown to invert, and when the shear stress is larger, then the thrust is correspondingly reduced.

Tangential Stress Distribution: The tangential shear stress distribution is shown in Fig. 7.18, where the largest stress occurs 30 to 45 deg from the crown and is zero at the crown and invert. The shear stress results from the shear stiffness multiplied by the relative tangential movement between the lining and medium, so the relative movement is largest in this high stress region and zero at the crown and invert due to symmetry. The tangential stress decreases with shear stiffness ratio in about the same proportions for both the highest and lowest flexibility ratios though the magnitudes are larger for the larger flexibility ratios, and consequently larger medium stiffness.

Radial Pressure Distribution: The external radial passive pressure on the medium results from the radial lining displacement multiplied by the radial stiffness. Therefore, the radial outward displacements are proportional to the radial pressure on the lining shown in Fig. 7.19 because the radial stiffness was taken as constant. When the shear stiffness ratio is high ( $K_t/K_r = 0.25$ ), most of the

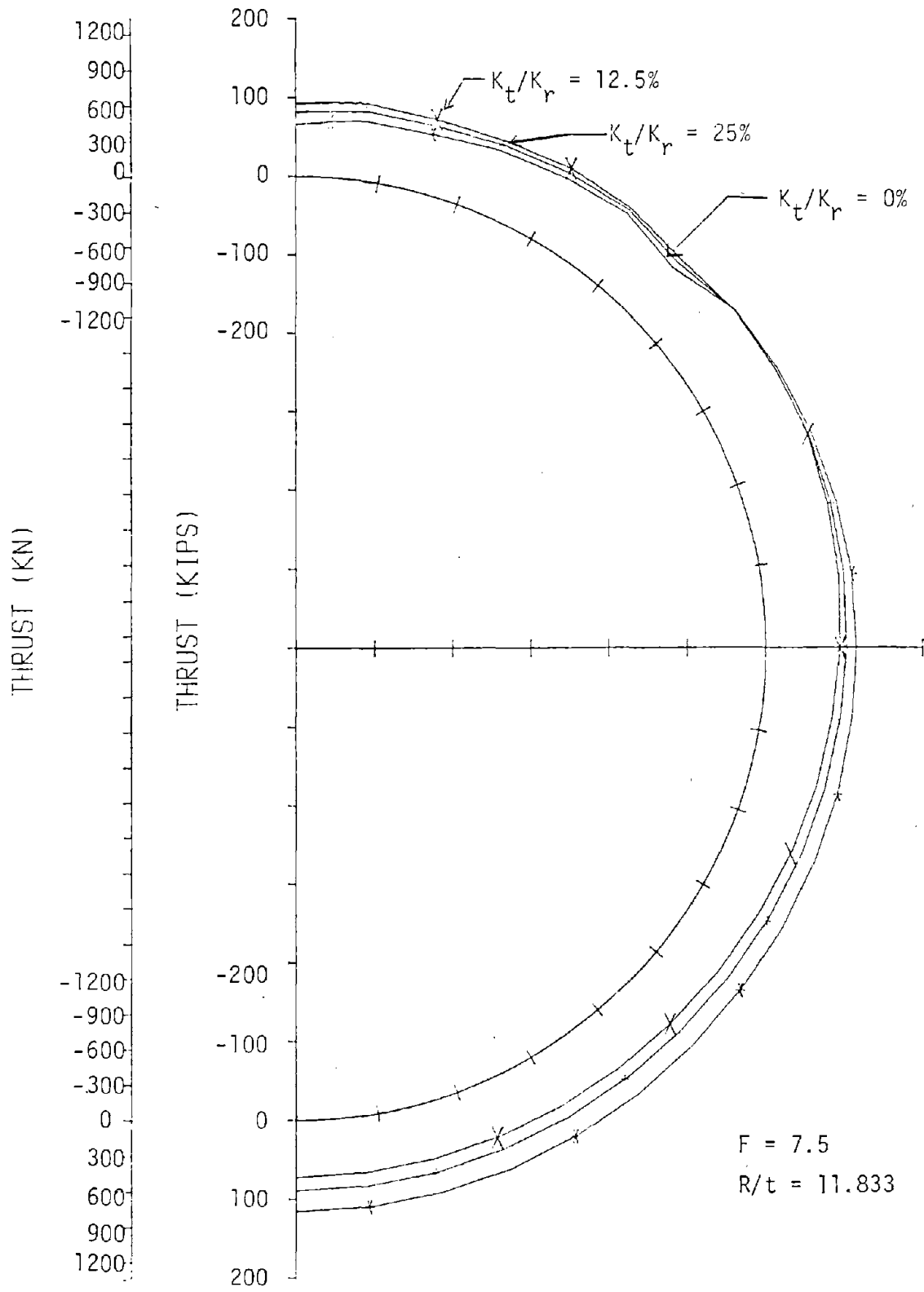


FIGURE 7.16 EFFECT OF  $K_t/K_r$  ON THRUST AT MAXIMUM LOAD



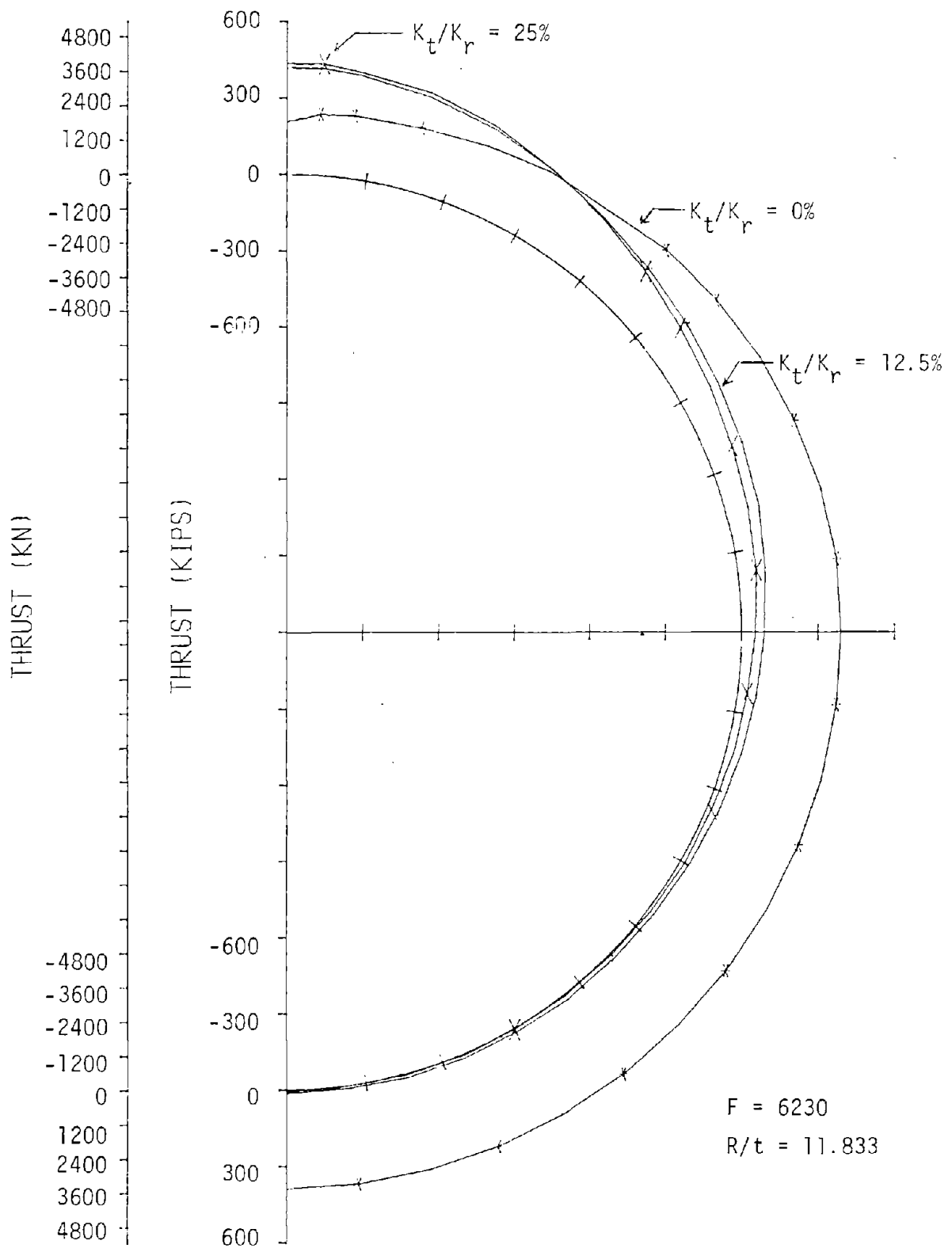


FIGURE 7.17 EFFECT OF  $K_t/K_r$  ON THRUST AT MAXIMUM LOAD

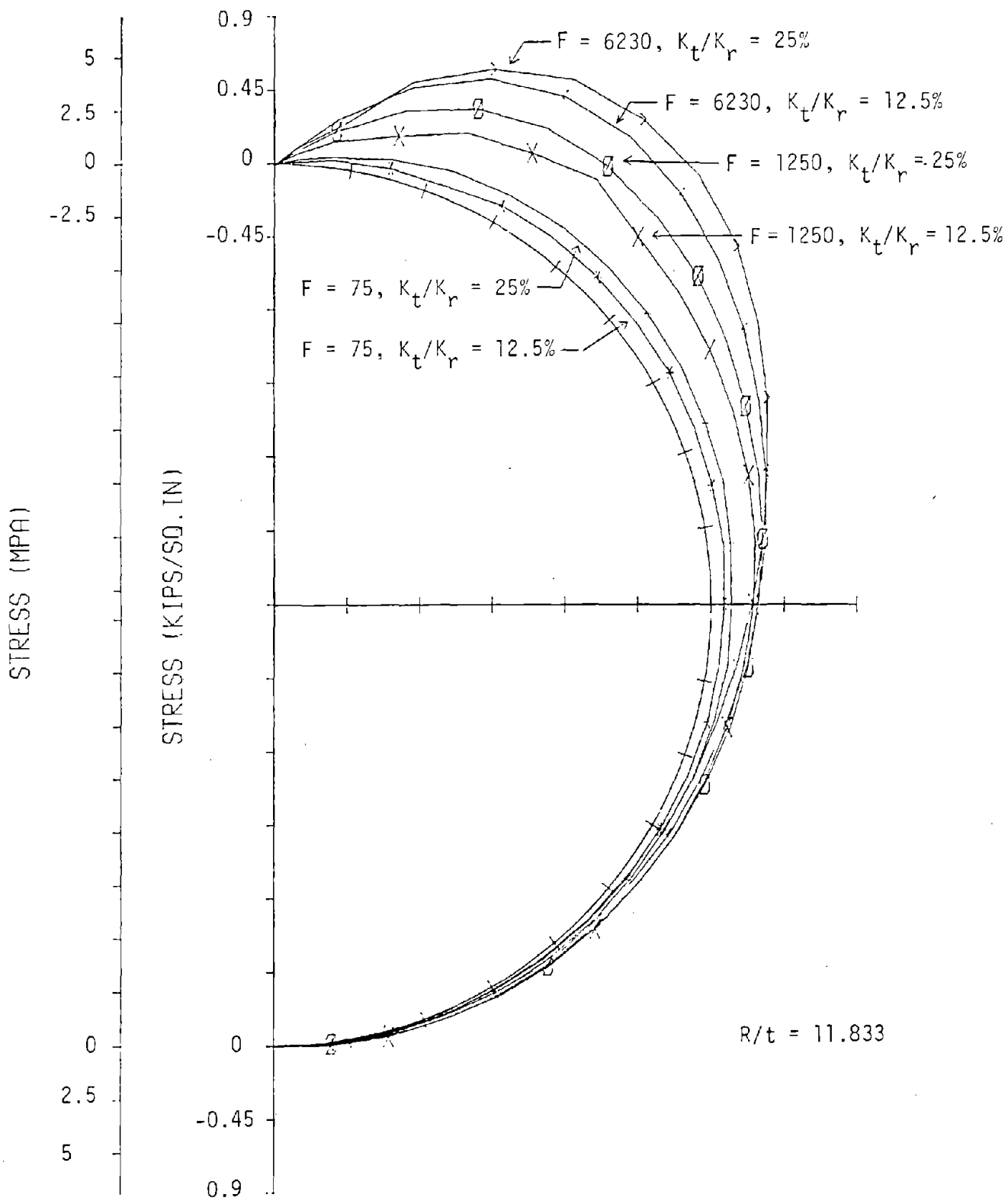


FIGURE 7.18 EFFECT OF  $K_t/K_r$  ON TANGENTIAL STRESS AT MAXIMUM LOAD

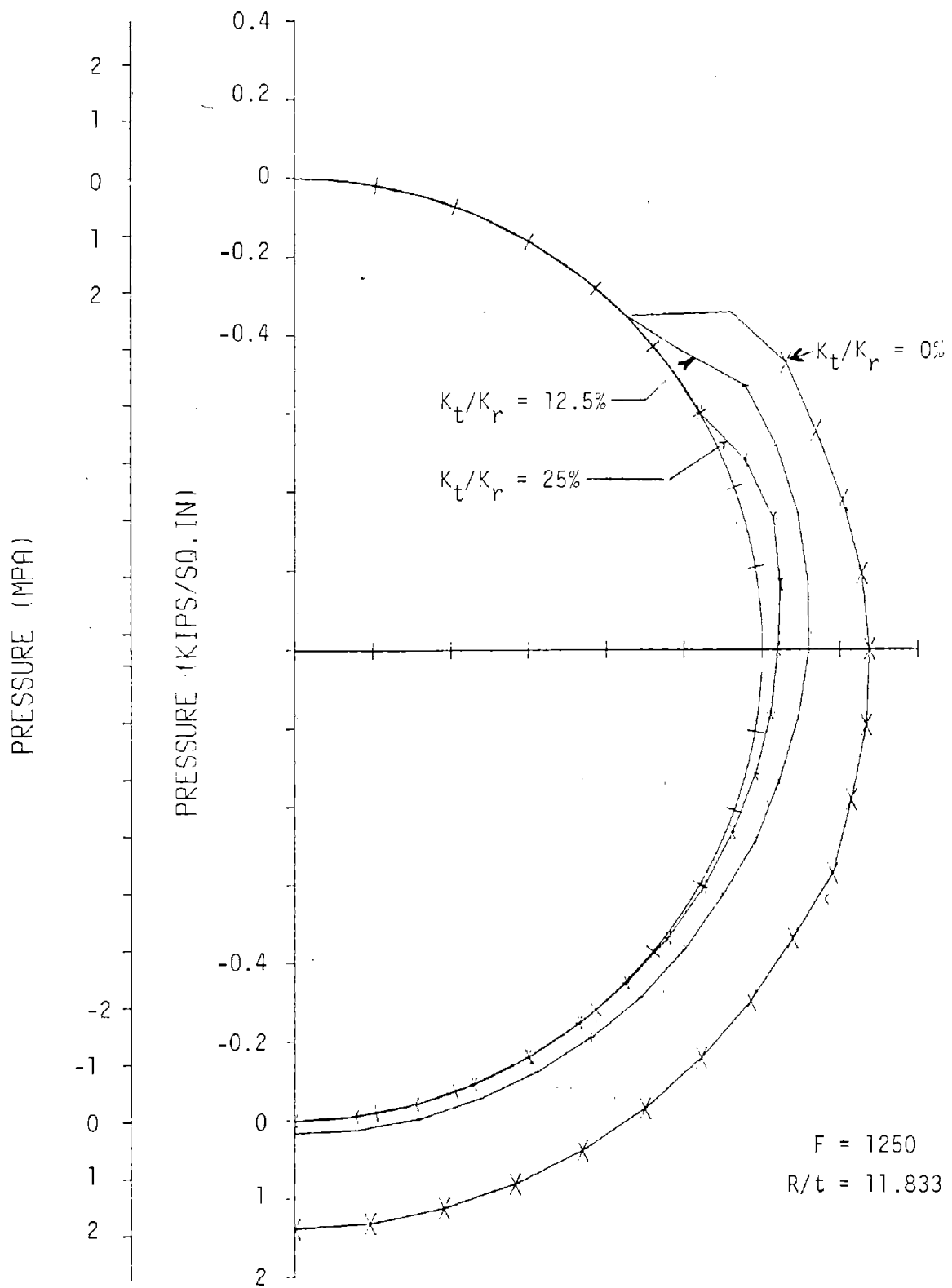


FIGURE 7.19 EFFECT OF  $K_t/K_r$  ON RADIAL STRESS AT MAXIMUM LOAD

active load is transferred to the medium through the tangential shear mechanism, there is little thrust transmitted to the lower portion of the lining, small rigid body movement of the lining occurs, and therefore, small radial pressure results in the region of the invert. When the tangential stiffness is zero, all the active load is transmitted to the lower portion of the lining, and a high pressure results. The radial pressure near the springlines depends on the outward movement or ovaling of the lining as well as the radial stiffness of the medium. Increased tangential shear stiffness reduces the amount of ovaling of the lining, which in turn reduces the radial pressure in the region of the springlines.

Moment Distribution: The distribution of moment around the lining at the peak loads are shown in Figs. 7.20 and 7.21. For a low flexibility ratio ( $F = 7.5$ ), the change in shear stiffness ratio does not change the peak moments a great deal, but causes a slight shift of the curves toward the crown as the shear stiffness ratio decreases. For a large flexibility ratio ( $F = 6230$ ), where the moment-thrust paths reach the failure envelope above the balance point, the maximum moments increase with decreasing  $K_t/K_r$  at the crown and in the region 30 to 50 deg from the crown. Beyond a point about 70 deg from the crown, the moment is very small and almost constant. The negative moment is slightly larger at the 30 to 50 deg region, than the positive moment at the crown. From these curves it is observed that when the medium is stiff, the maximum moment is increased by increasing the shear stiffness between the lining and medium, but when the medium is soft, the shear stiffness makes little difference. Generally, when the medium is soft only a small shear stress can be developed, however. Shifting of the negative moment region toward the crown as  $K_t/K_r$  becomes smaller is much more pronounced for the small flexibility ratio.

Internal Shear Distribution: Maximum internal shear forces of opposite signs occur near 20 deg and near the region 45 to 55 deg from

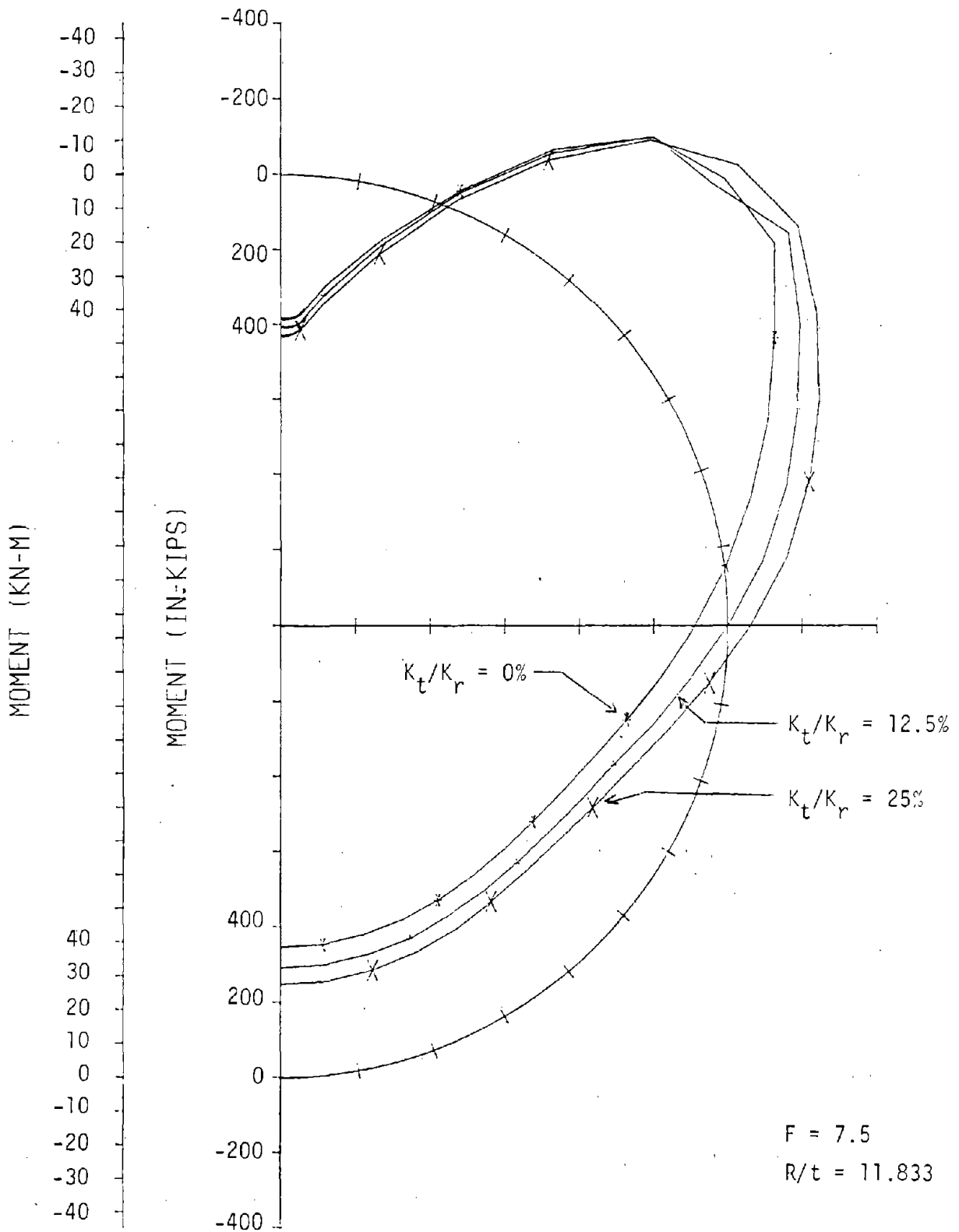


FIGURE 7.20 EFFECT OF  $K_t/K_r$  ON MOMENT DISTRIBUTION AT  
 MAXIMUM LOAD FOR  $F = 7.5$

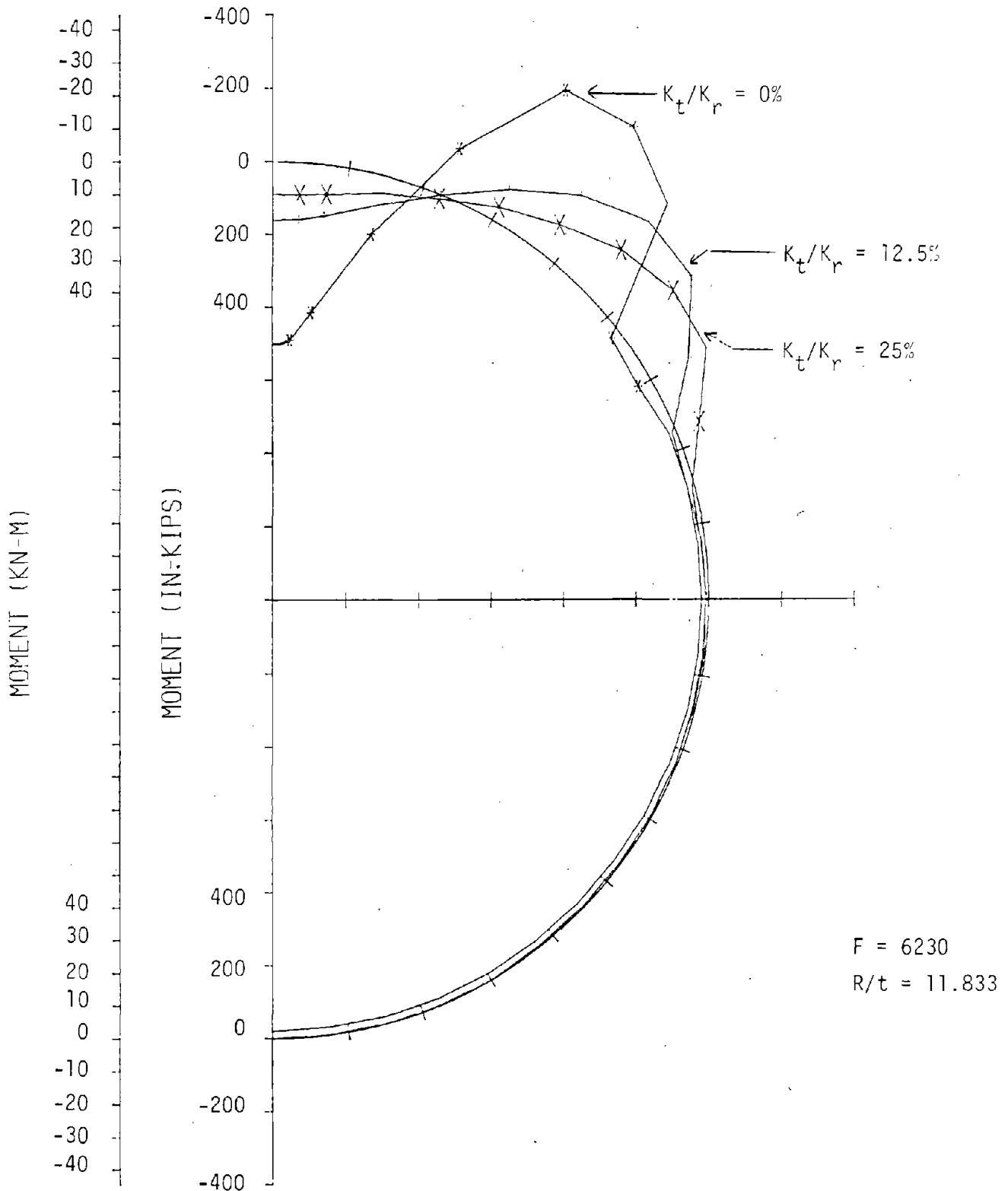


FIGURE 7.21 EFFECT OF  $K_t/K_r$  ON MOMENT DISTRIBUTION AT MAXIMUM LOAD FOR  $F = 6230$

the crown as shown in Fig. 7.22. The maximum shear increases with decreasing shear stiffness ratio  $K_t / K_r$ . The magnitude of peak shear is slightly larger at the 45 to 55 deg sections, but the section at 20 deg is likely to be more critical because it corresponds to inward punching of the crown region. The internal shear is almost zero for sections beyond 65 deg from the crown.

### 7.2.3 Effect of Radius to Thickness Ratio (R/t)

The effect of the radius to thickness ratio (R/t) on the strength of the lining was studied by plotting the thrust ratio ( $T_u / T_o$ ) against flexibility ratio (F) for different values of R/t, as shown in Fig. 7.2. Several problems were analyzed with different combinations of radius and thickness for a particular shear stiffness ratio ( $K_t / K_r$ ), while keeping both flexibility and R/t radius constant. For all these combinations of radius and thickness, a unique thrust ratio was obtained for a particular flexibility and shear stiffness ratios. The thrust ratio for several values of flexibility and R/t ratios were checked, to reach the conclusion that a unique curve can be drawn for each radius to thickness ratio.

Three such curves for R/t values of 8.2, 11.8 and 14, and  $K_t / K_r$  ratio of 25 percent are shown in Fig. 7.2. For the same flexibility and shear stiffness ratio, the thrust ratio increases with decrease of the R/t ratio. However, the variation of thrust ratio with R/t is less pronounced when the flexibility ratio is larger than about 2500, as the curves for different R/t ratios approach each other with increase of flexibility ratio.

### 7.2.4 Effect of Reinforcement

The parameter study included linings without reinforcement and with a reasonable area of deformed bars for tunnel linings; the effect of this reinforcement (0.5 percent near each face) on the strength is

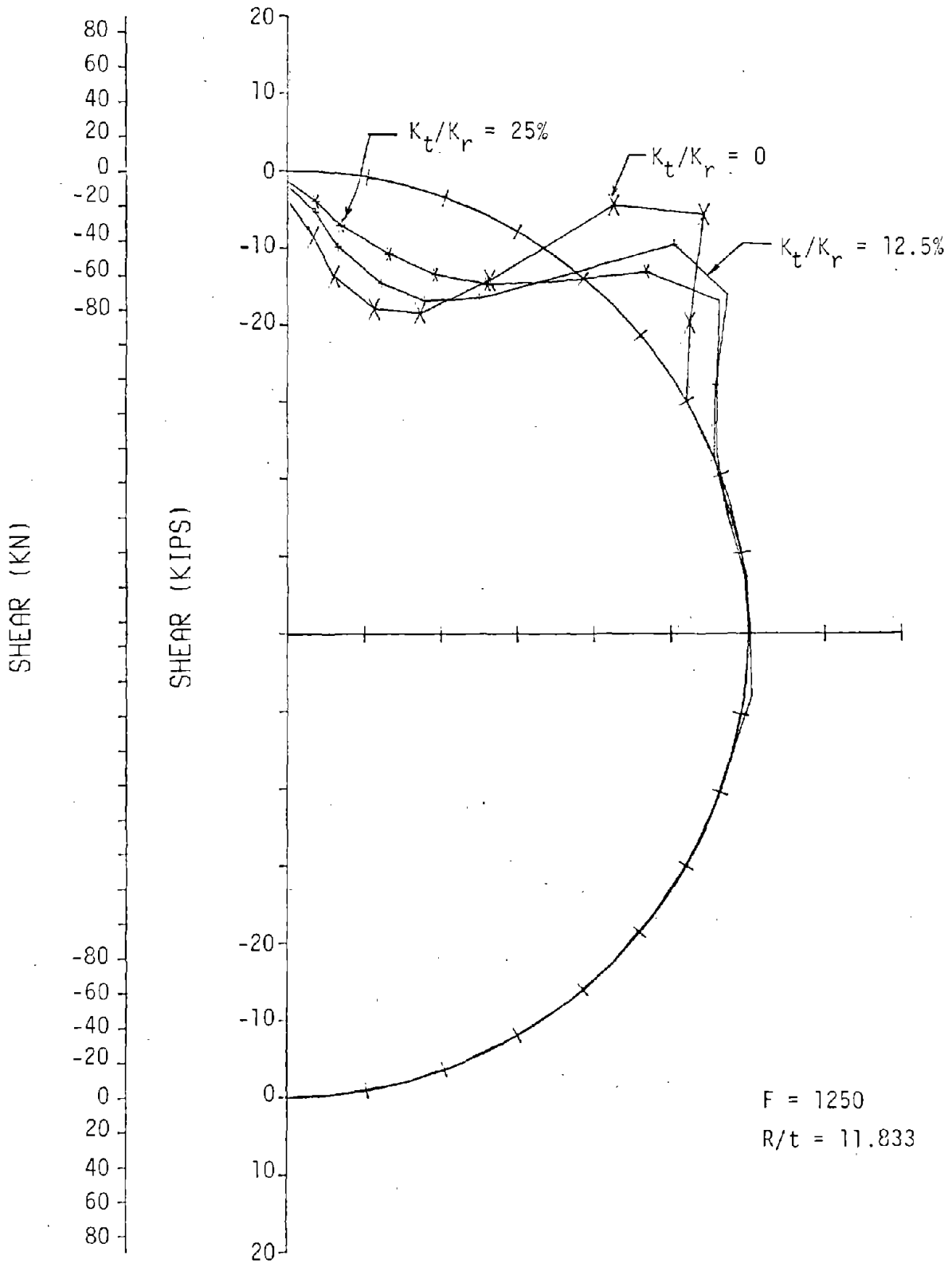


FIGURE 7.22 EFFECT OF  $K_t/K_r$  ON SHEAR AT MAXIMUM LOAD



shown in Fig. 7.13. In these graphs the thrust ratio  $T_u/T_o$  changes very little with the addition of reinforcement. The same conclusion was reached when comparing the laboratory test results in Section 4.5. In these analytic studies  $f'_c$  was increased for the unreinforced cases to compensate for the absence of reinforcing steel so that  $T_u$  would be constant for all cases. Thus, differences in strength and ductility are primarily the effect of reinforcement on the bending behavior. This effect can be observed in Fig. 7.23 where the load-diameter change curves are compared. For the stiffer mediums ( $F = 1250$  and  $6230$ ) or flexible linings, addition of reinforcement increased the strength a very slight amount, and it had a negligible effect on the stiffness of the system. Since the moment-thrust paths reached the failure envelope above the balance point, where the maximum load occurs due to compression failure, the reinforcement would not be expected to improve the strength or ductility an appreciable amount. For the low flexibility ratio ( $F = 7.5$ ) the addition of reinforcement does not increase the initial slope of the load deflection curve, but near maximum load the reinforced lining became somewhat more stiff and failed at a slightly lower deformation. The maximum loads are almost identical, however.

Moment-thrust paths are compared for several cases with and without reinforcement in Fig. 7.24. In addition, the paths are compared with the moment-thrust failure envelopes, which are the same in the high thrust range where failure occurs in compression, but different below 300 kips (1330 kN), where the moment capacity is increased by reinforcement since failure occurs in tension. Below the balance point the two envelopes are very nearly parallel. There is very little difference in the moment-thrust paths except for the lowest flexibility ratio; for this case the paths start to separate at a thrust of about 90 kips (400 kN) and each path approaches its respective moment-thrust envelope. The moment resisted by the reinforced section is therefore, larger, but both paths turn back toward the thrust axis and reach the same peak thrust so the load on the lining is the same. If the maximum

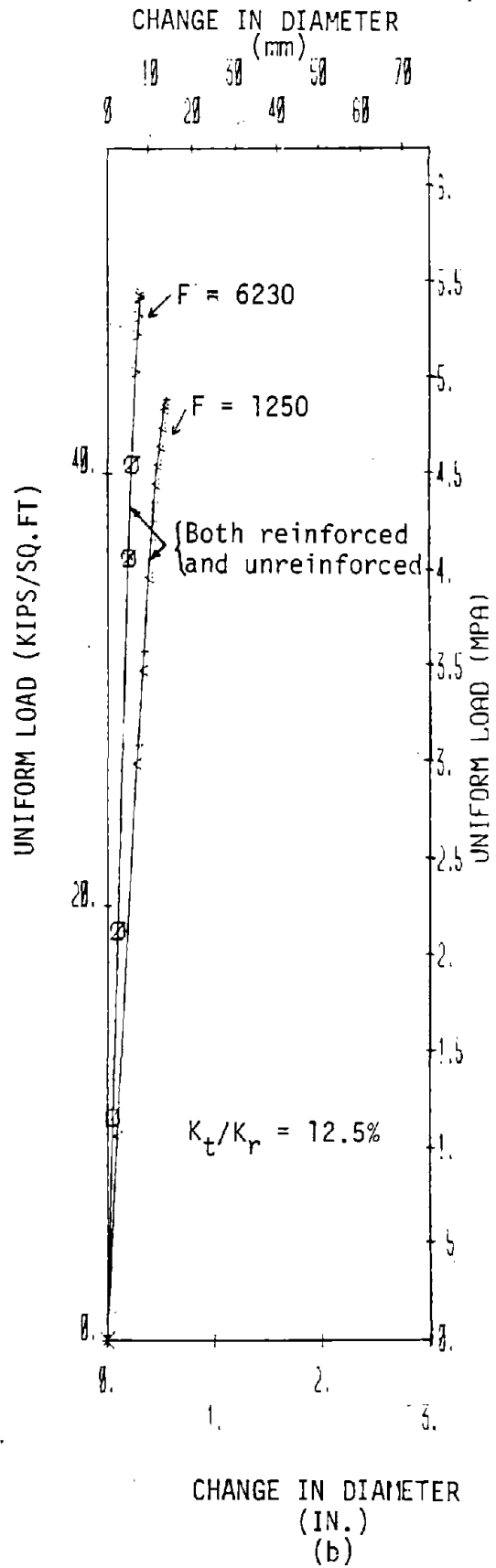
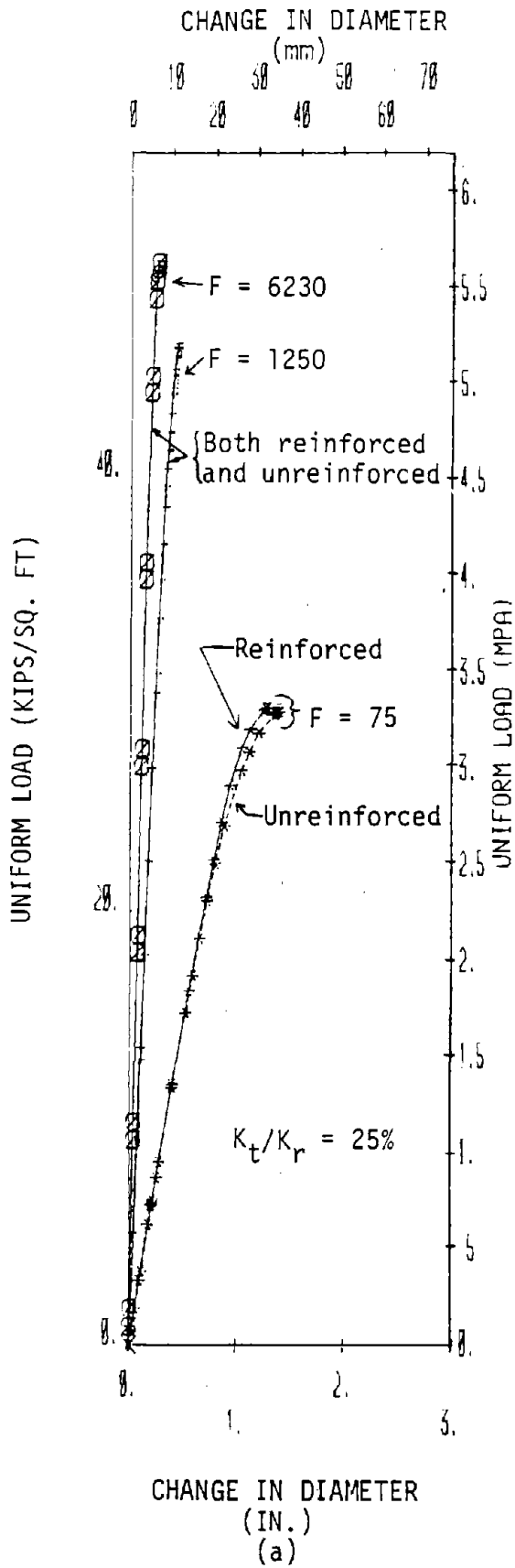


FIGURE 7.23 EFFECT OF REINFORCEMENT ON DIAMETER CHANGE

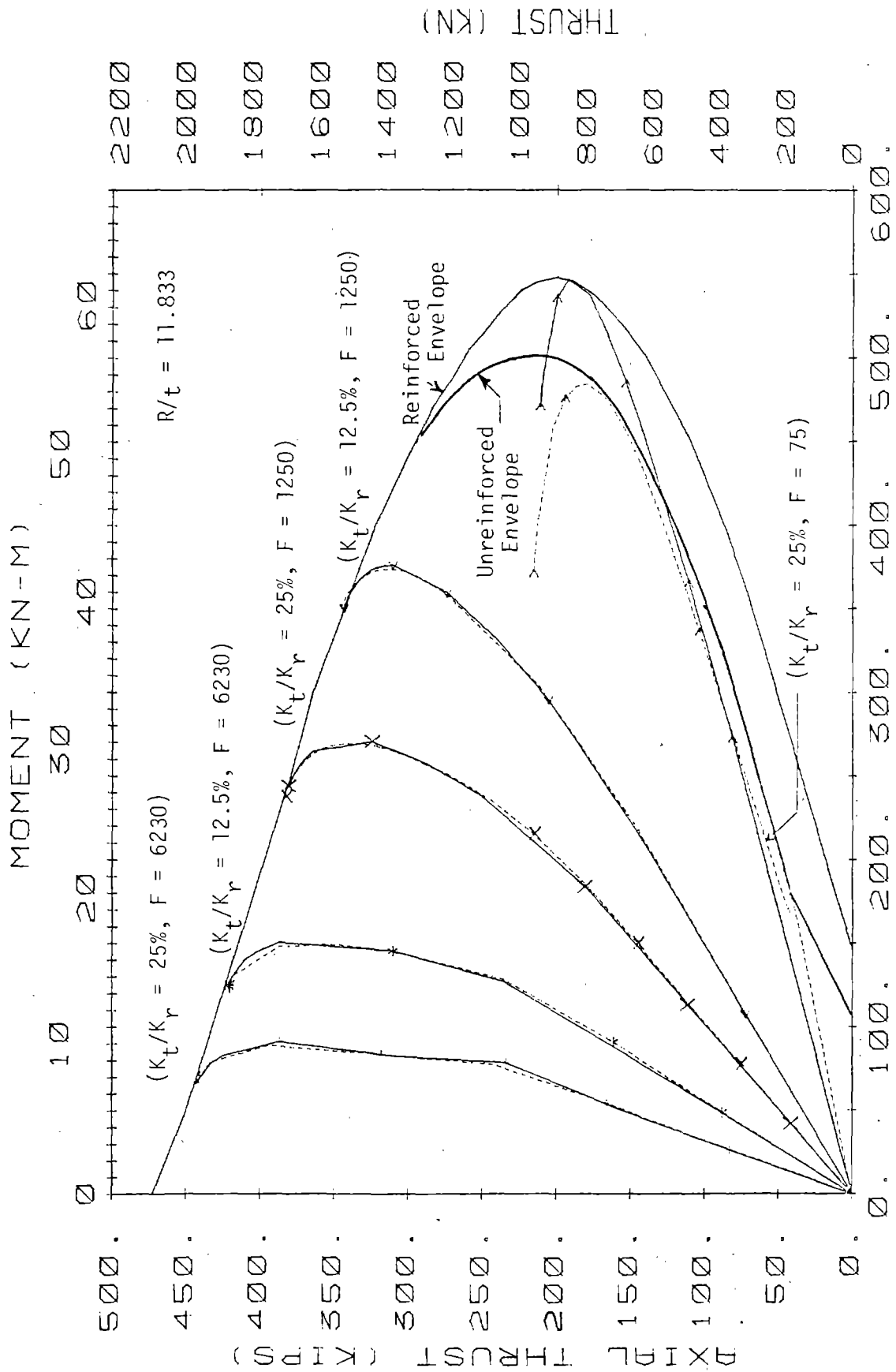


FIGURE 7.24 EFFECT OF REINFORCEMENT ON MOMENT-THRUST PATHS

load was assumed to occur when the envelope was first reached, the thrust in the reinforced lining would be about 20 kips (89 kN) larger.

The similarity of thrust distribution at maximum load for the reinforced and unreinforced cases shown in Fig. 7.25 is expected from the observations above. From these same observations the moment distribution at peak load are expected to be different for the low value of  $F = 7.5$  as shown in Fig. 7.26. The difference is largest at the crown and decreases toward the springline; from the springline to the invert the curves are very close. The moments are almost identical throughout for the larger value of  $F = 1250$ . The same comments may be made for the internal shear in the lining shown in Fig. 7.27. The external tangential shear shown in Fig. 7.28 and radial pressure in Fig. 7.29 show little difference between the reinforced and unreinforced cases. These quantities are sensitive to the lining deformation. Although for low flexibility ratios, the deformations are slightly larger for the unreinforced linings than for the reinforced ones (Fig. 7.23), the increase in passive radial and tangential pressures at the interface are negligible.

#### 7.2.5 Discussion of Results

Relationships Among the Parameters: Lining behavior is influenced by numerous parameters, as shown in the previous sections. The diameter change of the lining is dominated by the flexibility ratio and in turn by the medium stiffness when a particular  $R/t$  ratio is considered. Since the moments are related to the deformation, the moment to thrust ratio is dominated by medium stiffness. Thus, medium stiffness has a strong influence on the slope of the moment-thrust path and where the path intersects the moment-thrust failure envelope (Fig. 7.5). The ratio  $K_t / K_r$  influences the moment-thrust path in the same way but not as dramatically, while the addition of reinforcement or change in  $R/t$  ratio have little effect. If the moment-thrust path intersects the failure envelope below the balance point, additional

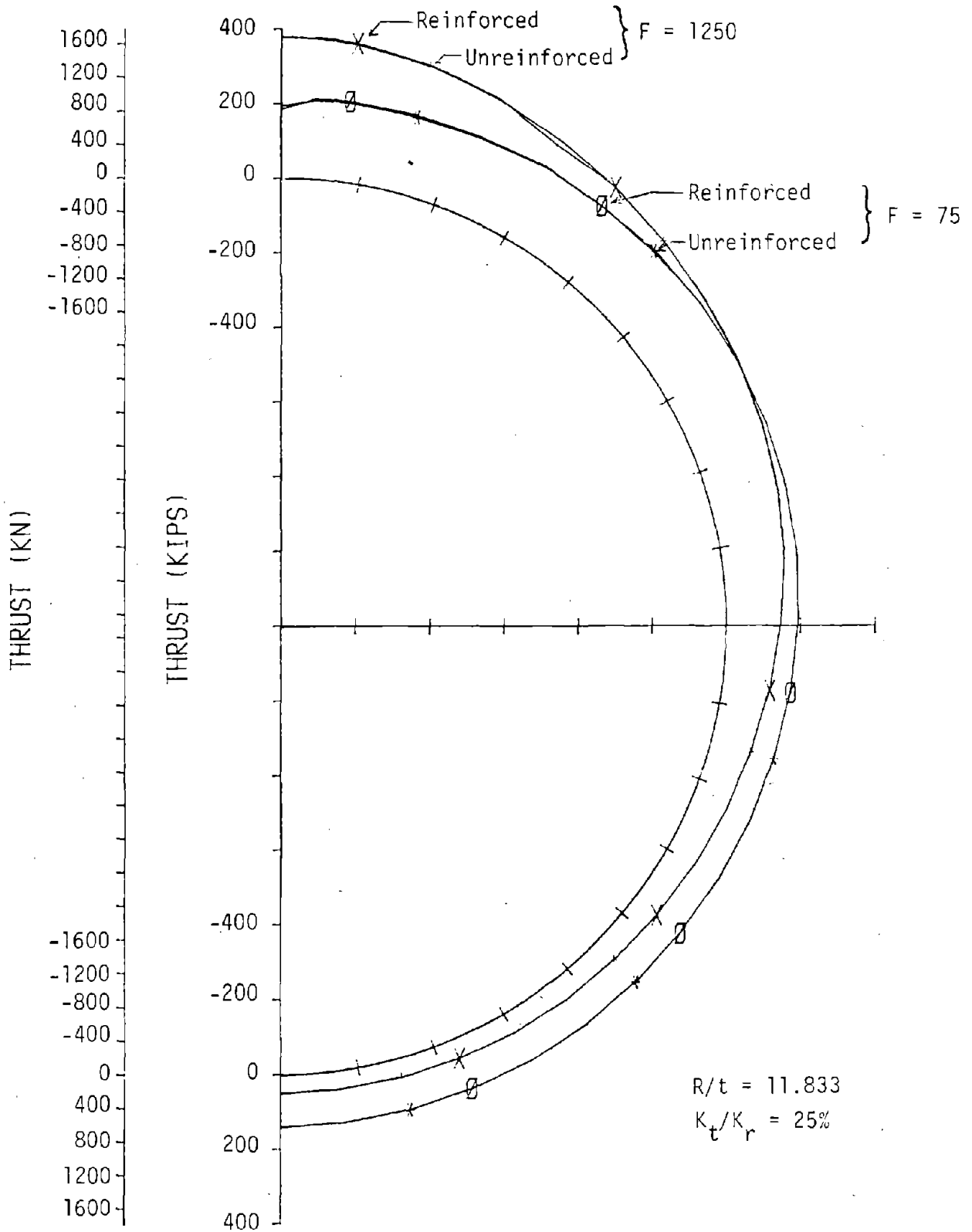


FIGURE 7.25 EFFECT OF REINFORCEMENT ON THRUST DISTRIBUTION AT MAXIMUM LOAD

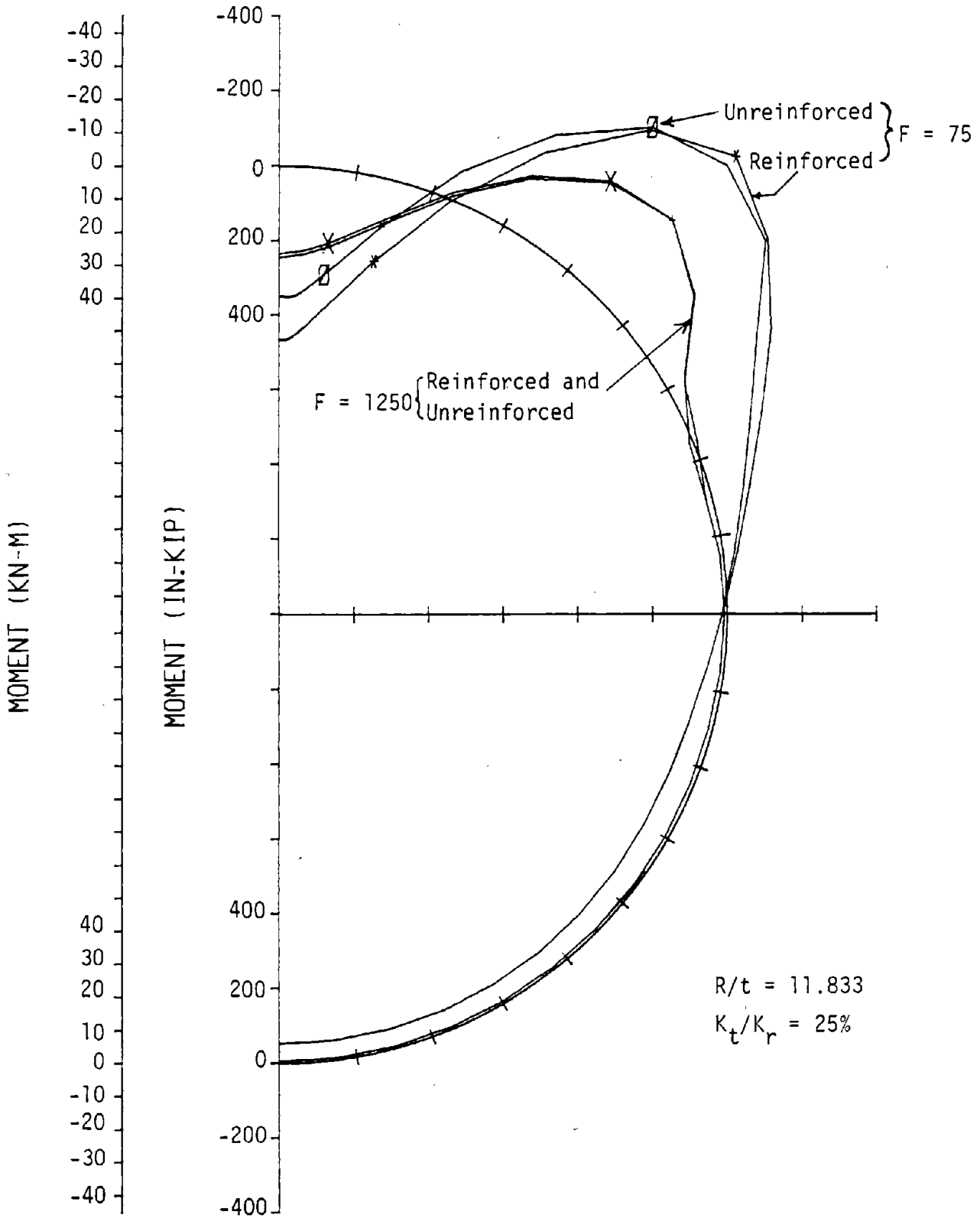


FIGURE 7.26 EFFECT OF REINFORCEMENT ON MOMENT DISTRIBUTION AT MAXIMUM LOAD

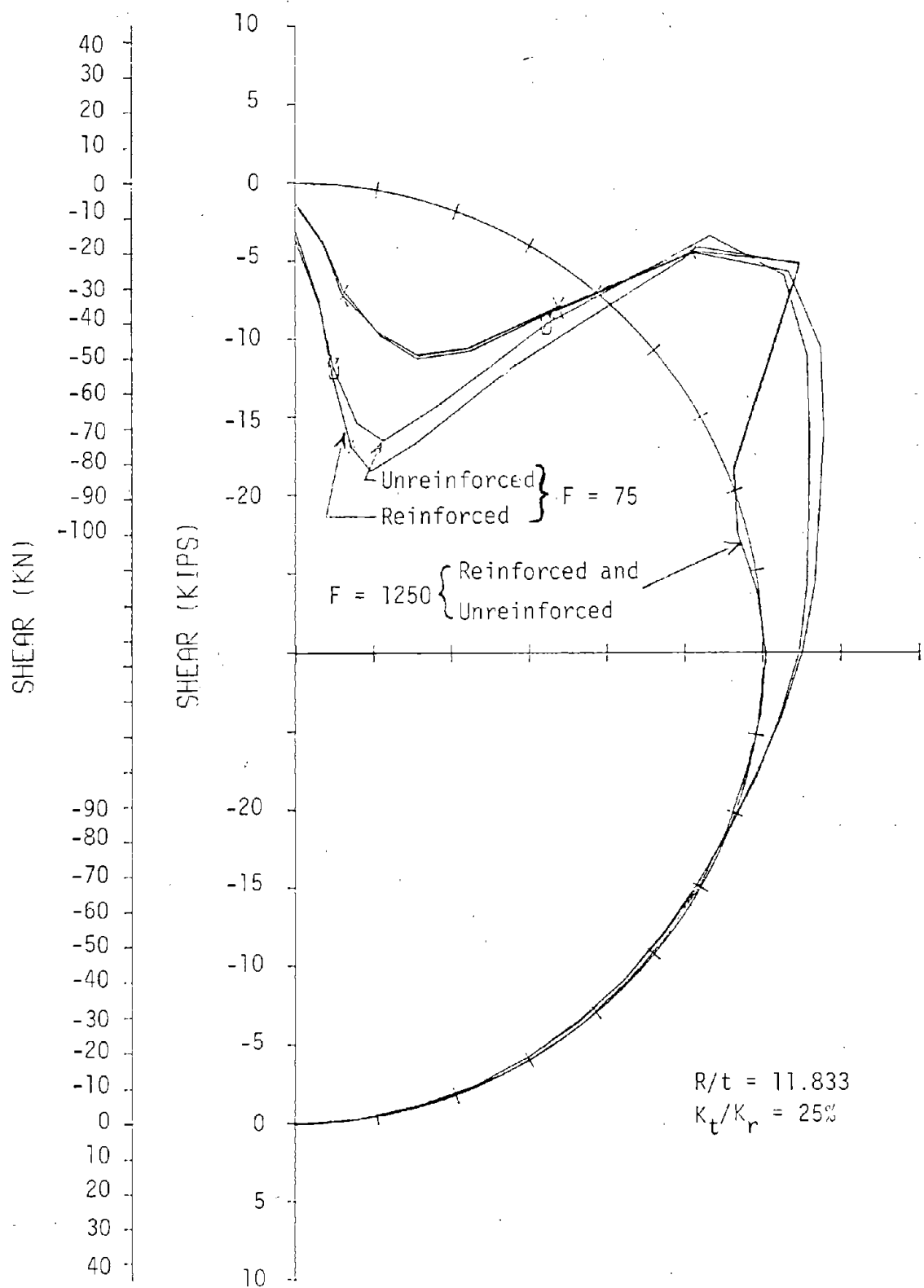


FIGURE 7.27 EFFECT OF REINFORCEMENT ON SHEAR DISTRIBUTION AT MAXIMUM LOAD

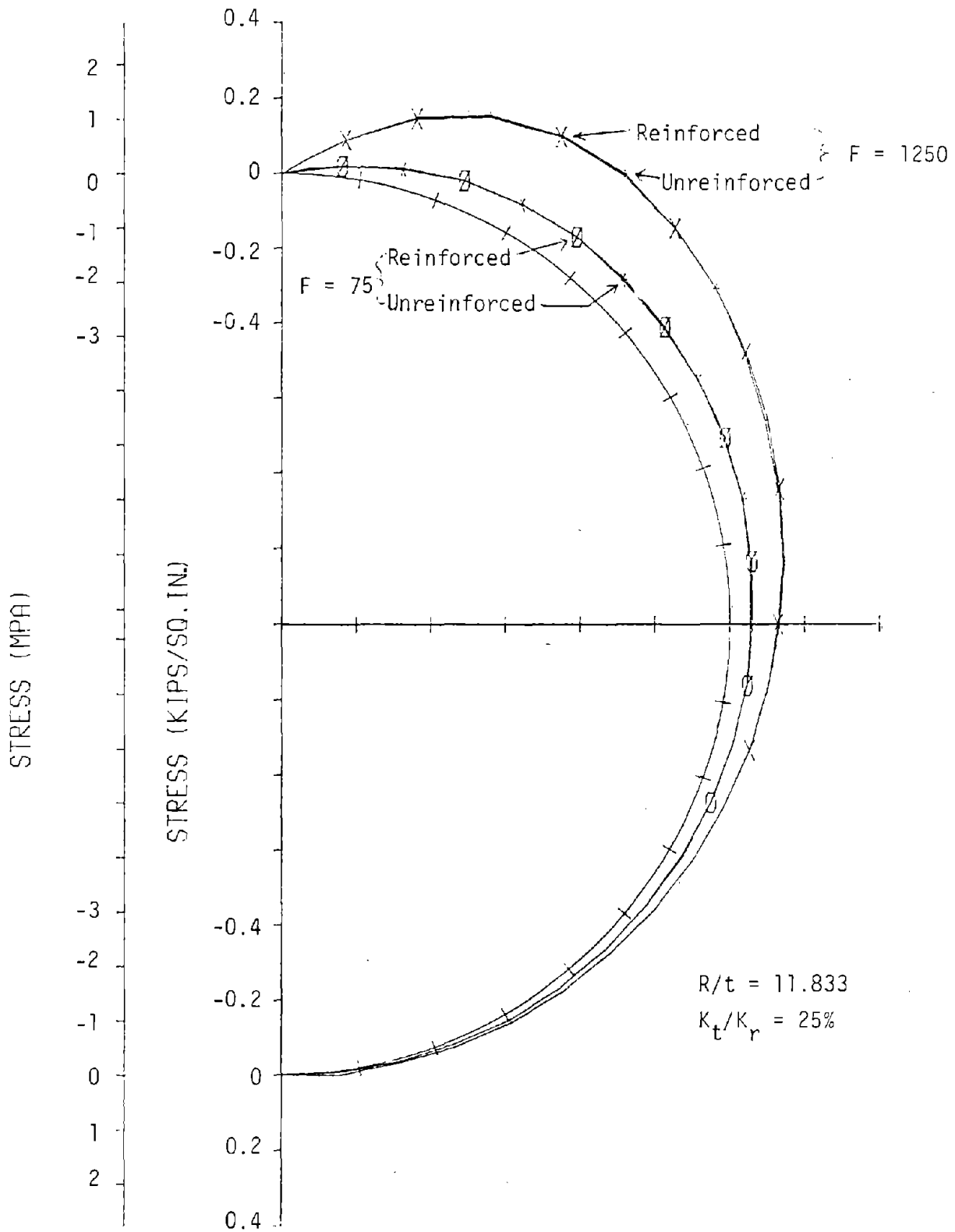


FIGURE 7.28 EFFECT OF REINFORCEMENT ON TANGENTIAL STRESS DISTRIBUTION AT MAXIMUM LOAD



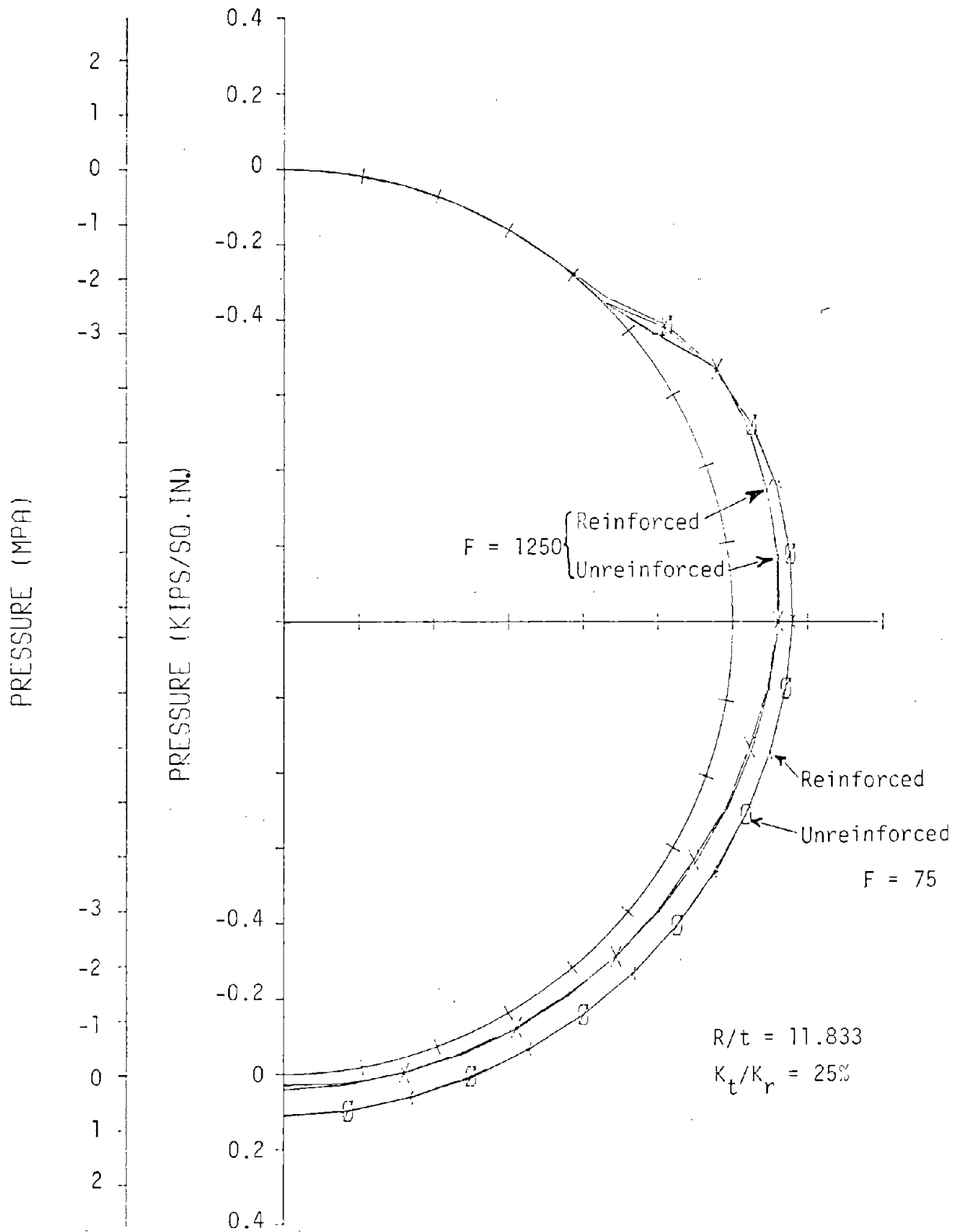


FIGURE 7.29 EFFECT OF REINFORCEMENT ON RADIAL PRESSURE DISTRIBUTION AT MAXIMUM LOAD

thrust increases the moment capacity, so additional load can be applied. The moment cannot become larger than that at the failure envelope, so the moment-thrust path must follow the envelope (Fig. 7.5); however, if the moment-thrust path had followed its original slope, the moment would be larger (outside the envelope). Thus, a redistribution of moment must occur that increases the rate at which other sections resist moment to compensate for the reduced rate at the critical section. This redistribution of moment and increase in moment capacity with increasing thrust accounts for the additional lining capacity when the moment-thrust path reaches the envelope below the balance point. When the path intersects the envelope above the balance point, there is some redistribution of moment because of the nonlinear behavior before the path reaches the envelope, but failure occurs essentially when the envelope is reached (Fig. 7.5).

Internal shear is related to the slope of the moment distribution diagram, and this slope is larger when the moment peaks are larger. Thus, the magnitude of peak shear increases with decreasing flexibility ratio as does the moment, and the influence on the shear distribution of the parameters under study is similar to that for moment.

At a given load the thrust at the crown of the lining depends very little on the parameters under study (Fig. 7.7), but if the thrusts are compared at the peak loads, they appear to increase with flexibility ratio because the peak load increases (Fig. 7.6). The reduction of thrust from the crown to invert increases with medium stiffness, however. When the medium stiffness in the radial direction increases, so does the tangential stiffness if  $K_t/K_r$  remains constant. The increased shear stiffness increases the tangential shear stress between lining and medium and thus, transfers thrust from the lining to the medium. Therefore, the largest medium stiffness case in Fig. 7.6 has the largest thrust at the crown and the smallest at the invert. When the tangential stiffness is zero, the thrust is essentially constant around the lining. The tangential shear stress and thrust are

therefore, closely related, with the largest shear stress occurring with the largest medium stiffness (which results in larger variation of thrust).

Design Implications: Lining strength depends on the moment-thrust relationship at various critical sections near the crown. The thrust in this region is nearly proportional to the load, but the moment depends heavily on the lining deformation; the deformation in turn depends heavily on the relative stiffness of the medium to the lining, or in other words, the flexibility ratio. A large flexibility ratio is desirable, and the ratio can be increased by increasing the medium stiffness or reducing the lining stiffness. Often there is little that can be done to change the medium; though sometimes its stiffness is increased by rock bolting or grouting. It is often easier to reduce the lining stiffness by using a segmented lining or using as thin a lining as possible that is consistent with the thrust considerations. This approach will also reduce cracking because the thinner lining will have smaller tensile strains with smaller moments and larger thrust strains to overcome those tensile strains that might exist. For larger flexibility ratios the strength of the lining as depicted by the thrust ratio ( $T_u / T_o$ ) varies little so that an estimate of the strength from Fig. 7.2 will not be subjected to great error. However, care must be exercised in estimating the thrust ratio for flexibility ratios below 1000 as a small change in  $F$  causes an appreciable change in the thrust ratio.

The shear stiffness ratio  $K_t / K_r$  has little effect on the lining strength when the medium stiffness is low relative to the lining, but the effect increases with increasing relative medium stiffness (Fig. 7.13). For  $F = 6230$ , the thrust ratio  $T_u / T_o$  increases from 0.5 to 0.95 when the  $K_t / K_r$  ratio increases from zero to 0.25.

Even the presence of a small amount of tangential shear stress at the interface between the lining and the medium increases the thrust

ratio substantially from its value for the full-slip case. In hard ground (rock), the full-slip case can be ruled out, so a reliable estimate of the value of  $K_t/K_r$  is important. However, the increase in thrust ratio is small for practical purposes for values of  $K_t/K_r$  greater than about 12.5 percent and even smaller for values greater than 25 percent. Thus, for flexibility ratios greater than about 1250 (representing tunnels in medium quality rock) an estimate of the thrust ratio considering  $K_t/K_r$  as 25 percent will not be unreasonable.

The variation of radius to thickness ratio ( $R/t$ ) has little effect, for all practical purposes, on the strength of the lining when the flexibility ratio is higher than 1250. However, for lower values of flexibility ratio, the radius to thickness ratio ( $R/t$ ) can make appreciable difference as shown in Fig. 7.2. It should be kept in mind that an increase in thickness may not always be beneficial as the section may not satisfy the cracking criterion.

The addition of reinforcement to the lining does not increase the thrust ratio  $T_u/T_o$  (Fig. 7.13), but the absolute strength is increased slightly for some flexibility ratios. Reinforcement increases the ultimate moment in the low thrust range (Fig. 7.24) so the effect on the capacity might be expected to be larger. The unreinforced lining is slightly more ductile when  $F = 75$  so the moment-thrust path reaches the envelope near the balance point (Figs. 7.23 and 7.24). However, nominal reinforcement (1/4-1/2 percent) does distribute cracks in those cases where cracking may be a problem, and if there is a sufficient amount it will reduce the amount of creep deformation that occurs.

### 7.3 DESCRIPTION OF THE STUDY FOR LININGS IN SOFT GROUND

Analysis of ground-lining interaction for the soft ground case is substantially different from that in rock, especially from the point

view of the the ground loads reach the lining. The beam-continuum and the beam-spring models described in Chapter 3 were used for nonlinear analysis with the three types of loading conditions described in Section 2.1, and closed-form analytic solutions obtained by Ranken, Ghaboussi and Hendron (1978) were used for linear analyses with the overpressure and excavation loadings. In the parametric studies the lining behavior under these loading conditions was studied and compared at both ultimate and first cracking load levels. Comparison of the linear solutions obtained by the beam-continuum models and closed-form solutions served to verify the computer program, while that with the nonlinear solutions also resulted in an evaluation of the effect of nonlinearity of the problem on the distribution of internal forces and additional strength over that predicted by linear analyses. Loading conditions consisting of water pressure or removal of internal air pressure were also investigated. Besides loading condition other variables used in the parametric studies were the interface properties (cohesion  $c$ , internal frictional angle  $\phi$ , shear modulus  $G$ ), coefficient of earth pressure at rest  $K$ , radius to thickness ratio  $R/t$ , lining reinforcement and the effect of joints in the dimensionless parameter flexibility ratio  $F$  has been selected as the variable to reflect variation of ground conditions on other parameters.

For most of the parameter study a typical uniform cast-in-place 10 in. (254 mm) thick lining with a diameter of 19 ft 8 in. (6 m) was considered. In some of the problems the thickness, radius and reinforcement were varied to study the effects of  $R/t$  and reinforcement. The finite element model used for analysis with overpressure and excavation loadings is shown in Fig. 7.30 and that used for loosening loads, in Fig. 7.31. The reinforced concrete lining had 0.5 percent reinforcement in each face, 3.5 in. (89 mm) from the surfaces, and concrete with compressive strength of 4000 psi (28 MPa) with a stress-strain curve as shown in Fig. 5.1b.

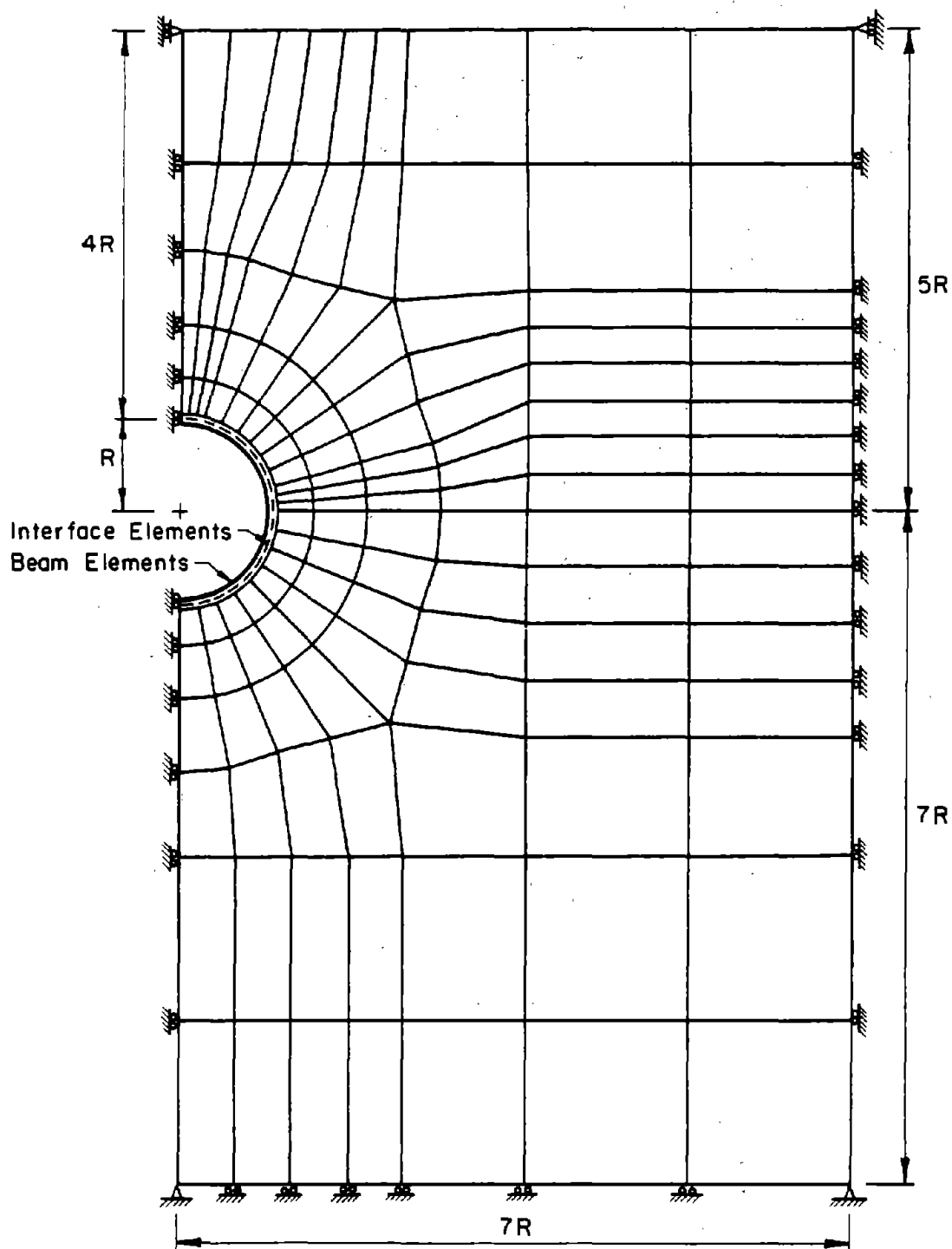


FIGURE 7.30 F.E. MODEL FOR PARAMETER STUDIES

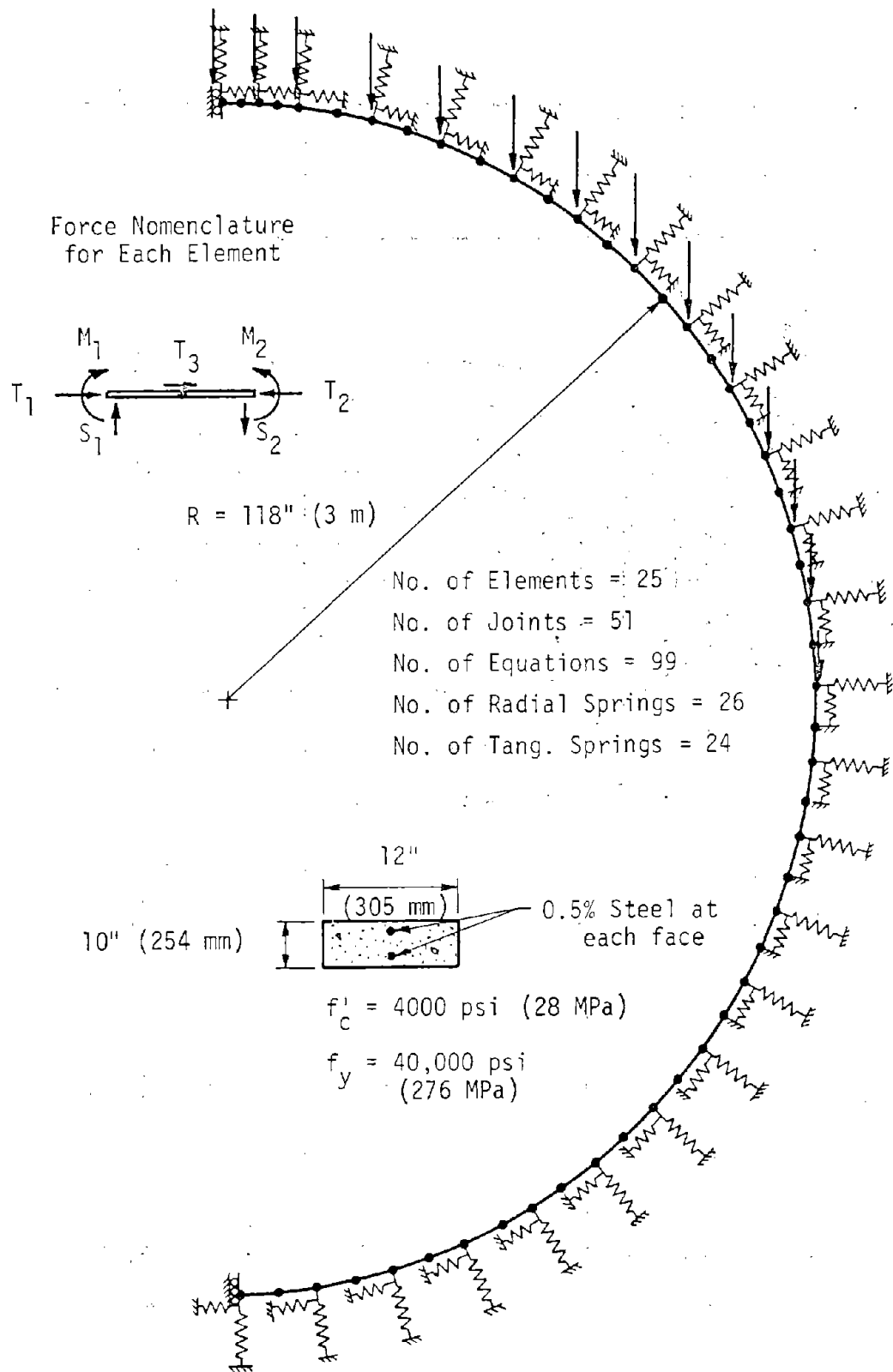


FIGURE 7.31 FINITE ELEMENT MODEL OF CIRCULAR LINING FOR PARAMETRIC STUDIES IN SOFT GROUND FOR LOOSENING LOAD

For the overpressure and excavation loading, the medium was represented by linear elastic continuum elements and the elastic modulus,  $E$ , was varied from 2.5 ksi to 57 ksi (17.2 to 393 MPa) to cover the <sup>m</sup> range of soft ground properties. For the beam-spring model used for loosening loads, the spring stiffnesses were computed, using Eq. 7.1. Since the use of tangential springs has little effect on the solution at low flexibility ratios as discussed in Section 7.2.2, and since full-slip at the interface is closer to the actual condition than no-slip in soft ground, the tangential springs were not used in the beam-spring model for soft ground in this study.

In the analysis with overpressure loading, uniform vertical pressure was applied at the top surface of the initially unstressed medium with the lining in place. The excavation loading condition was obtained by applying the in-situ stresses (Fig. 7.32) at the interface between the lining and medium on the medium nodes. In the beam-spring model, uniform vertical pressure was applied directly to the lining to represent loosening load.

### 7.3.1 Effect of Interface Properties

The slip condition at the ground-lining interface in the beam-continuum model is controlled by three parameters, defining the material properties for the interface element, cohesion  $c$ , angle of internal friction  $\phi$ , and shear modulus  $G$ . Variation of cohesion within reasonable limits (0 to 5 psi, 0 to 35 kPa) did not have an appreciable effect on the solutions. There is very little difference in the crown deflection, tangential and radial pressure distribution on the lining, or moment and thrust distributions as shown in Figs. 7.33 and 7.34. For this reason a small value of  $c$  has been used in most of the problems for parametric studies, as it facilitates obtaining convergence in the computations. Variation of the angle of internal friction did show an appreciable effect; with high  $\phi$  (= 45 deg), the shear strength of the interface increases and larger tangential shear



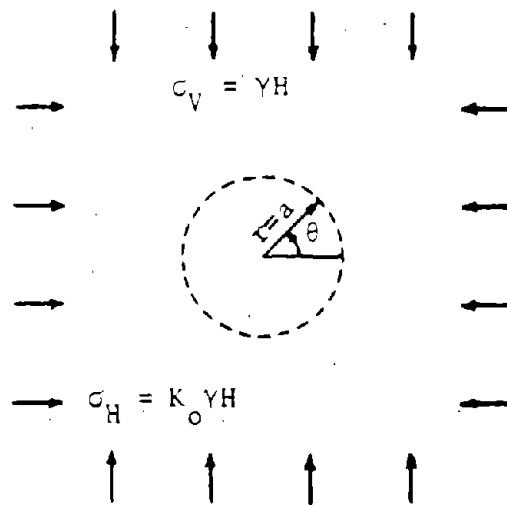
a) In-situ stress state

In polar coordinates:

$$\sigma_r = \frac{1}{2}YH[(1 + K_o) - (1 - K_o) \cos 2\theta]$$

$$\sigma_\theta = \frac{1}{2}YH[(1 + K_o) + (1 - K_o) \cos 2\theta]$$

$$\tau_{r\theta} = \frac{1}{2}YH(1 - K_o) \sin 2\theta$$



b) Distribution of pressures acting on cylinder of ground to be replaced by liner

$$K_o = 0.5$$

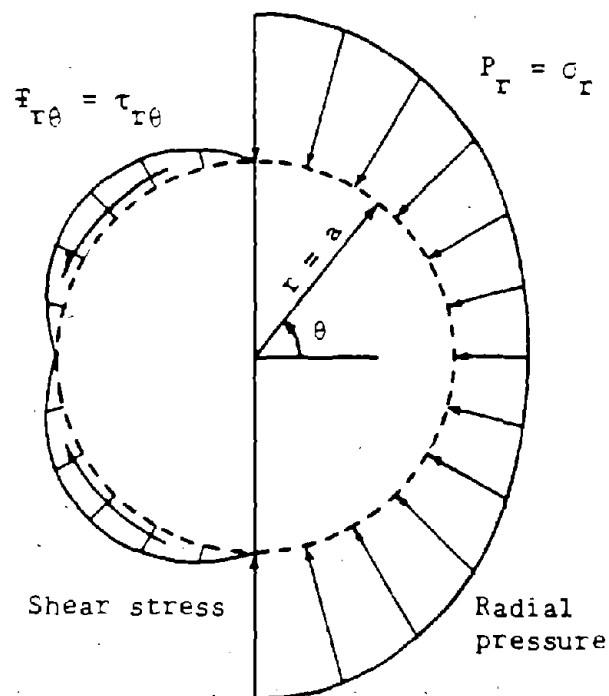


FIGURE 7.32 THE IN-SITU STRESS STATE

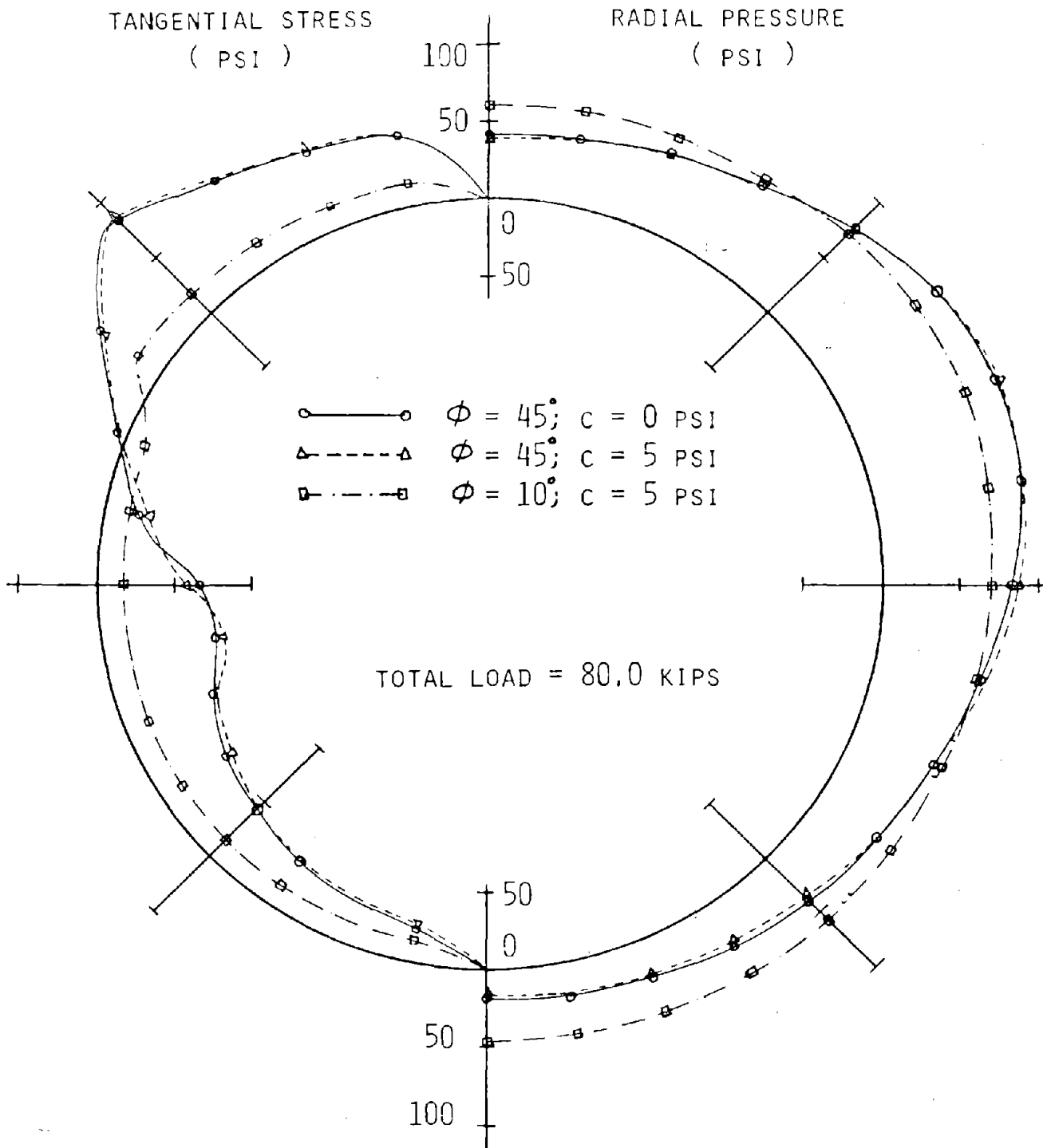


FIGURE 7.33 EFFECT OF  $\phi$  AND  $c$  ON RADIAL PRESSURE AND TANGENTIAL STRESS

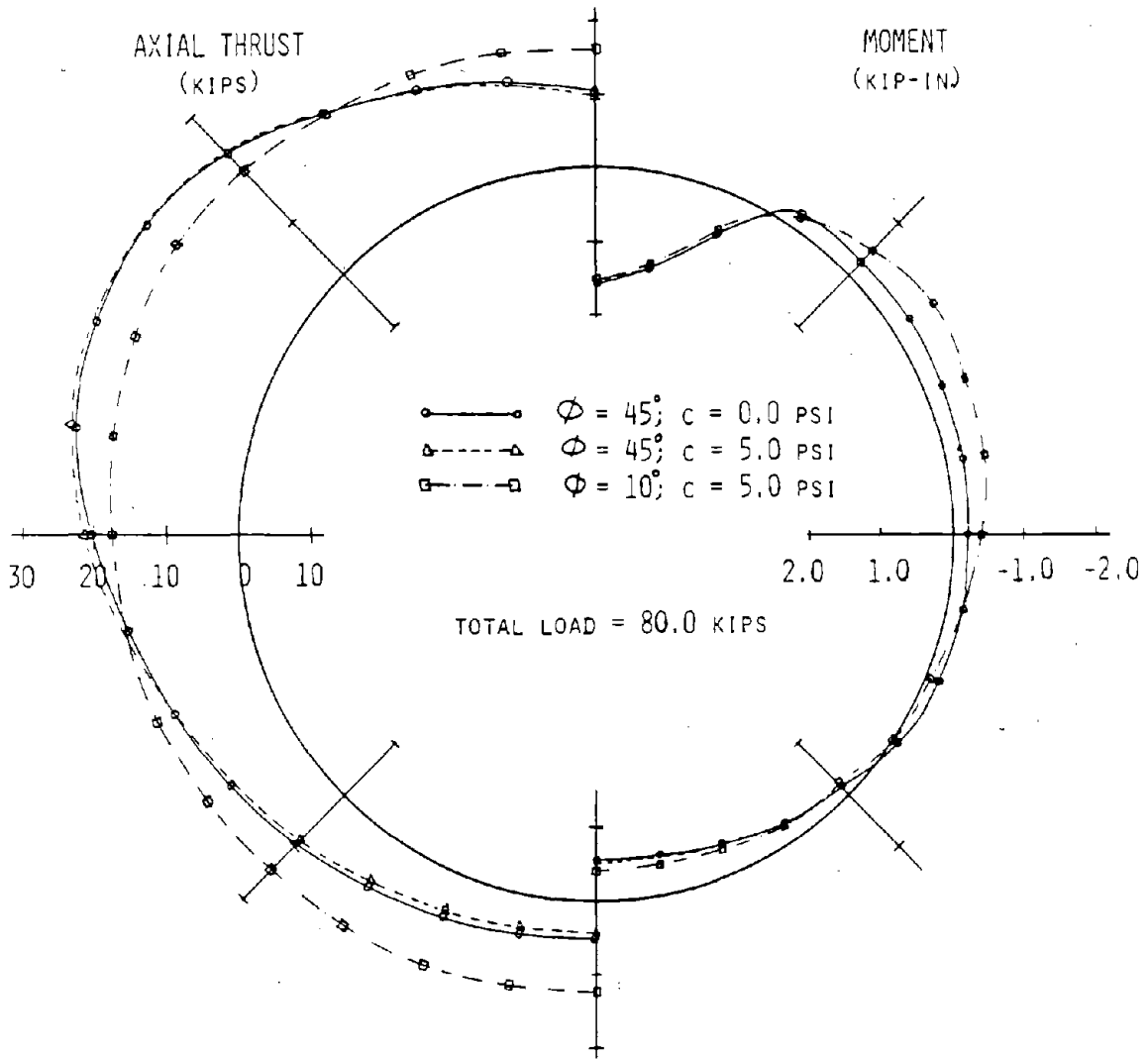


FIGURE 7.34 EFFECT OF  $\phi$  AND  $c$  ON AXIAL THRUST AND MOMENT

stresses result, which reduces the thrust at the crown and invert. The thrust distribution for a small  $\phi$  remains fairly uniform, since the tangential shear strength remains low at the interface, which leads to a condition near full-slip as most of the interface elements become plastic in shear at the load level shown. On the other hand for higher  $\phi$  a partial slip or nearly no-slip situation arises. Moments are larger for low  $\phi$ , and since crown thrust is lower, the critical section is at the crown for low flexibility ratios ( $F < 7$ ). However, the total load does not differ appreciably between full-slip and partial slip or no-slip conditions as shown in Fig. 7.35. On the other hand for higher flexibility ratios ( $F > 7$ ), the thrust at the springline becomes so much higher for the partial slip case that the failure section changes to the springline and failure occurs at a lower load than in the full-slip case. Thus the load capacity is lower for the partial or no-slip case and the difference increases with the increase in flexibility ratio (Fig. 7.35). The same trend occurs for excavation loading also.

### 7.3.2 Effect of Water Pressure

For studying the effect of water pressure on the lining behavior and on the total load capacity, uniform all-around water pressure was added to the ground loads in the incremental solution process until an estimated service load was reached and then the incremental ground loading was continued but not the water pressure. The moment-thrust paths shown in Fig. 7.36 for three different water pressures (0,  $2.5 \gamma_w D$  and  $5 \gamma_w D$ , where  $\gamma_w$  is the unit weight of water and  $D$  is the tunnel diameter), show the beneficial effects of water pressure. Since a uniform pressure does not induce moment, only the thrust is increased with the increase in water pressure, which reduces the slope of the moment-thrust paths (eccentricity) and helps in avoiding or reducing cracks in the lining and increases slightly the thrust when the path reaches the interaction diagram. Table 7.1 summarizes the effect of water pressure on various other parameters and indicates that although

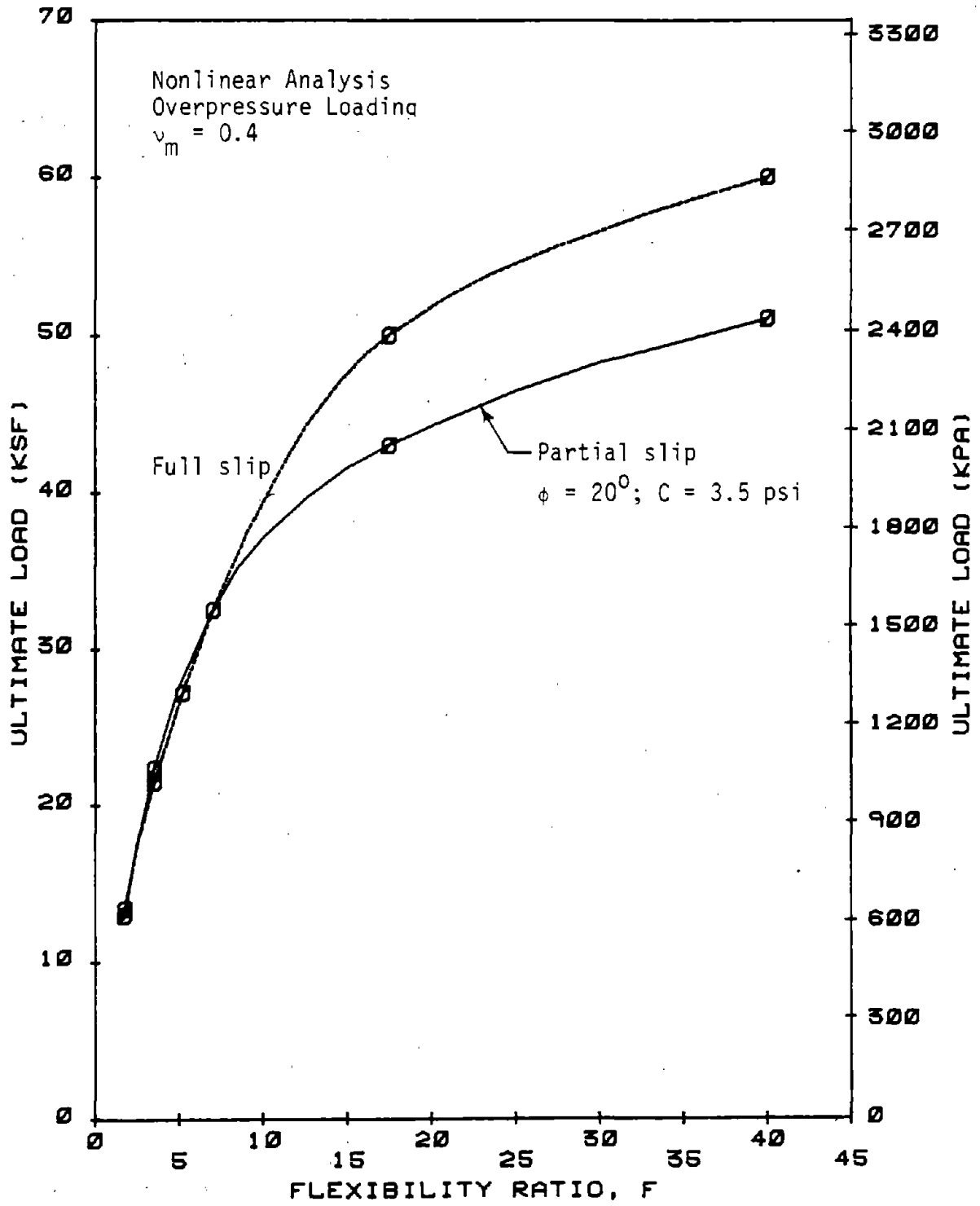


FIGURE 7.35 EFFECT OF SLIPPAGE ON ULTIMATE LOAD

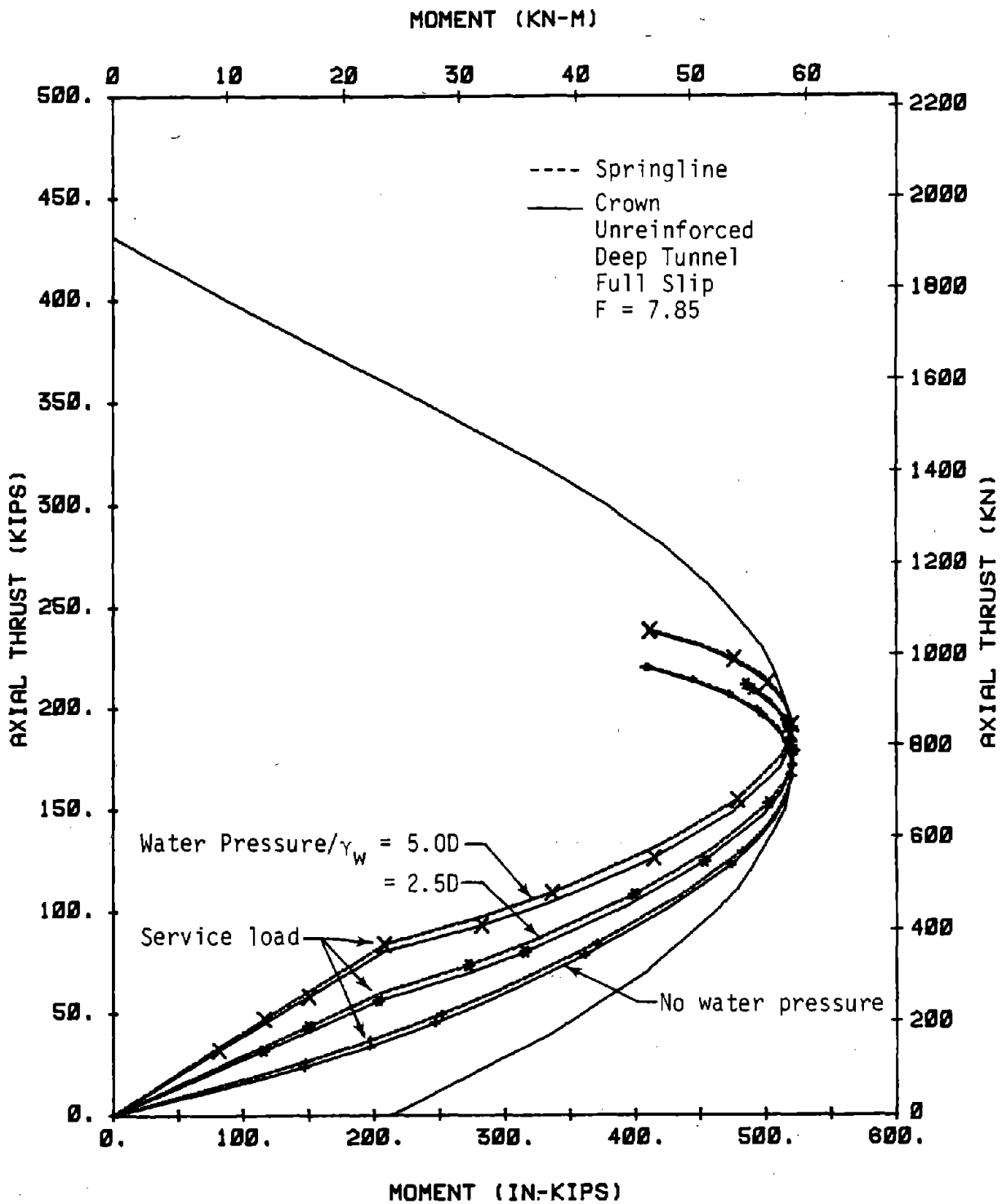
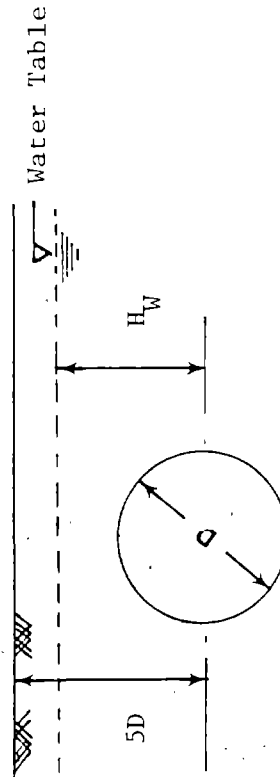


FIGURE 7.36 EFFECT OF WATER PRESSURE ON MOMENT-THRUST PATHS

TABLE 7.1 EFFECT OF WATER PRESSURE ON VARIOUS PARAMETERS

$H_w^1$	Total Ultimate Load ksf	Factor of Safety	$T_u/T_o$	$\Delta D_{cr}/D$ at Ultimate	$\epsilon_{sp}$ at Ultimate	$\Delta D/D$ at Service Load	Vertical Load at Cracking ksf
0.	22.8	5.36	.419	2.0	.0048	.313	2.394
2.5D	21.4	5.02	.449	1.879	.0045	.317	3.098
5 D	20.0	4.69	.478	1.916	.0045	.325	4.26
Effect of Increase in Water Pr.	No Appreciable Change	No Appreciable Change	Increases	No Appreciable Change	---	No Appreciable Change	Increases

<sup>1</sup>  $H_w$  is defined as below:



$F = 7.85$ ;  $E_m = 10$  ksi;  $D = 17.75$  ft.;  $t = 9$  in. unreinforced;  $f'_c = 4000$  psi;  $\gamma_s =$  unit weight of soil = 120 lbs/ft<sup>3</sup>; service load =  $2D \cdot \gamma_s = 4.26$  ksf

the thrust ratio increases with the increase in water pressure, total ultimate vertical load is not changed appreciably.

### 7.3.3 Effect of Loading Conditions

Three different loading conditions were investigated to determine their effect on the lining behavior under different conditions of slip for several flexibility ratios. The overpressure loading condition was modeled by applying uniform pressure at the top surface of the initially unstressed medium with the lining in place. The excavation loading condition, explained in Section 2.1, was obtained by applying the shape of the in situ stresses at the interface on the medium nodes and increasing the magnitude proportionally. The excavation and overpressure loading were applied to a lining in a linear medium with joint elements between the lining and medium having properties corresponding on an angle of internal friction  $\phi$  of 20 deg and cohesion of 3.5 psi (0.024 MPa). The beam-spring model was used for the gravity loading cases. A wide range of variables and loadings were investigated for these loading conditions for a 10 in. (254 mm) thick lining with 118 in. (3.0 m) radius and 0.5 percent reinforcement in each face. For selected cases for the gravity loadings the problems were also run for the same lining but without reinforcement. The compressive strength of the concrete was 4000 psi (27.6 MPa).

Some of the gravity loading cases are quite severe as a result of large moment at the crown while the corresponding thrust is small, because horizontal forces result only from passive resistance due to ovaling. The manner in which the gravity forces act on the lining in any particular case, depends on the soil condition and the excavation and support procedure. Several loading shapes were investigated with the beam-spring model while varying the tangential spring stiffness relative to the radial values between zero and 40 percent. It is believed that the case with full slip is far too conservative for this loading case and a significant shear stress would always be present. Four load shapes were considered: (1) a uniform vertical load across the full lining (2) only the radial components of a vertical uniform



load across the full lining acting on the lining, (3) uniform radial load around the upper 180 deg of the lining and (4) radial load over the upper 60 deg segment centered at the crown (See Fig. 7.37).

The result of particular interest for design is shown in Fig. 7.37 and contains all the data at failure of the lining in terms of the ultimate thrust at failure ( $T_u$ ) divided by the axial failure thrust ( $T_o$ ) plotted against the linear eccentricity ( $e_\ell$ ) divided by the lining thickness ( $t$ ). All the failure points fall in a rather narrow band and provide a means of obtaining the strength that includes the nonlinear behavior of the concrete by performing a linear analysis to obtain the eccentricity  $e_\ell$  (by dividing the moment at the critical section by the corresponding thrust). The criteria used to determine failure was a concrete compressive strain of 0.004 or failure to converge in the analysis if this strain was not reached. Failure by this criteria always occurred after the interaction diagram was reached; for the largest eccentricity, failure occurred on the interaction diagram but for others the strain of 0.004 was reached shortly after the moment-thrust path turned inward after leaving the interaction diagram; normally there was some capacity of the lining remaining in the latter cases that was larger as the flexibility ratio increased. Also failure occurred at a higher thrust after leaving the interaction diagrams for the unreinforced lining than for the reinforced linings; that is, there was more reserve capacity remaining. The variation of compressive strain for a typical reinforced lining is shown in Figs. 7.38 where the interaction diagram and moment-thrust paths are shown with the compressive strains indicated on the paths.

Figures 7.39 and 7.40 compare the various loading conditions in terms of  $p/f'_c$  and flexibility ratio ( $F$ ). The pressure  $p$  for the excavation loading and overpressure loading are the full overburden pressure at the level of the tunnel rather than that acting on the lining (part of this pressure arches around the lining), while that for the gravity loadings is the pressure of a certain height of soil above the lining acting directly on the lining. Though these loadings are not directly comparable it is convenient to place them on the same plot

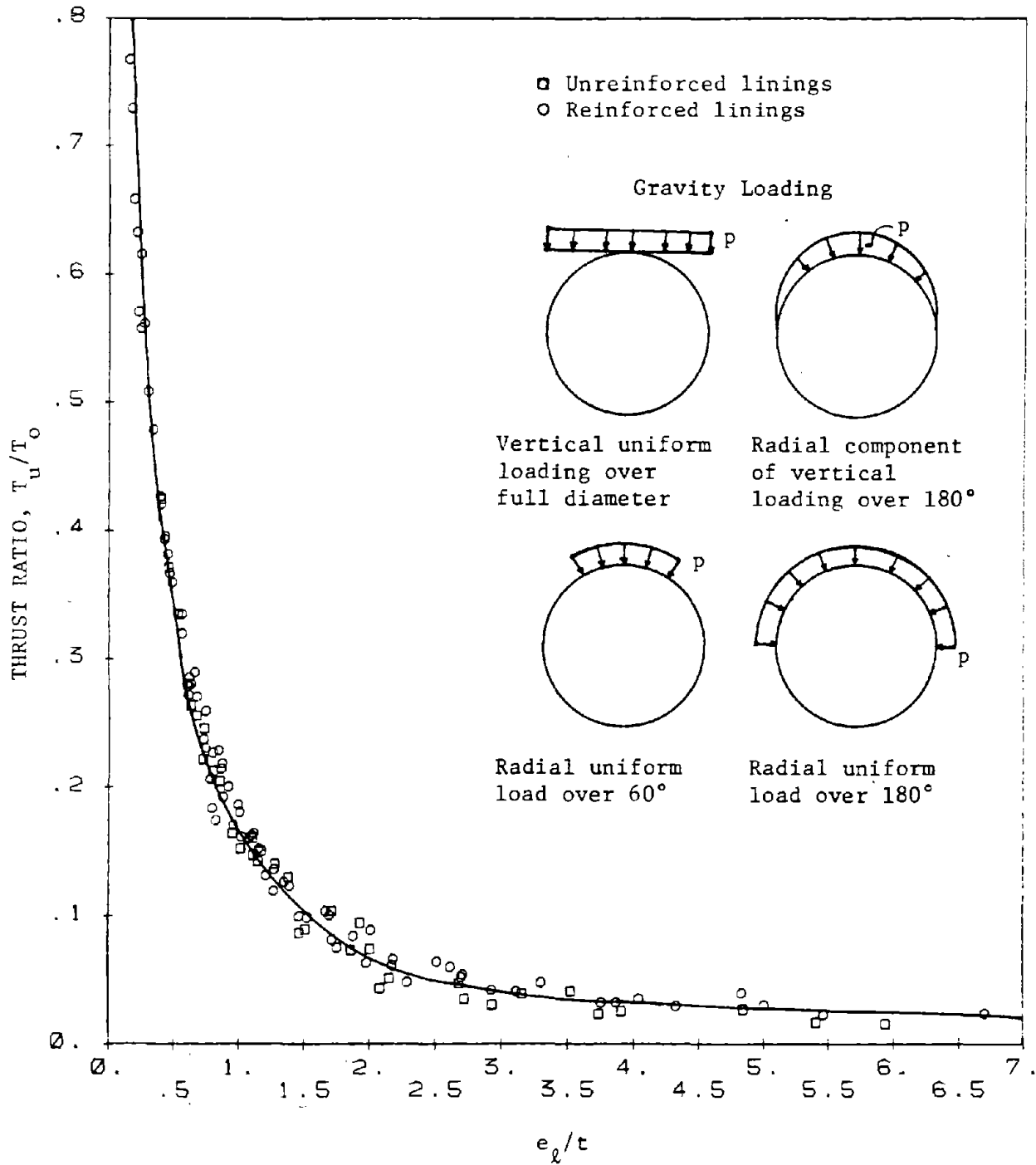


FIGURE 7.37 PREDICTION OF FAILURE OF LININGS BY THE NONLINEAR ANALYSIS AS A FUNCTION OF THE LINEAR ECCENTRICITY DIVIDED BY THICKNESS

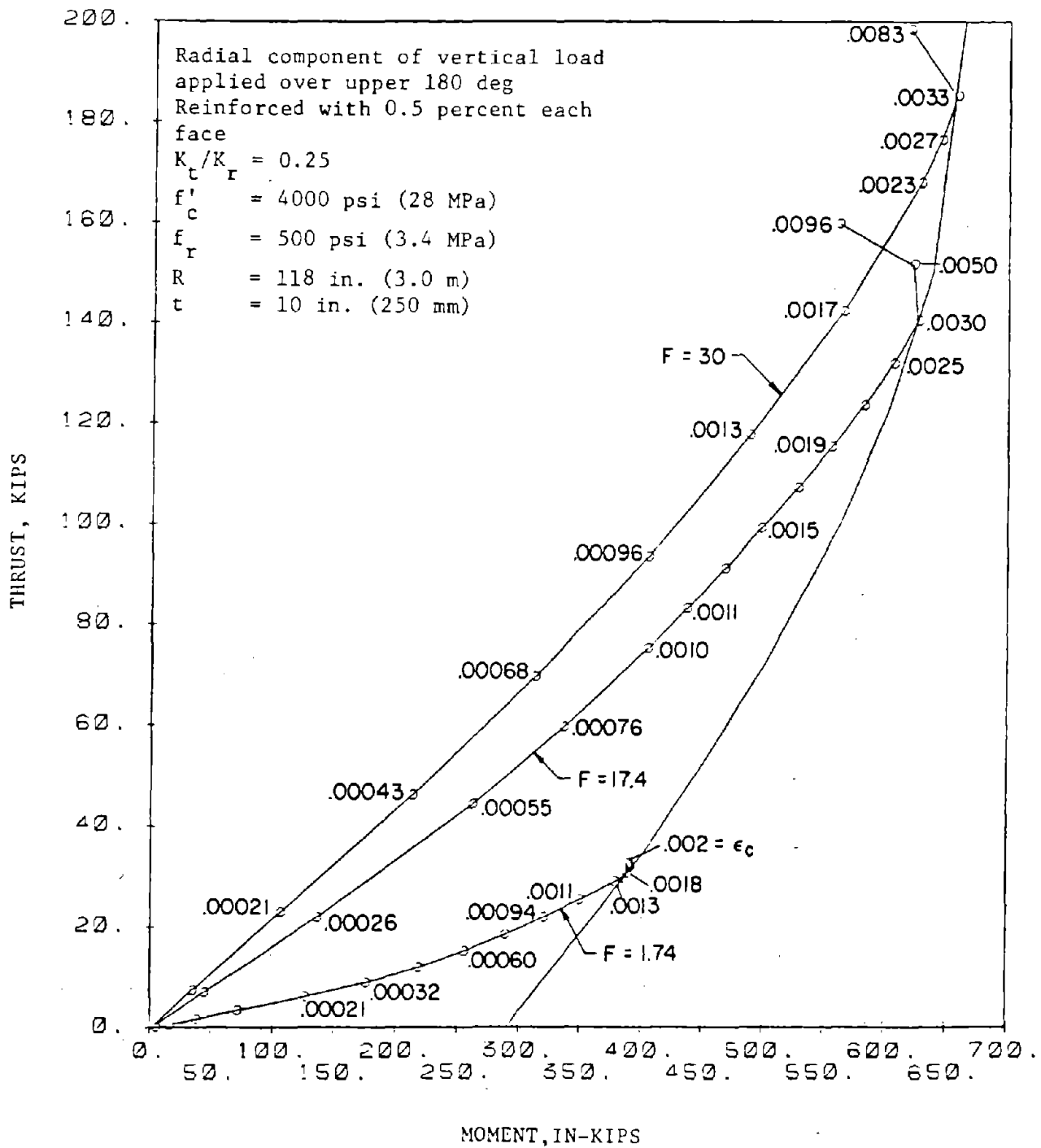
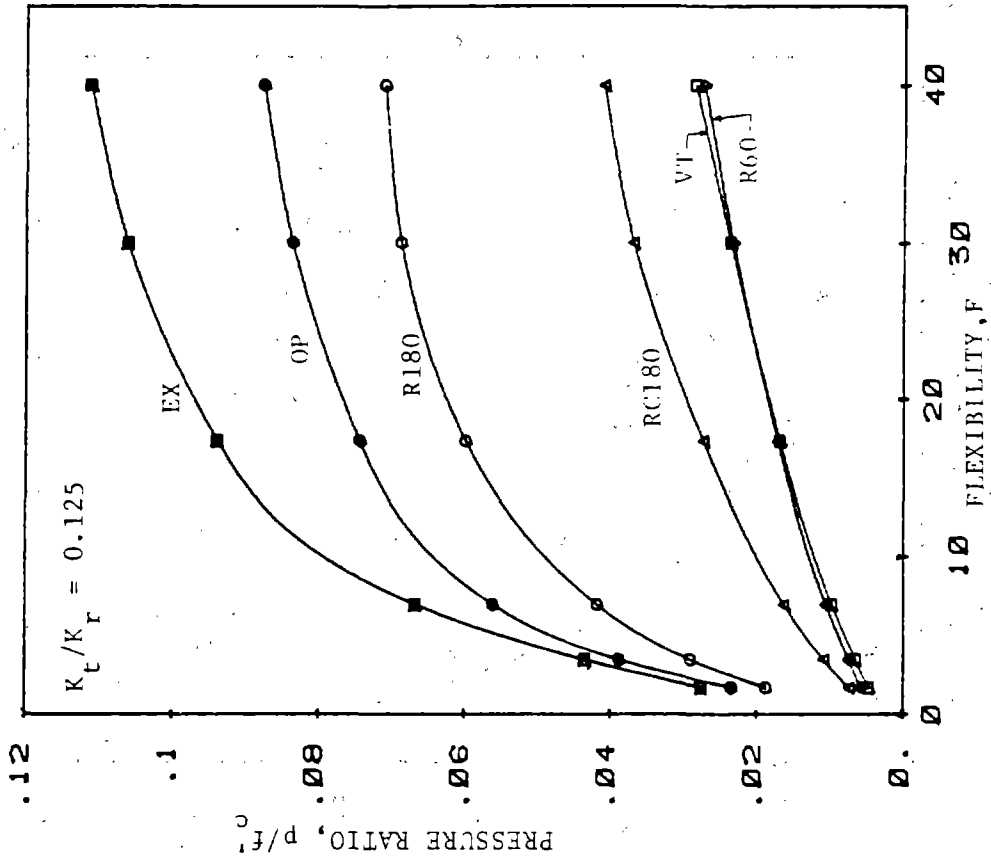


FIGURE 7.38 COMPRESSION STRAIN VARIATION ALONG THE MOMENT-THRUST PATH

RC180 = Radial Component of vertical loading over 180°  
 R60 = Radial uniform load over 60°  
 VT = Vertical load across full diameter



EX = Excavation loading  
 OP = Overpressure loading  
 R180 = Radial uniform loading over 180°

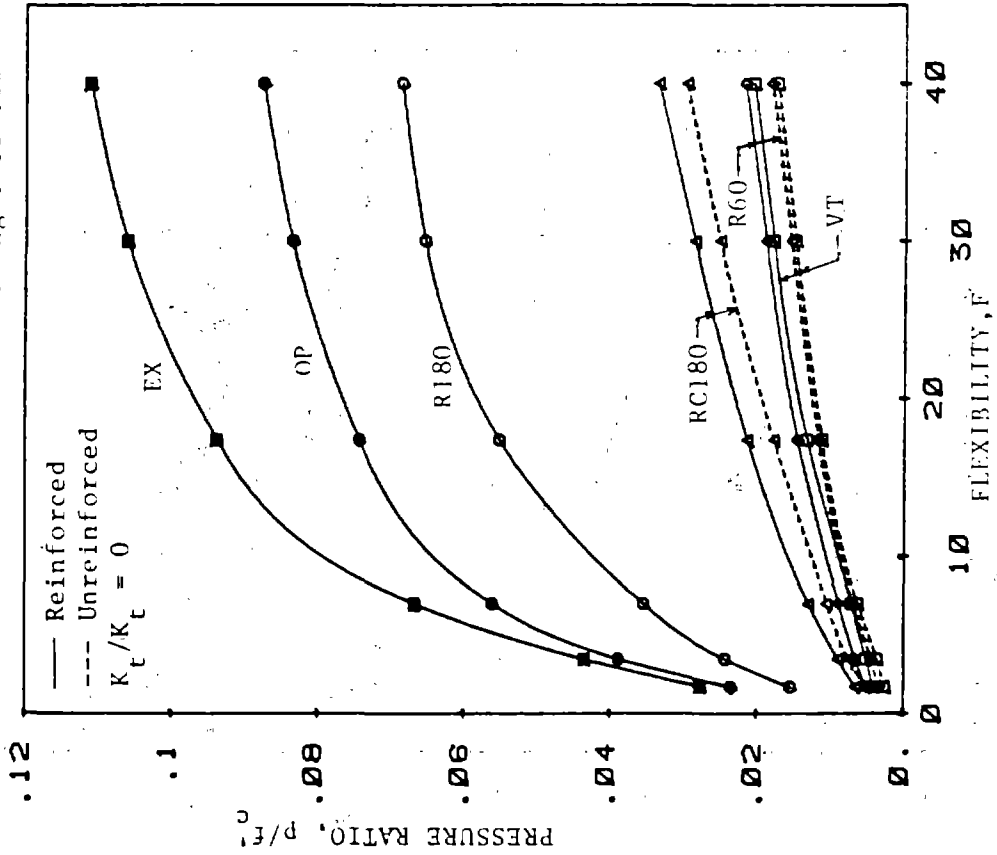
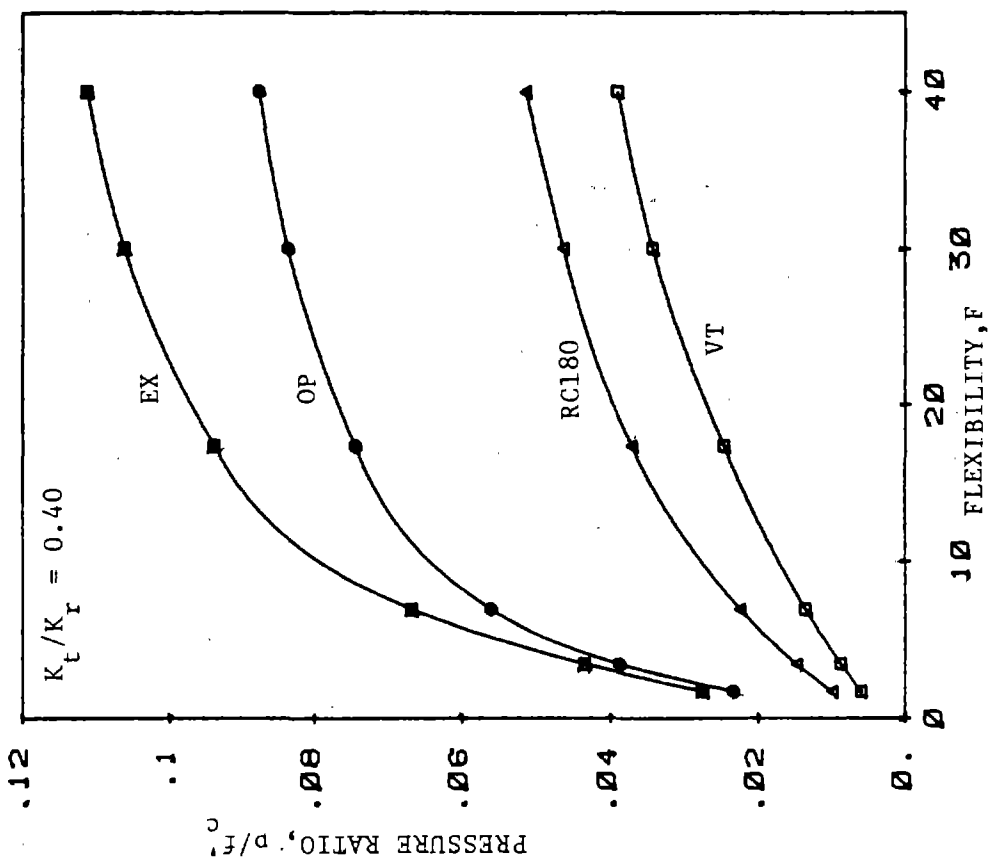


FIGURE 7.39 COMPARISON OF LOADING CONDITIONS FOR  $K_t/K_r$  OF 0 AND 0.125 FOR GRAVITY LOADING IN TERMS OF  $p/f_c$ .

RC180 = Radial Component of vertical loading over 180°  
 R60 = Radial uniform load over 60°  
 VT = Vertical load across full diameter



EX = Excavation loading  
 OP = Overpressure loading  
 R180 = Radial uniform loading over 180°

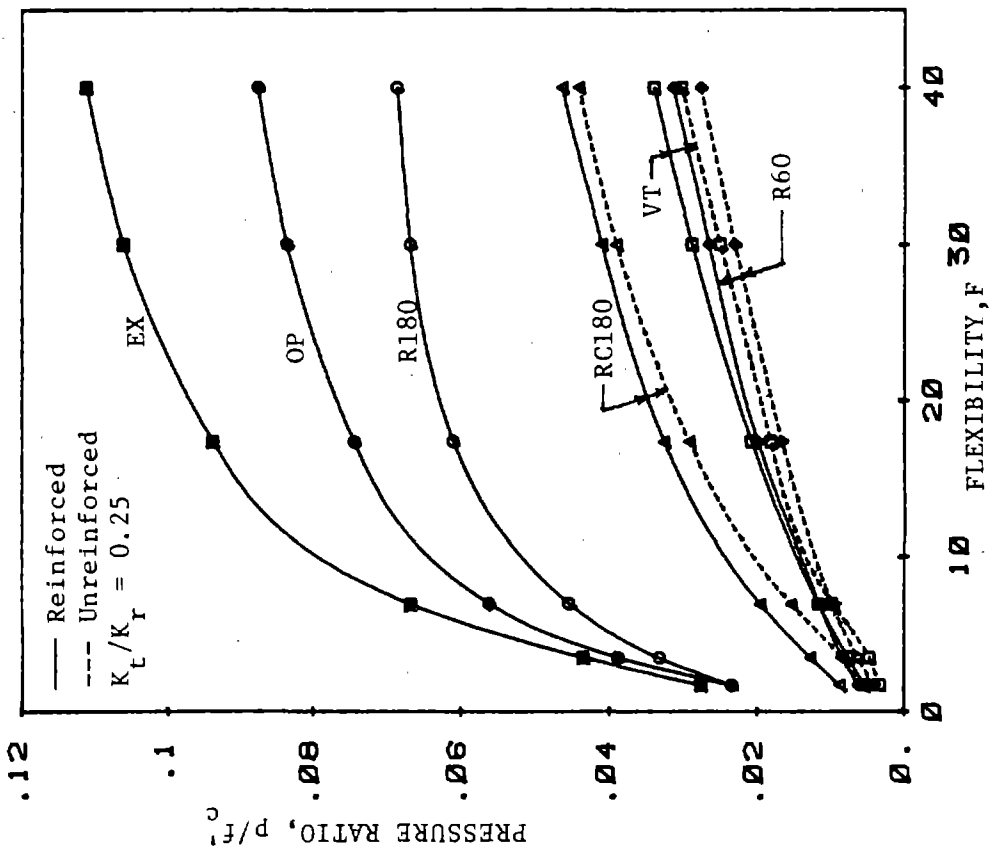


FIGURE 7.40 COMPARISON OF LOADING CONDITIONS FOR  $K_t/K_r$  OF 0.25 AND 0.40 FOR GRAVITY LOADING IN TERMS OF  $p/f_c$

and instructive to compare them. It is clear that if full overburden pressure is used for the design for all the loading conditions, the gravity loadings would always govern, but this would be reasonable only for very shallow tunnels. For deeper tunnels the gravity loading would be limited to some depth of soil above the tunnel on the order of two diameters in the worst case and less in most cases as discussed in Section 2.1.

The excavation and overpressure loading cases were analyzed with joint elements between the linear medium and the lining to represent the shear stress on this surface. In the gravity loading cases where tangential springs are used to represent this shear stress, four different values were investigated and it is clear from Figs. 7.39 and 7.40 that increasing the tangential spring stiffness relative to the radial stiffness increased the lining strength, and the increase is greater as the flexibility ratio increases.

Figures 7.39 and 7.40 also show that reinforcement increases the pressures on a lining required to cause failure, because the reinforcement increases the thrust capacity, but this thrust capacity can easily be replaced by a very small increase in concrete strength or thickness. The curves of Figs. 7.41 and 7.42 show the data in the previous figures except that the flexibility ratio is plotted against  $T_u/T_o$  defined earlier, and the difference between the reinforced and unreinforced cases is reduced. This shows that the reduction in thrust capacity by moment is essentially the same for a reinforced and unreinforced lining.

The results for the vertical, radial component of vertical and radial over 60 deg loadings are shown in Fig. 7.43 in terms of  $p/f'_c$  vs  $F$ . Here it is clear what effect the tangential shear has. Above  $F = 20$ , for example, the shear spring stiffness of 40 percent of the radial values can increase the lining capacity by 50 to 100 percent. The effect of reinforcement is also shown, and its influence appears to be fairly constant throughout the range of  $F$  except for values below about 10.

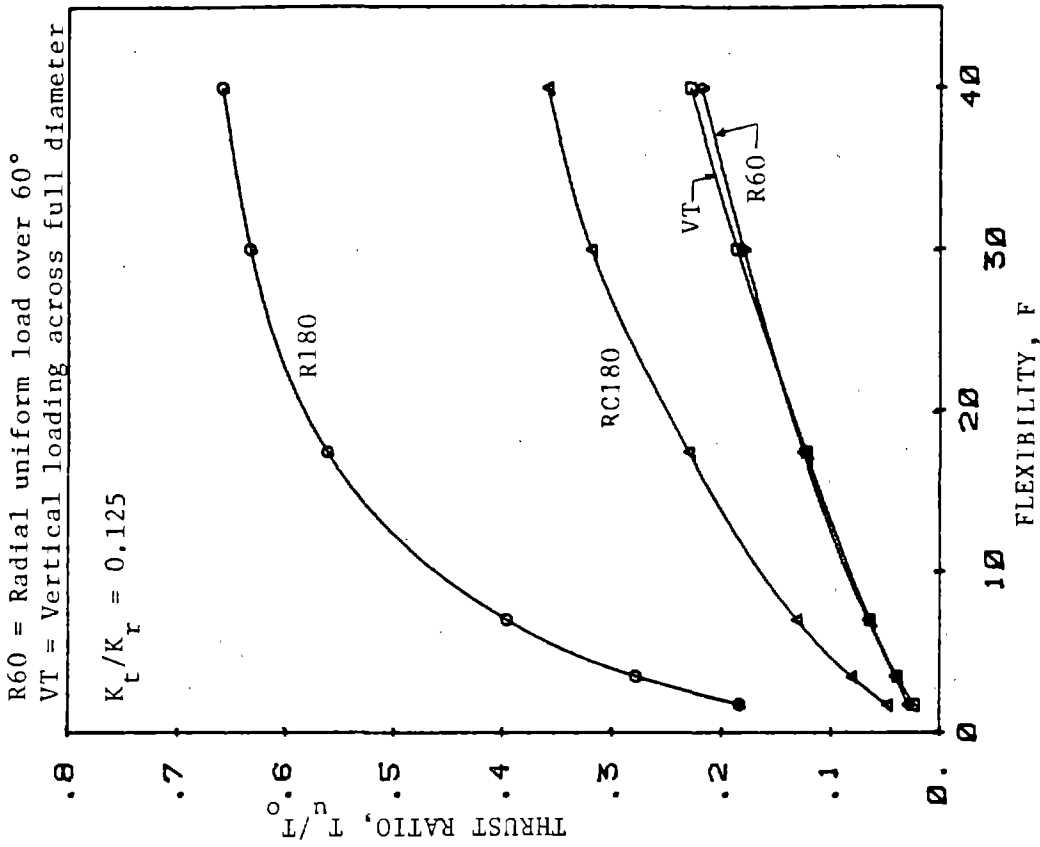
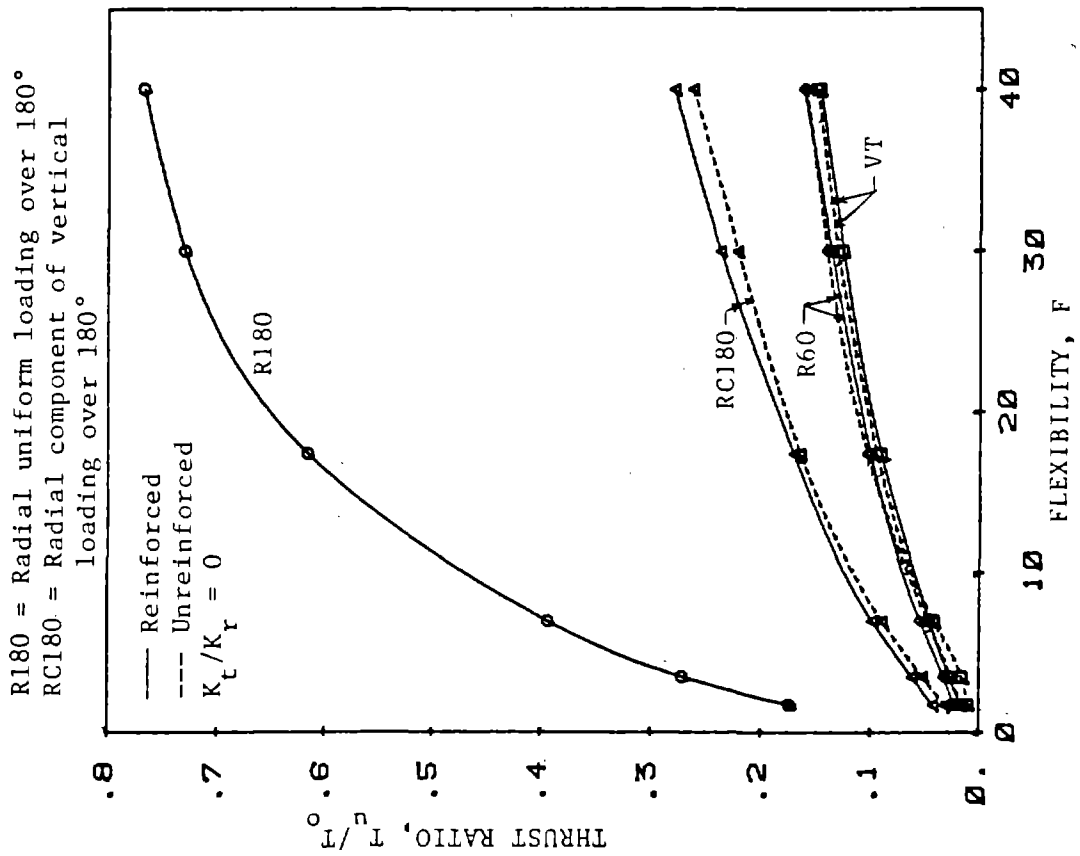
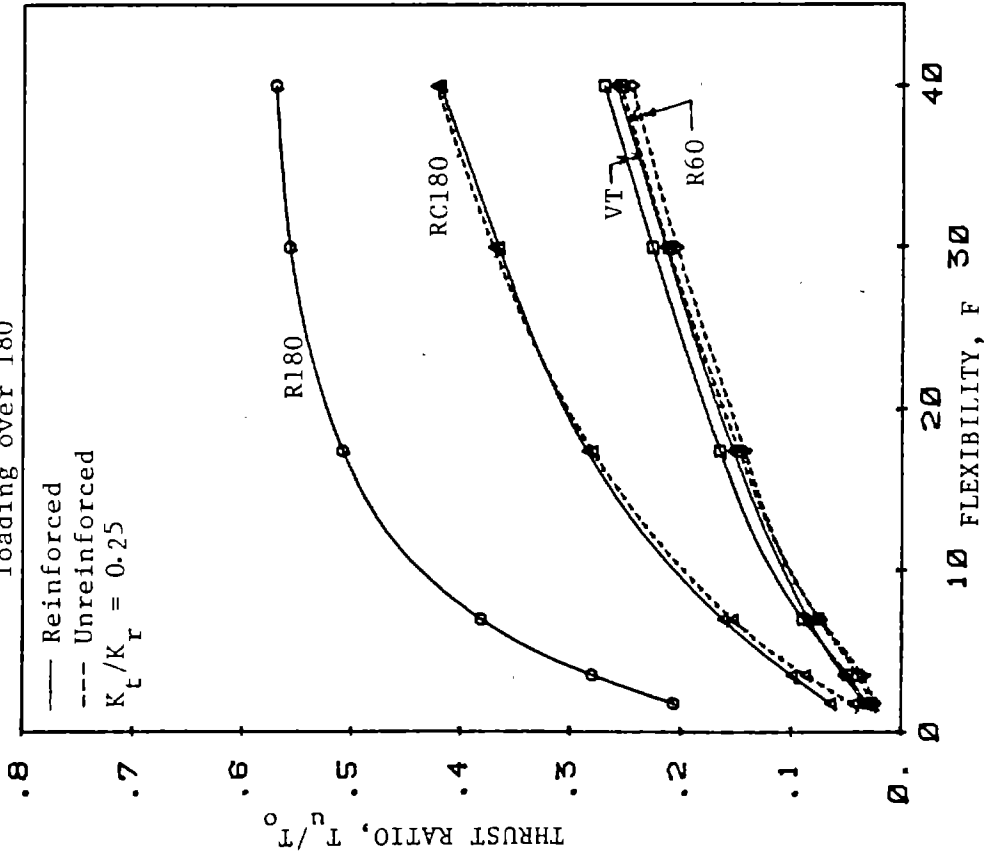


FIGURE 7.41 COMPARISON OF GRAVITY LOADING SHAPES FOR  $K_t/K_r$  OF 0 AND 0.125

R180 = Radial uniform loading over 180°  
 RC180 = Radial component of vertical  
 loading over 180°



R60 = Radial uniform load over 60°  
 VT = Vertical loading across full diameter

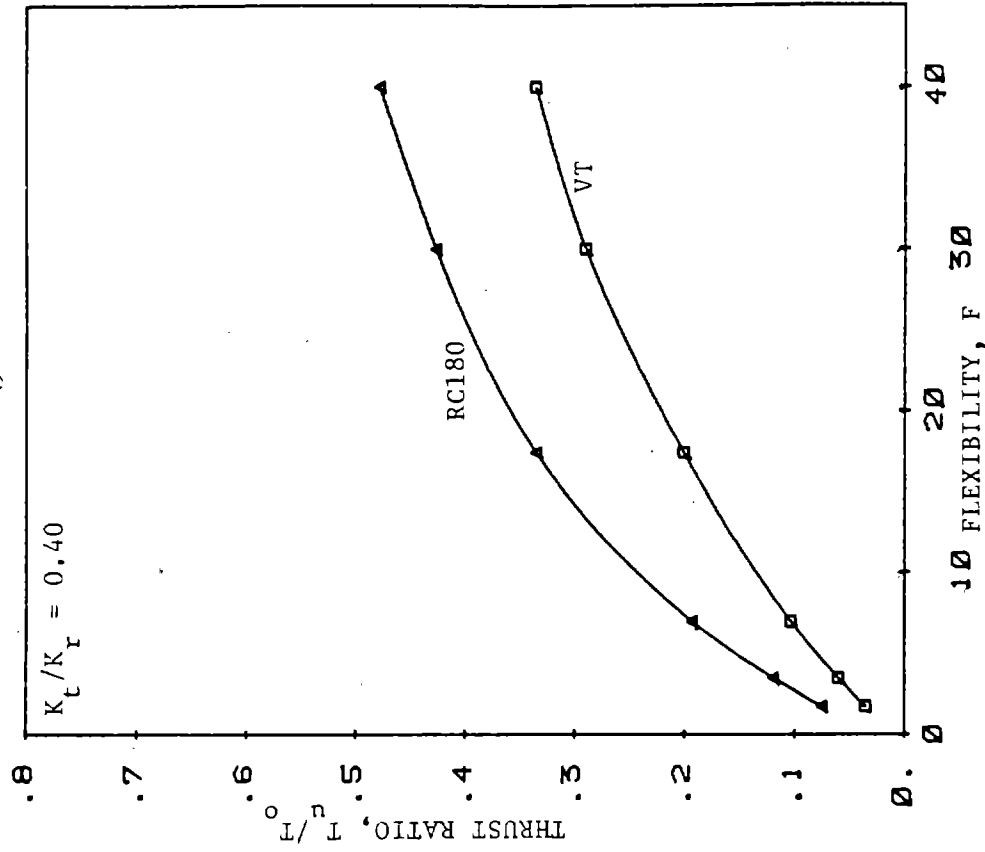


FIGURE 7.42 COMPARISON OF GRAVITY LOADING SHAPES FOR  $K_t/K_r$  OF 0.25 AND 0.40



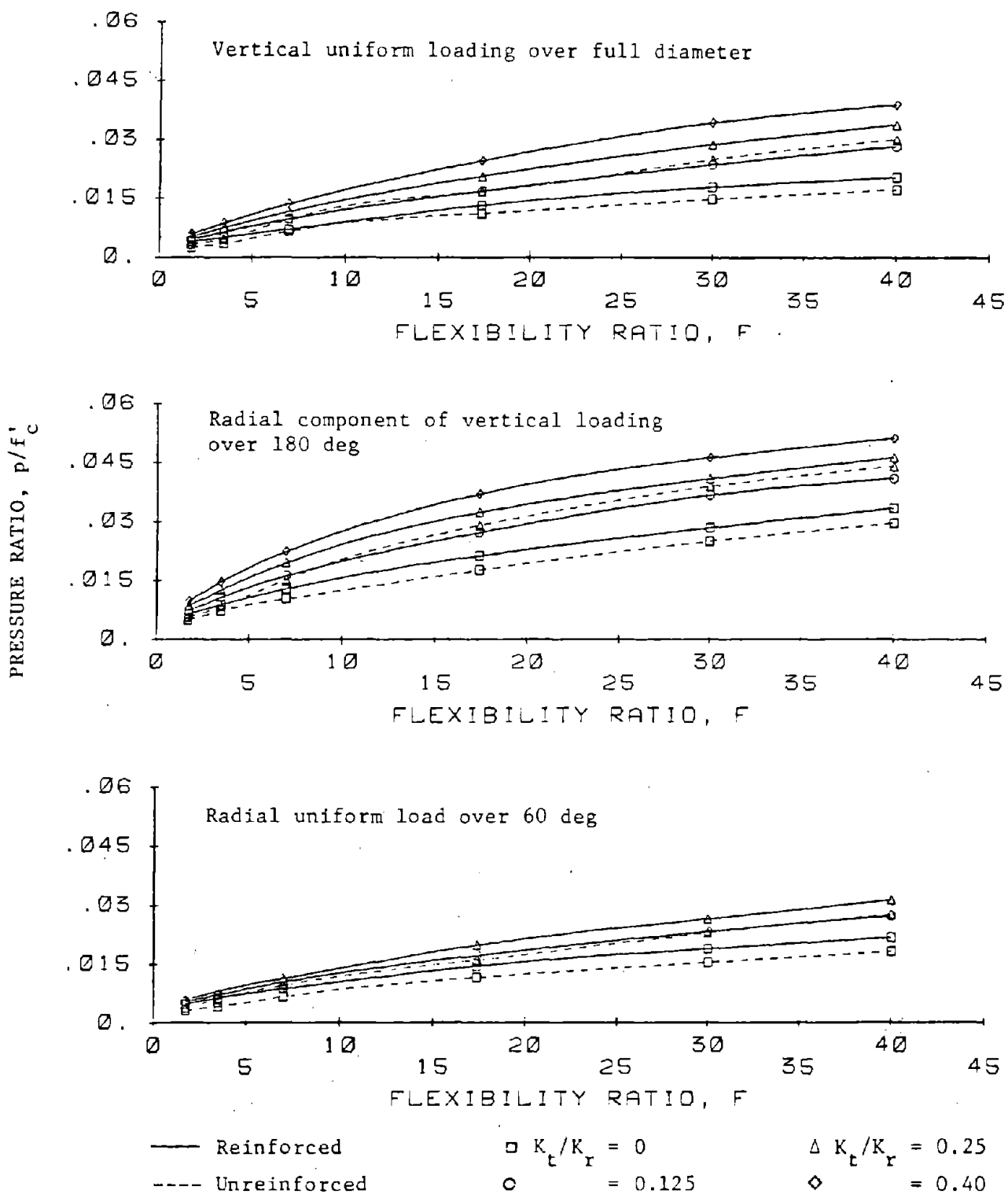


FIGURE 7.43 EFFECT OF  $K_t/K_r$  FOR THE VARIOUS GRAVITY LOADING SHAPES

Cracking in linings can be evaluate by studying the strains that occur at critical sections during loading; in Fig. 7.44 contours of tensile strain at the tension face of the concrete are shown on the moment-thrust paths for the radial component of vertical loading,  $K_t/K_r = 0.25$  and the reinforced and unreinforced linings. From these curves the thrust level can be seen relative to the ultimate thrust for a particular strain reached. Flexural cracking is generally considered to occur at about 0.00015 strain for a fairly rapid loading, but if the loading is slow it is reasonable to double this. Therefore, the 0.0003 contours in these figures may be considered to approximately indicate cracking in linings. In that case cracking occurs at about 25 to 30 percent of the ultimate thrust for the reinforced lining for the range of  $F$  shown; for the unreinforced lining the cracking thrust is about the same level relative to the ultimate for the two larger values of  $F$ , and is about 40 percent for the smallest  $F$ . The range remains the same (25 to 30 percent) for the reinforced linings for the other loading conditions, and for the unreinforced lining it is between 20 and 37 percent for the larger values of  $F$  and 40 to 50 percent for the smallest.

After cracking the width of cracks can be estimated. For the reinforced lining a strain of 0.0006 at the critical section and crack spacing of 10 in. (254 mm) would correspond approximately to a crack width of 0.006 in. (0.15 mm), and the thrust level at which this would occur can be observed on Fig. 7.44. The width would likely be larger for the unreinforced lining because the spacing would be larger.

#### 7.3.4 Effect of Reinforcement

Three different reinforcement ratios (0, 0.5 and 1.0 percent) were used to investigate their effect on the lining behavior. The moment-thrust paths of the critical sections for overpressure loading are shown in Fig. 7.45 for different flexibility ratios. It will be noted that the paths for different reinforcement ratios do not change

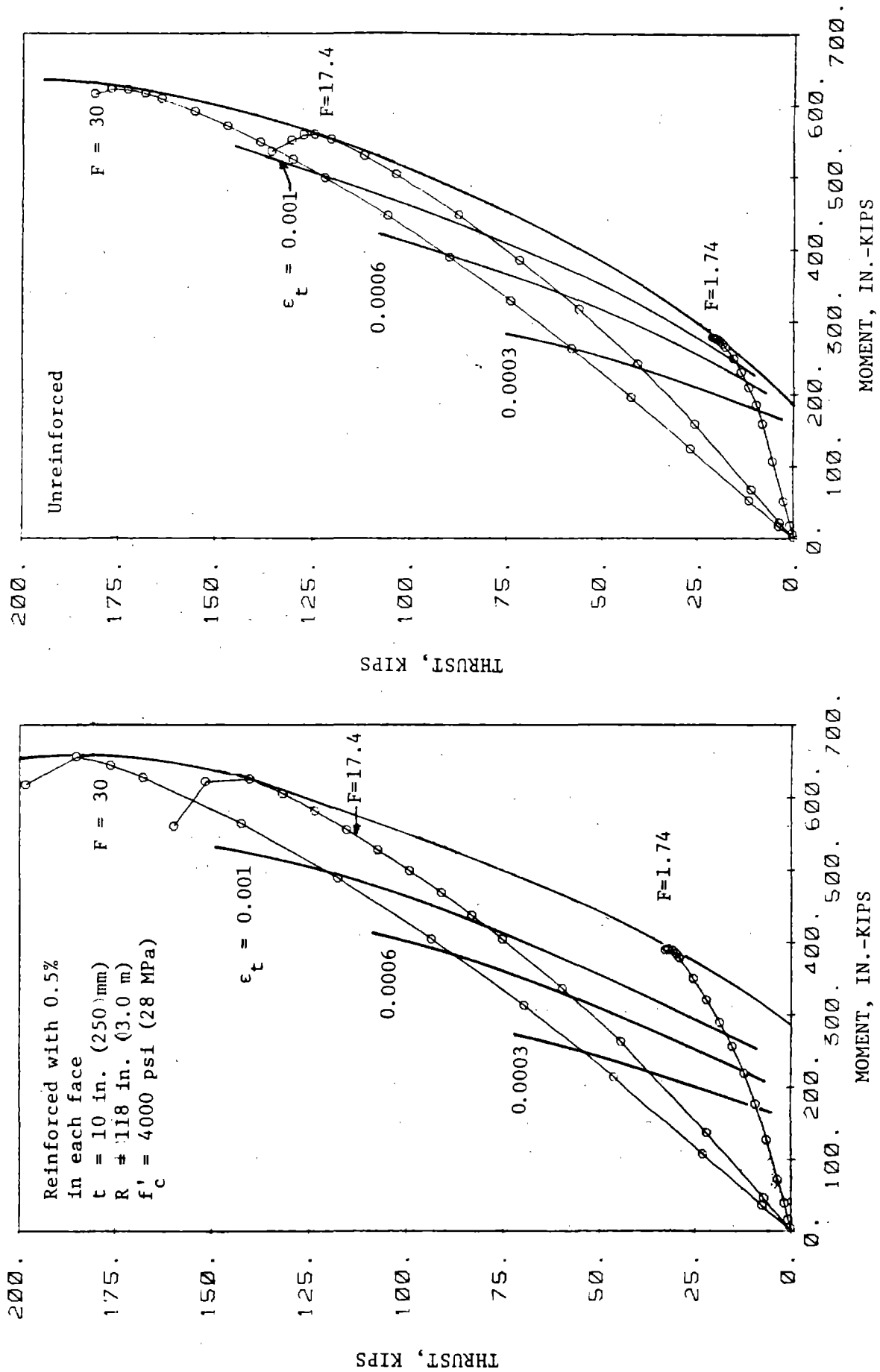


FIGURE 7.44 TENSION STRAINS ALONG THE M-T PATH FOR A REINFORCED AND UNREINFORCED LINING

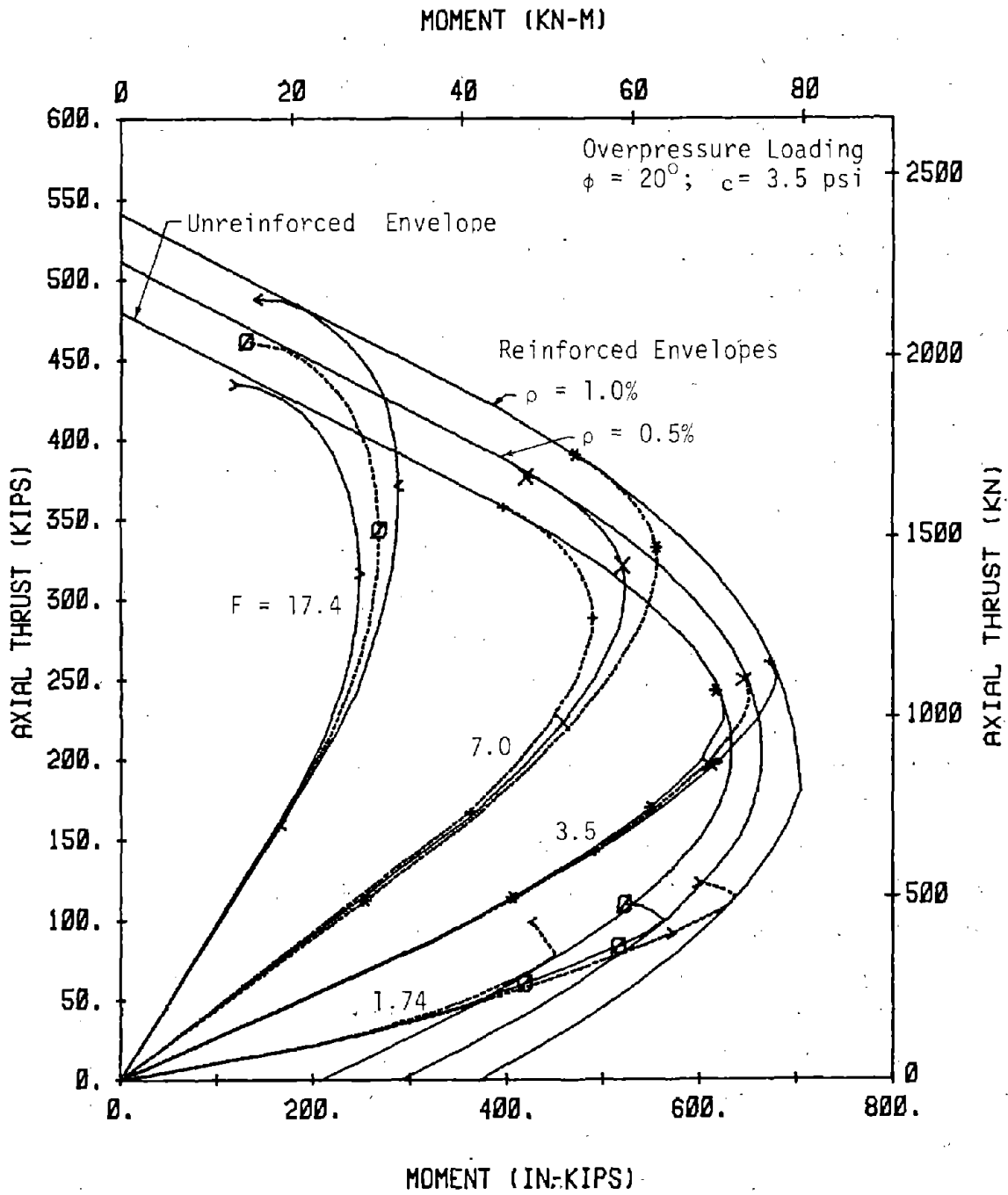


FIGURE 7.45 EFFECT OF REINFORCEMENT ON MOMENT-THRUST PATHS FOR OVERPRESSURE LOADING

in the linear range. Although they approach their respective envelopes showing higher ultimate thrust for higher reinforcement ratios, the ultimate load does not vary appreciably (Fig. 7.46). The moment-thrust paths for the critical section for cracking at the crown are plotted in Fig. 7.47, which also includes the cracking envelope according to a cracking strain of 0.00015. Moment-thrust paths do not reach the failure envelope because the crown is not the failure section for these cases. Since the cracking envelope remains essentially the same for all three reinforcement ratios, the cracking loads are also not affected appreciably by variation in reinforcement. This diagram also points out that cracking may be a problem for low flexibility ratios but if the cracking strain is increased to 0.0003 as a result of creep resulting from the slow application of load, the cracking problem is greatly reduced as shown in Fig. 7.47 for overpressure loading and Fig. 7.48 for excavation loading. Since the opening is stable from initial support when the final lining is placed, it is reasonable to assume that the load will reach the final lining slowly due to relaxation of the ground with time or deterioration of the initial supports. In this case the thrust at first cracking is still somewhat less than one-half that at failure (thrust is nearly proportional to load); but if the thrust at failure is assumed to be that from a linear projection of the moment-thrust path to the failure envelope, the cracking moment is less than one-half the failure moment for all cases. Therefore, a safety factor of about two and a prediction of failure based on a linear analysis will normally preclude flexural cracking in the lining at service load. Only below a flexibility ratio of about 10 is flexural cracking likely to be a problem, and the relative values of cracking load and ultimate load are shown in Fig. 7.46 in terms of uniform surface pressure. The effect of doubling the cracking criterion is shown, where the ultimate load shown is the actual ultimate based on the nonlinear analysis. Minor cracking due to flexure is not likely to create problems of leakage because the compression zone of concrete remains an effective barrier to water passage. Also, cracking reduces the lining stiffness and increases the flexibility ratio, which reduces

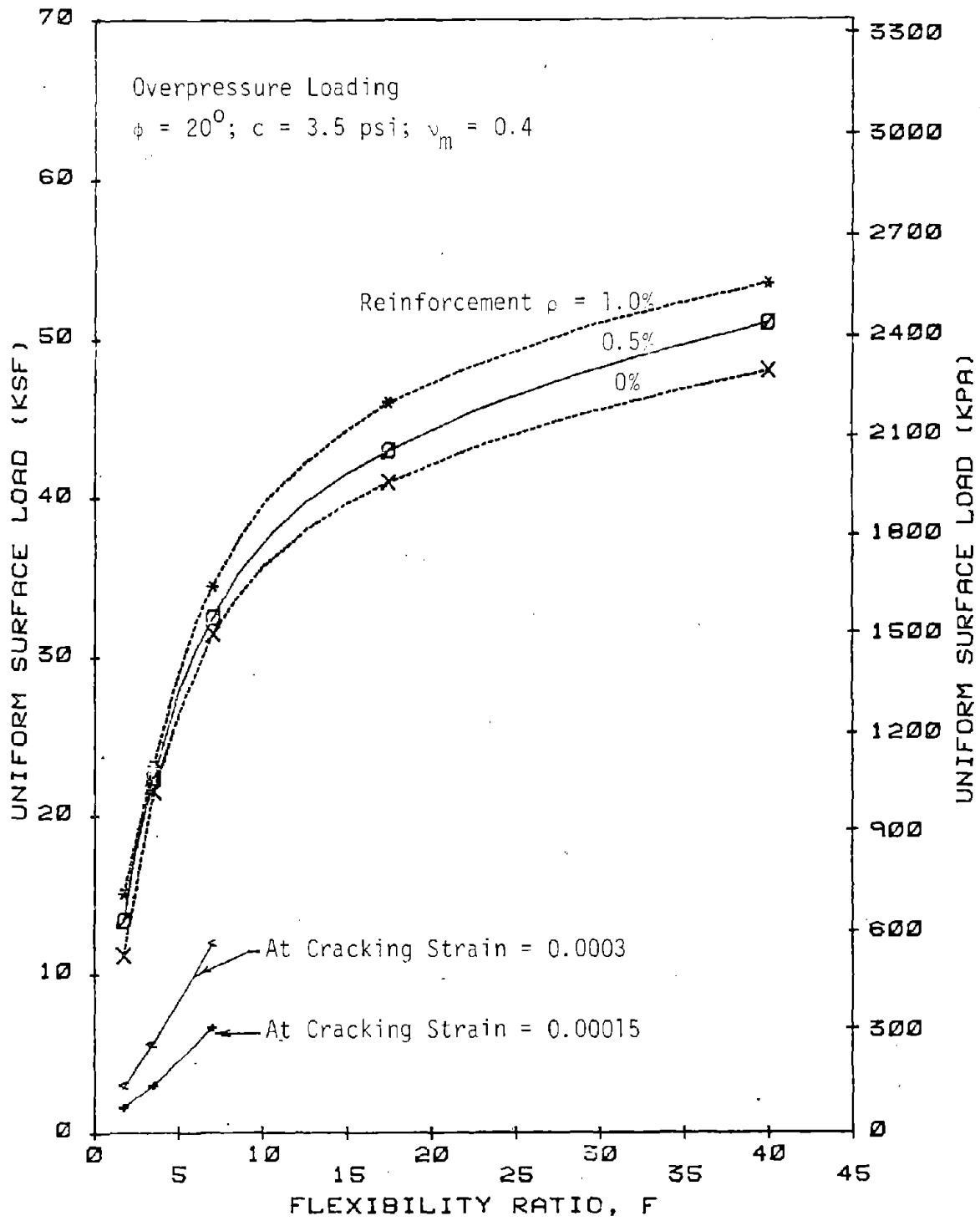


FIGURE 7.46 EFFECT OF REINFORCEMENT ON TOTAL LOAD AND CRACKING LOAD

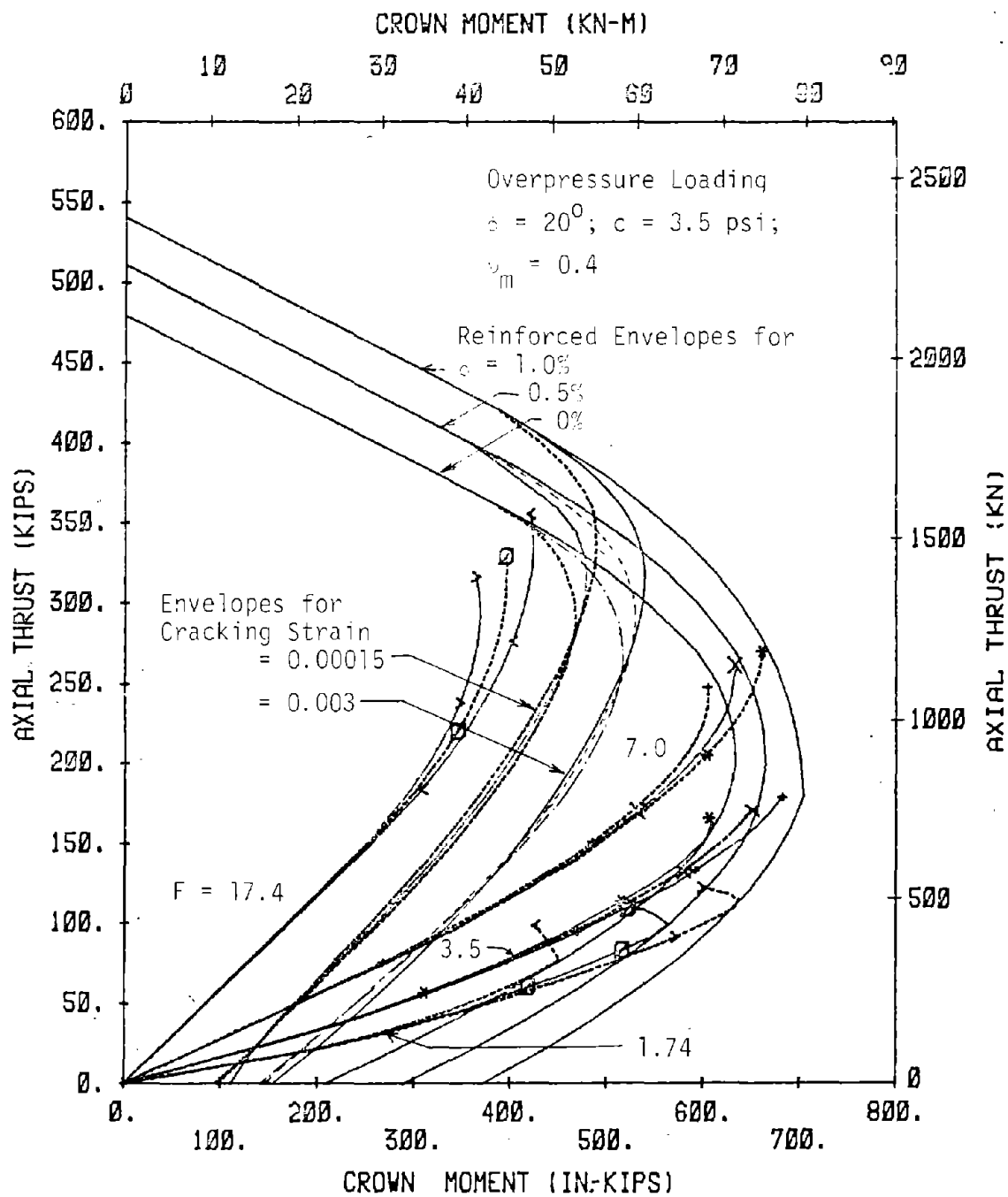


FIGURE 7.47 EFFECT OF REINFORCEMENT ON FIRST CRACKING FOR OVERPRESSURE LOADING

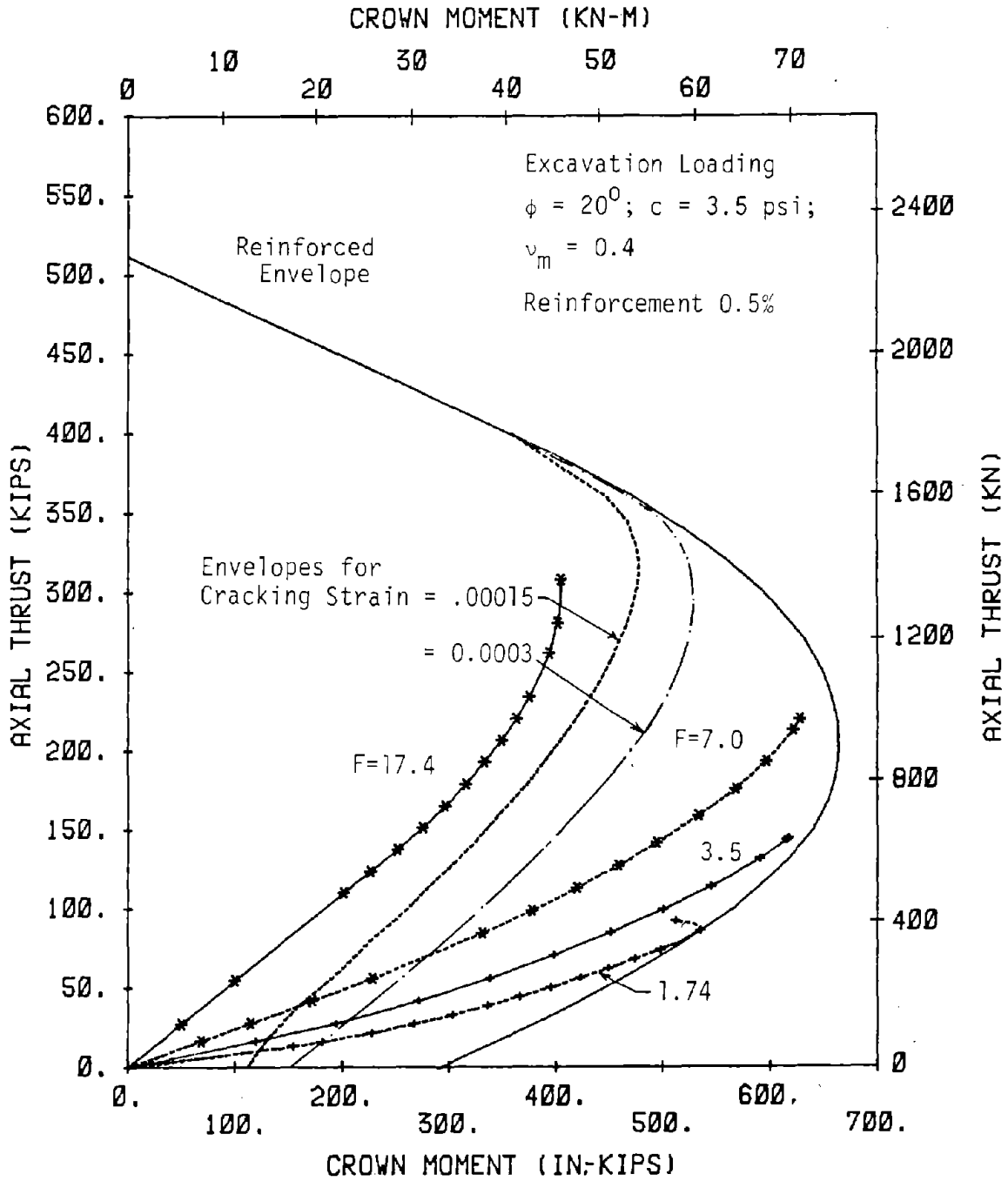


FIGURE 7.48 EFFECT OF FLEXIBILITY RATIO ON FIRST CRACKING FOR EXCAVATION LOADING



further cracking. The same trend has been noticed for excavation loading as well (Fig. 7.48).

### 7.3.5 Effect of Joints in Segmented Linings

The presence of joints in segmented linings causes reduction in the stiffness of the lining which in turn increases the flexibility ratio and thus reduces the moments in the lining. The objective of this study was to evaluate the reduction in lining stiffness caused by the presence of joints. This reduction in the lining stiffness is incorporated into an equivalent modulus of the lining ( $E_{eq}$ ) and can be expressed as a fraction of the modulus of a monolithic lining of the same thickness ( $E_l$ ). First, the closed-form analytic solution descr by Ranken, Ghaboussi and Hendron (1978) for linear analysis with excavation loading and full-slip conditions was used to obtain the curves shown in Fig. 7.49 for monolithic linings. The mean diameter of the lining was 19 ft 8 in. (6 m), the thickness 8 in. (200 mm) and the coefficient of earth pressure at rest  $K_0 = 0.5$ . The critical moment coefficient ( $M/pR^2$ ) was obtained for different values of the modulus of the lining ( $E_l$ ) and the modulus of the medium ( $E_m$ ). Similar curves were obtained for linings with thicknesses of 10 in. (250 mm) and 12 in. (300 mm) covering the range of flexibility ratios from zero to 10.

The beam-continuum model shown in Fig. 7.30 was used to analyze the segmented linings for excavation loading, full-slip conditions and  $K_0 = 0.5$ . All problems were run using the same stress level since it was found that the moment coefficient is not affected significantly by variations in stress level. The same radius and lining thickness as in the monolithic cases were used. The lining was represented by a series of one-dimensional beam elements, described in Section 3.2, with a linear concrete stress-strain curve having a slope of  $3.3 \times 10^6$  psi (22700 MPa). The joints were represented by short beam elements, 0.25 in. (6.5 mm) long with a red thickness 1.0 in. (25 mm) less than that of the segment, and with no tension in the concrete. Two cases were

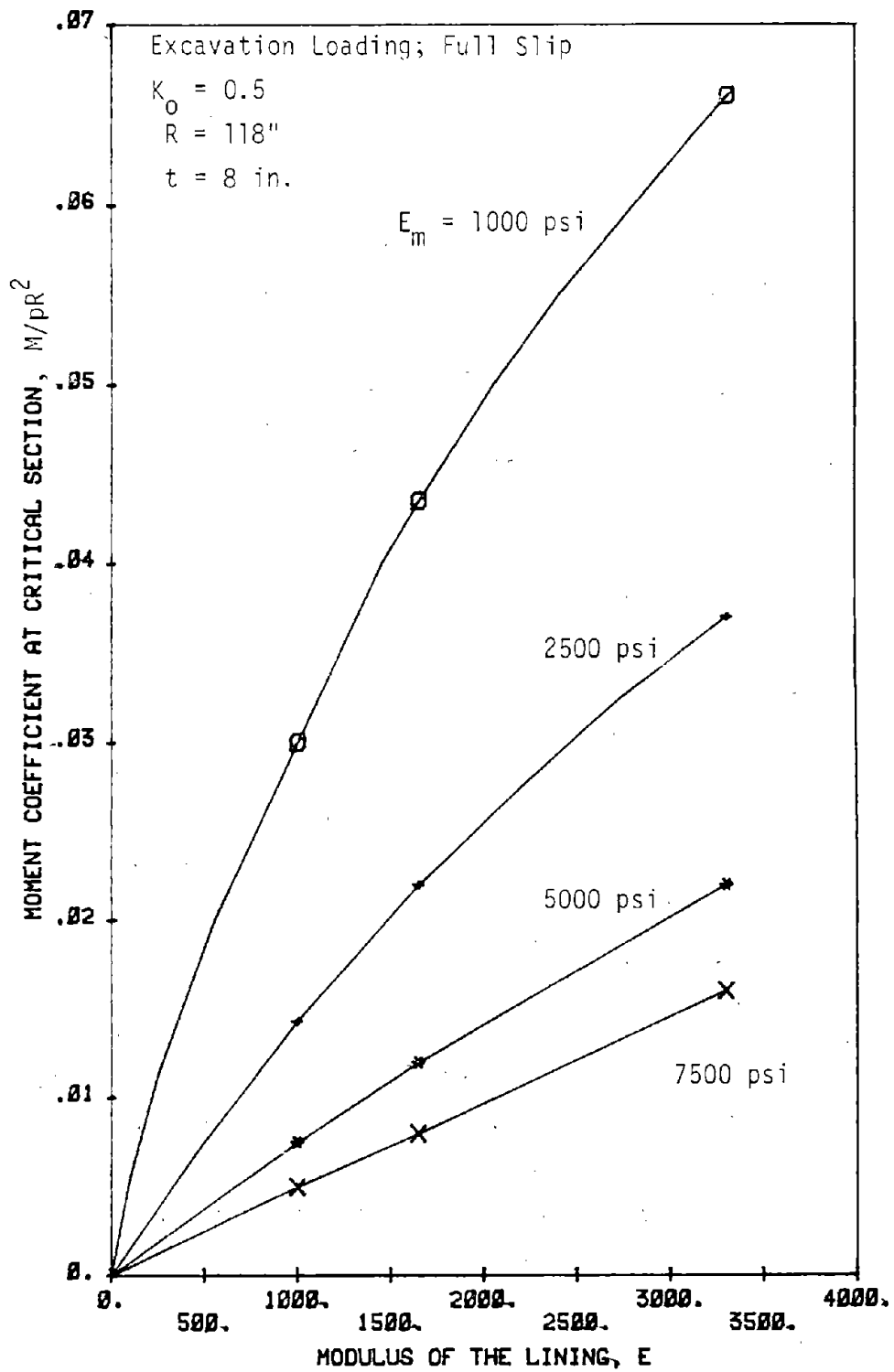


FIGURE 7.49 MOMENT COEFFICIENT VS MODULUS OF LINING FOR A MONOLITHIC LINING IN DIFFERENT SOIL MEDIA

examined, one with eight segments per ring (45 deg segments) and another with four segments per ring (90 deg segments) with a joint always present at the crown. For every thickness examined the value of the modulus of the medium was varied and the moment coefficient at the critical section (springline) obtained. The corresponding curves in Fig. 7.49 were used to obtain a value for the modulus of elasticity of the lining ( $E_l$ ) that would give the same moment coefficient as obtained for the monolithic lining. The ratio of this modulus to the original modulus of the segmented lining was plotted as  $E_{eq} / E_l$  versus the modulus of elasticity of the medium in Fig. 7.50. Thus, for a specific modulus of elasticity of the medium and for a specific thickness of the lining an equiv value of the lining modulus is obtained. This equivalent modulus can be used to the flexibility ratio for the segmented lining and then the expected moments in the lining. The graph in Fig. 7.50 was obtained for a lining with eight segments per ring. The results for four segments per ring were almost identical with slightly higher values of  $E_{eq} / E_l$  obtained in the lower range of medium modulus. Beyond a certain level of medium modulus the joints became ineffective in reducing the lining modulus as indicated by the flattening of the curves.

The values of  $E_{eq} / E_l$  shown in Fig. 7.50 should only be used as a guide in actual design problems, because of the numerous assumptions made in obtaining them (i.e., linear analysis, modeling of the joints, excavation loading,  $K_o$  value, specific radius of the opening, specific joint orientation). Nevertheless, they provide an indication of the effect of joints, in conjunction with other parameters, on the lining stiffness and the order of magnitude of the reduction to be expected.

### 7.3.6 Discussion of Results

Lining behavior in soft ground is greatly influenced by the loading conditions assumed. The loosening load proves to be the most severe while excavation loading gives the maximum capacity or is the least

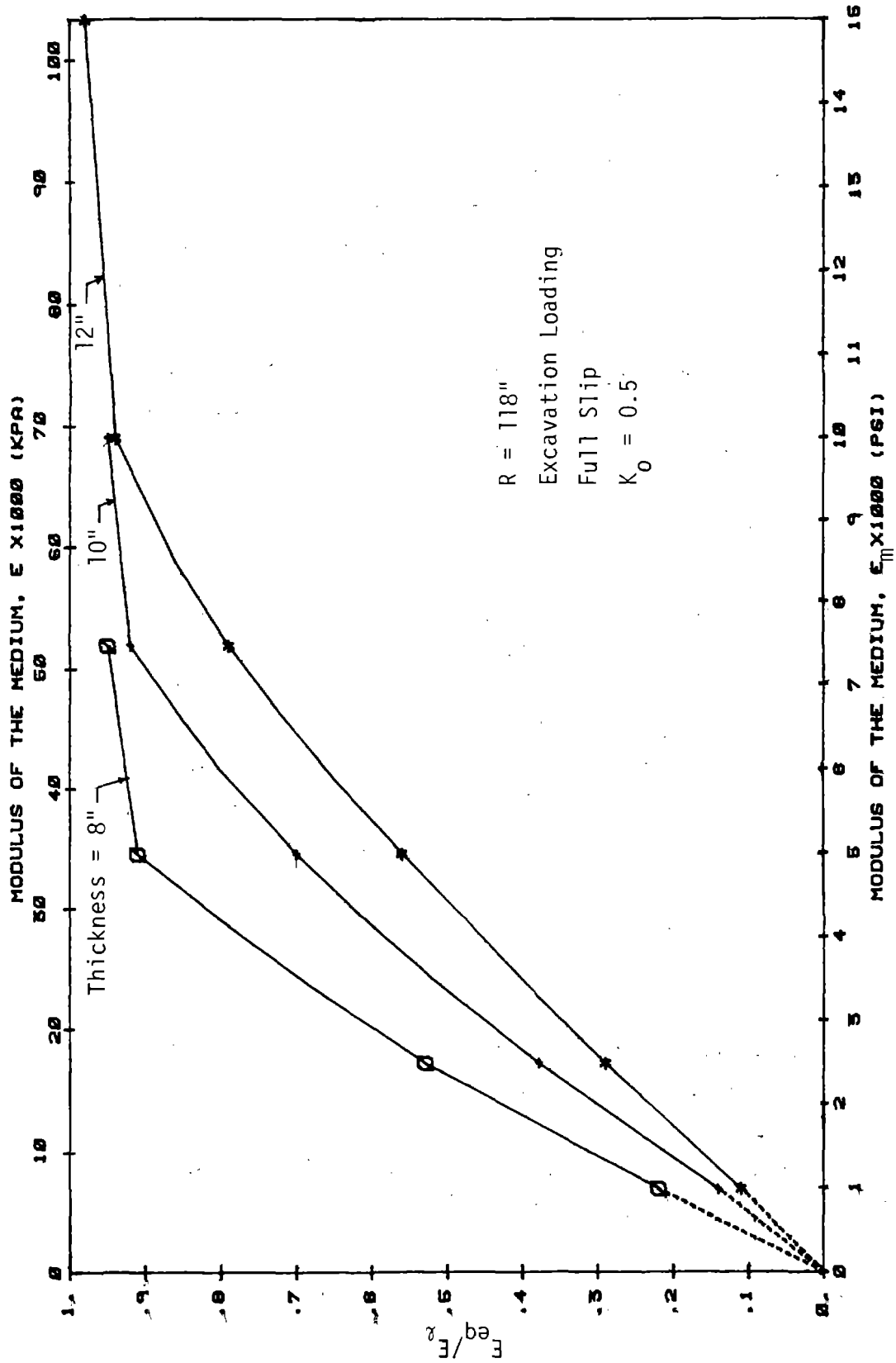


FIGURE 7.50 EQUIVALENT MODULUS OF ELASTICITY OF SEGMENTED LININGS

severe. The difference in capacity between the overpressure loading and excavation loading increases with flexibility ratio up to a flexibility ratio of about 20, and then remains fairly constant. Since the loosening load is likely to be limited in its magnitude to the weight of some fixed depth of soil above the crown, this loading will not govern the design in all cases. However, because of its severity it should be checked if there is any possibility that it could occur. The overpressure loading probably leads to an overly conservative design and the excavation loading is more suitable in most cases. The study of the variation of  $K$  shows that at low flexibility ratios the ultimate load is increased greatly by increasing  $K$ , but the difference decreases as  $F$  becomes large.

The lining capacity is improved by its nonlinear behavior from its value obtained by a linear analysis. For loosening loads it improves by a factor that ranges from about 1.5 to 1.9, depending on the flexibility ratio. On the other hand, for excavation loading this factor is only 1.15 to 1.35 except at flexibility ratios below about 7. Since the difference between actual ultimate strength and that predicted by linear analysis is fairly high and consistent for loosening loads, it may be desirable to take advantage of this extra strength if a linear analysis is used by employing a smaller load factor.

The slip condition at the interface between the lining and the medium has little effect on the behavior of most soft ground linings. The critical section is usually at the crown for low flexibility ratios ( $F < 7$ ) because of larger moments and smaller thrust. However, for higher flexibility ratios ( $F > 7$ ), the thrust at the springline becomes so much higher for the partial slip case that the failure section changes to the springline and failure occurs at a lower load than in the full-slip case. Thus, the load capacity is lower for the partial or no-slip case, and the difference increases with the increase in flexibility ratio (Fig. 7.35).

Uniform all-around water pressure or removal of internal air pressure only increases the lining thrust and does not induce moment. This increases the thrust ratio, but the total ultimate vertical load does not change appreciably. However, the overall effect is beneficial from the point of view of cracking in the lining as a higher thrust reduces the slope of the moment-thrust paths (eccentricity) which helps in avoiding or reducing cracks in the lining. Cracking could be a problem for very low flexibility ratios as noted in the discussion of the effect of reinforcement in Section 7.3.4, but if the effect of creep of the concrete on the cracking criterion is considered the calculations indicate that cracking is unlikely to occur. However, since reinforcement does help in reducing crack widths by distributing them, it may be advisable to use it in the amount required from the cracking point of view if it is calculated to occur and will create serious problems. Addition of a reasonable amount of reinforcement does not appreciably improve the load carrying capacity of the lining, however.

The presence of joints in segmented linings greatly influences the stiffness of the lining, which in the practical range of soft ground modulus could vary from 30 to 25 percent of that of a monolithic lining with the same thickness. Once the modulus of the medium reaches a certain value, however, the joints become ineffective in terms of reducing the stiffness (Fig. 7.50) and thus the moments in the lining, because of high thrust values that do not allow the joints to open. Thus, for certain combinations of lining thickness and medium modulus, segmented linings could be treated as monolithic from an analysis point of view. The number of joints per ring did not significantly influence the magnitude of moments in the lining for the particular joint orientations selected.

## 8. SUMMARY OF RESULTS OF MODEL TESTS AND PARAMETRIC STUDIES

The research associated with this project consisted of a series of model tests on arch and circular concrete linings and development of a computer-based analysis that was used to study effects of parameter variation on arch linings in rock and circular linings in rock and in soft ground. This volume contains detailed descriptions of these studies as well as background information and implications on design. A summary of the findings is presented below.

### 8.1 MODEL TEST RESULTS

Arches in "Rock": The model arch tests provided information about the behavior of arch-shaped concrete linings in a medium representing rock and their implications to design. In particular the effects of loading shape, rock modulus, lining thickness, lining reinforcement and amount of tangential shear between the lining and the medium were examined.

Table 4.1 summarizes the variables and Table 4.8 provides a summary of the most significant test results. In these comparisons strength is normalized as the ultimate thrust in the lining at failure divided by the ultimate thrust that would occur if there was no moment,  $T_u/T_o$ . The load shape that gave the lowest  $T_u/T_o$  ratio at  $F = 1200$  and interlocking between the lining and medium was the symmetrical triangle with load concentrated at the center. The largest  $T_u/T_o$  resulted from the uniform load. The range was from 0.60 to 0.69 or a difference of 15 percent. At  $F = 120$  loads were applied uniformly or from a rigid block, and the  $T_u/T_o$  values were 0.42 and 0.37 for a difference of 14 percent. Failure of the specimen with triangular loading that peaked at the crown was ductile and resulted from flexure at the crown. Comparable tests with other shapes of loading failed more suddenly and at or near the edges of the loaded area. Load shape also had an effect

on the deformability of the lining with the rigid block loading (Arch-6) exhibiting the smallest ductility as shown in Table 4.5.

The effect of tangential shear is shown by comparing Arch-1 with full interlock and Arch-5 with no interlock, and both with the same  $F$  of 1200. Removal of interlock reduced  $T/T$  from 0.69 to 0.52 or 33 percent. Removal of tangential shear  $\frac{u}{o}$  leads to larger deflections, which allows the crown region to flatten more and creates a larger moment; it also increases greatly the force reaching the base of the arch. With interlocking, the base force was from 5 to 30 percent of the total load, but without interlock, this base force was slightly over 100 percent.

The rock modulus and lining stiffness are incorporated in the flexibility ratio, which has a marked effect on  $T/T$ . There is a problem with the comparison, because at  $F = 1200$  the full interlock and no interlock cases were tested, while at  $F = 120$  and 3650 neoprene was used between the lining and medium, which would be equivalent to a partial interlock between these extremes. By trial and error, in trying to match the analysis with experimental results, it was determined that these latter cases with the neoprene corresponded to a tangential shear stiffness that was about 33 percent of the radial stiffness, so the curve shown in Fig. 4.86 is drawn 1/3 of the way between Arch-5 (no interlock) and Arch-1 (full interlock) at  $F = 1200$ . The resulting curve is then for the same tangential shear condition and uniform loading. Though exceptions can be taken with the value used, the curve appears reasonable, and for this loading case  $T/T$  varied from 0.42 at  $F = 120$  to 0.62 at  $F = 3650$ . Also, the curve  $\frac{u}{o}$  is rather flat beyond  $F = 2000$ , which would indicate that there is an upper limit for  $T/T$  which is about 0.62 for the uniform load case in good quality rock.  $\frac{u}{o}$  This conclusion is based on the assumption made at  $F = 1200$  to draw the curve, but any assumption made will result in a fairly flat curve. It may reasonably be expected that there is a similar limit for other load shapes or other tangential shear conditions. A minimum



amount of moment should be expected in the lining, no matter how high the value of rock modulus. This moment causes the thrust ratio to drop from 1.0 (no moment) to 0.62 in this case.

Flexural tension cracks did not occur in 4 of the tests, and in all tests that had cracking except Arch-7, it first appeared at or above 50 percent of the ultimate load. There is a definite increase in the tendency toward cracking as the flexibility ratio becomes smaller, as shown in Fig. 4.87. This results from larger deformation and larger moment, which is consistent with the effect of flexibility ratio discussed above. In Arch-7 where cracking occurred at 40 percent of the ultimate load, the smallest flexibility ratio was combined with the rigid block loading that provided the greatest load concentration. In most of the tests in which cracking occurred, the width of the crack remained small during a considerable part of the remaining loading, and only started to open significantly near failure.

Reinforcement had little influence on the strength of Arch-10, which was the companion test of uniformly loaded Arch-9 that did not have reinforcement. The normalized load for Arch-9 was 44 kips (196 kN) while that for Arch-10 was 45 kips (200 kN). With the reinforcement ratio of 1 percent used, if all the bars reached their yield stress they could resist a thrust of 2.5 kips (11 kN), so it is reasonable that this thrust would result in a small increase in load. By comparing the general appearance of the cracks for the reinforced specimen with those for the comparable unreinforced ones, it appears that the reinforcement serves to distribute the cracks and by so doing keep them finer. When no reinforcement was present, only one or two cracks appeared in the high moment region near the crown, and when there were more than one, generally only one of them opened significantly while the others remained small. However, in Arch-10 with reinforcement, 4 cracks formed that were approximately evenly spaced and each of them opened at about the same rate. Also near

failure reinforcement helped the failed region hold together for a little more deflection at nearly constant load.

Circles in Soft Medium:The purpose of the circle tests was to investigate the effects of reinforcement, medium stiffness and joints between segments on the overall structural behavior of concrete tunnel linings in a medium with comparable deformability to soil.

The effects of the amount of circumferential reinforcement on the load carrying capacity of the lining are examined by comparing Circle-2 with 1.0 percent reinforcement to Circle-3 with 0.6 percent reinforcement. The capacity of Circle-3 was higher even though the amount of reinforcement was lower, because of the slightly higher modulus of the medium, 40,000 psi (275.6 MPa) for Circle-3 and 35,000 psi (241.1 MPa) for Circle-2. Thus, the load carrying capacity of the lining is more sensitive to variations in the modulus of the medium than the amount of reinforcement present. Because of the lower initial modulus (25,000 psi (172.2 MPa)) for the unreinforced Circle-1, direct comparison with Circle-2 and Circle-3 is not possible. This comparison is carried out in the parametric study, and it is concluded, as in the case of the Circle-2 and Circle-3 results, that reinforcement does little to improve the load carrying capacity of the lining, because the reinforcement is most effective in tension, and for this flexibility ratio range most of the lining section is in compression.

The two major flexure related cracks appeared at the crown and at the springline in all three monolithic lining tests. Overall additional cracking was more severe in Circle-1, than in Circle-2 and Circle-3. Comparing Circle-2 to Circle-3, it is observed that fewer cracks are present in Circle-3, even though the modulus of the medium is slightly higher. Thus, the larger amount of reinforcement in Circle-2 distributed the cracks and in so doing kept them finer. The crack size for crown and invert in Circles-1, 2 and 3 was compared, and the higher the amount of reinforcement, the smaller the size of the

crack. The larger amount of cracking observed in Circle-1, is not only the result of lack of reinforcement but also the result of lower modulus of the medium.

The time of appearance of first cracks is not affected by the amount of reinforcement, since it is a function of the cracking strain of the concrete. First cracks appeared at about 32 to 42 percent of the peak load in all three monolithic tests. First cracks in the two segmented linings Circle-4 and Circle-5 appeared at 91 and 93 percent of the peak load. However, this was the result of the presence of the joints rather than of the reinforcement in the lining. It should be remembered that all the conclusions regarding reinforcement concern short term load-related cracking. The effects of reinforcement on temperature related cracking or the long-term behavior of the lining cannot be obtained from these relatively short term tests. If the loads were applied slowly and the concrete could creep during the load application, the cracks would occur at higher loads and would not open as much.

The stiffness of the medium is the most important parameter in determining the load carrying capacity of the lining. The higher the modulus of the medium, the higher the capacity of the lining. The same observation is made for the two segmented linings, Circles-4 and 5. The stiffness of the medium greatly overshadows the amount of reinforcement in the lining.

A stiffer medium also decreases the moments in the lining as related by the thrust ratio  $T_u/T_o$ . As observed in Table 6.1, the higher the modulus of the medium, and thus the flexibility ratio, the higher the thrust ratio because the moment is less.

Some indication of the effects of the joints on lining behavior may be obtained by comparing the load-deflection curves of Circle-2 (monolithic) and Circle-5 (segmented) with the same medium modulus in

Fig. 6.19; the capacities of the linings were comparable with the segmented lining exhibiting a slightly lower capacity due to the reduction of the cross-section at the joints. Furthermore, the change in diameter at peak load  $\Delta D/D$  was higher for the segmented lining, 1.9 percent for Circle-5 vs 1.2 percent for Circle-2.

The joints between the segments act as pre-formed cracks, and thus by rotating during loading they decrease the moment in the lining. This in turn results in fewer cracks. Furthermore, first cracks appeared at over 90 percent of the peak load, and their size was only a fraction of that in the monolithic linings (0.002 in. (0.05 mm) for segmented vs an average width of 0.004 in. (0.1 mm) for the monolithic linings). The effect of joints in reducing moments in the lining is magnified as the stiffness of the medium becomes lower, since the joint rotations increase.

Failure of the lining occurred between 60 and 80 deg from the crown with the exception of Circle-5, where it occurred 120 deg from the crown at a joint. All the model lining failures resulted from crushing of concrete that began at the inside surface in some small region, and with additional load it spread both through the depth of the section and longitudinally in the lining. The initiation of crushing was generally accompanied by cracking parallel to the direction of compressive stress (circumferential in the lining) typical of compression failures in concrete and to be expected in a specimen only one inch thick. Crushing began on one side of a joint in both segmented lining models, and in Circle-4 spread to both sides of the joint while in Circle-5 it remained only on one side. The joints constitute a weak section because of the reduced cross-section and the lack of reinforcement. There was no indication of high shear stress contributing to the initiation of failure or contributing to the spread of failed concrete after initiation (as might be indicated by a radial offset in each side of the failure region if shear were a contributing factor).

## 8.2 PARAMETRIC STUDIES

The analysis program described in Chapter 3 was used for parametric studies of arches in rock and circular linings in rock and soft grounds. An existing nonlinear finite element program that used springs to represent the medium in a plain strain analysis was modified to provide a better representation of softer ground conditions, by incorporating two dimensional isoparametric elements and a newly devised interface element. The solution method was also modified to use a multiple-level substructuring scheme for efficient handling of large problems. The coding of the modified program was verified by comparing the finite element solutions with similar analytic closed-formed solutions and excellent agreement was obtained. Besides using the program for parametric studies, it also simulated the laboratory tests of arches and circles quite satisfactorily.

For the parametric studies two numerical models were used. The finite element model that used springs to represent the medium is termed the beam-spring model and that using continuum element as the beam-continuum model. In both models the lining was represented by the same beam elements.

Parameter Study of Arches: The response of semicircular arches to interaction with the surrounding ground mass was examined in Chapter 5 for the case of loosening loading on a typical full scale configuration. The beam-spring model, with material and geometric nonlinearities taken into account, was used to show the effect of flexibility ratio  $F$ , radius to thickness ratio  $R/t$ , ratio of tangential to radial stiffness of the springs  $K_t/K_r$  and load shapes.

The parameter study indicates that a uniform loading across the entire arch has the smallest safety factor against collapse for the particular conditions investigated. Though a triangular and unsymmetrical uniform loading provide lower values of  $T_u/T_o$  they still have larger safety factors for the rock-block dimensions selected. The thrust ratio and consequently the load capacity of lining is quite sensitive to flexibility ratio (F) for values less than 1000. However, in the higher range of F, as the curves flatten, selection of accurate values of rock and lining stiffness for calculating F are not as critical as it is in the low range.

An increase in shear stress between the lining and medium results in a definite increase in strength of the lining. Therefore, it is essential to include the shear stress in the analysis of the lining to obtain a realistic prediction of strength, especially for larger values of F, but the strength is not highly sensitive to the ratio of tangential to radial stiffness,  $K_t/K_r$ , of springs representing the medium.

The effect of reinforcement on  $T_u/T_o$  has been found to be small. Although addition of reinforcement improves the lining strength, the total load does not increase appreciably. However, the absence of reinforcement does not lead to premature failure due to other causes such as lack of ductility, for example, because of the high degree of indeterminacy of the structure. From the point of view of cracking, small amounts of reinforcement may be desirable to help distribute cracks and reduce crack width as observed in the model tests.

Parameter Study of Circular Linings: As described in Chapter 7 a series of finite element analyses was performed to study the behavior of circular linings in both rock and soft ground. The analyses for the two ground conditions are different in the way the loading and the interaction components are handled. Loosening rock loading was represented by the beam-spring model in which uniform load was applied

directly to the lining. However, for analysis of linings in soft ground the beam-continuum model was used in order to study other loading conditions in which the loading on the lining depends on the ground-lining interaction.

Parameters of interest in the analysis of circular linings in rock (Section 7.2) are: flexibility ratio  $F$ , relative stiffness of the tangential to radial springs  $K_t/K_r$ , radius to thickness ratio of the lining  $R/t$ , and the lining reinforcement. The most important parameters affecting lining strength were found to be medium stiffness and tangential to radial spring stiffness ratio; the effects of these parameters on the lining strength in terms of the thrust ratio  $T_u/T_o$  are shown in Fig. 7.2. In the low range of flexibility ratios ( $< 300$ ) the  $T_u/T_o$  ratio can become low and is sensitive to the medium modulus. In this range care must be exercised in selecting the loading and the medium properties. If the lining cracks, its stiffness is immediately reduced relative to that of the medium; and if the cracked moment of inertia is one-half the uncracked value for example, the value of  $F$  is doubled and shifts to the right on the curves, increasing the strength of the lining appreciably. When  $F$  is larger than 300, which corresponds to a deformation modulus of the medium of about 500,000 psi (3450 MPa) for the particular lining considered, the curves become rather flat, indicating a greatly reduced sensitivity to the medium modulus. The diameter change of the lining is dominated by the flexibility ratio and in turn by the medium stiffness when a particular radius to thickness ratio is considered. Since the moments are related to the deformation, the moment to thrust ratio is dominated by medium stiffness. Thus, medium stiffness has a strong influence on the slope of the moment-thrust path and where the path intersects the moment-thrust failure envelope. The ratio  $K_t/K_r$  influences the moment-thrust path the same way but not as dramatically, while the addition of reinforcement or change in  $R/t$  ratio have little effect.

The tangential to radial spring stiffness ratio  $K_t/K_r$  has little effect on the lining strength when the medium stiffness is low relative to the lining, but the effect increases with increasing relative medium stiffness. However, there is very little change in strength for all values of  $F$  when  $K_t/K_r$  is larger than about 0.12. Most designers agree that the effective  $K_t/K_r$  in the actual tunnel in rock is at least this large, so the analysis is not greatly sensitive to the value selected. The range normally used is from 0.10 to 0.50. If the value selected is smaller than 0.12 because the opening walls are smooth or a large amount of wood blocking remains between the final lining and the rock, then the effect of the value selected depends on the flexibility ratio; for low values of  $F$  the sensitivity remains small, and becomes larger as  $F$  increases.

The lining-medium system is not defined completely by the flexibility ratio as the thrust ratio has been found to vary with  $R/t$  ratio for a particular flexibility ratio. The reason for the variation with  $R/t$  is the effect of thickness on the nonlinear behavior of the lining, where the thicker lining has a larger  $T_u/T_o$  ratio at the same  $F$ . This is misleading, however, because in the same medium the thicker lining would result in a smaller  $F$  and therefore, a smaller  $T_u/T_o$ .

The study of moment-thrust paths combined with the failure envelope for the critical sections is very useful in understanding how the flexibility ratio affects strength. When the flexibility ratio is small and therefore the deformation and moments are large, the moment-thrust paths reach the failure envelope below the balance point. The concrete and steel in the section are fairly ductile so the moment-thrust path follows the failure envelope until the concrete starts to crush on the compression side of the section. When crushing occurs, the internal-thrust resultant shifts inward toward the center of the section, reducing the lever arm and therefore the moment, but the thrust can continue to increase as more concrete toward the tension side starts to resist compression. The reduction in moment causes the



moment-thrust path to turn inward toward the thrust axis. The maximum thrust and thus the peak load is obtained when the rotational capacity of the critical section is finally reached. A value of  $F$  equal to 70 is about the lower limit for linings in rock, and for this value the path normally approaches the interaction diagram near the balance point.

For large flexibility ratios, ( $> 200$ ) the lining deformation and therefore, the moment at the critical sections are smaller, so the moment-thrust path reaches the failure envelope above the balance point where the rotational capacity of the section is much smaller due to the large thrust. In this case the limiting rotation of the section is reached when the failure envelope is reached and there is no following of the envelope, but the thrust and therefore the load on the lining is considerably larger.

Since the ultimate load is nearly proportional to the thrust capacity, and the thrust capacity depends on where the moment-thrust path reaches the failure envelope, the strength of the lining is affected by the flexibility ratio. The moment-thrust paths start as if the problem solution is linear, before the nonlinear effects begin. If the initial path is projected linearly to intersection with the failure envelope, the linear prediction of failure thrust would be obtained. The difference between the linear and nonlinear prediction of failure increases as the flexibility ratio decreases, and above the balance point a linear prediction of the failure thrust is much more accurate than below the balance point.

The moment distribution around the lining is particularly severe in the loaded crown region because of low thrust which magnifies the effects of the moment. Although the larger moments may occur at about 45 deg from the crown, the moment-thrust combination is more favorable than at the crown. Internal shear induced in the lining peaks near 20 deg and from 45 to 60 deg from the crown. The shear is larger at 45 to

60 deg for the high flexibility ratio and at 20 deg for the low values. The section closer to the crown is likely to be more critical, however, because the direction of diagonal tension at this section leads to movement into the tunnel.

A comparison of reinforced and unreinforced linings reveals that there is essentially no effect on the thrust ratio. Reinforcement had a negligible effect on the stiffness (EI) of the lining for the larger values of F and increased the stiffness only slightly near failure for the low values of F due to cracking and nonlinear effects. In the range of flexibility ratio appropriate for linings in rock, reinforcement in the lining adds negligible strength or ductility in circular linings. If the lining actually receives the design loads, reinforcement to control cracking should seldom be needed, because at service loads the thrust is large enough to prevent appreciable tensile stresses except in the softest rock.

Parameter studies of linings in soft ground were conducted using the beam-continuum model. The loading condition was one of the variables, since a great deal of uncertainty lies in the way the ground loads reach the lining in this case, and this model will include this variable in the interaction. The lining behavior under three commonly used loading conditions (overpressure, excavation and loosening or gravity loading) was studied and compared in view of the degree of their severity at both ultimate and cracking load levels. Water pressure or removal of internal air pressure was also considered. Besides loading conditions, other variables of interest examined are the properties of the interface between lining and medium, the coefficient of earth pressure at rest,  $K_0$  and the amount of lining reinforcement.

The slip condition at the ground-lining interface is controlled by three parameters defining the material properties for the interface element: cohesion  $c$ , angle of internal friction  $\phi$ , and shear modulus of

the medium  $G$ . Variation of cohesion within reasonable limits (0 to 5 psi, 0 to 35 kPa) did not have an appreciable effect on the solutions. For this reason a small value of  $c$  has been used in most of the problems for parametric studies as it facilitates obtaining convergence. Variation of the angle of internal friction did show an appreciable effect, however; with high  $\phi$  ( $= 45$  deg), the shear strength of the interface increases, and larger tangential shear stresses result, which reduces the thrust at the crown and invert. The thrust distribution for a small  $\phi$  remains fairly uniform, since the tangential shear strength remains low at the interface, which leads to a condition near full-slip, as most of the interface elements become plastic. On the other hand, for higher  $\phi$  a partial slip or nearly no-slip situation arises. Moments are larger for low  $\phi$  and since crown thrust is lower, the critical section is at the crown for low flexibility ratios ( $F < 7$ ). However, the total load does not differ appreciably between full-slip and partial slip or no-slip conditions. On the other hand for higher flexibility ratios ( $F > 7$ ), the thrust at the springline becomes so much higher for the partial slip case that the failure section changes to the springline and failure occurs at a lower load than in the full-slip case. Thus the load capacity is lower for the partial or no-slip case, and the difference increases with the increase in flexibility ratio. The same trend occurs for excavation loading as well.

The study of the influence of water pressure clearly indicated its beneficial effects on strength. Since a uniform pressure does not induce moment, only the thrust is increased with the increase in water pressure until service load. This reduces the slope of the moment-thrust paths (eccentricity) which helps in avoiding or reducing cracking in the lining. The study also indicates that although the thrust ratio increases with the increase in water pressure, total ultimate vertical load is not changed appreciably.

Different finite element models were used for the representation of the various loading conditions. Using the beam-continuum model, the overpressure loading condition was modeled by applying uniform pressure at the top surface of the initially unstressed medium with the lining in place. The excavation loading condition was obtained by applying the in-situ stresses at the interface on the medium nodes. The spring model was used for the loosening load condition, and uniform vertical pressure was applied directly to the lining. A comparison of the effects of the three loading conditions indicates that the loosening load is the most severe, while excavation loading gives the maximum capacity or is the least severe. The difference in capacity between the overpressure loading and excavation loading increases with flexibility ratio up to a flexibility ratio of about 20, and then remains fairly constant. Since the loosening load is likely to be limited in its magnitude to the weight of some fixed depth of soil above the crown, this loading will not govern the design in all cases even though it provides the largest moment-thrust ratio. Nevertheless because of its severity it should be checked if there is any possibility that it could occur. The overpressure loading may lead to an overly conservative design and the excavation loading is more suitable. The study of the variation of  $K$  shows that at low flexibility ratios the ultimate load is increased<sup>o</sup> greatly by increasing  $K$ , but the difference decreases as  $F$  increases.

The lining capacity is improved by its nonlinear behavior from its value obtained by a linear analysis. For loosening loads it improves by a factor that ranges from about 1.7 to 1.9 depending on the flexibility ratio. On the other hand, for excavation loading this factor is much smaller except at flexibility ratios below about 7. A large difference between the actual ultimate strength and the linear prediction occurs because the moment-thrust paths for the critical sections are well below the balance point and very near the moment axis; this is the case for loosening loads in soft grounds, and it is the case for the excavation loading when the flexibility ratio is below

5 to 7. Since the difference between actual ultimate strength and that predicted by linear analysis is fairly consistent for loosening loads, a lower load factor may be used for design by linear analysis to take advantage of the extra strength.

Three different reinforcement ratios (0, 0.5 and 1.0 percent) were used to investigate their effect on the lining behavior. The moment-thrust paths of the critical sections for different reinforcement ratios do not change in the linear range. Although the paths approach their respective envelopes in the nonlinear range at higher ultimate thrusts for higher reinforcement ratios, the total ultimate load does not vary appreciably (Fig. 7.40). When the moment-thrust paths for the section that cracks first, which is the crown, is compared with the cracking envelope, it is found that reinforcement has little effect on the cracking load because the cracking envelope remains essentially the same for all three reinforcement ratios. Cracking may be a problem for low flexibility ratios, however.

## APPENDIX A

### DETAILED DESCRIPTION OF EXISTING DESIGN PRACTICE FOR CONCRETE TUNNEL LININGS

#### A.1 Bechtel Incorporated, San Francisco, CA

Designers Interviewed: Walter Ferris, Chief Engineer, Soils  
Division

Art Arnold, Chief Geologist

Chris Gardner, Project Engineer

The firm is primarily involved with the design and construction of water conveyance tunnels in hydroelectric applications. In most cases the firm acts as construction manager rather than as designer.

##### A.1.1 Loading

SOFT GROUND: Not discussed.

ROCK

Running Tunnels: Initial support is generally provided by steel ribs and/or rock bolts. Their design is based on judgment, size of the tunnel opening and evaluation of the geologic exploration data. The initial support is assumed to carry all the loads, so the final concrete lining is primarily to provide a smooth surface and to resist internal water pressures. Therefore, the minimum constructable lining is considered adequate.

In pressure tunnels, if the rock cover is 75 percent or less than the internal pressure, the tunnel is lined with steel, especially near the portal. Otherwise, the final concrete lining is reinforced to resist the internal water pressure.

Stations (Large Openings): The amount of exploration for large underground openings in rock is more extensive than is required for

tunnels. The orientation of the opening will be adjusted to fit the geologic conditions as favorably as possible. The stability of the opening for construction and long-term loading is assured by a systematic excavation and support sequence. Primarily rock bolts are used although lightweight steel sets might be installed over the crown to prevent small rock blocks from falling. Resin bonded rock bolts are favored over the grouted type, since they are easier and faster to install. If a concrete lining is placed over the crown, its purpose is to act as a "security blanket" against rock falls rather than to take rock loads.

#### A.1.2 Analysis

An analysis in the usual sense of load determination, computations and member sectioning is not performed for the ground loads. Primarily judgment is used in the determination of support requirements and the final result is substantiated by reference to design charts.

To select the amount of reinforcement needed to resist the internal pressure in pressurized tunnels, elastic theory of interaction of rock and reinforcement is used; the reinforcement is designed to resist (a) a portion of the load required to close the shrinkage gap between the lining and the rock, and (b) that portion of the water pressure that the rock could not carry without causing the concrete ring to exceed its tensile strength. The procedure is a compromise between the theory of radially cracked rock cylinders and the theory of uniform undisturbed elastic mass.

#### A.1.3 Design and Performance Criteria

All design parameters, both hydraulic and structural, used in the analysis and construction procedures will be specified and enforced (i.e., joints, grouting procedures, curing of concrete, design

strength, minimum dimensions, A-line and B-line, deviation in dimensions, and finished surfaces).

Leakage and cracking of the concrete lining can be controlled by effective grouting since concrete linings are grouted for contact between them and the rock. In internal pressure tunnels, if they are reinforced as described in Section A.1.2, there will be no cracking.

The minimum thickness for a tunnel without steel rib initial supports is approximately 8 in. (203 mm) for diameters less than about 10 ft (3 m) and 12 in. (305 mm) for larger diameters. For a steel rib supported tunnel it will be the thickness of the ribs plus 4 in. (102 mm).



A.2 DeLeuw, Cather and Company, Washington, DC

Designers Interviewed: Dah Fwu Fine, Assistant Chief Engineer  
Kuldip Singh, Principal Structural Engineer

Bechtel Incorporated, Bethesda, MD

Designer Interviewed: Carl Bock, Chief-Geotechnical Group

These two firms are listed together because of their involvement in the Washington Metro, the former as General Engineering Consultant and the latter as Construction Consultant.

The Washington Metro, when completed, will be a 101 mile (162.5 km) system with 86 stations. As of July 1980, 1/3 of the system was in operation, 1/3 under construction and 1/3 under final design. Assuming funding availability, the system's completion is planned for 1990. The major tunneled portion of the system consists of a pair of running tunnels about 20 ft (6.1 m) outside diameter and arch shaped stations 65 ft (19.8 m) wide by 45 ft (13.7 m) high. The average overburden depth is 40 to 60 ft (12.2 to 18.3 m). During the tunneling operations many types of ground conditions were encountered varying from rock (primarily, foliated quartz, mild schist or gneiss) to soft ground (water bearing silty-clays, sandy-clays and gravels) to mixed face.

Design contracts were awarded to many different firms and as a consequence the design procedures used vary. Nevertheless, some degree of uniformity exists because all designs were submitted to the General Engineering Consultant for final approval. In the following pages the overall design philosophy is being described, even though differences in particular designs will be pointed out when appropriate.

### A.2.1 Loading

#### SOFT GROUND

Precast Segmented Linings: A standard design for a prefabricated circular concrete lining for a single-track earth tunnel has been prepared, although not used yet, by the General Engineering Consultant. It consists of seven bolted reinforced concrete segments five of 60 deg, one of 40 deg and a 20 deg key. The segments are of the waffle type 3 ft (0.9 m) wide, 10 in. (254 mm) thick at the flanges and 4 in. (102 mm) thick between the edges. The segment thickness was also considered suitable for 18 x 150 tons (18 x 1334 kN) jacking load in the longitudinal direction. To prevent water leakage into the tunnel through joints between segments, neoprene gasket ring is provided around each segment.

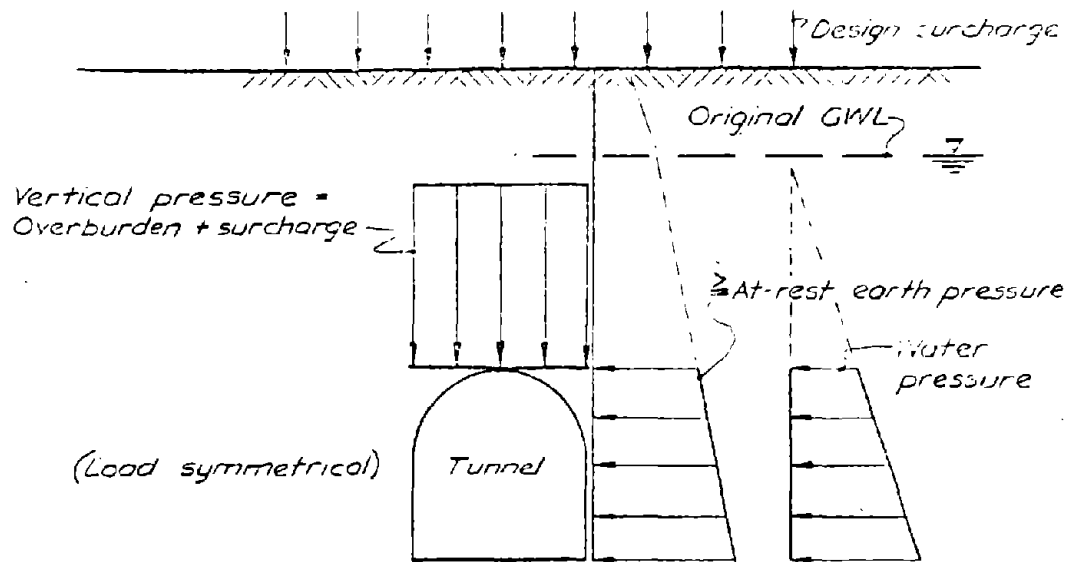
To check the adequacy of the lining for ground loads it is recommended that the total soil overburden pressure be applied over the crown. As a result of this loading the lining would deflect at the springlines and would result in horizontal reactive pressures that are estimated generally to be in the range of 0.90 to 0.97 times the average vertical pressure at the crown.

As an alternative, it is suggested that the designer could estimate the magnitude of side pressure by assuming that the horizontal diameter of the lining increases by 1/2 to 1-1/2 in. (13 to 38 mm) and then utilize the modulus of subgrade reaction of the soil. The smaller deflection value applies to compact coarse grained pleistocene materials, cretaceous strata or decomposed rock and the larger value to fills, clays or organic soils.

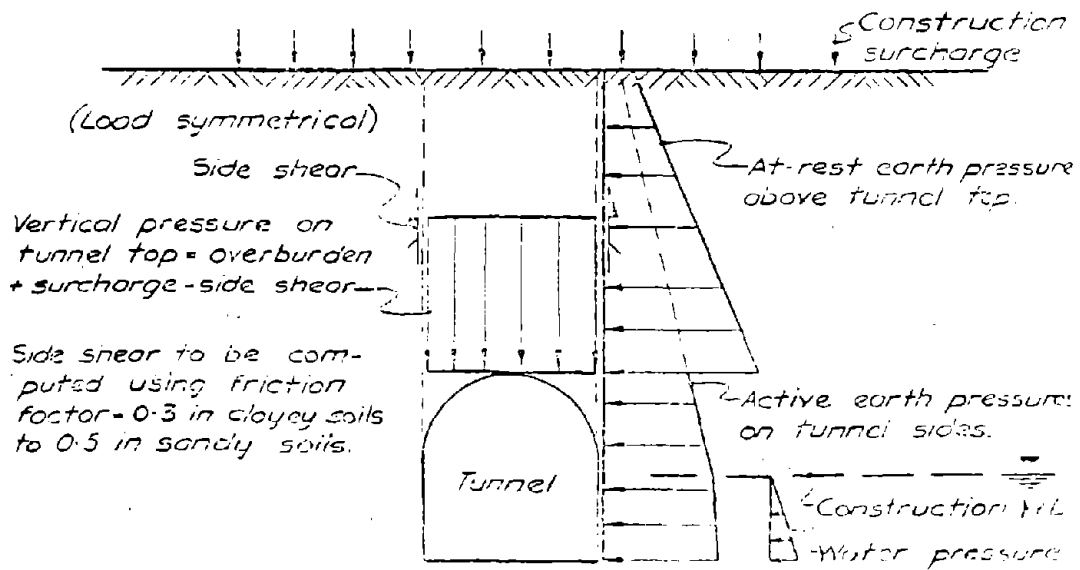
Cast-in-Place Monolithic Linings: Two different loading criteria are used for cast-in-place final linings that depend on whether the shape of the opening is horseshoe or circular.

a) Horseshoe-Shaped Tunnels: Horseshoe tunnels in soft ground are not generally recommended. However, in mixed face soil conditions such tunnels have been constructed. The method of driving these tunnels is generally with a mechanical excavator and/or hand mining. The initial support is provided by steel ribs and lagging, for which the loading (construction and short term loading) is based on the assumption that the method of construction will tend to permit inward movement of the surrounding soil between springline and invert, and that the temporary supporting system may settle vertically to some extent; thus, consideration is given to the probable decrease in vertical pressure over the crown of the tunnel due to development of "side shears" in the overburden as shown in Fig. A.1b. The magnitude of these side shears can be computed by assuming at rest earth pressures above the tunnel and a coefficient of friction ranging between approximately 0.3 in clayey soils to 0.5 in sandy soils. Horizontal earth pressure acting on the tunnel supports is taken as the active value plus water pressure consistent with the assumed construction drawdown level. If substantial inward earth movements are expected below the springline, the vertical effective pressure applied to the active wedge at the tunnel sides is reduced by taking into account vertical shear in the overburden above the wedge. Consideration is also given to the possible settlement of tunnel supports, the mining of adjacent tunnels and the construction procedure in evaluating this reduction of vertical stresses above the active wedge.

Vertical loading of the final concrete lining (long-term loading) is taken as the full overburden weight plus surcharge without side-shear restraint, as shown in Fig. A.1a. Surcharge or roadway live loads are superimposed on the ground loads based on the HS20-44 loading of AASHTO for depths to 4 ft (1.2 m); at depths between 4 ft (1.2 m) and 8 ft (2.4 m), a graduated uniform live load of 440 psf (21 kPa) to 300 psf (14.4 kPa) is used; for depths greater than 8 ft (2.4 m) a uniform live load of 300 psf (14.4 kPa) is used. Final linings of all



A.1.a Long-Term Loading



A.1.b Construction and Short Term Loading

FIGURE A.1 WMATA LOADING CRITERIA FOR HORSESHOE SHAPED TUNNELS IN SOFT GROUND

underground structures having less than 8 ft (2.4 m) of earth cover are designed for two conditions:

i) The actual depth of cover plus superimposed HS20-44 wheel load distributed in accordance with the above.

ii) An assumed future cover of 8 ft (2.4 m) plus a uniform live load of 300 psf (14.4 kPa). The same live load criteria apply to circular tunnels as well.

Horizontal soil pressure for a single-track horseshoe tunnel is taken as 0.75 to 0.85 times the average total vertical pressure. For the double-track tunnel this ratio of horizontal to vertical pressures is somewhat lower. It is not intended to consider an average horizontal total pressure greater than the average vertical pressure on the top of a tunnel where the cover over the tunnel is equal to 1.5 times the tunnel height or more.

b) Circular Tunnels: The initial support for circular tunnels usually consists of steel ribs and timber lagging. It is assumed that during construction the initial support will deflect downward at the crown and outward at the springline. This is in contrast with that for horseshoe-shaped tunnels where inward movements are assumed during construction between springline and invert. For loading on the initial support some allowance is made for the development of side shears in the overburden, which reduce the vertical pressure caused by the total overburden plus surcharge, as shown in Fig. A.2b. These shears ordinarily are less than for the horseshoe tunnel where settlement of the arch footings is expected. A reasonable vertical soil design pressure for the initial support corresponds to a pressure caused by a column of soil one-half the tunnel diameter. Horizontal soil pressures are taken as reasonable values after considering the outward deflection of the supporting structure, ordinarily not less than at rest values, and generally in the range of  $2/3$  to  $3/4$  of the effective vertical

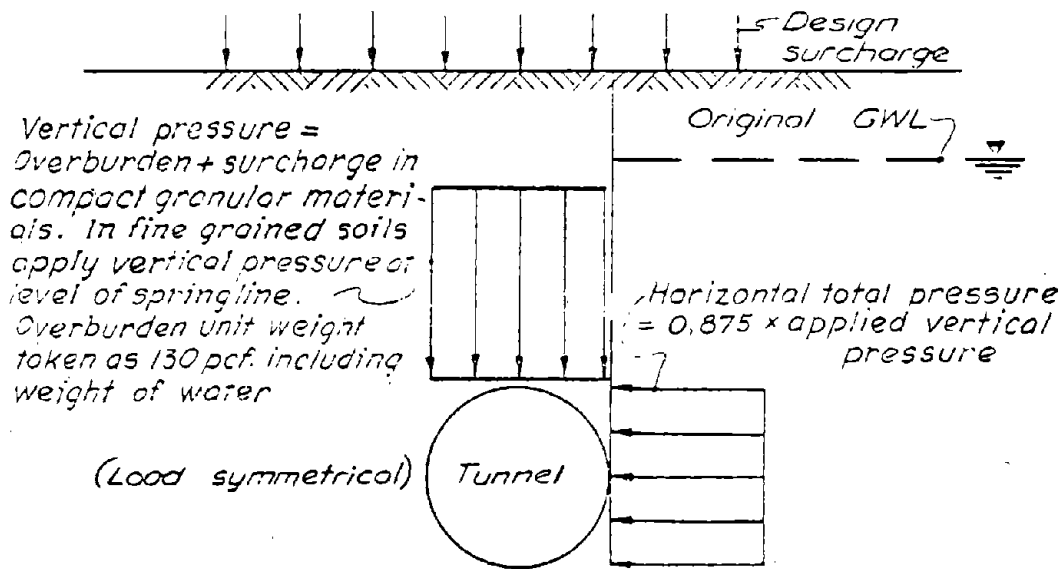
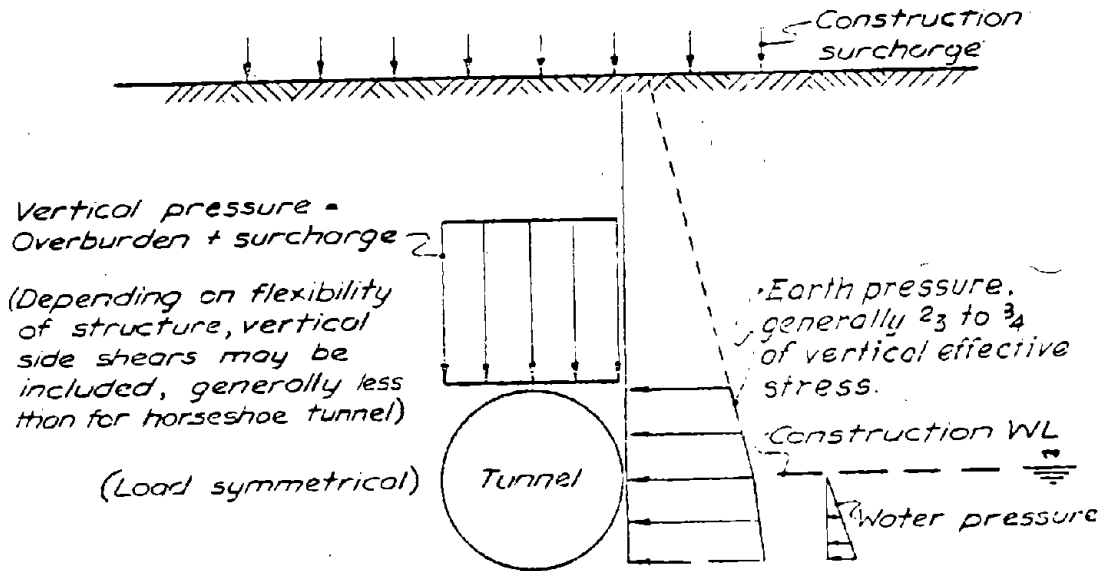


FIGURE A.2a Long-Term Loading



A.2.b Construction and Short Term Loading

FIGURE A.2 UMTA LOADING CRITERIA FOR CIRCULAR SHAPED TUNNELS IN SOFT GROUND

pressures acting at the springline during construction. Water pressures used are those corresponding to the probable construction drawdown condition. Total pressures which are computed in vertical and horizontal diagrams may be applied as all-around, radially directed pressures varying smoothly between vertical and horizontal values.

The final concrete lining loads do not include a reduction in vertical pressures for side shears. Thus, the full overburden and surcharge loads are used. For relatively favorable ground conditions where overburden consists predominately of compact coarse grained soils, the total vertical pressure is taken as the height of overburden above the crown of the tunnel plus surcharge. For relatively unfavorable ground conditions where the overburden consists primarily of fine grained plastic soils, the total overburden is taken as the weight of materials above the springline plus surcharge. These criteria do not make a distinction between effective earth and ground water pressure, and consequently the overburden unit weight is taken as  $130 \text{ lb/ft}^3$  ( $2082 \text{ kg/m}^3$ ) including the weight of the water, as shown in Fig. A.2a. The horizontal total pressure, applied to the sides of the tunnel, is equal to 0.875 times the vertical total pressure.

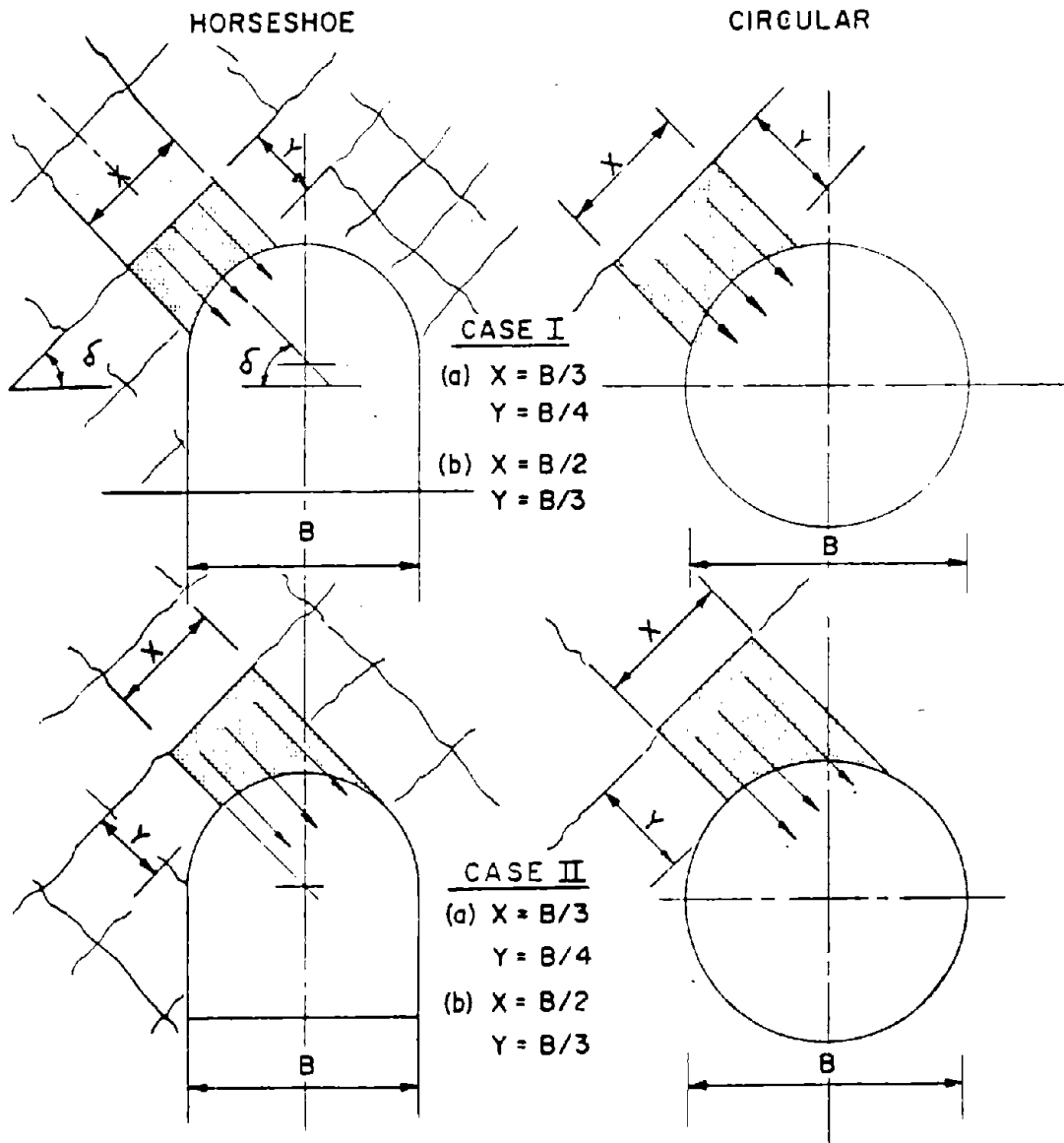
The structural design of final concrete linings for both the horseshoe-shaped and circular tunnels is based on working stresses, as described in Section A.2.3. However, the design is checked using ultimate strength design methods with a load factor of one and horizontal total pressure factors of 0.45 for the poorer ground conditions and 0.65 for the most favorable ground conditions. If the spacing of two parallel running tunnels is less than two tunnel diameters from center line to center line, unequal side loadings are considered.

## ROCK

Running Tunnels: Cast-in-Place Monolithic Linings: The design of initial support such as rock bolts, steel ribs, shotcrete and combinations thereof is specified as the contractor's responsibility. However, it is to be erected as close to the face as possible and in the case of steel ribs, tight blocking must be installed without delay. The rock loads assumed for the design of final concrete linings are shown in general fashion without magnitudes in Figs. A.3, A.4, and A.5. These diagrams include a series of rock wedges formed by characteristic jointing patterns in the Washington, D.C. area. The magnitude and direction of the loads are primarily influenced by the joint attitudes and their effective friction angles. These in turn are determined by the specific geologic conditions along the tunnel line. Generally, the pressure for the vertical, symmetrical loading of Fig. A.5 ranges from about 0.25 to 0.6 times  $B$ , where  $B$  is the total unit weight of the rock and  $B$  is the width of the tunnel opening. In the Washington, D.C. area these vertical pressures correspond to 1 to 2 ksf (48 to 96 kPa). Joint friction angles range from 20 to 25 deg in the diorite gneiss to a minimum of 10 to 15 deg in zones of shear or movement in the amphibolite or chloritic rocks.

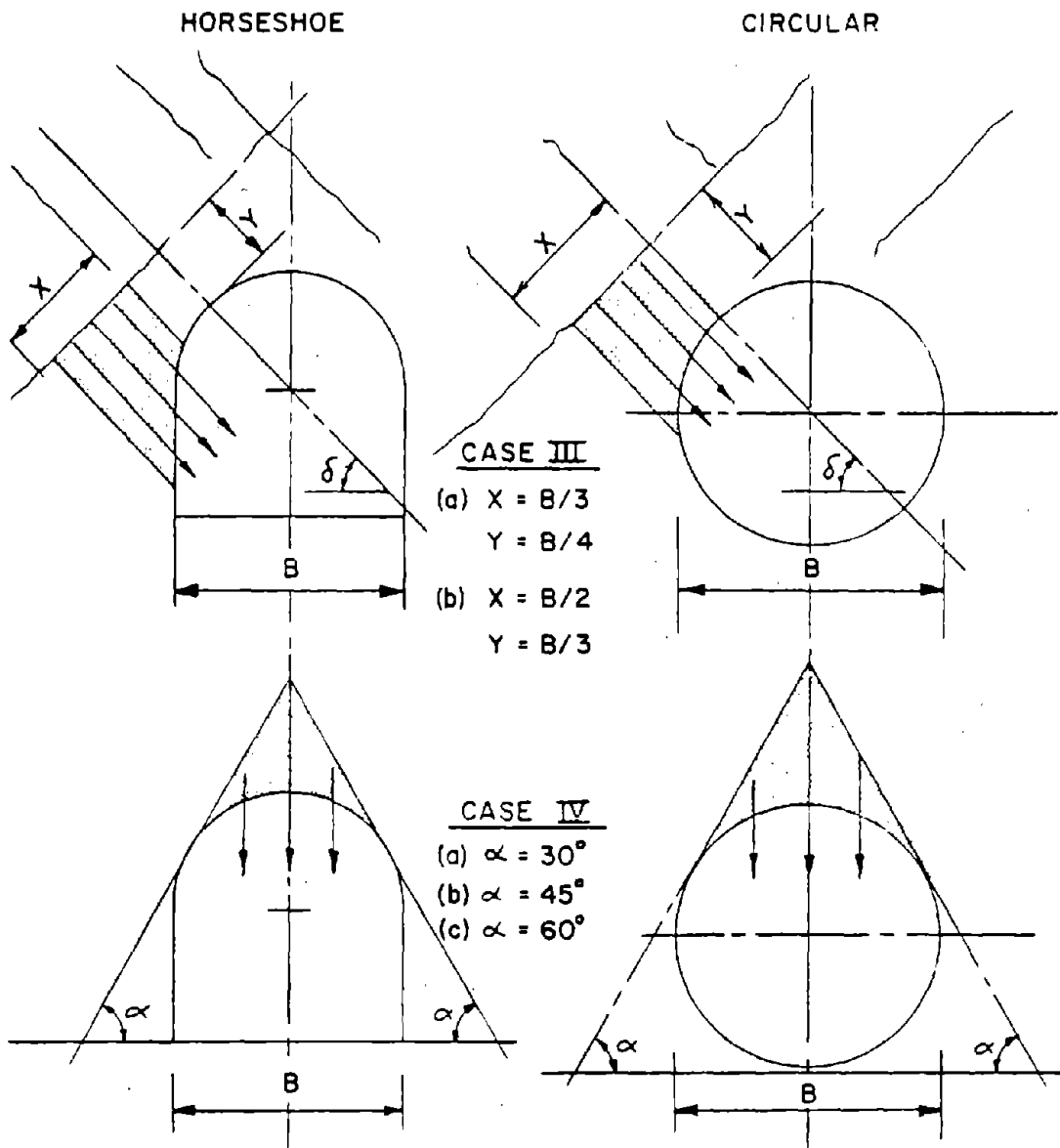
Circular running tunnels in rock are designed for full external water pressure without permanent drainage. The metamorphic rocks of the Washington, D.C. area contain extensive thin calcite deposits in their joint systems and as a consequence drainage pipes which have been installed in some completed tunnels have been subjected to substantial flow of calcium carbonate in solution, leading to clogging and continual maintenance problems. Therefore, the final lining is designed for short term drained rock load (full unit weight without hydrostatic pressures) and it is checked for the long-term restoration of ground water pressures with bouyant rock unit weight and full hydrostatic pressure.





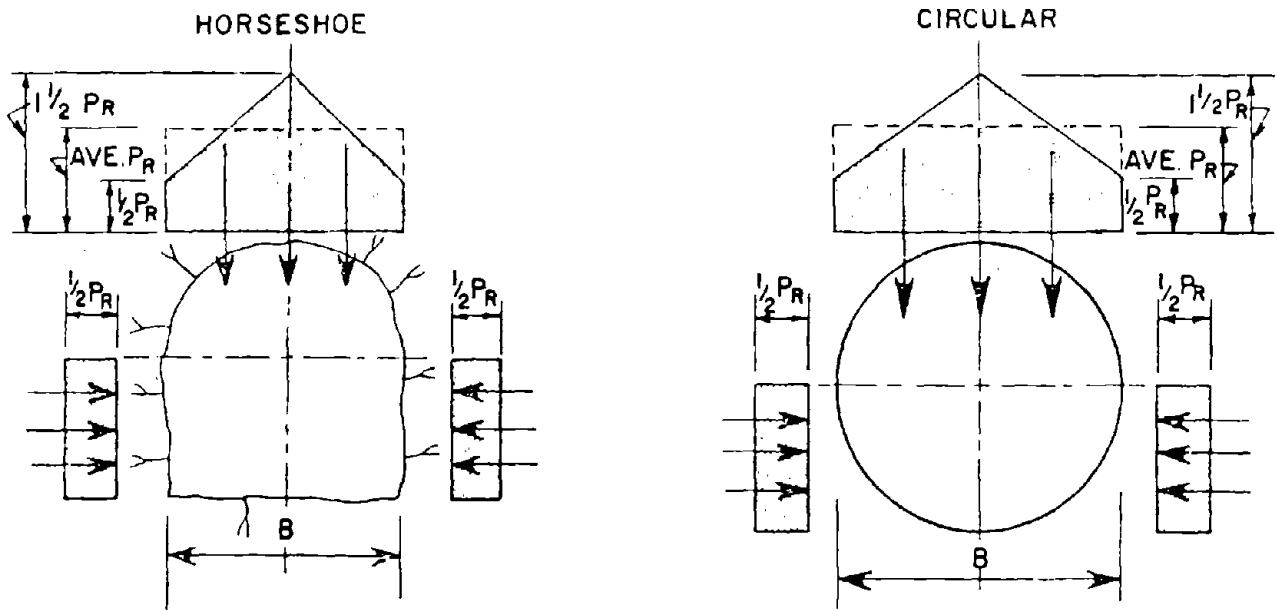
FOR CASES I & II, ANGLE  $\delta$  TO BE DETERMINED FROM SUBSURFACE DATA  
 Note: FRICTION ANGLE OF 15° AT SLIDING JOINTS CASE I THRU III.

FIGURE A.3 WMATA LOADING CRITERIA FOR RUNNING TUNNELS IN ROCK -- CASES I AND II



FOR CASE III, ANGLE  $\delta$  TO BE DETERMINED FROM SUBSURFACE DATA.

FIGURE A.4 WMATA LOADING CRITERIA FOR RUNNING TUNNELS IN ROCK -- CASES III AND IV



CASE V

$P_R$  = TABULATED AVERAGE VERTICAL ROCK PRESSURE.

FIGURE A.5 WMATA LOADING CRITERIA FOR RUNNING TUNNELS IN ROCK -- CASE V

Because of the existence of long straight walls in horseshoe-shaped running tunnels and the possibility of high bending moments due to water pressures, full permanent drainage is provided with a carefully monitored and maintained drainage system.

Running Tunnels: Precast Segmented Linings: A standard design for a segmented concrete lining for circular tunnels in rock has also been developed by DeLeuw Cather. The lining consists of five 72 deg solid segments, 7 in. (178 mm) thick and 4 ft (1.2 m) wide. The segments are equipped with a non-bolted key joint with a gasket to stop leakage. This lining has not been used, although there is the feeling it will be in the near future before its counterpart for soft ground tunnels.

Stations (Large Openings): The typical single chamber station in the Washington, D.C. area is 65 ft (19.8 m) wide and 45 ft (13.7 m) high with 40 to 60 ft (12.2 to 18.3 m) of cover. The newer double chamber stations have comparable width and are 30 ft (9.1 m) high with 60 to 80 ft (18.3 to 24.4 m) of rock cover. The stations are excavated in stages, with initial support designed to maintain integrity of the rock arch over the crown during construction. The initial support normally consists of 2 in. (51 mm) of shotcrete within 2 hrs of the excavation and 4 to 6 rock bolts about 20 ft (6.1 m) long within 24 hrs of the excavation. Steel ribs are installed within 15 ft (4.6 m) of the excavation face and blocked with shotcrete. The final concrete lining is formed by shotcreting (with option to use cast-in-place concrete) between and over the steel ribs to form a sufficient thickness to support the rock loads specified in Figs. A.6 and A.7. The size of rock wedges is determined by local geologic conditions prevailing at the site of the individual station. The size and spacing of the steel ribs used for initial and final support depend on the geotechnical assessment of design rock loads and the assumptions made by the designer with respect to excavation procedures. In the Zoological Park Station, for instance, the steel ribs used were W14 x 119 at 4 ft (1.2 m) centers; in the Bethesda Station, with similar

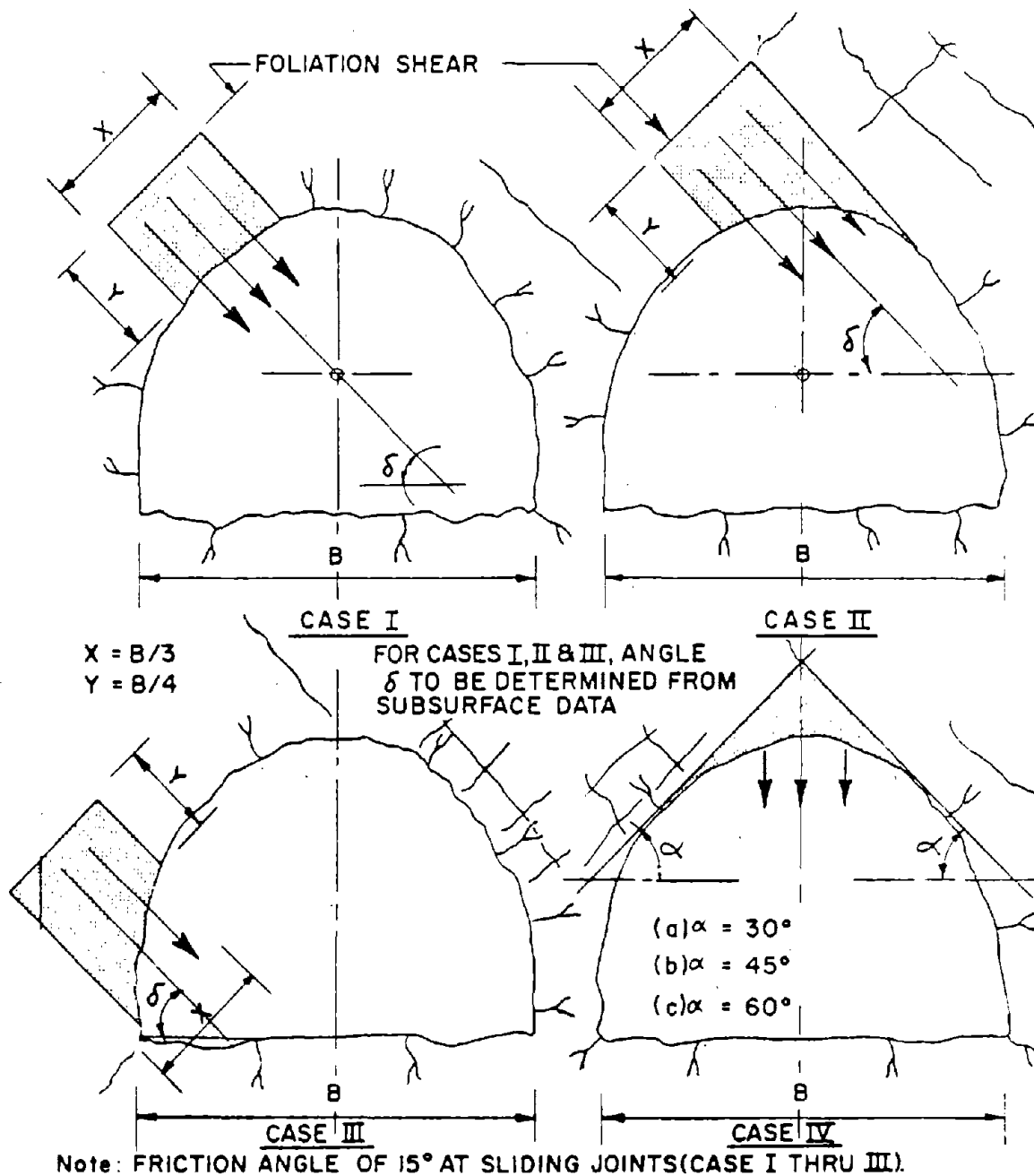
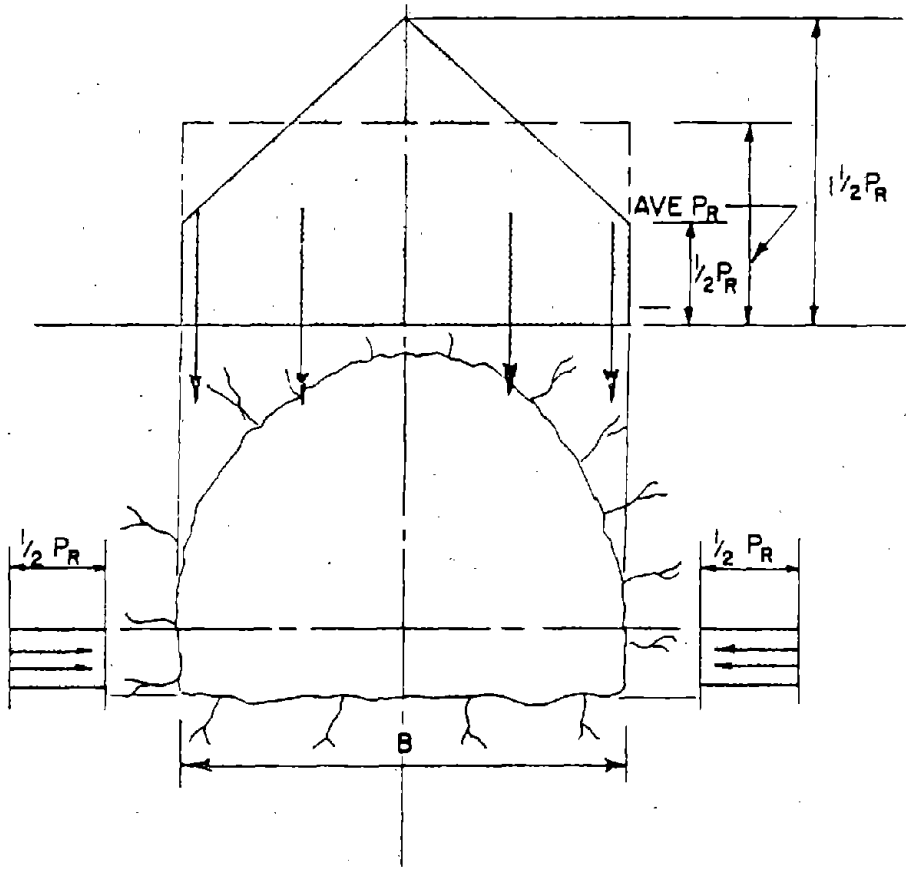


FIGURE A.6 WMATA LOADING CRITERIA FOR STATION IN ROCK -- CASES I THRU IV



CASE V

$P_R$  = TABULATED AVERAGE VERTICAL ROCK PRESSURE

FIGURE A.7 WMATA LOADING CRITERIA FOR STATIONS  
IN ROCK -- CASE V

geology and size, W14 x 61 steel ribs at 5 ft (1.5 m) centers were used; both being single chamber stations.

Initially the designs of final linings were based on complete drainage of hydrostatic pressure. However, because of difficulties experienced with hydrostatic pressure relief systems for tunnels in rock already constructed, the total rock loads have been modified to account for partial bouyant effects and water pressure applied in later designs.

For a design at normal working stresses, hydrostatic pressure is applied to the permanent structure which varies from 25 percent of the total potential water pressure acting on the crown of the tunnel to ten percent of the total water pressure acting at the bottom of the tunnel. The pressure is applied normal to the lining surface, varying smoothly from the maximum at the crown to the minimum at the base of the vertical sides.

Design calculations based on ultimate conditions in the lining section are based on the full potential water pressure at the crown and smooth variation to ten percent of the potential water pressure acting at the base. Full permanent underdrainage is provided for a flat invert slab on rock in station structures (or horseshoe tunnels) so that no uplift pressures are created beyond those negated by the slab weight.

#### MIXED FACE CONDITIONS

In cases where part of the tunnel face is in soft ground and part of it is in rock, no set loading criteria exist. These conditions are handled on a case by case basis.

### A.2.2 Analysis

Analyses of the final concrete lining are performed using different combinations of vertical loads, side pressures and ground water elevations. Depending on the section designer, linear elastic programs like STRESS, STRUDL, SAP-IV, have been used. The lining is modeled as a series of beam elements and the ground by springs; in soft ground only radial springs are used for the medium, while in rock both radial and tangential springs are generally used. All spring supports must be in compression. The tangential spring stiffness is taken as some percentage of the radial spring stiffness, usually between 0 and 50 percent.

In soft ground the radial spring stiffness is estimated by transforming the mass of soil surrounding the liner into equivalent radial concrete members emanating from the liner joints. The length and cross sectional area of these members is being determined as follows:

$$k = \frac{A_c \cdot E_c}{L_c}$$

where

$k$  = modulus of subgrade reaction of the soil (load per unit deformation)

$A_c$  = cross sectional area of equivalent concrete mass

$E_c$  = modulus of elasticity of concrete

$L_c$  = length of equivalent concrete member.

In rock, the stiffness is related to the in-situ modulus of elasticity of the rock mass by:

$$K_r = \frac{E_m}{(1 + \nu_m)} b \cdot \theta ,$$



where

$b$  = tunnel length that is represented by the spring

$\vartheta$  = angular segment for which the medium is represented by a spring

$E$  = elastic modulus of the medium (rock)

$\nu_m$  = Poisson's ratio of the medium (rock)

$K_r^m$  = radial spring stiffness for the medium (rock)

The average rock properties in the Washington area are an elastic modulus of 100,000 psi (689 MPa) and modulus of subgrade reaction (pressure/unit deformation) that varies from a minimum of about 40 to 70 ksf/in. (75 to 132 kPa/mm) in weathered and jointed rock to a maximum of 150 to 200 ksf/in. (283 to 377 kPa/mm) in relatively sound rock.

If during the analysis process any of the springs go into tension both radial and tangential springs are disconnected at that location and the analysis repeated until no springs show tension. In the analysis of segmented linings the stiffness in the joint region is reduced to 20 to 30 percent of that of the segment.

### A.2.3 Design and Performance Criteria

Designs for final concrete linings in both tunnels and stations are based on working stress design methods. The recommended compressive strength of concrete for monolithic cast-in-place linings is 3,500 psi (24.1 MPa) whereas for precast linings not less than 5,000 psi (34.5 MPa) is used. The recommended steel is A36. The allowable flexural design strengths are  $(0.4) f'_c$  for concrete and  $0.66 f_y$  for steel. As described in Section A.2.1, the results of the working stress design for linings in soft ground are checked using the ultimate strength design method with a load factor of one and reduced side earth pressures.

The minimum recommended design thickness for cast-in-place concrete linings in soft ground is 15 in. (381 mm) whereas for linings in rock it is 12 in. (305 mm). Cracking of the final concrete lining is allowed as long as it does not cause excessive leakage. The allowable leakage criteria for running tunnels is at 0.2 gal per minute per 250 ft (0.8  $\ell$ /min/76 m) length, whereas for stations no leakage is permitted. In segmented concrete linings the gasket is specified to be under compression after the lining deformation occurs with a maximum allowed opening of the joints of 1/8 in. (3 mm).

Whenever drainage of the tunnel is desired drain holes 10 ft (3 m) long and 2 in. (51 mm) in diameter are provided with spacing dictated by the local ground water conditions. To make the invert slab underdrainage system for a horseshoe or a station tunnel as effective as possible, additional grouting cut-off beneath the vertical walls of the structure is recommended. There may be circumstances in which efficient underdrainage will require the placing of filter sand or filter fabric material where zones of weathered or decomposed rock cannot be completely cleaned and material of essentially soil-like consistency appears in joints or fractures.

For crack control one layer of circumferential reinforcement (#6 at 12 in. (305 mm) typical) is placed on the inside face of rock tunnel linings, whereas one layer (#6 at 12 in. (305 mm)) in each face of the soft ground linings is used.

In soft ground tunnels, longitudinal temperature and shrinkage reinforcement for the 50 ft (15 m) long cast units should not be less than 0.15 percent of the gross concrete areas with a maximum of #7 bars at 18 in. (457 mm) spacing in each face. For casts longer than 50 ft (15 m) between joints construction procedures should be specified and reinforcement provided to reduce cracking to a minimum. Stripping of concrete lining forms is allowed after the concrete has attained 40

percent of its design strength. Both vertical and sloping joints between concrete pours have been used.

A.3 Denver Board of Water Commissioners, Denver, CO

Designers Interviewed: John Parsons, Project Manager  
Verne Hornback, Geologist  
Jim Batt, Project Engineer  
Walt Colwell, Chief Civil Engineer  
with DMJM Phillips-Reister-Haley, Inc.,  
consultant to Denver Water Board

This organization is exclusively involved with the design of water conveyance tunnels with a typical diameter of 10 ft (3.1 m).

A.3.1 Loading

SOFT GROUND: Not discussed.

ROCK

Running Tunnels: Rock loads are a result of geologic conditions and the size and geometry of the tunnel opening. Alignment of the tunnel is dictated by geologic conditions and engineering requirements. A pilot tunnel is very effective, although not always feasible, in predicting ground conditions. Drilling ahead of the tunnel face is desirable to provide necessary geologic data to estimate anticipated support and water conditions.

The geologic reports, available at bidding time, include estimates of whether the required amount of initial support will be light, medium or heavy and the percentage of total length that these classifications might apply. The initial support usually consists of steel ribs (W6 x 20 typical), shotcrete or rock bolts or a combination of the three. Generally specifications are set up so that the type of initial support to be used is selected by the contractor. In essence, the owner provides an estimate of the initial support required but not where to place it. The units of initial support is then bid by unit price. The resident engineer and the contractor decide on the exact quantity of support needed, as excavation proceeds.

The final concrete lining is not designed to take ground loads except in unusual ground conditions. Its thickness is determined by construction and hydraulic rather than geologic considerations and is usually unreinforced. However, special geologic conditions may require reinforcing and/or a thicker than normal section. Furthermore, the final lining may not be designed to take the external water loads, which might be quite high in the Rocky Mountains area, but rather a drainage system of weep holes is provided. A maintenance and inspection program is then instituted to ensure the proper functioning of the drainage system. When internal water pressure is a design consideration, either a steel lining is installed on the inside of the final concrete lining or the lining is reinforced with conventional bar reinforcement, especially near the portal areas.

Stations (Large Openings): Not discussed.

#### A.3.2 Analysis

In pressure tunnels, an analysis is performed with the water pressures applied radially on the inside surface of the lining to determine the amount of reinforcement or the thickness of the steel plate required.

#### A.3.3 Design and Performance Criteria

The minimum thickness of cast-in-place concrete linings is 6 to 9 in. (152 to 229 mm) to accommodate the concrete placing pipe. If shotcrete is used, the minimum design thickness is 3 in. (76 mm). Backfill grouting is performed between the lining and the rock to ensure good contact. Concrete linings are not reinforced except in pressure tunnels near the portal areas.

The strength of the concrete is specified at 4,000 psi (27.6 MPa) and the form stripping time at 24 hours after casting.

A tunnel maintenance program is enforced which involves dewatering and inspection of the tunnel every 5 years on the average, or sooner as might be required.

#### A.3.4 Comments

Geologic data will generally dictate the choice of alternative excavation methods although the final decision is made by the contractor based on his experience and available equipment. The possibility of encountering squeezing ground conditions is quite high in tunnels through the Rocky Mountains; this has favored drill and blast methods over the TBM in the past. For the Roberts tunnel for instance (bid in 1956), a 23.3 miles (37.5 km) long, 10 ft 3 in. (3.1 m) inside diameter pressure tunnel through the continental divide, out of 9 bids submitted only one involved the use of a TBM.

A.4 Daniel, Mann, Johnson & Mendenhall/Kaiser Engineers

DMJM/KE a joint venture, Baltimore, MD

Designers Interviewed: David Hammond, Vice President

Drupad Desai, Chief Engineer

This firm is the General Engineering Consultant for the 8 miles (13 km) long Baltimore Region Rapid Transit System. It has 9 stations of which 6 are underground and 3 are aerial, and of the 8 miles (13 km) of track, 4-1/2 (7.2 km) are subway, 2-1/2 (4 km) are aerial and one mile (1.6 km) is at grade. About 1-1/2 miles (2.4 km) of subway identical twin tunnels will be through soft earth using a hydraulic shield which is jacked against an erected steel lining. Compressed air is forced into the tunnel to stabilize the surrounding earth while the shield advances. Another 1-3/4 miles (2.8 km) of tunnel will be through rock, which will be removed with small explosive charges. Depending on the location, tunneling operations will take place between 25 to 60 ft (7.6 to 18.3 m) underground. Construction began in December 1976 and the system is expected to go into revenue service in late 1982.

A.4.1 Loading

SOFT GROUND

Precast Segmented Linings: The concrete segments are designed to withstand jacking, erection and ground loads resulting from a depth of soil on the order of 1.2 to 2 tunnel diameters over the crown of the opening. If the tunnel is located deeper than 2 diameters, the inherent ability of the soil to arch around the opening and support itself is recognized, and thus the same design criterion is applied. The external water pressure is superimposed on the ground loads.

Cast-in-Place Monolithic Linings: The initial lining (usually steel ribs and timber lagging) is designed for a vertical load equivalent to a height of 1.5 to 2 diameters of soil above the crown. To control the inflow of water during excavation the use of compressed

air is recommended, provided that the required air pressure does not exceed 12 psi (82.7 kPa); for higher air pressures a cost analysis is recommended to determine the most effective and economical excavation and support sequence. The final concrete lining is designed for about 60 percent of the ground loads used to design the initial lining. The external water pressures are superimposed on the ground loads.

## ROCK

Running Tunnels: The magnitude of rock loads depend on the quality of the rock, the method of excavation and the size of tunnel opening. In order to assess the rock quality, percent of core recovery, unconfined compressive and RQD values are determined. Normally the initial support is provided by rock bolts. Their design is based on the size and orientation of the rock wedges around the tunnel opening. If the quality of the rock is poor, shotcrete or steel ribs are used as well.

In the case of rock tunnels it is easier to change the support type and sequence than in soil tunnels; therefore, it is recommended that an alternative support method be available during excavation that can be used if problems arise with the original method.

The stability of the rock pillar between parallel tunnels is a source of great concern. It is desirable to have the thickness of the pillar at least one tunnel diameter wide. On the Baltimore project, as noted in Desai (1979), this pillar width varied from 14 to 40 ft (4.3 to 12.2 m) for the 17 ft 10 in. (5.4 m) inside diameter tunnels. In order to maintain integrity of the pillar, reinforcement consisting of #11 steel reinforcing bars was inserted and grouted in the pillar. The bars extended from the face of the pillar in the first tunnel to within one foot (0.3 m) of the face in the adjacent tunnel; they were untensioned and were installed prior to excavation of the second tunnel.



The final concrete lining is designed to withstand only nominal rock loads resulting from combination of rock wedges since the opening is assumed to be stable by the time the final lining is installed. At first the design of the final concrete lining in the Baltimore system was based on the assumption that a hydrostatic pressure relief system resulting from properly installed drains would exist. However, the design was later changed to allow the lining to resist partial hydrostatic pressures because of uncertainties associated with the proper functioning of the drains.

Stations (Large Openings): The design philosophy for large openings in rock is similar to that described for running tunnels in rock, but in the case of large openings rock cover relative to the opening size becomes more important. The depth of the station and the quality of the ground over the crown determine its adequacy to provide arching of part of the ground loads around the opening. Even though the final concrete lining is designed for nominal ground loads determined from rock wedges and excavation method, it is more likely to be reinforced either with steel ribs that provide initial support or with additional deformed bar reinforcement to control shrinkage.

#### A.4.2 Analysis

Segmented concrete linings are modeled by a series of straight beams with the joints between the beam elements modeled as pins at the actual joint locations. The ground is represented by radial springs attached to each node of the lining model and a linear analysis is performed. The analysis is performed on the individual segments first for the worst combinations of loads that are likely to occur during erection of the segmental rings. These loadings generally represent the most severe conditions that the lining will experience, so additional analysis for ground loads generally does not result in a change of the design.

Only radial springs are used to model soft ground, with a stiffness determined by performing one-dimensional consolidation and/or simple shear laboratory tests. The value of the soil spring stiffness to be used in the analysis is then determined by correlating the modulus of subgrade reaction or modulus of elasticity of the soil with the expected radial deformations and pressures at each joint. In rock, the stiffness of the radial springs is determined from the results of in situ plate load tests, and tangential springs are added at each node with a stiffness equal to 20 percent of the radial stiffness, to simulate interlocking between the concrete lining and the rock mass. In the case of large openings in rock, the size of rock wedge that loads the linings will determine the number of nodes that need to be provided in the analytical model. The larger the size of the wedge, the larger the number of nodes needed to monitor the behavior of the lining in the region of the rock wedge. Loads are applied at the nodes, and their magnitude is determined from the geotechnical data as described in Section A.4.1; for soft ground tunnels a portion of the ground over the crown and for rock tunnels a combination of rock wedges. A dynamic analysis is performed for segmented linings in seismic zones to ensure that the joints can withstand the earthquake induced displacements.

#### A.4.3 Design and Performance Criteria

Load factors are not directly applied to the ground loads determined by evaluation of geotechnical data. However, if the available geotechnical data are insufficient to determine the magnitude of ground loads with the desired degree of assurance, the geotechnical data are interpreted conservatively and larger loads are applied to the concrete linings. Nevertheless, there is not a predetermined load factor which is applied per se, and the working strength design method is used.

The final concrete lining thickness should not be less than 6 to 8 in. (152 to 203 mm). This minimum thickness is dictated by construction limitations and by the fact that if the final concrete lining is thinner there is greater likelihood of "bleeding" of ground water through it. Within that thickness a single layer of reinforcement at variable locations is recommended (i.e., on the inside face at the crown and on the outside at the springline). A construction joint is placed whenever a crack is expected for crack control. A control joint is provided at the end of each casting cycle. The final concrete lining should be cast at least 7 days (or about 350 ft (107 m)) behind the face of the excavation to allow ground movements to stabilize.

The amount of acceptable leakage is defined by the owner. In the case of the Baltimore subway, leakage was limited to 0.07 gallons per min per 100 linear feet of tunnel (0.26 /min/30 m). The designer should have the authority to monitor leakage and a grouting program should be available to control excess infiltration.

Finally, an overall tunnel maintenance plan should be developed by the designer and enforced during the life of the structure.

A.5 Goldberg-Zoino Associates of New York, Buffalo, NY

Designer Interviewed: Richard Flanagan, Chief Engineer

Hatch Associates Consultants, Inc.

Designer Interviewed: Wesley Terry, Structural Engineer

These two firms are grouped together because of their involvement with the design of the Light Rail Rapid Transit System in Buffalo, NY, the former as Geotechnical Consultant, and the latter as Principal Engineering Consultant, designer for station and running tunnels through the rock section. The first line of the Buffalo system now under construction is 6.4 miles (10.3 km) long. Of those, 1.2 miles (1.9 km) are on the surface, 1.7 miles (2.7 km) in soft ground (all cut and cover construction) and 3.5 miles (5.6 km) in rock (tunneled). The system also includes 14 stations of which 8 are to be constructed underground. The opening of the line is targeted for 1984.

A.5.1 Loading

SOFT GROUND: All soft ground sections are constructed using the cut and cover method.

ROCK

Running Tunnels: The twin running tunnels 18 ft (5.5 m) nominal outside diameter are entirely in the Bertie formation, a 50 to 60 ft (15.2 to 18.3 m) thick massive dolostone, laminated with dark shale bands. The rock is generally competent and unweathered, except near the bedrock surface. The upper portion of the formation consists of discrete blocks separated by weathered horizontal and vertical joints 5 to 18 ft (1.5 to 5.5 m) apart, occasionally filled with silt and clay. A 15 ft (4.6 m) minimum rock cover was arrived at in setting the alignment. Because of environmental restrictions the TBM method of construction was specified over the drill and blast. Furthermore, because of the high unconfined compressive strength of the rock (average 25,000 psi (172 MPa)), a full face TBM is used.

The high permeability of the rock zone underlying the invert required deep well dewatering during construction to draw the water level from 30 ft (9.1 m) above the crown of the tunnel to at least 2 ft (0.6 m) below the invert.

Initial support consists primarily of rock bolts 8 ft (2.4 m) long (4 by 4 ft (1.2 by 1.2 m) spacing is typical). Where such initial support is determined inadequate, steel ribs are used for support (W6 x 25 at 5 ft (1.5 m) centers typical). The contractor is responsible for determining the need for and location of the various initial supports.

For the final support a 12 in. (305 mm) thick cast-in-place unreinforced concrete lining is used. Its thickness was determined after careful analysis and due regard for construction and placement considerations.

Stations (Large Openings): The two station platform tunnels in rock are first excavated by the TBM forming twin 18 ft (5.5 m) diameter openings; these openings are then supported with rock bolts and finally enlarged by drill and blast to a flat-bottom elliptical shape 22 ft (6.7 m) high and 28 ft (8.5 m) wide. Rectangular cross passages connect the two platform tunnels, and an inclined escalator shaft connecting with one of these cross passages ascends between the platform tunnels to a cut-and-cover concourse structure just below street level. Initial support for the twin TBM openings is provided by rock bolts 8 ft (2.4 m) long with 4 by 4 ft (1.2 by 1.2 m) spacing. The station platform tunnels and connecting cross passages will be constructed first, and then the 30 deg inclined escalator shafts.

Rock loads for the final concrete lining were determined by evaluating the geotechnical data from borings, the RQD value and the effective width between the two closely spaced parallel tunnels. An average load of about 16 ft (4.9 m) of rock resulted after accounting for the rock bolts. The steel ribs in the inclined escalator shaft

were taken into account in designing the final concrete lining only when a predetermined pattern was specified in the design documents. The final concrete lining, 1 ft 6 in. (457 mm) thick, was designed to take full water pressure.

#### A.5.2 Analysis

An analysis was performed to determine the most cost effective thickness and reinforcement for the station linings. A linear finite element program called ANSYS was used. Rock and water pressure loads were applied separately and the results superimposed.

In most cases, the lining was modeled by using beam elements and the rock by radial and tangential springs when analyzing for rock loads and radial springs only when analyzing for water pressure. In the more complex areas, plane strain plate elements were used to model both the lining and rock.

The stiffness of radial springs used to represent the rock was determined from Dixon's formula, Dixon (1971):

$$K_r = \frac{E_m}{(1 + \nu_m)} \cdot b \cdot \phi,$$

where:

b = tunnel length that is represented by the spring

$\phi$  = angular segment (in a plane perpendicular to the tunnel axis) for which the rock (medium) is represented by a spring

$E_m$  = elastic modulus of the rock (medium)

$\nu_m$  = Poisson's ratio of the rock (medium)

The tangential spring stiffness was taken as 10 percent of the radial stiffness. The design value for bulk elastic modulus of the

rock was varied from 200 ksi (1380 MPa) to 4000 ksi (27,560 MPa), resulting in 20 percent difference in the magnitude of moments and shears in the lining.

#### A.5.3 Design and Performance Criteria

The ultimate strength method was used in designing the station linings and cross passages with a load factor of 1.7 for rock loads and 1.4 for water pressures. The rock loads at intersections were generally twice that estimated for adjacent tunnels. Material design strengths were 4,000 psi (27.6 MPa) for concrete and 60,000 psi (413.4 MPa) for reinforcing steel. The minimum concrete lining thickness was set at 12 in. (305 mm) to allow proper placement in those areas with steel ribs. The running tunnel lining and station platform tunnel arches were generally unreinforced, whereas the station cross passages, inverters and inclined escalator shafts were reinforced throughout. Crack control was provided in accordance with the 1977 ACI Code (#5 bars at 12 in. (305 mm) typical), in the reinforced sections. In the unreinforced areas, it was considered more cost effective to accept a minimum amount of seepage and design a permanent drainage system. To ensure good contact between the lining and to reduce inflows into the permanent drainage system, grouting was specified over the crown region.

In addition to the permanent drainage system (channel water to the track drains and pump it into the city's sewer system), water infiltration was controlled by instituting a grouting program to reduce post construction leakage.

Sulfate resistant cement was used to ensure the long-term integrity of the concrete lining.

A.6 Haley and Aldrich of N.Y., Rochester, NY

Designer Interviewed: Gary Brierley, Manager

A.6.1 Loading

SOFT GROUND: Not discussed.

ROCK

Running Tunnels: For initial support, the use of shotcrete and/or rock bolts is recommended. If initial support is used, it should be taken into account when determining the loads on the final lining, though its primary function is to make the load reaching the final lining uniform.

Steel ribs are not favored as initial support because they allow movement of the surrounding ground, provide limited shearing resistance with the surrounding ground and are expensive and time-consuming to install.

The type and magnitude of loads that will eventually reach the final lining is not considered to be a major design concern. A 6 to 8 in. (152 to 203 mm) unreinforced (except in pressure tunnels where reinforcement is necessary) concrete lining is considered to be adequate to support the loads induced in a rock tunnel up to 20 ft (6.1 m) in diameter. However, the need for demonstration of this adequacy is recognized and generally requires an analysis. Water loads should be added as a uniform pressure to the ground loads. Rock loads should be obtained from investigation of local geology and selecting reasonable rock wedges.

Stations (Large Openings): The loads for the design of linings for large underground openings in rock are illustrated by the design of the Porter Square Station in Cambridge, Massachusetts. The main station is a 500 ft (152.4 m) long 70 ft (21.3 m) wide by 45 ft (13.7 m) high mined chamber in moderately jointed hard argillite. The



station is located about 75 ft (23 m) below the ground surface under 30 ft (9.1 m) of rock cover. The ground water level is 30 ft (9.1 m) over the crown of the station. Fully grouted non-tensioned bolts were used for initial support. The final support consisted of shotcrete and W8 x 40 wide flange steel ribs at 5 ft (1.5 m) centers. Though this design does not involve the use of concrete itself the same philosophy would apply if, after the initial layer of shotcrete and steel ribs were installed, the remaining area of the lining cross-section was cast-in-place concrete. Rock loads were estimated from the most unfavorable rock wedges anticipated along the entire station site based on available subsurface and geologic information. These rock loads were used for design of the upper arched portion only; different criteria were employed for the walls.

Lining design for the arch was based primarily on the "concentrated" rock loadings and the "full width" loading of 4250 psf (203 kPa) in this case. "Concentrated" rock loadings were obtained from the combinations of bedding planes, joint sets and shear zones over the crown of the opening. "Full width" loading represents a combination of rock wedge loads spread uniformly over the entire width of the opening. The resulting lining was checked for the "maximum" rock loading, conceivably the overburden, with a reduced load factor (8800 psf (421 kPa) in this case).

The station will have a permanent ground water drainage system and a drained invert and thus the lining was not designed for water loads.

#### A.6.2 Analysis

If an analysis is to be performed (in the case of running tunnels in rock just to check the adequacy of the 6 to 8 in. (152 to 203 mm) lining) it should be kept as simple as possible. For instance, instead of using a nonlinear analysis to account for geometric and material nonlinearities, a linear one may be performed and the results adjusted

to account for the nonlinear effects. This, of course, presupposes that a relationship has been developed between the linear and the nonlinear case.

For the design of Porter Square Station, a linear frame analysis, using the "STRESS" program was used. The lining was modeled as a series of beam elements and the rock mass as a series of linear radial and tangential springs or bar elements connected to the joints between beam elements. Radial spring stiffnesses were based on the modulus of subgrade reaction assuming a laterally loaded area of one-third the opening's diameter. These springs were disconnected from the joints when they went into tension. Modulus of elasticity of the bar in compression was taken as  $1.0 \times 10^6$  psi (6,890 MPa) as determined from in situ plate load tests. The tangential spring modulus was taken as 50 percent of the radial spring modulus. Full moment transmission was provided at the joints, where the rock loads were applied.

To check the adequacy of the lining a moment-thrust interaction diagram was constructed according to the basic assumptions recommended by the ACI Code (318-71), but the basic material strengths were reduced rather than using  $\phi$  factors as specified in the Code. It was recommended that the envelope be constructed using  $(0.67) f'_c$  for the shotcrete and  $(0.9) f_y$  for the steel capacities.

The design procedure employed can then be outlined as follows:

- 1) Select lining dimensions
- 2) Construct thrust-moment diagram as previously recommended
- 3) Load lining with a "full width" or "concentrated" loading
- 4) Estimate thrusts and moments using a linear frame analysis

5) Multiply moments and thrust from the analysis at the critical sections by a load factor of 3 and plot the points on the moment-thrust interaction diagram. Check areas of high positive and high negative moments, for both loading conditions.

6) If a line of constant eccentricity ( $e = 3M/3T$ ) passing through the plotted point intersects the interaction envelope below the balance point, the balance point thrust will be the lining thrust capacity and  $3T$  must be less than the balance point thrust. If the line of constant eccentricity intersects the envelope above the balance point, the thrust at the point of intersection is the limiting thrust and  $3T$  must be less than the limiting thrust.

If the assumed lining geometry proved to be acceptable, steps 1 to 6 were repeated for all the different loading configurations. The final lining was also checked by applying the "maximum" rock loading, but applying a factor of 1.2 to the maximum moment and thrust.

#### A.6.3 Design and Performance Criteria

As a rule, "above-ground" specifications do not apply to "below-ground" projects. However, the existing construction and material codes should be examined to see which sections do apply.

With regard to serviceability of the Porter Square Station, the recommended load factors of 3.0 for "full width" loading and "concentrated" rock loading and of 1.2 for "maximum" rock loading should keep the lining stresses at service loads within acceptable levels to satisfy serviceability requirements such as cracking and deflections. Strength design for shear was satisfied by specifying W8 x 40 steel ribs at 5 ft (1.5 m) centers and a minimum shotcrete

thickness of 8 in. (203 mm) between the ribs. The design parameters recommended for the station chamber are given below:

Shotcrete: Maximum strain at extreme compression fiber = 0.003  
No tensile strength  
 $f'_c = 4,000$  psi (27.6 MPa, average strength of cored samples)  
Design strength =  $(0.67) f'_c$   
Minimum design thickness: behind ribs: 4 in. (102 mm)  
between ribs: 8 in. (203 mm)  
cover on ribs: 3 in. (76 mm)

Steel ribs:  $f_y = 36,000$  psi (248 MPa)  
Design yield strength =  $(0.9) f_y$

In Porter Square Station, leakage will be controlled by a permanent drainage system and a drained invert. Furthermore, the false architectural inner lining would provide an additional barrier for incoming water.

#### A.6.4 Comments

The major problem with the lining design lies with the fact that it is left to the structural engineer who might have considerable experience in the design of above-ground structures, but no tunnel design experience. The lining is treated as an above-ground structure and consequently a considerably thicker and more costly lining results. Thus, one of the owner's most crucial responsibilities may be the selection of his design team. The owner of the tunnel should demand expert assistance from a qualified tunnel design engineer and a qualified geotechnical consultant since the earliest stages of planning. Once a competent and experienced design team has been selected, the tunnel lining design philosophy can be described under three different headings:

- a) Interaction
- b) Arch action
- c) Design criteria

Interaction between the lining and the surrounding ground should be taken into account in the analysis. The ground mass supports the lining restraining it radially and resisting slip along the tunnel walls. Thus, interaction is recognized both in the radial and tangential directions. Tangential interaction causes the maximum thrust to occur near the crown, rather than toward the springline when no tangential interaction is considered. Higher thrust near the crown is beneficial for the concrete lining because it reduces or eliminates tensile stresses caused by higher positive moments in that region.

Arch action should be considered during the analysis of lining behavior. A curved structural element confined by the ground (i.e., lining) subjected to both moment and thrust has a broader range of stability than the same element subjected only to moment. Furthermore, in many cases the primary function of the lining is to provide continuity to the surrounding soil or rock mass so that the ground can maintain its full strength. To ignore such actions in lining design is overly conservative.

Today, the tunneling industry needs standard design criteria for different types of tunnels. Thus, excessively conservative local standards may be identified and steps taken to reduce the added cost.

Another major problem with regard to tunnel lining design in the U.S. is the existing contractual practices. The inflexibility of the design specifications and the allocation of risks do not provide room for modifications during construction. However, instead of trying to change the contractual methods in order to accommodate observational

approaches (such as the so called New Austrian Tunneling Method), the thrust of the effort should be directed toward improving the design procedures so that modification during construction is not needed. In the final analysis very few tunnels in the U.S.A. are built under squeezing ground conditions where observational approaches are more beneficial.

A.7 Harza Engineering, Chicago, IL

Designers Interviewed: Jan Veltrop, Vice President  
& Chief Engineer

Arvids Zagars, Vice President & Staff  
Civil Engineer

William Bristow, Vice President & Deputy  
Chief Engineer

William Shieh, Head Structural Analysis  
and Design Section

Jerry Hahn, Structural Design Division

Ed Cikanek, Chief Field Engineer-TARP

Harza is the engineering consultant to the Metropolitan Sanitary District of Greater Chicago for the Mainstream System of the Tunnel and Reservoir Plan (TARP). The Company is one of the Section Designers for the Washington, D.C. Metro and also serves other clients in the U.S.A. and abroad on projects related to the development of water resources.

TARP is designed to intercept the flow of combined sewers (sewers that carry both raw sewage and stormwater), when excessive stormwater runoff exceeds the capacity of the sewers, and store it until it can be pumped to treatment plants, purified and released into the waterways as clean water. When completed, TARP will consist of 131 miles (211 km) of deep tunnels, 251 vertical drop shafts, 4 pumping stations and 126,000 acre-ft (155 km<sup>2</sup>-m) of storage in 5 reservoirs. The portion of the TARP Mainstream System (which Harza designed) includes in part 29 miles (46.7 km) of 35 ft (10.7 m) diameter and 11.5 miles (18.5 km) of 32 ft (9.7 m) diameter machine bored tunnels in flat bedded sedimentary rocks (dolomites and shales) about 250 ft (76.2 m) below ground surface. This portion of the project is 75 percent complete and is expected to go into operation by 1985.

The METRO work involved approximately 4 miles (6.4 km) of single track, 16 ft 8 in. (5.1 m) finished diameter concrete lined, machine

bored running tunnels. Three subway stations, each arch-shaped, 58 ft (17.7 m) wide, 44 ft (13.4 m) high and 800 ft (243.8 m) long, varying from 60 to 110 ft (18.3 to 33.5 m) below the surface with inclined access tunnels, ventilation shafts and handicapped elevator shafts were also designed.

Harza has designed some 70 tunnels totaling approximately 50 miles (80.5 km) in length for hydroelectric projects. Additionally, five subsurface caverns for power stations have been designed and constructed. One cavern design that the Company was associated with in an advisory capacity is located 2100 ft (640 m) below the surface.

#### A.7.1 Design Loadings

##### A. Excavation (Initial) Support Systems in Rock

1. General. The design of excavation (initial) support systems usually consists of rock bolts and shotcrete or steel ribs, and is based on the rock conditions. Temporary support during construction is normally the responsibility of the contractor and would include any support considered necessary over and above the permanent support which is specified. For permanent support, rock bolts and shotcrete are generally favored over steel ribs; steel ribs are more likely to be used as the tunnel size increases, or in zones of weak rock. Rock bolt length and spacing is based on past experience, judgment and an assessment of rock conditions to be encountered.

2. Tunnels. Steel ribs for hydroelectric tunnels are usually designed according to the method described in Proctor and White (1968). Rock loadings are estimated on the basis of the spacing and orientation of the prevailing jointing and physical condition of the rock stratigraphy which the tunnel excavation is penetrating. The joint spacing, orientation and rock condition is interpreted from exploratory drill holes and exploratory adits. In those exceptional cases in which



rock jointing is well developed a combination of rock bolts and shotcrete is used as temporary support until the steel ribs can be placed and adequately blocked. A second layer of shotcrete is generally recommended then to be applied over and around the blocking and behind much of the top flange of the steel sets to fix the sets in place and minimize the potential for overbreak and fallout.

When rock bolts and shotcrete are used as the support, the length of rock bolt is determined as that necessary to maintain the natural bridging and arching action of the rock in the roof of the tunnel. This is, of course, influenced by the orientation of the joint sets and stratigraphy, but in general rock bolts of length equal to  $1/2$  the tunnel diameter are placed in the tunnel crown with the length reducing to  $1/3$  the tunnel diameter above the springline, with spacing in the order of 5 ft (1.5 m) each way.

3. Large Underground Caverns. The selection of the rock loads for the support of a large opening and the degree of conservatism in the selection of the loads depends upon the detail of the geologic investigations.

METRO Stations: Harza designed three subway stations of the Washington Metro (Zoo Park, Cleveland Park and Van Ness U.D.C.). They are arch-shaped openings 58 ft (17.7 m) wide, 44 ft (13.4 m) high and 800 ft (243.8 m) long, 60 to 110 ft (18.3 to 33.5 m) below ground surface, excavated in moderately jointed diorite and granitic gneiss with occasional chlorite schist bands and shear zones. Because of the requirement that the stations be located within the Right of Way of Connecticut Avenue, it was not possible to orient the stations in the most favorable direction to minimize rock loads and support requirements. Station excavation started with a small pilot tunnel at the crown and two running tunnel bores next to the bases of the arch in the first construction contract. The exposed rock in the pilot tunnel at the crown was supposed to be supported immediately by resin-grouted,

tensioned rock bolts. The remaining portion of the opening was excavated in the second construction contract by drill and blast in three lifts across the width of the station. The rock was supported immediately by 1-1/8 in. (29 mm) diameter resin-grouted, tensioned and untensioned rock bolts of varying length (5 to 25 ft (1.5 to 7.6 m)). An initial 2 in. (51 mm) layer of shotcrete was also applied on the rock surface. Steel ribs (W 14 x 119) with varying spacing, determined on the basis of exploratory drilling and inspection of the pilot and running tunnels, were installed in segments from the crown to the base of the arch and blocked with shotcrete. Finally the steel ribs were covered with 2 in. (51 mm) additional shotcrete. The steel ribs and shotcrete combination served both as the initial and the final support. The design rock loads were determined by studying the relative orientation of rock joints and shear zones with relation to the stations. Symmetric and asymmetric rock wedges were considered as well as full overburden loads. From the largest possible rock blocks horizontal and vertical components of pressure were determined assuming an angle of internal friction of the rock joints ( $\phi$ ) equal to 15 deg. Drainage of ground water was accomplished by installing 2-1/2 in. (63 mm) diameter, 10 ft (3.1 m) long PVC pipes into the rock for collecting the infiltrating water.

Underground Hydroelectric Power Stations: Harza has designed five underground power station caverns and advised on the design of one underground power station that is 2100 ft (640 m) below the surface. There is generally some flexibility in locating the powerhouse cavern and tailrace tunnels to take advantage of the most competent rock available and in orientating the caverns in the most favorable direction with respect to stratigraphy and jointing to attempt to minimize support requirements. Caverns for power stations range from 60 to 75 ft (18.3 to 23 m) across, 75 to 90 ft (23 to 27.5 m) in height, and the length is dependent upon the number of generating units installed.

Rockbolts, shotcrete and wire mesh are provided as temporary and permanent support of the cavern roof. The length of rock bolts provided is that necessary to maintain the natural rock arch in the roof.

#### B. Concrete Linings in Rock (Final Lining)

In general, the design of concrete linings is treated separately from the design of various rock support systems whose principal purpose is to either reinforce or support the rock mass surrounding the tunnel or shaft lining. However, in cases where the surrounding rock mass is of poor quality (i.e., in shear, fault zones, etc.) the lining may be designed to resist also rock loads in composite action with the supports (principally steel supports). Principally, concrete lining is provided in hydroelectric project tunnels to:

- (1) provide smooth surface to obtain greater hydraulic efficiency,
- (2) ensure watertightness where such is of concern and feasible to obtain with a concrete lining alone (plain concrete or reinforced), i.e., without the provision of steel liner,
- (3) protect the tunnel faces against erosion or progressive degradation during the life of the project if rock conditions so dictate and if other methods (such as shotcrete) are deemed inappropriate because of insufficient smoothness of the resulting surface (see item (1) above).

Concrete linings without steel liners are provided only where the depth of rock cover is more than 40 to 50 percent of the internal pressure head. Concrete encased steel liners are provided in regions of lesser rock cover and in weak rock zones. Concrete linings may be provided for relatively low heads, for small-diameter tunnels in good

rock, and for shallower rock covers provided the lining can be designed and reinforced to be watertight.

Tunnel linings for hydroelectric developments are designed, where appropriate, for:

- internal pressure effects
- external pressures.

Internal Pressure Design. The internal pressures consist of static pressure head and dynamic water hammer effects. Where the lining is provided only to obtain a smooth tunnel surface and where the surrounding mass is watertight and of sufficient cover, the internal pressures are resisted by the rock mass.

In tunnels surrounded by rock mass which is not watertight and which exhibits low modulus of deformation, the lining is designed to resist the internal pressures in combined action with the rock mass. In such cases the lining will require reinforcement for crack control.

External Pressure Design. External pressures on lining consist of pressures from existing ground water and/or of pressures developed from saturation of rock by reservoir water seeping under pressure through joints and fractures in the surrounding rock. The external pressures become effective during unwatering of the tunnel.

Circular linings of nominally provided thickness are able to resist external pressures developed under appreciably high heads because of the intimate contact between the rough excavated rock face and the lining after contact grouting. Excessive pressures can be expected to be relieved through shrinkage cracks.

Design that considers nonuniformly distributed pressures for bending moment effects is not usually warranted, because the

assumptions made in such analyses are incompatible with the actual behavior of the concrete lining which is virtually interlocked with the rock mass at the excavated face.

Noncircular sections, however, are avoided when high external pressures can be expected to develop during dewatering. The TARP tunnels' 12 in. (305 mm) thick circular unreinforced concrete lining was checked against full external hydrostatic load. In addition, the lining was investigated for an asymmetrical loading of a 5 ft by 5 ft by 10 ft (1.5 by 1.5 by 3.1 m) high rock block.

#### A.7.2 Analysis

##### A. Excavation (Initial) Support Systems

As defined previously, the determination of loadings and the design of support systems used for tunnels follows relatively conventional procedures. The analysis and design of excavation support systems for large underground caverns requires more detailed studies.

The STRUDL program was used in analyzing the three Washington subway stations, and the composite steel-shotcrete lining was modeled by plane frame elements 2 ft (0.6 m) in length. To simplify the analysis and modeling of the lining it was determined by calculations that the composite section could be reflected in the analysis by increasing the allowable steel stress from  $(0.75) f_y$  to  $(0.90) f_y$  to account for the presence of the shotcrete.

The passive support offered by the rock periphery was modeled by providing blocking points every 2 ft (0.6 m) on the outer face of the steel ribs. For purposes of analysis, imaginary steel compression members of equal length were considered hinged to the steel rib supports at the blocking points, to represent the deformability of the rock surface. The cross sectional area of the link was computed by

equating the outward deformation behind the blocking point to the deformation of an equivalent imaginary steel link 2 ft (0.6 m) long. The modulus of the rock was taken as 1,000,000 psi (6890 MPa) and 100,000 psi (689 MPa). The rock loads were derived by initially computing the vertical rock loads at the lining joints, resulting from the rock wedges considered; the joint loads were then resolved into radial and tangential components at the blocking points along the steel set. In the analysis, only the radial components were considered, the tangential component was assumed to be carried by the rock. Next, the radial components were resolved into vertical and horizontal joint loads. The ends of the arch at the base of the vertical legs were considered pinned, and were not allowed to move horizontally or vertically. In the region where inward deflections were determined by the initial computer run, the link was considered inactive and was not included in the subsequent computer runs. Runs were performed considering the effects of symmetric and asymmetric loadings and of the two different rock moduli. The design was termed satisfactory if the allowable steel stress of 32.4 ksi (223 MPa) was not exceeded in any of the runs.

In recent designs of large underground openings in rock, elastoplastic finite element analyses of the unlined opening are performed. The rock is modeled by two-dimensional plane strain elements or three-dimensional solid elements (isoparametric) whose stiffness is reduced after a certain amount of deformation has occurred. Rock bolts are modeled as truss elements. The purpose of these analyses is to determine the movements in the rock mass and around the opening and the formation of plastic zones under the influence of in-situ and excavation induced stresses. The horizontal in situ stresses are taken as 1/3 of the vertical unless more accurate in situ measurements are available. Normally this type of analysis is performed to check the design assumptions rather than to serve as a design tool by itself.

## B. Concrete Linings (Final Lining)

The purpose of the concrete linings and the procedure for analyzing them for either internal or external design pressures has been defined previously.

### A.7.3 Design and Performance Criteria

Allowable stress design is used. The minimum concrete lining thickness is generally set at 12 in. (305 mm), for ease in concrete placement.

Linings for tunnels in rock are reinforced only at intersections, areas of weak geologic zones (i.e., shear zones) where bridge action is needed and in pressurized tunnels when the overburden cover in feet is less than 50 percent of the internal pressure in psi. Reinforcement, when provided, is placed only in the inside face of the tunnel. The longitudinal reinforcement is placed near the lining face so as to minimize the exposure of transverse reinforcement to flow in case concrete erosion has taken place. Exposure of the transverse reinforcement is conducive to aggravate concrete erosion. In general, concrete linings and shafts for hydroelectric developments are unreinforced and cracking resulting from shrinkage and temperature effects is accepted providing the surrounding rock mass is reasonably watertight. Nominal reinforcement is, however, provided in areas upstream of steel liners to effect transition from steel lined to the non-reinforced concrete zone, in shaft elbows, bifurcations, at portals and in geologically disturbed zones of rock mass.

In transportation tunnels, watertightness over the crown region is desirable. Leakage control is achieved by grouting around the opening and then draining the tunnel in a controlled manner through weep holes if necessary. In areas of high external water pressure, anchoring by rock bolts of the concrete lining to the rock mass is also recommended

to reduce the length of the "free span." Anchoring is particularly useful in non-circular shaped tunnels. Cracking is permitted as long as it does not violate the leakage criteria.

Concrete linings can be placed either with vertical construction joints or in long continuous pours with sloping face joints. Except where crack control for watertightness is required, the latter method is more economical than the former. Linings with vertical joints require water stops in such joints only when the lining is designed for crack control. In tight rock, no water stops are needed.

The concrete casting sequence is not prespecified. In the TARP tunnels for instance, one contractor requested permission and was allowed to cast the upper portion of the concrete lining first by anchoring it to the rock mass every 10 ft (3.1 m) near the bottom of the pour. The invert will be cast later after the entire tunnel has been excavated. This was done so that the train rail could stay in place and the traffic of muck cars could continue uninterrupted through the lining and form without inhibiting the excavation process. Removal of forms is recommended at 10 to 12 hrs after casting or when the concrete has reached a strength of more than 500 psi (3.4 MPa).

#### A.7.4 Comments

Concrete lining costs continue to escalate relative to the excavation costs because excavation techniques become more and more cost effective, whereas concrete lining placement techniques have not. It is very difficult to define the actual lining costs since they depend so much on the site conditions and the efficiency of the construction. However, ratios of lining to excavation costs for certain tunnel diameters, lining thicknesses and excavation methods are given below. These figures illustrate the importance of trying to improve design and construction of concrete linings, as they are such a major cost item in a tunneling project:



10 ft (3.1 m) I.D. - Drill and Shoot - 12 in. (305 mm) nominal lining thickness; lining is 80-90% of excavation cost

20 ft (6.1 m) I.D. - Drill and Shoot - 12 in. (305 mm) nominal lining thickness; lining is 40-50% of excavation cost

13 ft (4 m) I.D. - TBM excavated - 12 in. (305 mm) nominal lining thickness; lining is 30-35% of excavation cost

32 ft (9.8 m) I.D. - TBM excavated - 12 in. (305 mm) nominal lining thickness; lining is 25-30% of excavation cost

It is obvious that a change in lining thickness would give other ratios. These figures are for an unreinforced lining; inclusion of reinforcement will further increase the lining cost.

A.8 Jacobs Associates, San Francisco, CA

Designer Interviewed: James Wilton, President

This firm is primarily working with contractors in developing designs for tunnel projects whose support is not prespecified by the owner.

A.8.1 Loading

SOFT GROUND

Precast Segmented Linings: Not discussed.

Cast-in-Place Monolithic Linings: For initial support loads, a portion of the overburden pressure is applied to the crown and invert. The magnitude of this pressure depends on the type of ground and the diameter of tunnel opening. The maximum value of side pressure is the passive earth pressure (i.e., the coefficient of the passive earth pressure times the overburden pressure at that depth).

The final concrete lining is usually designed for the full overburden pressure. Limited arching and thus reduced design loads is recognized if the overburden depth is more than 80 ft (24.4 m) from the crown of the tunnel. The side pressure value is between the at rest and passive earth pressure values but normally greater than that used in the design of the initial support system.

ROCK

Running Tunnels: For initial support Terzaghi's loads described by Proctor and White (1968) or the RSR (Rock Structure Rating) concept described by Wickham, et al. (1974) are used. In swelling ground the circular tunnel shape is favored, with rock bolt presupport; the ground is then allowed to expand before the final support is installed.

The initial support is not taken into account when designing the final concrete lining. In essence, the final lining is designed for the same loads as the initial support except in the case of swelling ground where the loads on the final lining might be even higher. The final concrete lining is designed for thrust alone, since it is assumed that the combination of active and passive rock loads result in an almost uniform all-around rock pressure. In a horseshoe shaped opening with sharp angles and a flat invert rock bolts are used to stabilize the opening and thus eliminate the bending moments in the vertical walls of the final concrete lining.

In pressure tunnels, the final concrete lining is reinforced to take internal pressures only if the overburden is less than about 60 percent of the internal pressure.

To accommodate external water loads, either the ground around the rock opening is grouted to prevent the water from reaching the lining or a drain system is installed to relieve the hydrostatic pressures.

Stations (Large Openings): Not discussed.

#### A.8.2 Analysis

Final concrete linings in rock tunnels are designed for thrust only. For soft ground tunnels, the combination of loads are applied on the final lining as described in Section A.8.1 and the resulting moments are computed. In other instances, the design moments are estimated by allowing the lining to undergo a prespecified amount of deformation. The amount of allowable deformation is usually a function of the tunnel diameter.

In the recent design of initial support for Section N-1 of the San Francisco waste water tunnel system, ground-lining interaction was considered. Section N-1 is a 500 ft (152.4 m) long, 50 ft (15.2 m)

deep, 9 ft (2.7 m) finished diameter tunnel driven through soft shales and loose water-bearing sands. The relative stiffness of the lining with respect to the ground was determined as described in Peck, Hendron, and Mohraz (1972). The compressibility ratio, a measure of the extensional stiffness of the medium relative to the lining, is related to the maximum thrust in the lining section. The flexibility ratio, a measure of the flexural stiffness of the medium relative to the lining is related to the maximum moment in the lining. These values of the maximum thrust and maximum moment, multiplied by an appropriate safety factor, are then used for the design of the support system. In this case, for an average modulus of elasticity of 4,000 psi (27.5 MPa) for the soil, the analysis resulted in an initial support consisting of W6 x 19 ribs at 5 ft (1.5 m) centers with 2 in. (51 mm) timber lagging.

#### A.8.3 Design and Performance Criteria

The ultimate strength procedure is used in the lining design, with a recommended concrete strength of 4,000 psi (27.5 MPa) for cast-in-place linings and 5,000 psi (34.5 MPa) for shotcrete linings. The minimum concrete lining thickness is set at 8 in. (203 mm) for an unreinforced cast-in-place lining.

Though reinforcement may not be required from a strength point of view, a nominal amount of 0.4 percent is considered a good measure to control cracking. To avoid landslides in areas close to the portals, the final concrete lining should be heavily reinforced in pressure tunnels. This will limit tension cracks in the lining, exfiltration of water and thus build up of the porewater pressures which in turn will reduce the factor of safety of the slope. In addition to other guidelines, at least 5 tunnel diameters of cover are recommended for pressure tunnels running parallel to sloping ground surfaces.

Allowable leakage should be specified in terms of pounds (kg) of water per minute per linear foot (m) and is a function of the type of tunnel.

Grouting is recommended between the final concrete lining and the surrounding ground to ensure good contact. However, before casting the final concrete lining the bottom of the tunnel should be relatively clean from muck and about 50 percent of the timber lagging should be removed.

#### A.8.4 Comments

Small design firms do not have the resources to develop new recommendations for tunnel lining design. They usually adopt or modify the ones initiated by the larger organizations such as WMATA (Washington Metropolitan Area Transit Authority), NYCTA (New York City Transit Authority), and BART (Bay Area Rapid Transit).

A.9 Jenny Engineering Corporation, South Orange, NJ  
Milwaukee, WI

Designers Interviewed: Prakash Donde, Structural Engineer  
Lloyd Monroe, Vice President

This firm is involved primarily with the design of smaller diameter sewer tunnels.

#### A.9.1 Loading

##### SOFT GROUND

Precast Segmented Linings: The lining is designed for the full overburden pressure applied uniformly at the crown over the width of the tunnel. An equal and opposite reaction is applied at the invert. Side pressures are applied on the sides of the lining using a coefficient of at rest lateral earth pressure  $K$  so that:

$$P_h = K \cdot P_v$$

where

$P_v$  = vertical earth pressure at that depth, using the submerged soil unit weight when applicable

$K$  = coefficient of at rest lateral earth pressure

$P_h$  = horizontal earth pressure at that depth

The value of coefficient of lateral earth pressure is related to the angle of shearing resistance of the soil (determined from uniaxial or triaxial shear tests) and to the degree of overconsolidation (determined from past experience in the area and by reviewing the literature on the regional geology). Additional interaction between the lining and ground due to deformation of the lining is taken into account by considering the deformation modulus of the soil, as explained in Section A.9.2. Adequacy of the concrete segments to

withstand jacking stresses is also checked. External hydrostatic pressures are added to the ground loads.

Live loads are considered only if the crown of the tunnel is within 10 to 15 ft (3.1 to 4.6 m) from the ground surface. Secondary linings, often cast inside the segmented one for hydraulic reasons, are not designed to take any loads except in the case that internal water pressures might exist. The secondary lining is then reinforced adequately to resist the difference between the internal and overburden pressures.

Cast-in-Place Monolithic Linings: Temporary support usually consists of steel ribs and timber lagging or of steel liner plates with a monolithic lining cast within. The same design philosophy is applied to these initial supports as for segmented linings with one exception; when applying the active ground loads at the crown and invert, they are reduced from the full overburden loads. This reduction is justified by accounting for the shearing resistance of the column of soil over the crown of the tunnel. As excavation of the tunnel takes place, this column of soil tends to displace downward and shearing resistance is mobilized. The magnitude of the shearing resistance and thus the magnitude of the reduction of full overburden pressures depends on the characteristics of the soil. For a clayey material the shearing resistance will be a function of the undrained shear strength whereas for a granular material a function of the angle of internal friction.

This arching allowance is permitted in designing the final lining also, provided that the final cast-in-place concrete lining will be installed within a short period (about 3 days) after installation of the initial support. Otherwise, the final concrete lining is designed for the full overburden.

## ROCK

Running Tunnels: For the design of initial support in good quality rock, rock bolts are installed so that they will form a rock arch around the opening which can sustain the ground loads. To account for fractures and discontinuities in the rock mass, the effective modulus of elasticity of the rock arch is taken as one-fifth of the laboratory value. In horseshoe shaped tunnels in bad quality rock steel ribs and Terzaghi's rock loads, described in Proctor and White (1968), are used.

The final concrete lining is not designed to take any ground loads, other than the water pressure.

Stations (Large Openings): Not discussed.

### A.9.2 Analysis

A computer program is used for analysis of the ground-lining system that assumes linear stress-strain behavior of the materials. The ground is modeled by a series of two-force bar elements attached radially to the lining by a pin connection. The number of elements used depends on the size of the tunnel. The properties of the bar elements are obtained by considering the deformation modulus of the soil and the tributary area of each spring. Bar elements that go into tension are released.

The lining is modeled as a series of beam elements whose properties depend on the shape and the material of the lining. The transformed reinforced concrete section analysis is used for the beam element properties.

In the case of a segmented lining the joints are modeled by reducing the bending stiffness of the lining to almost zero in the



region where a physical joint exists. A joint is always placed at the crown, where bending is high and the presence of the joint will be more beneficial in reducing cracking and redistributing moments.

Loading on the lining is applied as described in Section A.9.1. All loadings are represented as concentrated loads on the nodes based on the tributary areas for the joint.

Because of the uncertainty in determining a value for the at rest earth pressure coefficient and because of the great influence of the value of the side pressure on the overall behavior of the lining, analyses are performed using different estimated values of side pressure. The interpretation of the analysis results and the writing of the design specifications are done more conservatively when the estimated value of the side pressures is lower.

### A.9.3 Design and Performance Criteria

Working stress and ultimate strength methods are used, depending on the owner's criteria. The desired compressive strengths for concrete are 4,000 psi (27.5 MPa) for monolithic linings and 5,000 to 7,000 psi (34.5 to 48.2 MPa) for segmented. The minimum design thickness for monolithic linings is set at 8 in. (203 mm) for construction reasons, plus 2 to 3 in. (51 to 76 mm) for alignment allowance. Deflection of the initial support is limited to 2.5 to 3.0 percent of the diameter of the opening. If the analysis indicates that higher deformations result, the lining should be stiffened.

Reinforcement is provided as dictated by the analysis. Usually the minimum amount specified by the ACI Code is provided, and it is normally placed in one layer near the inside face (#4 bars at 12 in. (305 mm) is typical), with the outside face reinforced only around the springline region. In pressure tunnels enough reinforcement is provided to resist the difference between the internal and overburden

pressures. To control width of cracking in the final concrete lining, the reinforcing steel stress under internal pressure is limited to 15 ksi (103.3 MPa). For sanitary applications the use of sulfate resistant cement is recommended.

To facilitate casting, the area of the lining over the crown is flattened. Construction joints are provided with a shear key and neoprene water stops.

The secondary lining, cast inside the segmented concrete linings for hydraulic purposes, is designed with minimum thickness and minimum amount of reinforcement. However, if internal pressures exist, then more reinforcement might be needed.

If compressed air is used during the excavation phase it should be left on until the concrete lining has reached the 28 day strength.

Stripping of the forms is specified once the concrete has reached 25 percent of its compressive strength or about 24 hours after casting.

#### A.9.4 Comments

In a recent invitation to bid for a 5 mile (8 km) long 6 ft (1.8 m) diameter sewer tunnel in Milwaukee, WI all the bidders preferred the steel ribs and timber option for initial support, even though other alternatives such as precast segments and steel plates were provided as well. This could be explained by the fact that U.S. contractors feel more comfortable with the steel ribs-timber lagging support system and furthermore, it is believed to be more economical than precast segments for depths up to 100 ft (30.5 m).

A.10 Leeds, Hill and Jewett, Inc., San Francisco, CA

Designer Interviewed: John Bischoff, Principal Engineer

A.10.1 Loading

SOFT GROUND: Not discussed.

ROCK

Running Tunnels: The magnitude of the loadings developing on the lining of a rock tunnel is influenced by a number of factors, including the size of the tunnel, the strength and physical characteristics of the rock mass, and the stresses developing in the rock subsequent to excavation. Other factors also enter in. For example, the structure of the rock mass often plays a significant role in the development of these loadings. Major discontinuities present in the rock mass (i.e., shears, joints, etc.), form rock wedges which, in turn, may load the lining both in the crown and the sidewalls of the tunnel. To check for the possibility of this condition, extensive surface investigations are performed along the alignment of the tunnel, as part of the overall geologic investigations. Detail line surveys of existing rock outcrops are made to develop stereoplots of the measured discontinuities which enable the frequency and orientation of the discontinuities in the rock mass to be properly assessed. Oriented cores are sometimes used as well.

Once geologic investigations have been completed, and the rock mass has been classified, initial or primary tunnel stabilization systems can be designed using as a guide several different methods. Assessments of stabilization requirements based on estimates of rock loads, using methods such as those devised by Terzaghi and described in Proctor and White (1968), or classification systems based on observation, such as have been proposed by Bieniawski (1979) and Barton (1974, 1976), have proven reasonable. Experience gained from other tunnels driven in similar ground under similar conditions has also proven to be quite helpful in design. Primary stabilization usually

consists of rock reinforcement, including patterned rock bolts, shotcrete (reinforced with wire mesh), spiling and grouting. Steel sets in combination with rock reinforcement have also been used successfully, depending on ground conditions.

It is assumed that the rock mass surrounding the opening is fully stabilized by the time the final concrete lining is installed and, thus, the final lining generally is not designed to take ground loads. Depending on the purpose of the tunnel, that is, whether it is a roadway tunnel, sewer, etc., the primary function of the lining may be to prevent infiltration of ground water or to provide an architecturally finished tunnel surface.

If the ground water pressures are expected to be large, a system of drains or collector pipes is used to help relieve the hydrostatic pressures on the final lining. In planning such a system, the possibility of blockage of the drains should be investigated. Alternatively, if the anticipated water pressures are small, a drainage system may not be needed, and the final concrete lining is designed for the full hydrostatic pressure. It should be recognized that leakage through a concrete lining cannot be entirely eliminated, and that provisions should be made to intercept this leakage. The specifications should set a reasonable limit for the quantity of infiltration flows that will be allowed.

Stations (Large Openings): Not discussed.

#### A.10.2 Analysis

Closed-form elastic analyses for openings in a semi-infinite elastic medium are performed as a check for stress concentrations around the tunnel opening under the influence of in situ stresses. Finite element analysis methods may also be employed providing that the rock mass elastic properties and structure can be reasonably defined.

Such analyses are often useful for parametric and sensitivity studies. For rock reinforcement system design, arch theory calculation techniques can be used, if reliable test data relating to the shear strength of the jointed rock mass is available.

#### A.10.3 Design and Performance Criteria

Design specifications should be clearly written and should be enforced by close supervision during the construction stage. The minimum design thickness for a reinforced concrete final lining is that which can be reasonably constructed. A 12 in. (305 mm) lining thickness is not unreasonable. It should be recognized that concrete linings crack, and careful monitoring of the tunnel is recommended to determine whether observed cracks are shrinkage or stress induced. Allowable tolerances for cracking should be included in the specifications, and methods for treating cracks should also be specified.

Reinforcement of the final lining is usually minimal, primarily for shrinkage control. Bending moments should be included to handle localized bending only, such as that caused by zones of loosened rock. Large bending moments usually do not develop, because of the rigidity of the rock mass compared to the more flexible lining.

The spacing of construction joints depends to a large extent on the construction methods employed for casting the concrete. Sloped joints provide better protection against leakage than do vertical joints, and should be used if possible.

A.11 New York City Transit Authority, NY

Designers Interviewed: Mel Oberter, Deputy Chief Engineer,  
Civil Engineering and Architectural  
Division  
Abe Blumberg, Administrative Structural  
Engineer  
Richard Mitchell, Administrative  
Structural Engineer

The New York City Transit System opened in 1904 with 9.3 route miles (15 Km) of subway in lower Manhattan. Today the system has 230 route miles (370 Km), more than half underground, and 458 stations, Ziegler and Loshinsky (1979). Design of the New York subway tunnels has been evolving with time. The design philosophy described here primarily reflects the one used in the recent route 131-A (section 5A) extension, consisting of 1240 ft (378 m) of rock tunnel along 63rd Street from Park Avenue to 3rd Avenue. The drill and blast method is being used to construct a four track double level subway (two in the lower and two in the upper level) with a horseshoe configuration of about 48 ft (14.6 m) high by 58 ft (17.7 m) wide. The rise in the middle of the arch is usually 0.25 to 0.28 the width of the opening.

Two 18 by 18 ft (5.5 by 5.5 m) drifts were excavated first at the base of the tunnel opening, for the entire length of the tunnel. Then the sides of the entire height were excavated to permit the vertical initial steel posts to be installed. Then the top arch was opened up to permit completion of the blocked steel rib support. Finally, the center rock core was removed. The section includes 900 ft (274 m) of cut and cover construction to accommodate the two-level platforms for the Lexington Avenue Station. Rock in this area is very good quality schist and gneiss varying from granite-like at some locations to shistose at others; foliation is nearly vertical. Average depth to the lower track in the structures is 130 ft (39.6 m) below street level and almost entirely below the water table.

The rock cover varies between 15 ft (4.6 m) to 65 ft (19.8 m). Additional complications were introduced by the need to tunnel and support two operating railroads.

Construction started in 1976 and the section is expected to be completed in mid-1982.

#### A.11.1 Loading

SOFT GROUND: Not discussed.

ROCK

Running Tunnels: Because of the size of the tunnels and for purposes of this study, the design philosophy for running tunnels could easily be applied to stations (larger openings) in rock.

The Rock Quality Designation (RQD) value is used in determining the magnitude of rock loads in the following way:

RQD > 85% use  $(0.35) B$

40% < RQD < 85% use  $(0.5) B$

RQD < 40% use full overburden

where:  $B$  = width of tunnel opening

$\gamma$  = rock unit weight.

The minimum permitted rock cover is 10 ft (3.1 m). Steel ribs (with typical spacing of 2.5 to 5 ft (0.8 to 1.5 m)) are primarily used for initial support. They are designed by a computerized program based on the method outlined in Rock Tunneling with Steel Supports by Proctor & White (1968).

The New York City Transit Authority has been aware of the fact that the loading on the initial tunnel supports outlined above may be conservative particularly if the support installation closely follows the tunnel excavation. An instrumentation program was undertaken on an

earlier tunnel section along the same route involving the initial steel tunnel supports, rock bolts and the final concrete lining. The instrumentation data obtained on the stresses indicated less than 50 percent of the design load on the initial tunnel supports. This enabled the Authority designers to increase the permissible stresses in the tunnel supports for subsequent tunnel sections thereby reducing the size of the steel members used in the tunnel ribs.

Rock bolts, with a minimum length of 10 ft (3.1 m) are used as required to support loose rock wedges between the steel ribs. Shotcrete is only used to provide blocking for the steel ribs. The same rock loads are used for design of the initial and the final support; the initial support is not considered when designing the final concrete lining for the following reasons:

a) Rusting in the long run will most likely destroy the initial support (steel ribs or rock bolts).

b) Steel ribs get distorted during their installation and thus their structural adequacy cannot be assured.

c) Steel ribs may occasionally not be placed at the specified location.

d) Tunnels are under city streets sometimes extending from Building Line to Building Line and must last for an indefinite life. Site location thereby dictates the degree of conservatism.

Hydrostatic loads, applied perpendicular to the permanent lining surface, are superimposed on the ground loads when designing for the final concrete lining. If the RQD value is greater than 85 percent, half of the hydrostatic load is used, whereas if the RQD value is less than 85 percent, the full hydrostatic load is used. Dead load is considered to be the weight of the lining plus the overbreak backfilled



with concrete applied vertically. Live loads are taken into account if the total overburden is less than 20 ft (6.1 m).

Stations (Large Openings): The one station included in the 131-A (section 5A) extension was excavated by the cut and cover method.

#### A.11.2 Analysis

The permanent (final) concrete lining for the horseshoe section is analyzed taking rib shortening and arch deformation into account and programmed by finite element linear elastic analysis. The steel ribs and the concrete between them are not considered when computing the capacity of the concrete lining. "Net structure" is considered the section between the inside surface of the steel ribs to the inside surface of the concrete lining.

Rock loads are applied vertically over the crown of the tunnel. The magnitude of uniform rock load is selected by following the guidelines described in Section A.11.1. However, for analysis purposes in order to check the effects of asymmetric and symmetric loadings, the rock load is applied within the 3/8 portion of one side adjacent to the center line and alternatively within the center half of the crown section. The rock mass on the sides of the tunnel opening is accounted for by not allowing the lining walls to move outward. Hydrostatic loads are applied uniformly around the surface of the lining.

The base of the arch is modeled as fixed and hinged connections. Also the structure is analyzed with a hinge and without a hinge where the arched roof portion and the straight walls meet. An envelope of maximum stress around the lining is then constructed to include both fixed and hinged conditions. This stress envelope is used as the basis for design.

### A.11.3 Design and Performance Criteria

Working stress design procedures, based on the provisions of the ACI Code (318-63), are used. However, NYCTA used 55 psi (379 kPa) as allowable tension and  $(0.25) f'_c$  on full bearing as allowable compression limits. The compressive strength of the concrete varies as to needs.

The minimum concrete lining thickness is set at 9 in. (229 mm) for circular tunnels and 12 in. (305 mm) for horseshoe tunnels. In the 63rd Street extension, epoxy coated reinforcing steel bars have been used. Unreinforced concrete sections are favored, because of concerns over rusting of the steel bars and creation of leakage paths through the lining.

Cracking is not allowed except on the inside faces of the vertical walls; since leakage is not allowed either, a grouting program is at hand to treat cracks as they appear and to prevent leakage. Vertical construction joints are provided every 30 ft (9.1 m) to control shrinkage in the concrete. Concrete form stripping time is specified at 24 hours after casting. The bases of the arch are cast first followed by the invert, the straight walls and then the crown.

### A.11.4 Comments

The basic rationale behind the design philosophy used in the New York City Subways was that the tunnels ought to be as maintenance free as possible, since the design life of the system is for an indefinite time.

A.12 Parsons-Brinckerhoff, Inc., New York City, NY

Designers Interviewed: Tom Kuesel, Sr. Vice President, P.E.

Dan Wallace, Structural Engineer

Bill Daly, Geotechnical Engineer

William Hansmire, Geotechnical Engineer

A.12.1 Loading

SOFT GROUND

Precast Segmented Linings: The principal loads on segmented linings are the longitudinal forces required to shove the shield and normally they dictate the design of the segments. In addition, the adequacy of the lining to resist grouting pressures, required to establish good contact between the lining and the ground, should be checked. Once construction and handling loads have been accounted for, the influence of permanent ground loads on lining performance is usually of secondary importance. Linings that have been selected on the basis of the above criteria may be analyzed for their behavior under certain assumed ground loads but they are rarely designed for such loads, Kuesel (1979).

Cast-in-Place Monolithic Linings: Generally the gross dimensions of the lining will be determined by practical construction requirements. However, in exceptional cases such as very soft, squeezing or swelling ground, the thickness of the tunnel lining may be determined by consideration of ground loads. Also in water conveyance tunnels, where the internal water pressure may exceed the ground water pressure, the thickness and reinforcing of the lining will be determined by the internal water pressure.

If an initial lining is used its function is to deform and redistribute the ground loads thus stabilizing the opening before the final concrete lining is installed. The minimum practical thickness of the final concrete linings that will provide clearance for concrete

placement will almost invariably be sufficient to support the ground loads. Initial and final linings need not be designed for the same loads. However, the usual legal/contractual arrangements say that the contractor is responsible for the initial support and the owner for the final concrete lining, which results in the design of both systems for the same loads. Where steel ribs are used for initial support for instance, and later they are embedded in the final concrete lining, they should be counted on as part of the permanent support system and thus able to carry loads during the life of the structure.

The greatest structural danger to a lining is not high ground loads or nonuniform loading but absence of passive support. Properly designed and constructed tunnel linings derive great strength from deforming to mobilize passive pressures from the surrounding ground, thereby smoothing nonuniform loading. The absence of this passive resistance reduces the load carrying capacity of the lining-ground system and induces large deformations in the lining which may result in excessive cracking and leakage.

## ROCK

Running Tunnels: Lining thickness for running tunnels in rock is usually determined by nonstructural considerations like function of the tunnel, leakage considerations, and minimum constructable thickness. The method of construction has a major affect on the initial support requirements, which in turn influence the final lining. Tunnel boring machines, for example, reduce the requirements for temporary support and make the single-stage segmented linings more attractive.

Stations (Large Openings): Ground loads are much more important in large openings in rock than in running tunnels, unless the rock is of excellent quality. Whether ground loads must be considered depends on the local geology and construction and functional requirements. In Atlanta's Peachtree Center Station, for instance, described by Kuesel

and King (1979), a 770 ft (235 m) long by 60 ft (18 m) wide and a maximum height of 45 ft (14 m) opening in very good quality biotite gneiss and hornblende, the final concrete lining has been totally abolished from a large portion of the walls. The natural rock with the rock dowels used for initial support will serve both structural and architectural purposes. The nominal 16 in. (400 mm) thick final concrete lining, specified over the crown portion of the station, was designed for the grouting pressures only and was included primarily as insurance against possible rock falls in the future.

#### A.12.2 Analysis

For an analysis to be meaningful the processes and sequence of construction need to be realistically considered. Because of great difficulties in determining the parameters and of modeling the entire construction sequence, practical experience offers a surer guide than abstract theory in determining the adequacy of a support system.

Provided that the void between the lining and the ground is properly filled, the lining will be able to conform to the ground distortion without undergoing unrestrained ring bending. The computation of bending stresses in tunnel linings is usually a waste of time, because the assumptions on which the calculations are based usually bear no resemblance to the actual conditions in the tunnel. Nevertheless, all linings in rock and in soft ground should have a minimum bending strength to resist stochastic point loads. Specifically, concrete tunnel linings should be able to resist in axial compression the average effective overburden and the ground water loads that are imposed after the lining is installed. Concrete linings should also have a bending capacity equivalent to a thrust eccentricity of 1 to 4 percent of the radius of the opening. The ability to withstand construction loads should also be checked in segmented concrete linings.

In essence, the purpose of the analysis is to check whether the thickness and reinforcement determined from other considerations are adequate to support ground loads.

#### A.12.3 Design and Performance Criteria

The minimum suggested concrete lining thickness is set at 12 in. (300 mm) inside the A-line, when no steel ribs are used as initial support, and the same distance inside the ribs, when they are used. This is based on allowing sufficient space behind the reinforcing steel for concrete placement.

Leakage control is the most important performance criterion, since a "satisfactory lining" is one that does not leak. There are two ways to control leakage: 1) Intercept the water with drain pipes, collect it and pump it out, or 2) limit water infiltration or exfiltration from the tunnel. In the latter case, setting a requirement for a zero leakage tunnel is unrealistic, and a maintenance and sealing program should be available to handle unexpected leakage. Leakage paths usually lie at the location of steel ribs since they cause shrinkage cracking of the concrete lining. Cracking of the final concrete lining is allowed as long as it does not form leakage paths. The quantity of allowable leakage depends on the function of the tunnel with stricter requirements for highway tunnels.

The criterion for the design of initial supports should not be bending stress but ductility. The initial support should be able to absorb the imposed ground distortion without fracture.

The location of construction joints is determined by the pumping distance. Sloping joints, if properly cleaned before the next casting, are preferable.

A single layer of nominal steel reinforcement (#5 bars at 12 in. (300 mm) or #6 bars at 18 in. (450 mm)) near the inside face is considered a good investment in terms of keeping the lining from cracking and inhibiting concrete spalls from falling into the tunnel. For concrete linings in soft ground, both faces should be reinforced to ensure the required bending capacity of the lining. (Embedded steel ribs may serve as extrados reinforcing.)

Form stripping time is set at 24 hours or when the concrete reaches 15 to 40 percent of the design compressive strength, the higher percentage applying to the ceiling and the lower one to the walls of the lining.

If segmented concrete linings are used, bolting of the segments should be specified only in earthquake zones or in areas of ground water pressures to ensure the tightness of the joints.

A.13 Parsons Brinckerhoff/Tudor, Atlanta, GA

Designers Interviewed: Douglas J. Mansfield, Manager for  
Engineering

Zdenek Zachar, Structural Engineer

Perry M. Lin, Structural Engineer

Parsons Brinckerhoff/Tudor, a joint venture, is the general engineering consultant for the Metropolitan Atlanta Rapid Transit Authority's rail transit system. The majority of the system is at grade but it does include about one mile (1.6 km) of twin running tunnels and one mined (tunneled) station at Peachtree Center. Seven hundred feet of the tunneled portion is in soft ground, three hundred feet is in mixed face, and the rest is in rock. The 54 mile (87 km) system has nearly 12 miles (19.3 km) in operation at this time (October 1980).

A.13.1 Loading

SOFT GROUND: Not discussed. In the soft ground and mixed face tunneled portions no concrete lining was involved because prefabricated steel liner segments were used for both initial and final support.

ROCK

Running Tunnels: The 16 ft (4.9 m) high by 16 ft (4.9 m) wide horseshoe shaped rock tunnels were constructed by the drill and blast method. Rock in the area is moderately jointed gneiss with RQD values ranging from 80 to 90 percent and core recovery ratios close to 100 percent.

Initial support was provided by a system of rock dowels and post-tensioned rock bolts in fallout areas with spacing varying from 8 to 25 ft (2.4 to 7.6 m). The rock support design was based on RQD values and Deere's recommendations, Deere, et al. (1969). About one-half the rock tunneled portion was lined with 4 in. (102 mm) of shotcrete which serves as the final lining. In areas of high water



leakage and in the region of progressively weathered rock a final concrete lining, sometimes in combination with steel ribs, was used.

In stairways and escalatorways, where steel ribs were used for initial support, the final concrete lining-steel rib system was analyzed as a composite section by applying Terzaghi's loads over the crown region and a portion of the crown loads along the sides.

Stations (Large Openings): The station design philosophy reflects the procedure used in the design of the Peachtree Center Station by Parsons Brinckerhoff offices in New York and San Francisco and described in Kuesel and King (1979). The Station, 900 ft (274.3 m) long with a 58 ft (17.7 m) maximum width and 46 ft (14 m) maximum height lies in a massive gneiss formation with widely spaced joints. Of the 100 ft (30.5 m) of overburden, 50 ft (15.2 m) directly above the arched crown is good quality rock, 5 to 15 ft (1.5 to 4.6 m) is weathered rock, and 20 to 50 ft (6.1 to 15.2 m) is fill and sands. The Station was excavated in stages by drilling and blasting. Untensioned resin grouted rock dowels supplemented with tensioned and grouted rock bolts were used to stabilize the opening. The good quality of the rock in conjunction with the well coordinated excavation and support sequence allowed major parts of the exposed rock walls to serve as the architectural finish material. The great economy resulting from this is obvious in the comparison of the bid prices per linear foot: \$15,100 for the station, \$12,800 for the twin shield driven soft ground and mixed face tunnels, and \$7,100 for the twin single track rock tunnels. The final concrete lining, installed only over the crown portion of the opening, was supported by abutment niches formed in the rock at the junction of the arched and straight portions of the opening. The primary purpose of the final concrete lining was to preclude the fall of small rocks that might dry out and spall between dowels. The principal design load was the pressure of contact grouting between the lining and the overlying rock, which was limited to 10 psi (69 kPa). The final lining thickness, controlled by placement

considerations, was 16 in. (406 mm) at the crown increasing to 24 in. (610 mm) at the abutments.

#### A.13.2 Analysis

For the analysis of the Peachtree Center Station, computer, manual, and judgmental analyses were used. The computer program used, JRCSTF, was developed at the University of California and is a finite element program with modeling capabilities for the rock joints and the rock bolts. The joints were activated or locked by altering their material properties. Parametric studies were run by using lower frictional values in the joints than indicated by the geotechnical data, hydrostatic stresses in the steeply dipping joints, high initial horizontal in situ stresses in the rock mass, and low friction and hydrostatic stresses in the flat-dipping joints.

Manual analyses included the design of steel ribs in escalator shafts by the Proctor and White method, Proctor and White (1968), and design of the concrete arch by varying the degree of fixity at the abutments between free and fixed and selecting an optimum condition.

Although computer and manual analyses were used, the final design decisions were reached by "intuitive design," "feel" for the conditions, and a great deal of engineering judgment.

#### A.13.3 Design and Performance Criteria

A minimum concrete lining thickness of 12 to 14 in. (305 to 356 mm) is recommended for running tunnels in areas where quality of rock is not suitable for less expensive protection (i.e., shotcrete). If the final concrete lining is not designed for structural support, a nominal amount of reinforcement in the inside face is recommended to ensure the long-term integrity of the concrete. If the final concrete lining is

used to provide structural support, then both faces should be reinforced as dictated by the analysis results.

For leakage control of tunnels in rock, a drainage system of pipes should be provided to collect infiltrating ground water. Vertical construction joints with water stops are recommended every 25 ft (7.6 m).

Concrete forms over the crown portion may be removed after the concrete has reached 50 percent of its 28 day design strength but no sooner than 72 hours. Forms from the walls may be removed after the concrete has reached 25 percent of its 28 day strength but no sooner than 24 hours.

A.14 Tudor Engineering Company, San Francisco, CA

Designers Interviewed: Don Rose, Project Manager  
Heinz Mueller, Supervising Engineer  
Richard Mayes, Structural Engineer

Tudor Engineering Company does not have a company-wide policy on concrete/shotcrete linings. Each project is designed by the staff assigned to the work and some individual variation exists within the firm. However, the following principles generally apply.

A.14.1 Loading

SOFT GROUND

Precast Segmented Linings: Instead of trying to predict ground loads a deflection criterion is established for the design of precast segments in soft ground. The lining must withstand a certain amount of deformation. The magnitude of allowable deformation will depend on the size and function of the tunnel. The adequacy of the lining should also be checked by evaluating its ability to withstand jacking and grouting stresses.

Cast-in-Place Monolithic Linings: Design and construction of the initial support is left to the contractor. Normally, the final concrete lining is not designed for any specific loads, because it is assumed that the opening has stabilized itself by the time the final lining is installed. If the tunnel is to be subjected to internal pressure the final lining should be designed to withstand them.

ROCK

Running Tunnels: Tunnel designs in rock can proceed logically as follows:

- a) Obtain representative rock samples.
- b) Classify rock based on jointing, weathering, etc.
- c) Calculate the load this rock will exert on tunnel.
- d) Design initial support for this rock load.
- e) Make a cost estimate of this tunnel support system.

The final concrete lining is not designed for any specific loads. For design of the initial support system (step d above), Tudor has made parametric studies for 10 to 30 ft (3 to 9.1 m) diameter tunnels using Terzaghi's method as described in Proctor and White (1968), and the formulas for rock load determination presented by Deere, et al. (1969), Wickham, et al. (1974), and Barton (1974, 1976). The findings of this study have been summarized by Rose, et al. (1980). The study was made with the Wickham and Barton methods assuming values for "reasonably good" and "reasonably poor" rock, "reasonably" referring to what an optimistic geologist and a pessimistic geologist might call the same rock. The study concluded that because Wickham and Barton have such a large number of input parameters, the spread of rock loads computed by "reasonably good" versus "reasonably poor" descriptions of the rock is too large. It also confirmed the conclusion reached by Einstein, et al. (1979), that Terzaghi's method is not conservative compared to other methods.

For rock load determination Tudor uses Terzaghi's classification without increasing the rock loads (in classes 4, 5, and 6) below the water table. This is in accordance with Brekke's (1968) observations that tunnels below the water table behave quite well and that Terzaghi's assumption that the water acts to increase the rock loads is conservative. Furthermore, all Terzaghi's loads are reduced by 20 percent in accordance with Deere's (1969) recommendations, since it is

well-known that Terzaghi's concept of a loose rock mass lying on the steel ribs is an extreme condition and it is not always going to develop. The resulting rock loads are used for designing steel ribs but may be applied where appropriate to other initial support systems.

By using shotcrete and/or rock bolts for instance, to prevent ravelling, very little force is required to hold the tunnel open safely. Thus, the rock load must be very low initially, and in fact, cannot be computed. Shotcrete works in spite of the fact that theoretically a thin 4 in. (102 mm) layer of irregular, rough "concrete" cannot act as an arch. Because of this, shotcrete lining design computations are not as clean and logical as those involving steel ribs.

A joint venture of Parsons-Brinckerhoff and Tudor designed a shotcrete lining as final support in a pair of running tunnels in the Atlanta subway system. In one of these tunnels, a lining of steel-fiber reinforced shotcrete was also installed for the first time in the U.S.A. However, these linings were not designed in the sense of rock load determination, analysis, lining dimensioning. The standard 4 in. (102 mm) thick shotcrete was applied to the rock to prevent ravelling and thus, to hold the tunnel open before a large rock load developed.

There is no need to design the final lining for full hydrostatic pressure. As Terzaghi showed in his work on the Chicago subway, all tunnels act as drains no matter how slight the amount of leakage. Therefore, it is assumed that the hydrostatic water load is reduced by drainage to a level that is not critical for lining designs; as a rule no calculations are made (involving soil permeability, etc.) for water pressure loading.

Excavation sequence and construction technique outweigh all other factors in their effect on the ground loads that actually occur.

However, it is considered essentially impossible to forecast them at the design stage with the exception of longitudinal thrust on shield driven tunnels and other standard construction/erection stresses. To account for this uncertainty, field inspection during construction by highly experienced personnel is heavily emphasized.

Stations (Large Openings): Use of the observational approach (coordinating excavation with support) is favored. The combination of rock bolts and shotcrete 4 to 6 in. (102 to 152 mm) thick will be adequate in most cases where the rock is sound. In these cases the need for a final cast-in-place concrete lining is debatable (see Atlanta's Peachtree Station, Kuesel and King (1979)).

#### A.14.2 Analysis

Several methods of analysis are available which may be based on loads or on allowable deflections of the lining. Common sense is also used. In other words, Tudor tries to avoid designing overconservative linings merely because some mathematical formulas suggest so. As lining computations for the BART system showed a decade ago, a deformed lining is not necessarily near dangerous collapse, but instead it redistributes the loads in new ways which are not always easy to compute or predict.

In the analysis, the initial support is taken into account when designing the final support and soil-structure interaction is included. There are finite element approaches that account for soil-structure interaction and they have been used occasionally. However, it is generally felt that the ground conditions will change often in a long tunnel and idealized finite element assumptions are unlikely to be valid. Furthermore, most finite element studies rely on in situ stress information which in fact, along a real tunnel, will vary considerably and are almost impossible to predict. Finite element solutions are usually employed in very uniform ground conditions.

#### A.14.3 Design and Performance Criteria

On each tunnel project the practical details, which will depend on the site and the function of the tunnel, will get the most attention. For instance, in precast segmented concrete linings, which Tudor has considered favorably for several tunnels still in the planning stage, the joints, bolts and water-stop details are critical. For cast-in-place concrete linings sloping or vertical joints may be used, depending on the function of the tunnel. Reinforcement is only favored in pressure tunnels close to the portal areas or where rock strength is insufficient.

The amount of acceptable leakage again will depend on the function of the tunnel, with transportation type tunnels requiring stricter criteria. The minimum concrete lining thickness is set at 8 in. (203 mm) for construction considerations. The ultimate strength design is favored, because an understanding of the failure mode will provide more insight into the behavior of the lining.

The concrete strength should be over 5,000 psi (34.5 MPa) for precast and over 3,000 psi (20.7 MPa) for cast-in-place linings. The time before form removal should not be less than 24 hours.

#### A.14.4 Comments

Tudor Engineering has initiated conversations with the Associated General Contractors (AGC) examining the possibility of applying the NATM (New Austrian Tunneling Method) in the U.S. West coast contractors were found reluctant to use NATM because of possible excessive interference by the engineer during construction, which would upset the construction cycle. Nevertheless, Tudor intends to try a modified version of NATM suitable to American conditions in future tunneling projects.



The potential use of the Bernold Method is also being investigated. Tudor routinely designs a system and then estimates its cost using a comprehensive contractor-style cost estimating system with all crews, equipment, supplies, land and rights-of-way, etc. included. It appears that some NATM-type designs are not as cost-effective in the U.S. as they are in Europe, because of different labor and contract practices. Today they are unsure of Bernold Method costs in the U.S.

Tudor's interest in cost estimating is very intense, and in some respects designs are selected by "cost estimate" to produce the least expensive design, regardless of the latest trends in the literature. On the other hand, active steps have been taken to promote serious consideration of NATM and Bernold Methods, where these appear to be cost effective, as might be the case in badly fractured Franciscan Formation and Monterey Formation rocks but not in California Sierra hard granitic rocks.

A.15 U.S. Army Corps of Engineers, Missouri River Division, Omaha,  
Nebraska

Designer Interviewed: Dan Hokens, Chief Engineer-  
Structures and Bridges Section

The U.S. Army Corps of Engineers is primarily involved with the design and construction of water conveyance tunnels.

A.15.1 Loading

SOFT GROUND: Not discussed.

ROCK

Running Tunnels: The main factors that determine the type and magnitude of rock loads are the local geology, size of opening and construction procedure. The type and nature of rock, the state of stress in the rock mass and the relative orientation of the tunnel axis with respect to the bedding and jointing patterns will determine the shape and size of rock blocks that in turn will load the lining. The stability of a tunnel lining through a particular rock formation tends to decrease as the tunnel size increases. It is suggested that the effect of size may be taken into account by adjusting the rock classification at a particular site. For example, the same rock that might be classified as moderately blocky and seamy for a 7 ft (2.1 m) diameter tunnel can be classified as very blocky and seamy for a 30 ft (9.1 m) diameter tunnel.

During construction care should be exercised in preserving the integrity of the rock around the opening, because it is the most effective load carrying member of the rock-lining system. Initial support should be installed immediately behind the tunnel face regardless of whether the support consists of rock bolts, shotcrete or steel sets. However, construction procedure normally requires that steel sets be placed after mucking is completed and at a sufficient distance from the face to prevent damage when the next round is

removed. Rock bolts and shotcrete can be installed from a muck pile when necessary. In this manner, further rock loosening is prevented or minimized and maximum advantage is taken of the rock's inherent ability to support itself. The volume of damaged rock due to excavation, that must be supported by the initial support, could be different by a factor of two depending on the excavation and initial support methods. The length and spacing of rock bolts are determined by the condition of the rock and the necessary strengthening required to create an intact rock arch of sufficient strength and thickness to support itself and any additional rock loads outside the arch.

For the determination of rock loads on steel ribs, the following methods are recommended in the Corps of Engineer's Manual (1978). If the depth of cover is less than 2.5 times the width of the opening, full overburden pressure (Szechy (1967)) should be used. For greater values of depth of cover Terzaghi's loads described in Proctor and White (1968), should be used. As an alternative Deere's (1969) support requirements, based on RQD, may be used for the latter case.

Eventually loads are transferred to the final concrete lining due to creep in the rock mass but the ribs will continue to support some load. It is suggested that the loads for the design of the final concrete lining should be taken as 50 to 100 percent of those used in the design of the steel ribs. The value of 50 percent would be more applicable to a tunnel driven in hard limestone, whereas the 100 percent value would be more appropriate for a tunnel driven in soft shale. If in addition to steel ribs, rock reinforcement or shotcrete or a combination of the two with sufficient strength and durability for long-term stability is used for initial support, smaller loads will develop on the final concrete lining. It is then recommended that the unbalanced vertical load for design of the final concrete lining be taken as 25 to 75 percent of that used for the design of steel ribs. The actual percentage will be determined by evaluation of the local geology and of in situ measurements during construction.

It is further recommended that rock loads for machine excavated tunnels be taken 25 percent lower than tunnels excavated by conventional drilling and blasting. If wood sets are used for initial support, then the same loads used to design the initial support are recommended for final supports also.

Concrete linings should be designed to resist external hydrostatic loads equal to the full ground water load in addition to the rock load. However, if the lining required to resist the combined load becomes unreasonably thick (over 3 ft (0.9 m)), hydrostatic pressure must be reduced by installing drains behind and through the lining or by constructing a separate drainage tunnel above the main tunnel.

Stations (Large Openings): Not discussed.

#### A.15.2 Analysis

Computation of moments in the concrete lining is performed by using Bougayeva's method described in Szechy (1967) based on the analysis of an elastically embedded ring. The coefficient of subgrade reaction (pressure per unit of deformation) is used to represent the reaction of the medium. Once bending moments have been calculated, the resulting stress in the concrete lining can be determined from linear beam theory.

The axial stress due to rock load, acting uniformly across the lining section is determined from:

$$f_w = \frac{w \cdot R_2}{R_2 - R_1}$$

where

$f$  = axial stress due to rock load  
 $w$  = uniform unit rock load on the lining

$R_2$  = radius to outer surface of lining  
 $R_1$  = radius to inner surface of lining

The combined stress acting on the concrete lining section due to rock load is then found by adding algebraically that due to axial load and that due to bending.

In order to get an estimate of the foundation modulus (coefficient of subgrade reaction) to be used in the analysis, the modulus of deformation of the rock (similar to the modulus of elasticity, but accounting for the geologic discontinuities in the rock mass) must be determined. Methods for estimating the modulus of deformation by large scale in situ tests are described in Stagg and Zienkiewicz (1978).

Once an estimate of the modulus of deformation is made, the foundation modulus can be estimated in the following way. The rock deformation due to a uniform internal pressure on the walls of an opening in an elastic medium

$$\Delta r_o = \frac{P \cdot R_2 (1 + \nu_R)}{E_R}$$

where

$p$  = internal pressure  
 $R_2$  = radius to excavated surface of opening  
 $\nu_R$  = Poisson's ratio of rock (if unknown, use  $\nu_R = 0.25$ )  
 $E_R$  = modulus of deformation for rock

If  $\Delta r_o$  is set equal to one inch, then the foundation modulus  $K$  can be calculated from:

$$p/\text{inch of deformation} = K = \frac{E_R}{R_2 (1 + \nu_R)}$$

It is noted that although errors are introduced by assuming that the rock mass is a continuum, the magnitude of error does not exceed the limits of accuracy of the method used to estimate the modulus of deformation of the rock.

It is recommended that the lining be designed to resist water loads (applied as a uniform load on the exterior concrete surface) alone, ground loads alone and the combined effects of ground and water loads. In pressure tunnels, if the internal pressure is higher than the overburden (especially near the portal area) there should be an additional steel lining inside the concrete lining.

Shear stresses should be considered for any tunnel shape which is not circular. In this instance the possibility of large blocks transmitting the load directly to the lining exists. Also, hydrostatic loads will develop shear stresses in the side walls. Consequently, the lining thickness should be adequate to resist the shear stresses created by this loading.

Dynamic analysis is not considered necessary because most well-designed tunnels in hard rock can withstand the dynamic effects of earthquakes.

#### A.15.3 Design and Performance Criteria

The working stress design method is used with design strengths of  $(0.45) f'_c$  for concrete and 20,000 psi (138 MPa) for 40,000 psi (276 MPa) steel. For high water velocity tunnels concrete with  $f'_c = 4,500$  psi (31 MPa) should be used, whereas for normal applications  $f'_c = 3,000$  psi (21 MPa) is adequate.

The minimum recommended concrete lining thickness, for concrete placing considerations, is set at 9 in. (229 mm). For 1.5 in. (38 mm)

maximum size aggregate, a 6 in. (152 mm) concrete placing pipe is recommended.

Concrete linings crack approximately every 10 ft. (3.1 m). Cracking cannot be eliminated but it can be controlled by placing continuous reinforcement, about 1/4 percent, near the inside face of the lining (#9 bars at 12 in. (305 mm) spacing is considered maximum). A 3 in. (76 mm) minimum concrete cover should be provided as a safeguard against corrosion of the bars.

Concreting is recommended after the entire tunnel is mined so that it will not interfere with the mucking operation. However, when poor rock or slaking is encountered concreting might follow soon after the excavation. The length of a tunnel monolith is controlled by limitations in concrete placing procedures and equipment. Reusable forms normally have lengths of 20 to 40 ft (6.1 to 12.2 m). The form stripping time is set at 16 hours after concreting.

A.16 Bureau of Reclamation, Denver, CO

Designers Interviewed: Paul Tilp, Head, Tunnels Section

Tim Smirnoff, Technical Specialist,  
Tunnels

Ken Schoeman, Unit Head in Tunnel Section

The Tunnels Section of the Bureau of Reclamation deals with the design of access and water conveyance tunnels in rock with typical inside diameter ranging from 7 to 28 ft (2.1 to 8.5 m) and length from 1 to 3 miles (1.6 to 4.8 km). Spillway and outlet type tunnels are designed by a different division (Dams Branch) within the Bureau of Reclamation and they are not included in this design summary. A few soft ground tunnels have been designed by the agency.

A total of 179 water conveyance tunnels (1,399,257 linear ft (426.5 km)), have been designed by this organization, 171 constructed and 8 under construction as of September 1979.

A.16.1 Loading

SOFT GROUND: Not discussed.

ROCK

Running Tunnels:

Cast-in-Place Monolithic Linings: Terzaghi's rock loads given in Proctor and White (1968) or procedures described by, Wickham, et al. (1974), Deere, et al. (1969), Barton (1974,1976), and Bieniawski (1976), are used in estimating the amount of initial support needed. The type and exact amount of initial support, the method of excavation and the shape of the excavated tunnel are the responsibility of the contractor, subject to approval by the designer. In most cases, steel ribs have been used as initial support. Occasionally, ungrouted rock bolts and rock anchors have been used as well. In the very few instances that shotcrete was used, it served primarily as protective



coating to prevent deterioration of exposed shales. Shotcrete was, however, used as initial support and final lining in 5 small water collection tunnels on the Fryingpan-Arkansas Project in Colorado. Steel liner plates are sometimes used adjacent to tunnel portals.

Squeezing ground conditions have been handled by overmining around the steel ribs and allowing the ground to move inward. In squeezing ground conditions a cost-plus or a negotiated contract is now being considered to encourage more dialogue between the owner and the contractor before award of contract.

Since most of the tunnels designed are gravity flow type, the external water is allowed to drain through the concrete lining into the tunnel. Furthermore, it is assumed that by the time of installation of the final concrete lining the opening has stabilized; therefore, with the exception of tunnels in squeezing ground conditions and pressure tunnels, the final concrete lining is designed mainly for reasons of constructability and not for ground or water loads.

Precast Concrete Segmented Linings: Ground loads for the design of precast segmented linings are generally based on the weight of a portion of the overburden. Depending on the ground conditions, Terzaghi's loads, a number of tunnel diameters or full overburden, has been used. The segments are also checked for handling and jacking loads.

Segmented linings have been designed and used by the Bureau of Reclamation with mixed success. The Buckskin Mountains Tunnel in Arizona, a 22 ft (6.7 m) inside diameter, 6.8 mile (10.9 km) long tunnel bored through tuffs and lava, was successfully completed in 1980. A 7 in. (178 mm) thick, 60 in. (152.4 cm) wide precast segmented (4 segments per ring) lining was used as initial and final support.

On the other hand, construction of the Stillwater tunnel in Central Utah, a 7.5 to 8.5 ft (2.3 to 2.6 m) inside diameter tunnel, 8 miles (12.9 km) long was terminated in September 1979 with only 2.6 miles (4.2 km) completed. Maximum overburden on this tunnel is about 2500 ft (762 m) and most of the tunnel excavation was in shale. The 24 ft (7.3 m) long tunnel boring machine (TBM) remains stalled in the mountain. The machine was unable to propel itself and overcome the friction between the shield and the surrounding ground. Near the stalled TBM intensely fractured and sheared rock was encountered with an 18 ft (5.5 m) long fault zone just ahead of it. A system of four 5 in. (127 mm) thick unbolted segments, 36 in. (915 mm) long, reinforced with two layers of 4 x 10 - W 6.5 by W 5.7 wire fabric was used for initial and final support. The 3 in. (76 mm) annular void between the lining and the ground was specified to be filled with pea gravel and backfill grouting as close to the face as possible. Before the final stalling, the TBM had encountered advancement problems and had caused damage to segments already in-place by pushing against them. The reasons for the TBM stalling which lead to termination of the contract are unclear. However, both the Bureau of Reclamation (designer), Marushack and Tilp (1980) and Harrison Western Corporation (contractor), Morton and Provost (1980), agree that more interaction is needed prior to the start of construction in the future in designing the TBM and in defining the most effective excavation-lining system. This case history demonstrates that, in addition to ground loads, many construction related details must be evaluated before an excavation, lining and support can be termed satisfactory.

Stations (Large Openings): Not discussed.

#### A.16.2 Analysis

Two approaches to the selection of a preliminary precast concrete segment thickness are used and described in Selander, et al. (1980). In estimating the ground pressures for tunnels in rock, Terzaghi's

loads are normally used. Following the ground pressure determination, one of the analysis and design approaches is described in Deere, et al. (1969); namely, provide for ring thrust, design for anticipated distortions (usually 0.5 percent of the diameter change), consider the possibility of buckling and make allowance for other external conditions (i.e., jacking loads, asymmetrical loads, etc.). To account for the effects of the joints between the segments a reduced effective stiffness of the lining is used (EI). The effective stiffness calculation is based on the ACI Code (318-77) equations 10-10, 10-9 or 9-7. Once an effective EI has been selected, the magnitude of the moments and shears are determined from the expressions relating the moment and shear to the design distortions. The computed values of moment and shear are then multiplied by 1.7 to obtain the ultimate design values. The ultimate thrust is computed by multiplying the design earth pressure by the radius of the tunnel and the 1.7 "load" factor. Thrust capacity of the segments is reduced to account for bolt or gasket pockets at the joints. Shear and moment capacities are not reduced, since moment and shear are directly proportional to the moment of inertia which will be reduced by such a blockout, therefore reducing moment and shear proportionately. Joint thrust capacity is reduced to account for joint geometry and the presence of the sealant material. This reduction should be based on tests of the proposed joint and sealant material.

A second analysis approach is also used in which the computer program "TUNNEL" of the U.S. Army Corps of Engineers is used. The ground pressures are determined as in the first approach. The ground is modeled by a series of linear elastic resisting elements attached to certain points on the lining. The value of the modulus of subgrade reaction for these elastic elements depend on the type of ground. Dead load of the concrete of the lining, and the locomotive wheel loads at the invert of the tunnel are taken into account. Handling and jacking loads are used to estimate an initial amount of reinforcement. Load factors of 1.7 for live loads and 1.4 for dead loads are used. With

this amount of steel as a starting point, a neutral axis for a cracked section is assumed. Then the moment of inertia of the cracked cross-section and the equivalent modulus of elasticity are found. These values, representing the lining as a series of beam elements, are used as input to the "TUNNEL" program. The program solution is used to determine internal moments and thrusts from which the depth of cracking (location of the neutral axis) and corresponding moment of inertia of the cracked section can be calculated. The moment and thrust capacities are checked to see if they are adequate for the computed values. The process is repeated until the assumed and computed moments of inertia are the same.

#### A.16.3 Design and Performance Criteria

The ultimate strength design method of ACI Code (318-77) is used with load factors of 1.7 for dead loads and 1.4 for live loads. In the first method of analysis, the load factors are applied to the thrust resulting from the unfactored ground loads and to the moments and shears resulting from the induced design distortion. In the second method (computer based analysis) the load factors are applied directly to the loads.

The minimum cast-in-place concrete lining thickness is a function of the diameter of the tunnel. A minimum cover of 4 in. (102 mm) should be provided over the steel ribs and an 8 in. (203 mm) spacing over the crown of the lining to accommodate the concrete discharge pipe (slick line). A "rule of thumb" used for smaller tunnels is minimum cover over rib should be 1/2 in. (13 mm) per ft (0.3 m) of finished tunnel diameter.

Usually cast-in-place linings for free-flow water tunnels are not reinforced, except near the portal region. Precast linings are reinforced in accordance with the design calculations to take ground

and construction loads. Reinforcement to resist internal pressure is always considered for pressure tunnels.

No cracking, deflection or leakage criteria for the final concrete lining have been formalized. However, precast linings should not deflect more than the design distortions.

Sloping type joints are permitted for unreinforced cast-in-place linings, provided that the contractor will thoroughly consolidate the concrete in such joints and form uniform and stable slopes while the concrete is still plastic. For reinforced cast-in-place linings bulkhead type joints are specified with cold casting of the next batch. All cold joints should be wet, sandblasted, washed with air-water jets, and surface dried prior to placement of the adjoining concrete. Concrete mixes used for the tunnel lining are subject to the approval of the agency and the slump of the concrete during placement is usually specified to be between 2 and 4 in. (51 and 102 mm). The recommended concrete strength is 3,000 psi (21 MPa) for cast-in-place linings. Cleanup of the tunnel excavation should be performed before placing the concrete. Immediately before the concrete is placed the contractor is required to remove all timber material within the A-line except steel ribs and spiling. Timber lagging, timber blocking and timber wedges outside the A-line should all be removed as completely as practicable. Furthermore, all loose material on surfaces of excavation on the sidewalls of the tunnel above the invert, except loose material behind lagging or blocking, should be removed before concrete is placed. Loosened material between the bases of each tunnel side wall and outside of the B-line may be allowed to remain in place provided that such material is thoroughly compacted. Forms should be left in place for at least 16 hours after casting or until there is no danger of fallout from the crown or damage to the inside surface of the lining by construction operations.

It is desirable to control excessive leakage out of water conveyance tunnels lined with precast segments. The sealant system used in the Stillwater tunnel was a strip of impregnated felt, 1/8 in. (3.2 mm) thick placed on each face of the longitudinal joints. Rubberized bitumén sealant strips were placed in the shiplap circumferential joints. A caulking groove 5/8 in. (16 mm) deep was provided on all inside surfaces of longitudinal and circumferential joints that was filled with a single component urethane sealant. The Bureau of Reclamation has prepared standard specifications for this sealant.

Backfill grouting of all spaces between any type of concrete lining and the rock should be specified. Approximately 4 grout holes per 20 linear ft (6.1 m) are needed for the grouting operation with grouting pressures limited to 30 psi (207 kPa).

#### A.16.4 Comments

Adverse geologic conditions or excessive amount of tunnel drainage might cause difficulties in the functioning of a TBM in machine excavated tunnels. The contractor should therefore submit a contingency plan showing methods to adapt the machine to geologic conditions or to be able to shift to an alternate excavation and support system should the machine become stalled.

Although the number of segments to be used in a precast concrete lining ring is not widely standardized, four segments per ring appears to be the most appropriate (Selander, et al. 1980). Use of only four segments decreases the number of joints and still permits reasonable handling ease. The width of the tunnel segment may be a function of the ground conditions. For instance, in squeezing ground conditions, shorter segments may be preferable to reduce the time that the ground remains unsupported. A detailed discussion of precast concrete segment

support and lining used in tunnels throughout the world is given in Selander, et al. (1980).

## APPENDIX B

### FORMULATION OF INTERFACE ELEMENT

#### B.1 INTRODUCTION

Joints and interfaces between dissimilar materials are inherent characteristics of most geotechnical problems. Finite element representation of such discontinuities in a continuous system requires special provisions that handles such physical phenomenons as debonding or separation between adjacent elements and slippage as the shearing strength is exceeded. Even a linear elastic problem that contains such joint behavior requires a multiphase or iterative solution process making the overall problem a nonlinear one. Several finite element models have been developed in the past to simulate rock discontinuities. A brief review of a few of the widely used joint elements will be given here.

Goodman Element: Goodman, Taylor and Brekke (1968), describe simple joint elements used in the context of stability of jointed rock masses. These authors represent a joint element as a one-dimensional tube which offers resistance to compressive and shear forces acting normal and parallel to its axis. This is a simple two-dimensional element with four nodes, rectangular but no thickness, and has eight degrees of freedom. It was designed to be compatible with the constant strain triangle continuum element. However, this element has the disadvantage that elements adjacent to both sides of the joint can penetrate into each other if there is compression on the joint element because it is compressible but has no thickness. However, this problem is minimized with a large stiffness normal to the joint.

Zienkiewicz Model: To represent complex joint shapes, Zienkiewicz, et al. (1970) introduced the isoparametrically specified joint elements. Uniform strain in the thickness direction is assumed



and simple nonlinear material property for shear and normal stresses can be assigned. However, these authors point out that in certain cases these elements generate very large off diagonal terms or very small diagonal terms in the stiffness matrix. This leads to numerical problems due to such ill-conditioning of the stiffness matrix.

Relative Displacement Model: Ghaboussi, Wilson and Isenberg (1973), introduced a joint element that uses relative displacements between two faces of the joint as the independent degrees of freedom. This is achieved by recognizing only one of the faces of a joint explicitly as a line of nodal points in the mesh; the opposite joint face is considered to belong to one of the adjoining block or element as an internal feature. These elements allow debonding in the direction normal to the joint plane and an elastic-perfectly plastic stress-strain relationship along the slip surface. Although this element overcomes some theoretical difficulties of other elements, ambiguity with respect to nodal displacements does arise at kink points in a slip surface where a kink occurs. A kink in a slip surface may arise when a curved joint or interface is discretized by the representation of the adjacent elements by straight edge finite elements. A tunnel lining represented by straight beam elements would develop such kinks at the node points where the curvature changes.

## B.2 INTERFACE ELEMENT

The joint element that is described herein is based to a large extent on the same formulation as developed by Ghaboussi, Wilson and Isenberg (1973) with the main purpose to use the element for representing the ground-lining interface in a tunnel problem. The ambiguity with respect to the nodal displacements as associated with the joint element developed by those authors, as mentioned earlier, is avoided by approximating the joint geometry to be concentrated at the nodes and using relative displacements at the nodes in the direction tangent to the original curved surface.

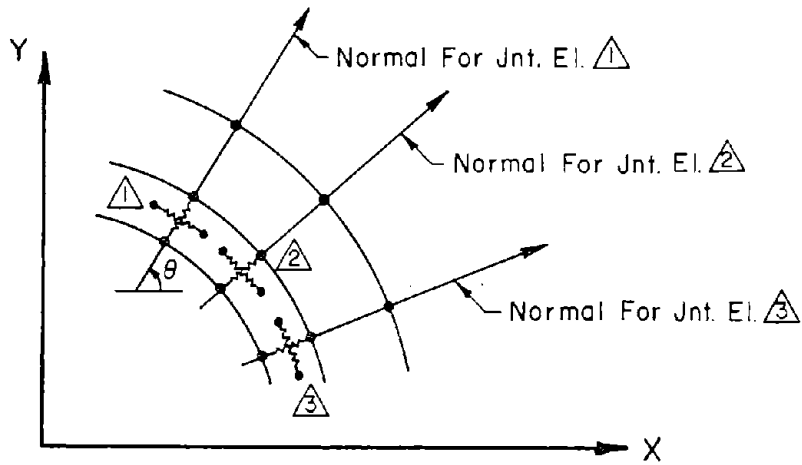


FIGURE B.1 NODAL INTERFACE ELEMENT VISUALIZED AS A SET OF NORMAL AND TANGENTIAL SPRINGS

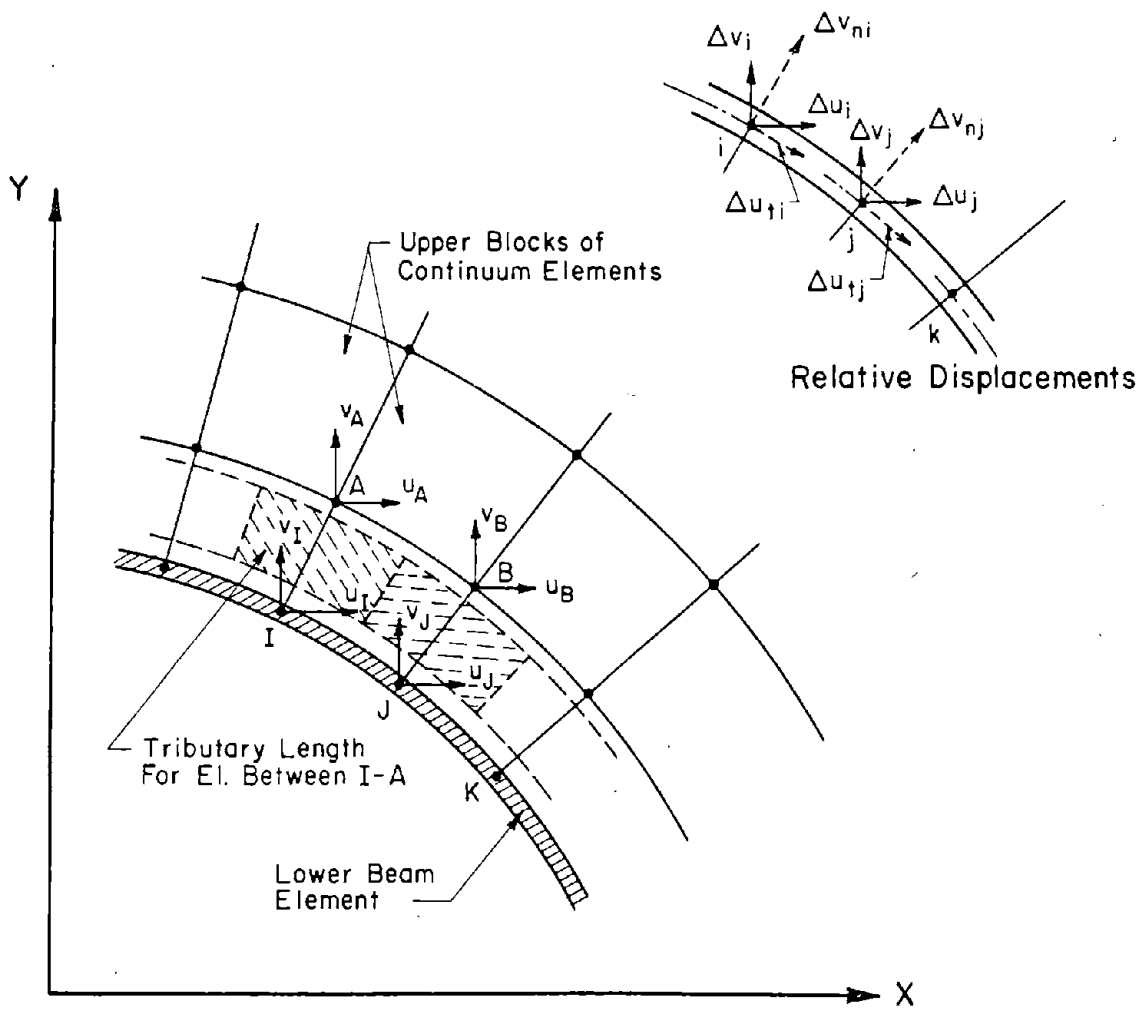


FIGURE B.2 GLOBAL ABSOLUTE DISPLACEMENT

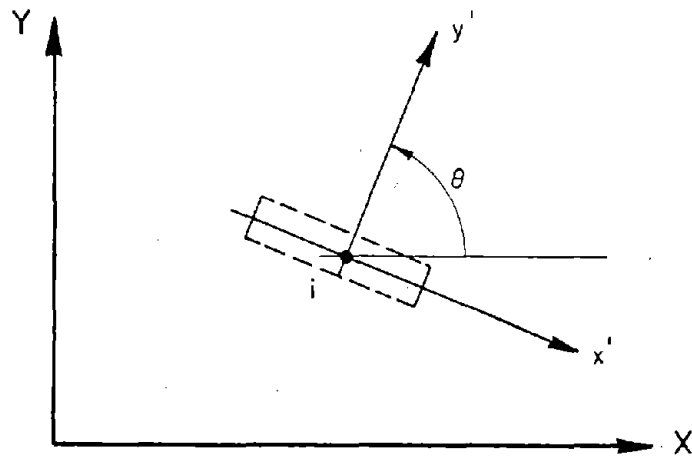


FIGURE B.3 ORIENTATION OF THE NODAL INTERFACE ELEMENT

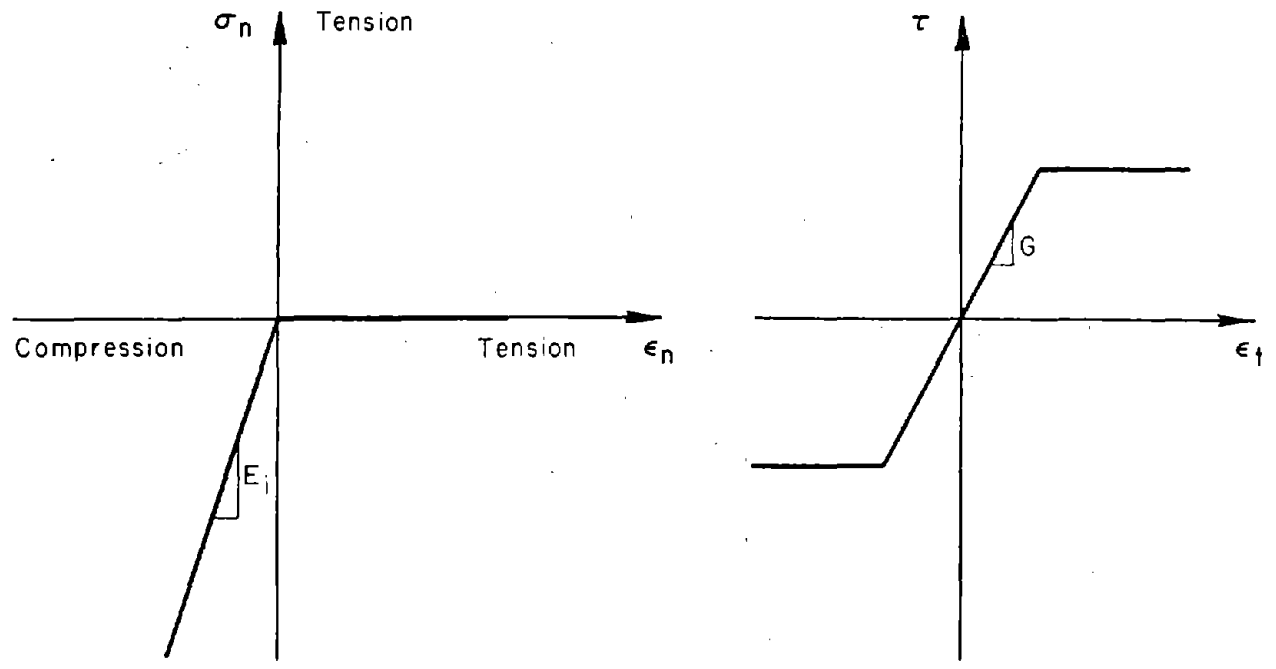


FIGURE B.4 MATERIAL PROPERTIES FOR INTERFACE ELEMENTS

Interface Element Stiffness: The nodal interface element may be visualized as being composed of two springs, normal and tangential, connecting the nodes between the two faces of a slip surface (Fig. B.1). Thus, it essentially has two nodes, one at each face of the joint. One such interface element is required for each nodal connection at the slip surface. The normal direction for each interface element is specified and a tributary length over which the stresses are assumed to be constant is also assigned to each interface element. Generally, this length will be one-half the distance to adjacent nodes.

Transformation of the absolute displacements of one side of the interface into the relative displacements between the two sides of the interface is carried out according to the following relations (Fig. B.2):

$$u_A = u_I + \Delta u_i$$

$$v_A = v_I + \Delta v_i \tag{B.1}$$

The interface element stiffness matrix is based on relative displacement. Its independent degrees of freedom at the two nodes are  $\Delta u_t$  and  $\Delta v_n$  in the tangential and normal directions, respectively. For nondilatant joints the shear and normal components of deformations are uncoupled as there is no volume change due to shearing strains. Thus, the nodal joint force-relative displacement relationship can be written in the element coordinate system (Fig. B.3) as:

$$\{ F \} = [k_{x'y'}] \{ \Delta u \}$$

$$\begin{Bmatrix} T_i \\ N_i \end{Bmatrix} = \begin{bmatrix} k_t & 0 \\ 0 & k_n \end{bmatrix} \begin{Bmatrix} \Delta u_t \\ \Delta u_n \end{Bmatrix}$$

B.2

where

- $k_n$  = normal spring stiffness of the interface element
- $k_t$  = tangential spring stiffness of the interface element
- $N_i$  = normal force in the interface element at node i
- $T_i$  = tangential force in the interface element at node i

The interface stiffness matrix  $[k_{x'y'}]$  is transformed into the global coordinate system using the orientation of the normal of the interface element as follows:

$$k = T^T k_{x'y'} T$$

B.3

where

$T$  = matrix for coordinate transformation

$$= \begin{bmatrix} \sin & -\cos \\ \cos & \sin \end{bmatrix}$$

Thus, in the global system:

$$k = \begin{bmatrix} S^2 k_t + C^2 k_n & SC(k_n - k_t) \\ SC(k_n - k_t) & S^2 k_n + C^2 k_t \end{bmatrix}$$

B.4

where

$$S = \sin \theta \quad ; \quad C = \cos \theta.$$

The interface stiffness parameters  $k_n$  and  $k_t$  can be defined from the stress-strain relationships of the joint material. The normal and tangential strain components are assumed to be related to the relative displacements in the following manner:

$$\begin{aligned} \epsilon_n &= \frac{1}{t} \Delta v_n \\ \epsilon_t &= \frac{1}{t} \Delta u_t \end{aligned} \tag{B.5}$$

where

$t$  = thickness of the joint in the normal direction.

The material property matrix,  $[C]$ , relates the stresses to the strains as below:

$$\begin{Bmatrix} \sigma_t \\ \sigma_n \end{Bmatrix} = \begin{bmatrix} C_{tt} & 0 \\ 0 & C_{nn} \end{bmatrix} \begin{Bmatrix} \epsilon_t \\ \epsilon_n \end{Bmatrix} \tag{B.6}$$

Substituting Eq. B.5 in B.6 and multiplying B.6 by the tributary length ( $L$ ) and width ( $B$ ) of the element yields:

$$(L \times B) \begin{Bmatrix} \sigma_t \\ \sigma_n \end{Bmatrix} = \frac{L \times B}{t} \begin{bmatrix} C_{tt} & 0 \\ 0 & C_{nn} \end{bmatrix} \begin{Bmatrix} \Delta u_t \\ \Delta v_n \end{Bmatrix}$$

or

$$\begin{Bmatrix} T_i \\ N_i \end{Bmatrix} = \frac{L \times B}{t} \begin{bmatrix} C_{tt} & 0 \\ 0 & C_{nn} \end{bmatrix} \begin{Bmatrix} \Delta u_t \\ \Delta v_n \end{Bmatrix} \quad \text{B.7}$$

Comparison of Eqs. B.4 and B.1 gives for  $k_t$  and  $k_n$

$$k_t = \frac{L \times B}{t} C_{tt}$$

$$k_n = \frac{L \times B}{t} C_{nn} \quad \text{B.8}$$

Finally to assemble the element stiffness matrix into the stiffness matrix of the entire structure, a transformation from the relative displacements to absolute nodal displacements is carried out using the following relationship:

$$K_{(4 \times 4)} = T_{1(4 \times 2)}^T \cdot k_{(2 \times 2)} \cdot T_1_{(2 \times 4)} \quad \text{B.9}$$

where

$$T_1 = \text{Transformation matrix}$$

$$= \begin{bmatrix} -1 & 0 & 1 & 0 \\ 0 & -1 & 0 & 1 \end{bmatrix}$$

Iterative Solution to Simulate Interface Properties: The first solution of the system of linear equations developed with the nodal displacements at any given load increment will presume tension in some joints or interface elements or excessive shear in others. Subsequent second or more iterations are thus necessary to compute deformations and stresses consistent with the interface mechanics. The existing computer program uses an incremental iterative solution scheme for nonlinear problems as described in Section 3.4. Hence, the simulation of the interface properties has been programmed to comply with this solution procedure. Debonding is recognized by detecting tension in

the normal stress in the interface element. In such a case the interface element is not assembled in the global stiffness matrix in subsequent iteration. In case of contact, the proportionality constant for normal stress-strain relationship of the interface material,  $C_{nn}$ , can be assigned large values without any numerical problem. Usually a very high stiffness term on the diagonal tends to fix a nodal point. However, in the relative displacement scheme adopted here, a high joint stiffness will force only the relative displacement between the two nodes of the interface element to be nearly zero.

The interface material properties are specified in the interface element coordinates for convenience (Fig. B.4). The Mohr-Coulomb criterion has been adopted to represent the behavior of the interface in shear which establishes an elastic-perfectly plastic tangential stress-strain relationship. The material constants  $C_{nn}$  and  $C_{tt}$  are assigned values according to states of strain and stress in the interface element in the following manner:

a) Separation:  $C_{nn} = C_{tt} = 0$  for  $\xi_n \geq 0$   
 (in fact, the element becomes nonexistent)

b) Contact:

For  $\xi_n \leq 0$  i)  $C_{nn} = E_i$

ii) Elastic in Shear:

$$C_{tt} = G \text{ for } T < c + \sigma_n \tan \phi$$

Plastic in Shear:

$$C_{tt} = 0 \text{ for } T = c + \sigma_n \tan \phi$$

(Beyond the shear strength)

in which  $c$  and  $\phi$  are joint cohesion and angle of informal friction respectively, read in as data.



## APPENDIX C

### REPORT OF NEW TECHNOLOGY

The work performed under this contract, while leading to no new technology, has led to the development of improved practical design tools to provide more accurate representations of the ground-structure interaction in tunneling. They range from simple analytical and empirical methods to sophisticated finite element techniques which satisfy the requirements of concrete tunnel lining design.

#### REFERENCES

ACI Committee 224, (1972), "Control of Cracking in Concrete Structures," Journal of the American Concrete Institute, Vol. 69, No. 12, pp. 717-757.

ACI Committee 318, (1977), "Building Code Requirements for Reinforced Concrete," ACI Standard 318-77, American Concrete Institute, Detroit, Michigan.

ACI Committee 444, (1979), "Models of Concrete Structures, State-of-the-art," Report No. ACI 444 R-79, Concrete International, Jan. 1979, pp. 77-95.

Ady, N. and J.E. Carpenter, (1970), "Models for Concrete Structures-Bibliography," ACI Publication SP-24, Models for Concrete Structures, pp. 449-487.

Alami, Z.Y. and P.M. Ferguson, (1963), "Accuracy of Models Used in Research on Reinforced Concrete," Journal American Concrete International, Proc. Vol. 60, No. 11, November 1963, pp. 1643-1663.

Allgood, J.R. and J.B. Ciani, (1968), "The Influence of Soil Modulus on the Behavior of Cylinders in Sand," Highway Research Record, No. 249, pp. 1-13.

Anderson, R.H., R.T. Haelsig and M.D. Reifel, (1966), Structural Behavior of Ring Sections under Nonuniform External Pressure, Technical Report No. AFWL-TR-65-145, Air Force Weapons Laboratory Research and Technology Division, Air Force Systems Command, Kirkland Air Force Base, New Mexico, March.

Atkinson, J.H., E.T. Brown and M. Potts, (1975), "Collapse of Shallow Unlined Tunnels in Dense Sand," Tunnels and Tunnelling, Vol. 7, No. 3, pp. 81-87.

Atkinson, J.H., T.L.L. Orr and D.M. Potts, (1975), Research Studies into the Behavior of Tunnels and Tunnel Linings in Soft Ground, Department of Environment, TRRL Report SR176UC, Growthorne.

Barton, N., R. Lien and J. Lunde, (1974), "Engineering Classification of Rock Masses for the Design of Tunnel Support," Rock Mechanics, Vol. 6, No. 4, pp. 189-236.

Benito, C., (1960), "Building of Models (Scales, Materials and Manufacturing Processes)," Bull. RILEM, No. 8, September 1960, pp. 5-14.

Blomeier, G.A. and J.E. Breen, (1975), "Effect of Yielding of Restraints on Slender Concrete Columns with Sidesway Prevented," Reinforced Concrete Columns, SP-50, ACI, Detroit, pp. 41-66.

Borges, J.R. and J.A. Lima, (1960), "Crack and Deformation Similitude in Reinforced Concrete," Bull. RILEM, No. 7, June 1960, pp. 79-90.

Brierley, G., (1975), The Performance During Construction of the Liner for a Large, Shallow Underground Opening in Rock, Ph.D. Thesis, University of Illinois, Urbana.

Burns, J.Q. and R.M. Richards, (1964), "Attenuation of Stresses for Buried Cylinders," Proceedings, Symposium on Soil-Structure Interaction, Tucson, pp. 378-392.

Caincross, A.M., (1973), Deformations Around Model Tunnels in Stiff Clay, Ph.D. Thesis, Cambridge University.

Carpenter, J.E., F. Roll and M.I. Zelman, (1970), "Techniques and Materials for Structural Models," ACI Publication SP-24, Models for Concrete Structures, pp. 41-63.

Christian, J.T. and H.W. Ing, (1973), "Errors in Simulating Excavation in Elastic Media by Finite Elements," Soils and Foundations (Japan), Vol. 13, No. 1, pp. 1-10.

Clough, R.W. and R.J. Woodward, III, (1967), "Analysis of Embankment Stresses and Deformations," Journal of the Soil Mechanics and Foundation Division, ASCE, Vol. 93, No. SM4, pp. 529-549.

Cording, E.J., (1974), "Geologic Considerations in Shotcrete Design," Use of Shotcrete for Underground Structural Support, ASCE and ACI, SP-45, pp. 175-199.

Cording, E.J. and D.U. Deere, (1972), "Rock Tunnel Supports and Field Measurements," Chapter 33, Proc. RETC, Vol. 1, pp. 601-622.

Cording, E.J. and J.W. Mahar, (1978), "Index Properties and Observations for Design of Chambers in Rock," Engineering Geology, Vol. 12, pp.113-142.

Craig, R.N. and A.M. Muirwood, (1978), A Review of Tunnel Lining Practice in the United Kingdom, Supplementary Report 335, Transport and Road Research Laboratory, Growthorne, Berkshire.

Curtis, D.J., (1976), Discussion of: Muir Wood, A.M., "The Circular Tunnel in Elastic Ground," Geotechnique, Vol. 26, No. 2, pp. 231-237.

Dar, S.M. and R.C. Bates, (1974), "Stress Analysis of Hollow Cylindrical Inclusions," Journal of the Geotechnical Engineering Division, ASCE, Vol. 100, No. GT2, pp. 123-138.

Deere, D.U., R.B. Peck, J.B. Monsees and B. Schmidt, (1969), "Design of Tunnel Liners and Support Systems," Report to OHSGT-U.S. DOT from University of Illinois, Urbana.

Dixon, J.D., (1969a), Analysis of Tunnel Support Structures with Consideration of Support-Rock Interaction, Report of Investigations 7526, U.S. Bureau of Mines, June.

Dixon, J.D., (1969b), Structural Design Data for Unreinforced Concrete Tunnel Linings, Report of Investigations 7297, U.S. Bureau of Mines, October.

Dixon, J.D., (1971), Analysis of Tunnel Support Structures with Consideration of Support-Rock Interaction, Report of Investigations 7526, U.S. Bureau of Mines.

Dixon, J.D., (1973), Structural Design Data for Concrete Drift Linings in Block Stopes, Report of Investigations 7792, U.S. Bureau of Mines.

Dolcetta, M., (1971), "Problems with Large Underground Stations in Italy," Proceedings, 13th Symposium of Rock Mechanics, ASCE, pp. 243-286.

Duncan, J.M., (1979), "Behavior and Design of Long-span Metal Culverts," Journal of the Geotechnical Engineering Division, pp. 399-418 (March).

Duncan, J.M. and P. Dunlop, (1968), Slopes in Stiff-Fissured Clays and Shales, Contract Report No. TE 68-6, U.S. Army Engineer Waterways Experiment Station, Vicksburg, Mississippi.

Ebaid, G.S. and M.E. Hammad, (1978), "Of Circular Tunnel Design," *Tunnels and Tunnelling*, July, pp. 59-63.

Einstein, H.H. and C.W. Schwartz, (1979), "Simplified Analysis for Tunnel Supports," *Journal of the Geotechnical Engineering Division, Proceedings of the ASCE*, Vol. 105, No. GT4, April, pp. 499-518.

Einstein, H.H., W. Steiner and G.B. Baecher, (1979), "Assessment of Empirical Design Methods for Tunnels in Rock," *Proc. RETC*, Vol. 1, Chapter 40, AIME-ASCE, pp. 683-706.

Ferguson, P.M. and J.E. Breen, (1966), "Investigation of the Long Concrete Column in a Frame Subject to Lateral Loads," *Symposium on Reinforced Concrete Column*, SP-13, ACI, Detroit, pp. 75-120.

Fernandez-Delgado, G., E.J. Cording, J.W. Mahar and M.L. Van Sint Jan, (1979), "Thin Shotcrete Linings on Loosening Rock," *RETC, Proc.*, Vol. 1, pp. 750-813.

Ferrera-Boza, R.A. and S.L. Paul, (1978), Structural Behavior of Monolithic Concrete Tunnel Liner Models, Contract No. DOT FR 30022, Report for U.S. Department of Transportation, (December).

Fumagalli, E., (1968), "Model Simulation of Rock Mechanics Problems," Chapter 11, in Rock Mechanics in Engineering Practice, Ed. Stagg and Zienkiewicz, pp. 353-384, John Wiley and Sons, Ltd.

Furlong, R.W. and P.M. Ferguson, (1966), "Tests on Frames with Columns in Single Curvature," *Symposium on Reinforced Concrete Columns*, SP-13, ACI, Detroit, pp. 55-74.

Ghaboussi, J. and R.E. Ranken (1974), Tunnel Design Considerations: Analysis of Medium-Support Interaction, Report No. FRA-ORDD 75-24, Federal Railroad Administration, U.S. Department of Transportation.

Ghaboussi, J., E.L. Wilson and J. Isenberg, (1973), "Finite Elements for Rock Joints and Interface," Journal Soil Mechanics and Foundation Division, Proceedings, ASCE, Vol. 99, No. SM10, pp. 833-848.

Glanville, W.H. and F.G. Thomas, (1939), "Moment Redistribution in Reinforced Concrete," in Studies in Reinforced Concrete, Technical Paper No. 22, Building Research, Department of Scientific and Industrial Research.

Goodman, R.E., (1966), "On the Distribution of Stresses around Circular Tunnels in Non-homogeneous Rocks," Proc. 1st Cong. ISRM, Lisbon, Vol. 2, pp. 249-255.

Goodman, R.E., R. Taylor and T.L. Brekke, (1968), "A Model for the Mechanics of Jointed Rock," Journal of the Soil Mechanics and Foundation Division, ASCE, Vol. 94, No. SM3, pp. 637-659.

Harris, H.G., G.M. Sabnis and R.N. White, (1970), "Reinforcement for Small Scale Direct Models of Concrete Structures," ACI Publication, SP-24, Models for Concrete Structures, pp. 141-158.

Hayashi, M. and S. Hibino, (1970), "Visco-Plastic Analysis on Progressive Relaxation of Underground Excavation Works," Proceedings 2nd Congress of the International Society for Rock Mechanics, Belgrad, pp. 565-575.

Hendron, A.J. and P. Engeling, (1973), Model Tests of Lined Tunnels in a Jointed Rock Mass, Technical Report M-41, Construction Engineering Research Laboratory, Champaign, Illinois, May.

Hendron, A.J., Jr., P. Engeling, A.K. Aiyer and S.L. Paul, (1972), Geomechanical Model Study of the Behavior of Underground Opening in Rock Subjected to Static Loads, Contract Report N-69-1, U.S. Army

Engineer Waterways Experiment Station, Vicksburg, Mississippi, Report 3, June.

Heuer, R.E. and A.J. Hendron, Jr., (1969), Geomechanical Model Study of the Behavior of Underground Openings in Rock Subjected to Static Loads, Report 1, Development of Modeling Techniques, Contract Report N-69-1, U.S. Army Engineer Waterways Experiment Station, Vicksburg, Mississippi, October.

Hoeg, K., (1968), "Stresses Against Underground Structural Cylinders," *Journal of the Soil Mechanics and Foundation Division, ASCE*, Vol. 94, No. SM4, p. 833-858.

Hubert, M.K., (1937), "Theory of Scale Models as Applied to the Study of Geologic Structures," *Bull. GSA*, Vol. 48, pp. 1459-1520.

Judd, W.R. and W.H. Perloff, (1971), "Predicted and Measured Displacements for Tunnels," *Proceedings, 13th Symposium of Rock Mechanics, ASCE*, pp. 487-514.

Karshenas, M. and J. Ghaboussi, (1979), "Modeling and Finite Element Analysis of Soil Behavior," *Civil Engineering Studies, Geotechnical Research Series No. 17, University of Illinois at Urbana-Champaign*.

Kennedy, T.C. and H.E. Lindberg, (1978), "Model Tests for Plastic Response of Lined Tunnels," *Journal Engineering Mechanics Division, Proceedings, ASCE*, Vol. 104, No. 2, April, pp. 399-420.

Kennedy, T.E. and J.T. Ballard, (1967), Dynamic Test of a Model Flexible-Arch-Type Protective Shelter, Report 1, Pilot Test, Technical Report No. 1-768, U.S. Army Engineer Waterways Experiment Station, Vicksburg, Mississippi, April.



Kulay, F.H., J.M. Duncan and H.B. Seed, (1969), Finite Element Analysis of Stresses and Movements in Embankments During Construction, Contract Report S-69-8, U.S. Army Engineers Waterways Experiment Station, Vicksburg, Mississippi.

Ladangi, B., (1974), "Use of Long-term Strength Concept in the Determination of Ground Pressure on Tunnel Linings," Proc. 3rd Congr. ISRM, Denver, 1974, Vol. II, part B, pp. 1150-1156.

Langhaar, H.L., (1951), Dimensional Analysis and Theory of Models, John Wiley and Sons, Inc., New York, 166 pages.

Litle, W.A., E. Cohen and G. Somerville, (1970), "Accuracy of Structural Models," ACI Publication SP-24, Models for Concrete Structures, pp. 65-124.

Mandel, J., (1963), "Tests on Reduced Scale Models in Soil and Rock Mechanics--A Study of the Conditions of Similitude," Int. J. Rock Mechanics Mining Science, Vol. 1, pp. 31-42.

Massey, B.S., (1971), "Units, Dimensional Analysis and Physical Similarity," Van Nosttrand Reinhold Co., 140 pages.

Meyer, G.D. and W.J. Flathau, (1967), Static and Dynamic Laboratory Tests of Unreinforced Concrete Fixed-End Arches Buried in Dry Sand, Technical Report No. 1-758, U.S. Army Engineer Waterways Experiment Station, Vicksburg, Mississippi, February.

Morgan, H.D., (1971), "A Contribution to the Analysis of Stress in a Circular Tunnel," Geotechnique, Vol. 11, March, pp. 37-46.

Muirwood, A.M., (1975), "The Circular Tunnel in Elastic Ground," Geotechnique, Vol. 25, No. 1, pp. 115-127.

Muller, L., (1978), "Removing Misconceptions on the New Austrian Tunneling Method," Tunnels and Tunneling, October 1978, pp. 29-32.

Munn, J.F., G.L. Carre and T.E. Kennedy, (1970), Failure of Footing-Supported Buried Steel Arches Loaded Staticly, Miscellaneous Paper N-70-2, U.S. Army Engineer Waterways Experiment Station, Vicksburg, Mississippi, March.

Murphy, G., (1950), Similitude in Engineering, Ronald Press, New York, 302 pages.

Neville, A.M., (1971), Hardened Concrete: Physical and Mechanical Aspects, ACI Monograph No. 6, American Concrete Institute, 260 pages.

Newmark, N.M. and Associates, (1965), Feasibility of Modeling Cavity Behavior in Jointed Rock Masses, Contract Report No. 1-135, U.S. Army Engineer Waterways Experiment Station, Vicksburg, Mississippi, November.

Norman, C.D. and J.D. Predergast, (1973), Behavior of Stiff Cylinders Buried in Sand under Static Loading, Technical Report No. N-73-1, U.S. Army Engineer Waterways Experiment Station, Vicksburg, Mississippi, April.

Obert, L. and W.I. Durvall, (1967), Rock Mechanics and the Design of Structures in Rock, Chapter 7, Dimensional Analysis, pp. 191-201.

O'Rourke, T.D., (1978), "Tunneling for Urban Transportation: A Review of European Construction Practice," Report for U.S. DOT, UMTA-IL-06-0041-78-1.

Orr, T.L.L., (1976), The Behavior of Lined and Unlined Model Tunnels in Stiff Clay, Ph.D. Thesis Submitted to the Cambridge University (Churchill College), 188 pages.

Peck, R.B., A.J. Hendron, Jr. and B. Mohraz, (1972), "State of the Art of Soft Ground Tunneling," Proc., First North American Rapid Excavation and Tunneling Conference, Chicago, Vol. 1, pp. 259-286.

Potts, D.M., (1976), Behavior of Lined and Unlined Tunnels in Sand, Ph.D. Thesis, Cambridge University, (Churchill College).

Proctor, R.V. and T.L. White, (1946) Revised (1968), Rock Tunneling with Steel Supports, Commercial Shearing and Stamping Company, Youngstown, Ohio.

Rabcewicz, L.V., (1964), "The New Austrian Tunneling Method," Water Power, pp. 453-457, 511-515, 1965, pp. 19-24.

Rabcewicz, L.V., (1969), "Stability of Tunnels under Rock Load," Water Power, pp. 225-229, 266-273, 297-302.

Ranken, R.E. and J. Ghaboussi, (1976), Analysis of Interaction Between Two Parallel Tunnels, Report No. DOT-TST-76T-16, U.S. Department of Transportation, Office of the Secretary and Federal Railroad Administration, Washington, D.C. (August).

Ranken, R.E., J. Ghaboussi and A.J. Hendron, Jr., (1978), Analysis of Ground-Liner Interaction for Tunnels, Report No. UMTA-IL-06-0043-78-3, Urban Mass Transportation Administration, U.S. Department of Transportation, October.

Roberds, W.J. and H.H. Einstein, (1978), "Comprehensive Model for Rock Discontinuities," Journal of Geotechnical Division, Proceedings, ASCE, Vol. 104, No. GT5, pp. 553-569.

Rocha, M., (1955), "Analysis of Concrete Dams by Model Tests," Trans. 5th Int. Congress on Large Dams, Vol. IV, pp. 1307-1344.

Rocha, M., (1957), "The Possibility of Solving Soil Mechanics Problems by the Use of Models," Proc. 4th Int. Conf. on Soil Mechanics and Found. Engineering, London, Vol. 1, pp. 183-188.

Rocha, M., (1958), "Model Tests in Portugal," Civil Engineering and Public Works Review, Vol. 53, No. 619, January 1958, pp. 49-53 and No. 620, February 1958, pp. 179-182.

Rocha, M., (1961), "Practical Application of Models," Bun, RILEM, No. 12, September 1961, pp. 5-28.

Rocha, M., (1965), "Structural Model Techniques--Some Recent Developments," Chapter 16, pp. 395-424 in Stress Analysis ed. by Zienkiewicz and Hollister, John Wiley and Sons, Ltd.

Rodriguez Perez, C.E., (1980), Analysis of an Underground Opening in Jointed Rock, Ph.D. Thesis, University of Illinois, Urbana.

Roscoe, K.H., (1963), "A Fundamental Principle of Similarity in Model Tests for Earth Pressure Problems," Proc. 2nd Asian Regional Conf. on Soil Mechanics and Found. Engineering, Vol. 1, pp. 134-140.

Roscoe, K.H., (1968), "Soils and Model Tests," Journal Strain Analysis, Vol. 3, No. 1, pp. 57-64.

Salamon, M.D.G., (1970), "A Note on the Design of Tunnel Lining," Proc. S. African Tunneling Conference, Vol. 1, pp. 115-119.

Schultze, H. and H. Duddeck, (1964), "Stresses in Shield Driven Tunnels," Beton and Stahlbetonbau, August, pp. 169-175.

Serafim, J.L. and M.C. Azevedo (1961), "Methods in Use at the LNEC for the Stress Analysis in Models of Dams," Bull. RILEM, No. 11, June, 1961, pp. 12-24.

Stagg, K.G. and O.C. Zienkiewicz, (1978), Rock Mechanics in Engineering Practice, John Wiley and Sons, New York.

Szechy, K., (1967), The Art of Tunneling, Akademiai Kiado, Budapest.

Tener, R.K., (1964), Model Study of a Buried Arch Subjected to Dynamic Loading, Technical Report No. 1-660, U.S. Army Engineer Waterways Experiment Station, Vicksburg, Mississippi, November.

Terzaghi, K., (1942), "Liner-Plate Tunnels on the Chicago Subway," Proceedings, ASCE, Vol. 68, No. 6, pp. 862-899.

Terzaghi, K., (1968), "Rock Defects and Loads on Tunnel Supports," in Proctor and White, Rock Tunneling with Steel Supports, Youngstown, Ohio, pp. 17-102.

Timoshenko, S.P. and J.N. Goodier, (1970), Theory of Elasticity, Third Edition, McGraw-Hill Book Company, New York.

Voegele, M., C. Fairhurst and P. Cundall, (1977), "Analysis of Tunnel Support Loads using a Large Displacement, Distinct Block Model," Proc. 1st Int. Symp. on Storage in Excavated Rock Caverns, Stockholm, pp. 247-252.

Wagner, M., (1970), "The New Austrian Tunneling Method," Proc. S. African Tunneling Conf., Vol. 1, pp. 121-127.

Waldorf, W.A., J. Veltrou and J.J. Curtis, (1963), "Foundation Module Tests for Kardj Arch Dam," Journal of Soil Mechanics and Foundations Division, ASCE, Vol. 89, pp. 91-124.

Wallace, J.G., (1973), Behavior of Lined Openings in Jointed and Unjointed Model Rock Masses, Technical Report No. N-73-6, U.S. Army Engineer Waterways Experiment Station, Vicksburg, Mississippi, September.

Zia, P., R.N. White and D.A. Vanhorn, (1970), "Principles of Model Analysis," ACI-Publication SP-24, Models for Concrete Structures, pp. 19-39.

Zienkiewicz, O.C., (1977), The Finite Element Method, McGraw Hill Book Co.

Zienkiewicz, O.C., B. Best, C. Dullage and K.G. Stagg, (1970), "Analysis of Nonlinear Problems in Rock Mechanics with Particular Reference to Jointed Rock Systems," Proc. 2nd Congress on Rock Mechanics, Belgrade.

